Universidad Miguel Hernández de Elche

Análisis de la contribución de los genes *MAS2*, *SMO4* y *RRP7* al metabolismo del ARN ribosómico en *Arabidopsis thaliana*

Rosa Micol Ponce

Elche, 2017

Análisis de la contribución de los genes *MAS2*, *SMO4* y *RRP7* al metabolismo del ARN ribosómico en *Arabidopsis thaliana*

Trabajo realizado por la Licenciada Rosa Micol Ponce, en la Unidad de Genética del Instituto de Bioingeniería de la Universidad Miguel Hernández de Elche, para optar al grado de Doctora.

Elche, 7 de junio de 2017.

MARÍA ROSA PONCE MOLET, Catedrática de Genética de la Universidad Miguel Hernández de Elche,

HACE CONSTAR:

Que el presente trabajo ha sido realizado bajo mi dirección y recoge fielmente la labor desarrollada por la Licenciada Rosa Micol Ponce para optar al grado de Doctora. Las investigaciones reflejadas en esta Tesis se han desarrollado íntegramente en la Unidad de Genética del Instituto de Bioingeniería de la Universidad Miguel Hernández de Elche.

María Rosa Ponce Molet

Elche, 7 de junio de 2017.

Instituto de Bioingeniería
Universidad Miguel Hernández

Avenida de la Universidad s/n
03202 ELCHE (Alicante)
Telf: 96 591 8817 - Fax: 96 522 2033
e-mail: bioingenieria@umh.es

A quien corresponda:

Eugenio Vilanova Gisbert, Catedrático de Toxicología y Director del Instituto de Bioingeniería,

HACE CONSTAR:

Que da su conformidad a la lectura de la Tesis Doctoral presentada por Doña **Rosa Micol Ponce**, titulada "Análisis de la contribución de los genes *MAS2*, *SMO4* y *RRP7* al metabolismo del ARN ribosómico en *Arabidopsis thaliana*", que se ha desarrollado dentro del Programa de Doctorado en Bioingeniería de este Instituto, bajo la dirección de la profesora Dra. María Rosa Ponce Molet.

Lo que firmo en Elche, a instancias de la interesada y a los efectos oportunos, a siete de junio de dos mil diecisiete.

Eugenio Vilanova Gisbert
Catedrático de Toxicología
Director del Instituto de Bioingeniería

A mi familia y amigos

ÍNDICE DE MATERIAS

ÍNDICE DE FIGURAS

ÍNDICE DE TABLAS

I.- PREFACIO

I.- PREFACIO

Este documento se ha elaborado siguiendo la normativa de la Universidad Miguel Hernández de Elche para la "Presentación de Tesis Doctorales con un conjunto de publicaciones" y se ha dividido en las partes siguientes:

1.- Un apartado de *Resumen y conclusiones*.

2.- Una *Introducción*, en la que se presenta el tema de la Tesis, el organismo experimental elegido y los antecedentes y objetivos del trabajo realizado.

3.- Una *Bibliografía de la introducción*.

4.- Un apartado de *Publicaciones,* que contiene las cuatro siguientes, dos de ellas publicadas en revistas del primer cuartil de su categoría (se indica el índice de impacto [IF] del año de su publicación) y otras dos pendientes de envío.

Micol-Ponce, R., Aguilera, V., y Ponce, M.R. (2014). A genetic screen for suppressors of a hypomorphic allele of Arabidopsis *ARGONAUTE1*. *Scientific Reports* **4**, 5533. IF (2014): 5,578.

Sánchez-García, A.B., Aguilera, V., Micol-Ponce, R., Jover-Gil, S., y Ponce, M.R. (2015). Arabidopsis *MAS2*, an essential gene that encodes a homolog of animal NF-Kappa B activating protein, is involved in 45S ribosomal DNA silencing. *Plant Cell* **27**, 1999-2015. IF (2015): 8,538.

Micol-Ponce, R., Sarmiento-Mañús, R., y Ponce, M.R. The ribosomal biogenesis factor SMALL ORGAN 4 functions in 5.8S and 18S rRNA maturation in Arabidopsis. Pendiente de envío (a).

Micol-Ponce, R., Sarmiento-Mañús, R., Ruiz-Bayón, A., y Ponce, M.R. Arabidopsis RIBOSOMAL RNA PROCESSING 7 participates in 45S rDNA transcriptional regulation and 45S pre-rRNA processing. Pendiente de envío (b).

5.- Un *Anexo*, que incorpora 30 comunicaciones a congresos: 14 nacionales y 16 internacionales.

Durante mi periodo predoctoral en el laboratorio de M.R. Ponce también he publicado tres artículos que no se incluyen en esta Tesis:

Ferrández-Ayela, A., Alonso-Peral, M.M., Sánchez-García, A.B., Micol-Ponce, R., Pérez-Pérez, J.M., Micol, J.L., y Ponce, M.R. (2013). Arabidopsis *TRANSCURVATA1* encodes NUP58, a component of the nucleopore central channel. *PLOS ONE* **8**, e67661. IF (2013): 4,490. Destacado en Faculty of 1000.

Ferrández-Ayela, A., Micol-Ponce, R., Sánchez-García, A.B., Alonso-Peral, M.M., Micol, J.L., y Ponce, M.R. (2013). Mutation of an Arabidopsis NatB N-alpha-terminal acetylation complex component causes pleiotropic developmental defects. *PLOS ONE* **8**, e80697. IF (2013): 4,490.

Micol-Ponce, R., Sánchez-García, A.B., Barrero, J.M., Micol, J.L., y Ponce, M.R. (2015). Arabidopsis INCURVATA2 regulates salicylic acid and abscisic acid signaling, and oxidative stress responses. *Plant and Cell Physiology* **56**, 2207-2219. IF (2015): 4,319.

La introducción de esta Tesis no incluye un apartado de materiales y métodos, que están descritos en las publicaciones. Todas las citas que se intercalan en la introducción de esta memoria se corresponden con referencias que aparecen en la bibliografía del mismo apartado. Algunas de dichas citas se repiten en la bibliografía de los artículos. Las Figuras 8, 10 y 13 de la introducción de esta Tesis se corresponden total o parcialmente con otras de Micol-Ponce *et al.* (2014) y Micol-Ponce *et al.*, pendiente de envío (a y b).

En esta memoria se mencionan genes, mutaciones, alelos, mutantes y proteínas de *Homo sapiens*, *Arabidopsis thaliana* y *Saccharomyces cerevisiae* (a la que también se llama comúnmente "la levadura"), y en menor medida, de *Drosophila melanogaster*, *Caenorhabditis elegans* y *Schizosaccharomyces pombe*. Las comunidades de investigadores en estos seis sistemas modelo han desarrollado nomenclaturas diferentes, que hemos procurado respetar (Cherry, 1995; Meinke y Koornneef, 1997; Wain *et al.*, 2002). Así, se escriben con mayúscula inicial los acrónimos de los genes y proteínas de la levadura, pero no se emplean las minúsculas para los humanos y de Arabidopsis. Para facilitar la lectura de esta memoria hemos omitido la p final de los acrónimos de las proteínas de la levadura, práctica que se considera aceptable (Cherry, 1995). Se escriben en cursiva todos los nombres de genes, omitiendo prefijos descriptores de especie, como *At* (por *Arabidopsis thaliana*), que fueron desaconsejados por Meinke y Koornneef (1997).

Para la redacción de esta memoria se han seguido las mismas pautas que en Tesis anteriores del laboratorio de M.R. Ponce. Se ha preferido usar los acrónimos castellanizados ADN y ARN —de uso común en los medios de comunicación españoles—, en lugar de los recomendados por la International Union of Pure and Applied Chemistry, DNA y RNA, para los ácidos desoxirribonucleico y ribonucleico, respectivamente. Esta elección no está basada en ningún argumento que se considere incontestable; ambas opciones son aceptadas por el *Diccionario de la Lengua Española* (vigesimotercera edición, 2015) de la Real Academia Española (RAE). Tal como recomienda la RAE en su *Ortografía de la lengua española* (2010), en esta memoria no se realiza el plural de las siglas añadiendo al final una s minúscula: se escribe "el ARN" y también "los ARN". Se emplean aquí algunos extranjerismos de uso común que carecen de una traducción al español generalmente aceptada, como *splicing* —el procesamiento de los intrones—, que solo algunos autores traducen como "ayuste", la unión de dos cuerdas o trozos de madera por sus extremos. El carácter foráneo de estas palabras se ha destacado en cursiva. No hemos traducido al español muchos de los nombres de genes y proteínas que se mencionan en esta memoria; en estos casos solo hemos usado la cursiva para los genes.

II.- RESUMEN Y CONCLUSIONES

II.- RESUMEN Y CONCLUSIONES

Se considera metabolismo del ARN a cualquier evento en el ciclo de vida de estas moléculas, como su síntesis, plegamiento, procesamiento, modificación y degradación. Una de las facetas más antiguas y complejas del metabolismo del ARN es la biogénesis del ribosoma citoplásmico eucariótico, también llamado ribosoma 80S, en la que intervienen los productos de más de 350 genes, que sintetizan, modifican, ensamblan y transportan unas 80 proteínas ribosómicas (PR) y cuatro ARN ribosómicos (ARNr).

Otro aspecto del metabolismo del ARN es el silenciamiento postranscripcional mediado por microARN (miARN), en el que la proteína ARGONAUTE1 (AGO1) juega un papel central en Arabidopsis. Los alelos de insuficiencia de función del gen *AGO1* causan un fenotipo pleiotrópico —letal en los casos más severos— que parece deberse a la alteración de numerosos aspectos del desarrollo. En el laboratorio de M.R. Ponce se han identificado alelos hipomorfos y viables de *AGO1* y de otros genes de la maquinaria de los miARN, inducidos mediante metanosulfonato de etilo (EMS), uno de los cuales es *ago1-52*, portador de una mutación puntual que perturba el *splicing* de su transcrito primario.

ago1-52 fue mutagenizado con EMS en una tesis anterior a esta, con el objetivo de aislar dobles mutantes con fenotipos sinérgicos, que permitiesen identificar genes relacionados funcionalmente con *AGO1*. El escrutinio de 56.810 semillas M_2 nos ha permitido aislar, entre otras, 23 líneas viables en las que el fenotipo morfológico de *ago1-52* se suprime casi totalmente. Hemos denominado *morphology of argonaute1-52 suppressed* (*mas*) a las segundas mutaciones de las que son portadoras estas líneas, todas las cuales, salvo una, son supresores extragénicos. Hemos considerado a las mutaciones *mas* candidatas a ser alelos de genes funcionalmente relacionados con *AGO1*.

Mediante análisis iterativo del ligamiento a marcadores moleculares se identificaron transiciones G→A —las mutaciones que con más frecuencia causa el EMS— en los genes AT4G02720 y AT1G80070, a los que hemos denominado *MAS2* y *MAS5*, respectivamente. *MAS2* es un gen esencial de copia única que codifica una proteína homóloga de las NKAP (NF-kappa B Activating Proteins) de los metazoos. Hemos demostrado que MAS2 participa en el control de la transcripción del ADNr 45S y el procesamiento de su transcrito primario, cuyos productos finales son los ARNr 25S, 18S y 5.8S. *MAS5* es un gen esencial que codifica la proteína PRP8 (PRE-MRNA-PROCESSING SPLICING FACTOR 8) de Arabidopsis. PRP8 es el elemento central del espliceosoma en todos los eucariotas en los que se ha estudiado. La caracterización de *MAS5* se completará más adelante.

Hemos realizado una búsqueda de interactores de MAS2 basada en el ensayo del doble híbrido de la levadura. Varios de los interactores identificados son ortólogos de proteínas cuya implicación en el control del *splicing* y en la biogénesis del ribosoma se ha demostrado en otros eucariotas. En esta tesis se han analizado dos de los genes que codifican interactores de MAS2: AT2G40430 y AT5G38720. El ortólogo de AT2G40430 en la levadura codifica la Nucleolar protein 53 (Nop53), que participa en la maduración del pre-ARNr 5.8S y en la biogénesis y exportación del núcleo al citoplasma de la subunidad mayor del ribosoma 80S. AT5G38720 es ortólogo del gen que codifica la Ribosomal RNA-processing protein 7 (Rrp7) de la levadura, que participa en la maduración del ARNr 18S. Durante el desarrollo de esta Tesis, otros autores han denominado *SMALL ORGAN 4* (*SMO4*) a AT2G40430; hemos llamado *RRP7* a AT5G38720. La insuficiencia de función de *SMO4* causa un fenotipo similar al de las mutaciones en algunos genes que codifican PR: sus hojas son ligeramente dentadas y apuntadas. Los alelos mutantes de *RRP7* alteran la filotaxia y la venación de los órganos laterales, retrasan la floración, reducen la fertilidad y causan hipersensibilidad al ácido abscísico durante el establecimiento de la plántula.

Hemos demostrado que SMO4 es una proteína nucleolar y nucleoplásmica y que RRP7 es nucleolar y perinucleolar. En los mutantes *smo4* y *rrp7* se acumulan intermediarios del procesamiento del pre-ARNr 45S, que indican que SMO4 participa en la maduración de los ARNr 5.8S y 18S, y RRP7 en la del ARNr 18S. Los niveles de las variantes *VAR* del pre-ARNr 45S están alterados en los mutantes *rrp7* y *smo4*, lo que evidencia la participación de RRP7 y SMO4 en el control, directo o indirecto, de la transcripción del ADNr 45S. Hemos demostrado que *rrp7-1* es epistático sobre *smo4-3*, y que ambos interaccionan con *mas2-1* y con alelos hipomorfos o nulos de genes que participan en el procesamiento del pre-ARNr 45S y en la regulación epigenética de la transcripción del ADNr 45S.

En conclusión, en esta tesis se han identificado supresores extragénicos de un alelo hipomorfo y viable del gen *AGO1* y se ha iniciado la caracterización de uno de ellos, *MAS5*, que muy probablemente juega un importante papel en el *splicing*, tal como hacen sus ortólogos en otros eucariotas. También se ha contribuido a la caracterización de otro, *MAS2*, que regula la transcripción del ADNr 45S y participa en la maduración del pre-ARNr 45S. Se ha confirmado que *SMO4* y *RRP7* codifican interactores de MAS2 y se ha demostrado a niveles genético, citológico y molecular que estos dos genes están implicados en la biogénesis del ribosoma citoplásmico de Arabidopsis y presentan actividades evolutivamente conservadas a la vez que divergentes. Nuestros resultados sugieren que *SMO4* y *RRP7* también participan en otras rutas del metabolismo del ARN.

III.- INTRODUCCIÓN

III.- INTRODUCCIÓN

III.1.- *Arabidopsis thaliana*: nacimiento y crecimiento de un sistema modelo

Arabidopsis thaliana (en adelante, Arabidopsis) es una brasicácea como la colifor, las mostazas o el rábano. Carece de interés agronómico pero ha atraído la atención de una comunidad científica numerosa. Fue descrita por primera vez en 1570 por Johannes Thal, médico y botánico alemán al que esta planta debe parte de su nombre. Uno de los primeros científicos que mostró interés por Arabidopsis en el siglo XX fue Friedrich Laibach, un discípulo de Edward Strasburger. Laibach determinó en su tesis doctoral (Laibach, 1907) el número de cromosomas de esta planta, a los que consideró demasiado pequeños para merecer la atención de un citólogo (Endersby, 2009). No obstante, reconoció más tarde el potencial de Arabidopsis: destacó su pequeño tamaño, que hace posible su cultivo a gran escala en cualquier laboratorio dotado de una cámara de crecimiento, sin recurrir a invernaderos; su ciclo de vida corto, que permite completar una generación en 6-8 semanas; su genoma diploide —a diferencia de muchas plantas cultivables, que son poliploides—, que facilita el análisis de las mutaciones recesivas; y su autogamia, que simplifica el mantenimiento de estirpes homocigóticas (Meyerowitz, 2001).

Arabidopsis se ha convertido en el sistema modelo de elección preferente para el estudio de la genética y la biología molecular de las plantas (Provart *et al.*, 2016). Aunque se celebraron simposios internacionales en 1965 (Göttingen) y 1976 (Frankfurt), la comunidad científica dedicada a su estudio no comenzó a crecer hasta la década de los ochenta (Meyerowitz, 2001). El espectacular ascenso de su popularidad se evidencia en la base de datos bibliográfica PubMed: se publicaron solo 4 artículos en la década de los 50 con la palabra “Arabidopsis” en su título o resumen, valor que pasó a ser de 31, 46, 237, 4.878 y 21.011 en cada una de las cinco décadas siguientes, y de 25.986 de 2010 a 2016.

El primer centro de conservación y distribución de semillas y clones de ADN de Arabidopsis (The Arabidopsis Biological Resource Center; ABRC) se constituyó en 1991 en Columbus (Ohio, Estados Unidos). La base de datos más usada actualmente es The Arabidopsis Information Resource (TAIR; Berardini *et al.*, 2015), que probablemente sea reemplazada a corto plazo por el Arabidopsis Information Portal (Araport; Krishnakumar *et al.*, 2015), financiado desde 2013 por la National Science Foundation de Estados Unidos. Araport posee una estructura modular que posibilita el acceso directo a diversas plataformas, que a su vez permiten obtener información y hacer pedidos de semillas y diversas herramientas genéticas y moleculares. Sus creadores lo han definido como *a one-stop-shop for* Arabidopsis thaliana *genomics* (https://www.araport.org).

III.2.- Estructura del genoma y manipulación genética de Arabidopsis

III.2.1.- Herramientas para la disección de la función de los genes

La secuencia genómica más completa y mejor anotada de Arabidopsis es la de Columbia-0 (Col-0), estirpe a la que se considera de referencia (The Arabidopsis Genome Initiative, 2000). Incluye 38.194 genes en tan solo 135,7 Mb (Tabla 1). Se trata por tanto de un genoma muy compacto, con 27.655 genes que codifican proteínas, el 39% de los cuales producen transcritos primarios que sufren *splicing* alternativo (Cheng *et al.*, 2017). Se ha publicado recientemente la secuenciación y anotación detallada de Landsberg *erecta* (L*er*), otra línea de uso común en los laboratorios (Zapata *et al.*, 2016).

Tabla 1.- Clasificación de los genes de Col-0 en función de la naturaleza de sus productos

Productos (si los tienen)	Número	Productos (si los tienen)	Número
Proteínas	27.655	ARN ribosómicos	15
ARN no codificantes intergénicos largos	2.444	Otros ARN	221
Transcritos antisentido naturales	1.115	Pequeños ARN (20-24 nt)	35.846
microARN	325	Pseudogenes	952
ARN pequeños nucleolares	287	Elementos transponibles	3.901
ARN transferentes	689		
ARN pequeños nucleares	82	Número total de genes	38.194

Estos datos corresponden a la anotación Araport11 del genoma de Col-0 (Cheng *et al.*, 2017).

Entre las numerosas herramientas genéticas, moleculares y bioinformáticas con que cuenta la comunidad de investigadores en Arabidopsis cabe destacar la disponibilidad de más de 1.200 ecotipos (también denominados accesos o razas), que difieren en morfología, respuestas a estímulos o tolerancia a diferentes tipos de estrés (Weigel, 2012). En 2008 se constituyó el “1001 Genomes Consortium”, cuyo objetivo fue el análisis a gran escala de la variación natural en Arabidopsis (http://1001genomes.org/index.html). Este consorcio ha secuenciado los genomas de más de mil accesos (Cao *et al.*, 2011; The 1001 Genomes Consortium, 2016), analizado su epigenoma (Kawakatsu *et al.*, 2016) y deducido su proteoma (Joshi *et al.*, 2012; http://1001proteomes.masc-proteomics.org/). Estos análisis a gran escala de la variación natural facilitarán la identificación de los genes que contribuyen a un determinado carácter mediante estudios de asociación a todo el genoma (GWAS, *genome-wide association studies*; The 1001 Genomes Consortium, 2016).

Los centros de germoplasma de Arabidopsis conservan y distribuyen miles de mutantes múltiples y centenares de miles de mutantes simples, la mayoría de los cuales pertenecen a colecciones indexadas (Alonso *et al.*, 2003): no han sido estudiados pero se

sabe qué gen está mutado en cada uno de ellos. Una de las razones —según algunos autores, la razón decisiva (Endersby, 2009)— de la aceptación de Arabidopsis como sistema modelo fue la eficacia de su transformación mediante infección con *Agrobacterium tumefaciens*, que incorporó la transgénesis al inventario de herramientas cotidianas para el análisis funcional de los genes de esta planta (Provart *et al.*, 2016).

A la obtención de mutantes insercionales mediante transgénesis se han añadido recientemente las técnicas de silenciamiento génico postranscripcional (mediante miARN artificiales [amiARN]; Schwab *et al.*, 2006) y de edición genómica (CRISPR; Feng *et al.*, 2013; Li *et al.*, 2013) que permiten ampliar el catálogo de mutantes disponibles, así como inactivar simultáneamente varios genes, además de poder hacerlo exclusivamente en determinados tejidos o ante ciertos estímulos ambientales, estrategias que resultan de gran utilidad para el análisis de las funciones postembrionarias de los genes letales embrionarios (Lowder *et al.*, 2016).

Las aproximaciones a gran escala, denominadas genéricamente “ómicas”, como la genómica, la transcriptómica o la proteómica, han producido cantidades ingentes de datos, cuya minería y análisis han requerido el desarrollo de nuevas herramientas bioinformáticas que se han hecho cotidianas para el análisis funcional de los genes (Toloti Carneiro *et al.*, 2015). Pese a la disponibilidad de este vasto repertorio de técnicas experimentales y recursos bioinformáticos aún no se ha predicho la función de unos 13.500 genes de Arabidopsis y no se sabe en qué proceso participan 7.500 de ellos (Provart *et al.*, 2016).

III.2.2.- Análisis mutacional

La agricultura se ha basado secularmente en la selección masal, que ya se aplicó en las etapas iniciales de la domesticación de las plantas cultivables (Hillman y Davies, 1990). Este método consiste en la selección de las plantas aparentemente más aptas, productivas o resistentes, a fin de propagarlas, de manera que constituyan la fuente de las semillas para la siembra en la estación siguiente. En una población de plantas cultivadas obtenidas mediante polinización abierta, la heterogeneidad fenotípica intrapoblacional se debe a la preexistencia de mutaciones espontáneas. Las líneas puras que se han obtenido tras milenios de selección en muchas especies cultivables han reducido su diversidad genética y han generado la necesidad de incrementarla (Sikora *et al.*, 2011).

A principios del siglo XX se obtuvieron varias conclusiones de especial relevancia para el análisis causal del desarrollo de los animales y las plantas: que los mutantes morfológicos resultaban especialmente útiles para comprender determinados procesos, que eran portadores de mutaciones espontáneas que dañaban genes responsables del

proceso a estudio, y que dichas mutaciones ocurrían naturalmente con una frecuencia muy baja, que convenía incrementar mediante procedimientos artificiales (Smartt y Simmonds, 1995). Estas ideas fundamentaron el descubrimiento del primer mutágeno, los rayos X, de la mano de Hermann J. Müller, un discípulo de Thomas H. Morgan, lo que le valió el Premio Nobel de Fisiología o Medicina en 1946 (Carlson, 2013). A los rayos X les siguieron los gamma y los neutrones rápidos (Sikora *et al.*, 2011). Tras la Segunda Guerra Mundial, a los mutágenos físicos se añadieron los químicos, como el gas mostaza (Auerbach y Robson, 1946) y los metanosulfonatos de alquilo, que siguen siendo de uso común en muchos laboratorios (Westergaard, 1957). Los mutágenos químicos son fáciles de obtener y usar, no requieren equipamiento pesado ni instalaciones de seguridad, y son muy efectivos, causando muchas mutaciones que son habitualmente sencillas, ya que afectan a solo una o unas pocas bases nucleotídicas y no producen reorganizaciones cromosómicas (Sikora *et al.*, 2011).

El mutágeno químico más popular en Arabidopsis y muchas otras especies —por su gran mutagenicidad y baja mortalidad— es el metanosulfonato de etilo (EMS; $C_3H_8O_3S$). El EMS alquila la guanina, convirtiéndola en O-6-etilguanina, que no es complementaria de la citosina sino de la timina. En consecuencia, durante la replicación del ADN mutado se incorpora a la cadena naciente, frente a la O-6-etilguanina, una timina en lugar de una citosina. Se inducen así, en cualquier parte del genoma, transiciones G/C→A/T; este tipo de mutación supone el 99% de las que causa el EMS (Till *et al.*, 2004; Kim *et al.*, 2006; Till *et al.*, 2007). En base a la frecuencia en el uso de codones que contienen G o C en Arabidopsis, se ha estimado que la mayoría de las mutaciones que genera el EMS en regiones codificantes del genoma (≈ 65%) son hipomorfas y de cambio de sentido en la proteína mutante. Las mutaciones sin sentido aparecerían con una frecuencia mucho menor (≈ 5%; Kim *et al.*, 2006). A lo anterior debe añadirse que el EMS también puede dañar las señales donantes y aceptoras del *splicing*, ya que la primera y la última base nucleotídica de los exones y los intrones es una guanina. La alteración de la maduración del pre-ARN mensajero (ARNm) como consecuencia de una transición G→A en una señal donante o aceptora del *splicing* puede reducir o anular la actividad del gen afectado. La gran efectividad del EMS como mutágeno y su capacidad de acceder a cualquier parte de un cromosoma permite alcanzar la saturación de un genoma con mutaciones (Krieg, 1963).

La nomenclatura de uso habitual en las mutagénesis de Arabidopsis es la que muestra la Figura 1. La tasa de mutación del EMS en Arabidopsis, estimada en la generación M_2, oscila entre 1/1.000 y 1/5.000 nucleótidos, empleando concentraciones del mutágeno que varían en función del grado de saturación del genoma requerido (0,1-0,4%

v/v de EMS en agua) y tiempos de exposición de 3-15 horas (Page y Grossniklaus, 2002; Kim *et al.*, 2006; Weigel y Glazebrook, 2006; Qu y Qin, 2014). En consecuencia, tras una mutagénesis convencional cada planta M_1 sería portadora de más de 700 mutaciones (Jander *et al.*, 2003), y cada planta M_2 fenotípicamente mutante, de entre 2 y 75 mutaciones adicionales a la que causa su fenotipo (Feldmann *et al.*, 1994). Sin embargo, la secuenciación masiva de mutantes inducidos por EMS indica que las plantas M_2 son portadoras de unas 1.200 mutaciones (Ashelford *et al.*, 2011). La gran mutagenicidad del EMS permite completar el espectro de las mutaciones que pueden perturbar un proceso biológico, saturando en consecuencia el genoma a estudio, tras el escrutinio de solo unas decenas de miles de individuos M_2.

Se denomina mutagénesis de saturación a aquella en la que se obtiene al menos un alelo de cada gen implicado en el proceso a estudio (Pollock y Larkin, 2004). La eficacia de una mutagénesis se ha estimado habitualmente en Arabidopsis determinando la frecuencia de embriones letales (semillas que no completan su desarrollo dentro de la

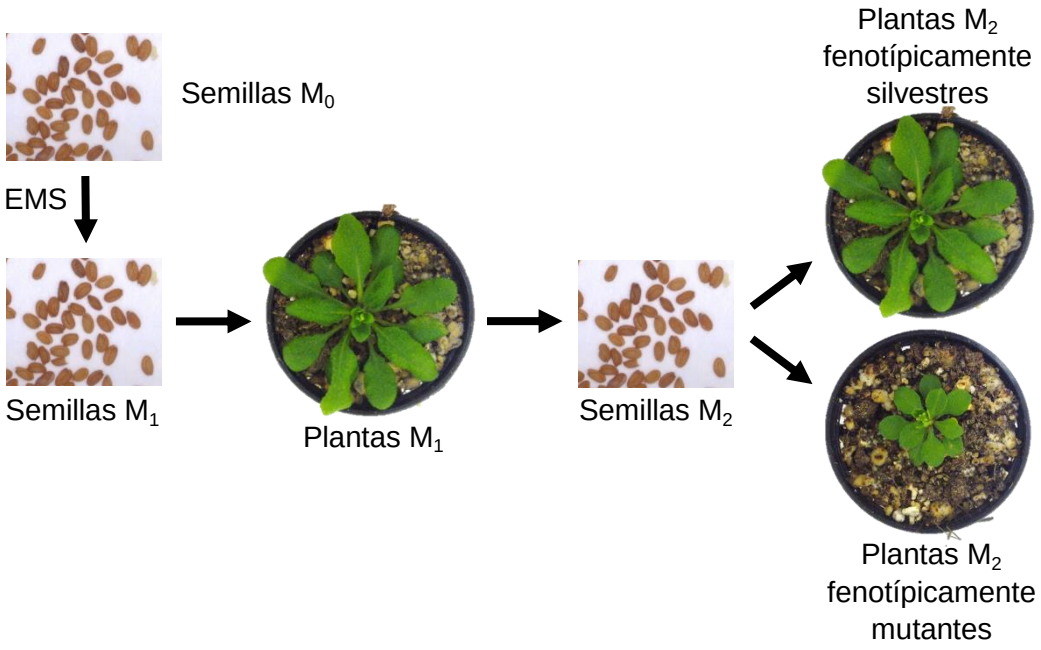

Figura 1.- Etapas de una mutagénesis con EMS en Arabidopsis. Las semillas que se mutagenizan con un mutágeno físico o químico se denominan M_0 y M_1, antes y después de su exposición al mutágeno, respectivamente. La germinación de las semillas M_1 rinde plantas M_1, que son heterocigóticas para cada una de las mutaciones producidas por el mutágeno, la mayoría de las cuales son recesivas. El fenotipo causado por estas últimas se manifestará en las plantas homocigóticas de la siguiente generación (M_2), derivadas de la autofecundación de las plantas M_1. El escrutinio del fenotipo de interés se realiza en la generación M_2. La mutación a estudio segregará en las plantas M_2, observándose en las homocigotas el fenotipo deseado.

silicua) y plántulas albinas, dos fenotipos de fácil escrutinio. Se consideran aceptables, por su equilibrio entre eficacia (tasa de mutación) y letalidad, las mutagénesis en las que entre el 5 y el 10% de las plantas M_1 muestran en sus silicuas algún embrión letal, y al menos una de cada 250 plántulas M_2 es albina (Feldmann *et al.*, 1994).

Se denomina mutagénesis de segundos sitios (*second site mutagenesis*; Peters *et al.*, 2003) a aquella que se realiza mutagenizando un mutante preexistente. Su objetivo es identificar genes funcionalmente relacionados, cuyas mutaciones pudieran incrementar o disminuir la severidad del fenotipo del mutante original. En esta tesis se ha realizado un escrutinio de los dobles mutantes obtenidos en una mutagénesis de segundos sitios del mutante *ago1-52*, que fue obtenido en una mutagénesis anterior, en la que el tipo silvestre L*er* fue tratado con EMS (Micol-Ponce *et al.*, 2014; página 61 y siguientes).

III.3.- Mecanismos de regulación de la expresión génica

III.3.1.- Regulación transcripcional, postranscripcional y postraduccional

El desarrollo está regulado genéticamente. La arquitectura corporal de un animal o una planta es el resultado final de un proceso complejo en el que las células toman decisiones asociadas a patrones de expresión génica espaciales y temporales que son específicos de tejido y estado de desarrollo (Davidson y Erwin, 2006). La regulación de la iniciación de la transcripción mediada por la actividad de factores de transcripción que se unen a sus secuencias diana en el ADN es común a muchos genes de todos los seres vivos. Esta lógica fue descubierta en los análisis bioquímicos y genéticos del operón de la lactosa de *Escherichia coli* realizados por Jacob y Monod (1961) y opera no solo en el desarrollo de los organismos pluricelulares, sino también en su fisiología y respuestas al ambiente.

La estructura de las células eucarióticas, en las que el núcleo y el citoplasma están compartimentados durante buena parte del ciclo celular, la compacidad de la cromatina en el núcleo y la existencia de exones e intrones exigen mecanismos de regulación de la expresión génica distintos de los procarióticos. El inicio de la transcripción eucariótica se regula, como en las bacterias, mediante la unión de factores de transcripción —activadores o represores— a sus secuencias diana, pero también mediante cambios estructurales en la cromatina. Estos últimos modulan el acceso de los factores de transcripción específicos y la maquinaria general de la transcripción a los promotores de los genes. Existen además mecanismos de regulación postranscripcionales, que intervienen en la maduración del pre-ARNm y la exportación, degradación, estabilización y traducción de los ARNm. Finalmente, existen mecanismos de regulación postraduccionales, que modifican

químicamente las proteínas para su activación o desactivación, integración en homo o heteromultímeros, desplazamiento entre compartimentos subcelulares, estabilización o degradación (Nestler y Hyman, 2002). Están recibiendo una atención creciente los mecanismos de silenciamiento génico transcripcional y postranscripcional mediados por pequeños ARN reguladores no codificantes, que no se traducen a proteínas.

III.3.2.- Silenciamiento génico mediado por ARN no codificantes

Muchos ARN de los eucariotas pluricelulares no codifican proteínas, y participan en procesos tan diversos como la maduración de los ARN ribosómicos (ARNr), el *splicing* y la traducción (Tabla 1, en la página 6). En las últimas dos décadas se han identificado varias especies de pequeños ARN reguladores (sARN; small RNAs), de 20-30 nt, que reprimen a nivel postranscripcional (PTGS; post-transcriptional gene silencing) o transcripcional (TGS; transcriptional gene silencing) la expresión de sus genes diana. Los sARN se unen por complementariedad a los ARNm, en complejos de silenciamiento denominados RISC (RNA-induced silencing complex) o RIST (RNA-induced transcriptional silencing complex; revisado en Xie *et al.*, 2004; Ding y Voinnet, 2008; Czech y Hannon, 2011; Pontes *et al.*, 2013). Los principales sARN son los miARN y los ARN pequeños interferentes (siARN; small interferent RNAs, siRNAs), que se generan a partir de ARN bicatenarios (dcARN), que son sustratos de ribonucleasas denominadas DICER-like (DCL; revisado en Ghildiyal y Zamore, 2009; Voinnet, 2009). Las dianas y la biogénesis de los miARN y los siARN son diferentes, pero sus mecanismos de silenciamiento son muy parecidos y las correspondientes maquinarias poseen componentes comunes (Figura 2, en la página 12).

Los precursores de los miARN son productos de la transcripción de genes endógenos y forman estructuras secundarias en horquilla. La transcripción de los genes de los miARN es llevada a cabo por la ARN polimerasa II (ARN pol II), dando lugar a un miARN primario (pri-miARN; revisado en Rogers y Chen, 2013) que es procesado en Arabidopsis por un complejo del que forman parte: la RNasa III DICER-LIKE1 (DCL1; Jacobsen *et al.*, 1999; Schauer *et al.*, 2002); HYPONASTIC LEAVES1 (HYL1; Han *et al.*, 2004; Tomari y Zamore, 2005), una proteína que se une a ARN bicatenario; SERRATE (SE; Grigg *et al.*, 2005; Lobbes *et al.*, 2006; Yang *et al.*, 2006a), una proteína con dedos de zinc que también participa en el *splicing* (Laubinger *et al.*, 2008); y TOUGH (TGH; Ren *et al.*, 2012b), una proteína de unión a ARN. La actividad de este complejo rinde un dúplex miARN/miARN*, que es metilado por la metiltransferasa HUA ENHANCER1 (HEN1; Yu *et al.*, 2005), que lo protege de su uridilación por HEN1 SUPPRESSOR1 (HESO1; Ren *et al.*, 2012a) y posterior degradación.

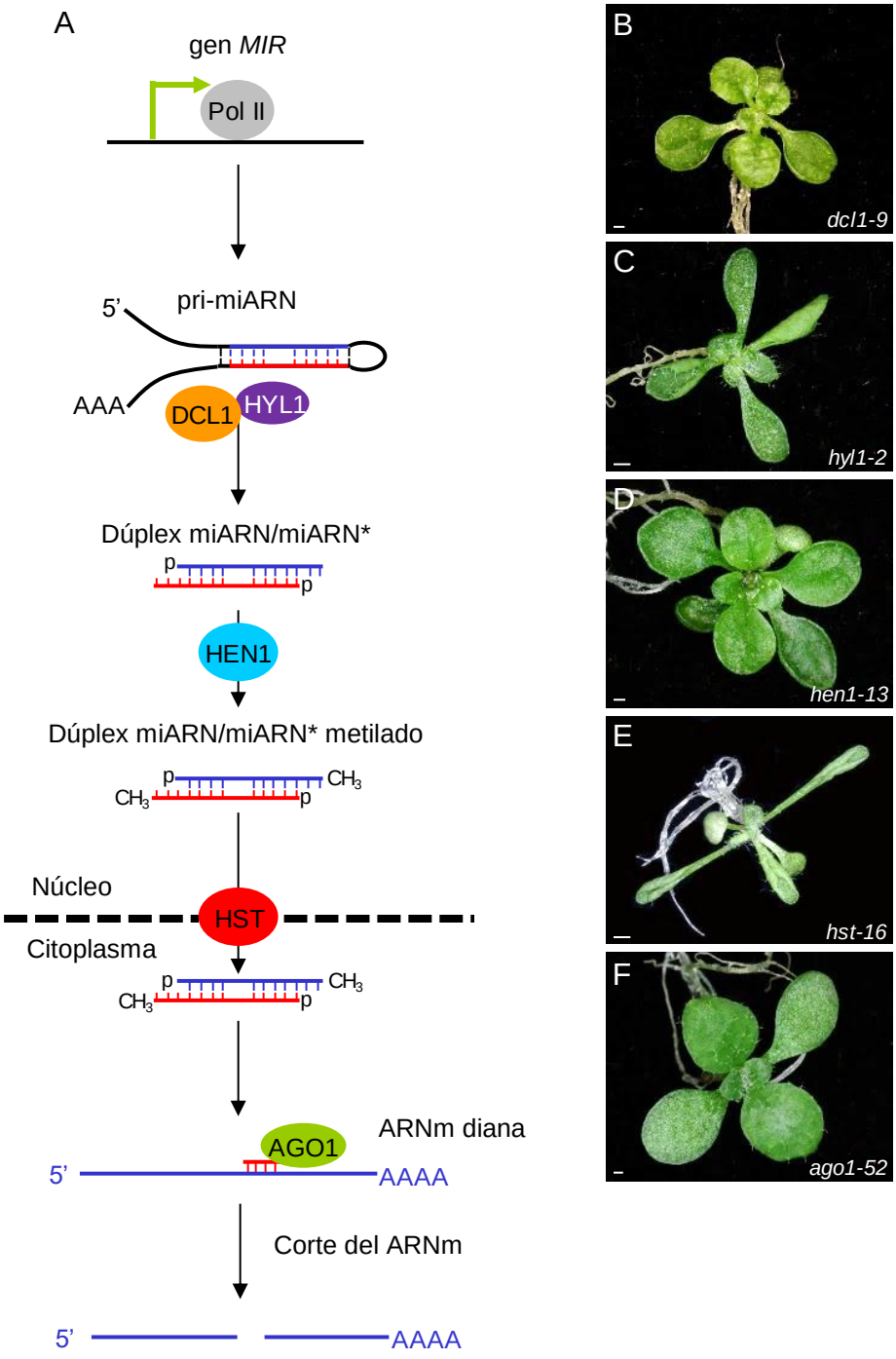

Figura 2.- Componentes de la maquinaria de los miARN: actividad y efectos fenotípicos de su insuficiencia de función. (A) Biogénesis y actividad de los miARN en las plantas. Se muestran solo algunos de los componentes de la maquinaria de los miARN. El símbolo ↱ indica el sitio de inicio de la transcripción de un gen (*MIR*) cuyo producto es un miARN. Pol II: ARN pol II. (B-F) Fenotipos morfológicos de plantas homocigóticas para los alelos nulos (C) *hyl1-2*, (D) *hen1-13* y (E) *hst-16* y los hipomorfos (B) *dcl1-9* y (F) *ago1-52* (los alelos nulos de *DCL1* y *AGO1* son letales). Las barras de escala indican 1 mm. Modificado a partir de Aguilera Díaz (2009), que a su vez se inspiró en Brodersen y Voinnet (2006).

Los dúplex miARN/miARN* maduros son transportados del núcleo al citoplasma por HASTY (HST; Telfer y Poethig, 1998; Park *et al.*, 2005), una proteína homóloga de la Exportina-5 humana. Una vez en el citoplasma, el miARN se incorpora al RISC, que contiene la endonucleasa ARGONAUTE1 (AGO1; Bohmert *et al.*, 1998). El silenciamiento de un ARNm por un miARN implica su unión por complementariedad y la actuación de AGO1 (Rogers y Chen, 2013). Se denomina componentes de la maquinaria de los miARN a las proteínas que participan en su biogénesis (DCL1, y HEN, que son perinucleolares, y HYL1, SE, TGH y HEN1) y a HST y AGO1 (Figura 2; Pontes *et al.*, 2013).

AGO1 es el principal componente de los RISC de Arabidopsis; se une a los miARN y a los siARN producidos por transgenes y virus para actuar sobre sus ARNm diana, cortándolos o inhibiendo su traducción. En Arabidopsis, como en otros organismos, los miARN reprimen a muchos genes que codifican factores de transcripción implicados en el control del desarrollo, el metabolismo y el estrés (revisado en Jover-Gil *et al.*, 2005).

Las dianas de los miARN son moléculas de ARNm resultantes de la transcripción de genes endógenos, que codifican proteínas implicadas en una gran variedad de procesos biológicos. El origen de los siARN de Arabidopsis es muy diverso, como la transcripción convergente de dos genes, o la de regiones intergénicas o intrones, así como ARNm aberrantes. También, de loci silenciados epigenéticamente como los transposones, retroelementos, genes de ADN ribosómico (ADNr) y las repeticiones pericentroméricas (Allen *et al.*, 2005; Xie y Qi, 2008). En todos estos casos se forman moléculas de dcARN que son precursoras de los siARN. Los siARN promueven la modificación del ADN y las histonas de sus loci originarios, reclutando desacetilasas de histonas, metiltransferasas de histonas y de ADN, y complejos remodeladores de la cromatina (Ossowski *et al.*, 2008; Vaucheret, 2008; Xie y Qi, 2008; revisado en Pontes *et al.*, 2013).

EL PTGS mediado por siARN podría ser un sistema inmune primitivo, para la protección del genoma frente a ácidos nucleicos invasores, como el ARN bicatenario viral, o endógenos, como los transgenes, los elementos genéticos móviles y las secuencias altamente repetitivas (Jensen *et al.*, 1999; Ratcliff *et al.*, 1999; Elbashir *et al.*, 2001; Wang y Metzlaff, 2005; Ossowski *et al.*, 2008; revisado en Borges y Martienssen, 2015).

III.3.3.- Funciones de la proteína ARGONAUTE1 de Arabidopsis

Los genes que codifican componentes clave de la maquinaria de silenciamiento génico mediado por siARN y miARN pertenecen a familias génicas más o menos numerosas, presentes en casi todas las especies en las que se han estudiado. Esta diversificación ha permitido su especialización en diferentes rutas (Shabalina y Koonin,

2008), que explica los muy distintos efectos fenotípicos de las mutaciones en los parálogos de los genes *AGO* y *DCL* (Okamura *et al.*, 2004). Dicha especialización es particularmente clara en Arabidopsis, ya que cuenta con 6 ARN polimerasas dependientes de ARN para la obtención de dcARN, 4 proteínas DCL y 10 AGO. Existe redundancia funcional parcial entre los miembros de cada una de estas familias (revisado en Vazquez, 2006; Mallory y Vaucheret, 2010). Se ha propuesto la existencia de diferentes complejos de silenciamiento, de los que formarían parte distintas proteínas AGO (revisado en Czech y Hannon, 2011).

AGO1, el miembro fundador de la familia génica AGO, fue identificado en una búsqueda de mutantes de desarrollo anormal (Bohmert *et al.*, 1998). Los primeros mutantes *ago1* eran enanos, estériles y portadores de alelos nulos. Los alelos *ago1* hipomorfos causan un fenotipo mutante menos severo (Morel *et al.*, 2002; Yang *et al.*, 2006b). La proteína AGO1 inmunoprecipita con moléculas de miARN y diversas clases de siARN, entre ellos los producidos por transgenes y virus (Baumberger y Baulcombe, 2005; Qui *et al.*, 2005; Zhang *et al.*, 2006; revisado en Mallory y Vaucheret, 2010). AGO1 se asocia preferentemente con sARN que presentan una uridina en su extremo 5', como la mayoría de los miARN. El severo fenotipo causado por las mutaciones de insuficiencia de función *ago1* confirma la importancia de AGO1 en el silenciamiento mediado por miARN, especialmente si se compara con el de los alelos de sus parálogos (Vaucheret, 2008; revisado en Borges y Martienssen, 2015). Los alelos hipomorfos y nulos de *DCL1*, *HYL1*, *HEN1* y *HST* también perturban el desarrollo, en particular la morfología, el momento de la floración y la fertilidad (Kidner y Martienssen, 2005).

Mediante secuenciación masiva de sARN que inmunoprecipitan con AGO1, se ha constatado que un 30% son de 24 nt y están probablemente implicados en el PTGS, ya que proceden de regiones intergénicas y heterocromatínicas, incluidas las centroméricas. Algunos de estos sARN de 24 nt también derivan de la maduración de ARN transferentes (ARNt), de ARN pequeños nucleolares (snoARN, por small nucleolar RNAs) implicados en el procesamiento de los ARNr, y de ARN pequeños nucleares (snARN) que intervienen en el *splicing* (Wang *et al.*, 2011). La localización subcelular de AGO1 es compatible con esta observación, ya que se encuentra en el citoplasma, en donde se produce el PTGS, y también en el núcleo (revisado en Vaucheret, 2008).

III.4.- Estructura, biogénesis y funciones del ribosoma

III.4.1.- Componentes estructurales de los ribosomas

El ribosoma es la maquinaria de traducción de los ARNm en todos los seres vivos. Fue descubierto por George E. Palade en 1955, que obtuvo por ello el Premio Nobel de

Fisiología o Medicina en 1974 (Palade, 1955; 1975). Su alto grado de conservación permite la traducción de proteínas heterólogas en cualquier organismo. Está formado por dos subunidades, que contienen proteínas ribosómicas (PR) y ARNr. Existen tres tipos de ribosomas eucarióticos: el citoplásmico, que es el más grande y complejo, y el mitocondrial y el cloroplástico, que son similares al bacteriano.

El ribosoma procariótico mejor estudiado es el de *Escherichia coli* (también denominado 70S, por su coeficiente de sedimentación), que contiene 3 ARNr y 54 PR, mientras que el eucariótico citoplásmico (80S) incluye 4 ARNr y unas 80 PR (Melnikov *et al.*, 2012). La subunidad mayor del ribosoma procariótico (50S) está formada por los ARNr 23S y 5S, con 33 PR, y la menor (30S), por el ARNr 16S y 21 PR (Ban *et al.*, 2000; Wimberly *et al.*, 2000; Yusupov *et al.*, 2001). La subunidad mayor (60S) del ribosoma eucariótico contiene el ARNr 25S (en las levaduras y las plantas) o el 28S (en los animales), así como los ARNr 5.8S y 5S. La subunidad menor (40S) contiene en todos los eucariotas un solo tipo de ARNr, el 18S. En *Saccharomyces cerevisiae* (en adelante, la levadura), la subunidad mayor contiene 47 PR, y la menor, 33 (Klinge *et al.*, 2011; Rabl *et al.*, 2011; Klinge *et al.*, 2012).

III.4.2.- Organización genómica, estructura y expresión de los ADNr

III.4.2.1.- Transcripción de los genes implicados en la biogénesis del ribosoma

La biogénesis del ribosoma citoplásmico 80S (en adelante, el ribosoma) es muy compleja y requiere la acción coordinada de las tres ARN polimerasas comunes a todos los eucariotas. La ARN pol I transcribe el ADNr 47S en los mamíferos, 45S en las plantas y 35S en la levadura, rindiendo un primer precursor (pre-ARNr 47S, 45S o 35S) que tras un procesamiento complejo rendirá los tres ARNr mayores (5.8S y 18S en todos los eucariotas, y 25S en la levadura y las plantas o 28S en los mamíferos). La ARN pol III transcribe el ADNr 5S, los genes de los ARNt y de algunos snoARN que intervienen en la maduración de los ARNr. La ARN pol II transcribe los genes que codifican las PR, así como todas las proteínas y la mayoría de los snoARN implicados en la biogénesis del ribosoma; en este proceso intervienen varios cientos de proteínas, de las que solo unas 80 forman parte finalmente del ribosoma maduro (Gerhardy *et al.*, 2014).

III.4.2.2.- Estructura, organización y expresión de los ADNr 47S, 45S y 35S

La biogénesis del ribosoma ocurre en el nucleolo, el nucleoplasma y el citoplasma. Comienza en el nucleolo con la transcripción del ADNr 47S, 45S o 35S (Komarova *et al.*, 2008), que es máxima en las fases S y G2 del ciclo celular, y nula en la M. Las repeticiones

del ADNr están dispuestas en tándem; son unas 150 en las células haploides de la levadura, 300-400 en las humanas diploides y 750 en las de Arabidopsis. Las repeticiones del ADNr 47S, 45S o 35S se sitúan en las constricciones secundarias de los cromosomas acrocénticos, que reciben el nombre de regiones organizadoras nucleolares (NOR, nucleolar organizer region). Las NOR se encuentran en el brazo corto de los cromosomas 13, 14, 15, 21 y 22 humanos (Henderson *et al.*, 1972), en el XII de la levadura (Nomura *et al.*, 2000) y en el brazo corto de los 2 y 4 de Arabidopsis (Copenhaver y Pikaard, 1996). Cada unidad de ADNr 47S contiene las secuencias de los ARNr 18S, 5.8S y 28S (25S en el ADNr 45S; Figura 3) maduros, a las que se denomina regiones codificantes, separadas por dos espaciadores internos que se transcriben (ITS1 e ITS2) y flanqueadas por los espaciadores externos, que también se transcriben (5'-ETS y 3'-ETS).

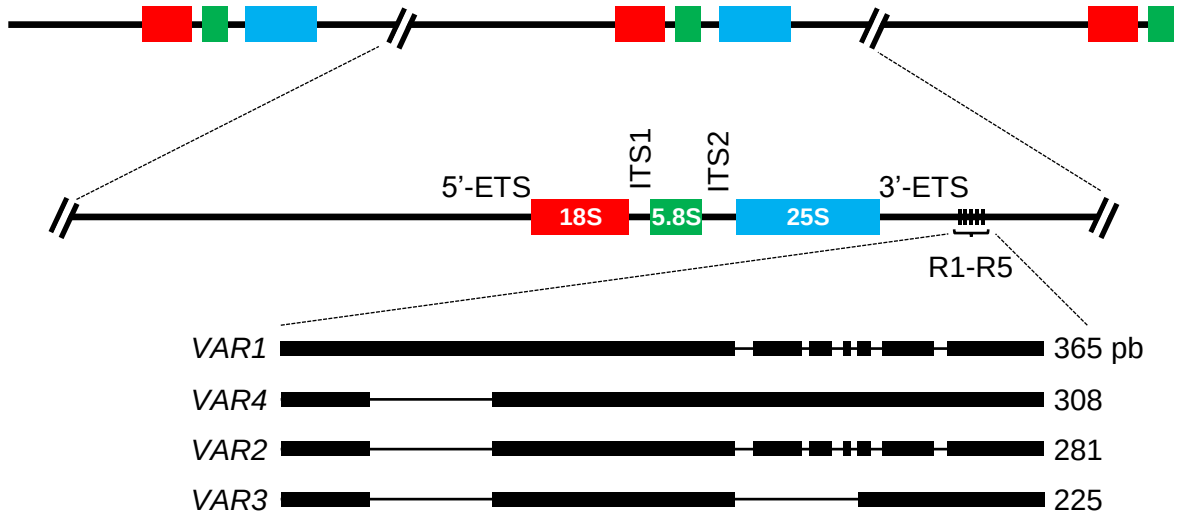

Figura 3.- Estructura y variantes de las unidades del ADNr 45S de Arabidopsis. Las regiones codificantes de los ARNr se destacan en rojo (18S), verde (5.8S) y azul (25S). Se indican las posiciones de los espaciadores externos (5'-ETS y 3'-ETS) e internos (ITS1 e ITS2). Se ha ampliado la región polimórfica entre distintas *VAR* del ADNr 45S, que difieren en secuencia y longitud. En el alineamiento de las cuatro *VAR* se representan con rectángulos y líneas, respectivamente, los segmentos presentes y ausentes en cada una de ellas. Modificado a partir de Pontvianne *et al.* (2010).

Cada unidad del ADNr 45S de Arabidopsis está separada de la siguiente por un espaciador intergénico (IGS; Rogers y Bendich, 1987; Jorgensen y Cluster, 1988), que no se transcribe. En Arabidopsis existen 4 variantes de las unidades del ADNr 45S, a las que se denomina *VARIANTS* (*VAR*), que difieren en la longitud y secuencia de un segmento de su extremo 3', que contiene distintas combinaciones de cinco secuencias repetidas de 47 pb (R1-R5). Cuatro de estas repeticiones son a su vez polimórficas, habiéndose descrito

las R1a, R1b, R1c, R2a, R2b, R3a, R3b, R4a y R4b. Las regiones polimórficas de las *VAR* de Arabidopsis difieren en longitud (Figura 3) y estructura, que es la siguiente, en sentido 5'→3': *VAR1*, R1a-R2a-R5-R3a; *VAR4*, R1c-R2a-R2b-R2b-R3a; *VAR2*, R1b-R3b-R3b; y *VAR3*, R1b-R4b-R4a-R3a (Abou-Ellail *et al.*, 2011).

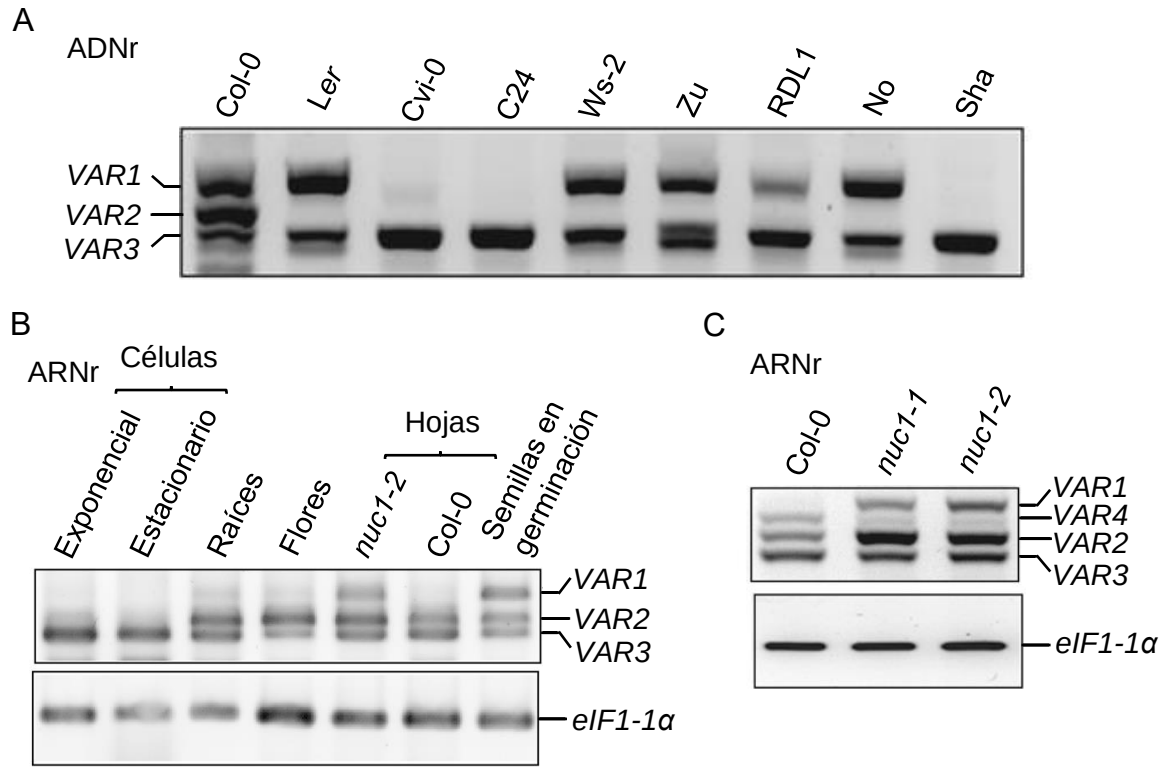

Figura 4.- Abundancia en el genoma y niveles de expresión de las variantes *VAR* del ADNr 45S de Arabidopsis. (A) Amplificación de las *VAR* del ADNr 45S en los accesos Col-0, L*er*, Cape Verde Islands (Cvi-0), C21, Wassilewskija-2 (Ws-2), Zurich (Zu), RDL1, Nossen (No) y Shahdara (Sha). (B, C) RT-PCR de las *VAR* del pre-ARNr 45S. (B) ARN extraído de células en cultivo en crecimiento exponencial o estacionario, raíces, flores, hojas y semillas en germinación. Todas las muestras son de Col-0, excepto la del mutante *nuc1-2*. Se utilizó como control el gen doméstico *eIF1-1α*, que codifica un factor de elongación de la traducción. (C) ARN extraído de Col-0 y los mutantes *nuc1-1* y *nuc1-2*. Modificado a partir de (A) Abou-Ellail *et al.* (2011) y (B, C) Pontvianne *et al.* (2010).

El número de copias de cada *VAR* en el genoma de Arabidopsis no se correlaciona con sus niveles de expresión (Figura 4). Las *VAR* se expresan además de modo distinto en diferentes accesos y etapas del desarrollo. Por ejemplo, la *VAR1* es la más abundante en el genoma de Col-0, pero no se expresa en las plantas adultas, en las que la más activa, *VAR4*, es la menos representada en el genoma (Abou-Ellail *et al.*, 2011). Las proporciones relativas de los transcritos de las *VAR* son modificadas por las mutaciones en algunos

genes, como *NUC1,* que codifica la NUCLEOLINA1, una proteína nucleolar implicada en la regulación de la expresión del ADNr 45S y del procesamiento del pre-ARNr 45S; *VAR1* se expresa en las plantas adultas *nuc1* (Pontvianne *et al.*, 2010). Los niveles de los ARNr mayores de Arabidopsis están controlados epigenéticamente, habiéndose observado diferencias en la metilación de las histonas de los promotores de las copias del ADNr 45S activas y silenciadas (Pontvianne *et al.*, 2012).

III.4.2.3.- Estructura, organización y expresión del ADNr 5S

Cada unidad del ADNr 5S de Arabidopsis tiene una longitud de 0,5 kb e incluye un espaciador intergénico (IGS) que no se transcribe, de unas 380 pb, y la región codificante del ARNr 5S, de 120 pb, que a su vez contiene un promotor interno (Figura 5). El IGS contiene tres motivos necesarios para la transcripción, entre ellos una caja TATATA, 28 pb aguas arriba de la región codificante. Aguas abajo de la región codificante, en el siguiente espaciador intergénico, se encuentra una señal de terminación de la transcripción, que incluye varias timidinas sucesivas (Cloix *et al.*, 2003). Existen dos variantes del ADNr 5S, solo una de las cuales (15-20% de los genes) se transcribe en plantas Col-0 de tres semanas. La variante que no se transcribe (80-85% de los genes) difiere de la anterior en 1-3 nt en la región codificante del ARNr 5S (Douet y Tourmente, 2007).

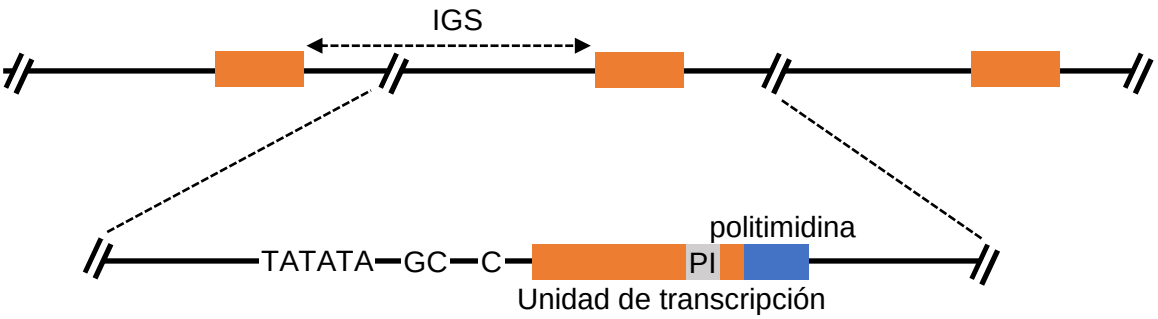

Figura 5.- Estructura de las unidades del ADNr 5S de Arabidopsis. Se representa en naranja la región codificante del ARNr 5S, y su promotor interno (PI), en gris. Las secuencias TATATA, GC y C no están representadas a escala. Modificado a partir de Douet y Tourmente (2007).

Existen 35-175 repeticiones del ADNr 5S en las células humanas (Stults *et al.*, 2008), 100-200 en las de la levadura (Petes, 1979) y unas 1.000 en las de Arabidopsis (por genoma haploide; Campell *et al.*, 1992). El ADNr 5S humano está situado en el brazo corto del cromosoma 1 (Sorensen *et al.*, 1991). Cada unidad del ADNr 5S de la levadura está dentro de una de ADNr 35S (Drouin y de Sa, 1995).

Los genes del ADNr 5S de Arabidopsis están agrupados en la heterocromatina pericentromérica de los cromosomas 3, 4 y 5, separados de los genes del ADNr 45S (Murata *et al.*, 1997; Fransz *et al.*, 1998; Tutois *et al.*, 1999; Cloix *et al.*, 2000). En el cromosoma 5 existen dos agrupaciones de genes del ADNr 5S, una en cada brazo cromosómico. La agrupación más corta de las dos del cromosoma 5 y la del 3 no se expresan; esta última no está presente en algunos ecotipos (Cloix *et al.*, 2002; 2003). Solo se transcriben las agrupaciones del cromosoma 4 y la más larga del 5, que tienen unas 150 kb e incluyen unas 300 unidades (Douet y Tourmente, 2007). En plantas de la familia de las Asteráceas el ADNr 5S está dentro del espaciador interno que separa las regiones codificantes de los ARNr 18S y 25S del ADNr 45S (Garcia *et al.*, 2010).

III.4.3.- Papel del nucleolo en la biogénesis del ribosoma

En el nucleolo de las plantas y los animales se sintetizan los ARNr y tiene lugar gran parte de la biogénesis de las subunidades ribosómicas (Brown y Shaw, 1998; Shaw y Brown, 2004). Aunque carece de membranas que lo separen del nucleoplasma o lo subdividan internamente, el nucleolo está compartimentado estructural y funcionalmente (Stepinski, 2014). En las plantas existen cuatro compartimentos nucleolares distinguibles mediante microscopía electrónica (Figura 6): los centros fibrilares (CF), el componente fibrilar denso (CFD), el componente granular (CG) y la vacuola (o vacuolas) o cavidad nucleolar (CN). Esta última está ausente en los nucleolos del resto de los eucariotas.

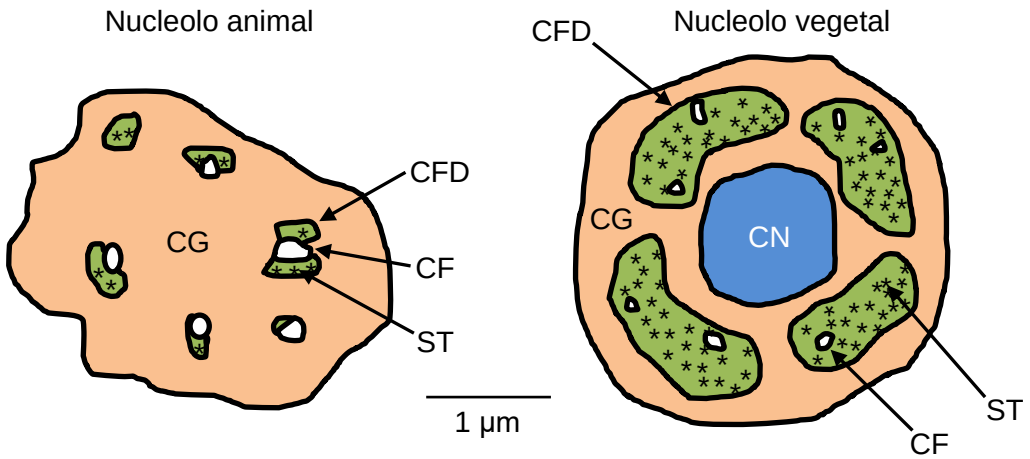

Figura 6.- Compartimentos del nucleolo animal y el vegetal. Los centros fibrilares (CF) se representan en blanco, el componente fibrilar denso (CFD) en verde, y el componente granular (CG) en naranja. La cavidad nucleolar (CN) aparece en azul. Los sitios de transcripción (ST) se destacan con asteriscos. En una célula vegetal típica, el CFD supone el 40-70% del nucleolo y puede distinguirse de los CF únicamente por su textura. Los CF suelen ser pequeños y están dispersos entre el CFD. Modificado a partir de Brown y Shaw (2008).

La transcripción del ADNr 45S y las primeras etapas de la maduración de las subunidades del ribosoma ocurren en el CFD (Shaw y Jordan, 1995; Stepinski, 2010) y las siguientes en el CG (Thiry y Lafontaine, 2005; Shaw y Brown, 2012). Se desconoce la función de la CN, en la que se propuso que se secuestraban temporalmente determinadas proteínas como los componentes del proteasoma (Moreno-Diaz de la Espina *et al.*, 1980). Se han detectado en la CN componentes de las ribonucleoproteínas nucleolares pequeñas (snoRNP) que modifican y procesan el pre-ARNr 45S (Brown y Shaw, 1998) como las de la snoRNP U1 (Moreno-Diaz de la Espina *et al.*, 1980; Lorkovic y Barta, 2008).

III.4.4.- Sinopsis de la biogénesis del ribosoma

La biogénesis del ribosoma es un proceso conservado en todos los eucariotas, con aspectos divergentes entre los hongos, plantas y animales. En la levadura comienza con la transcripción del ADNr 35S, durante la cual se asocian al pre-ARNr 35S en un orden determinado una parte de las PR y varios heteromultímeros proteicos y snoRNP. Estas últimas contienen un snoARN y varias proteínas que no son componentes estructurales del ribosoma maduro pero participan en su biogénesis. El procesamiento del pre-ARNr 35S consiste en su fragmentación y la eliminación de los ITS y ETS mediante cortes endonucleolíticos y la acción de exonucleasas, así como la metilación y pseudouridilación (conversión de uridina a pseudouridina) de algunos de sus nucleótidos (Weinstein y Steitz, 1999; Terns y Terns, 2002). El procesamiento de los pre-ARNr 47S, 45S y 35S es muy complejo, presentando numerosas etapas y algunas rutas alternativas, en las que se generan distintos precursores de los ARNr maduros (Henras *et al.*, 2015).

La partícula prerribosómica 90S o procesoma SSU (por *small subunit*, la subunidad 40S del ribosoma; Figura 7) contiene unas 70 proteínas (Turowski y Tollervey, 2015) y se va constituyendo cotranscripcionalmente en torno al pre-ARNr 35S, al que pliega y modifica, ensamblándolo con las PR y eliminando los ITS y ETS. Las rutas de biogénesis de las dos subunidades del ribosoma divergen tras el corte endonucleolítico del sitio A_2 del ITS1, que rinde la partícula prerribosómica pre-40S, que se exporta al citoplasma. La partícula prerribosómica pre-60S sufre etapas adicionales de procesamiento en el nucleolo y el nucleoplasma, una de las cuales es la incorporación del ARNr 5S maduro. El ADNr 5S se transcribe en el nucleoplasma, en donde su transcrito primario, el pre-ARNr 5S, sufre una maduración relativamente simple. Las partículas prerribosómicas pre-60S y pre-40S son exportadas a través de los nucleoporos de la membrana nuclear al citoplasma, en donde completan su maduración. Las subunidades 60S y 40S maduras se unen finalmente para formar el ribosoma 80S maduro (Thomas y Kutay, 2003).

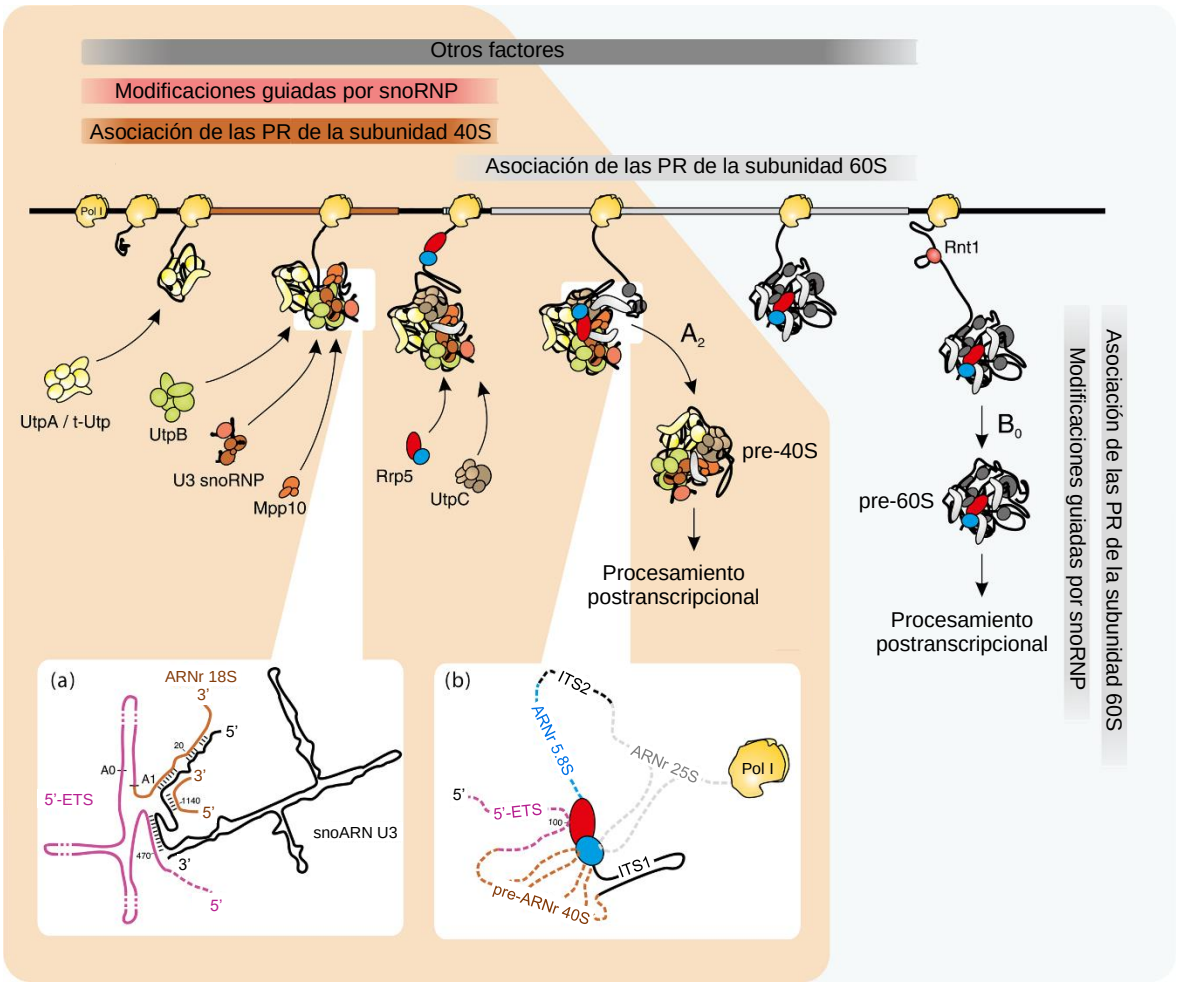

Figura 7.- Eventos cotranscripcionales en la biogénesis del ribosoma de la levadura. Se representa una versión simplificada del ensamblaje del procesoma SSU, así como del momento en que ocurren los cortes endonucleolíticos de los sitios A_2 y B_0 del pre-ARNr 35S, que liberan las partículas prerribosómicas pre-40S y pre-60S, respectivamente. Se amplían las uniones al pre-ARNr 35S de (a) el snoARN U3 (se destaca en marrón la región codificante del ARNr 18S) y (b) Rrp5, que son especialmente importantes para el plegamiento del pre-ARNr 35S. Tal como se aprecia en (a), el snoARN U3 se aparea por complementariedad con dos regiones de los extremos del pre-ARNr 35S, facilitando el plegamiento de este último. Modificado a partir de Turowski y Tollervey (2015).

III.4.5.- Maduración de los ARNr eucarióticos

III.4.5.1.- Procesamiento del pre-ARNr 35S en la levadura

Las primeras modificaciones que sufre el pre-ARNr 35S son la eliminación del 5'-ETS y el corte del ITS1 (Figura 7; Figura 8, en la página 23). En el procesamiento del 5'-ETS intervienen muchos componentes del procesoma SSU (Dragon *et al.*, 2002; Osheim *et al.*, 2004; Phipps *et al.*, 2011), y la mitad de las PR (O'Donohue *et al.*, 2010; Ferreira-Cerca *et al.*, 2005). La mayoría de los pre-ARNr 35S nacientes son procesados cotranscripcionalmente, eliminándose su 5'-ETS antes de que termine su transcripción,

mediante cortes sucesivos en los sitios A_0 y A_1 (Hughes y Ares, 1991; Beltrame *et al.*, 1994). La proteína nucleolar RNA 3'-terminal phosphate cyclase like (Rcl1) cataliza el corte del sitio A_2 del ITS1 (Udem y Warner, 1972; Billy *et al.*, 2000; Horn *et al.*, 2011), que libera la partícula pre-40S. Esta partícula contiene el pre-ARNr 20S y es exportada al citoplasma, en donde Nin one binding 1 (Nob1) corta el sitio D, generando el ARNr 18S maduro (Thoms *et al.*, 2015). La Ribonucleasa III Rnt1 corta el sitio B_0 del pre-ARNr 35S (Kufel *et al.*, 1999), situado a 20 nt del extremo 3' de la región codificante del ARNr 25S, generado la partícula pre-60S, que contiene el pre-ARNr $27SA_3$ y sufre etapas adicionales de maduración en el nucleoplasma. Algunos de los pre-ARNr 35S siguen la denominada ruta postranscripcional, en la que los cortes endonucleolíticos se producen en el orden B_0, A_0, A_1 y A_2. Tanto la ruta cotranscripcional como la postranscripcional rinden los pre-ARNr 20S y $27SA_2$. La extensión de 20 nt del extremo 3' del pre-ARNr $27SA_2$ es eliminada por la exonucleasa Rnase H 70 (Rnh70, también denominada Rex1; Kempers-Veenstra *et al.*, 1986).

En un 85-90% de los pre-ARNr $27SA_2$ sucede un corte en el sitio A_3, que es catalizado por la RNase for mitochondrial RNA processing (MRP), y en el B_{1L} en los restantes, obteniéndose los pre-ARNr $27SA_3$ y $27SB_L$, respectivamente. El pre-ARNr $27SA_3$ es procesado por la exorribonucleasa Ribonucleic acid trafficking 1 (Rat1) y la endonucleasa Ribosomal RNA processing 17 (Rrp17); esta última corta el sitio B_{1S}, generando el pre-ARNr $27SB_S$ (Henry *et al.*, 1994; Oeffinger *et al.*, 2009). El corte del sitio C_2 del ITS2 de los intermediarios alternativos $27SB_S$ y $27SB_L$ rinde dos productos: los pre-ARNr 26S y 7S, que a su vez puede ser $7S_S$ (de *short*, que es la forma mayoritaria) o $7S_L$ (de *large*).

La eliminación de los segmentos del ITS2 del extremo 3' del pre-ARNr $7S_{S/L}$ y el 5' del 26S es catalizada por exonucleasas. El extremo 5' del pre-ARNr 26S es degradado por Rat1 para formar el ARNr 25S maduro (Geerlings *et al.*, 2000), que es exportado al citoplasma. El pre-ARNr $7S_{S/L}$ tiene en su extremo 3' una extensión de 140 nt adicionales a la región codificante del ARNr 5.8S maduro, que son degradados por el exosoma en sentido 3'$\rightarrow$5', hasta una posición situada a 30 nt de esta última, generando el pre-ARNr 5.8S+30. Contribuye a este proceso la helicasa de ARN Mrna transport 4 (Mtr4), también llamada Dependent on elF4B (Dob1; de la Cruz *et al.*, 1998; Li *et al.*, 2016), que es reclutada por la Nucleolar protein 53 (Nop53; Thoms *et al.*, 2015). Mtr4 parece facilitar la actuación del exosoma desplazando las proteínas unidas al pre-ARNr $7S_{S/L}$ o deshaciendo las estructuras secundarias del precursor. A continuación, la exonucleasa Rrp6 elimina otros 22 nt del extremo 3' del precursor 5.8S+30, rindiendo el pre-ARNr 6S. Tras la exportación al citoplasma de la subunidad pre-60S, la exonucleasa Ngl2 acorta el extremo 3' del pre-ARNr 6S produciendo el ARNr 5.8S maduro (Thomson y Tollervey, 2010).

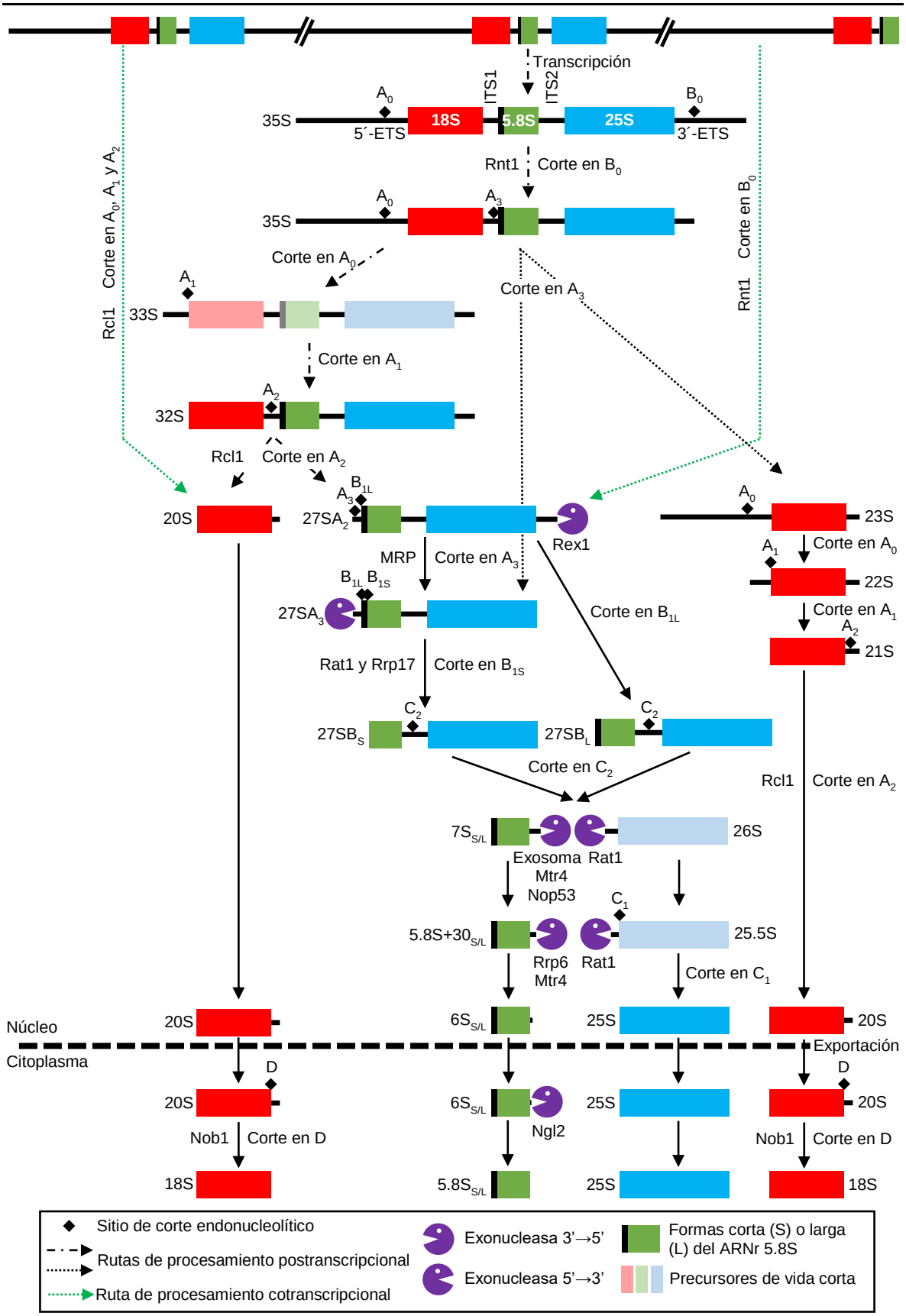

Figura 8.- Procesamiento del pre-ARNr 35S en la levadura. Se siguen las pautas definidas en el pie de la Figura 3, en la página 16. Las flechas indican las etapas del procesamiento. Las extensiones de los intermediarios no se han dibujado a escala. Modificado a partir de Henras *et al*. (2015).

III.4.5.2.- Procesamiento del pre-ARNr 47S en los mamíferos

En la mayoría de los pre-ARNr 47S de las células de mamífero en cultivo, el primer corte sucede en el sitio A_0 del 5'-ETS. En algunos animales y plantas ocurre antes un corte en el sitio llamado A' o 1, que contiene un motivo de 11 nt muy conservado, al que se unen la snoRNP U3 y la nucleolina (Enright *et al.*, 1996; Saez-Vasquez *et al.*, 2004).

Existen dos rutas alternativas de procesamiento del pre-ARNr 45S, a las que se denomina "del ITS1 primero" (*ITS1-first pathway*) y "del 5'-ETS primero" (*5'-ETS-first pathway*), en función de que el primer corte se produzca en el ITS1 o en el 5'-ETS. Estas dos rutas también se han descrito en las plantas (Figura 10, en la página 27). La mayoría de los transcritos nacientes del ADNr 47S siguen la ruta "del 5'-ETS primero" (Figura 9, Henras *et al.*, 2015). La sincronización de los procesos de eliminación del 5'-ETS y el ITS1, que se inicia mediante cortes en el sitio A_0 del pre-ARNr 30S y 2 del 41S, respectivamente, es crucial para el correcto procesamiento.

En la ruta "del ITS1 primero", el primer corte suele ocurrir en el sitio 2 del ITS1, obteniéndose el pre-ARN 30S, que es digerido en los sitios A_0 y 1 secuencialmente, rindiendo los precursores 26S y 21S, respectivamente. En la ruta "del 5'-ETS primero", se obtiene el pre-ARNr 41S, que es cortado en el sitio 2 o en el E del ITS1, iniciándose otras dos rutas de alternativas. El corte en el sitio 2 genera el pre-ARNr 21S, de cuyo extremo 3' el exosoma elimina unos 250 nt para rendir el pre-ARNr 21S-C, que a su vez sufre un corte en E, obteniéndose el precursor 18S-E. El corte en el sitio E es realizado por RCL1, ortóloga de la Rcl1 de la levadura. El extremo 3' del pre-ARNr 18S-E es procesado por exonucleasas aún desconocidas, primero en el núcleo y después en el citoplasma (Preti *et al.*, 2013). Una vez en el citoplasma, la endorribonucleasa NOB1 corta el sitio 3 del pre-ARNr 18S-E, dando lugar al ARNr 18S maduro (Preti *et al.*, 2013; Sloan *et al.*, 2013). Alternativamente, se degrada el extremo 3' del pre-ARNr 18S (Henras *et al.*, 2015).

En células humanas y del ratón, la exorribonucleasa 5'$\rightarrow$3' XRN2 procesa los precursores generados por los cortes en los sitios 2 y E (Preti *et al.*, 2013), así como el extremo 5' del pre-ARNr 32S (Wang y Pestov, 2011). El corte endonucleolítico de los sitios 4 humano y 4b del ratón en el ITS2 del pre-ARNr 32S rinde los intermediarios 12S y 28.5S. El extremo 5' del pre-ARNr 28.5S es digerido por XRN2 para formar el ARNr 28S. El procesamiento del ITS2 del pre-ARNr 12S da lugar al precursor 7S, cuya extensión 3' es digerida por el exosoma nuclear y sus factores asociados MTR4, M-Phase phosphoprotein 6 homolog (MPP6) y Nuclear receptor corepressor (C1D). Se obtiene así el pre-ARNr 5.8S+40, que contiene la región codificante del ARNr 5.8S y 40 nt adicionales en su

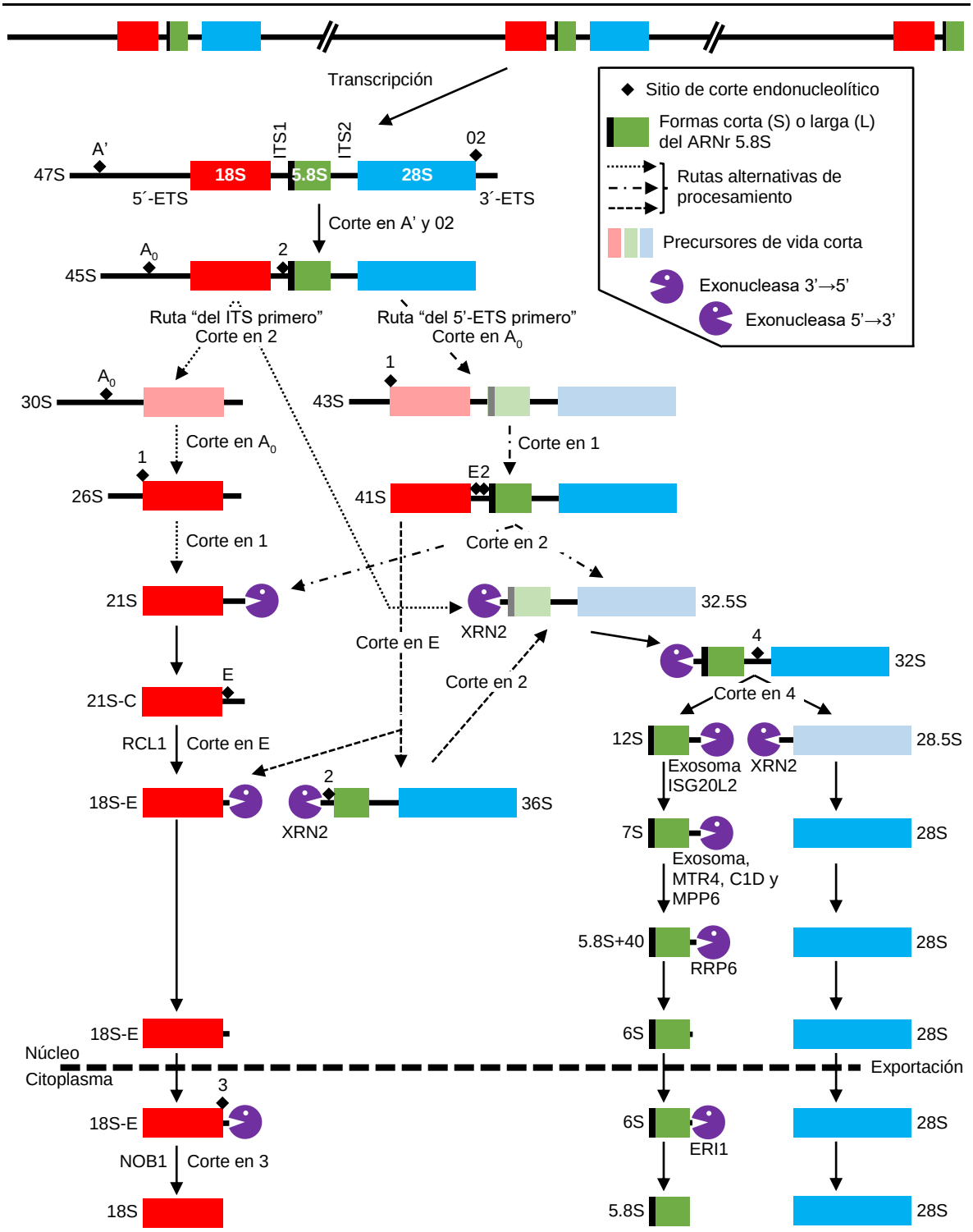

Figura 9.- Procesamiento del pre-ARNr 47S en los mamíferos. Se siguen las pautas definidas en los pies de las Figuras 3 y 8, en las páginas 16 y 23. Modificado a partir de Weis *et al.* (2015).

extremo 3´ y es muy similar al 5.8S+30 de la levadura, que es acortado por la exonucleasa RRP6, generándose el pre-ARNr 6S, que es a su vez convertido en ARNr 5.8S maduro por la Exoribonuclease 1 (ERI1) en el citoplasma (Ansel *et al.*, 2008).

III.4.5.3.- Procesamiento del pre-ARNr 45S en las plantas

El 5'-ETS de las plantas es más largo que el de la levadura, y contiene sitios de corte adicionales en el extremo 5' de la región codificante del ARNr 18S (P, P_1, P' y P_2; Figura 10). Se ha descrito un complejo denominado "*Brassica oleracea* snoRNP U3 (BoU3)", similar al procesoma SSU de la levadura, que se une al sitio $A_{123}B$, presente en las brasicáceas aguas arriba del P; BoU3 corta el sitio P (Caparros-Ruiz *et al.*, 1997; Saez-Vasquez *et al.*, 2004). En Arabidopsis también sucede el corte en P, pero no se ha demostrado la existencia de un complejo similar a BoU3. El 5'-ETS del pre-ARNr 45S de Arabidopsis contiene una inserción de 1.083 nt entre los sitios P y $A_{123}B$, de función desconocida (Saez-Vasquez *et al.*, 2004). Se han detectado intermediarios que contienen el sitio $A_{123}B$ pero carecen de dicha inserción, que al parecer es eliminada por un mecanismo similar al *splicing* (Weis *et al.*, 2015). De hecho, se han encontrado en el nucleolo de Arabidopsis proteínas relacionadas con el *splicing* (Beven *et al.*, 1995). En el 3'-ETS del pre-ARNr 45S de Arabidopsis se encuentran las secuencias polimórficas de las *VAR* (Figura 3, en la página 16), aguas abajo del sitio B_0, que presentan una región de 13 nt, complementaria de un segmento del snoARN U3 (Abou-Ellail *et al.*, 2011).

El procesamiento del pre-ARNr 45S de Arabidopsis comienza con el corte del sitio B_0, con el que finaliza la transcripción, catalizado por la RNasa III RTL2 (Comella *et al.*, 2008), homóloga de la Rnt1 de la levadura (Kufel *et al.*, 1999). El mecanismo de eliminación del extremo 5' del pre-ARN 45S también es similar al *splicing*. La EXORIBONUCLEASE2 (XRN2) y la snoRNP U3 están implicadas en el corte en el sitio P, que genera el pre-ARNr 35S(P) (Saez-Vasquez *et al.*, 2004; Zakrzewska-Placzek *et al.*, 2010; Weis *et al.*, 2015). A la vez que se elimina el 3'-ETS del pre-ARNr 45S se inician dos rutas alternativas: en la "del 5'-ETS primero" ocurren cortes sucesivos en los sitios P' y P_2, dando lugar a los pre-ARNr 33S(P') y 32S, respectivamente, que son muy similares a los 33S y 32S de la levadura, salvo por la presencia del 3'-ETS en estos últimos (Henras *et al.*, 2015). Tras la eliminación del 5'-ETS, un corte en el sitio A_2 rinde los pre-ARNr $27SA_2$ y 20S. En la ruta "del ITS1 primero", el corte en el sitio A_3 del ITS1 fragmenta el pre-ARNr 35S(P), rindiendo los pre-ARNr P-A_3 y $27SA_3$ (Weis *et al.*, 2015). Se elimina después el 5'-ETS, obteniéndose el pre-ARNr 18S-A_3, que a su vez da lugar al ARNr 18S maduro tras el corte del sitio D por NOB1 en el citoplasma (Veith *et al.*, 2012; Missbach *et al.*, 2013). El procesamiento de los pre-ARNr 25S y 5.8S es igual que en la levadura. RRP6, RRP46 y MTR4 están implicadas en la eliminación del ITS2 del extremo 3' del pre-ARNr $7S_{S/L}$ (Xi *et al.*, 2009; Lange *et al.*, 2011).

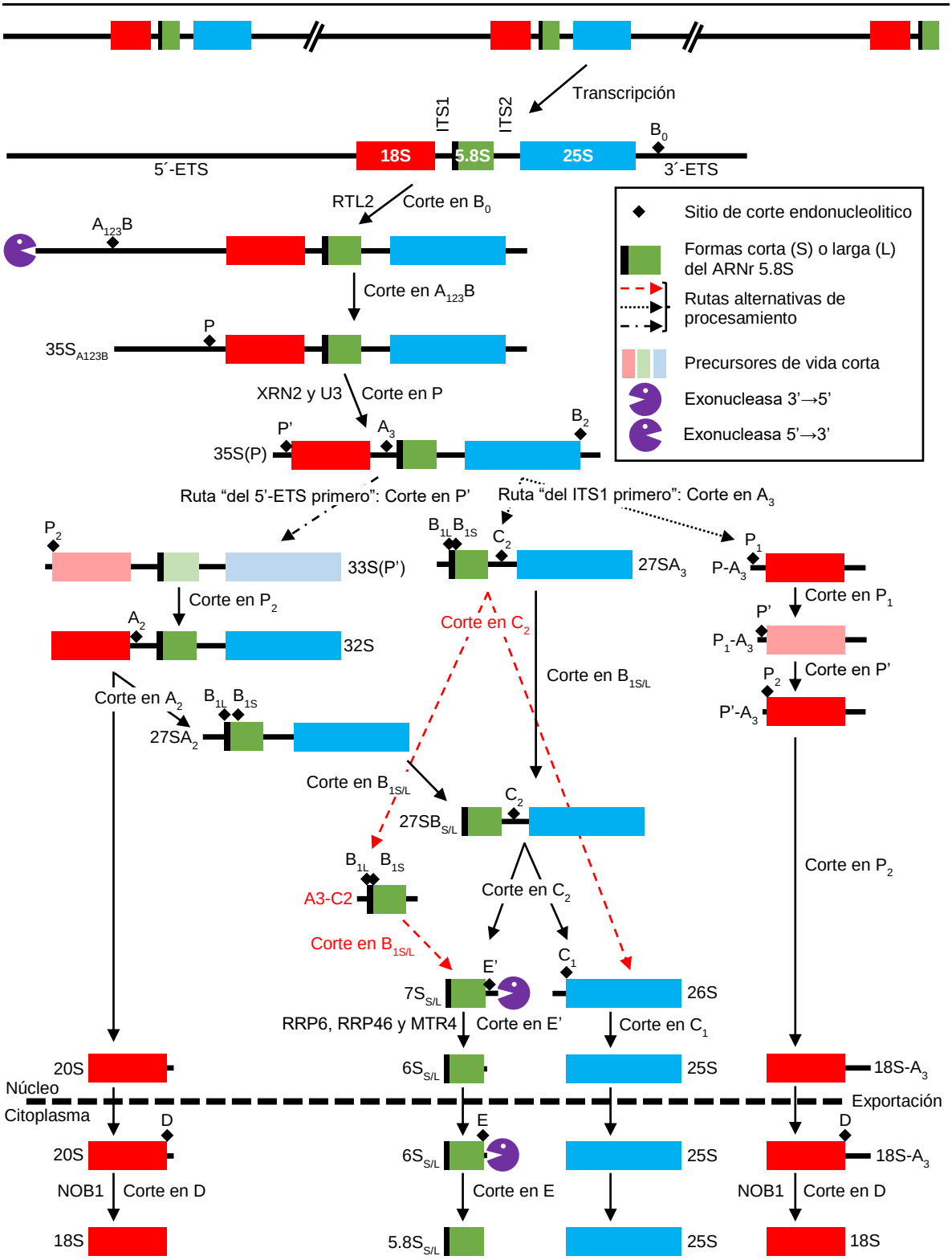

Figura 10.- Procesamiento del pre-ARNr 45S en las plantas. Se siguen las pautas definidas en los pies de las Figuras 3 y 8, en las páginas 16 y 23. Modificado a partir de Weis *et al.* (2015) y Zakrzewska-Placzek *et al*. (2010).

III.5.- Antecedentes y objetivos

III.5.1.- Diversidad y funciones no canónicas de los ribosomas

La estructura del ribosoma 80S está muy conservada en los eucariotas, lo que sugiere que todos sus componentes son importantes para su función (Carroll, 2013). En la levadura, cada PR está codificada por un solo gen o por dos parálogos (Komili *et al.*, 2007). Casi todas las PR de los mamíferos son productos de genes de copia única (Sugihara *et al.*, 2010). Resulta por tanto paradójico que el ribosoma 80S de Arabidopsis contenga 80 PR (Carroll *et al.*, 2008) y que existan en el genoma de esta planta 249 genes que las codifican (Barakat *et al.*, 2001), un número mucho mayor del aparentemente necesario. De hecho, si se combinasen de todas las formas posibles las PR de Arabidopsis, podrían formar más de 10^{34} ribosomas distintos (Carroll, 2013). La composición de los ribosomas vegetales varía dependiendo del tejido y el momento de desarrollo (Koyama *et al.*, 1996; Szick-Miranda y Bailey-Serres, 2001), y se ve afectada por determinados estímulos ambientales, que pueden inducir modificaciones postranscripcionales de las PR (Hummel *et al.*, 2012; Scharf y Nover, 1982; Perez *et al.*, 1990).

Los ribosomas ejecutan una función doméstica: la síntesis de proteínas. Esta función es igualmente necesaria para todas las células, por lo que es razonable suponer que no existan fenotipos específicos de órgano o tejido asociados a las mutaciones en genes que codifican componentes del ribosoma. Sin embargo, se han descrito varias decenas mutantes de Arabidopsis portadores de alelos de genes que codifican PR y manifiestan un fenotipo pleiotrópico similar: hojas apuntadas (Byrne, 2009; Creff *et al.*, 2010; Van Minnebruggen *et al.*, 2010; Horiguchi *et al.*, 2011; Szakonyi y Byrne, 2011; Stirnberg *et al.*, 2012) y reducción del crecimiento (Creff *et al.*, 2010) y la proliferación celular en la hoja (Horiguchi *et al.*, 2011).

Tampoco han tenido hasta ahora una explicación molecular satisfactoria las interacciones sinérgicas entre alelos de insuficiencia de función de genes que codifican PR y *ASYMMETRIC LEAVES1* (*AS1)* y *AS2* (Pinon *et al.*, 2008; Yao *et al.*, 2008), que son factores de transcripción de las familias MYB (MYELOBLASTOSIS) y LOB (LATERAL ORGAN BOUNDARIES), respectivamente (Byrne *et al.*, 2000; Iwakawa *et al.*, 2002). AS1 y AS2 participan en el establecimiento del eje adaxial-abaxial de la hoja (Husbands *et al.*, 2015). Las combinaciones dobles de alelos mutantes de genes que codifican PR y de *AS1* y *AS2* causan diferentes grados de abaxialización foliar (Pinon *et al.*, 2008; Yao *et al.*, 2008). Estos resultados sugieren que las PR participan en el desarrollo de la hoja, en la que contribuyen a regular el establecimiento de la identidad adaxial.

Es también digno de mención que se han descrito funciones de las PR humanas aparentemente no relacionadas con el ribosoma. Se sabe que participan en la tumorigénesis, la señalización inmune y el desarrollo. Estas funciones parecen tener un gran potencial para el desarrollo de algunas terapias contra el cáncer (Zhou *et al.*, 2015).

III.5.2.- El nucleolo es un compartimento nuclear multifuncional

El nucleolo es el compartimento nuclear más grande y está presente en todas las células eucarióticas. Se descubrió en el siglo XVIII y a lo largo del XIX muchos citólogos describieron la variabilidad de su morfología y tamaño en distintos organismos, histotipos y etapas del ciclo celular. La presencia de ARN en el nucleolo y de ADNr en las NOR se demostraron a mediados del siglo XX. Este orgánulo es visible por su gran tamaño y bajo contenido en ADN, ya que no se tiñe con agentes de tinción fluorescentes que se unen a este ácido nucleico, como el DAPI o el Hoechst 33342 (revisado en Sirri *et al.*, 2008). También puede distinguirse con naranja de acridina, una molécula fluorescente cuyos máximos de excitación y emisión son, respectivamente, 502 nm y 525 nm, o 460 nm y 650 nm, si está unida al ADN bicatenario, principalmente en el nucleoplasma, o al ARN, que se concentra en el nucleolo (Tafforeau *et al.*, 2013).

El nucleolo es un orgánulo multifuncional, que contiene muchas proteínas no relacionadas con la biogénesis del ribosoma, tanto en la levadura como en los animales y las plantas. Se ha establecido recientemente que el proteoma nucleolar de Arabidopsis incluye 1.602 proteínas (Palm *et al.*, 2016); estudios anteriores habían identificado solo 217 (Pendle *et al.*, 2005; Tabla 2, en la página 30). De la comparación de los proteomas nucleolares de Arabidopsis, humano y de la levadura se concluye que las proteínas específicas de Arabidopsis son 70 (Tabla 3, en la página 32): 25 de ellas están relacionadas con la transcripción, la remodelación de la cromatina o las histonas, o son proteínas de unión a ADN o ARN; 22 son de función desconocida; 17 son enzimas, componentes de rutas de transducción de señales o proteasas; y 6 son proteínas del citoesqueleto, de membranas u organulares (Palm *et al.*, 2016).

La proteómica del nucleolo evidencia su relación con el control de la calidad del ARNm. En efecto, este orgánulo alberga proteínas de las rutas de vigilancia de los ARNm defectuosos, en concreto las que reconocen las moléculas que contienen codones de terminación prematura (NMD: *nonsense-mediated decay;* decaimiento del ARNm mediado por secuencias sin sentido), en las que están implicados los factores UP-FRAMESHIFT1, (UPF1), UPF2 y UPF3. También se han identificado en el nucleolo varios miembros

Tabla 2.- Proteínas nucleolares aparentemente no relacionadas con la biogénesis del ribosoma

Categorías funcionales anotadas[a]	Código AGI de los genes que las codifican (denominación de la proteína, si la tiene)
Degradación o modificación de proteínas en el retículo endoplásmico	AT2G30050 (SC13B), AT3G53230 (CDC48B) y AT5G66680 (DGL1)
Estructura celular	AT1G18450 (ARP4), AT4G14960 (TUA6), AT5G09810 (ACT7) y AT5G62690 (TUB2)
Chaperona	AT3G13470 (CPN60BETA2), AT3G44110 (ATJ3), AT5G02500 (HSC70-1), AT5G42020 (HSP70-12/BIP2) y AT5G56010 (HSP81.3)
Helicasa de ARN	AT3G18600 (RH51), AT3G58510 (RH11), AT3G62310 y AT5G54910 (RH32)
Interacción con la cromatina	AT1G21690 (EMB1968), AT1G48620 (HON5), AT1G51060 (HTA10), AT1G54690 (H2AXB), AT2G19520 (FVE/MSI4), AT2G28740 (HIS4), AT2G30620 (H1.2), AT2G38810 (H2A 8), AT3G45980 (HTB9), AT3G51800 (EBP1), AT5G02570 (H2B9), AT5G22880 (HT2B), AT5G27670 (H2A.7), AT5G54640 (HTA1/RAT5), AT5G59870 (HTA6) y AT5G59910 (HTB4)
Complejo de unión de exones (EJC)	AT1G02140 (HAP1/MAGO), AT1G51510 (Y14) y AT3G19760 (EIF4A-III)
Exportación del ARNm	AT5G11170 (RH15) y AT5G37720 (ALY4)
Proliferación celular	AT5G40770 (EER3/PHB3)
Envuelta nuclear	AT1G68790 (LINC3)
Complejo del nucleoporo	AT1G14850 (NUP155), AT1G24310 (NUP54), AT1G79280 (NUA) y AT2G41620 (NUP93)
Transporte nucleocitoplásmico	AT3G06720 (IMPA1), AT4G16143 (IMPA-2) y AT5G20020 (RAN2)
Proteínas del cloroplasto	AT1G48850 (EMB1144), AT2G19940 (NAGPR), AT3G16950 (LPD1) y AT4G37870 (PCK1)
Proteínas de la mitocondria	AT2G07698(F4IMB5), AT2G33040 (ATP3), AT3G02090 (MPPBETA), AT3G08580 (AAC1), AT3G22330 (RH53/ PMH2), AT3G52300 (ATPQ), AT5G08690 (ATPBN), AT5G15090 (VDAC3) y AT5G50850 (MAB1)
Proteínas del peroxisoma	AT2G33150 (PKT3) y AT3G06860 (MFP2)
Unión a ARN y nucleótidos	AT3G15010 (UBA2C), AT3G16810 (PUM24), AT3G18130 (RACK1C), AT4G19610, AT4G39260 (GRP8), AT5G04280 (RZ-1C) y AT5G46070

[a]Modificado a partir de Brown *et al.* (2005); se han introducido nombres abreviados de proteínas, se han agrupado algunas categorías funcionales y se han actualizado las descripciones de los genes en base a la información depositada en Araport. [b]Arabidopsis Genome Initiative.

Tabla 2 (continuación).- Proteínas nucleolares aparentemente no relacionadas con la biogénesis del ribosoma

Categorías funcionales anotadas[a]	Código AGI[b] de los genes que las codifican (denominación de la proteína, si la tiene)
Splicing	AT1G04510 (MAC3A), AT1G16610 (SR45), AT1G20960 (BRR2/EMB1507), AT1G55310 (SR33), AT1G77180 (SKIP), AT2G18510 (EMB2444), AT2G24590 (RSZ22A), AT3G18165 (MOS4), AT3G49430 (SR34A), AT5G16780 (MDF) y AT5G57120
Componente del proteasoma	AT1G45000 (RPT4B)
Maduración de los miARN	AT2G27100 (SE)
Transcripción	AT1G60850 (RPAC42), AT1G54060 (ASIL1), AT1G61730, AT2G27840 (HDA1), AT2G28510 (DOF2.1), AT2G38250, AT2G45640 (SAP18), AT3G10490 (SGS1), AT3G44750 (HDA3), AT4G00238 (STKL1), AT4G00390, AT4G10710 (SPT16), AT4G25210, AT5G03740 (HDT3), AT5G22650 (HD2) y AT5G64680 (C34.5)
Traducción	AT1G07920, AT1G56070 (LOS1), AT3G13920 (EIF4A1), AT3G55620 (EIF6A) y AT4G20360 (RABE1B)
Enzimas citoplásmicas	AT1G13440 (GAPC2), AT3G17390 (MTO3/SAMS3), AT3G52930 (FBA8) y AT4G01850 (SAM2)
De función desconocida	AT1G65030, AT1G18850, AT1G54850, AT2G03510, AT2G21870, AT2G27730, AT2G44510, AT3G23620, AT3G53170, AT3G56990, AT3G62530, AT5G10010, AT5G40340 y AT5G48240

[a]Modificado a partir de Brown *et al.* (2005); se han introducido nombres abreviados de proteínas, se han agrupado algunas categorías funcionales y se han actualizado las descripciones de los genes en base a la información depositada en Araport. [b]Arabidopsis Genome Initiative.

Tabla 3.- Proteínas nucleolares específicas de Arabidopsis

Descripción	Código AGI[b] del gen que la codifica (denominación de la proteína, si la tiene)
Fosfolipasa D	AT1G52570 (PLDALPHA2)
Unión a carbohidratos	AT4G25900 y AT1G78850
Factor de transporte nuclear	AT3G25150 (NTF2)
ATPasa mitocondrial transportadora de aniones	AT5G60730 (GET3C)
Endopeptidasa aspártica	AT5G19100
Proteína de unión a ADN con un motivo de gancho AT (*AT-hook*)	AT3G55560 (AGF2/AHL15)
Tiorredoxina de tipo O	AT2G35010 (TRX-O1)
Glioxalasa de tipo I dependiente de níquel	AT1G67280 (GLYI6)
Factor remodelador de la cromatina dependiente de ATP	AT2G28290 (CHR3/SYD)
Componente de un complejo remodelador de la cromatina de tipo SWIB	AT1G31760 (SWIB5)
Factor de transcripción de tipo B3 de la familia REM	AT1G49480 (RTV1/REM19)
Componentes de la topoisomerasa Topo-IIb/tipo-VI	AT1G48380 (RHL1) y AT5G02820 (RHL2)
Proteínas de unión a ARN y ADN de función desconocida	AT1G29250 y AT2G34160
GDP-D-manosa 3',5'-epimerasa	AT5G28840 (GME)
Presunta fosfoglicerato/bisfosfoglicerato mutasa	AT5G64460
Desacetilasa de histonas de tipo HD2	AT2G27840 (HD2D/HDT4)
Inositol fosforilceramida glucuronosiltransferasa	AT5G18480 (IPUT1/PGSIP6)
Proteína de unión a calmodulina	AT1G14380 (IQD28)
Proteolisis	AT5G40200 (DEG9)
Degradación de ARNm en respuesta a estrés	AT5G21160 (LARP1a)
Ensamblaje de los nucleosomas	AT1G06760 (H1.1)
Familia de las O-fucosiltransferasas	AT3G26370
Edición del ARN mitocondrial	AT4G20020 (MORF1)

Modificado a partir de Palm *et al.* (2016). Las descripciones de los genes se han actualizado en base a la información depositada en Araport.

Tabla 3 (continuación).- Proteínas nucleolares específicas de Arabidopsis

Descripción	Código AGI[b] del gen que la codifica (denominación de la proteína, si la tiene)
Actividad oxidorreductasa	AT3G56460 y AT5G21105
Superfamilia de los inhibidores de la pectina metilesterasa	AT5G62350
Superfamilia de las peroxidasas	AT2G18980
Proliferación de los peroxisomas	AT3G61070 (PEX11E)
Edición del ARN del cloroplasto	AT2G37080 (RIP2)
Quinasa de serina/treonina regulada por calcio	AT5G21326 (CIPK26)
Factor de transcripción con homeodominio	AT1G28420 (HB-1)
Proteína arabinogalactano	AT1G28290 (AGP31)
Unión a ARN; implicada en la división celular	AT3G55340 (PHIP)
Helicasa de ARN de tipo DEAD BOX	AT3G01540 (DRH1)
Unión a ADN monocatenario	AT5G44785 (OSB3)
Superfamilia de las tioesterasas	AT1G35290 (ALT1)
Factores de transcripción	AT5G11260 (bZIP56), AT1G14510, AT2G17410, AT3G14180, AT3G22170 (CPD45/FHY3) y AT5G16470
Biosíntesis de celulosa	AT5G24710 (TWD40-2)
Similar a las transposasas de la familia hAT	AT3G42170 (DAYSLEEPER)
Endotransglucosilasa de xiloglucano	AT4G30280 (XTH18)
Desconocidas	AT1G50620, AT1G48610, AT1G13690, AT1G20970, AT1G56660, AT1G59710, AT2G22795, AT2G39020, AT2G41800 (TEB), AT2G45520, AT3G03590, AT3G04500, AT3G22520, AT4G24270 (EMB140), AT4G30150, AT4G37090, AT5G13020, AT5G17160, AT5G25090 (ENODL13), AT5G60030, AT5G60950 (COBL5) y AT5G64680

Modificado a partir de Palm *et al.* (2016). Las descripciones de los genes se han actualizado en base a la información depositada en Araport.

del complejo de unión de exones (EJC; Exon Junction Complex), como Mago, Y14, Eukaryotic translation Initiation Factor 4A3 (eIF4A3), Barentsz2, Barentsz1 y Partner of Y14 and Mago (PYM). Los EJC se unen a las uniones entre exones que se originan tras la eliminación de los intrones en el *splicing* de los pre-ARNm, y se desplazan con el ARNm hasta el citoplasma para su traducción. Los EJC cooperan con las rutas NMD de vigilancia de ARNm defectuosos, ya que su presencia en una unión entre exones situada aguas abajo de un codón de terminación indica que este último es prematuro. Los componentes de la ruta de la NMD se unen a los EJC en los ARNm que cuentan con un codón de terminación prematuro e inducen su degradación por el exosoma citoplásmico, evitándose así la síntesis de proteínas truncadas (Chang *et al.*, 2007). Se deriva también de la Tabla 3 que el nucleolo está relacionado con la actividad del espliceosoma y otros procesos.

III.5.3.- La ortóloga humana de Nop53 regula la respuesta al estrés nucleolar

La síntesis de los ribosomas consume una gran cantidad de energía: en la levadura, el ADNr supone el 10% del genoma y cada célula en cultivo (en crecimiento exponencial) cuenta con unos 200.000 ribosomas, dedica el 60% de la transcripción a la síntesis de ARNr y produce 2.000 ribosomas por minuto, que cada nucleoporo exporta al citoplasma a razón de 25 por minuto (Thomson *et al.*, 2013).

Tal como se ha comentado en el apartado anterior, análisis proteómicos han revelado la implicación del nucleolo en funciones adicionales a la biogénesis del ribosoma, como el control del ciclo celular. La ausencia de membrana alrededor del nucleolo permite el tránsito de proteínas y ARN entre el nucleolo y el nucleoplasma, por lo que el proteoma nucleolar es dinámico, tal como indican sus respuestas a diversos tipos de estrés celular, que causan cambios estructurales visibles de este orgánulo (Boulon *et al.*, 2010). Se considera al nucleolo un sensor de estrés general, ya que responde rápidamente a distintos tipos de estrés celular, incluido el estrés nucleolar.

Nop53 (Rout *et al.*, 2000) es una de las proteínas implicadas en el procesamiento del pre-ARNr 35S de la levadura (Figura 8, en la página 23). Nop53 está implicada en la maduración de los ARNr 25S y 5.8S, según evidencian sus alelos nulos, que acumulan el 7S pre-rRNA y otros precursores del ARNr 5.8S rRNA (Granato et al., 2005; Sydorskyy et al., 2005; Thomson and Tollervey, 2005). Nop53 también está implicado en la exportación de la subunidad 60S del ribosoma al citoplasma, pero no la acompaña en su tránsito a través del nucleoporo, permaneciendo en el núcleo y disociándose de la partícula pre-60S antes de su exportación al citoplasma(Thomson y Tollervey, 2005). La localización dual de

Nop53, en el nucleolo y la membrana nuclear, concuerda con su papel en el procesamiento del ARNr, que es un proceso nucleolar, y en la exportación de la partícula pre-60S.

La ortóloga humana de Nop53 es la proteína Glioma Tumor Suppressor Candidate Region Gene 2 (GLTSCR2), también denominada Protein Interacting with Carboxyl Terminus 1 (PICT1). La implicación de GLTSCR2 en la biogénesis del ribosoma se demostró en un análisis masivo del procesamiento del pre-ARNr 47S en líneas celulares humanas en las que se inhibió individualmente, mediante ARN interferentes, la expresión de 625 genes que codifican proteínas nucleolares (Tafforeau *et al.*, 2013). Este estudio concluyó que la GLTSCR2 humana interviene en la biogénesis del ARNr 5.8S, como Nop53, su ortóloga de la levadura.

Se denomina estrés nucleolar o ribosómico a cualquier alteración de la biogénesis del ribosoma que comprometa la homeostasis celular (James *et al.*, 2014). Por ejemplo, los mutágenos químicos o físicos causan estrés nucleolar (Llanos y Serrano, 2010). También causa estrés nucleolar la escasez de nutrientes, que desregula a los factores asociados a las ARN pol I y III, a los que procesan los pre-ARNr y a Split Finger Protein 1 (SFP1) y Fork Head-like 1 (FHL1), que son necesarios para la transcripción de los genes que codifican las PR y los factores de la biogénesis del ribosoma (Zhou *et al.*, 2015).

La biogénesis del ribosoma humano está controlada directa o indirectamente por los productos de oncogenes y genes supresores de tumores, entre ellos el factor de transcripción p53, al que se considera guardián de la integridad del genoma (Lane, 1992). En condiciones normales, la actividad de p53 es baja, ya que su activación induce la interrupción del ciclo celular, la apoptosis o la senescencia. La inactividad de p53 es necesaria para el mantenimiento de la homeostasis celular en condiciones no estresantes y es consecuencia de su interacción con la protooncoproteína Murine Double Minute 2 (MDM2). MDM2 es una ligasa de ubiquitina de tipo E3, que poliubiquitina a p53, que es entonces exportada al citoplasma y allí degradada por el proteasoma. En situaciones de estrés celular, como cuando el ADN es dañado, p53 se libera de MDM2, y al estabilizarse, incrementa su concentración, que a su vez induce la reparación del ADN; ante lesiones irreparables, p53 inhibe el ciclo celular o promueve la apoptosis (Vogelstein *et al.*, 2000).

El estrés nucleolar causa la acumulación de PR libres, no integradas en un ribosoma. En situaciones de estrés nucleolar son varias las PR, como RPL5 y RPL11, que pasan del nucleolo al nucleoplasma, en donde se unen a MDM2, inhibiendo su actividad ligasa de ubiquitina; se incrementa así la concentración de PR libres. El mismo efecto produce la inducción de la traducción de los ARNm que codifican PR en respuesta al estrés

nucleolar, muchos de los cuales contienen un tracto de pirimidinas en su región 5´ no traducida (5´-TOP; 5´-Track of pyrimidines), como el de RPL11 (Fumagalli *et al.*, 2009).

Las ribosomopatías son enfermedades genéticas muy pleiotrópicas, alguna de las cuales es poligénica, causadas por mutaciones en genes que codifican PR, factores de la biogénesis del ribosoma o proteínas nucleolares de función desconocida. Son ribosomopatías la disqueratosis congénita, la hipoplasia cartílago-cabello y los síndromes 5q, de Schwachman-Diamond y de Treacher Collins. Estas enfermedades congénitas son consecuencia de distintas alteraciones de la biogénesis del ribosoma y causan fenotipos clínicos distintos, algunos de los cuales tienen en común las disfunciones de la médula ósea y las alteraciones craneofaciales y de otras partes del esqueleto (Narla y Ebert, 2010).

La primera ribosomopatía descubierta y la mejor estudiada hasta ahora es la anemia de Diamond-Blackfan, que se manifiesta en individuos heterocigóticos para mutaciones nulas en más de 10 genes aparentemente haploinsuficientes que codifican PR, entre ellas RPL5 y RPL11 (Farrar y Dahl, 2011). RPL5, RPL11 y el ARNr 5S componen la partícula ribonucleoproteica 5S (5S RNP) de la subunidad mayor del ribosoma y son cruciales para la regulación de p53 en respuesta al estrés nucleolar. El descenso de los niveles de cualquiera de estas tres moléculas impide la estabilización y acumulación de p53. PICT1 se une directamente al ARNr 5S y retiene a RPL5 y RPL11 en el nucleolo; la reducción de la concentración de PICT1 favorece la traslocación de RPL11 al nucleoplasma y causa, en consecuencia, la acumulación de p53 (Figura 11). En este proceso intervienen otras proteínas: Promyelocytic Leukemia Tumor-Suppressor (PML), un activador de p53; Neural-Precursor-Cell-Expressed Developmentally Down-Regulated 8 (NEDD8), una proteína similar a la ubiquitina, que se conjuga a sus sustratos; Myb-Binding Protein 1A (MYBBP1A), que acetila y estabiliza a p53; Alternative Reading Frame (ARF), cuya unión a MDM2 inhibe su actividad ligasa de ubiquitina; y la chaperona de histonas Nucleophosmin 1 (NPM1), cuya implicación en este proceso está demostrada, aunque se desconoce su mecanismo de acción (Holmberg Olausson *et al.*, 2012).

Un efecto similar a la acumulación de p53 mediada por RPL11 es causado por la quinasa Ataxia Telangiectasia Mutated (ATM), un regulador maestro del ciclo celular. ATM juega un papel importante en la respuesta a los daños en el ADN, situación en la que fosforila a PICT1 en el nucleolo, induciendo su degradación y la acumulación de p53. Se considera a PICT1 un sensor importante en la señalización de la respuesta a los daños en el ADN (Chen *et al.*, 2016). La estabilización de p53 también se consigue inhibiendo con ARN interferentes la expresión de genes que codifican proteínas implicadas en el procesamiento del pre-ARNr 47S, una de los cuales es PICT1 (Tafforeau *et al.*, 2013).

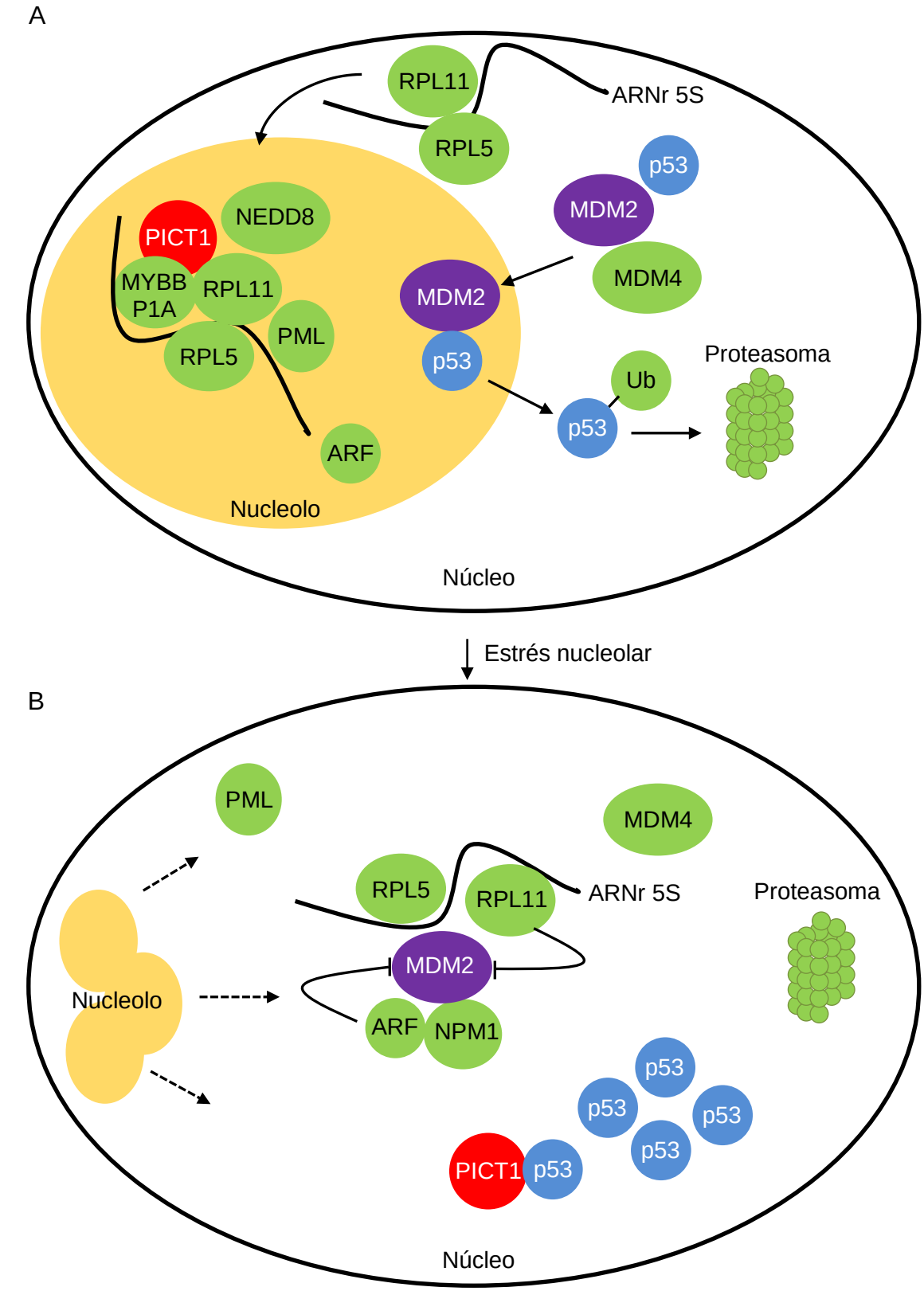

Figura 11.- Regulación del estrés nucleolar por la ruta de RPL11-MDM2-p53. Se representa el núcleo (A) en condiciones normales, y (B) durante el estrés nucleolar. Se destaca en rojo a PICT1 (GLTSCR2), la ortóloga humana de la Nop53 de la levadura. El símbolo ⊣ representa inhibición. Modificado a partir de Holmberg Olausson *et al.* (2012).

El estrés nucleolar también perturba la ruta de los miARN, que en condiciones normales impiden la traducción de sus ARNm diana. La reducción de la expresión de genes que codifican PR, que produce estrés nucleolar al desequilibrar las concentraciones de los componentes estructurales del ribosoma, incrementa los niveles de p53 y los ARNm diana de los miARN. Por el contrario, la inhibición simultánea de la expresión de *p53* y de genes de las PR reduce los niveles de las dianas de los miARN, lo que indica que p53 participa en la regulación de la ruta de los miARN. La desrepresión de las dianas de los miARN también se produce si se induce estrés nucleolar con actinomicina D, que inhibe la transcripción del ADNr y estabiliza a p53. En suma, el desequilibrio en la síntesis de los componentes de las subunidades ribosómicas produce estrés nucleolar, estabilización de p53 e inhibición de la represión de los ARNm diana de los miARN (Janas *et al.*, 2012).

La sobreexpresión de *PICT1* activa el promotor del gen de la telomerasa y en consecuencia eleva los niveles de su ARNm y su producto proteico en células normales y tumorales. Por el contrario, la inhibición de *PICT1* reduce los niveles de la telomerasa, y causa alteraciones en la morfología celular, incluida la del núcleo, probablemente por inestabilidad cromosómica, e induce apoptosis (Kim *et al.*, 2016).

Se sabe muy poco de otros miembros de la familia Nop53/GLTSCR2 en los animales y casi nada en las plantas, en las que no se ha demostrado experimentalmente su relación con la biogénesis del ribosoma. El ortólogo de Nop53 en *Caenorhabditis elegans*, denominado Y39B6A.33, es una proteína nucleolar (Meissner *et al.*, 2011); su inactivación con un ARN antisentido ha evidenciado que controla la función mitocondrial, ya que regula la respiración celular, como su ortólogo humano (Yoon *et al.*, 2014).

La ortóloga de Nop53 en *Schizosaccharomyces pombe* es rRNA processing protein 16 (Rrp16), que interacciona con Caffeine-induced death protein 14 (Cid14), una poli(A) polimerasa no canónica (Keller *et al.*, 2010). Cid14 se asocia con la subunidad 60S y con factores necesarios para su ensamblaje. Cid14 forma un complejo estable con Air1/2p, una helicasa de ARN, y con la antes mencionada Mtr4 (apartado III.4.5.1, en la página 21), que recluta al exosoma, tanto en la especie humana como en la levadura, a sus ARN diana, entre ellos los pre-ARNr. El complejo que conforman estas proteínas se denomina TRAMP (Trf4/Air2/Mtr4p Polyadenylation complex), está muy conservado en todos los eucariotas y tiene como sustratos múltiples tipos de ARN, a los que conduce al exosoma nuclear. Tanto el exosoma nuclear como el citoplásmico poseen actividad exonucleasa 3´→5 y son componentes importantes de las rutas de vigilancia de los ARN en todos los eucariotas (Schmidt y Butler, 2013). La unión entre Nop53 y Mtr4 es necesaria en *Saccharomyces cerevisiae* para el reclutamiento del exosoma al pre-ARNr 7S para su procesamiento

(Thoms *et al.*, 2015). Aunque no se ha demostrado el papel de Rrp16 en *Schizosaccharomyces pombe* como reclutador indirecto del exosoma, su interacción con Cid14 lo sugiere, ya que este último es un factor necesario para la poliadenilación del ARNr y de sus precursores, que a su vez induce su degradación por el exosoma. Las mutaciones en genes que codifican componentes del exosoma nuclear causan la acumulación de pre-ARNr poliadenilados en el nucleolo de *Schizosaccharomyces pombe* (Win *et al.*, 2006).

III.5.4.- Rrp7 es un componente del procesoma SSU de la levadura

El pre-ARNr 35S de la levadura se asocia cotranscripcionalmente con unos 50 factores de biogénesis del ribosoma, el snoARN U3 y algunas PR para formar el proceosoma SSU (Lin *et al.*, 2013; Figura 7, en la página 21). Uno de los subcomplejos que se incorporan al procesoma SSU es UtpC, que está integrado por la Caseína quinasa 2 (CK2; incluye cuatro subunidades), la U3 snoRNA-associated protein 22 (Utp22) y la Ribosomal RNA-processing protein 7 (Rrp7; Grandi *et al.*, 2002; Krogan *et al.*, 2004). Los componentes de UtpC también se asocian con el factor de transcripción Interacts with Fork Head 1 (Ifh1) para formar el complejo CURI (CK2, Utp22, Rrp7 e Ifh1), que coordina las dos rutas necesarias para la síntesis del ribosoma: por un lado, la producción del pre-ARNr, y por otro, la transcripción de los genes que codifican las PR (Rudra *et al.*, 2007; Figura 12).

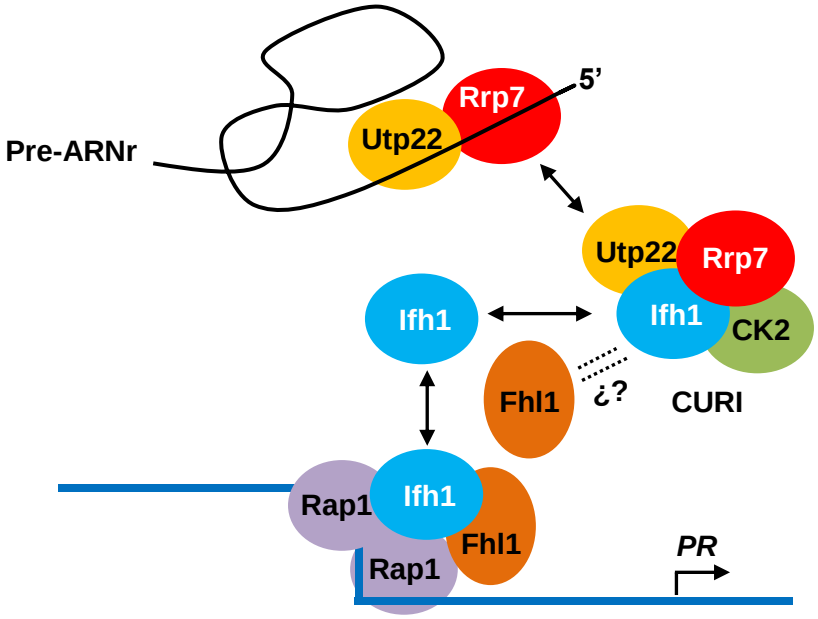

Figura 12.- Modelo propuesto para explicar la coordinación de la producción de los ARNr y las PR. Se destaca en rojo a Rrp7. El símbolo ↱ indica el sitio de inicio de la transcripción de un gen (*PR*) que codifica una PR. Modificado a partir de Rudra *et al.* (2007).

Según el modelo propuesto por Rudra *et al.* (2007), Ifh1 también forma parte de otro complejo, en el que se une a una molécula de Fhl1 y dos de Repressor/activator site binding protein1 (Rap1), que están a su vez unidas a los promotores de los genes que codifican RP. Este complejo desplaza a los nucleosomas para promover la transcripción de los genes de las RP. Cuando la transcripción de los ARNr es activa, las proteínas Utp22 y Rrp7 procesan precursores de ARNr y no pueden formarse complejos CURI, por lo que existe Ifh1 libre, que puede unirse a Rap1 y Fhl1. Si la transcripción del ADNr se ralentiza, se reduce la demanda de Utp22 y Rrp7, que pasan a estar disponibles para formar complejos CURI con CK2 e Ifh1, lo que a su vez merma la disponibilidad de este último para asociarse a Rap1 y Fhl1, reduciéndose en consecuencia la transcripción de los genes de las RP.

Rrp7 contiene un dominio aminoterminal (NTD; residuos 1-156), una región de unión (157-189) y un dominio carboxiterminal (CTD; 190-297). Ambos dominios terminales son esenciales (Lin *et al.*, 2013). Rrp7 también presenta en su región aminoterminal un RNA Recognition Motif (RRM), similar al de otras muchas proteínas que reconocen ARN monocatenario. Los dos residuos del dominio RRM implicados en la unión a ARN (Phe54 y Leu125) están conservados en Rrp7 (Lin *et al.*, 2013). Rrp7 se une a una región del ARN flanqueada por dianas del snoR30, un snoARN esencial de la familia H/ACA, que está implicado en la maduración del ARNr 18S (Vogelstein *et al.*, 2000; Atzorn *et al.*, 2004; Fayet-Lebaron *et al.*, 2009). El snoR30 es necesario para la incorporación de Rrp7 al procesoma SSU (Lin *et al.*, 2013).

III.5.5.- Las NKAP son proteínas multifuncionales muy conservadas

Los genes *NKAP* se encuentran en casi todos los eucariotas y son de copia única y esenciales, excepto en los mamíferos, que cuentan con dos parálogos (Sánchez-García *et al.*, 2015). La NKAP humana es el miembro fundador de la familia, cuya denominación, NF-κB activating protein, deriva de su capacidad de activar al factor de transcripción Nuclear factor kappa light chain enhancer of activated B cells (NF-κB) en cultivos celulares (Chen *et al.*, 2003). La proteína NF-κB juega un importante papel en la respuesta inflamatoria humana y del ratón, ya que se induce rápidamente ante cualquier daño celular o infección bacteriana y activa a los cientos de genes que actúan como guardianes en la respuesta inmune, cuyos productos son quimiocinas, citoquinas, moléculas de adhesión, mediadores de la inflamación e inhibidores de la apoptosis. En condiciones normales, el NF-κB se encuentra inactivo en el citoplasma y se trasloca al núcleo ante una señal de estrés celular (Horn *et al.*, 2011). Los estudios de las NKAP son escasos y en la mayoría se aborda exclusivamente su papel en la respuesta inmune de los mamíferos. Se han

publicado recientemente dos estudios funcionales en otros organismos: Arabidopsis (Sánchez-García *et al.*, 2015; página 123 y siguientes) y *Dictyostelium discoideum* (Burgute *et al.*, 2016; véase el último párrafo de este apartado).

Las proteínas de la familia NKAP presentan un dominio muy conservado en su extremo carboxilo, denominado SynMuv, y una región RS aminoterminal, de baja complejidad y rica en argininas (R) y serinas (S) (región RS), de interacción con otras proteínas y ARN (Burgute *et al.*, 2014; Jarvelin *et al.*, 2016). Las regiones RS son características de las proteínas de unión a ARN denominadas genéricamente factores SR, que actúan como activadores en el *splicing* constitutivo y alternativo, y en el control de la estabilidad, la exportación al citoplasma y la traducción de los ARNm. Los factores SR también están implicados en el procesamiento de los pre-miARN (Howard y Sanford, 2015).

Se considera a la NKAP humana una proteína relacionada con las SR (*SR-related protein*) por su dominio RS no canónico (Jarvelin *et al.*, 2016). Las proteínas que contienen un dominio RS son intrínsecamente desordenadas, es decir, incapaces de formar una estructura terciaria estable en condiciones fisiológicas. Las proteínas intrínsecamente desordenadas, también denominadas desestructuradas, son muy plásticas en su conformación, que varía dependiendo de las moléculas con las que se asocian, que pueden ser otras proteínas, ARN de diversos tipos, y componentes de membranas, como algunos lípidos u otras pequeñas moléculas (Dunker *et al.*, 2008; Uversky, 2015; Levine y Shea, 2016). La localización subcelular de algunas proteínas SR es dinámica: se les ha encontrado en dominios nucleares denominados manchas o motas (*speckles)* nucleares y en el nucleolo, en donde interaccionan con factores implicados en la biogénesis del ribosoma.

Es poco lo que se sabe acerca de las ortólogas de la NKAP humana en *Drosophila melanogaster* y *Caenorhabditis elegans*. Ambas son esenciales y la de *Drosophila melanogaster*, CG6066, interacciona con proteínas relacionadas con el espliceosoma (Giot *et al.*, 2003). Las NKAP humana, del ratón, Arabidopsis y *Dictyostelium discoideum* también son nucleares y esenciales. La NKAP humana es una proteína multifuncional con capacidad de unión a ARN y proteínas, que se asocia con la Desacetilasa de histonas 3 (HDAC3), con CBF1 interacting corepressor (CIR), que forma parte del complejo correpresor Notch, y con proteínas de unión a ARN, como algunas helicasas de ARN y factores implicados en el *splicing* (Davidson y Erwin, 2006; Burgute *et al.*, 2016). La inactivación condicional de la NKAP del ratón ha evidenciado que esta proteína reprime la transcripción de los genes diana de la ruta de Notch, y que se requiere para el desarrollo de las células citotóxicas T del sistema inmune (Thapa *et al.*, 2013). La NKAP humana está

asociada al espliceosoma (Hegele *et al.*, 2012) y participa en el control del *splicing* (Burgute *et al.*, 2014). Un estudio reciente de la NKAP humana evidencia una vez más su carácter multifuncional, ya que le asigna un papel regulador en la mitosis, al reclutar a la Centromere protein E (CENPE) al cinetocoro, una asociación clave para la localización polar de los cromosomas en la placa metafásica. En las células en las que la NKAP está inactivada, CENPE no se sitúa en el cinetocoro, y los cromosomas se alinean erróneamente en la prometafase, segregando de manera anómala y causando aneuploidías o la interrupción de la mitosis (Li *et al.*, 2016).

La NKAP de *Dictyostelium discoideum* se une a ARN y proteínas, como su ortóloga humana. Está presente en un patrón puntuado en el núcleo e interacciona con proteínas de unión a ARN, entre ellas algunas proteínas implicadas en el *splicing*, como Pre mRNA processing factor 19 (Prp19), y en la biogénesis del ribosoma, como la fibrilarina y varias PR de las dos subunidades del ribosoma. Prp19 es una ligasa de ubiquitina que forma parte del Nine Teen Complex (NTC), implicado en el ensamblaje y remodelación del espliceosoma en diferentes etapas del *splicing* (Chanarat y Strasser, 2013). La fibrilarina es una metiltransferasa nucleolar que se encuentra mayoritariamente en el CFD y en menor medida en los CF (Ochs *et al.*, 1985; Figura 6, en la página 19) por lo que se utiliza como marcador de este compartimento nucleolar; se asocia con varios snoARN, como U3 (apartado III.4.4, en la página 20), y participa en las primeras etapas del procesamiento del pre-ARNr 45S (Rodriguez-Corona *et al.*, 2015). La NKAP de *Dictyostelium discoideum* se une a diversos tipos de ARN codificantes y no codificantes, fundamentalmente a ARNr, pero también a los snARN U1 y U2, que participan en el *splicing* (Burgute *et al.*, 2016).

III.5.6.- Búsqueda de interactores genéticos de *ago1-52*

En el laboratorio de J.L. Micol se obtuvo una colección de varios cientos de mutantes de Arabidopsis con alteraciones en la morfología foliar, tras una mutagénesis con EMS de la estirpe silvestre L*er* (Berná *et al.*, 1999; Serrano-Cartagena *et al.*, 1999). Se denominó *incurvata* (*icu*) a 41 de estos mutantes, ya que presentaban hojas recurvadas hacia el haz, a diferencia de las silvestres, que son casi totalmente planas. La clonación posicional en el laboratorio de M.R. Ponce de 5 de ellas —*icu3*, *icu8*, *icu9-1*, *icu9-2* e *icu15*—, reveló que eran nuevos alelos hipomorfos o nulos de los genes *HASTY* (*HST*; Telfer y Poethig, 1998), *HYPONASTIC LEAVES1* (*HYL1*; Lu y Fedoroff, 2000), *ARGONAUTE1* (*AGO1*; Bohmert *et al.*, 1998) y *HUA ENHANCER1* (*HEN1*; Chen *et al.*, 2002), respectivamente. Los productos de estos genes son elementos clave de las rutas de PTGS mediadas por miARN (apartado III.3.2, en la página 11).

Con la intención de contribuir a una mejor comprensión del papel del PTGS en el desarrollo de las plantas, los mutantes descritos en el párrafo anterior fueron estudiados en el laboratorio de M.R. Ponce a nivel morfológico e histológico, y se obtuvieron sus combinaciones dobles, todas las cuales manifestaron un fenotipo sinérgico (Jover-Gil *et al.*, 2005). Esta observación sugirió que los alelos hipomorfos de *HST*, *HYL1*, *AGO1* o *HEN1* proporcionarían un fondo genético sensibilizado, útil para una búsqueda de mutantes con el propósito de identificar nuevos genes implicados en el PTGS. Se supuso que la aparición de sinergia, epistasia o supresión en una población derivada de una mutagénesis de segundos sitios (apartado III.2.2, en la página 7) realizada con un mutante *hst*, *hyl1*, *ago1 o hen1* constituiría un indicio de que la segunda mutación dañaba un gen relacionado funcionalmente con el anteriormente mutado y, en consecuencia, con el PTGS.

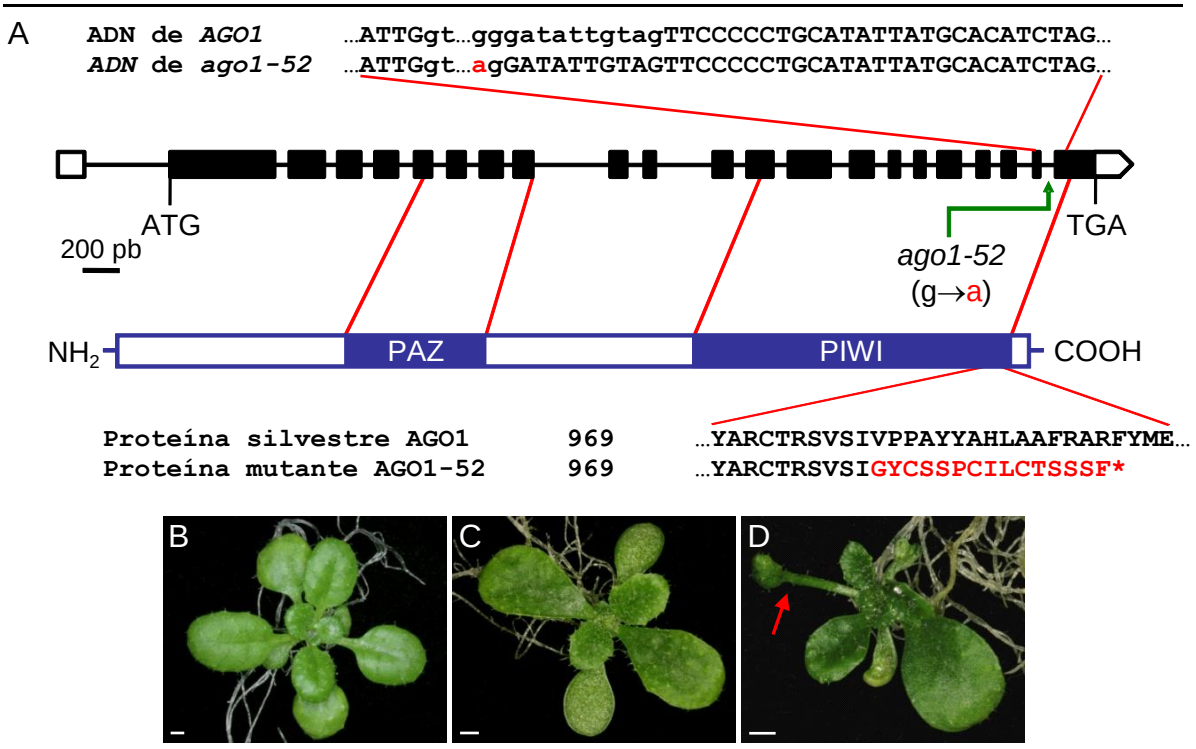

Figura 13.- Naturaleza molecular y fenotipo morfológico de la mutación *ago1-52*. Estructura del gen *AGO1* y su producto proteico, con indicación de la naturaleza de la mutación *ago1-52* (flecha verde) y sus consecuencias en la secuencia de la proteína. Los rectángulos negros representan a los exones, y las líneas que los separan, a los intrones. Se indican con rectángulos blancos las regiones no traducidas 5' y 3'. Los rectángulos azules destacan los dominios PAZ y PIWI de la proteína AGO1. En las secuencias nucleotídicas, se usan las letras minúsculas para los intrones y las mayúsculas para los exones. Las letras rojas destacan nucleótidos mutados o aminoácidos distintos a los silvestres. El asterisco indica un codón de terminación prematura. (B-D) Algunos rasgos fenotípicos del mutante *ago1-52*. Rosetas de (B) L*er* y (C, D) *ago1-52*, fotografiadas 21 días después de la estratificación. La flecha roja señala una hoja radializada en D. Las barras de escala indican 1 mm. Esta figura contiene elementos de las que aparecen en las páginas 62 y 70 de esta memoria.

Para llevar a cabo la mutagénesis de segundos sitios se eligió la mutación hipomorfa *ago1-52*, que altera el *splicing* y elimina 55 aa del extremo carboxilo de AGO1 (Figura 13), causa un fenotipo inequívocamente distinguible del silvestre y reduce solo parcialmente la viabilidad y la fertilidad. Las hojas de las plantas homocigóticas para esta mutación tienen una forma característica, ya que no muestran una delimitación clara entre el peciolo y el limbo (Aguilera Díaz, 2009).

Para la mutagénesis de segundos sitios del mutante *ago1-52*, se optó por el EMS dada su gran mutagenicidad, superior a la de los mutágenos físicos o insercionales, y su capacidad de generar alelos puntuales hipomorfos, usualmente más viables que los nulos (apartado III.2.2, en la página 7). La mutagénesis con EMS de 67.500 semillas M_0 *ago1-52* resultó fructífera, ya que tras el escrutinio de 36.810 semillas M_2 se identificaron 4.189 presuntos dobles mutantes en los que el fenotipo de *ago1-52* se debilitaba o acentuaba, o manifestaban rasgos no observados en su parental. 3.133 de ellos resultaron estériles o letales y mostraron un fenotipo muy severo, similar al de los dobles mutantes previamente obtenidos combinando alelos de genes de la maquinaria de los miARN. Solo 302 de las plantas M_2 seleccionadas resultaron viables y fértiles, de las que 92 transmitieron su fenotipo a su descendencia M_3 con penetrancia completa y expresividad poco variable. El mayor número de presuntos dobles mutantes M_2 viables y fértiles se encontró en la clase en la que el fenotipo de *ago1-52* se suprimió parcialmente. Se estudiaron en detalle las 17 líneas que mostraron mayor supresión, cuyas mutaciones recibieron la denominación de *mas* (*morphology of argonaute1-52 suppressed*). Se inició la clonación posicional de 6 genes *MAS* (*MAS1-MAS6*).

III.5.7.- Búsqueda de interactores físicos de MAS2

En esta Tesis y en otra anterior se ha contribuido a la identificación y caracterización de *MAS2*, cuyo estudio ha demostrado que es ortólogo del gen *NKAP* humano. También hemos demostrado que la proteína MAS2 participa en el control de la expresión del ADNr 45S y el procesamiento de su transcrito primario, el pre-ARNr 45S. Hemos aislado mutantes portadores de alelos de *MAS2* que son supresores informacionales del fenotipo morfológico del alelo *ago1-52* del gen *AGO1*.

Se sabe muy poco de las NKAP animales, a excepción de las de los mamíferos, y prácticamente nada de sus ortólogas vegetales (apartado III.5.5, en la página 40). La NKAP humana interacciona, en ensayos del doble híbrido de la levadura, con proteínas relacionadas con el *splicing* de los pre-ARNm, con factores que intervienen en el procesamiento del pre-ARNr 45S y el ensamblaje del ribosoma y con proteínas implicadas

en la reparación de rupturas dobles (en las dos cadenas) del ADN. Mediante inmunoprecipitación de proteínas asociadas a ARN, seguida de secuenciación masiva de ARN, se ha detectado la interacción de la NKAP humana con muchos tipos de ARN, entre ellos noARN implicados en el *splicing*, ARNr, snoARN implicados en el procesamiento del pre-ARNr 45S, ARN reguladores (como *XIST*, que inicia el silenciamiento del cromosoma X de las hembras de los mamíferos), y ARN largos no codificantes (Burgute *et al.*, 2014).

La determinación de la naturaleza molecular de la proteína MAS2 hizo posible una búsqueda de sus interactores basada en el ensayo del doble híbrido de la levadura, que se encargó a la empresa PANBIONET (Kyungbuk, Corea del Sur). Todas las interacciones detectadas por PANBIONET fueron confirmadas en el laboratorio de M.R. Ponce mediante ensayos dirigidos del doble híbrido de la levadura. Se identificaron en este escrutinio 14 interactores, 13 de los cuales no habían sido previamente estudiados en Arabidopsis. Se comprobó en la base de datos HomoloGene (http://www.ncbi.nlm.nih.gov/ homologene) que las ortólogas de 12 de estas 14 proteínas en los animales y los hongos son nucleares. Tres de estos interactores están probablemente relacionados con la regulación del *splicing*, otros tres con el procesamiento del pre-ARNr 45S y el ensamblaje del ribosoma y uno con la reparación de rupturas dobles en el ADN. Dada la localización de MAS2 en las NOR (apartado III.4.2.2, en la página 15), se inició la caracterización funcional de los genes cuyos productos interaccionaron con MAS2 y están presuntamente relacionados con la biogénesis del ribosoma. Nos interesaron particularmente dos de ellos, uno de los cuales es el producto de AT2G40430, aparentemente ortólogo de los genes *Nop53* de la levadura y *GLTSCR2* humano (apartado III.5.3, en la página 34). Durante el desarrollo de esta Tesis, se publicó la asignación del nombre *SMALL ORGAN4* (*SMO4*; Zhang *et al.*, 2015) a AT2G40430. El segundo interactor de MAS2 que hemos identificado y estudiado en esta Tesis, codificado por AT5G38720, es presuntamente ortólogo de la proteína Rrp7 de la levadura (apartado III.5.4, en la página 39), que es nucleolar y esencial en los eucariotas en que se ha estudiado, en los que está implicada en el procesamiento del pre-ARNr 45S (Baudin-Baillieu *et al.*, 1997; Rudra *et al.*, 2007).

III.5.8.- Objetivos de esta Tesis

En esta Tesis se ha completado una búsqueda de supresores de *ago1-52* previamente iniciada en el laboratorio de M.R. Ponce, sometiendo a escrutinio 20.000 semillas M_2 (Micol-Ponce *et al*., 2014; página 61 y siguientes), se han clonado y caracterizado parcialmente los genes *MAS2* (Sánchez-García *et al*., 2015; página 75 y siguientes) y *MAS5* (Micol-Ponce, Cabezas-Fuster y Ponce, sin publicar), y se ha

caracterizado a niveles genético, molecular, morfológico e histológico la función de los genes *SMO4* (Micol-Ponce *et al*., página 125 y siguientes) y *RRP7* (Micol-Ponce *et al*., página 179 y siguientes).

Los objetivos inicialmente planteados para esta Tesis fueron (1) completar la búsqueda de supresores del fenotipo morfológico de *ago1-52* (Aguilera Díaz, 2009), sometiendo a escrutinio 20.000 semillas M_2 que no habían sido sembradas anteriormente, y (2) contribuir a la clonación posicional de alguna de las mutaciones supresoras *mas*, cuya naturaleza molecular aún no se había determinado, con el fin de (3) caracterizar funcionalmente alguno de los genes mutados.

Durante la realización de las tareas asociadas al objetivo (2) del párrafo anterior, contribuí a la clonación de *MAS2* y cloné *MAS5*. La determinación de la identidad de *MAS2* nos permitió realizar una búsqueda de interactores de la proteína MAS2, en la que se identificaron varios presuntos interactores; la caracterización de los genes que codifican dos de estas proteínas se convirtió en los objetivos sobrevenidos (4) y (5) de esta Tesis, que consistieron en el análisis de la función de los genes *SMO4* (ortólogo del gen *Nop53* de la levadura y el *GLTSCR2* humano) y *RRP7* (ortólogo del gen *Rrp7* de la levadura y el *RRP7A* humano).

En esta introducción no se han hecho, deliberadamente, consideraciones en torno al *splicing*, proceso en el que probablemente juega un papel central *MAS5*, gen que como antes he dicho he clonado pero están estudiando otros miembros del laboratorio de M.R. Ponce. Durante el desarrollo de esta Tesis se han realizado algunas investigaciones sobre la función de *SMO4* y *RRP7* que aún no se han reflejado en manuscrito alguno, como las interacciones genéticas de sus alelos nulos con los de los genes de la maquinaria de los miARN *HST*, *HYL1*, *AGO1* y *HEN1*. El fenotipo de varios de los dobles mutantes que he obtenido es sinérgico, sugiere una relación funcional entre la ruta de los miARN y *SMO4* y *RRP7* y amplía el espectro de los procesos en los que participan estos dos genes. Este trabajo, ahora inconcluso, se publicará más adelante, junto con otros estudios que he iniciado o a los que he contribuido, como las interacciones genéticas entre *SMO4*, *RRP7*, *AS1* y *AS2* (apartado III.5.1, en la página 28), que revelan su relación funcional, el análisis mutacional del promotor del gen *AGO1* o la relación entre la ruta de los miARN y la formación de la cutícula en Arabidopsis.

IV.- BIBLIOGRAFÍA DE LA INTRODUCCIÓN

IV.- BIBLIOGRAFÍA DE LA INTRODUCCIÓN

Abou-Ellail, M., Cooke, R., y Saez-Vasquez, J. (2011). Variations in a team: major and minor variants of *Arabidopsis thaliana* rDNA genes. *Nucleus* **2,** 294-299.

Aguilera Díaz, V. (2009). Búsqueda de modificadores del fenotipo morfológico de un mutante *argonaute1* viable. Tesis doctoral. Universidad Miguel Hernández.

Allen, E., Xie, Z., Gustafson, A.M., y Carrington, J.C. (2005). MicroRNA-directed phasing during trans-acting siRNA biogenesis in plants. *Cell* **121,** 207-221.

Alonso, J.M., Stepanova, A.N., Leisse, T.J., Kim, C.J., Chen, H., Shinn, P., Stevenson, D.K., Zimmerman, J., Barajas, P., Cheuk, R., Gadrinab, C., Heller, C., Jeske, A., Koesema, E., Meyers, C.C., Parker, H., Prednis, L., Ansari, Y., Choy, N., Deen, H., Geralt, M., Hazari, N., Hom, E., Karnes, M., Mulholland, C., Ndubaku, R., Schmidt, I., Guzman, P., Aguilar-Henonin, L., Schmid, M., Weigel, D., Carter, D.E., Marchand, T., Risseeuw, E., Brogden, D., Zeko, A., Crosby, W.L., Berry, C.C., y Ecker, J.R. (2003). Genome-wide insertional mutagenesis of *Arabidopsis thaliana. Science* **301,** 653-657.

Ansel, K.M., Pastor, W.A., Rath, N., Lapan, A.D., Glasmacher, E., Wolf, C., Smith, L.C., Papadopoulou, N., Lamperti, E.D., Tahiliani, M., Ellwart, J.W., Shi, Y., Kremmer, E., Rao, A., y Heissmeyer, V. (2008). Mouse Eri1 interacts with the ribosome and catalyzes 5.8S rRNA processing. *Nature Structural and Molecular Biology* **15,** 523-530.

Atzorn, V., Fragapane, P., y Kiss, T. (2004). U17/snR30 is a ubiquitous snoRNA with two conserved sequence motifs essential for 18S rRNA production. *Molecular and Cellular Biology* **24,** 1769-1778.

Auerbach, C., y Robson, J.M. (1946). Action of mustard gas on the bone marrow. *Nature* **158,** 878.

Ban, N., Nissen, P., Hansen, J., Moore, P.B., y Steitz, T.A. (2000). The complete atomic structure of the large ribosomal subunit at 2.4 Å resolution. *Science* **289,** 905-920.

Barakat, A., Szick-Miranda, K., Chang, I.F., Guyot, R., Blanc, G., Cooke, R., Delseny, M., y Bailey-Serres, J. (2001). The organization of cytoplasmic ribosomal protein genes in the Arabidopsis genome. *Plant Physiology* **127,** 398-415.

Baudin-Baillieu, A., Tollervey, D., Cullin, C., y Lacroute, F. (1997). Functional analysis of Rrp7p, an essential yeast protein involved in pre-rRNA processing and ribosome assembly. *Molecular and Cellular Biology* **17,** 5023-5032.

Baumberger, N., y Baulcombe, D.C. (2005). *Arabidopsis* ARGONAUTE1 is an RNA slicer that selectively recruits microRNAs and short interfering RNAs. *Proceedings of the National Academy of Sciences USA* **102,** 11928-11933.

Beltrame, M., Henry, Y., y Tollervey, D. (1994). Mutational analysis of an essential binding site for the U3 snoRNA in the 5' external transcribed spacer of yeast pre-rRNA. *Nucleic Acids Research* **22,** 5139-5147.

Berardini, T.Z., Reiser, L., Li, D., Mezheritsky, Y., Muller, R., Strait, E., y Huala, E. (2015). The Arabidopsis information resource: Making and mining the "gold standard" annotated reference plant genome. *Genesis* **53,** 474-485.

Berná, G., Robles, P., y Micol, J.L. (1999). A mutational analysis of leaf morphogenesis in *Arabidopsis thaliana. Genetics* **152,** 729-742.

Beven, A.F., Simpson, G.G., Brown, J.W., y Shaw, P.J. (1995). The organization of spliceosomal components in the nuclei of higher plants. *Journal of Cell Science* **108,** 509-518.

Billy, E., Wegierski, T., Nasr, F., y Filipowicz, W. (2000). Rcl1p, the yeast protein similar to the RNA 3'-phosphate cyclase, associates with U3 snoRNP and is required for 18S rRNA biogenesis. *EMBO Journal* **19,** 2115-2126.

Bohmert, K., Camus, I., Bellini, C., Bouchez, D., Caboche, M., y Benning, C. (1998). *AGO1* defines a novel locus of *Arabidopsis* controlling leaf development. *EMBO Journal* **17,** 170-180.

Boulon, S., Westman, B.J., Hutten, S., Boisvert, F.M., y Lamond, A.I. (2010). The nucleolus under stress. *Molecular Cell* **40,** 216-227.

Brodersen, P., y Voinnet, O. (2006). The diversity of RNA silencing pathways in plants. *Trends in Genetics* **22,** 268-280.

Brown, J.W., y Shaw, P.J. (1998). Small nucleolar RNAs and pre-rRNA processing in plants. *Plant Cell* **10,** 649-657.

Brown, J.W., Shaw, P.J., Shaw, P., y Marshall, D.F. (2005). Arabidopsis nucleolar protein database (AtNoPDB). *Nucleic Acids Research* **33,** 633-636.

Brown, J.W., y Shaw, P.J. (2008). The role of the plant nucleolus in pre-mRNA processing. *Current Topics in Microbiology and Immunology* **326,** 291-311.

Burgute, B.D., Peche, V.S., Steckelberg, A.L., Glockner, G., Gassen, B., Gehring, N.H., y Noegel, A.A. (2014). NKAP is a novel RS-related protein that interacts with RNA and RNA binding proteins. *Nucleic Acids Research* **42,** 3177-3193.

Burgute, B.D., Peche, V.S., Muller, R., Matthias, J., Gassen, B., Eichinger, L., Glockner, G., y Noegel, A.A. (2016). The C-Terminal SynMuv/DdDUF926 domain regulates the function of the N-Terminal domain of DdNKAP. *PLoS One* **11,** e0168617.

Byrne, M.E., Barley, R., Curtis, M., Arroyo, J.M., Dunham, M., Hudson, A., y Martienssen, R.A. (2000). *Asymmetric leaves1* mediates leaf patterning and stem cell function in *Arabidopsis. Nature* **408,** 967-971.

Byrne, M.E. (2009). A role for the ribosome in development. *Trends in Plant Science* **14,** 512-519.

Campell, B.R., Song, Y., Posch, T.E., Cullis, C.A., y Town, C.D. (1992). Sequence and organization of 5S ribosomal RNA-encoding genes of *Arabidopsis thaliana*. *Gene* **112,** 225-228.

Cao, J., Schneeberger, K., Ossowski, S., Gunther, T., Bender, S., Fitz, J., Koenig, D., Lanz, C., Stegle, O., Lippert, C., Wang, X., Ott, F., Muller, J., Alonso-Blanco, C., Borgwardt, K., Schmid, K.J., y Weigel, D. (2011). Whole-genome sequencing of multiple *Arabidopsis thaliana* populations. *Nature Genetics* **43,** 956-963.

Caparros-Ruiz, D., Lahmy, S., Piersanti, S., y Echeverria, M. (1997). Two ribosomal DNA-binding factors interact with a cluster of motifs on the 5' external transcribed spacer, upstream from the primary pre-rRNA processing site in a higher plant. *European Journal of Biochemistry* **247,** 981-989.

Carlson, E.A. (2013). H.J. Muller's contributions to mutation research. *Mutation Research* **752,** 1-5.

Carroll, A.J., Heazlewood, J.L., Ito, J., y Millar, A.H. (2008). Analysis of the Arabidopsis cytosolic ribosome proteome provides detailed insights into its components and their post-translational modification. *Molecular and Cellular Proteomics* **7,** 347-369.

Carroll, A.J. (2013). The Arabidopsis cytosolic ribosomal proteome: from form to function. *Frontiers in Plant Science* **4,** 32.

Chanarat, S., y Strasser, K. (2013). Splicing and beyond: the many faces of the Prp19 complex. *Biochimica et Biophysica Acta* **1833,** 2126-2134.

Chang, Y.F., Imam, J.S., y Wilkinson, M.F. (2007). The nonsense-mediated decay RNA surveillance pathway. *Annual Review Biochemistry* **76,** 51-74.

Chen, D., Li, Z., Yang, Q., Zhang, J., Zhai, Z., y Shu, H.B. (2003). Identification of a nuclear protein that promotes NF-kappaB activation. *Biochemical and Biophysical Research Communications* **310,** 720-724.

Chen, H., Han, L., Tsai, H., Wang, Z., Wu, Y., Duo, Y., Cao, W., Chen, L., Tan, Z., Xu, N., Huang, X., Zhuang, J., y Huang, L. (2016). PICT-1 is a key nucleolar sensor in DNA damage response signaling that regulates apoptosis through the RPL11-MDM2-p53 pathway. *Oncotarget* **7,** 83241-83257.

Chen, X., Liu, J., Cheng, Y., y Jia, D. (2002). *HEN1* functions pleiotropically in *Arabidopsis* development and acts in C function in the flower. *Development* **129,** 1085-1094.

Cheng, C.Y., Krishnakumar, V., Chan, A., Thibaud-Nissen, F., Schobel, S., y Town, C.D. (2017). Araport11: a complete reannotation of the *Arabidopsis thaliana* reference genome. *Plant Journal* **89,** 789-804.

Cherry, J.M. (1995). Genetic nomenclature guide. *Saccharomyces cerevisiae. Trends in Genetics* **March,** 11-12.

Cloix, C., Tutois, S., Mathieu, O., Cuvillier, C., Espagnol, M.C., Picard, G., y Tourmente, S. (2000). Analysis of 5S rDNA arrays in *Arabidopsis thaliana*: physical mapping and chromosome-specific polymorphisms. *Genome Research* **10,** 679-690.

Cloix, C., Tutois, S., Yukawa, Y., Mathieu, O., Cuvillier, C., Espagnol, M.C., Picard, G., y Tourmente, S. (2002). Analysis of the 5S RNA pool in *Arabidopsis thaliana*: RNAs are heterogeneous and only two of the genomic 5S loci produce mature 5S RNA. *Genome Research* **12,** 132-144.

Cloix, C., Yukawa, Y., Tutois, S., Sugiura, M., y Tourmente, S. (2003). *In vitro* analysis of the sequences required for transcription of the *Arabidopsis thaliana* 5S rRNA genes. *Plant Journal* **35,** 251-261.

Comella, P., Pontvianne, F., Lahmy, S., Vignols, F., Barbezier, N., Debures, A., Jobet, E., Brugidou, E., Echeverria, M., y Saez-Vasquez, J. (2008). Characterization of a ribonuclease III-like protein required for cleavage of the pre-rRNA in the 3'ETS in Arabidopsis. *Nucleic Acids Research* **36,** 1163-1175.

Copenhaver, G.P., y Pikaard, C.S. (1996). Two-dimensional RFLP analyses reveal megabase-sized clusters of rRNA gene variants in *Arabidopsis thaliana*, suggesting local spreading of variants as the mode for gene homogenization during concerted evolution. *Plant Journal* **9,** 273-282.

Creff, A., Sormani, R., y Desnos, T. (2010). The two Arabidopsis *RPS6* genes, encoding for cytoplasmic ribosomal proteins S6, are functionally equivalent. *Plant Molecular Biology* **73,** 533-546.

Czech, B., y Hannon, G.J. (2011). Small RNA sorting: matchmaking for Argonautes. *Nature Reviews Genetics* **12,** 19-31.

Davidson, E.H., y Erwin, D.H. (2006). Gene regulatory networks and the evolution of animal body plans. *Science* **311,** 796-800.

de la Cruz, J., Kressler, D., Tollervey, D., y Linder, P. (1998). Dob1p (Mtr4p) is a putative ATP-dependent RNA helicase required for the 3' end formation of 5.8S rRNA in *Saccharomyces cerevisiae*. *EMBO Journal* **17,** 1128-1140.

Ding, S.W., y Voinnet, O. (2008). Antiviral immunity directed by small RNAs. *Cell* **130,** 413-426.

Douet, J., y Tourmente, S. (2007). Transcription of the 5S rRNA heterochromatic genes is epigenetically controlled in *Arabidopsis thaliana* and *Xenopus laevis*. *Heredity* **99,** 5-13.

Dragon, F., Gallagher, J.E., Compagnone-Post, P.A., Mitchell, B.M., Porwancher, K.A., Wehner, K.A., Wormsley, S., Settlage, R.E., Shabanowitz, J., Osheim, Y., Beyer, A.L., Hunt, D.F., y Baserga, S.J. (2002). A large nucleolar U3 ribonucleoprotein required for 18S ribosomal RNA biogenesis. *Nature* **417,** 967-970.

Drouin, G., y de Sa, M.M. (1995). The concerted evolution of 5S ribosomal genes linked to the repeat units of other multigene families. *Molecular Biology and Evolution* **12,** 481-493.

Dunker, A.K., Oldfield, C.J., Meng, J., Romero, P., Yang, J.Y., Chen, J.W., Vacic, V., Obradovic, Z., y Uversky, V.N. (2008). The unfoldomics decade: an update on intrinsically disordered proteins. *BMC Genomics* **9,** S1.

Elbashir, S.M., Lendeckel, W., y Tuschl, T. (2001). RNA interference is mediated by 21- and 22-nucleotide RNAs. *Genes and Development* **15,** 188-200.

Endersby, J. (2009). *A guinea pig's history of Biology*. Harvard University Press.

Enright, C.A., Maxwell, E.S., Eliceiri, G.L., y Sollner-Webb, B. (1996). 5'ETS rRNA processing facilitated by four small RNAs: U14, E3, U17, and U3. *RNA* **2,** 1094-1099.

Farrar, J.E., y Dahl, N. (2011). Untangling the phenotypic heterogeneity of Diamond Blackfan anemia. *Seminars in Hematology* **48,** 124-135.

Fayet-Lebaron, E., Atzorn, V., Henry, Y., y Kiss, T. (2009). 18S rRNA processing requires base pairings of snR30 H/ACA snoRNA to eukaryote-specific 18S sequences. *EMBO Journal* **28,** 1260-1270.

Feldmann, K.A., Malmberg, R.L., y Dean, C. (1994). Mutagenesis in *Arabidopsis*. En *Arabidopsis*, pp. 137-172. Meyerowitz, E.M., y Somerville, C.R., eds. Cold Spring Harbor Laboratory Press.

Feng, Z., Zhang, B., Ding, W., Liu, X., Yang, D.L., Wei, P., Cao, F., Zhu, S., Zhang, F., Mao, Y., y Zhu, J.K. (2013). Efficient genome editing in plants using a CRISPR/Cas system. *Cell Research* **23,** 1229-1232.

Ferreira-Cerca, S., Poll, G., Gleizes, P.E., Tschochner, H., y Milkereit, P. (2005). Roles of eukaryotic ribosomal proteins in maturation and transport of pre-18S rRNA and ribosome function. *Molecular Cell* **20,** 263-275.

Fransz, P., Armstrong, S., Alonso-Blanco, C., Fischer, T.C., Torres-Ruiz, R.A., y Jones, G. (1998). Cytogenetics for the model system *Arabidopsis thaliana. Plant Journal* **13,** 867-876.

Fumagalli, S., Di Cara, A., Neb-Gulati, A., Natt, F., Schwemberger, S., Hall, J., Babcock, G.F., Bernardi, R., Pandolfi, P.P., y Thomas, G. (2009). Absence of nucleolar disruption after impairment of 40S ribosome biogenesis reveals an rpL11-translation-dependent mechanism of p53 induction. *Nature Cell Biology* **11,** 501-508.

Garcia, S., Panero, J.L., Siroky, J., y Kovarik, A. (2010). Repeated reunions and splits feature the highly dynamic evolution of 5S and 35S ribosomal RNA genes (rDNA) in the Asteraceae family. *BMC Plant Biology* **10,** 176.

Geerlings, T.H., Vos, J.C., y Raue, H.A. (2000). The final step in the formation of 25S rRNA in *Saccharomyces cerevisiae* is performed by 5'→ 3' exonucleases. *RNA* **6,** 1698-1703.

Gerhardy, S., Menet, A.M., Pena, C., Petkowski, J.J., y Panse, V.G. (2014). Assembly and nuclear export of pre-ribosomal particles in budding yeast. *Chromosoma* **123,** 327-344.

Ghildiyal, M., y Zamore, P.D. (2009). Small silencing RNAs: an expanding universe. *Nature Reviews Genetics* **10,** 94-108.

Giot, L., Bader, J.S., Brouwer, C., Chaudhuri, A., Kuang, B., Li, Y., Hao, Y.L., Ooi, C.E., Godwin, B., Vitols, E., Vijayadamodar, G., Pochart, P., Machineni, H., Welsh, M., Kong, Y., Zerhusen, B., Malcolm, R., Varrone, Z., Collis, A., Minto, M., Burgess, S., McDaniel, L., Stimpson, E., Spriggs, F., Williams, J., Neurath, K., Ioime, N., Agee, M., Voss, E., Furtak, K., Renzulli, R., Aanensen, N., Carrolla, S., Bickelhaupt, E., Lazovatsky, Y., DaSilva, A., Zhong, J., Stanyon, C.A., Finley, R.L., Jr., White, K.P., Braverman, M., Jarvie, T., Gold, S., Leach, M., Knight, J., Shimkets, R.A., McKenna, M.P., Chant, J., y Rothberg, J.M. (2003). A protein interaction map of *Drosophila melanogaster*. *Science* **302,** 1727-1736.

Grandi, P., Rybin, V., Bassler, J., Petfalski, E., Strauss, D., Marzioch, M., Schafer, T., Kuster, B., Tschochner, H., Tollervey, D., Gavin, A.C., y Hurt, E. (2002). 90S pre-ribosomes include the 35S pre-rRNA, the U3 snoRNP, and 40S subunit processing factors but predominantly lack 60S synthesis factors. *Molecular Cell* **10,** 105-115.

Grigg, S.P., Canales, C., Hay, A., y Tsiantis, M. (2005). SERRATE coordinates shoot meristem function and leaf axial patterning in Arabidopsis. *Nature* **437,** 1022-1026.

Han, M.H., Goud, S., Song, L., y Fedoroff, N. (2004). The Arabidopsis double-stranded RNA-binding protein HYL1 plays a role in microRNA-mediated gene regulation. *Proceedings of the National Academy of Sciences USA* **101,** 1093-1098.

Hegele, A., Kamburov, A., Grossmann, A., Sourlis, C., Wowro, S., Weimann, M., Will, C.L., Pena, V., Luhrmann, R., y Stelzl, U. (2012). Dynamic protein-protein interaction wiring of the human spliceosome. *Molecular Cell* **45,** 567-580.

Henderson, A.S., Warburton, D., y Atwood, K.C. (1972). Location of ribosomal DNA in the human chromosome complement. *Proceedings of the National Academy of Sciences USA* **69,** 3394-3398.

Henras, A.K., Plisson-Chastang, C., O'Donohue, M.F., Chakraborty, A., y Gleizes, P.E. (2015). An overview of pre-ribosomal RNA processing in eukaryotes. *Wiley Interdisciplinary Reviews: RNA* **6,** 225-242.

Henry, Y., Wood, H., Morrissey, J.P., Petfalski, E., Kearsey, S., y Tollervey, D. (1994). The 5' end of yeast 5.8S rRNA is generated by exonucleases from an upstream cleavage site. *EMBO Journal* **13,** 2452-2463.

Hillman, G.C., y Davies, M.S. (1990). Measured domestication rates in wild wheats and barley under primitive cultivation, and their archaeological implications. *Journal of World Prehistory* **4,** 157-222.

Holmberg Olausson, K., Nister, M., y Lindstrom, M.S. (2012). p53 -dependent and -independent nucleolar stress responses. *Cells* **1,** 774-798.

Horiguchi, G., Mollá-Morales, A., Pérez-Pérez, J.M., Kojima, K., Robles, P., Ponce, M.R., Micol, J.L., y Tsukaya, H. (2011). Differential contributions of ribosomal protein genes to *Arabidopsis thaliana* leaf development. *Plant Journal* **65,** 724-736.

Horn, D.M., Mason, S.L., y Karbstein, K. (2011). Rcl1 protein, a novel nuclease for 18 S ribosomal RNA production. *Journal of Biological Chemistry* **286,** 34082-34087.

Howard, J.M., y Sanford, J.R. (2015). The RNAissance family: SR proteins as multifaceted regulators of gene expression. *Wiley Interdisciplinary Reviews: RNA* **6,** 93-110.

Hughes, J.M., y Ares, M., Jr. (1991). Depletion of U3 small nucleolar RNA inhibits cleavage in the 5' external transcribed spacer of yeast pre-ribosomal RNA and impairs formation of 18S ribosomal RNA. *EMBO Journal* **10,** 4231-4239.

Hummel, M., Cordewener, J.H., de Groot, J.C., Smeekens, S., America, A.H., y Hanson, J. (2012). Dynamic protein composition of *Arabidopsis thaliana* cytosolic ribosomes in response to sucrose feeding as revealed by label free MSE proteomics. *Proteomics* **12,** 1024-1038.

Husbands, A.Y., Benkovics, A.H., Nogueira, F.T., Lodha, M., y Timmermans, M.C. (2015). The ASYMMETRIC LEAVES complex employs multiple modes of regulation to affect adaxial-abaxial patterning and leaf complexity. *Plant Cell* **27,** 3321-3335.

Iwakawa, H., Ueno, Y., Semiarti, E., Onouchi, H., Kojima, S., Tsukaya, H., Hasebe, M., Soma, T., Ikezaki, M., Machida, C., y Machida, Y. (2002). The *ASYMMETRIC LEAVES2* gene of *Arabidopsis thaliana*, required for formation of a symmetric flat leaf lamina, encodes a member of a novel family of proteins characterized by cysteine repeats and a leucine zipper. *Plant and Cell Physiology* **43,** 467-478.

Jacob, F., y Monod, J. (1961). Genetic regulatory mechanisms in the synthesis of proteins. *Journal of Molecular Biology* **3,** 318-356.

Jacobsen, S.E., Running, M.P., y Meyerowitz, E.M. (1999). Disruption of an RNA helicase/RNAse III gene in Arabidopsis causes unregulated cell division in floral meristems. *Development* **126,** 5231-5243.

James, A., Wang, Y., Raje, H., Rosby, R., y DiMario, P. (2014). Nucleolar stress with and without p53. *Nucleus* **5,** 402-426.

Janas, M.M., Wang, E., Love, T., Harris, A.S., Stevenson, K., Semmelmann, K., Shaffer, J.M., Chen, P.H., Doench, J.G., Yerramilli, S.V., Neuberg, D.S., Iliopoulos, D., Housman, D.E., Burge, C.B., y Novina, C.D. (2012). Reduced expression of ribosomal proteins relieves microRNA-mediated repression. *Molecular Cell* **46,** 171-186.

Jarvelin, A.I., Noerenberg, M., Davis, I., y Castello, A. (2016). The new (dis)order in RNA regulation. *Cell Communication and Signaling* **14,** 9.

Jensen, S., Gassama, M.P., y Heidmann, T. (1999). Taming of transposable elements by homology-dependent gene silencing. *Nature Genetics* **21,** 209-212.

Jorgensen, R.A., y Cluster, P.D. (1988). Modes and tempos in the evolution of nuclear ribosomal DNA: new characters for evolutionary studies and new markers for genetic and population studies. *Annals of the Missouri Botanical Garden* **75,** 1238-1247.

Joshi, H.J., Christiansen, K.M., Fitz, J., Cao, J., Lipzen, A., Martin, J., Smith-Moritz, A.M., Pennacchio, L.A., Schackwitz, W.S., Weigel, D., y Heazlewood, J.L. (2012). 1001 Proteomes: a functional proteomics portal for the analysis of *Arabidopsis thaliana* accessions. *Bioinformatics* **28,** 1303-1306.

Jover-Gil, S., Candela, H., y Ponce, M.R. (2005). Plant microRNAs and development. *International Journal of Developmental Biology* **49,** 733-744.

Kawakatsu, T., Huang, S.S., Jupe, F., Sasaki, E., Schmitz, R.J., Urich, M.A., Castanon, R., Nery, J.R., Barragan, C., He, Y., Chen, H., Dubin, M., Lee, C.R., Wang, C., Bemm, F., Becker, C., O'Neil, R., O'Malley, R.C., Quarless, D.X., Genomes, C., Schork, N.J., Weigel, D., Nordborg, M., y Ecker, J.R. (2016). Epigenomic diversity in a global collection of *Arabidopsis thaliana* accessions. *Cell* **166,** 492-505.

Keller, C., Woolcock, K., Hess, D., y Buhler, M. (2010). Proteomic and functional analysis of the noncanonical poly(A) polymerase Cid14. *RNA* **16,** 1124-1129.

Kempers-Veenstra, A.E., Oliemans, J., Offenberg, H., Dekker, A.F., Piper, P.W., Planta, R.J., y Klootwijk, J. (1986). 3'-End formation of transcripts from the yeast rRNA operon. *EMBO Journal* **5,** 2703-2710.

Kidner, C.A., y Martienssen, R.A. (2005). The developmental role of microRNA in plants. *Current Opinion in Plant Biology* **8,** 38-44.

Kim, J.Y., An, Y.M., y Park, J.H. (2016). Role of GLTSCR2 in the regulation of telomerase activity and chromosome stability. *Molecular Medicine Reports* **14,** 1697-1703.

Kim, Y., Schumaker, K.S., y Zhu, J.K. (2006). EMS mutagenesis of Arabidopsis. *Methods in Molecular Biology* **323,** 101-103.

Klinge, S., Voigts-Hoffmann, F., Leibundgut, M., Arpagaus, S., y Ban, N. (2011). Crystal structure of the eukaryotic 60S ribosomal subunit in complex with initiation factor 6. *Science* **334,** 941-948.

Klinge, S., Voigts-Hoffmann, F., Leibundgut, M., y Ban, N. (2012). Atomic structures of the eukaryotic ribosome. *Trends in Biochemical Sciences* **37,** 189-198.

Komarova, N.Y., Grimm, G.W., Hemleben, V., y Volkov, R.A. (2008). Molecular evolution of 35S rDNA and taxonomic status of *Lycopersicon* within *Solanum* sect. *Petota. Plant Systematics and Evolution* **276,** 59-71.

Komili, S., Farny, N.G., Roth, F.P., y Silver, P.A. (2007). Functional specificity among ribosomal proteins regulates gene expression. *Cell* **131,** 557-571.

Koyama, K., Wada, A., Maki, Y., y Tanaka, A. (1996). Changes in the protein composition of cytoplasmic ribosomes during the greening of etiolated barley leaves. *Physiologia Plantarum* **96,** 85-90.

Krieg, D.R. (1963). Ethyl methanesulfonate-induced reversion of bacteriophage T4rII mutants. *Genetics* **48,** 561-580.

Krishnakumar, V., Hanlon, M.R., Contrino, S., Ferlanti, E.S., Karamycheva, S., Kim, M., Rosen, B.D., Cheng, C.Y., Moreira, W., Mock, S.A., Stubbs, J., Sullivan, J.M., Krampis, K., Miller, J.R., Micklem, G., Vaughn, M., y Town, C.D. (2015). Araport: the Arabidopsis information portal. *Nucleic Acids Research* **43,** D1003-D1009.

Krogan, N.J., Peng, W.T., Cagney, G., Robinson, M.D., Haw, R., Zhong, G., Guo, X., Zhang, X., Canadien, V., Richards, D.P., Beattie, B.K., Lalev, A., Zhang, W., Davierwala, A.P., Mnaimneh, S., Starostine, A., Tikuisis, A.P., Grigull, J., Datta, N., Bray, J.E., Hughes, T.R., Emili, A., y Greenblatt, J.F. (2004). High-definition macromolecular composition of yeast RNA-processing complexes. *Molecular Cell* **13,** 225-239.

Kufel, J., Dichtl, B., y Tollervey, D. (1999). Yeast Rnt1p is required for cleavage of the pre-ribosomal RNA in the 3' ETS but not the 5' ETS. *RNA* **5,** 909-917.

Laibach, F. (1907). Zur frage nach der individualität der chromosomen im pflanzenreich. *Beih Botanishes Centralblatt* **22,** 191-210.

Lane, D.P. (1992). Cancer. p53, guardian of the genome. *Nature* **358,** 15-16.

Lange, H., Sement, F.M., y Gagliardi, D. (2011). MTR4, a putative RNA helicase and exosome co-factor, is required for proper rRNA biogenesis and development in Arabidopsis thaliana. *Plant Journal* **68,** 51-63.

Laubinger, S., Sachsenberg, T., Zeller, G., Busch, W., Lohmann, J.U., Ratsch, G., y Weigel, D. (2008). Dual roles of the nuclear cap-binding complex and SERRATE in pre-mRNA splicing and microRNA processing in *Arabidopsis thaliana. Proceedings of the National Academy of Sciences USA* **105,** 8795-8800.

Levine, Z.A., y Shea, J.E. (2016). Simulations of disordered proteins and systems with conformational heterogeneity. *Current Opinion in Structural Biology* **43,** 95-103.

Li, J., Zhang, Y., Chen, K.L., Shan, Q.W., Wang, Y.P., Liang, Z., y Gao, C.X. (2013). [CRISPR/Cas: a novel way of RNA-guided genome editing]. *Yi Chuan* **35,** 1265-1273.

Li, T., Chen, L., Cheng, J., Dai, J., Huang, Y., Zhang, J., Liu, Z., Li, A., Li, N., Wang, H., Yin, X., He, K., Yu, M., Zhou, T., Zhang, X., y Xia, Q. (2016). SUMOylated NKAP is essential for chromosome alignment by anchoring CENP-E to kinetochores. *Nature Communications* **7,** 12969.

Lin, J., Lu, J., Feng, Y., Sun, M., y Ye, K. (2013). An RNA-binding complex involved in ribosome biogenesis contains a protein with homology to tRNA CCA-adding enzyme. *PLoS Biology* **11,** e1001669.

Llanos, S., y Serrano, M. (2010). Depletion of ribosomal protein L37 occurs in response to DNA damage and activates p53 through the L11/MDM2 pathway. *Cell Cycle* **9,** 4005-4012.

Lobbes, D., Rallapalli, G., Schmidt, D.D., Martin, C., y Clarke, J. (2006). SERRATE: a new player on the plant microRNA scene. *EMBO Reports* **7,** 1052-1058.

Lorkovic, Z.J., y Barta, A. (2008). Role of Cajal bodies and nucleolus in the maturation of the U1 snRNP in Arabidopsis. *PLoS One* **3,** e3989.

Lowder, L., Malzahn, A., y Qi, Y. (2016). Rapid evolution of manifold CRISPR systems for plant genome editing. *Frontiers in Plant Science* **7,** 1683.

Lu, C., y Fedoroff, N. (2000). A mutation in the *Arabidopsis HYL1* gene encoding a dsRNA binding protein affects responses to abscisic acid, auxin, and cytokinin. *Plant Cell* **12,** 2351-2366.

Mallory, A., y Vaucheret, H. (2010). Form, function, and regulation of ARGONAUTE proteins. *Plant Cell* **22,** 3879-3889.

Meinke, D., y Koornneef, M. (1997). Community standards for *Arabidopsis thaliana. Plant Journal* **12,** 247-253.

Meissner, B., Rogalski, T., Viveiros, R., Warner, A., Plastino, L., Lorch, A., Granger, L., Segalat, L., y Moerman, D.G. (2011). Determining the sub-cellular localization of proteins within *Caenorhabditis elegans* body wall muscle. *PLoS One* **6,** e19937.

Melnikov, S., Ben-Shem, A., Garreau de Loubresse, N., Jenner, L., Yusupova, G., y Yusupov, M. (2012). One core, two shells: bacterial and eukaryotic ribosomes. *Nature Structural and Molecular Biology* **19,** 560-567.

Meyerowitz, E.M. (2001). Prehistory and history of *Arabidopsis* research. *Plant Physiology* **125,** 15-19.

Missbach, S., Weis, B.L., Martin, R., Simm, S., Bohnsack, M.T., y Schleiff, E. (2013). 40S ribosome biogenesis co-factors are essential for gametophyte and embryo development. *PLoS One* **8,** e54084.

Morel, J.B., Godon, C., Mourrain, P., Beclin, C., Boutet, S., Feuerbach, F., Proux, F., y Vaucheret, H. (2002). Fertile hypomorphic *ARGONAUTE* (*ago1*) mutants impaired in post-transcriptional gene silencing and virus resistance. *Plant Cell* **14,** 629-639.

Moreno-Diaz de la Espina, S., Medina, F.J., y Risueno, M.C. (1980). Correlation of nucleolar activity and nucleolar vacuolation in plant cells. *European Journal of Cell Biology* **22,** 724-729.

Murata, M., Heslop-Harrison, J.S., y Motoyoshi, F. (1997). Physical mapping of the 5S ribosomal RNA genes in *Arabidopsis thaliana* by multi-color fluorescence in situ hybridization with cosmid clones. *Plant Journal* **12,** 31-37.

Narla, A., y Ebert, B.L. (2010). Ribosomopathies: human disorders of ribosome dysfunction. *Blood* **115,** 3196-3205.

Nestler, E.J., y Hyman, S.E. (2002). Regulation of gene expression. En *Neuropsychopharmacology: The Fifth Generation of Progress*, pp. 217-228. Davis, K.L., Charney, D., Coyle, J.T., y Nemeroff, C., eds. American College of Neuropsychopharmacology.

Nomura, M., Nogi, Y., y Oakes, M. (2000). Transcription of rDNA in the yeast *Saccharomyces cerevisiae*. En *Madame Curie Bioscience Database*, pp. Landes Bioscience.

O'Donohue, M.F., Choesmel, V., Faubladier, M., Fichant, G., y Gleizes, P.E. (2010). Functional dichotomy of ribosomal proteins during the synthesis of mammalian 40S ribosomal subunits. *Journal of Cell Biology* **190,** 853-866.

Ochs, R.L., Lischwe, M.A., Spohn, W.H., y Busch, H. (1985). Fibrillarin: a new protein of the nucleolus identified by autoimmune sera. *Biology of the Cell* **54,** 123-133.

Oeffinger, M., Zenklusen, D., Ferguson, A., Wei, K.E., El Hage, A., Tollervey, D., Chait, B.T., Singer, R.H., y Rout, M.P. (2009). Rrp17p is a eukaryotic exonuclease required for 5' end processing of Pre-60S ribosomal RNA. *Molecular Cell* **36,** 768-781.

Okamura, K., Ishizuka, A., Siomi, H., y Siomi, M.C. (2004). Distinct roles for Argonaute proteins in small RNA-directed RNA cleavage pathways. *Genes and Development* **18,** 1655-1666.

Osheim, Y.N., French, S.L., Keck, K.M., Champion, E.A., Spasov, K., Dragon, F., Baserga, S.J., y Beyer, A.L. (2004). Pre-18S ribosomal RNA is structurally compacted into the SSU processome prior to being cleaved from nascent transcripts in *Saccharomyces cerevisiae. Molecular Cell* **16,** 943-954.

Ossowski, S., Schwab, R., y Weigel, D. (2008). Gene silencing in plants using artificial microRNAs and other small RNAs. *Plant Journal* **53,** 674-690.

Page, D.R., y Grossniklaus, U. (2002). The art and design of genetic screens: *Arabidopsis thaliana. Nature Reviews Genetics* **3,** 124-136.

Palade, G. (1975). Intracellular aspects of the process of protein synthesis. *Science* **189,** 347-358.

Palade, G.E. (1955). A small particulate component of the cytoplasm. *Journal of Biophysical and Biochemical Cytology* **1,** 59-68.

Palm, D., Simm, S., Darm, K., Weis, B.L., Ruprecht, M., Schleiff, E., y Scharf, C. (2016). Proteome distribution between nucleoplasm and nucleolus and its relation to ribosome biogenesis in *Arabidopsis thaliana. RNA Biology* **13,** 441-454.

Park, M.Y., Wu, G., Gonzalez-Sulser, A., Vaucheret, H., y Poethig, R.S. (2005). Nuclear processing and export of microRNAs in Arabidopsis. *Proceedings of the National Academy of Sciences USA* **102,** 3691-3696.

Pendle, A.F., Clark, G.P., Boon, R., Lewandowska, D., Lam, Y.W., Andersen, J., Mann, M., Lamond, A.I., Brown, J.W., y Shaw, P.J. (2005). Proteomic analysis of the Arabidopsis nucleolus suggests novel nucleolar functions. *Molecular Biology of the Cell* **16,** 260-269.

Perez, L., Aguilar, R., Mendez, A.P., y de Jimenez, E.S. (1990). Phosphorylation of ribosomal proteins induced by auxins in maize embryonic tissues. *Plant Physiology* **94,** 1270-1275.

Peters, J.L., Cnudde, F., y Gerats, T. (2003). Forward genetics and map-based cloning approaches. *Trends in Plant Science* **8,** 484-491.

Petes, T.D. (1979). Yeast ribosomal DNA genes are located on chromosome XII. *Proceedings of the National Academy of Sciences USA* **76,** 410-414.

Phipps, K.R., Charette, J., y Baserga, S.J. (2011). The small subunit processome in ribosome biogenesis-progress and prospects. *Wiley Interdisciplinary Reviews: RNA* **2,** 1-21.

Pinon, V., Etchells, J.P., Rossignol, P., Collier, S.A., Arroyo, J.M., Martienssen, R.A., y Byrne, M.E. (2008). Three *PIGGYBACK* genes that specifically influence leaf patterning encode ribosomal proteins. *Development* **135,** 1315-1324.

Pollock, D.D., y Larkin, J.C. (2004). Estimating the degree of saturation in mutant screens. *Genetics* **168,** 489-502.

Pontes, O., Vitins, A., Ream, T.S., Hong, E., Pikaard, C.S., y Costa-Nunes, P. (2013). Intersection of small RNA pathways in *Arabidopsis thaliana* sub-nuclear domains. *PLoS One* **8,** e65652.

Pontvianne, F., Abou-Ellail, M., Douet, J., Comella, P., Matia, I., Chandrasekhara, C., Debures, A., Blevins, T., Cooke, R., Medina, F.J., Tourmente, S., Pikaard, C.S., y Saez-Vasquez, J. (2010). Nucleolin is required for DNA methylation state and the expression of rRNA gene variants in *Arabidopsis thaliana. PLoS Genetics* **6,** e1001225.

Pontvianne, F., Blevins, T., Chandrasekhara, C., Feng, W., Stroud, H., Jacobsen, S.E., Michaels, S.D., y Pikaard, C.S. (2012). Histone methyltransferases regulating rRNA gene dose and dosage control in Arabidopsis. *Genes and Development* **26,** 945-957.

Preti, M., O'Donohue, M.F., Montel-Lehry, N., Bortolin-Cavaille, M.L., Choesmel, V., y Gleizes, P.E. (2013). Gradual processing of the ITS1 from the nucleolus to the cytoplasm during synthesis of the human 18S rRNA. *Nucleic Acids Research* **41,** 4709-4723.

Provart, N.J., Alonso, J., Assmann, S.M., Bergmann, D., Brady, S.M., Brkljacic, J., Browse, J., Chapple, C., Colot, V., Cutler, S., Dangl, J., Ehrhardt, D., Friesner, J.D., Frommer, W.B., Grotewold, E., Meyerowitz, E., Nemhauser, J., Nordborg, M., Pikaard, C., Shanklin, J., Somerville, C., Stitt, M., Torii, K.U., Waese, J., Wagner, D., y McCourt, P. (2016). 50 years of Arabidopsis research: highlights and future directions. *New Phytologist* **209,** 921-944.

Qu, L.J., y Qin, G. (2014). Generation and identification of Arabidopsis EMS mutants. *Methods in Molecular Biology* **1062,** 225-239.

Qui, Y., Denli, A.M., y Hannon, G.J. (2005). Biochemical specialization within *Arabidopsis* RNA silencing pathways. *Molecular Cell* **19,** 421-428.

Rabl, J., Leibundgut, M., Ataide, S.F., Haag, A., y Ban, N. (2011). Crystal structure of the eukaryotic 40S ribosomal subunit in complex with initiation factor 1. *Science* **331,** 730-736.

Ratcliff, F.G., MacFarlane, S.A., y Baulcombe, D.C. (1999). Gene silencing without DNA. rna-mediated cross-protection between viruses. *Plant Cell* **11,** 1207-1216.

Ren, G., Chen, X., y Yu, B. (2012a). Uridylation of miRNAs by hen1 suppressor1 in Arabidopsis. *Current Biology* **22,** 695-700.

Ren, G., Xie, M., Dou, Y., Zhang, S., Zhang, C., y Yu, B. (2012b). Regulation of miRNA abundance by RNA binding protein TOUGH in Arabidopsis. *Proceedings of the National Academy of Sciences USA* **109,** 12817-12821.

Rodriguez-Corona, U., Sobol, M., Rodriguez-Zapata, L.C., Hozak, P., y Castano, E. (2015). Fibrillarin from Archaea to human. *Biology of the Cell* **107,** 159-174.

Rogers, K., y Chen, X. (2013). Biogenesis, turnover, and mode of action of plant microRNAs. *Plant Cell* **25,** 2383-2399.

Rogers, S.O., y Bendich, A.J. (1987). Heritability and variability in ribosomal RNA genes of *Vicia faba. Genetics* **117,** 285-295.

Rout, M.P., Aitchison, J.D., Suprapto, A., Hjertaas, K., Zhao, Y., y Chait, B.T. (2000). The yeast nuclear pore complex: composition, architecture, and transport mechanism. *Journal of Cell Biology* **148,** 635-651.

Rudra, D., Mallick, J., Zhao, Y., y Warner, J.R. (2007). Potential interface between ribosomal protein production and pre-rRNA processing. *Molecular and Cellular Biology* **27,** 4815-4824.

Saez-Vasquez, J., Caparros-Ruiz, D., Barneche, F., y Echeverria, M. (2004). A plant snoRNP complex containing snoRNAs, fibrillarin, and nucleolin-like proteins is competent for both rRNA gene binding and pre-rRNA processing in vitro. *Molecular and Cellular Biology* **24,** 7284-7297.

Sánchez-García, A.B., Aguilera, V., Micol-Ponce, R., Jover-Gil, S., y Ponce, M.R. (2015). Arabidopsis MAS2, an essential gene that encodes a homolog of animal NF-kappa B activating protein, is involved in 45S ribosomal DNA silencing. *Plant Cell* **27,** 1999-2015.

Scharf, K.D., y Nover, L. (1982). Heat-shock-induced alterations of ribosomal protein phosphorylation in plant cell cultures. *Cell* **30,** 427-437.

Schauer, S.E., Jacobsen, S.E., Meinke, D.W., y Ray, A. (2002). DICER-LIKE1: blind men and elephants in Arabidopsis development. *Trends in Plant Science* **7,** 487-491.

Schmidt, K., y Butler, J.S. (2013). Nuclear RNA surveillance: role of TRAMP in controlling exosome specificity. *Wiley Interdisciplinary Reviews: RNA* **4,** 217-231.

Schwab, R., Ossowski, S., Riester, M., Warthmann, N., y Weigel, D. (2006). Highly specific gene silencing by artificial microRNAs in *Arabidopsis. Plant Cell* **18,** 1121-1133.

Serrano-Cartagena, J., Robles, P., Ponce, M.R., y Micol, J.L. (1999). Genetic analysis of leaf form mutants from the *Arabidopsis* Information Service collection. *Molecular and General Genetics* **261,** 725-739.

Shabalina, S.A., y Koonin, E.V. (2008). Origins and evolution of eukaryotic RNA interference. *Trends in Ecology and Evolution* **23,** 578-587.

Shaw, P., y Brown, J. (2012). Nucleoli: composition, function, and dynamics. *Plant Physiology* **158,** 44-51.

Shaw, P.J., y Jordan, E.G. (1995). The nucleolus. *Annual Review of Cell and Developmental Biology* **11,** 93-121.

Shaw, P.J., y Brown, J.W. (2004). Plant nuclear bodies. *Current Opinion in Plant Biology* **7,** 614-620.

Sikora, P., Chawade, A., Larsson, M., Olsson, J., y Olsson, O. (2011). Mutagenesis as a tool in plant genetics, functional genomics, and breeding. *International Journal of Plant Genomics* **2011,** 314829.

Sirri, V., Urcuqui-Inchima, S., Roussel, P., y Hernandez-Verdun, D. (2008). Nucleolus: the fascinating nuclear body. *Histochemistry and Cell Biology* **129,** 13-31.

Sloan, K.E., Mattijssen, S., Lebaron, S., Tollervey, D., Pruijn, G.J., y Watkins, N.J. (2013). Both endonucleolytic and exonucleolytic cleavage mediate ITS1 removal during human ribosomal RNA processing. *Journal of Cell Biology* **200,** 577-588.

Smartt, J., y Simmonds, N.W. (1995). *Evolution of crop plants*. John Wiley & Sons.

Sorensen, P.D., Lomholt, B., Frederiksen, S., y Tommerup, N. (1991). Fine mapping of human 5S rRNA genes to chromosome 1q42.11-q42.13. *Cytogenetics and Cell Genetics* **57,** 26-29.

Stepinski, D. (2010). Organization of the nucleoli of soybean root meristematic cells at different states of their activity. *Micron* **41,** 283-288.

Stepinski, D. (2014). Functional ultrastructure of the plant nucleolus. *Protoplasma* **251,** 1285-1306.

Stirnberg, P., Liu, J.P., Ward, S., Kendall, S.L., y Leyser, O. (2012). Mutation of the cytosolic ribosomal protein-encoding RPS10B gene affects shoot meristematic function in Arabidopsis. *BMC Plant Biology* **12,** 160.

Stults, D.M., Killen, M.W., Pierce, H.H., y Pierce, A.J. (2008). Genomic architecture and inheritance of human ribosomal RNA gene clusters. *Genome Research* **18,** 13-18.

Sugihara, Y., Honda, H., Iida, T., Morinaga, T., Hino, S., Okajima, T., Matsuda, T., y Nadano, D. (2010). Proteomic analysis of rodent ribosomes revealed heterogeneity including ribosomal proteins L10-like, L22-like 1, and L39-like. *Journal of Proteome Research* **9,** 1351-1166.

Szakonyi, D., y Byrne, M.E. (2011). Ribosomal protein L27a is required for growth and patterning in *Arabidopsis thaliana. Plant Journal* **65,** 269-281.

Szick-Miranda, K., y Bailey-Serres, J. (2001). Regulated heterogeneity in 12-kDa P-protein phosphorylation and composition of ribosomes in maize (*Zea mays* L.). *Journal of Biological Chemistry* **276,** 10921-10928.

Tafforeau, L., Zorbas, C., Langhendries, J.L., Mullineux, S.T., Stamatopoulou, V., Mullier, R., Wacheul, L., y Lafontaine, D.L. (2013). The complexity of human ribosome biogenesis revealed by systematic nucleolar screening of Pre-rRNA processing factors. *Molecular Cell* **51,** 539-551.

Telfer, A., y Poethig, R.S. (1998). *HASTY*: a gene that regulates the timing of shoot maturation in *Arabidopsis thaliana. Development* **125,** 1889-1898.

Terns, M.P., y Terns, R.M. (2002). Small nucleolar RNAs: versatile trans-acting molecules of ancient evolutionary origin. *Gene Expression Patterns* **10,** 17-39.

Thapa, P., Das, J., McWilliams, D., Shapiro, M., Sundsbak, R., Nelson-Holte, M., Tangen, S., Anderson, J., Desiderio, S., Hiebert, S., Sant'angelo, D.B., y Shapiro, V.S. (2013). The transcriptional repressor NKAP is required for the development of iNKT cells. *Nature Communications* **4,** 1582.

The 1.001 Genomes Consortium (2016). 1.135 genomes reveal the global pattern of polymorphism in *Arabidopsis thaliana. Cell* **166,** 481-491.

The Arabidopsis Genome Initiative (2000). Analysis of the genome sequence of the flowering plant *Arabidopsis thaliana. Nature* **408,** 796-815.

Thiry, M., y Lafontaine, D.L. (2005). Birth of a nucleolus: the evolution of nucleolar compartments. *Trends in Cell Biology* **15,** 194-199.

Thomas, F., y Kutay, U. (2003). Biogenesis and nuclear export of ribosomal subunits in higher eukaryotes depend on the CRM1 export pathway. *Journal of Cell Science* **116,** 2409-2419.

Thoms, M., Thomson, E., Bassler, J., Gnadig, M., Griesel, S., y Hurt, E. (2015). The exosome is recruited to RNA substrates through specific adaptor proteins. *Cell* **162,** 1029-1038.

Thomson, E., y Tollervey, D. (2005). Nop53p is required for late 60S ribosome subunit maturation and nuclear export in yeast. *RNA* **11,** 1215-1224.

Thomson, E., y Tollervey, D. (2010). The final step in 5.8S rRNA processing is cytoplasmic in *Saccharomyces cerevisiae. Molecular and Cellular Biology* **30,** 976-984.

Thomson, E., Ferreira-Cerca, S., y Hurt, E. (2013). Eukaryotic ribosome biogenesis at a glance. *Journal of Cell Science* **126,** 4815-4821.

Till, B.J., Reynolds, S.H., Weil, C., Springer, N., Burtner, C., Young, K., Bowers, E., Codomo, C.A., Enns, L.C., Odden, A.R., Greene, E.A., Comai, L., y Henikoff, S. (2004). Discovery of induced point mutations in maize genes by TILLING. *BMC Plant Biology* **4,** 12.

Till, B.J., Cooper, J., Tai, T.H., Colowit, P., Greene, E.A., Henikoff, S., y Comai, L. (2007). Discovery of chemically induced mutations in rice by TILLING. *BMC Plant Biology* **7,** 19.

Toloti Carneiro, J.M., Chacón-Madrid, K., Miranda Maciel, B.C., y Zezzi Arruda, M.A. (2015). *Arabidopsis thaliana* and omics approaches: a review. *Journal of Integrated OMICS* **5,** 1-16.

Tomari, Y., y Zamore, P.D. (2005). Perspective: machines for RNAi. *Genes and Development* **19,** 517-529.

Turowski, T.W., y Tollervey, D. (2015). Cotranscriptional events in eukaryotic ribosome synthesis. *Wiley Interdisciplinary Reviews: RNA* **6,** 129-139.

Tutois, S., Cloix, C., Cuvillier, C., Espagnol, M.C., Lafleuriel, J., Picard, G., y Tourmente, S. (1999). Structural analysis and physical mapping of a pericentromeric region of chromosome 5 of *Arabidopsis thaliana. Chromosome Research* **7,** 143-156.

Udem, S.A., y Warner, J.R. (1972). Ribosomal RNA synthesis in *Saccharomyces cerevisiae. Journal of Molecular Biology* **65,** 227-242.

Uversky, V.N. (2015). The multifaceted roles of intrinsic disorder in protein complexes. *FEBS Letters* **589,** 2498-2506.

Van Minnebruggen, A., Neyt, P., De Groeve, S., Coussens, G., Ponce, M.R., Micol, J.L., y Van Lijsebettens, M. (2010). The *ang3* mutation identified the ribosomal protein gene *RPL5B* with a role in cell expansion during organ growth. *Physiologia Plantarum* **138,** 91-101.

Vaucheret, H. (2008). Plant ARGONAUTES. *Trends in Plant Science* **13,** 350-358.

Vazquez, F. (2006). Arabidopsis endogenous small RNAs: highways and byways. *Trends in Plant Science* **11,** 460-468.

Veith, T., Martin, R., Wurm, J.P., Weis, B.L., Duchardt-Ferner, E., Safferthal, C., Hennig, R., Mirus, O., Bohnsack, M.T., Wohnert, J., y Schleiff, E. (2012). Structural and functional analysis of the archaeal endonuclease Nob1. *Nucleic Acids Research* **40,** 3259-3274.

Vogelstein, B., Lane, D., y Levine, A.J. (2000). Surfing the p53 network. *Nature* **408,** 307-310.

Voinnet, O. (2009). Origin, biogenesis, and activity of plant microRNAs. *Cell* **136,** 669-687.

Wain, H.M., Bruford, E.A., Lovering, R.C., Lush, M.J., Wright, M.W., y Povey, S. (2002). Guidelines for human gene nomenclature. *Genomics* **79,** 464-470.

Wang, H., Zhang, X., Liu, J., Kiba, T., Woo, J., Ojo, T., Hafner, M., Tuschl, T., Chua, N.H., y Wang, X.J. (2011). Deep sequencing of small RNAs specifically associated with Arabidopsis AGO1 and AGO4 uncovers new AGO functions. *Plant Journal* **67,** 292-304.

Wang, M., y Pestov, D.G. (2011). 5'-end surveillance by Xrn2 acts as a shared mechanism for mammalian pre-rRNA maturation and decay. *Nucleic Acids Research* **39,** 1811-1822.

Wang, M.B., y Metzlaff, M. (2005). RNA silencing and antiviral defense in plants. *Current Opinion in Plant Biology* **8,** 216-222.

Weigel, D., y Glazebrook, J. (2006). EMS mutagenesis of arabidopsis seed. *Cold Spring Harbor Protocols* **2006,** doi: 10.1101/pdb.prot4621.

Weigel, D. (2012). Natural variation in Arabidopsis: from molecular genetics to ecological genomics. *Plant Physiology* **158,** 2-22.

Weinstein, L.B., y Steitz, J.A. (1999). Guided tours: from precursor snoRNA to functional snoRNP. *Current Opinion in Cell Biology* **11,** 378-384.

Weis, B.L., Kovacevic, J., Missbach, S., y Schleiff, E. (2015). Plant-specific features of ribosome biogenesis. *Trends in Plant Science* **20,** 729-740.

Westergaard, M. (1957). Chemical mutagenesis in relation to the concept of the gene. *Experientia* **13,** 224-234.

Wimberly, B.T., Brodersen, D.E., Clemons, W.M., Jr., Morgan-Warren, R.J., Carter, A.P., Vonrhein, C., Hartsch, T., y Ramakrishnan, V. (2000). Structure of the 30S ribosomal subunit. *Nature* **407,** 327-339.

Win, T.Z., Draper, S., Read, R.L., Pearce, J., Norbury, C.J., y Wang, S.W. (2006). Requirement of fission yeast Cid14 in polyadenylation of rRNAs. *Molecular and Cellular Biology* **26,** 1710-1721.

Xi, L., Moscou, M.J., Meng, Y., Xu, W., Caldo, R.A., Shaver, M., Nettleton, D., y Wise, R.P. (2009). Transcript-based cloning of RRP46, a regulator of rRNA processing and R gene-independent cell death in barley-powdery mildew interactions. *Plant Cell* **21,** 3280-3295.

Xie, Z., Johansen, L.K., Gustafson, A.M., Kasschau, K.D., Lellis, A.D., Zilberman, D., Jacobsen, S.E., y Carrington, J.C. (2004). Genetic and functional diversification of small RNA pathways in plants. *PLoS Biology* **2,** 642-652.

Xie, Z., y Qi, X. (2008). Diverse small RNA-directed silencing pathways in plants. *Biochimica et Biophysica Acta* **1779,** 720-724.

Yang, L., Huang, W., Wang, H., Cai, R., Xu, Y., y Huang, H. (2006a). Characterizations of a hypomorphic *argonaute1* mutant reveal novel *AGO1* functions in *Arabidopsis* lateral organ development. *Plant Molecular Biology* **61,** 63-78.

Yang, L., Liu, Z., Lu, F., Dong, A., y Huang, H. (2006b). SERRATE is a novel nuclear regulator in primary microRNA processing in Arabidopsis. *Plant Journal* **47,** 841-850.

Yao, Y., Ling, Q., Wang, H., y Huang, H. (2008). Ribosomal proteins promote leaf adaxial identity. *Development* **135,** 1325-1334.

Yoon, J.C., Ling, A.J., Isik, M., Lee, D.Y., Steinbaugh, M.J., Sack, L.M., Boduch, A.N., Blackwell, T.K., Sinclair, D.A., y Elledge, S.J. (2014). GLTSCR2/PICT1 links mitochondrial stress and Myc signaling. *Proceedings of the National Academy of Sciences USA* **111,** 3781-3786.

Yu, B., Yang, Z., Li, J., Minakhina, S., Yang, M., Padgett, R.W., Steward, R., y Chen, X. (2005). Methylation as a crucial step in plant microRNA biogenesis. *Science* **307,** 932-935.

Yusupov, M.M., Yusupova, G.Z., Baucom, A., Lieberman, K., Earnest, T.N., Cate, J.H., y Noller, H.F. (2001). Crystal structure of the ribosome at 5.5 Å resolution. *Science* **292,** 883-896.

Zakrzewska-Placzek, M., Souret, F.F., Sobczyk, G.J., Green, P.J., y Kufel, J. (2010). *Arabidopsis thaliana* XRN2 is required for primary cleavage in the pre-ribosomal RNA. *Nucleic Acids Research* **38,** 4487-4502.

Zapata, L., Ding, J., Willing, E.M., Hartwig, B., Bezdan, D., Jiao, W.B., Patel, V., Velikkakam James, G., Koornneef, M., Ossowski, S., y Schneeberger, K. (2016). Chromosome-level assembly of *Arabidopsis thaliana* L*er* reveals the extent of translocation and inversion polymorphisms. *Proceedings of the National Academy of Sciences USA* **113,** E4052-E4060.

Zhang, B., Pan, X., Cobb, G.P., y Anderson, T.A. (2006). Plant microRNA: a small regulatory molecule with big impact. *Developmental Biology* **289,** 3-16.

Zhou, X., Liao, W.J., Liao, J.M., Liao, P., y Lu, H. (2015). Ribosomal proteins: functions beyond the ribosome. *Journal of Molecular Cell Biology* **7,** 92-104.

V.- PUBLICACIONES

SCIENTIFIC REPORTS

OPEN

SUBJECT AREAS:
PLANT SCIENCES
GENETICS

Received
14 May 2014

Accepted
13 June 2014

Published
2 July 2014

Correspondence and requests for materials should be addressed to M.R.P. (mrponce@umh.es)

* These authors contributed equally to this work.

† Current address: Centro Nacional de Biotecnología, Consejo Superior de Investigaciones Científicas, 28049 Madrid, Spain.

A genetic screen for suppressors of a hypomorphic allele of Arabidopsis *ARGONAUTE1*

Rosa Micol-Ponce*, Verónica Aguilera*† & María Rosa Ponce

Instituto de Bioingeniería, Universidad Miguel Hernández, Campus de Elche, 03202 Elche, Spain.

***ARGONAUTE1* (*AGO1*) encodes a key component of the complexes mediating microRNA (miRNA) function in Arabidopsis. To study the regulation, action and interactions of *AGO1*, we conducted a genetic screen to identify second-site mutations modifying the morphological phenotype of *ago1-52*, a partial loss-of-function allele of *AGO1*. Unlike null *ago1* mutations, the hypomorphic *ago1-52* allele does not cause lethality or sterility; however, *ago1-52* does produce a morphological phenotype clearly distinct from wild type. In our screen for modifiers of *ago1-52*, we identified suppressor mutations that partially restore wild-type morphology in the *ago1-52* background and we termed these *mas* (*morphology of argonaute1-52 suppressed*). We focused on 23 of these putative suppressors. Linkage analysis of the *mas* mutations together with sequencing of the *AGO1* gene in genomic DNA and cDNA from *ago1-52 mas* plants indicated that 22 of the *mas* lines contain extragenic suppressors, and one contains an intragenic suppressor that affects splicing of *ago1-52*. In the presence of the wild-type allele of *AGO1*, most of the *mas* mutations cause a mild or no mutant phenotype on their own, indicating that the *ago1-52* mutant may provide a sensitized background for examining the interactions of AGO1.**

The existence of RNA molecules with repressor[1] or activator[2] functions was proposed in the first models of gene expression regulation. Despite these early predictions, however, experimental evidence of the existence of chromosomally encoded small regulatory RNAs was not published until the last two decades of the XX century in prokaryotes and eukaryotes, with the discovery of *MicF*[3] and *lin-4*[4,5], respectively. *lin-4* belongs to a class of small RNAs that has received more attention in recent years, the microRNAs (miRNAs), single-stranded molecules of about 22 nt in length that hybridize by complementarity to their mRNA targets, and then induce the degradation and/or attenuation of the translation of these mRNA targets. These processes take place in the cytoplasm, in ribonucleoprotein complexes named RISC (RNA-Induced Silencing Complexes), whose catalytic component in all species studied so far is a protein of the ARGONAUTE (AGO) family[6–8]. Since the discovery of *lin-4*, hundreds of eukaryotic genes have been found to be negatively regulated by miRNAs in many organisms, including humans, and thousands have been predicted as miRNA targets using many different algorithms.

A collection of *Arabidopsis thaliana* (hereafter, Arabidopsis) mutants with morphologically abnormal leaves was obtained in the laboratory of J.L. Micol[9,10], and 41 of these mutants were dubbed *incurvata* (*icu*), because of their upwardly curved leaves[11–15]. We positionally cloned the *icu3*, *icu8*, *icu9-1*, *icu9-2* and *icu15* mutations[16,17], which were found to be novel loss-of-function alleles of the genes encoding HASTY (HST)[18], HYPONASTIC LEAVES1 (HYL1)[19], ARGONAUTE1 (AGO1)[20] and HUA ENHANCER1 (HEN1)[21]; these proteins are known components of the miRNA pathway[22,23].

The above mentioned *icu* mutants were renamed as *hst-21*, *hyl1-12*, *ago1-51*, *ago1-52* and *hen1-13*, respectively, and intercrossed and crossed to *dcl1-9* (*dicer-like1-9*)[24], a line carrying a mutant allele of *DCL1*, another gene encoding a component of the miRNA machinery. All of the double mutant combinations obtained in this way showed a strong, synergistic phenotype[16]. This observation led us to presume that loss-of-function alleles of *HST*, *HYL1*, *AGO1*, *HEN1* or *DCL1* would provide a sensitized genetic background, useful for a second-site mutagenesis aimed to identify novel genes directly or indirectly related to the miRNA pathway.

To study the regulation, action and interactions of *AGO1*, we decided to perform a second-site mutagenesis with the *ago1-52* mutant. The *ago1-52* hypomorphic allele causes a morphological phenotype easily distinguishable from wild type[16], and only partially reduces viability and fertility, unlike null *ago1* alleles, which are completely sterile[20]. *ago1-52* carries a G→A transition mutation 12 bp upstream of the 3′ end of its 21th intron[17]. The mutation creates a splicing acceptor signal that causes mis-splicing and gives rise to an mRNA 10 nt longer than

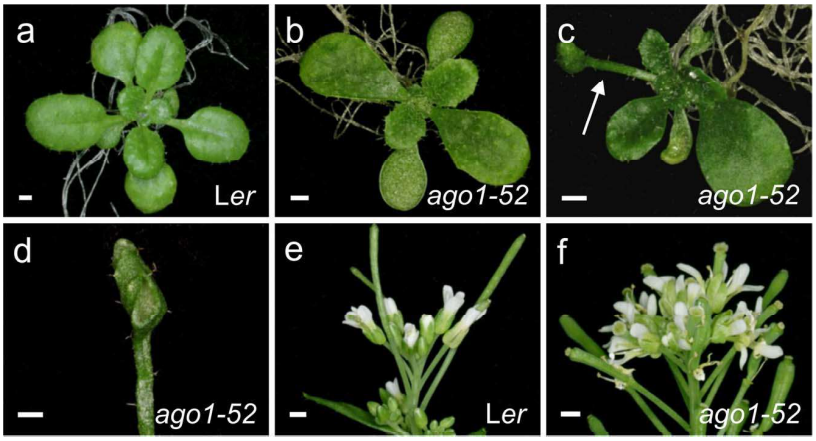

Figure 1 | Some phenotypes of the *ago1-52* mutant. (a–c) Rosettes from (a) the wild type L*er* and (b, c) *ago1-52*. An arrow in c highlights a trumpet-shaped, radialised leaf. (d) Detail of a radialised *ago1-52* leaf. (e, f) Terminal region of the inflorescences of (e) L*er* and (f) *ago1-52*. Scale bars: 1 mm. Pictures were taken (a–d) 21 das and (e, f) 42 das.

that of the wild type; the *ago1-52* mutant mRNA is translated into a mutant protein with 15 aa different than those of the wild type at the carboxyl terminus, and with 55 fewer residues than the wild type (Figure S1). For the mutagen, we chose ethyl methanesulfonate (EMS) for its strong mutagenicity and its capacity to generate hypomorphic alleles, which might provide a broader range of suppressor mutations than null alleles[25–27].

Results and Discussion

Morphological phenotype of the *ago1-52* mutant. The *ago1-52* recessive mutation causes a pleiotropic phenotype with complete penetrance and variable expressivity (Figure 1). At 21 days after stratification (das) the *ago1-52* plants have an average of 4.07 ± 0.25 vegetative leaves, in contrast to the L*er* plants, which have an average of 8.33 ± 0.84 leaves (n=30). As in other *ago1* mutants, leaves of *ago1-52* show no clear boundary between petiole and lamina[17]. Juvenile *ago1-52* leaves (the first three) exhibit abaxial trichomes, which are seen in the wild type only in adult leaves (fourth and following). Leaf adaxialisation is apparent in some *ago1-52* plants, which exhibit different extents of radialisation of the two first leaves[17]. The *ago1-52* plants do not exceed 20 cm in height (13.79 ± 1.82 cm in *ago1-52* versus 25.5 ± 1.73 cm in L*er*; n=20) and possess a short, compact inflorescence. The *ago1-52* plants have shorter siliques than the wild type (5.77 ± 1.52 mm in *ago1-52 versus* 10.10 ± 1.54 mm in L*er*; n=30), and have fewer seeds than wild type (10.79 ± 8.49 in *ago1-52 versus* 44.14 ± 16.92 in L*er*; n=30).

Screen design and mutagenesis. To isolate modifiers of the morphological phenotype of the *ago1-52* mutant, we mutagenised homozygous *ago1-52* plants with EMS. The procedure followed to isolate and characterise new mutants (Figure 2) was similar to that described by Berná *et al.*[9]. Approximately 67,500 seeds of *ago1-52* were sent to Lehle Seeds (www.arabidopsis.com) to be mutagenized. Mutagenized seeds (M_1 generation) were sown on soil and grown in a growth chamber to obtain M_2 seeds, which were harvested in bulk to form 15 parental groups; these groups were then sent to our laboratory for screening.

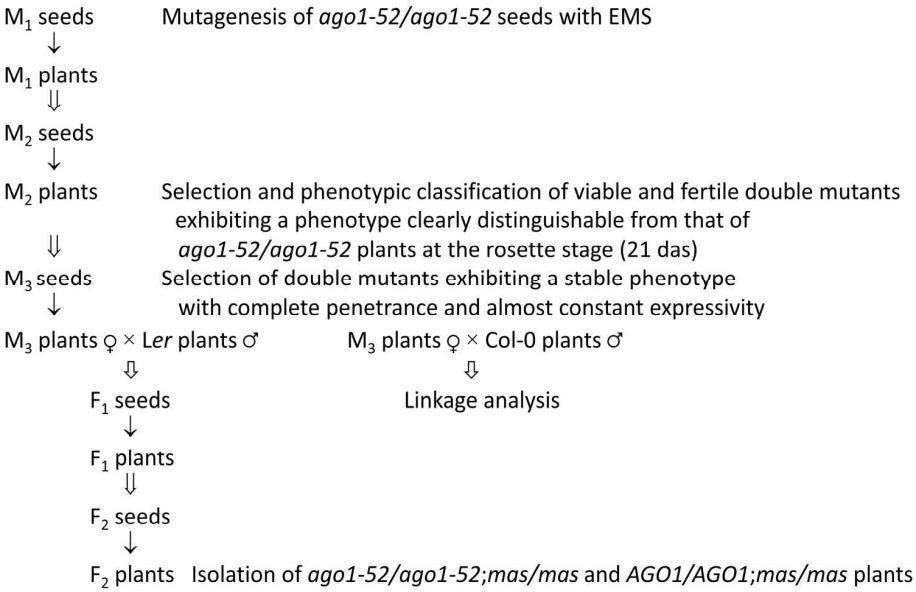

Figure 2 | Flowchart describing the screening strategy for the isolation and genetic analysis of suppressors of *ago1-52*. The ↓ and ⇓ symbols indicate growth and selfing, respectively. The ⇩ symbol indicates outcrossing or backcrossing.

www.nature.com/scientificreports

Table 1 | Modifiers of the mutant phenotype of *ago1-52* identified in the M_2 population screened

Parental group[a]	Number of M_2 seeds screened	Early lethality	Albino seedlings	Putative double mutant plants			
				Fertile	Sterile	Lethal	Total
1	3,891	1,215	92	113	148	102	363
2	2,373	1,035	56	26	68	222	316
3	4,212	1,651	29	47	89	422	558
4	6,002	2,422	11	28	75	709	812
5	4,984	1,893	12	11	41	478	530
6	6,310	2,302	24	32	51	675	758
7	4,594	1,851	7	20	22	401	443
8	4,444	1,752	18	25	27	357	409
Total	36,810	14,121	249	302	521	3,366	4,189

Values indicate the number of seeds, seedlings or plants of each type. [a]The number of M_1 plants in each parental group was 1,283.

Estimation of the efficiency of the mutagenesis. One of the methods used in Arabidopsis to estimate the efficiency of mutagenesis is based on determining the frequency of initial cells with mutations (P) and the mean number of mutations per initial cell (M)[28]. The values of P and M are calculated from the frequency of M_1 plants that show siliques with some sort of mutation (m_a) or from the frequency of siliques with mutations (m_b), which, in turn, are determined according to the appearance of easily-observable mutant phenotypes in the silique, phenotypes such as embryo lethality or albinism, which occur very rarely in wild-type populations. P and M are then calculated as follows[28,29]:

$$P = 1 - \sqrt[n]{1 - m_a} = m_b \quad (1)$$

$$M = -\ln(1 - m_a)n^{-1} = -\ln(1 - m_b) = -\ln(1 - P) \quad (2)$$

where n is the mean number of initial cells, whose most widely accepted value is 2–3. About 50 M_1 plants are usually examined, and 5–6 siliques in each plant, to count the presence of albino embryos. Any mutagenesis with EMS that leads to a P value of above 0.3 can be considered effective. Indeed, using the equation in which the P value was defined, it can be seen that, assuming $n = 2$, P will = 0.3 when half the M_1 plants show at least one mutation that causes embryo albinism ($m_a = 0.5$).

Ninety siliques from 18 M_1 plants were examined, and albino embryos were found in all of them. As a consequence, the proportion of siliques revealing the existence of a mutation causing albinism was $m_b = 90/90 = 1$, which implies $P = 1$. From the above, we can deduce that the frequency of M_1 plants with siliques showing some mutation was $m_a = 1$. In other words, all the M_1 plants were carriers of at least one mutation causing embryo albinism. This value is surprisingly high, since in a similar mutagenesis carried out by Lehle Seeds for J.L. Micol on a wild type L*er* genetic background, the value of P was 0.54[9,30]. Perhaps in the sensitized *ago1-52* genetic background many phenotypes, including albinism, arise that are much less visible in a wild-type background.

Of the M_2 seeds studied, 38% showed no or abortive germination. The causal mutations for such lethal phenotypes in mature embryos (seeds) or seedlings seem to occur in all the M_1 parental lines. This conclusion is based on the assumption that almost all these mutations were recessive, as is common for hypomorphic or null mutations, and that each of them was homozygous in one of the three M_2 seeds representing by each average M_1 parental.

The number of albino seedlings also indicates the presence of mutations in the genomes of the plants screened. We found one case of albinism per every 91 M_2 plants that did not show early lethality, which indicates that the mutagenesis was very effective. We use the term albinism here to refer to the absence of a green colour in the cotyledons of the seedlings, some of which were completely white and others yellowish.

Characterisation of the mutants. *Phenotypic classification of putative double mutants.* The screen for modifiers of the phenotype of *ago1-52* was carried out in two steps, using eight and seven parental groups, respectively. We first screened 36,810 M_2 seeds, the progeny of 10,264 M_1 plants (parental groups P1–P8; Table 1) sowing seeds in plates in a controlled number with L*er* and *ago1-52* seeds as controls (see Methods). Whereas the *ago1-52* and L*er* seeds germinated at a rate of 93.0% and 97.2%, respectively, and developed into viable plants, we observed no or abortive germination in 38.0% (14,121) of the M_2 seeds sown. Such a high percentage of early lethality shows the sensitivity of the *ago1-52* genetic background to EMS. Another indicator of the efficiency of the mutagenesis was the large number (249) of seedlings with albino cotyledons and no or only rudimentary leaves; all these seedlings died before 21 das (Table 1).

About 11% of the M_2 seeds sown produced plants that survived more than 21 das and were considered double mutants because they showed unexpected phenotypes or an increased or reduced mutant phenotype compared to that of *ago1-52* plants. Among the 4,189 double mutants isolated, 3,366 exhibited lethality after 21 das and died before completing their life cycle, 521 completed their life cycle but did not produce seeds, and only 302 produced M_3 seeds (Table 1).

M_2 double mutants of the most represented class showed a strong synergistic phenotype, in some cases reminiscent of those of the double mutant combinations of mutations in two miRNA machinery genes, and almost all showed a lethal phenotype. We also defined six phenotypic classes based on morphological traits, all of which included viable double mutants (Table 2 and Figure S2). Although some showed more than one of the traits considered characteristic of each class, we provisionally assigned each mutant to only one class. Plants showing leaf variegation or generalized chlorosis were assigned to the "De-pigmented plants" class. The "Severe Ago1-52 phenotype" and "Weak Ago1-52 phenotype" classes included plants

Table 2 | Assignment of M_2 putative double mutants to phenotypic classes

Phenotypic classes	Viability and fertility			
	Fertile	Sterile	Lethal	Total
Synergistic phenotypes	0	3	3,130	3,133
De-pigmented plants	34	70	68	172
Reticulate leaves	48	19	7	74
Compact rosette	25	104	37	166
Severe Ago1-52 phenotype	42	67	23	132
Weak Ago1-52 phenotype	93	91	29	213
Other phenotypes	60	167	72	299
Total	302	521	3,366	4,189

Values indicate the number of plants of each type.

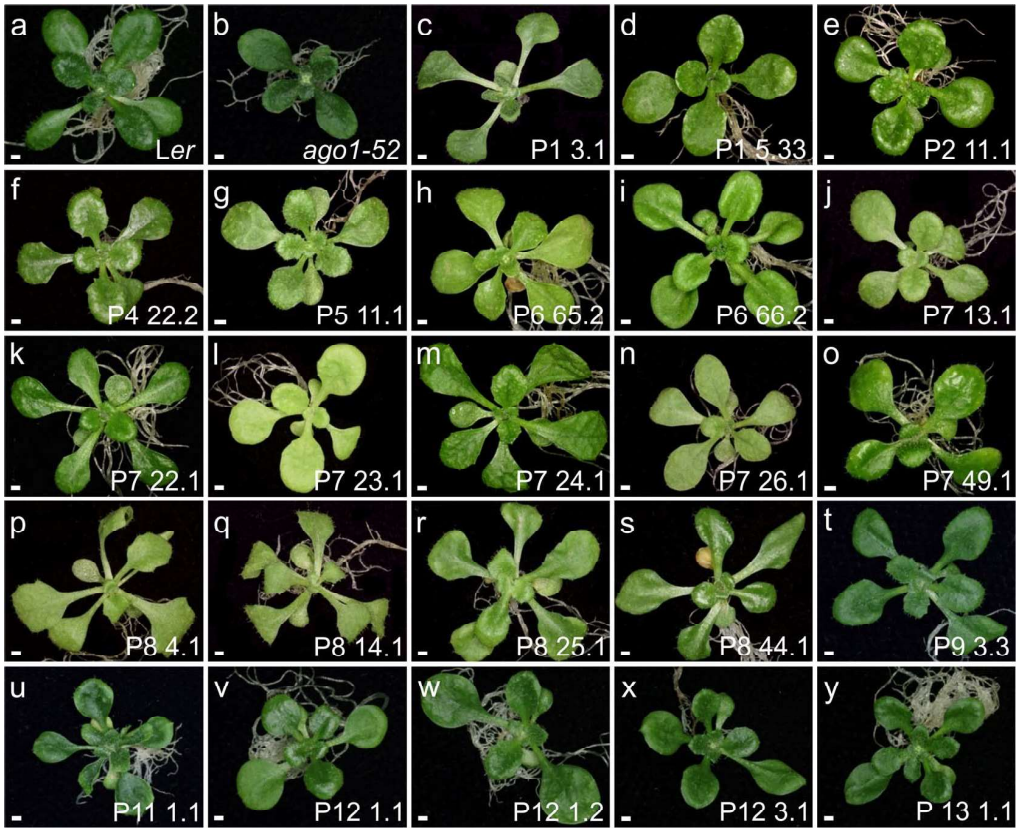

Figure 3 | Vegetative phenotype of the suppressor lines identified in this work. Rosettes of M_3 plants are shown from 23 of the double mutants isolated, in which the morphological phenotype of *ago1-52* is partially suppressed by a second-site mutation. Pictures were taken 21 das. Scale bar: 1 mm.

in which the phenotype of *ago1-52* was accentuated or alleviated, respectively. The "Reticulate leaves" class included plants with leaves in which the veins stood out because of their colour compared with a pale lamina. Plants with small vegetative leaves or short petioles were included in the "Compact rosette" class. The "Other phenotypes" class included a number of mutants with phenotypes that could not be categorized into the other classes.

Analysis of the transmission of the suppression of the phenotype of ago1-52. To study the inheritance of the suppressed phenotype, we examined the progeny of the isolated M_2 plants. We sowed several tens of M_3 seeds derived from each M_2 plant self-pollination. Transmission of the mutant phenotype was unequivocally Mendelian in only 92 of the 302 M_2 putative mutants that were fertile. We observed variable expressivity in 104 M_3 families, a phenotype weaker than that of their M_2 parentals in 21 M_3 families, and in 85 families the M_2 phenotype did not reappear in the M_3 generation.

Of the 92 M_2 putative double mutants that showed complete penetrance and almost invariable expressivity in the M_3 progeny, we focused on studying 17 lines of the 21 that we initially assigned to the class we denominate "Weak Ago1-52 phenotype" (Figure 3c-s). All these M_3 lines exhibited suppression of the *ago1-52* phenotypes during their vegetative and reproductive development. Leaves of the M_3 plants were less spatulated than those of *ago1-52*, with a well-defined boundary between petiole and lamina. No radialized leaves were seen in these suppressor lines, which exhibited in addition more vegetative leaves than *ago1-52*. Suppression was also shown by these plants after bolting: they exhibited increased stature and number of stems compared to *ago1-52*, from which they also differ in having a less compact inflorescence (Figure 4). The number of seeds in the siliques of these suppressor lines was also higher than that of *ago1-52* plants.

We hypothesized that partial suppression of the phenotype of the *ago1-52* mutation shown by these lines may have been caused by loss of function in genes whose products have an antagonistic effect on *AGO1*, or by gain of function alleles of genes that act together with *AGO1* in the silencing of miRNA targets. We did not study the lines of the remaining phenotypic classes, most of which were poorly viable and semi-fertile or sterile. We also did not study lines with phenotypes that seemed merely additive to that of *ago1-52*, since the corresponding double mutants were considered likely carriers of novel alleles of genes involved in processes unrelated to *AGO1*[31].

We also screened an additional set of about 20,000 M_2 seeds later, belonging to the P9–P15 parental groups. In this case we sowed the seeds at high density (500 seeds for plate) in top agar and directly looked for plants with a weak Ago1-52 phenotype. We found six additional suppressor lines in this way (Figure 3t–y), which were studied together with the 17 lines already chosen in our first screen.

To exclude the possibility of contamination with wild-type seeds, we sequenced the *AGO1* gene in all the suppressor lines, confirming the presence of the original, homozygous *ago1-52* mutation in all of the lines when genomic DNA was used as template. We also confirmed the effect of *ago1-52* on splicing when cDNA was used as template. The genomic and cDNA sequences revealed that one of the lines, P9 3.3, carried an intragenic suppressor mutation (which we termed *ago1-52S*), since it carries a G to A transition adjacent to the *ago1-52* mutation (Figure 5a). Sequencing of *AGO1* cDNA from P9 3.3 showed that the splicing acceptor (AG) site of the 21st intron had been shifted 1 nt downstream, causing the inclusion in the mutated mRNA of 9 nt that are intronic in the wild type, instead of 10 nt as occurs in *ago1-52* mRNA; this restored the wild-type reading frame, although inserting three additional codons that were not present in the wild-type mRNA (Figure 5b, c).

www.nature.com/scientificreports

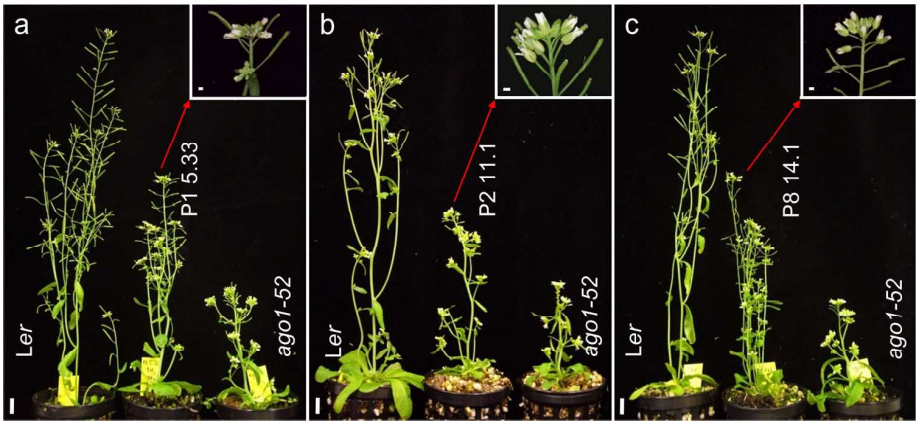

Figure 4 | Examples of other phenotypes of the suppressor lines identified in this work. Plant height of the (a) *ago1-52 mas1-1* (P1 5.33), (b) *ago1-52 mas2-1* (P2 11.1) and (c) *ago1-52 mas3-1* (P8 14.1) double mutants was intermediate between those of the wild type L*er* and the *ago1-52* single mutant. As shown in the insets, the structure of the terminal region of the inflorescence in the double mutants was also intermediate between those of L*er* (Figure 1e) and *ago1-52* (Figure 1f). Pictures were taken (a) 54 das, (b) 43 das and (c) 48 das. Scale bars: (a–c) 1 cm and (insets) 1 mm.

We named the genes whose mutations suppressed the morphological phenotype of *ago1-52* as *MORPHOLOGY OF argonaute1-52 SUPPRESSED* (*MAS*). We backcrossed the *ago1-52 mas* suppressor lines to L*er* twice. We transferred 1–5 F_1 plants derived from each backcross into pots to complete their life cycle and collected the F_2 seeds resulting from self-pollination. Between 150 and 450 seeds of several F_2 families from each line were sown and the morphological phenotypes of the corresponding plants were examined to identify *ago1-52/ago1-52;mas/mas* and *AGO1/AGO1;mas/mas* plants.

We assumed that, as is usual for EMS-induced mutations, the suppressor mutations would be recessive, in most if not all cases. Hence, we expected to find four phenotypic classes in the F_2 progeny: (1) the wild type (*AGO1/-;MAS/-*) class, (2) that of the mutation to be identified (*AGO1/-;mas/mas*), (3) Ago1-52 (*ago1-52/ago1-52;MAS/-*) and (4) the double mutant (*ago1-52/ago1-52;mas/mas*) class. As seen in Table S2, some of the *mas* mutations did not show any visible morphological phenotype in the *AGO1/-;mas/mas* genotype (P1 5.33, P2 11.1, P4 22.2, P5 11.1 and P8 14.1) whereas others do (P7 13.1, P7 23.1, P7 26.1 and P8 25.1).

We also note that in 6 of the 9 F_2 derived from the first backcrosses to L*er* we found mutant phenotypes additional to those initially seen in the M_2 (Table S2). This suggests the presence of mutations in different genes in the M_2 individual initially selected as a double mutant, and reinforces the importance of backcrossing to L*er* several times to reduce the number of mutations not relevant to the phenotype. In addition, the proportions of the phenotypes that we observed in the F_2 did not fit any known Mendelian segregation. No or abortive seed germination contributed to this, as well as lethality and plants showing phenotypes that had not been seen in the M_2 or M_3.

In all the lines studied except two (P5 11.1 and P7 26.1), the double mutant class is more numerous than that of the single mutants. Given that the mutations under study normalise the body architecture of the *ago1-52* mutant, it is reasonable to suppose that they also increase its fertility. As previously shown, the number of seeds per silique of the *ago1-52* mutant is 25% that of the wild type, which explains why the *ago1-52/ago1-52;mas/mas* plants are more numerous than *ago1-52/ago1-52;MAS/-* plants. The absence of the *AGO1/-;mas/mas* class in some of the lines suggests that plants of this genotype are included in the phenotypically wild-type class. As a consequence, the populations of the first three lines in Table S2 should fit a 12 : 3 : 1 segregation (*AGO1/-;-/-* : *ago1-52/ago1-52;MAS/-* : *ago1-52/ago1-52;mas/mas*), but they do not because of the much better viability of the suppressed plants compared with the plants showing the full *ago1-52* mutant phenotype.

We chose for subsequent study the P1 5.33, P2 11.1 and P8 14.1 lines for several reasons. Lines P1 5.33 and P2 11.1 were the first to be isolated in our screen and, therefore, the first ones to be studied. Line P8 14.1 was chosen because it showed a more pronounced suppression of the phenotype of *ago1-52* during the reproductive phase. In the F_2 of the backcrosses involving P1 5.33, P2 11.1 and P8 14.1 we only found three phenotypic classes: entirely wild type phenotype, *Ago1-52* and double mutants, which indicates that the suppressor mutations did not cause a mutant phenotype on their own, either as homozygotes or heterozygotes in the presence of the wild type allele of *AGO1*. We did not perform complementation analyses by intercrossing the suppressor lines. Rather, we first used linkage analysis to determine their genetic map positions (see examples in Table S3), and then crossed for allelism tests only the lines carrying mutations with neighbouring map positions. Linkage analyses demonstrated in all cases that the suppressor mutations are extragenic suppressors that map to chromosomes 2, 3, 4 or 5, or on chromosomes 1 but far from *AGO1*; the only exception was the above-mentioned *ago1-52S* intragenic suppressor mutation. The genetic and molecular characterization of each of these suppressors will be described elsewhere.

Concluding remarks. EMS has been widely used to induce mutations in forward and second-site genetic screens with many experimental organisms, but also to increase crop diversity. Further, EMS has been used in saturation mutagenesis in several TILLING (Targeting Induced Local Lesions in Genomes)[32,33] projects with different animal and plant species, including Arabidopsis, because it causes randomly distributed point mutations and only rarely produces DNA rearrangements that could result in lethality[26]. Mutagenesis in Arabidopsis predominantly relies on EMS and its non-lethal dose treatment has been well established. Therefore, it was striking that our *ago1-52* mutagenesis led to a very high percentage of lethality. EMS mainly induces alkylation of G residues, which then pair with T instead of with C; if these G:T mismatches are not repaired, they produce G/C to A/T transitions.

Universal repair mechanisms, such as the mismatch repair pathway that recognizes G:T mismatches, as well as repair of alkylated nucleotides by DNA glycosylases, act in Arabidopsis[34–36]. The apparently high sensitivity to EMS that we observed in the *ago1-52* background could be the result of defects in these DNA repair mechanisms. If this were true, *ago1-52* plants should accumulate mutations at a higher density than wild-type plants or other non-sensitive backgrounds under similar non-lethal EMS doses. Another interpretation of our results could be that since *AGO1* affects many pivotal processes, these processes are all de-regulated in the *ago1-52* mutant and second-site mutations in genes involved in other pivotal processes could result in lethality. Comparative analysis of whole-genome sequences of M_2 plants obtained from either *ago1-*

www.nature.com/scientificreports

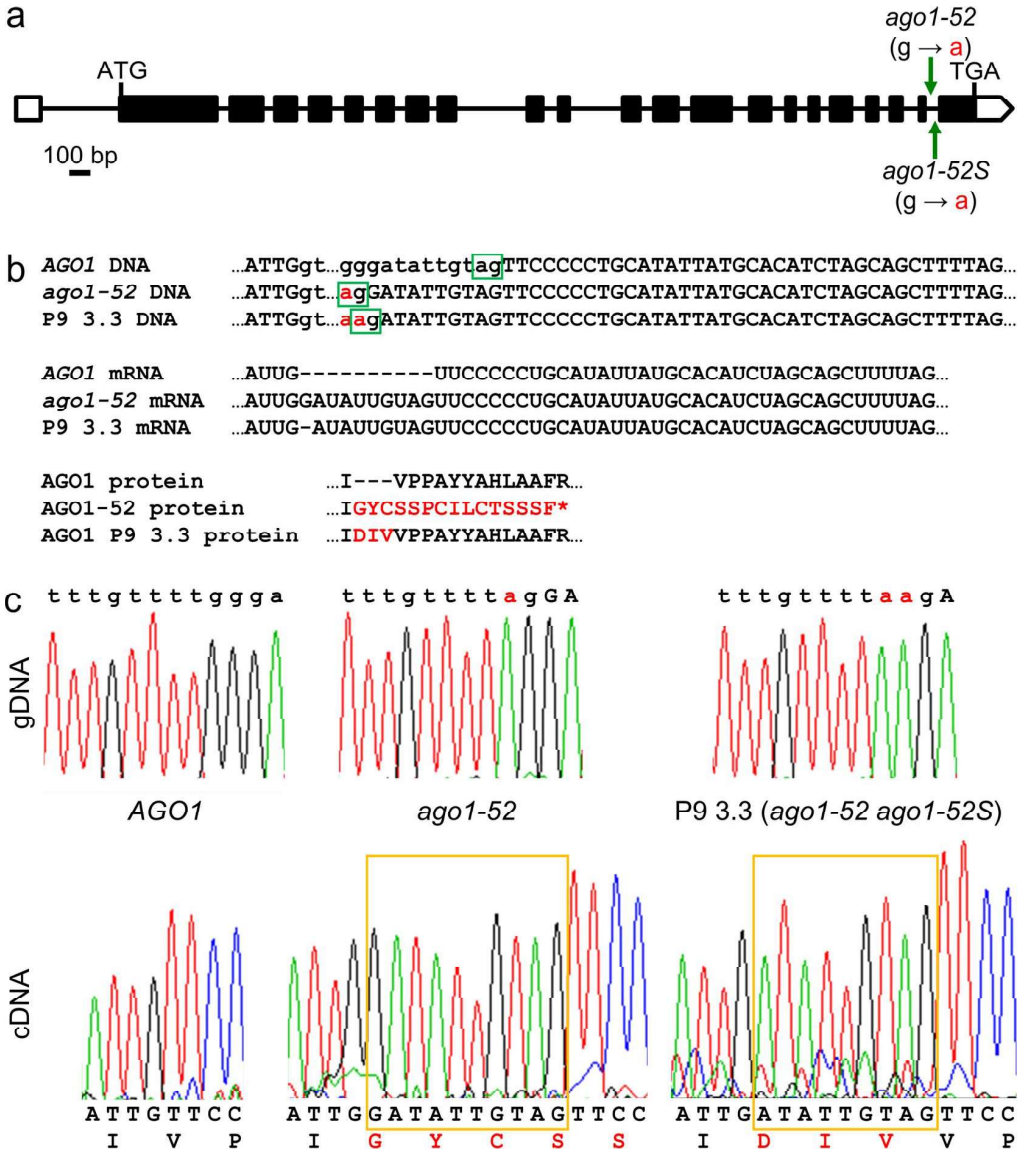

Figure 5 | The P9 3.3 line carries an intragenic suppressor mutation of *ago1-52*. (a) Structure of the *AGO1* gene with indication of the nature of the *ago1-52* and *ago1-52S* mutations (green arrows and red letters). Positions of the start (ATG) and stop (TGA) codons are also indicated. Exons are shown as boxes, and introns as lines between boxes. Open boxes represent untranslated exon sequences. (b) Effects of the *ago1-52* and *ago1-52S* mutations on splicing and mRNA translation. Intron sequences are shown in small case, and exon sequences in capital letters. The preferred splicing acceptor sites are boxed in green. Amino acids different from those of the wild type are shown in red. The asterisk indicates a premature stop codon. (c) Sequencing electropherograms obtained from L*er* (*AGO1*), *ago1-52* and P9 3.3 genomic DNA (gDNA; top) and cDNA (bottom). Nucleotide sequences that are intronic in the *AGO1* wild type allele but exonic in the *ago1-52* mutant and the *ago1-52 ago1-52S* double mutant are boxed in orange.

52 or wild-type plants both treated with EMS could settle this question.

Second-site mutagenesis screens are common strategies for finding functionally related genes. The pleiotropic phenotype of the *ago1* mutants results from the alteration of many biological processes, which involve many genes that are directly or indirectly regulated by the miRNA pathway. It may, therefore, seem surprising that we obtained *ago1-52 mas* double mutants with morphological phenotypes very close to that of the wild type. Suppressor mutations usually fall into two classes: informational suppressors and functional suppressors. Informational suppressors act through a generic mechanism, such as the transcription machinery, RNA processing and translation, and they can also suppress a premature stop codon, modify aberrant splicing of mRNA or control mRNA translation or protein degradation. For example, in *Caenorhabditis elegans*, three kinds of informational suppression have been described so far: nonsense suppression, suppression by modified splicing and suppression by loss of nonsense-mediated decay. By contrast, functional suppressors act through mechanisms directly related to the process of interest[37,38]. Since informational suppressors generally are allele-specific but not gene-specific, we will test allele- and gene-specificity in all our *mas* mutations.

Methods

Plant material and growth conditions. *Arabidopsis thaliana* (L) Heynh. Landsberg *erecta* (L*er*) and Columbia-0 (Col-0) wild-type accessions were obtained from the Nottingham Arabidopsis Stock Center (NASC; Nottingham, UK) and then propagated at our laboratory for further analysis. Seed sterilization and sowing, plant culture and crosses were performed as previously described[9,39]. In brief, seeds were sown on plates containing MS agar medium (half-strength Murashige and Skoog salts, 0.7% plant agar [Duchefa], pH 5.7, and 1% sucrose) and stratified (4°C in the

dark) for 48 h and then transferred to either Conviron TC16 or TC30 growth chambers set to our standard conditions (continuous light at approximately 75 μmol·m^{-2}·s^{-1}, 20 ± 1°C, 60–70% relative humidity). When required, plants were transferred into pots containing a 2 : 2 : 1 mixture of perlite : vermiculite : sphagnum moss and grown in walk-in growth chambers set to our standard conditions.

Mutagenesis and mutant isolation. ≈67,500 *ago1-52* seeds (1 g) were sent to a commercial supplier, Lehle Seeds (http://www.arabidopsis.com), where they were mutagenised by immersion in a solution of 0.23% (v/v) EMS for 12 hours at 25°C, stratified for 7 days, and then sown in pots. The M_2 progeny obtained from selfed M_1 plants was sent to us as 15 envelopes, each of which contained the pooled M_2 seed progeny of a parental group: 1,283 M_1 plants developed from seeds exposed to EMS.

Seeds were sown in 15 cm-diameter Petri dishes containing solid MS medium. Each dish was sown with 94 M_2 seeds, together with 8 L*er* and 8 *ago1-52* seeds, which served as controls. Selection of putative double mutants was carried out 21 days after stratification (das) by eliminating all the M_2 plants not showing clear morphological differences from *ago1-52*. All plants distinguishable from *ago1-52* were presumed to be double mutants, and they were transplanted into pots and allowed to complete their life cycles. Putative double mutants were given protocol numbers, as PN X.Y: PN indicates the corresponding parental group, X refers to the number of the plate where the mutant was isolated and Y is an ordinal assigned to each of the mutants found in a given plate.

Linkage analysis, RNA isolation, and genomic DNA and cDNA sequencing. Low-resolution mapping of the suppressor mutations was performed by linkage analysis as described in Ponce *et al.*[40,41]. Genomic DNA was isolated as previously described[42]. Total RNA from 20–30 mg of rosette leaves, collected 21 das, was isolated using TRI Reagent (Sigma), and first-strand cDNA synthesis was performed as described in Jover-Gil *et al.*[17]. Genomic DNA and cDNA PCR amplification and sequencing were performed as previously described[14,42]. Primers for PCR amplifications and sequencing were ago1-52-27-F (5′-TTACCACGTTCTTTGGGATGAG-3′) and ago1-52-27-R (5′-GCAGTAGAACATGACACGCTTC-3′). The chromatograms shown in Figure 5 were obtained with Chromas Lite 2.1.1. (http://technelysium.com.au/).

1. Jacob, F. & Monod, J. Genetic regulatory mechanisms in the synthesis of proteins. *J. Mol. Biol.* **3**, 318–356 (1961).
2. Britten, R. J. & Davidson, E. H. Gene regulation for higher cells: a theory. *Science* **165**, 349–357 (1969).
3. Esterling, L. & Delihas, N. The regulatory RNA gene *micF* is present in several species of gram-negative bacteria and is phylogenetically conserved. *Mol. Microbiol.* **12**, 639–646 (1994).
4. Lee, R. C., Feinbaum, R. L. & Ambros, V. The *C. elegans* heterochronic gene *lin-4* encodes small RNAs with antisense complementarity to *lin-14*. *Cell* **75**, 843–854 (1993).
5. Wightman, B., Ha, I. & Ruvkun, G. Posttranscriptional regulation of the heterochronic gene *lin-14* by *lin-4* mediates temporal pattern formation in *C. elegans*. *Cell* **75**, 855–862 (1993).
6. Höck, J. & Meister, G. The Argonaute protein family. *Genome Biol.* **9**, 210 (2008).
7. Meister, G. Argonaute proteins: functional insights and emerging roles. *Nat. Rev. Genet.* **14**, 447–459 (2013).
8. Peters, L. & Meister, G. Argonaute proteins: mediators of RNA silencing. *Mol. Cell* **26**, 611–623 (2007).
9. Berná, G., Robles, P. & Micol, J. L. A mutational analysis of leaf morphogenesis in *Arabidopsis thaliana*. *Genetics* **152**, 729–742 (1999).
10. Serrano-Cartagena, J., Robles, P., Ponce, M. R. & Micol, J. L. Genetic analysis of leaf form mutants from the *Arabidopsis* Information Service collection. *Mol. Gen. Genet.* **261**, 725–739 (1999).
11. Serrano-Cartagena, J. *et al.* Genetic analysis of *incurvata* mutants reveals three independent genetic operations at work in *Arabidopsis* leaf morphogenesis. *Genetics* **156**, 1363–1377 (2000).
12. Ochando, I. *et al.* Mutations in the microRNA complementarity site of the *INCURVATA4* gene perturb meristem function and adaxialize lateral organs in Arabidopsis. *Plant Physiol.* **141**, 607–619 (2006).
13. Pérez-Pérez, J. M. *et al.* A role for *AUXIN RESISTANT3* in the coordination of leaf growth. *Plant Cell Physiol.* **51**, 1661–1673 (2010).
14. Barrero, J. M., González-Bayón, R., del Pozo, J. C., Ponce, M. R. & Micol, J. L. *INCURVATA2* encodes the catalytic subunit of DNA polymerase alpha and interacts with genes involved in chromatin-mediated cellular memory in *Arabidopsis thaliana*. *Plant Cell* **19**, 2822–2838 (2007).
15. Esteve-Bruna, D., Pérez-Pérez, J. M., Ponce, M. R. & Micol, J. L. *incurvata13*, a novel allele of *AUXIN RESISTANT6*, reveals a specific role for auxin and the SCF complex in Arabidopsis embryogenesis, vascular specification, and leaf flatness. *Plant Physiol.* **161**, 1303–1320 (2013).
16. Jover-Gil, S., Candela, H. & Ponce, M. R. Plant microRNAs and development. *Int. J. Dev. Biol.* **49**, 733–744 (2005).
17. Jover-Gil, S. *et al.* The microRNA pathway genes *AGO1*, *HEN1* and *HYL1* participate in leaf proximal-distal, venation and stomatal patterning in Arabidopsis. *Plant Cell Physiol.* **53**, 1322–1333 (2012).
18. Telfer, A. & Poethig, R. S. *HASTY*: a gene that regulates the timing of shoot maturation in *Arabidopsis thaliana*. *Development* **125**, 1889–1898 (1998).
19. Lu, C. & Fedoroff, N. A mutation in the *Arabidopsis HYL1* gene encoding a dsRNA binding protein affects responses to abscisic acid, auxin, and cytokinin. *Plant Cell* **12**, 2351–2366 (2000).
20. Bohmert, K. *et al. AGO1* defines a novel locus of *Arabidopsis* controlling leaf development. *EMBO J.* **17**, 170–180 (1998).
21. Chen, X., Liu, J., Cheng, Y. & Jia, D. *HEN1* functions pleiotropically in *Arabidopsis* development and acts in C function in the flower. *Development* **129**, 1085–1094 (2002).
22. Park, W., Li, J., Song, R., Messing, J. & Chen, X. CARPEL FACTORY, a Dicer homolog, and HEN1, a novel protein, act in microRNA metabolism in *Arabidopsis thaliana*. *Current Biol.* **12**, 1484–1495 (2002).
23. Han, M. H., Goud, S., Song, L. & Fedoroff, N. The Arabidopsis double-stranded RNA-binding protein HYL1 plays a role in microRNA-mediated gene regulation. *Proc. Natl. Acad. Sci. USA* **101**, 1093–1098 (2004).
24. Jacobsen, S. E., Running, M. P. & Meyerowitz, E. M. Disruption of an RNA helicase/RNAse III gene in Arabidopsis causes unregulated cell division in floral meristems. *Development* **126**, 5231–5243 (1999).
25. Weigel, D. & Glazebrook, J. EMS mutagenesis of Arabidopsis seed. *Cold Spring Harb. Protoc.* **2006** (2006).
26. Kim, Y., Schumaker, K. S. & Zhu, J. K. EMS mutagenesis of Arabidopsis. *Methods Mol. Biol.* **323**, 101–103 (2006).
27. Qu, L. J. & Qin, G. Generation and identification of Arabidopsis EMS mutants. *Methods Mol. Biol.* **1062**, 225–239 (2014).
28. Mednik, I. G. On methods evaluating the frequencies of induced mutations in Arabidopsis based on embryo-test data. *Arabidopsis Inf. Serv.* **26**, 67–72 (1988).
29. Ivanov, V. I. Estimation of induced mutation rate in Arabidopsis. *Arabidopsis Inf. Serv.* **9**, 31–32 (1973).
30. Quesada, V., Ponce, M. R. & Micol, J. L. Genetic analysis of salt-tolerant mutants in *Arabidopsis thaliana*. *Genetics* **154**, 421–436 (2000).
31. Pérez-Pérez, J. M., Candela, H. & Micol, J. L. Understanding synergy in genetic interactions. *Trends Genet.* **25**, 368–376 (2009).
32. McCallum, C. M., Comai, L., Greene, E. A. & Henikoff, S. Targeted screening for induced mutations. *Nat. Biotechnol.* **18**, 455–457 (2000).
33. McCallum, C. M., Comai, L., Greene, E. A. & Henikoff, S. Targeting induced local lesions IN genomes (TILLING) for plant functional genomics. *Plant Physiol.* **123**, 439–442 (2000).
34. Culligan, K. M. & Hays, J. B. Arabidopsis MutS homologs-AtMSH2, AtMSH3, AtMSH6, and a novel AtMSH7-form three distinct protein heterodimers with different specificities for mismatched DNA. *Plant Cell* **12**, 991–1002 (2000).
35. Dany, A. L. & Tissier, A. A functional *OGG1* homologue from *Arabidopsis thaliana*. *Mol. Genet. Genom.* **265**, 293–301 (2001).
36. Garcia-Ortiz, M. V., Ariza, R. R. & Roldan-Arjona, T. An *OGG1* orthologue encoding a functional 8-oxoguanine DNA glycosylase/lyase in *Arabidopsis thaliana*. *Plant Mol. Biol.* **47**, 795–804 (2001).
37. Hodgkin, J. in *WormBook* (2005), pp. 1–13.
38. Fay, D. & Johnson, W. in *WormBook* (2006), pp. 1–4.
39. Ponce, M. R., Quesada, V. & Micol, J. L. Rapid discrimination of sequences flanking and within T-DNA insertions in the *Arabidopsis* genome. *Plant J.* **14**, 497–501 (1998).
40. Ponce, M. R., Robles, P. & Micol, J. L. High-throughput genetic mapping in *Arabidopsis thaliana*. *Mol. Gen. Genet.* **261**, 408–415 (1999).
41. Ponce, M. R., Robles, P., Lozano, F. M., Brotons, M. A. & Micol, J. L. Low-resolution mapping of untagged mutations. *Methods Mol. Biol.* **323**, 105–113 (2006).
42. Pérez-Pérez, J. M., Ponce, M. R. & Micol, J. L. The *ULTRACURVATA2* gene of Arabidopsis encodes an FK506-binding protein involved in auxin and brassinosteroid signaling. *Plant Physiol.* **134**, 101–117 (2004).

Acknowledgments

The authors wish to thank J.L. Micol for helpful discussions and comments on this manuscript, and for the use of his facilities. We wish also thank J.M. Serrano, F.M. Lozano, T. Trujillo and L. Serna for technical assistance. This work was supported by research grants from the Ministerio de Economía y Competitividad of Spain (BIO2008-01900) and the Generalitat Valenciana (Prometeo/2009/112) to M.R.P.

Author contributions

M.R.P. conceived and designed the research. R.M.-P. and V.A. performed the research. M.R.P. and R.M.-P. wrote the article.

Additional information

Supplementary information accompanies this paper at http://www.nature.com/scientificreports

Competing financial interests: The authors declare no competing financial interests.

How to cite this article: Micol-Ponce, R., Aguilera, V. & Ponce, M.R. A genetic screen for suppressors of a hypomorphic allele of Arabidopsis *ARGONAUTE1*. *Sci. Rep.* **4**, 5533; DOI:10.1038/srep05533 (2014).

A genetic screen for suppressors of a hypomorphic allele of Arabidopsis *ARGONAUTE1*

Rosa Micol-Ponce, Verónica Aguilera and María Rosa Ponce

Supplementary Information

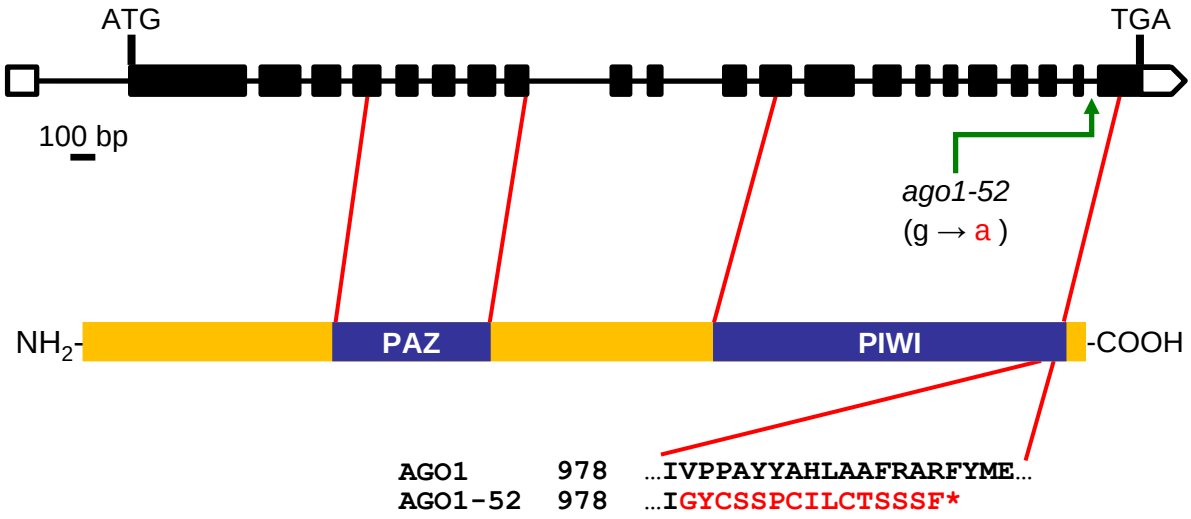

Figure S1 Schematic representation of the structure of the *AGO1* gene and the AGO1 protein, with indication of the nature of the *ago1-52* mutation and its impact on the mRNA and protein products of the mutated gene. Boxes and lines between boxes represent exons and introns, respectively. White boxes represent untranslated 5' and 3' regions. The PAZ and PIWI domains of the AGO1 protein are shown in blue. Lower case letters are used for intron sequences. Red letters indicate mutated nucleotides or amino acids. The asterisk indicates a stop codon.

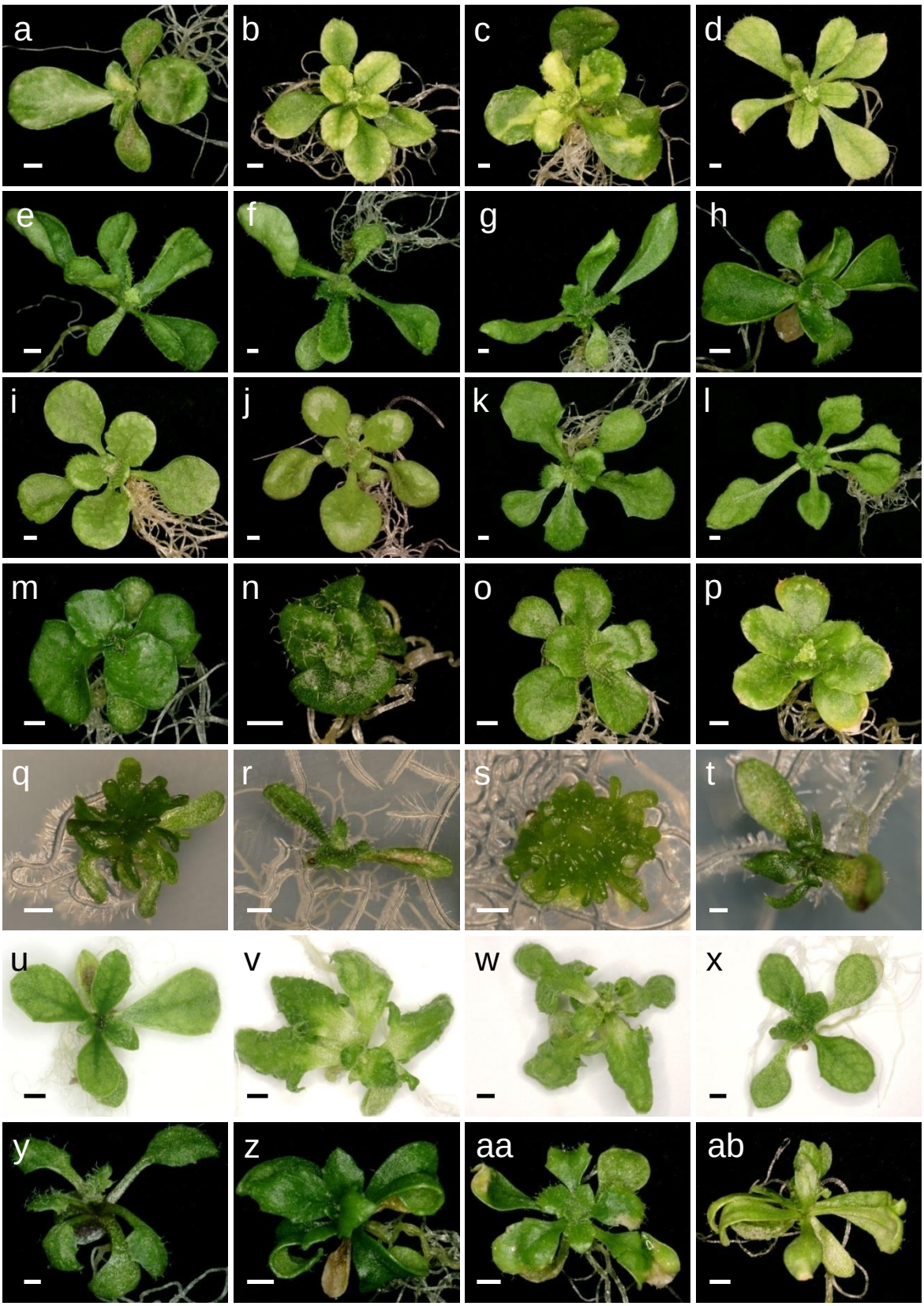

Figure S2 Double mutants representative of the phenotypic classes defined in this work. (a-d) Depigmented plants: (a) P5 25.1, (b) P6 9.2, (c) P6 9.3 and (d) P6 23.3. (e-h) Severe Ago1-52 mutant phenotype: (e) P2 3.4, (f) P3 39.1, (g) P3 40.3 and (h) P5 26.1. (i-l) Weak Ago1-52 mutant phenotype: (i) P6 3.2, (j) P6 29.1, (k) P8 6.2 and (l) P8 35.3. (m-p) Compact rosette: (m) P4 48.1, (n) P6 3.6, (o) P6 5.1 and (p) P6 8.1. (q-t) Synergistic phenotypes: (q) P1 6.3, (r) P1 10.13, (s) P1 15.11 and (t) P1 23.4. (u-x) Reticulate leaves: (u) P6 65.1, (v) P8 7.1, (w) P8 16.1 and (x) P8 21.1. (y-ab) Other phenotypes: (y) P3 3.5, (z) P3 28.1, (aa) P3 36.4 and (ab) P6 2.4. Pictures were taken at 21 das. Scale bars: 1 mm.

Table S1 Expressivity of the mutant phenotypes in M_3 families, classified by phenotypic class

Phenotypic class	M_2 double mutants	Expressivity in the M_3 generation			
		constant	reduced	variable	null
Severe Ago1-52 phenotype	42	11	4	18	9
Weak Ago1-52 phenotype	93	21	6	39	27
Compact rosette	25	3	2	7	13
Depigmented plants	34	8	4	14	8
Reticulate leaves	48	45	0	2	1
Other phenotypes	60	4	5	24	27
Total	302	92	21	104	85

Values indicate the number of individuals of each type.

Table S2 Phenotypic segregation in the F_2 progeny of several *mas ago1-52* × L*er* backcrosses

	Phenotypic classes in the F_2						
mas ago1-52 line backcrossed	WT[a]	Putative *mas* single mutant[b]	Ago1-52	Putative double mutant[c]	Lethal seeds[d]	Lethal seedlings[e]	Other phenotypes
P1 5.33 (*mas1*)[h]	122	0	16	27			
P2 11.1 (*mas2*)[i]	121	0	8	14			
P4 22.2[j]	107	0	3	12	15		11[f]
P5 11.1[k]	113	0	28	3	3		17[f]
P7 13.1 (*mas7*)[l]	160	26	13	27	62	22	
P7 23.1[m]	284	14	13	77			18[g]
P7 26.1 (*mas4*)[n]	125	20	31	22	20	18	9[g]
P8 14.1 (*mas3*)[o]	308	0	49	101			
P8 25.1 (*mas5*)[p]	136	13	14	24		54	

Values indicate the number of plants from each phenotypic class. [a]Phenotypically wild type class, including *MAS/MAS;AGO1/-* plants. If the *mas* mutation was recessive or dominant but had no morphological phenotype on its own, the *MAS/mas;AGO1/-* plants would also be included in this class. The *mas/mas;AGO1/-* plants would also be included in this class if the *mas* mutation is recessive but has no phenotype on its own. [b]Plants that share some phenotypes with the putative double mutants but not with *ago1-52*. [c]Plants that show a partially suppressed Ago1-52 phenotype. [d]Seeds exhibiting no or abortive germination. [e]Seedlings in which only the cotyledons and the first pair of leaves expand. [f]Plants with mutant phenotypes different among themselves and from that of *ago1-52*. [g]Plants with a phenotype other than that observed in M_2 and M_3. [h-p]See Figure [h]3d, [i]3e, [j]3f, [k]3g, [l]3j, [m]3l, [n]3n, [o]3q and [p]3r.

Table S3 Low-resolution mapping of *MAS1*, *MAS2* and *MAS3*

Marker	Chromosome - Physical map position (bp)	Chromosomes studied			Recombination frequency ($r \pm S_r$)[a]		
		MAS1	*MAS2*	*MAS3*	*MAS1*	*MAS2*	*MAS3*
nga59	1 - 2,768,000	116	84	76	35.34±4.44	50.00±5.46	32.89±5.39
JV18/19	1 - 5,160,595	116	84	54	**24.14±3.97**	31.71±5.14	38.89±6.63
AthZFPG	1 - 8,727,056	104	84	50	**16.35±3.63**	**21.43±4.48**	38.00±6.86
SNP10026	1 - 11,562,061	100	74	74	**11.00±3.13**	**20.27±4.67**	36.49±5.60
F1L21	1 - 15,993,202	116	84	74	**6.03±2.21**	**8.33±3.02**	**27.03±5.16**
nga128	1 - 20,695,113	116	84	76	**15.52±3.36**	**8.33±3.02**	31.58±5.33
SNP10490	1 - 24,344,448	116	84	76	23.28±3.92	20.24±4.38	30.26±5.27
nga111	1 - 27,418,736	116	84	76	34.48±4.41	42.86±5.40	25.00±4.97
nga1145	2 - 682,624	116	84	74	30.17±4.26	47.62±5.45	48.65±5.81
SNP8895	2 - 7,860,251	116	84	74	**12.93±3.12**	46.43±5.44	51.35±5.81
nga1126	2 - 11,670,000	110			**3.64±1.78**		
nga168	2 - 16,240,385	116	84	74	**18.10±3.58**	44.05±5.42	64.86±5.55
nga126	3 - 3,713,432	112	76	74	48.21±4.72	55.26±5.70	47.30±5.80
MYF24	3 - 6,466,772	98	50	74	43.88±5.00	56.00±7.02	43.24±5.76
AthGAPab	3 - 9,796,450	116	84	76	46.55±4.63	58.33±5.38	46.05±5.72
T32N15	3 - 16,986,906	108	84	74	41.67±4.74	47.62±5.45	50.00±5.81
F28P10	3 - 21,398,175	96	82	62	51.04±5.10	47.56±5.52	50.00±6.35
nga6	3 - 23,040,009	114	84	74	42.11±4.62	44.05±5.42	48.65±5.81
nga1111	4 - 5,074,681	116	84	76	40.52±4.56	**14.29±3.82**	**11.84±3.71**
AthF28J12.3	4 - 9,166,451	112	84	76	40.18±4.63	30.95±5.04	**6.58±2.84**
nga1139	4 - 15,408,641	116	84	76	43.10±4.60	42.86±5.40	**18.42±4.45**
AthCTR1	5 - 979,763	104			49.04±4.90		
nga151	5 - 4,669,932	106	76	76	48.11±4.85	46.05±5.72	43.42±5.69
nga76	5 - 10,375,531	104		74	50.96±4.90		39.19±5.67
AthPHYC	5 - 13,721,807	104	84	56	46.15±4.89	50.00±5.46	46.43±6.66
MNF13	5 - 17,908,612	116	84	52	49.14±4.64	50.00±5.46	40.38±6.80
MNB8	5 - 23,120,770	114	84	76	51.75±4.68	52.38±5.45	42.11±5.66
MUA2	5 - 23,956,127	106	84	74	53.77±4.84	50.00±5.46	54.05±5.79
K8K14	5 - 28,518,213	114	84	74	53.51±4.67	48.81±5.45	56.76±5.76

Genotyping results obtained for mapping populations of F_2 plants derived from crosses involving the wild type Col-0 and a *mas ago1-52* double mutant with a L*er* genetic background. *r*: recombination frequency. S_r: Standard error of recombination frequency. Physical map positions of the markers were obtained from the Munich Information Center for Protein Sequences (MIPS) Arabidopsis database. Data corresponding to $r < 30\%$ are highlighted in bold and were considered unequivocal evidence of linkage. The linkage found for chromosome 1 corresponds to the *ago1-52* mutation, whose physical map position is 17,885,633 bp.

The Plant Cell, Vol. 27: 1999–2015, July 2015, www.plantcell.org

Arabidopsis *MAS2*, an Essential Gene That Encodes a Homolog of Animal NF-κ B Activating Protein, Is Involved in 45S Ribosomal DNA Silencing

Ana Belén Sánchez-García,[1] Verónica Aguilera,[1,2] Rosa Micol-Ponce, Sara Jover-Gil, and María Rosa Ponce[3]

Instituto de Bioingeniería, Universidad Miguel Hernández, 03202 Elche, Alicante, Spain

ORCID IDs: 0000-0002-1315-8400 (A.B.S.-G.); 0000-0003-3885-6624 (V.A.); 0000-0001-9389-2906 (R.M.-P.); 0000-0003-0770-4230 (M.R.P.)

Ribosome biogenesis requires stoichiometric amounts of ribosomal proteins and rRNAs. Synthesis of rRNAs consumes most of the transcriptional activity of eukaryotic cells, but its regulation remains largely unclear in plants. We conducted a screen for ethyl methanesulfonate-induced suppressors of *Arabidopsis thaliana ago1-52*, a hypomorphic allele of *AGO1* (*ARGONAUTE1*), a key gene in microRNA pathways. We identified nine extragenic suppressors as alleles of *MAS2* (*MORPHOLOGY OF AGO1-52 SUPPRESSED2*). Positional cloning showed that *MAS2* encodes the putative ortholog of NKAP (NF-κ B activating protein), a conserved eukaryotic protein involved in transcriptional repression and splicing in animals. The *mas2* point mutations behave as informational suppressors of *ago1* alleles that cause missplicing. *MAS2* is a single-copy gene whose insertional alleles are embryonic lethal. In yeast two-hybrid assays, MAS2 interacted with splicing and ribosome biogenesis proteins, and fluorescence in situ hybridization showed that MAS2 colocalizes with the 45S rDNA at the nucleolar organizer regions (NORs). The artificial microRNA *amiR-MAS2* partially repressed *MAS2* and caused hypomethylation of 45S rDNA promoters as well as partial NOR decondensation, indicating that MAS2 negatively regulates 45S rDNA expression. Our results thus reveal a key player in the regulation of rRNA synthesis in plants.

INTRODUCTION

The regulation of eukaryotic gene expression involves multiple precisely controlled and coordinated transcriptional and post-transcriptional processes. For example, nuclear rRNA genes are tightly regulated, as transcription of rRNAs involves a vast amount of cell resources, representing ~50% of transcription in many eukaryotic cells (reviewed in Grummt, 2003). Assembly of the ribosome requires stoichiometric amounts of rRNAs and ribosomal proteins (Laferté et al., 2006). *Arabidopsis thaliana* contains ~1000 tandemly arrayed copies of the 5S rRNA gene and 570 to 750 copies of the 45S rRNA gene per haploid genome (Layat et al., 2012). Not all rRNA genes are transcribed at a given cell; active genes are enriched in euchromatin and silenced genes in heterochromatin (Lawrence et al., 2004). Transcription of the genes in rDNA depends on the action of enzymes that regulate histone methylation and acetylation, DNA methylation, and nucleosome positioning (Layat et al., 2012).

In humans, the NF-κ B activating protein (NKAP) activates nuclear factor-κ B (Chen et al., 2003) and is a component of the Notch corepressor complex (Pajerowski et al., 2009). NOTCH proteins are transmembrane receptors involved in several conserved pathways that regulate cellular differentiation, proliferation, and apoptosis in animals (Bray, 2006). Human NKAP has also been found bound to different spliceosomal complexes (Jurica and Moore, 2002; Bessonov et al., 2008, 2010; Ilagan et al., 2013) and to pre-mRNAs and spliced mRNAs (Burgute et al., 2014). A role has been proposed for human NKAP in regulating constitutive splicing. NKAP interacts with several RNA binding proteins, including splicing factors; it binds to exons in pre-mRNAs as well as to small nuclear RNAs, small nucleolar RNAs, rRNAs, and long intergenic noncoding RNAs. *XIST* (*X-inactive-specific transcript*) regulatory RNA, the major effector of X chromosome epigenetic inactivation, has also been found bound to NKAP (Burgute et al., 2014).

NKAP is a conserved eukaryotic protein that was first discovered in *Caenorhabditis elegans* and named E01A2.4 or LET-504 (Howell and Rose, 1990). Based on the interactions of its mutant alleles and their effects on vulvar development, *let-504* was classified as a class B Synthetic Multivulva (SynMuv) gene (Poulin et al., 2005); genes of this class encode proteins involved in epigenetic repression of gene expression (Saffer et al., 2011). The NKAP family is defined by the presence of a domain that was initially named DUF926 and later SynMuv.

One posttranscriptional regulatory mechanism is mediated by microRNAs, a class of eukaryotic endogenous small RNAs (20 to 24 nucleotides) that modulate a wide variety of processes (Jones-Rhoades et al., 2006; Bartel, 2009; Voinnet, 2009). Plant microRNAs play their regulatory role in the cytoplasm, through their selective loading into an ARGONAUTE (AGO) protein, the best known of which is AGO1 (Bartel, 2009; Mallory and Vaucheret, 2010). AGO proteins form the core component of RNA-induced silencing complexes (Voinnet, 2009; Rogers and Chen, 2013).

Here, we describe a characterization of *MORPHOLOGY OF AGO1-52 SUPPRESSED2* (*MAS2*), the Arabidopsis putative

[1] These authors contributed equally to this work.
[2] Current address: Centro Nacional de Biotecnología, Consejo Superior de Investigaciones Científicas, 28049 Madrid, Spain.
[3] Address correspondence to mrponce@umh.es.
The author responsible for distribution of materials integral to the findings presented in this article in accordance with the policy described in the Instructions for Authors (www.plantcell.org) is: María Rosa Ponce (mrponce@umh.es).
www.plantcell.org/cgi/doi/10.1105/tpc.15.00135

ortholog of human *NKAP*. We isolated 11 *mas2* alleles, nine of which behave as informational suppressors of two hypomorphic *ago1* alleles that exhibit missplicing. We found *MAS2* to be an essential gene whose protein product colocalizes with and regulates expression of the 45S rDNA.

RESULTS

The *mas2-1* Mutation Is an Extragenic Suppressor of *ago1-52*

We previously isolated and studied *ago1-52* (Berná et al., 1999; Jover-Gil et al., 2005; Jover-Gil et al., 2012), a hypomorphic, viable allele of *AGO1*. To study the regulation, action, and interactions of *AGO1*, we conducted a genetic screen to identify ethyl methanesulfonate (EMS)-induced second-site mutations suppressing the morphological phenotype of *ago1-52*; we termed these extragenic suppressors *morphology of argonaute1-52 suppressed* (*mas*) mutations (Micol-Ponce et al., 2014). One of the lines isolated was given the P2 11.1 protocol number and carried a suppressor mutation that we named *mas2-1*.

The *ago1-52* mutant exhibits a pleiotropic phenotype, consisting of leaves with no clear boundary between petiole and lamina, partial loss of adaxial-abaxial polarity in leaves and floral organs, compact inflorescences, moderately low fertility, slow growth, reduced plant size and number of vegetative leaves, and late flowering (Jover-Gil et al., 2012; Micol-Ponce et al., 2014). The *ago1-52 mas2-1* plants were closer in phenotype to the wild-type Landsberg *erecta* (L*er*) than to the *ago1-52* mutant. In these double mutant plants, we observed a clear boundary between leaf lamina and petiole (Figures 1A to 1D). Also, their growth rate, height, flowering time, and fertility were intermediate between those of *ago1-52* and L*er*, and their general body architecture, inflorescences, and fruits looked almost wild type (Figures 1E to 1I).

To reduce the number of EMS-induced mutations, we backcrossed P2 11.1 twice to L*er*. In the progeny of these backcrosses, the *mas2-1* mutation did not cause any visible phenotype on its own in an *AGO1/AGO1* background (Figure 1B), and its suppressor effect seemed to be dominant.

MAS2 Encodes the Putative Arabidopsis Ortholog of Human NKAP

To identify the *MAS2* gene, we subjected the *ago1-52 mas2-1* (P2 11.1) double mutant to iterative linkage analysis (Supplemental Table 1), as previously described (Ponce et al., 1999, 2006). The results indicated that *mas2-1* is a dominant mutation that maps to the upper telomere of chromosome 4, within a 157-kb candidate region encompassing 39 annotated genes (Supplemental Figure 1). A G→A mutation in the coding region of one of the candidate genes, At4g02720, was present in *ago1-52 mas2-1* plants but absent from L*er* and *ago1-52* plants (Supplemental Figure 2).

At4g02720 is an intronless, single-copy gene that encodes a protein of 422 amino acids, which contains the SynMuv domain characteristic of NKAP family members. The G→A mutation

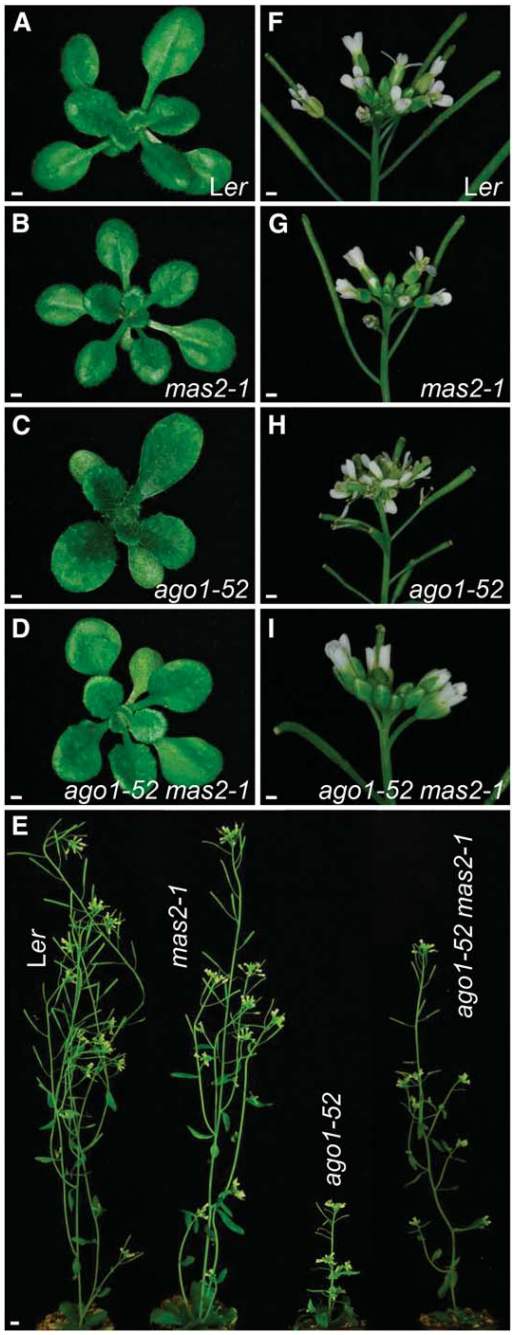

Figure 1. Suppression of the Phenotype of *ago1-52* by *mas2-1*.

(A) to **(D)** Rosettes of L*er* **(A)**, *mas2-1* **(B)**, *ago1-52* **(C)**, and *ago1-52 mas2-1* **(D)** plants.
(E) Adult plants of L*er*, *mas2-1*, *ago1-52*, and *ago1-52 mas2-1*.
(F) to **(I)** Inflorescences of L*er* **(F)**, *mas2-1* **(G)**, *ago1-52* **(H)**, and *ago1-52 mas2-1* **(I)** plants.
Pictures were taken at 21 (**[A]** to **[D]**) and 48 **(E)** DAS. Bars = 1 mm **(A)** to **(D)** and **(F)** to **(I)** and 1 cm in **(E)**.

carried by *mas2-1* is predicted to cause an Ala312→Trp substitution within the SynMuv domain (Figure 2). We also sequenced At4g02720 in the remaining 22 suppressor lines that we isolated, finding that nine of them bore additional *mas2* alleles, which we named *mas2-4* to *mas2-11*. All these alleles, except *mas2-11*, carry missense mutations mapping to a narrow (32 bp) region of At4g02720 encoding the SynMuv domain (Figure 2A; Supplemental Figure 2). Such a large allelic series found in a single genetic screen strongly supports the hypothesis that At4g02720 (hereafter, *MAS2*) is the causal gene for the suppression of the phenotype of *ago1-52* exhibited by P2 11.1.

All EMS-Induced *mas2* Alleles Carry Point Mutations Affecting Conserved Regions of MAS2

To ascertain whether the *mas2* mutations affect residues conserved among NKAP family members, we aligned MAS2 with other NKAP proteins. Full-length MAS2 has 32.4% identity to human NKAP, 30.0% to *Drosophila melanogaster* CG6066, and 33.5% to *C. elegans* LET-504. The SynMuv domain, which is 109 amino acids in the human NKAP, showed sequence similarities of 81 to 82%. By selecting putative NKAPs from a single representative of each of the supergroups identified in recent phylogenies based on massive sequencing (He et al., 2014), we only found conservation in the SynMuv domain: Its identity was 43.2% between Arabidopsis and the fungus *Mucor circinelloides* and 57.8% between *Homo sapiens* and the protozoan *Eimeria mitis*. All *mas2* mutations, except *mas2-11*, affected SynMuv domain residues that were highly conserved among all eukaryotes (Figures 2B and 2C; Supplemental Figure 3).

We also found very high conservation in a multiple alignment of several angiosperm NKAPs, to which we added that of the moss *Physcomitrella patens*: Only four of the 106 amino acids of the SynMuv domain differed between Arabidopsis and *P. patens* or rice (*Oryza sativa*). We detected a short conserved region, at the N terminus of MAS2 (residues 42 to 68), to which the *mas2-11* mutation maps (Pro64→Leu; Figure 2B; Supplemental Figure 4). The latter domain seems to be unique to moss and chlorophyta, as animals, red algae, and protists lack this domain. The conservation of this region suggests its relevance for NKAP function in plants.

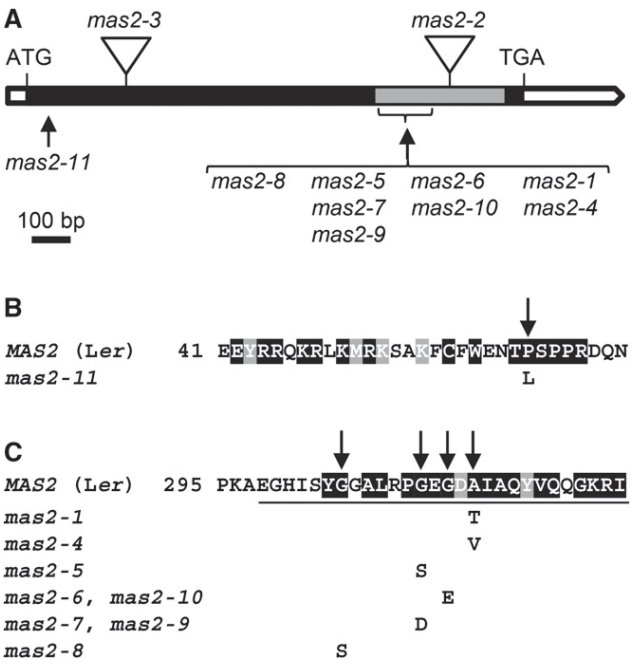

Figure 2. *MAS2* Gene Structure and Alleles.

(A) Schematic representation of the *MAS2* (At4g02720) gene, showing the nature and position of the *mas2* mutant alleles. White and black boxes represent untranslated and coding regions, respectively. The region encoding the SynMuv domain is shown in gray. Arrows indicate nucleotide substitutions, and triangles indicate T-DNA insertions.
(B) and **(C)** Predicted effects of the *mas2* mutations on the MAS2 protein. Residues conserved among plants **(B)** or eukaryotes **(C)** are shaded black (identical) and gray (similar). The full-length alignments are shown in Supplemental Figures 3 and 4. The amino acids underlined belong to the SynMuv domain.

mas2-1 Suppresses the Phenotype of Two *ago1* Alleles That Exhibit Missplicing

To ascertain if suppression of *ago1-52* by *mas2-1* is allele specific, we crossed *mas2-1* single mutant plants to the *ago1-25*, *ago1-27* (Morel et al., 2002), and *ago1-51* (Jover-Gil et al., 2012) single mutants. Both *ago1-25* and *ago1-27* carry missense mutations, whereas *ago1-51* and *ago1-52* exhibit missplicing of the *AGO1* pre-mRNA (Supplemental Figure 5).

The *ago1-25 mas2-1* and *ago1-27 mas2-1* double mutants were indistinguishable from their *ago1-25* and *ago1-27* single mutant F2 siblings (Figures 3A to 3D). By contrast, the *ago1-51 mas2-1* double mutant exhibited suppression, though to a lesser extent than that seen in *ago1-52 mas2-1* plants (Figures 3E to 3H). For example, one of the most conspicuous traits of hypomorphic *ago1* mutants, the absence of a well-defined petiole (Jover-Gil et al., 2012), is suppressed in *ago1-51 mas2-1* leaves. In addition, *ago1-51 mas2-1* plants were slightly taller than the *ago1-51* plants, but the inflorescences and fruits of the double mutant were less compact and longer, respectively, than those of *ago1-51* (Supplemental Figure 6). These results indicate that *mas2-1* suppresses the mutant phenotype of *ago1-51* and *ago1-52*, which carry mutations causing missplicing, but not those of *ago1-25* and *ago1-27*, which carry missense mutations.

The *mas2* Mutations Modify the Ratio between Splice Variants from *ago1-51* and *ago1-52*

The G→A transition carried by *ago1-51* and *ago1-52* (Supplemental Figure 5) causes missplicing. Two abnormal splice forms are detectable by RT-PCR from *ago1-51* mRNA: The short splice form (*ago1-51.1*) is 3468 nucleotides long and lacks the last 39 nucleotides of the 7th exon and the 7th intron, and the long form (*ago1-51.2*) is 3578 nucleotides long and includes the entire 7th intron. Translation of the short splice form should produce an AGO1 protein similar to wild type but lacking

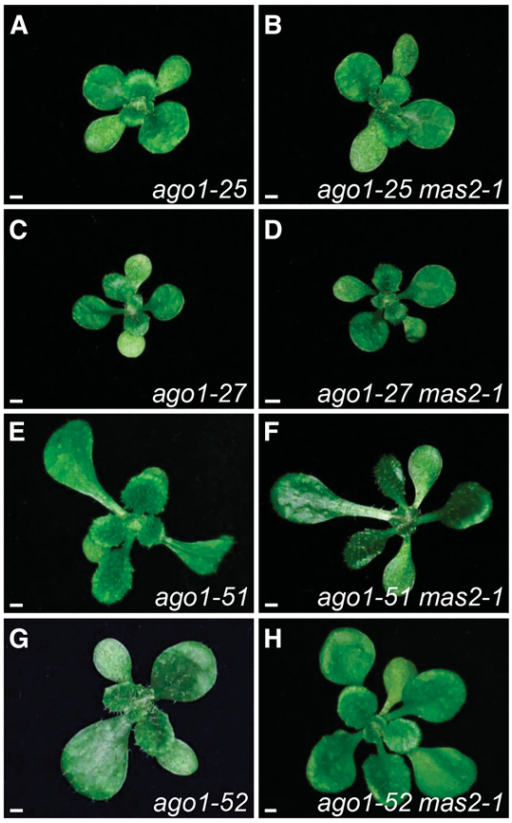

Figure 3. Genetic Interactions of *mas2-1* with *ago1-25*, *ago1-27*, *ago1-51*, and *ago1-52*.

Rosettes of *ago1-25* **(A)**, *ago1-25 mas2-1* **(B)**, *ago1-27* **(C)**, *ago1-27 mas2-1* **(D)**, *ago1-51* **(E)**, *ago1-51 mas2-1* **(F)**, *ago1-52* **(G)**, and *ago1-52 mas2-1* **(H)** plants. Pictures were taken at 21 DAS. Bars = 1 mm.

13 amino acids of the PAZ domain, but translation of the long splice form should produce a truncated protein. A single splice form of *AGO1* was detected from *ago1-52* RNA; this form is 3517 nucleotides long and includes 10 nucleotides of the 20th intron (Jover-Gil et al., 2012).

The *mas2-1* mutation suppresses the morphological phenotype of *ago1-51* and *ago1-52*; therefore, we wondered if *mas2-1* modifies the number and/or relative amounts of *AGO1* splice variants in these *ago1* mutants. We designed PCR primers to amplify the wild type (abbreviated as *wAGO1*) and mutant (*ago1-51.1*, *ago1-51.2*, and *ago1-52*) splice forms (Supplemental Table 2). Using primers designed to amplify all possible splice forms (total *AGO1* mRNAs, abbreviated as *tAGO1*), we could not detect the *wAGO1* splice form in *ago1-51* plants by RT-PCR, as previously reported (Jover-Gil et al., 2012) (Supplemental Figure 7A). However, using primers that selectively amplify *wAGO1*, we did detect this splice form at a very low level in the *ago1-51* mutant (Supplemental Figure 7A). We confirmed the presence of the *wAGO1*, *ago1-51.1*, and *ago1-51.2* mRNA variants by reverse transcription and quantitative PCR (RT-qPCR). These results indicated that the *wAGO1* splice form represents 0.8 and 2.1% of *tAGO1* in *ago1-51* and *ago1-51 mas2-1* plants, respectively (Figure 4A).

We also detected *wAGO1* in *ago1-52* and *ago1-52 mas2-1* plants by RT-PCR using specific primers (Supplemental Figure 7B and Supplemental Table 2) and found by RT-qPCR that *wAGO1* represents 2.5 and 14.8% of *tAGO1* in *ago1-52* and *ago1-52 mas2-1*, respectively (Figure 4B).

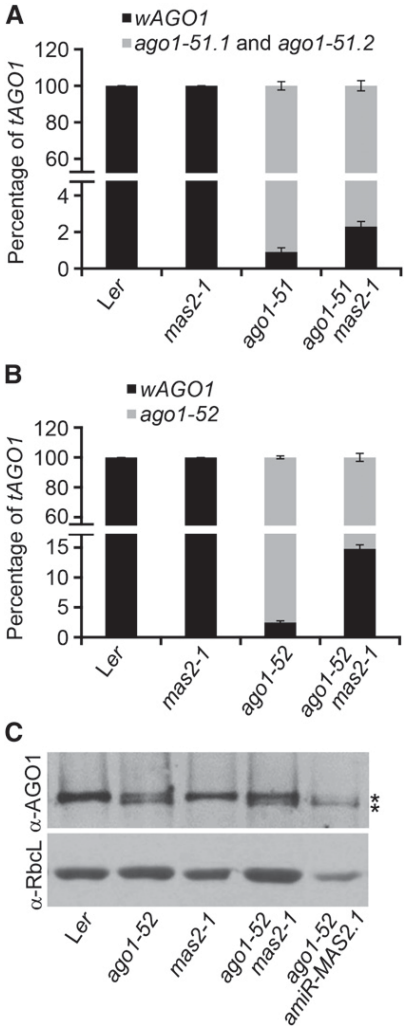

Figure 4. Effects of *mas2-1* on the Levels of *ago1-51* and *ago1-52* mRNA and Protein Products.

(A) and **(B)** RT-qPCR analyses using primers to amplify all of the splice forms of *AGO1* (*tAGO1*) or specifically the wild-type *AGO1* mRNA (*wAGO1*). The percentages of *wAGO1* and the mutant splice forms with respect to *tAGO1* were estimated in L*er*, *mas2-1*, *ago1-51*, and *ago1-51 mas2-1* plants **(A)** and in L*er*, *mas2-1*, *ago1-52*, and *ago1-52 mas2-1* plants **(B)**.

(C) Detection of AGO1 proteins by immunoblot using a primary antibody against AGO1 (α-AGO1). Total proteins from L*er*, *mas2-1*, *ago1-52*, *ago1-52 mas2-1*, and *ago1-52 amiR-MAS2.1* plants were used. Asterisks indicate the AGO1 (upper band) and the AGO1-52 (lower band) proteins. α-RbcL was used as the loading control.

To study the effects of *mas2-4* to *mas2-11* on the splicing of *ago1-52* in all the *ago1-52 mas2* lines isolated in our screen, we used RT-qPCR to measure the ratio between the *wAGO1* and *ago1-52* splice forms, which remained as in *ago1-52 mas2-1*. The only exception was the P1 5.33 (*ago1-52 mas2-5*) line, in which the ratio was the same as in the *ago1-52* mutant (Supplemental Figure 7C).

The *mas2* Mutations Modify the Ratio between Protein Variants Encoded by *ago1-51* and *ago1-52*

The increased *wAGO1* level we observed in *ago1-51 mas2-1* and *ago1-52 mas2-1* plants compared with *ago1-51* and *ago1-52*, respectively, seemed to be too modest to explain the strong phenotypic suppression observed. Hence, we performed immunoblot assays using an α-AGO1 antibody, extracting proteins from plants carrying different *ago1* alleles: the null *ago1-2* (Bohmert et al., 1998) and the hypomorphic *ago1-25*, *ago1-27* (Morel et al., 2002), *ago1-51*, and *ago1-52* (Jover-Gil et al., 2012) alleles. As expected, we detected no AGO1 protein in the *ago1-2* mutant; a single protein of ~130 kD in *ago1-25* and *ago1-27*, likely the AGO1-25 and AGO1-27 proteins, respectively; and ~130- and ~60-kD proteins in *ago1-51* plants, likely the AGO1-51.1 and AGO1-51.2 mutant proteins, respectively (Supplemental Figure 8). Due to the difference between the wild-type (AGO1) and the AGO1-51.1 protein, which is only 13 amino acids smaller than AGO1, we could not discriminate them in immunoblots. The largest amount of protein corresponded to the ~130-kD band, while the ~60-kD band was very weak (Supplemental Figure 8), suggesting that the truncated AGO1-51.2 protein is degraded or is less translatable than AGO1-51.1 or the wild-type protein. In *ago1-52* plants, two different proteins were also detected: one of ~130 kD, the size of the wild-type AGO1 protein, and another of ~125 kD, likely the AGO1-52 protein (Figure 4C; Supplemental Figure 8). Both AGO1 and AGO1-52 proteins were present in similar amounts in *ago1-52* (Figure 4C; Supplemental Figure 8), which suggests a greater translatability of the wild-type *AGO1* splice form compared with the *ago1-52* form or a higher stability of AGO1 protein.

These results suggest that *mas2-1* suppresses the phenotypes of *ago1-51* and *ago1-52* by increasing the translatability of *wAGO1* mRNA and/or stability of AGO1 protein more than modifying the splicing of *ago1-51* and *ago1-52* mRNAs. This assumption is also consistent with our results with the other *mas2* suppressor alleles described above, because one of them (*mas2-5*) does not change the ratio between *wAGO1*/*ago1-52* splice forms in *ago1-52 mas2-5* plants.

Overexpression of *mas2-1*, but Not *MAS2*, Suppresses *ago1-52* and *ago1-51*

To further examine the effect of *mas2-1* on the phenotypes of *ago1-51* and *ago1-52*, and to compare the effects of the overexpression of the *MAS2* and *mas2-1* alleles in wild-type *AGO1*/*AGO1* and mutant *ago1*/*ago1* backgrounds, we generated $35S_{pro}$*:MAS2* and $35S_{pro}$*:mas2-1* constructs, which were transferred into L*er*, *ago1-51*, and *ago1-52* plants. The $35S_{pro}$*:MAS2*, $35S_{pro}$*:mas2-1*, and L*er* plants were indistinguishable (Supplemental Figures 9A to 9C), and the $35S_{pro}$*:MAS2* transgene did not suppress the mutant phenotype of *ago1-51* and *ago1-52* plants (Supplemental Figures 9E to 9H). By contrast, $35S_{pro}$*:mas2-1* suppressed the mutant phenotype of *ago1-52* (Supplemental Figures 9I and 10) and *ago1-51*. Suppression of *ago1-51* by *mas2-1* was stronger in the $35S_{pro}$*:mas2-1 ago1-51* transgenic plants (Supplemental Figures 9F and 11) than in the *ago1-51 mas2-1* double mutant (Figure 3F). These results reconfirm that *mas2-1* is a true extragenic suppressor of *ago1-51* and *ago1-52* and that it is antimorphic, rather than hypermorphic, as suggested by the absence of suppression seen in $35S_{pro}$*:MAS2 ago1* plants.

Insertional *mas2* Alleles Are Embryonic Lethal

We also searched for insertional alleles of *MAS2* and identified three publicly available lines. The GABI_318G03 line (Supplemental Figure 12A) was phenotypically wild type and not studied further. SAIL_335_C06, which we named *mas2-2*, is in the Col-3 background and carries a T-DNA insertion 1074 bp downstream of the translation start codon of At4g02720, in the region encoding the SynMuv domain (Figure 2A). We found no *mas2-2*/*mas2-2* homozygotes among 274 T4 genotyped plants. Aborted seeds accounted for 0.28% ± 0.97% of seeds (n = 353, n being the number of embryos from fertilized ovules) in the siliques from six *MAS2*/*MAS2* plants, where no unfertilized ovules were seen. By contrast, the siliques of six *MAS2*/*mas2-2* plants showed 29.78% ± 8.38% aborted seeds (n = 339) and 3.42% ± 4.68% unfertilized ovules (n = 351, n being the sum of the number of unfertilized ovules plus the number of embryos from fertilized ovules; Supplemental Figure 13).

We named the At4g02720 allele carried by CSHL_GT188551 (in a L*er* background) *mas2-3* and found the coding region in *mas2-3* is interrupted by a T-DNA insertion 233 bp downstream of the translation start codon (Figure 2A). We genotyped 31 CSHL_GT188551 plants, none of which was *mas2-3*/*mas2-3*. Aborted seeds were found in dissected siliques from five *MAS2*/*MAS2* (0.75% ± 1.3%; n = 532) and five *MAS2*/*mas2-3* plants (26.33% ± 5.19%; n = 433). No unfertilized ovules were found in the *mas2-3*/*MAS2* plants studied or in their *MAS2*/*MAS2* siblings. Taken together, these results suggest that *MAS2* is an essential gene whose null alleles are embryonic lethal.

Partial Silencing of *MAS2* by *amiR-MAS2* Causes a Pleiotropic Phenotype

The recessive embryonic lethality exhibited by the null *mas2-2* and *mas2-3* alleles, together with the likely antimorphic effects of the *mas2* suppressor mutations, prompted us to attempt to obtain viable plants with a partial loss of *MAS2* function. To this end, we designed and constructed a transgene carrying an artificial microRNA targeting At4g02720 ($35S_{pro}$*:amiR-MAS2*), which was transferred into wild-type Col-0, L*er*, and En-2 plants, producing 72, 15, and 13 independent T1 transformant lines, respectively. Among these transformants, we identified 10 (Col-0), 3 (L*er*), and 6 (En-2) plants with pointed and serrated leaves, to a greater or lesser extent (Supplemental Figure 14; Figure 5B). We analyzed by RT-qPCR the degree of *MAS2* silencing in several of these *amiR-MAS2* lines in the Col-0 background.

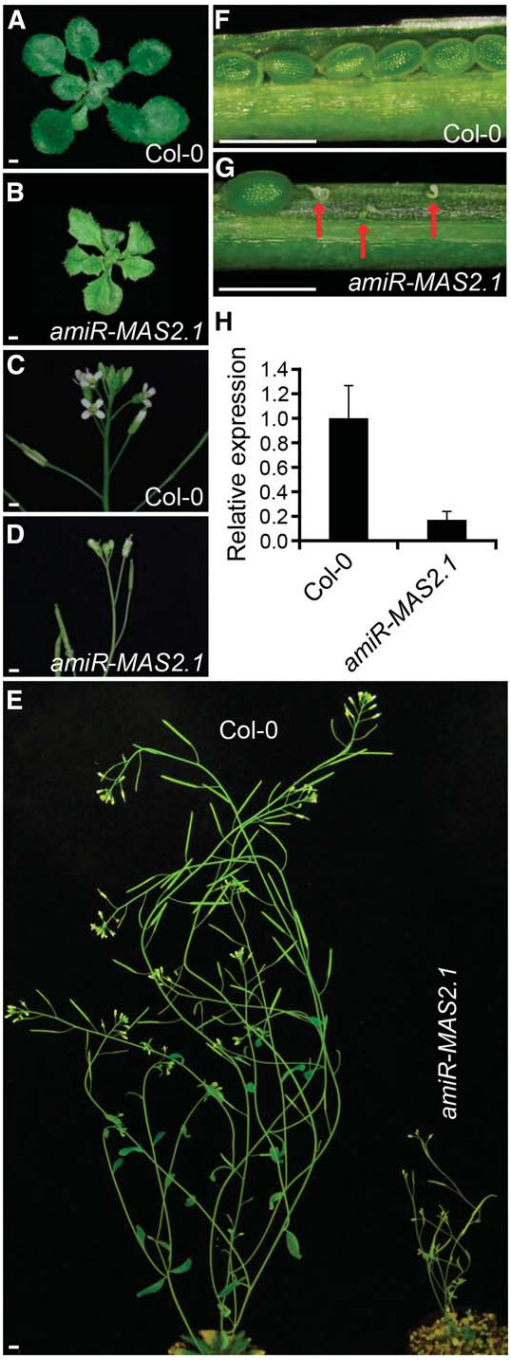

Figure 5. Phenotypic Effects of the *amiR-MAS2.1* Transgene in the Col-0 Background.

(A) and **(B)** Rosettes of Col-0 **(A)** and *amiR-MAS2.1* **(B)** (in the Col-0 background) plants.
(C) and **(D)** Inflorescences of Col-0 **(C)** and *amiR-MAS2.1* **(D)** plants.
(E) Adult Col-0 and *amiR-MAS2.1* plants.
(F) and **(G)** Dissected siliques from Col-0 **(F)** and *amiR-MAS2.1* **(G)** plants. Red arrows indicate unfertilized ovules.
(H) *MAS2* expression levels in Col-0 and *amiR-MAS2.1* plants. Three biological replicas with three technical replicas each were performed. Error bars represent standard deviations.

Homozygous plants of the line that we termed *amiR-MAS2.1* displayed the strongest mutant phenotype and also exhibited a 5-fold reduction of *MAS2* mRNA levels compared with the wild type (Figure 5H); these were chosen for further studies.

First- and third-node leaves of *amiR-MAS2.1* plants exhibited a vein pattern with reduced complexity (Supplemental Figures 15A to 15D), an increased number of air spaces in the palisade mesophyll (Supplemental Figures 15E to 15H), fewer vegetative leaves (7.82 $\pm$ 0.56 in *amiR-MAS2.1* and 12.87 $\pm$ 0.61 in Col-0, scored at 27 d after stratification [DAS]; $n \geq 47$), and early flowering (bolting was apparent in 51.3% of *amiR-MAS2.1* plants and 2.1% of Col-0 at 20 DAS; $n \geq 39$). These transgenic plants were also dwarfed, with thinner stems and fewer flowers than Col-0 (Figures 5A to 5E). We dissected siliques from 10 *amiR-MAS2.1* homozygous plants and found 18.46% $\pm$ 16.87% aborted seeds (n = 260) and 17.46% $\pm$ 23.05% unfertilized ovules (n = 315; Figure 5G).

The pleiotropic phenotype exhibited by *amiR-MAS2.1* plants suggests a role for *MAS2* in Arabidopsis development. In particular, *amiR-MAS2.1* leaves are reminiscent of the leaves of mutants carrying loss-of-function alleles of genes encoding ribosomal proteins (Van Lijsebettens et al., 1994; Ito et al., 2000; Creff et al., 2010; Horiguchi et al., 2011; Casanova-Sáez et al., 2014).

amiR-MAS2.1 Increases the Severity of the Mutant Phenotype of *ago1-52*

To study the effects of *MAS2* partial loss of function on the phenotype of *ago1-52*, we crossed *ago1-52/ago1-52* to *amiR-MAS2.1/amiR-MAS2.1* and sowed the F2 progeny on plates supplemented with hygromycin. Only two phenotypic classes of *ago1-52/ago1-52* plants were obtained: (1) lethal seedlings that only produced cotyledons and a few rod-like leaves (Figure 6C), which we inferred to be *ago1-52/ago1-52; amiR-MAS2.1/amiR-MAS2.1*; and (2) viable seedlings that developed into plants with narrow and strongly serrated leaves that exhibited fasciated stems and aberrant flowers (Figures 6D to 6H) and yielded few seeds, which we inferred to be *ago1-52/ago1-52; amiR-MAS2.1*. In the F3 and F4 progeny of the latter plants, a 3:1 (Hyg^r:Hyg^s) segregation was observed, confirming that they were homozygous for *ago1-52* but hemizygous for *amiR-MAS2.1*. The phenotype of the *ago1-52/ago1-52; amiR-MAS2.1/amiR-MAS2.1* lethal seedlings resembled that of plants homozygous for null alleles of *AGO1*, whereas the *ago1-52/ago1-52; amiR-MAS2.1* plants were very similar to those homozygous for the *ago1-103* mutation, a very strong but viable allele of *AGO1* (Fernández-Nohales et al., 2014).

We also quantified the percentage of *AGO1* mRNAs in the *ago1-52/ago1-52; amiR-MAS2.1/amiR-MAS2.1* lethal seedlings. In these plants, the *wAGO1* and *ago1-52* splice forms represented 0.7 and 99.3% of *tAGO1*, respectively (Supplemental Figure 16). The percentage of *wAGO1* in *ago1-52/ago1-52; amiR-MAS2.1/amiR-MAS2.1* (0.7%) is almost half of that found

Pictures were taken at 21 (**[A]** and **[B]**) and 48 (**[C]** to **[G]**) DAS. Bars = 1 mm in **(A)** to **(D)**, **(F)**, and **(G)**, and 1 cm in **(E)**.

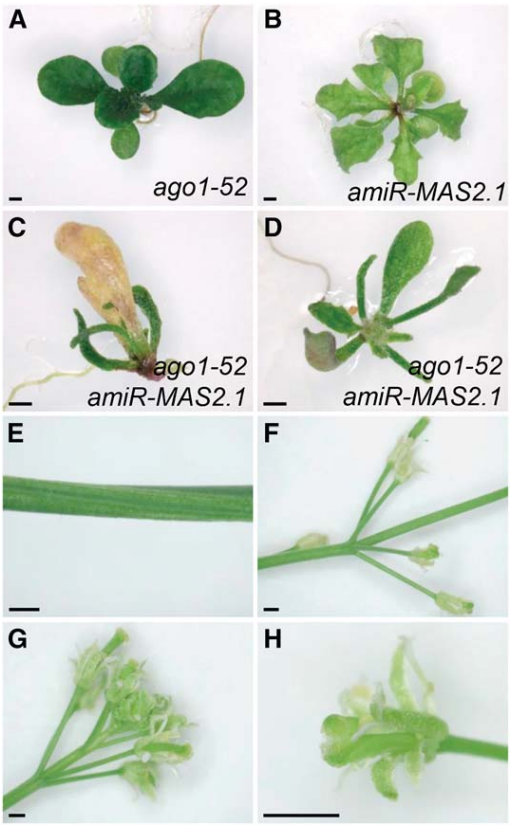

Figure 6. Phenotypic Effects of the *amiR-MAS2.1* Transgene in the *ago1-52* Background.

(A) to **(C)** Rosettes of *ago1-52/ago1-52* **(A)**, *amiR-MAS2.1/amiR-MAS2.1* **(B)**, and *ago1-52/ago1-52; amiR-MAS2.1/amiR-MAS2.1* **(C)** plants.
(D) to **(H)** Rosette **(D)**, stems (**[E]** and **[F]**), inflorescence **(G)**, and flower **(H)** of *ago1-52/ago1-52*; *amiR-MAS2.1* plants.
Pictures in **(A)** to **(D)** were taken at 21 DAS. Bars = 1 mm.

in *ago1-52* plants (1.2%) and could explain their extreme phenotype.

We also detected both the AGO1 and AGO1-52 proteins in the immunoblot assay of *ago1-52 mas2-1* and *ago1-52 amiR-MAS2.1* homozygous plants. The AGO1 protein was more abundant than AGO1-52 in *ago1-52 mas2-1* plants, whereas *ago1-52 amiR-MAS2.1* plants displayed an opposite pattern, with the AGO1-52 protein as the predominant variant (Figure 4C).

MAS2 Interacts in a Yeast Two-Hybrid Assay with Proteins Involved in Splicing and Translation

To better understand the function of MAS2, we decided to look for its interactors in a yeast two-hybrid (Y2H) assay. Two Arabidopsis cDNA libraries obtained from whole Arabidopsis plants, totaling 21 million prey clones, were used in the screening, which was performed at PanBioNet (http://www.panbionet.com). The bait contained the full-length coding region of *MAS2*. The screen identified 91 prey clones, representing 14 different genes, and these clones were confirmed by directed Y2H assays (Supplemental Table 3). These genes have not been previously studied in Arabidopsis, except for At1g20920, but their annotated functions are related to RNA processing and ribosome-related processes, as indicated by sequence similarity to known proteins.

Three of the interactors were related to ribosome biogenesis, including RPS24B, the second most represented interactor, which is one of the two Arabidopsis S24-type proteins in the 40S ribosomal subunit. Two other interactors, the putative ortholog of the Nucleolar protein 53 (NOP53) of *Saccharomyces cerevisiae* and RRNA-processing Protein 7 (RRP7), are nucleolar proteins involved in pre-rRNA processing and ribosome assembly in yeast (Granato et al., 2008).

The most represented interactor in the Y2H-based screen, in 23 of the 55 clones (Supplemental Table 3), was CAX INTERACTING PROTEIN4 (CXIP4), a protein of unknown function that was previously identified as interacting with the high-affinity vacuolar calcium antiporter CAX1 (Cheng et al., 2004). CXIP4 occurs exclusively in plants and 30 amino acids of its N-terminal region show 70% similarity to the mammalian splicing factor SREK1-interacting protein 1, as shown in the Aramemnon database (http://aramemnon.botanik.uni-koeln.de/index.ep; Schwacke et al., 2003). Other interactors were also involved in pre-mRNA splicing (Supplemental Table 3), including REGULATOR OF CBF GENE EXPRESSION1/RH42, a DEAD box RNA helicase (Guan et al., 2013).

The interaction between MAS2 and the protein encoded by At4g33690, annotated as an unknown protein, has also been found among the more than 6200 Y2H interactions included in the Arabidopsis interactome map (http://interactome.dfci.harvard.edu/A_thaliana/index.php; Arabidopsis Interactome Mapping Consortium, 2011).

Our results suggest a role for MAS2 in the regulation of pre-mRNA alternative splicing and translation. Our results also agree with those obtained with the mammalian NKAPs, which localize to nuclear speckles and interact with nuclear ribonuclear proteins, splicing factors, several RNA helicases, and other factors involved in the maturation of 45S pre-rRNA and ribosome biogenesis (Burgute et al., 2014).

MAS2 Expression and MAS2 Nuclear Localization

To determine the spatial expression pattern of *MAS2*, we generated a $MAS2_{pro}$*:GUS* construct in which the *MAS2* promoter drives the expression of the β-glucuronidase gene and transferred this construct into Col-0. Homozygous $MAS2_{pro}$*:GUS* plants were selected and used to detect GUS activity, which was found in roots, cotyledons, young vegetative and cauline leaves, stems, and flower buds (Supplemental Figure 17). GUS activity changed depending on the developmental stage, being more intense in seedlings and young plants; we did not detect GUS staining in vegetative leaves after bolting (48 DAS) or in fully expanded cauline leaves (Supplemental Figures 17F and 17H). Additionally, we performed RT-qPCR amplifications using cDNA from assorted organs of L*er* and Col-0 and found that *MAS2* was expressed in all the studied tissues at similar levels (Supplemental Figure 18).

To ascertain if MAS2 is nuclear, similar to all animal NKAP proteins already studied, we generated $35S_{pro}$*:MAS2:GFP* and

MAS2$_{pro}$:MAS2:GFP constructs, which we transformed into Col-0 and L*er* plants. As expected, we detected GFP signal in the nucleus for both constructs (Figure 7; Supplemental Figures 19A and 19B). MAS2 subcellular localization depended on the cell cycle: In cells with a high rate of nuclear division, such as those located at the root apex or emerging lateral roots, MAS2:GFP occurred in a diffuse pattern throughout the nucleus (Figures 7A to 7C). By contrast, in cells of the root elongation zone, MAS2:GFP was nuclear with an exclusion zone at the nucleolus (Supplemental Figure 20). Furthermore, MAS2:GFP had a punctuate distribution (Figures 7D to 7F; Supplemental Figure 20), which became more evident in differentiated cells where it appeared only in discrete foci in the nucleus (Figures 7G to 7I). These perinucleolar foci perfectly matched the heterochromatic chromocenters, which were visualized as bright fluorescent dots by 4',6-diamidino-2-phenylindole (DAPI) staining. These regions contain centromeric and other heterochromatic repeats, including those corresponding to silent rRNA 45S genes (Costa-Nunes et al., 2010). We obtained identical results with the *35S$_{pro}$:MAS2:GFP* and *MAS2$_{pro}$:MAS2:GFP* transgenes (Supplemental Figures 19A and 19B).

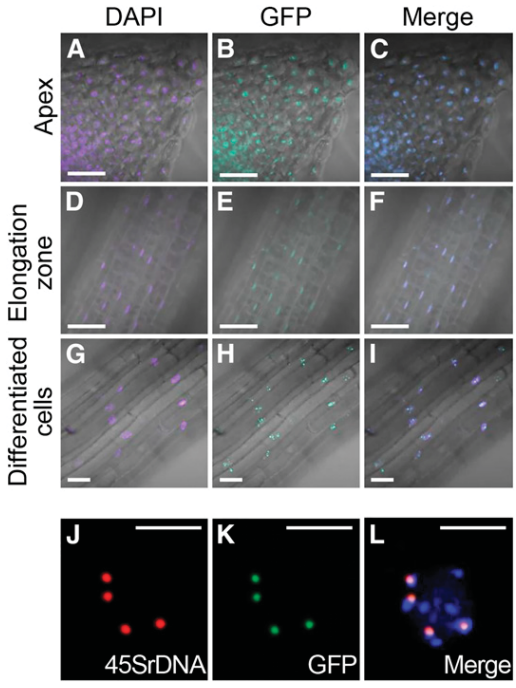

Figure 7. Subcellular Localization of the MAS2 Protein.

Confocal laser scanning microscopy of plants homozygous for the *35S$_{pro}$:MAS2:GFP* transgene.

(A) to **(I)** Different root zones from root apex (**[A]** to **[C]**), root elongation zone (**[D]** to **[F]**), and differentiated root cells (**[G]** to **[I]**). Fluorescence signals are DAPI (**[A]**, **[D]**, and **[G]**), GFP (**[B]**, **[E]**, and **[H]**), and their overlay (**[C]**, **[F]**, and **[I]**). Fluorescence and transmitted light contrast images were merged in **(A)** to **(I)**.

(J) to **(L)** Mitotic prophase nucleus from a flower bud cell showing the fluorescent signals from a hybridized 45S rDNA probe **(J)**, GFP **(K)**, and their overlay **(L)** with DAPI.

Bars = 30 μm in **(A)** to **(I)** and 50 μm in **(J)** to **(L)**.

To ascertain if the subcellular localization of MAS2 is modified by the *mas2-1* mutation, we generated the *MAS2$_{pro}$:mas2-1:GFP* construct, finding the fluorescent emission of MAS2-1:GFP indistinguishable from that of MAS2:GFP (Supplemental Figures 19C and 19D). These results indicate that overexpression of *MAS2* and the *mas2-1* mutation do not alter the nuclear localization of the MAS2 protein.

MAS2 Colocalizes with the 45S rDNA

In eukaryotes, tandem arrays of the genes encoding the four classes of nuclear rRNAs occur in different clusters. In the Arabidopsis Col-0 accession, the 5S rRNA genes occur within the pericentromeric heterochromatin of chromosomes 3, 4, and 5 (Campbell, 1992), and the 45S rRNA genes occur in the nucleolar organizer regions (NORs) at the tips of the short arms of the acrocentric chromosomes 2 and 4 (NOR2 and NOR4) (Lam et al., 2005; Layat et al., 2012). Transcription of the 5S rRNA gene by RNA polymerase III (Pol III) produces a 5S rRNA transcript (Cloix et al., 2002), and transcription of the 45S rRNA gene by RNA polymerase I (Pol I) produces a long polycistronic 45S pre-rRNA that is processed into the 5.8S, 18S, and 25S rRNA mature forms (Gruendler et al., 1989, 1991; Unfried et al., 1989).

The nuclear localization of MAS2 in discrete foci, together with the Y2H results, prompted us to analyze whether MAS2 colocalized with the 45S rRNA genes. To answer this question, we performed a fluorescence in situ hybridization (FISH) assays with plants expressing *35S$_{pro}$:MAS2:GFP*. In the root cells of these plants, the GFP signal perfectly matched the signal of a 45S rDNA probe (Sanchez Moran et al., 2001), indicating that MAS2 colocalizes with 45S rDNA (Figures 7J to 7L).

mas2-1 and *amiR-MAS2.1* Genetically Interact with *nuc-L1*

In Arabidopsis, *HISTONE DEACETYLASE6* (*HDA6*) and *NUCLEOLIN-LIKE PROTEIN1* (*NUC-L1*; also known as *PARALLEL1* [*PARL1*]) have been implicated in nuclear organization and transcriptional regulation of the 45S rDNA (Petricka and Nelson, 2007; Layat et al., 2012). The *amiR-MAS2.1* plants share some phenotypes, including reticulated and serrated leaves and altered leaf vein patterning, with the *nuc-L1* and *parl1* mutants and with mutants in genes encoding ribosomal proteins (Petricka and Nelson, 2007; Pontvianne et al., 2007).

Based on our interaction, localization, and phenotypic data for *MAS2*, we tested for a genetic interaction by crossing *mas2-1* and *amiR-MAS2.1* plants to the *parl1-2* nucleolin mutant (Petricka and Nelson, 2007). Although *mas2-1*/- plants show no morphological phenotype, the *mas2-1 parl1-2* double mutant plants displayed a synergistic phenotype, with small rosettes and pointed, serrated, and reticulated leaves resembling those of strong loss-of-function alleles of genes encoding ribosomal proteins (Van Lijsebettens et al., 1994; Ito et al., 2000; Creff et al., 2010; Horiguchi et al., 2011; Casanova-Sáez et al., 2014) (Figure 8E). Furthermore, the *mas2-1 parl1-2* double mutant had flowers with abnormal numbers of petals (5 to 6) and/or stamens (4 to 5), traits that we did not observe in either *mas2-1* or *parl1-2* single mutants (Figures 8J to 8L).

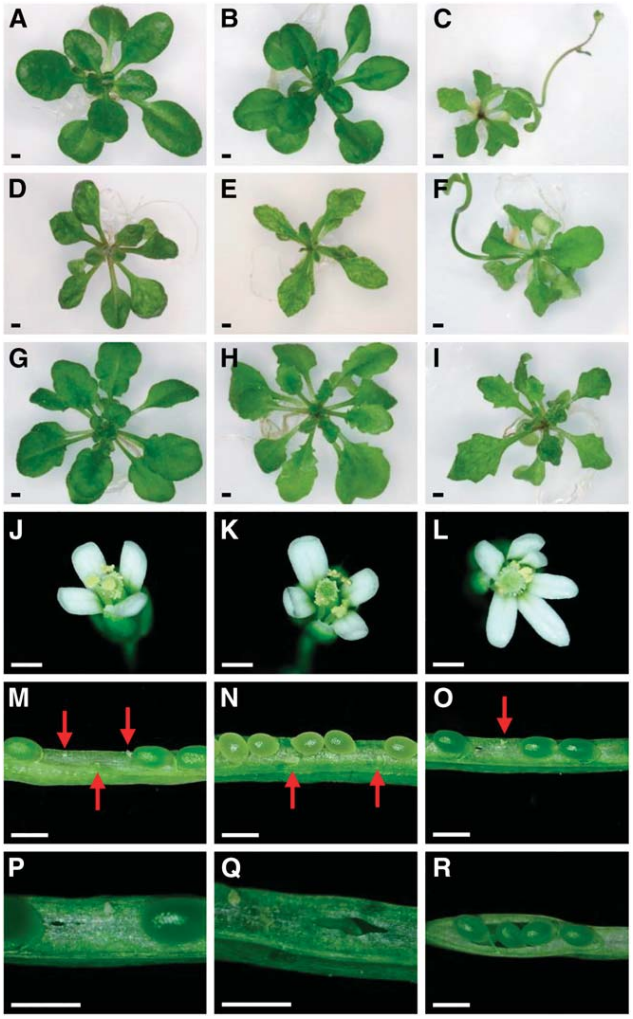

Figure 8. Genetic Interactions of *mas2-1* and *amiR-MAS2.1* with *parl1-2* and *hda6*.

(A) to **(I)** Rosettes of L*er* **(A)**, *mas2-1* **(B)**, *amiR-MAS2.1* **(C)**, *parl1-2* **(D)**, *mas2-1 parl1-2* **(E)**, *amiR-MAS2.1/amiR-MAS2.1; PARL1/parl1-2* **(F)**, *hda6-7* **(G)**, *mas2-1 hda6-7* **(H)**, and *amiR-MAS2.1 hda6-7* **(I)** plants.
(J) to **(L)** Flowers of *mas2-1* **(J)**, *parl1-2* **(K)**, and *mas2-1 parl1-2* **(L)** plants.
(M) to **(O)** Dissected siliques of *amiR-MAS2.1* **(M)**, *parl1-2* **(N)**, and *amiR-MAS2.1/amiR-MAS2.1; PARL1/parl1-2* **(O)** plants. Red arrows indicate unfertilized ovules.
(P) to **(R)** *amiR-MAS2.1/amiR-MAS2.1; PARL1/parl1-2* siliques exhibiting interrupted septa.
Pictures in **(A)** to **(I)** were taken at 28 DAS. Bars = 1 mm in **(A)** to **(I)** and 0.5 mm in **(J)** to **(R)**.

After genotyping 84 plants of different F2 and F3 families, we did not find any *amiR-MAS2.1/-; parl1-2/parl1-2* plant, and the *amiR-MAS2.1/amiR-MAS2.1; PARL1/parl1-2* and *amiR-MAS2.1/amiR-MAS2.1* plants were indistinguishable (Figures 8C and 8F). Since combined loss-of-function of *MAS2* and *PARL1* seemed to be lethal, we dissected siliques of *amiR-MAS2.1/amiR-MAS2.1*, *parl1-2/parl1-2*, and *amiR-MAS2.1/amiR-MAS2.1; PARL1/parl1-2* plants (Figures 8M to 8O), in which the unfertilized ovules and undeveloped seeds represented 42.9, 31.5, and 33.7% of the total, respectively. Moreover, around 25% of the siliques of *amiR-MAS2.1/amiR-MAS2.1; PARL1/parl1-2* plants displayed a disrupted septum between the two valves, a trait that we never observed in *amiR-MAS2.1/-* or *parl1-2/parl1-2* plants (Figures 8P to 8R). These results indicate that the combined loss of function of *MAS2* and *PARL1* is synergistic in *amiR-MAS2.1; PARL1/parl1-2* plants.

We also found that *mas2-1 hda6-7* leaves were strongly serrated (Figure 8H), suggesting that *HDA6* and *MAS2* are functionally related. The phenotype of *mas2-1 hda6-7* leaves is reminiscent of those of double mutants involving alleles of the *ASYMMETRIC LEAVES1* (*AS1*) or *AS2* genes and *axe1-5*, another loss-of-function allele of *HDA6* (Murfett et al., 2001). HDA6, AS1, and AS2 form a complex to repress *KNOX* genes and regulate leaf development (Luo et al., 2012). The morphological phenotype of *hda6-7* was hard to distinguish from the wild type in our growth conditions. The *amiR-MAS2.1/amiR-MAS2.1; hda6-7/hda6-7* and *amiR-MAS2.1/amiR-MAS2.1* plants were also indistinguishable (Figure 8I).

The phenotype of the *mas2-1 parl1-2* double mutant and, in particular, that of *amiR-MAS2.1/amiR-MAS2.1; PARL1/parl1-2* plants suggest that *MAS2* and *PARL1* are functionally related. The observation that both the *mas2-1* allele and the partial silencing of *MAS2* caused by *amiR-MAS2.1* synergistically interact with *parl1-2* reinforces the hypothesis that *mas2-1* is an antimorphic rather than a gain-of-function allele of *MAS2*.

amiR-MAS2.1 Alters Transcription of 45S rDNA, 45S Pre-rRNA Processing, and NOR Condensation

In Arabidopsis, each 45S rDNA unit has an intergenic spacer (IGS), two external transcribed spacers (ETSs), and the rRNA genes (18S, 5.8S, and 25S), which are separated by two internal transcribed spacers (ITSs) (Figure 9A). The IGS region separates adjacent genes and includes three repeat elements containing *Sal*I restriction sites that are separated by two spacer promoters, the promoter region, and the 5′ETS. The 3′ETS contains five repeated sequences (R1-R5) whose polymorphisms generate different variants of 45S rDNA genes (Abou-Ellail et al., 2011). The number of these variants differs among Arabidopsis accessions, with four (VAR1-VAR4) in Col-0 and other related accessions (Abou-Ellail et al., 2011). VAR2, VAR3, and VAR4 are expressed in Col-0 adult plants, while VAR1 is only expressed in germinating seeds or in mutants of genes involved in epigenetic regulation of the expression of 45S rDNA, such as *nuc-L1* and *hda6* (Pontvianne et al., 2010). We examined the expression of the 45S rDNA variants in *amiR-MAS2.1/amiR-MAS2.1* and *mas2-1/mas2-1* plants using p3/p4 primers (Figure 9A; Supplemental Table 2), which amplify the 3′ETS region of the 45S pre-rRNA and allow detection of all VAR variants (Pontvianne et al., 2010). RT-PCR amplifications showed no differences in the number or amount of rRNA variants between *amiR-MAS2.1/amiR-MAS2.1* and *mas2-1/mas2-1* plants and their respective backgrounds, Col-0 and L*er* (Figure 9B).

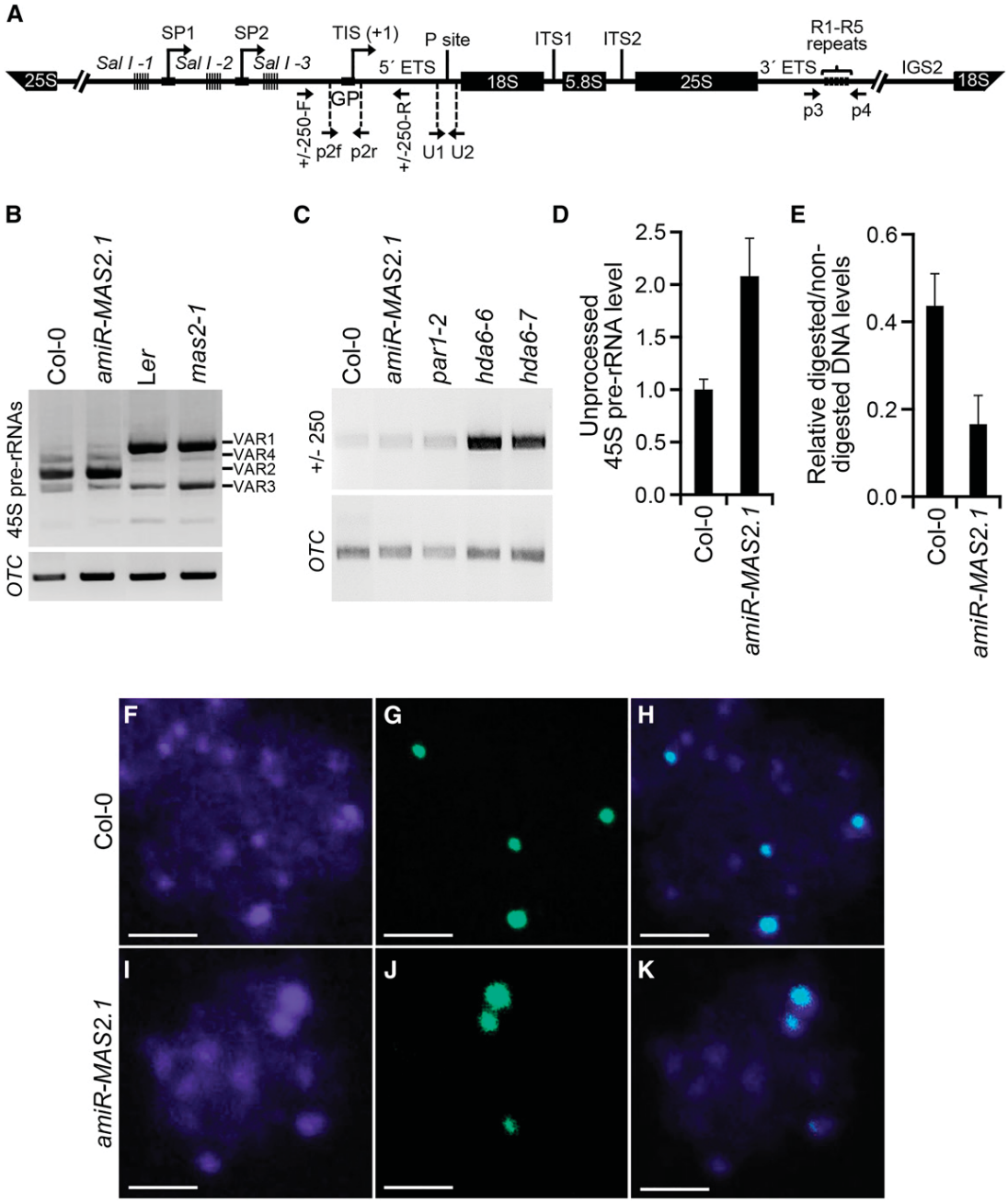

Figure 9. Effects of the *amiR-MAS2.1* Transgene on 45S Pre-rRNA Expression and NOR Condensation.

(A) Schematic representation of a 45S rDNA unit, modified from Pontvianne et al. (2010). GP, gene promoter; SP1 and SP2, spacer promoters; TIS, transcription initiation site. *Sal*I, repeat elements containing *Sal*I restriction sites. Upwards arrows with tip rightwards, transcription initiation sites. ITS1 and ITS2, internal transcribed spacers. Horizontal arrows indicate the positions of primers (not drawn to scale) used to detect pre-rRNA sequences.
(B) RT-PCR analysis of the expression of the VAR1-VAR4 45S rRNA variants in Col-0, *amiR-MAS2.1/amiR-MAS2.1*, L*er*, and *mas2-1/mas2-1* plants using the p3 and p4 primers (Supplemental Table 2).
(C) RT-PCR analysis of 45S pre-rRNA accumulation in Col-0, *amiR-MAS2.1/amiR-MAS2-1*, *parl1-2*, *hda6-6*, and *hda6-7* plants using the +/−250-F and +/−250-R primers.
(D) RT-qPCR analysis of unprocessed 45S pre-rRNAs in Col-0 and *amiR-MAS2.1/amiR-MAS2.1* plants using the U1 and U2 primers.
(E) Quantitative PCR analysis of 45S rDNA gene promoter methylation in Col-0 and *amiR-MAS2.1/amiR-MAS2.1* plants.
(D) and **(E)** Two biological replicas with three technical replicas each were performed. Error bars represent standard deviations.

In the *nuc-L1* and *hda6* mutants, NORs are decondensed (Probst et al., 2004; Pontvianne et al., 2007) and 45S pre-rRNA accumulates due to spurious transcription from the IGS region by Pol I and Pol II (Earley et al., 2010; Pontvianne et al., 2010), which in turn leads to the overproduction of small interfering RNAs (siRNAs) from the IGS region as a consequence of RNA-directed DNA methylation (Earley et al., 2010; Pontvianne et al., 2010). We also analyzed the accumulation of the 45S pre-rRNA transcripts produced by spurious transcription from the IGS region and the processing of these transcripts at the first step of cleavage (P site; Figure 9A). To amplify the 45S pre-rRNA, we used the +/−250-F and +/−250-R primers (Supplemental Table 2), which amplify the −250 to +250 region (Figure 9A; Earley et al., 2010). The 45S pre-rRNA processing was analyzed with the U1 + U2 primer pair (Supplemental Table 2), which amplify the sequences flanking the P site at the 5′ETS (Figure 9A; Shi et al., 2005). *amiR-MAS2.1*/*amiR-MAS2.1* and Col-0 plants accumulated comparable amounts of 45S pre-rRNA, while in *parl1-2* the level was far lower than that of *hda6* mutants (Figure 9C). Additionally, RT-qPCR analysis revealed that *amiR-MAS2.1*/*amiR-MAS2.1* plants accumulated approximately twice the amount of unprocessed 45S pre-rRNAs compared with Col-0 (Figure 9D). Mature rRNAs from processed 45S pre-rRNA were similar in *amiR-MAS2.1* and Col-0 plants (Supplemental Figure 21).

To study the effects of the silencing on NOR condensation, we analyzed NOR status in *amiR-MAS2.1*/*amiR-MAS2.1* plants by FISH assays, using a 45S rDNA probe (Sanchez Moran et al., 2001). Similar to the phenotype observed in *nuc-L1* and *hda6* mutants, we observed NOR decondensation in *amiR-MAS2.1* plants compared with Col-0 (Figures 9F to 9K).

amiR-MAS2.1 Affects Cytosine Methylation in the 45S Pre-rRNA 5′ETS

DNA methylation and histone modification epigenetically regulate the levels of rRNAs (Lawrence et al., 2004). Loss of *NUC-L1* and *HDA6* function in *nuc-L1* and *hda6* mutants leads to hypomethylation at the 5′ETS region affecting mainly the CG and, to a lesser extent, CHG contexts (where H indicates non-G nucleotides) (Earley et al., 2010; Pontvianne et al., 2010). To determine the DNA methylation status of the 5′ETS region in *amiR-MAS2.1* plants, we digested genomic DNA with the methylation-sensitive endonuclease *Hpa*II. Digested or non-digested DNA was used as template for quantitative PCR amplification using primers that flank the restriction sites (p2f and p2r) and hybridize downstream of the transcription initiation site (Figure 9A; Harscoët et al., 2010). We found that the ratio between digested and nondigested DNA was strongly reduced in *amiR-MAS2.1*/*amiR-MAS2.1* plants compared with Col-0 (Figure 9E), indicating that the promoter was hypomethylated in *amiR-MAS2.1*/*amiR-MAS2.1* plants, as occurred in the *nuc-L1* and *hda6* mutants.

DISCUSSION

Mutation of the SynMuv Domain of Arabidopsis MAS2 Causes Informational Suppression of *ago1* Alleles That Undergo Missplicing

The existence of SynMuv genes was first shown in *C. elegans* by screens for mutants deficient in vulval development (Ferguson and Horvitz, 1985, 1989; Ferguson et al., 1987; Howell and Rose, 1990). SynMuv genes act redundantly to prevent inappropriate vulval development (Horvitz and Sulston, 1980; Ferguson and Horvitz, 1989) and were initially classified into SynMuv A and B categories, based on their genetic interactions. SynMuv A and B single mutants are phenotypically wild type, but the AB double mutant combinations exhibit a synergistic, multivulva phenotype (Ferguson and Horvitz, 1989). Most SynMuv B genes encode epigenetic repressors, such as LHP1, the putative ortholog of Heterochromatin Protein 1, or are components of the NuRD (Nucleosome Remodeling Deacetylase) or DREAM (2DP, Retinoblastoma, E2F, and MuvB) repressor complexes (Saffer et al., 2011). The NuRD lysine deacetylase complex acts in a wide variety of cells (Yildirim et al., 2011), while DREAM is more specific and represses most cell cycle genes in mammalian quiescent G0 cells (Sadasivam and DeCaprio, 2013). Several genes encoding components of the splicing machinery behave as SynMuv B genes; their role in this process is still unknown (Ceron et al., 2007).

Second-site mutagenesis screens allow the identification of genes functionally related to a given gene of interest; the phenotype caused by a mutation can be modified, enhanced, or suppressed by a second-site mutation. One type of extragenic modifier that can be isolated by second-site mutagenesis is informational suppressors, mutations affecting any molecule involved in the transmission of information from DNA to protein (Prelich, 1999). Informational suppressors include those modifying pre-mRNA splicing, which suppress the splicing defects of some alleles of different genes. Some of these suppressors have helped in the elucidation of the regulation of alternative splicing in *C. elegans* (Hodgkin, 2005).

Here, we describe our characterization of the *MAS2* gene, which we identified from a second-site mutagenesis screen for suppressors of the morphological phenotype of *ago1-52*. *MAS2* is the putative Arabidopsis ortholog of human *NKAP* and *let-504* (*E01A2.4*), a SynMuv B gene of *C. elegans* (Poulin et al., 2005). MAS2 orthologs exist in almost all eukaryotes, and their sequence similarity is almost exclusively restricted to the SynMuv domain. NKAP family members encode nuclear proteins and, in most organisms except mammals, they exist as single-copy genes. Eight out the nine *mas2* suppressor mutations that we isolated affect conserved residues within the SynMuv domain; the remaining *mas2* mutation maps to another conserved region that seems to be exclusive to plants.

Figure 9. (continued).

(F) to **(K)** FISH assay. Representative mitotic prophase nuclei from Col-0 (**[F]** to **[H]**) and *amiR-MAS2.1* (**[I]** to **[K]**) cells. Fluorescent emissions are DAPI (**[F]** and **[I]**), hybridized 45S rDNA probe (**[G]** and **[J]**), and their overlay (**[H]** and **[K]**). Bars = 2.5 μm.

We found that *mas2* point alleles function as true extragenic suppressors of *ago1-52*, partially correcting *AGO1* missplicing in the *mas2 ago1-52* double mutants, hence increasing the ratio of AGO1 wild-type and mutant proteins. *mas2-1* also partially suppresses *ago1-51* missplicing. Immunoblot assays using an α-AGO1 antibody showed that the amount of wild-type AGO1 protein in *ago1-51* and *ago1-52* plants increased in the presence of *mas2-1* and decreased in the presence of the *amiR-MAS2.1* transgene.

Human NKAP interacts with pre-mRNAs and intronless mRNAs; it also interacts with FUSED IN SARCOMA (Burgute et al., 2014), a multifunctional protein involved in the regulation of alternative splicing and mRNA export from the nucleus to the cytoplasm. Taking together the recent results on human NKAP and our study of Arabidopsis MAS2, it seems plausible that NKAPs function in the regulation of the translation of aberrant or unspliced mRNAs, by regulating their nuclear export. This hypothesis provides an explanation for the observed suppression of *ago1-51* and *ago1-52* by the EMS-induced *mas2* alleles studied here, which seems to be due to partial correction of missplicing.

MAS2 Is an Essential Gene That Encodes a Multifunctional Protein

Whereas mammalian genes encoding NKAPs have been studied in some depth, little is known about NKAPs in *C. elegans* (LET-504) and Drosophila (CG6066). Human NKAP seems to be a multifunctional protein: It is a component of the Notch corepressor complex, it is required for proper T cell development (Pajerowski et al., 2009), and it plays an unknown role in splicing (Burgute et al., 2014).

Insertional disruption of the coding region of *MAS2* in the *mas2-2* and *mas2-3* lines caused embryonic lethality, as expected from the lethal phenotypes described for the lack-of-function mutations of *C. elegans*, Drosophila, and mammalian NKAP orthologs (Giot et al., 2003; Poulin et al., 2005; Pajerowski et al., 2009). The generation of transgenic plants carrying an artificial microRNA targeting *MAS2* mRNA allowed us to study the effects of the partial loss of function of *MAS2*; these plants displayed altered leaf morphology, early flowering, dwarfism, and partial loss of fertility. The embryonic lethality of *mas2-2* and *mas2-3* and the pleiotropic phenotype of *amiR-MAS2.1* plants indicate that *MAS2* is an essential gene required in multiple developmental processes.

MAS2 Is a Perinucleolar Protein That Interacts with Splicing and Ribosome Biogenesis Factors and Negatively Regulates 45S rRNA Expression

We found expression of *MAS2* was higher in cells undergoing active division, which require a continuous provision of proteins. MAS2 localized to the nucleus in a pattern that changed depending on the cell cycle: It was diffuse through the entire nucleus in actively dividing cells but became punctuate in differentiated cells. FISH analysis showed that MAS2 is a perinucleolar protein that colocalizes with the 45S rDNA genes.

The nucleolus is a multifunctional cellular compartment. In addition to ribosomal proteins, the Arabidopsis nucleolar proteome includes factors involved in mRNA biogenesis, splicing factors, and components of the exon-junction complex and the nonsense-mediated decay pathway, which participate in the degradation of aberrant mRNAs (Pendle et al., 2005). Aberrantly spliced mRNAs have been found to be enriched in the Arabidopsis nucleolus (Kim et al., 2009).

Perinucleolar localization of MAS2 is in agreement with our Y2H screen, which detected proteins predicted to function in nucleolar processes (Supplemental Table 3); this finding reinforces the hypothesis of a role for MAS2 in ribosome biogenesis and splicing. An indirect role for MAS2 in splicing is also plausible, as MAS2 interacts with factors directly acting in splicing or in regulation of splicing. MAS2 might also participate in mRNA quality control, preventing the translation of aberrant mRNAs. Further research will be required to analyze these possibilities.

The reduced methylation at the 45S rDNA promoters and the accumulation of unprocessed 45S pre-rRNAs observed in *amiR-MAS2.1* plants suggest that MAS2 participates in the regulation of 45S rDNA transcription and pre-45S rDNA processing. These molecular phenotypes are shared by the *nuc-L1* and *hda6* mutants; NUC-L1 and HDA6 participate in the silencing, transcription, and processing of 45S rDNA genes (Probst et al., 2004; Pontvianne et al., 2007; Earley et al., 2010; Pontvianne et al., 2010).

In addition, the similarity of the phenotype of *amiR-MAS2.1* plants and the phenotypes of mutants affecting ribosomal proteins and nucleolin as well as the synergistic interactions of *mas2* alleles and *nuc-L1* strongly suggest that MAS2 plays a key role in ribosome biogenesis together with or in parallel to nucleolin. The effects of *amiR-MAS2.1* on the methylation and accumulation of unprocessed 45S pre-rRNA were not as strong as those observed in the *nuc-L1* and *hda6* mutants, probably because *MAS2* expression is not completely abolished in *amiR-MAS2.1* plants.

NUC-L2 is a partially redundant paralog of *NUC-L1.* In contrast to the consequences of loss of function of *NUC-L1* and *MAS2*, loss of *NUC-L2* function causes hypermethylation of the 45S rDNA (Durut et al., 2014). Since our results suggest a functional relationship between *MAS2* and *NUC-L1*, and since loss of function of *NUC-L2* causes late flowering, a phenotype that is also opposite to that of *amiR-MAS2.1* plants, it should be interesting to examine whether MAS2 and NUC-L2 play antagonistic roles in the regulation of the expression of 45S rDNA and perhaps in the control of the transcription of other genes regulating flowering.

MAS2 and Human NKAP Likely Share DNA, RNA, and Protein Binding Preferences

Several lines of evidence indicate that MAS2 and human NKAP might share DNA, RNA, and protein binding preferences. A chromatin immunoprecipitation sequencing analysis revealed that human NKAP mainly binds to heterochromatic sequences, including those of centromeres (Burgute et al., 2014). Our FISH assays allowed us to visualize the colocalization of MAS2 and

the Arabidopsis NORs, which contain 45S rDNA linked to other heterochromatic regions, including the telomeric ends.

With regard to RNA binding preferences, several noncoding RNAs (ncRNAs), mainly small nucleolar RNAs and rRNAs, immunoprecipitate with human NKAP (Burgute et al., 2014). We did not carry out RNA binding assays, but we found that our suppressor *mas2* mutations modified the splicing and/or translational efficiency of the different *AGO1* or *ago1* mRNAs present in the *ago1-51* and *ago1-52* mutants. Additionally, MAS2 seems to be involved in the methylation of the promoters of 45S rDNA genes, which involves siRNAs (Earley et al., 2010). The SynMuv domain of human NKAP binds to RNA, and it has been suggested that the regulatory role of NKAP is mediated by its interaction with ncRNAs (Burgute et al., 2014). Due to the high sequence similarity between the SynMuv domains of MAS2 and human NKAP, we think it likely that MAS2 binds rRNAs, siRNAs, and other regulatory ncRNAs.

Finally, with regard to protein-protein interactions, human NKAP interacts with several types of RNA binding proteins, nuclear ribonuclear proteins, splicing factors, and RNA helicases involved in rRNA processing and splicing (Burgute et al., 2014). Our Y2H assays showed that MAS2 interacts with the previously mentioned classes of proteins (Supplemental Table 3). NKAP homologs have also been found in corepressor complexes in Drosophila and mammals. Drosophila CG6066 interacts with the ortholog of human CBF1-interacting corepressor (CIR) (CG6843) (Hsieh et al., 1999), a Notch corepressor complex component. NKAP associates with CIR and histone HDAC3 in human cells and its repressor activity depends on the interaction between its SynMuv domain and HDAC3 (Pajerowski et al., 2009). The Biological General Repository for Interaction Data sets (BioGRID; http://thebiogrid.org/; Stark et al., 2006) includes the interactions found in Y2H assays between E01A2.4, the *C. elegans* NKAP ortholog, and CIR-1 and the ribosomal protein RPL-22 (Boxem et al., 2008). In agreement with these results, we found that MAS2 physically interacts in a Y2H assay with a protein containing a CIR domain (encoded by At2g44200) and with the ribosomal protein RPS24B (Supplemental Table 3). Although we have not detected any physical interaction between MAS2 and any other protein with a known epigenetic role, our results suggest that MAS2 functions in both epigenetic regulation and splicing site selection or regulation of mRNA translation.

In conclusion, our study shows that MAS2, the single NKAP homolog present in the Arabidopsis genome, is a perinucleolar protein that colocalizes with 45S rDNA repeats and regulates 45S rRNA expression. The functional similarity between human NKAP and MAS2 seems to be very high. We consider that our work contributes to the characterization of a conserved factor that likely plays a key role in the regulation of plant gene expression.

METHODS

Plant Material and Growth Conditions

Arabidopsis thaliana L*er* and Col-0 wild-type accessions were obtained from the Nottingham Arabidopsis Stock Center (NASC) and then propagated at our institute for further analysis. Seeds of the SAIL_335_C06 and GABI_318G03 lines and the *parl1-2*, *hda6-6*, and *hda6-7* mutants were provided by NASC, and those of the CSHL_GT188551 line were provided by R. Martienssen. Seed sterilization and sowing, plant culture, and crosses were performed as previously described (Ponce et al., 1998; Berná et al., 1999). When required, culture media were supplemented with kanamycin (50 $\mu g \cdot mL^{-1}$), hygromycin (15 $\mu g \cdot mL^{-1}$), or Basta (5 $\mu g \cdot mL^{-1}$).

Positional Cloning and Molecular Characterization of *MAS2* and Its Mutant Alleles

Genomic DNA was extracted as described by Ponce et al. (2006). Fine mapping of the *mas2-1* mutation was performed by iterative linkage analysis as previously described (Ponce et al., 1999, 2006) using the primers listed in Supplemental Table 1. The *mas2* point mutations were identified by sequencing, using the At402720_F1, At402720_R1, At402720_F2, and At402720_R2 primers (Supplemental Table 2). Sequencing reactions and electrophoresis were performed with ABI PRISM BigDye Terminator Cycle Sequencing kits and on an ABI PRISM 3130xl Genetic Analyzer (Applied Biosystems), respectively. The presence of T-DNA insertions was verified by PCR using the SAIL_LB1 and At402720_R2 primers (SAIL_335_C06; *mas2-2*) and At402720_F1, Ds3_1, At402720_F1, and At402720_1R (CSHL_GT188551; *mas2-3*) primers (Supplemental Table 2). Discrimination between *MAS2* and *mas2-1* alleles was done by PCR amplification with At402720_F2 and At402720_R1 primers followed by digestion with *Bsa*HI, as the *mas2-1* mutation (GACGCC→GACACC) eliminates the *Bsa*HI restriction site.

RNA Isolation, Reverse Transcription, and RT-qPCR Analysis

Total RNA was isolated from 50 to 100 mg of rosettes with the TRI RNA isolation reagent (Sigma-Aldrich). Since *MAS2* lacks introns, prior to cDNA synthesis the RNA was treated with TURBO DNase (Ambion). Reverse transcription and RT-qPCR analyses were performed as described by Jover-Gil et al. (2012). RT-qPCR amplifications were performed on a Step-One Real-Time PCR System (Applied Biosystems). The *OTC* housekeeping gene (Quesada et al., 1999) was used as an internal control, as previously described (Cnops et al., 2004).

Construction of Transgenes and Transgenic Lines

To generate constructs for Gateway cloning, we performed PCR amplifications with the Phusion High-Fidelity DNA Polymerase (Finnzymes) and primers containing the attB1 (forward) or attB2 (reverse) sequences at their 5′ ends (Supplemental Table 2). Before being cloned into the pGEM-T Easy221 entry vector, PCR products were purified with the Illustra GFX PCR DNA and Gel Band Purification Kit (GE Healthcare Bio-Sciences). The entry and destination clones were obtained in 2.5-μL reactions using 1 μL of the BP and LR Clonase II kit (Life Technologies), respectively. Chemically competent *Escherichia coli* DH5α cells were transformed by the heat shock method; *Agrobacterium tumefaciens* C58C1 cells carrying the pSOUP helper plasmid were electroporated.

To obtain the $35S_{pro}$*:MAS2*, $35S_{pro}$*:mas2-1*, and $35S_{pro}$*:MAS2:GFP* overexpression constructs, the full-length coding sequences of *MAS2* and *mas2-1* were PCR amplified from L*er* and *ago1-52 mas2-1* plants, respectively. The destination vector pMDC32 was used for $35S_{pro}$*:MAS2* and $35S_{pro}$*:mas2-1*, and pMDC85 for $35S_{pro}$*:MAS2:GFP*. A 1.1-kb DNA region upstream of the translation start codon of the *MAS2* gene was used as promoter in the $MAS2_{pro}$*:GUS* and $MAS2_{pro}$*:MAS2:GFP* constructs. The fragments were obtained by PCR and subcloned into the pMDC162 and pMDC111 destination vectors, respectively. To obtain GFP translational fusions, the coding regions of *MAS2* and *mas2-1* lacking their stop codons were PCR amplified from L*er* and *ago1-52 mas2-1* plants,

respectively. All constructs were sequence verified before being transferred into plants, which was performed by the floral dip method (Clough and Bent, 1998). Primers used for obtaining these constructs and for sequencing them are described in Supplemental Table 2.

Arabidopsis transgenic lines expressing the *amiR-MAS2* artificial microRNA (5′-UAUACGUUUACCUUGCUGGAC-3′) were obtained as described in Jover-Gil et al. (2014).

Plant Gross Morphology and Histology, and Histochemical Assays

Leaf venation diagrams were obtained from first- and third-node leaves as described previously (Candela et al., 1999; Alonso-Peral et al., 2006). For histological analyses, first- and third-node leaves were fixed with FAA/Triton (1.85% formaldehyde, 45% ethanol, 5% acetic acid, and 1% Triton X-100) as described by Serrano-Cartagena et al. (2000). After dehydration, tissues were embedded in Technovit 7100 resin (Heraeus Kulzer) following the manufacturer's instructions. Sections of 7-mm thickness were cut on a Microm International HM350S microtome and stained with 0.1% (w/v) Toluidine blue. GUS assays were performed as described by Robles et al. (2010). In vivo visualization of MAS2 subcellular localization was performed in root cells of plants carrying MAS2-GFP fusion proteins. For nuclear staining, plant tissue was submerged in 1 $\mu g \cdot mL^{-1}$ DAPI for 30 s and then rinsed in water. Micrographs were taken on a Nikon D-Eclipse C1 confocal microscope.

Immunoblot Assay

Proteins were extracted with TRI reagent (Sigma-Aldrich) from 50 to 100 mg of material of plants collected at 15 DAS, precipitated with isopropanol, washed three times with 0.3 M guanidine-HCl (96% ethanol), and resuspended into resuspension buffer (8 M urea, 40 mM Tris-HCl, pH 6.8, 0.1 mM EDTA, and 1% SDS). Each protein extract (160 µg) was loaded in a 7% polyacrylamide gel. SDS-PAGE and electrotransfer to nitrocellulose were performed as previously described (Esteve-Bruna et al., 2013). Two primary antibodies were used: against AGO1 (Agrisera; AS09 527P) at 1:500 dilution and against the large subunit of Rubisco (Agrisera; AS03 037) at 1:500 to 1:2500 dilution.

FISH

Tissue preparation and FISH were performed as previously described (Armstrong and Hultén, 1998; Fransz et al., 1998; Sanchez Moran et al., 2001) with minor modifications. Flower buds were collected into a 50-mL Falcon tube and kept in ice-cold water at 4°C for 64 h to accumulate cells in mitotic metaphase. After three washes in citrate buffer (pH 4.5), tissue was incubated with a mixture of 2% (w/v) Cellulase Onozuka R-10 and 2% (w/v) Macerozyme R-10 (Duchefa Biochemie) in citrate buffer at 37°C for 2 h in a humid hybridization chamber before being macerated with a needle. A biotin-labeled 45S rDNA probe (pTa71; Gerlach and Bedbrook, 1979) and a 1:260 dilution of streptavidin-Cy3 (Roche) antibody in TNB buffer (100 mM Tris-HCl, pH 7.5, 150 mM NaCl, and 0.5% nonfat dry milk as a blocking reagent) were used. Confocal laser scanning microscopy images were obtained and digitally processed using the EZ-C1 operation software for a Nikon D-Eclipse C1 microscope.

Analysis of the Methylation Status of the 45S rDNA Promoter

Genomic DNA was extracted and digested with the methylation-sensitive *Hpa*II restriction endonuclease. Cleavage by *Hpa*II of the 5′-CCGG-3′ tetranucleotide is blocked by the presence of 5-MeC at this site (5′-C^{me}CGG-3′). Digested and nondigested DNA was used as template for quantitative PCR amplifications using the p2f and p2r primers, which flank the restriction sites (Supplemental Table 2; Harscoët et al., 2010). The 25S rRNA gene was amplified with the 25SrRNA_F/R primer set and used as an endogenous control for quantitative PCR experiments. Bars represent the ratio between levels of PCR amplification products representing digested and nondigested fragments.

Accession Numbers

Sequence data from this article can be found in The Arabidopsis Information Resource (http://www.arabidopsis.org/) under the following accession numbers: *MAS2* (At4g02720), *AGO1* (At1g48410), *NUC-L1* (At1g48920), and *HDA6* (At5g63110).

Supplemental Data

Supplemental Figure 1. Positional cloning of the *MAS2* gene.

Supplemental Figure 2. Molecular nature and position of *mas2* point mutations.

Supplemental Figure 3. Sequence conservation among eukaryotic NKAPs.

Supplemental Figure 4. Sequence conservation among plant NKAPs.

Supplemental Figure 5. *ago1* alleles used in this work.

Supplemental Figure 6. Morphological phenotype of *ago1-51 mas2-1* adult plants.

Supplemental Figure 7. Effects of the *mas2* mutations on the levels of *AGO1* splice variants.

Supplemental Figure 8. Visualization of AGO1 protein isoforms in *ago1* mutants.

Supplemental Figure 9. Phenotypic effects of the overexpression of *MAS2* and *mas2-1* on the L*er*, *ago1-51*, and *ago1-52* backgrounds at the rosette stage.

Supplemental Figure 10. Phenotypic effects of the overexpression of *mas2-1* on the *ago1-52* background in adult plants.

Supplemental Figure 11. Phenotypic effects of the overexpression of *mas2-1* on the *ago1-51* background in adult plants.

Supplemental Figure 12. Analysis of the of GABI_318G03 insertional line.

Supplemental Figure 13. Seeds and embryos of *MAS2/mas2-2* plants.

Supplemental Figure 14. Morphological phenotypes caused by the *amiR-MAS2* transgene in different genetic backgrounds.

Supplemental Figure 15. Histology of *amiR-MAS2.1* leaves.

Supplemental Figure 16. Levels of the *AGO1* splice variants in *ago1-52 amiR-MAS2.1* plants.

Supplemental Figure 17. Visualization of $MAS2_{pro}$*:GUS* activity in wild-type plants.

Supplemental Figure 18. Spatial pattern of expression of *MAS2*.

Supplemental Figure 19. Subcellular localization of the MAS2:GFP and MAS2-1:GFP proteins.

Supplemental Figure 20. Subcellular localization of the MAS2:GFP protein in cells of the root elongation zone from homozygous $35S_{pro}$*:MAS2:GFP* plants.

Supplemental Figure 21. Effects of *amiR-MAS2.1* on 45S rRNA processing.

Supplemental Table 1. Primer sets used for the fine mapping of *MAS2*.

Supplemental Table 2. Other primer sets used in this work.

Supplemental Table 3. Results of a Y2H-based screen using MAS2 as a bait.

Supplemental References.

ACKNOWLEDGMENTS

We thank R. Sarmiento-Mañús, J.M. Serrano, F.M. Lozano, T. Trujillo, and D. Navarro for their excellent technical assistance, J.L. Santos, M. Pradillo, and F.J. Medina for their help and advice, J.L. Micol for useful discussions and comments on the article as well as for the use of his facilities, B. Scheres for the pGEM-T Easy221 vector, and J. Simorowski and R. Martienssen for the CSHL_GT188551 line. This research was supported by grants from the Ministerio de Economía y Competitividad of Spain (BIO2008-01900 and BIO2014-56889-R) and the Generalitat Valenciana (PROMETEO/2009/112 and PROMETEOII/2014/006) to M.R.P.

AUTHOR CONTRIBUTIONS

M.R.P. conceived and designed research. M.R.P., A.B.S.-G., V.A., R.M.-P., and S.J.-G. performed research and analyzed data. M.R.P., R.M.-P., S.J.-G., and A.B.S.-G. wrote the article.

Received February 12, 2015; revised June 2, 2015; accepted June 12, 2015; published July 2, 2015.

REFERENCES

Abou-Ellail, M., Cooke, R., and Sáez-Vásquez, J. (2011). Variations in a team: major and minor variants of *Arabidopsis thaliana* rDNA genes. Nucleus **2:** 294–299.

Alonso-Peral, M.M., Candela, H., del Pozo, J.C., Martínez-Laborda, A., Ponce, M.R., and Micol, J.L. (2006). The *HVE/CAND1* gene is required for the early patterning of leaf venation in Arabidopsis. Development **133:** 3755–3766.

Arabidopsis Interactome Mapping Consortium (2011). Evidence for network evolution in an Arabidopsis interactome map. Science **333:** 601–607.

Armstrong, S.J., and Hultén, M.A. (1998). Meiotic segregation analysis by FISH investigations in sperm and spermatocytes of translocation heterozygotes. Eur. J. Hum. Genet. **6:** 430–431.

Bartel, D.P. (2009). MicroRNAs: target recognition and regulatory functions. Cell **136:** 215–233.

Berná, G., Robles, P., and Micol, J.L. (1999). A mutational analysis of leaf morphogenesis in *Arabidopsis thaliana.* Genetics **152:** 729–742.

Bessonov, S., Anokhina, M., Will, C.L., Urlaub, H., and Lührmann, R. (2008). Isolation of an active step I spliceosome and composition of its RNP core. Nature **452:** 846–850.

Bessonov, S., Anokhina, M., Krasauskas, A., Golas, M.M., Sander, B., Will, C.L., Urlaub, H., Stark, H., and Lührmann, R. (2010). Characterization of purified human Bact spliceosomal complexes reveals compositional and morphological changes during spliceosome activation and first step catalysis. RNA **16:** 2384–2403.

Bohmert, K., Camus, I., Bellini, C., Bouchez, D., Caboche, M., and Benning, C. (1998). *AGO1* defines a novel locus of *Arabidopsis* controlling leaf development. EMBO J. **17:** 170–180.

Boxem, M., et al. (2008). A protein domain-based interactome network for *C. elegans* early embryogenesis. Cell **134:** 534–545.

Bray, S.J. (2006). Notch signalling: a simple pathway becomes complex. Nat. Rev. Mol. Cell Biol. **7:** 678–689.

Burgute, B.D., Peche, V.S., Steckelberg, A.L., Glöckner, G., Gaßen, B., Gehring, N.H., and Noegel, A.A. (2014). NKAP is a novel RS-related protein that interacts with RNA and RNA binding proteins. Nucleic Acids Res. **42:** 3177–3193.

Campbell, D.A. (1992). *Bodo caudatus* medRNA and 5S rRNA genes: tandem arrangement and phylogenetic analyses. Biochem. Biophys. Res. Commun. **182:** 1053–1058.

Candela, H., Martínez-Laborda, A., and Micol, J.L. (1999). Venation pattern formation in *Arabidopsis thaliana* vegetative leaves. Dev. Biol. **205:** 205–216.

Casanova-Sáez, R., Candela, H., and Micol, J.L. (2014). Combined haploinsufficiency and purifying selection drive retention of *RPL36a* paralogs in Arabidopsis. Sci. Rep. **4:** 4122.

Ceron, J., Rual, J.F., Chandra, A., Dupuy, D., Vidal, M., and van den Heuvel, S. (2007). Large-scale RNAi screens identify novel genes that interact with the *C. elegans* retinoblastoma pathway as well as splicing-related components with synMuv B activity. BMC Dev. Biol. **7:** 30–45.

Chen, D., Li, Z., Yang, Q., Zhang, J., Zhai, Z., and Shu, H.B. (2003). Identification of a nuclear protein that promotes NF-kappaB activation. Biochem. Biophys. Res. Commun. **310:** 720–724.

Cheng, N.H., Liu, J.Z., Nelson, R.S., and Hirschi, K.D. (2004). Characterization of CXIP4, a novel *Arabidopsis* protein that activates the H^+/Ca^{2+} antiporter, CAX1. FEBS Lett. **559:** 99–106.

Cloix, C., Tutois, S., Yukawa, Y., Mathieu, O., Cuvillier, C., Espagnol, M.C., Picard, G., and Tourmente, S. (2002). Analysis of the 5S RNA pool in *Arabidopsis thaliana*: RNAs are heterogeneous and only two of the genomic 5S loci produce mature 5S RNA. Genome Res. **12:** 132–144.

Clough, S.J., and Bent, A.F. (1998). Floral dip: a simplified method for *Agrobacterium*-mediated transformation of *Arabidopsis thaliana.* Plant J. **16:** 735–743.

Cnops, G., Jover-Gil, S., Peters, J.L., Neyt, P., De Block, S., Robles, P., Ponce, M.R., Gerats, T., Micol, J.L., and Van Lijsebettens, M. (2004). The *rotunda2* mutants identify a role for the *LEUNIG* gene in vegetative leaf morphogenesis. J. Exp. Bot. **55:** 1529–1539.

Costa-Nunes, P., Pontes, O., Preuss, S.B., and Pikaard, C.S. (2010). Extra views on RNA-dependent DNA methylation and MBD6-dependent heterochromatin formation in nucleolar dominance. Nucleus **1:** 254–259.

Creff, A., Sormani, R., and Desnos, T. (2010). The two Arabidopsis *RPS6* genes, encoding for cytoplasmic ribosomal proteins S6, are functionally equivalent. Plant Mol. Biol. **73:** 533–546.

Durut, N., et al. (2014). A duplicated *NUCLEOLIN* gene with antagonistic activity is required for chromatin organization of silent 45S rDNA in Arabidopsis. Plant Cell **26:** 1330–1344.

Earley, K.W., Pontvianne, F., Wierzbicki, A.T., Blevins, T., Tucker, S., Costa-Nunes, P., Pontes, O., and Pikaard, C.S. (2010). Mechanisms of HDA6-mediated rRNA gene silencing: suppression of intergenic Pol II transcription and differential effects on maintenance versus siRNA-directed cytosine methylation. Genes Dev. **24:** 1119–1132.

Esteve-Bruna, D., Pérez-Pérez, J.M., Ponce, M.R., and Micol, J.L. (2013). *incurvata13*, a novel allele of *AUXIN RESISTANT6*, reveals a specific role for auxin and the SCF complex in Arabidopsis embryogenesis, vascular specification, and leaf flatness. Plant Physiol. **161:** 1303–1320.

Ferguson, E.L., and Horvitz, H.R. (1985). Identification and characterization of 22 genes that affect the vulval cell lineages of the nematode *Caenorhabditis elegans.* Genetics **110:** 17–72.

Ferguson, E.L., and Horvitz, H.R. (1989). The multivulva phenotype of certain *Caenorhabditis elegans* mutants results from defects in two functionally redundant pathways. Genetics **123:** 109–121.

Ferguson, E.L., Sternberg, P.W., and Horvitz, H.R. (1987). A genetic pathway for the specification of the vulval cell lineages of *Caenorhabditis elegans.* Nature **326:** 259–267.

Fernández-Nohales, P., Domenech, M.J., Martínez de Alba, A.E., Micol, J.L., Ponce, M.R., and Madueño, F. (2014). AGO1 controls arabidopsis inflorescence architecture possibly by regulating *TFL1* expression. Ann. Bot. (Lond.) **114:** 1471–1481.

Fransz, P., Armstrong, S., Alonso-Blanco, C., Fischer, T.C., Torres-Ruiz, R.A., and Jones, G. (1998). Cytogenetics for the model system *Arabidopsis thaliana.* Plant J. **13:** 867–876.

Gerlach, W.L., and Bedbrook, J.R. (1979). Cloning and characterization of ribosomal RNA genes from wheat and barley. Nucleic Acids Res. **7:** 1869–1885.

Giot, L., et al. (2003). A protein interaction map of *Drosophila melanogaster.* Science **302:** 1727–1736.

Granato, D.C., Machado-Santelli, G.M., and Oliveira, C.C. (2008). Nop53p interacts with 5.8S rRNA co-transcriptionally, and regulates processing of pre-rRNA by the exosome. FEBS J. **275:** 4164–4178.

Gruendler, P., Unfried, I., Pointner, R., and Schweizer, D. (1989). Nucleotide sequence of the 25S-18S ribosomal gene spacer from *Arabidopsis thaliana.* Nucleic Acids Res. **17:** 6395–6396.

Gruendler, P., Unfried, I., Pascher, K., and Schweizer, D. (1991). rDNA intergenic region from *Arabidopsis thaliana*. Structural analysis, intraspecific variation and functional implications. J. Mol. Biol. **221:** 1209–1222.

Grummt, I. (2003). Life on a planet of its own: regulation of RNA polymerase I transcription in the nucleolus. Genes Dev. **17:** 1691–1702.

Guan, Q., Wu, J., Zhang, Y., Jiang, C., Liu, R., Chai, C., and Zhu, J. (2013). A DEAD box RNA helicase is critical for pre-mRNA splicing, cold-responsive gene regulation, and cold tolerance in *Arabidopsis.* Plant Cell **25:** 342–356.

Harscoët, E., Dubreucq, B., Palauqui, J.C., and Lepiniec, L. (2010). *NOF1* encodes an Arabidopsis protein involved in the control of rRNA expression. PLoS ONE **5:** e12829.

He, D., Fiz-Palacios, O., Fu, C.J., Fehling, J., Tsai, C.C., and Baldauf, S.L. (2014). An alternative root for the eukaryote tree of life. Curr. Biol. **24:** 465–470.

Hodgkin, J. (2005). Genetic suppression. In WormBook: The Online Review of *C. elegans* Biology, doi/10.1895/wormbook.1.59.1.

Horiguchi, G., Mollá-Morales, A., Pérez-Pérez, J.M., Kojima, K., Robles, P., Ponce, M.R., Micol, J.L., and Tsukaya, H. (2011). Differential contributions of ribosomal protein genes to *Arabidopsis thaliana* leaf development. Plant J. **65:** 724–736.

Horvitz, H.R., and Sulston, J.E. (1980). Isolation and genetic characterization of cell-lineage mutants of the nematode *Caenorhabditis elegans.* Genetics **96:** 435–454.

Howell, A.M., and Rose, A.M. (1990). Essential genes in the *hDf6* region of chromosome I in *Caenorhabditis elegans.* Genetics **126:** 583–592.

Hsieh, J.J., Zhou, S., Chen, L., Young, D.B., and Hayward, S.D. (1999). CIR, a corepressor linking the DNA binding factor CBF1 to the histone deacetylase complex. Proc. Natl. Acad. Sci. USA **96:** 23–28.

Ilagan, J.O., Chalkley, R.J., Burlingame, A.L., and Jurica, M.S. (2013). Rearrangements within human spliceosomes captured after exon ligation. RNA **19:** 400–412.

Ito, T., Kim, G.T., and Shinozaki, K. (2000). Disruption of an *Arabidopsis* cytoplasmic ribosomal protein S13-homologous gene by transposon-mediated mutagenesis causes aberrant growth and development. Plant J. **22:** 257–264.

Jones-Rhoades, M.W., Bartel, D.P., and Bartel, B. (2006). MicroRNAS and their regulatory roles in plants. Annu. Rev. Plant Biol. **57:** 19–53.

Jover-Gil, S., Candela, H., and Ponce, M.R. (2005). Plant microRNAs and development. Int. J. Dev. Biol. **49:** 733–744.

Jover-Gil, S., Candela, H., Robles, P., Aguilera, V., Barrero, J.M., Micol, J.L., and Ponce, M.R. (2012). The microRNA pathway genes *AGO1, HEN1* and *HYL1* participate in leaf proximal-distal, venation and stomatal patterning in Arabidopsis. Plant Cell Physiol. **53:** 1322–1333.

Jover-Gil, S., Paz-Ares, J., Micol, J.L., and Ponce, M.R. (2014). Multi-gene silencing in Arabidopsis: a collection of artificial microRNAs targeting groups of paralogs encoding transcription factors. Plant J. **80:** 149–160.

Jurica, M.S., and Moore, M.J. (2002). Capturing splicing complexes to study structure and mechanism. Methods **28:** 336–345.

Kim, S.H., Koroleva, O.A., Lewandowska, D., Pendle, A.F., Clark, G.P., Simpson, C.G., Shaw, P.J., and Brown, J.W. (2009). Aberrant mRNA transcripts and the nonsense-mediated decay proteins UPF2 and UPF3 are enriched in the Arabidopsis nucleolus. Plant Cell **21:** 2045–2057.

Laferté, A., Favry, E., Sentenac, A., Riva, M., Carles, C., and Chédin, S. (2006). The transcriptional activity of RNA polymerase I is a key determinant for the level of all ribosome components. Genes Dev. **20:** 2030–2040.

Lam, S.Y., Horn, S.R., Radford, S.J., Housworth, E.A., Stahl, F.W., and Copenhaver, G.P. (2005). Crossover interference on nucleolus organizing region-bearing chromosomes in Arabidopsis. Genetics **170:** 807–812.

Lawrence, R.J., Earley, K., Pontes, O., Silva, M., Chen, Z.J., Neves, N., Viegas, W., and Pikaard, C.S. (2004). A concerted DNA methylation/histone methylation switch regulates rRNA gene dosage control and nucleolar dominance. Mol. Cell **13:** 599–609.

Layat, E., Sáez-Vásquez, J., and Tourmente, S. (2012). Regulation of Pol I-transcribed 45S rDNA and Pol III-transcribed 5S rDNA in Arabidopsis. Plant Cell Physiol. **53:** 267–276.

Luo, L., Ando, S., Sasabe, M., Machida, C., Kurihara, D., Higashiyama, T., and Machida, Y. (2012). Arabidopsis ASYMMETRIC LEAVES2 protein required for leaf morphogenesis consistently forms speckles during mitosis of tobacco BY-2 cells via signals in its specific sequence. J. Plant Res. **125:** 661–668.

Mallory, A., and Vaucheret, H. (2010). Form, function, and regulation of ARGONAUTE proteins. Plant Cell **22:** 3879–3889.

Micol-Ponce, R., Aguilera, V., and Ponce, M.R. (2014). A genetic screen for suppressors of a hypomorphic allele of Arabidopsis *ARGONAUTE1.* Sci. Rep. **4:** 5533.

Morel, J.B., Godon, C., Mourrain, P., Béclin, C., Boutet, S., Feuerbach, F., Proux, F., and Vaucheret, H. (2002). Fertile hypomorphic *ARGONAUTE* (*ago1*) mutants impaired in post-transcriptional gene silencing and virus resistance. Plant Cell **14:** 629–639.

Murfett, J., Wang, X.J., Hagen, G., and Guilfoyle, T.J. (2001). Identification of Arabidopsis histone deacetylase HDA6 mutants that affect transgene expression. Plant Cell **13:** 1047–1061.

Pajerowski, A.G., Nguyen, C., Aghajanian, H., Shapiro, M.J., and Shapiro, V.S. (2009). NKAP is a transcriptional repressor of notch signaling and is required for T cell development. Immunity **30:** 696–707.

Pendle, A.F., Clark, G.P., Boon, R., Lewandowska, D., Lam, Y.W., Andersen, J., Mann, M., Lamond, A.I., Brown, J.W., and Shaw, P.J. (2005). Proteomic analysis of the Arabidopsis nucleolus suggests novel nucleolar functions. Mol. Biol. Cell **16:** 260–269.

Petricka, J.J., and Nelson, T.M. (2007). Arabidopsis nucleolin affects plant development and patterning. Plant Physiol. **144:** 173–186.

Ponce, M.R., Quesada, V., and Micol, J.L. (1998). Rapid discrimination of sequences flanking and within T-DNA insertions in the *Arabidopsis* genome. Plant J. **14:** 497–501.

Ponce, M.R., Robles, P., and Micol, J.L. (1999). High-throughput genetic mapping in *Arabidopsis thaliana.* Mol. Gen. Genet. **261:** 408–415.

Ponce, M.R., Robles, P., Lozano, F.M., Brotóns, M.A., and Micol, J.L. (2006). Low-resolution mapping of untagged mutations. Methods Mol. Biol. **323:** 105–113.

Pontvianne, F., Matía, I., Douet, J., Tourmente, S., Medina, F.J., Echeverria, M., and Sáez-Vásquez, J. (2007). Characterization of *AtNUC-L1* reveals a central role of nucleolin in nucleolus organization and silencing of *AtNUC-L2* gene in *Arabidopsis.* Mol. Biol. Cell **18:** 369–379.

Pontvianne, F., et al. (2010). Nucleolin is required for DNA methylation state and the expression of rRNA gene variants in *Arabidopsis thaliana.* PLoS Genet. **6:** e1001225.

Poulin, G., Dong, Y., Fraser, A.G., Hopper, N.A., and Ahringer, J. (2005). Chromatin regulation and sumoylation in the inhibition of Ras-induced vulval development in *Caenorhabditis elegans.* EMBO J. **24:** 2613–2623.

Prelich, G. (1999). Suppression mechanisms: themes from variations. Trends Genet. **15:** 261–266.

Probst, A.V., Fagard, M., Proux, F., Mourrain, P., Boutet, S., Earley, K., Lawrence, R.J., Pikaard, C.S., Murfett, J., Furner, I., Vaucheret, H., and Mittelsten Scheid, O. (2004). Arabidopsis histone deacetylase *HDA6* is required for maintenance of transcriptional gene silencing and determines nuclear organization of rDNA repeats. Plant Cell **16:** 1021–1034.

Quesada, V., Ponce, M.R., and Micol, J.L. (1999). *OTC* and *AUL1*, two convergent and overlapping genes in the nuclear genome of *Arabidopsis thaliana.* FEBS Lett. **461:** 101–106.

Rogers, K., and Chen, X. (2013). Biogenesis, turnover, and mode of action of plant microRNAs. Plant Cell **25:** 2383–2399.

Robles, P., Fleury, D., Candela, H., Cnops, G., Alonso-Peral, M.M., Anami, S., Falcone, A., Caldana, C., Willmitzer, L., Ponce, M.R., Van Lijsebettens, M., and Micol, J.L. (2010). The *RON1/FRY1/SAL1* gene is required for leaf morphogenesis and venation patterning in Arabidopsis. Plant Physiol. **152:** 1357–1372.

Sadasivam, S., and DeCaprio, J.A. (2013). The DREAM complex: master coordinator of cell cycle-dependent gene expression. Nat. Rev. Cancer **13:** 585–595.

Saffer, A.M., Kim, D.H., van Oudenaarden, A., and Horvitz, H.R. (2011). The *Caenorhabditis elegans* synthetic multivulva genes prevent ras pathway activation by tightly repressing global ectopic expression of *lin-3* EGF. PLoS Genet. **7:** e1002418.

Sanchez Moran, E., Armstrong, S.J., Santos, J.L., Franklin, F.C., and Jones, G.H. (2001). Chiasma formation in *Arabidopsis thaliana* accession Wassilewskija and in two meiotic mutants. Chromosome Res. **9:** 121–128.

Schwacke, R., Schneider, A., van der Graaff, E., Fischer, K., Catoni, E., Desimone, M., Frommer, W.B., Flügge, U.I., and Kunze, R. (2003). ARAMEMNON, a novel database for Arabidopsis integral membrane proteins. Plant Physiol. **131:** 16–26.

Serrano-Cartagena, J., Candela, H., Robles, P., Ponce, M.R., Pérez-Pérez, J.M., Piqueras, P., and Micol, J.L. (2000). Genetic analysis of *incurvata* mutants reveals three independent genetic operations at work in Arabidopsis leaf morphogenesis. Genetics **156:** 1363–1377.

Shi, D.Q., Liu, J., Xiang, Y.H., Ye, D., Sundaresan, V., and Yang, W.C. (2005). *SLOW WALKER1*, essential for gametogenesis in Arabidopsis, encodes a WD40 protein involved in 18S ribosomal RNA biogenesis. Plant Cell **17:** 2340–2354.

Stark, C., Breitkreutz, B.J., Reguly, T., Boucher, L., Breitkreutz, A., and Tyers, M. (2006). BioGRID: a general repository for interaction datasets. Nucleic Acids Res. **34:** D535–D539.

Unfried, I., Stocker, U., and Gruendler, P. (1989). Nucleotide sequence of the 18S rRNA gene from *Arabidopsis thaliana* Col-0. Nucleic Acids Res. **17:** 7513.

Van Lijsebettens, M., Vanderhaeghen, R., De Block, M., Bauw, G., Villarroel, R., and Van Montagu, M. (1994). An S18 ribosomal protein gene copy at the *Arabidopsis PFL* locus affects plant development by its specific expression in meristems. EMBO J. **13:** 3378–3388.

Voinnet, O. (2009). Origin, biogenesis, and activity of plant microRNAs. Cell **136:** 669–687.

Yildirim, O., Li, R., Hung, J.H., Chen, P.B., Dong, X., Ee, L.S., Weng, Z., Rando, O.J., and Fazzio, T.G. (2011). Mbd3/NURD complex regulates expression of 5-hydroxymethylcytosine marked genes in embryonic stem cells. Cell **147:** 1498–1510.

Arabidopsis *MAS2*, an essential gene that encodes a homolog of animal NF-kappa B Activating Protein, is involved in 45S ribosomal DNA silencing

Ana Belén Sánchez-García, Verónica Aguilera, Rosa Micol-Ponce, Sara Jover-Gil and María Rosa Ponce

Instituto de Bioingeniería, Universidad Miguel Hernández, Campus de Elche, 03202 Elche, Alicante, Spain.

Supplemental figures, tables and references

Supplemental Data. Sánchez-García et al. Plant Cell (2015) 10.1105/tpc.15.00135

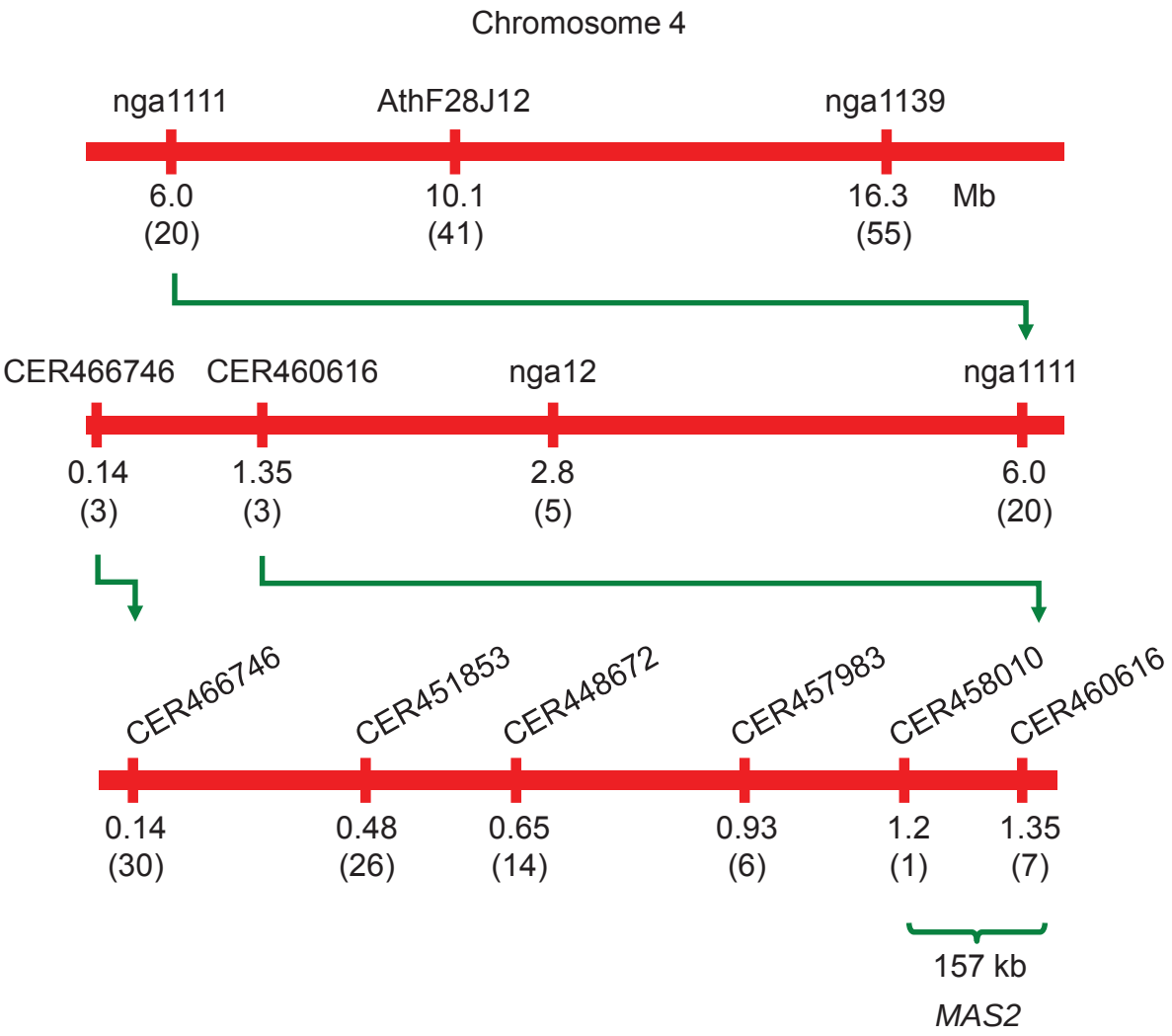

Supplemental Figure 1. Positional cloning of the *MAS2* gene.
The molecular markers used for linkage analysis, their map positions (in Mb) and the number of informative recombinants identified (in parentheses) are indicated. F_2 mapping populations were obtained from two P2 11.1 x Col-0 crosses. A total of 319 F_2 plants, exhibiting either the Ago1-52 suppressed or Ago1-52 phenotypes, were separately subjected to linkage analysis. Linkage to the L*er* alleles of the markers tested was detected at the proximity to the *AGO1* locus (at chromosome 1), among plants from both phenotypic classes. Unequivocal linkage to the Col-0 alleles of the markers under study was only seen at the top of chromosome 4 in plants of the Ago1-52 class, as expected for the wild-type allele (*MAS2*) of a dominant mutation (*mas2-1*; Micol-Ponce et al., 2014). The genotypes of the Ago1-52 suppressed and Ago1-52 phenotypic classes were then inferred to be *ago1-52/ago1-52; mas2-1/-* and *ago1-52/ago1-52; MAS2/MAS2*, respectively.

Supplemental Data. Sánchez-García et al. Plant Cell (2015) 10.1105/tpc.15.00135

```
Ler      (MAS2)      162 GCCAAGTTCTGCTTTTGGGAGAACACACCGAGTCCACCTAGAGATCAGAACGTTCAGCA
P7 13.l (mas2-11)        GCCAAGTTCTGCTTTTGGGAGAACACACTGAGTCCACCTAGAGATCAGTATGTTCAGCA

Ler      (MAS2)      898 AGTTATGGTGGTGCTTTAAGACCCGGTGAAGGAGACGCCATAGCACAGTATGTTCAGCA
P2 11.1 (mas2-1)         AGTTATGGTGGTGCTTTAAGACCCGGTGAAGGAGACACCATAGCACAGTATGTTCAGCA
Pl 3.1  (mas2-4)         AGTTATGGTGGTGCTTTAAGACCCGGTGAAGGAGACGTCATAGCACAGTATGTTCAGCA
Pl 5.33 (mas2-5)         AGTTATGGTGGTGCTTTAAGACCCAGTGAAGGAGACGCCATAGCACAGTATGTTCAGCA
P6 65.2 (mas2-6a)        AGTTATGGTGGTGCTTTAAGACCCGGTGAAGAAGACGCCATAGCACAGTATGTTCAGCA
P6 66.2 (mas2-6b)        AGTTATGGTGGTGCTTTAAGACCCGGTGAAGAAGACGCCATAGCACAGTATGTTCAGCA
P8 44.1 (mas2-7)         AGTTATGGTGGTGCTTTAAGACCCGATGAAGGAGACGCCATAGCACAGTATGTTCAGCA
Pll 1.1 (mas2-8)         AGTTATAGTGGTGCTTTAAGACCCGGTGAAGGAGACGCCATAGCACAGTATGTTCAGCG
P12 1.l (mas2-9)         AGTTATGGTGGTGCTTTAAGACCCGATGAAGGAGACGCCATAGCACAGTATGTTCAGCA
Pl3 1.l (mas2-10)        AGTTATGGTGGTGCTTTAAGACCCGGTGAAGAAGACGCCATAGCACAGTATGTTCAGCA
```

Supplemental Figure 2. Molecular nature and position of *mas2* point mutations.
Multiple alignment of the sequences of the regions of the *MAS2* gene where the *mas2* point mutations map. Numbers (162 and 898) indicate nucleotide positions, counting from the start codon. The mutated nucleotides are shown in red. Both protocol numbers (PX Y.Z) and allele names are indicated for each suppressor line. The *mas2-6* allele was isolated twice (*mas2-6a* and *mas2-6b*); it was carried by two different suppressor lines (P6 65.2 and P6 66.2) obtained from seeds of the same parental group (P6).

Supplemental Data. Sánchez-García et al. Plant Cell 2015 10.1105/tpc.15.00135

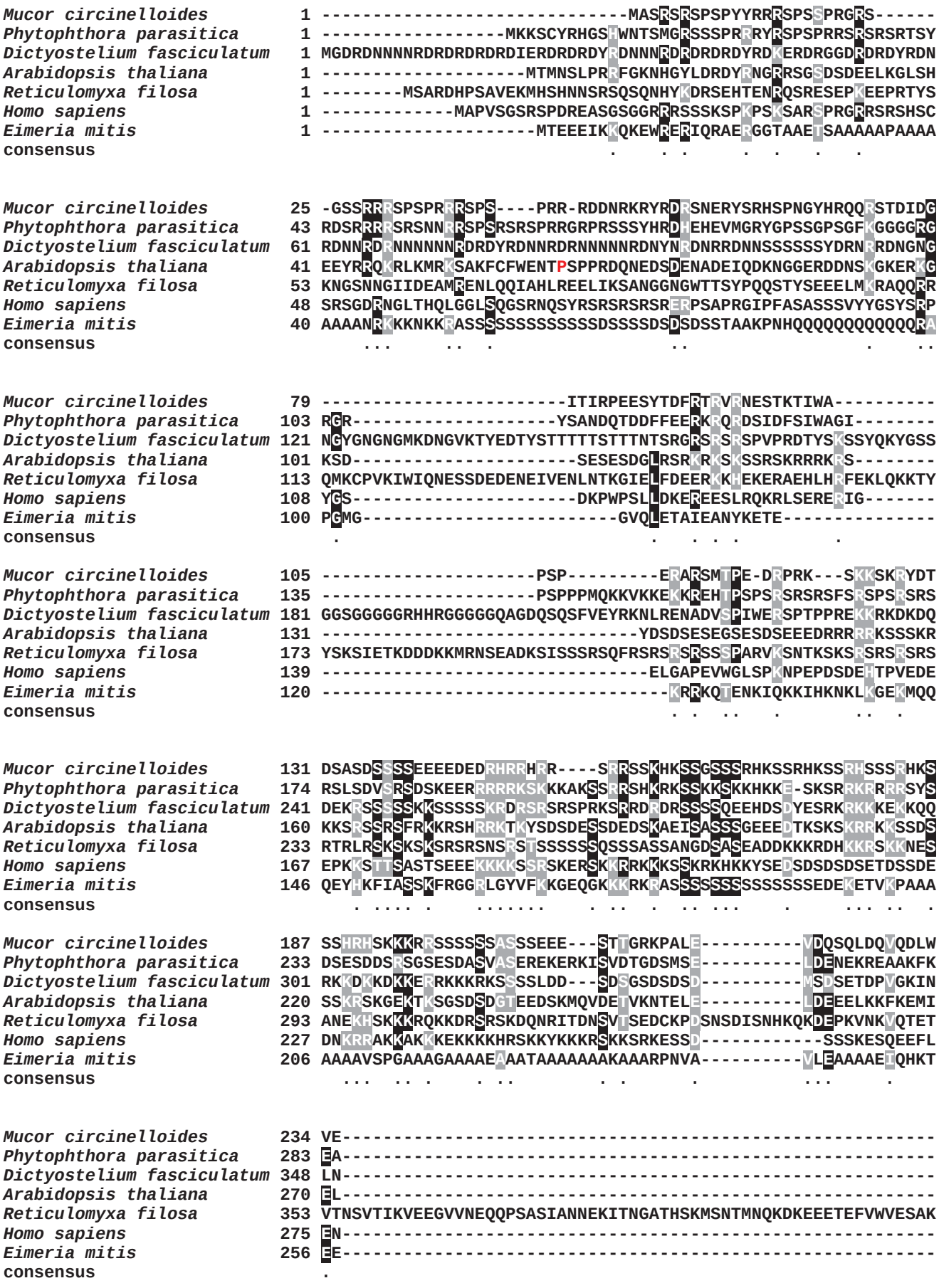

Supplemental Data. Sánchez-García et al. Plant Cell 2015 10.1105/tpc.15.00135

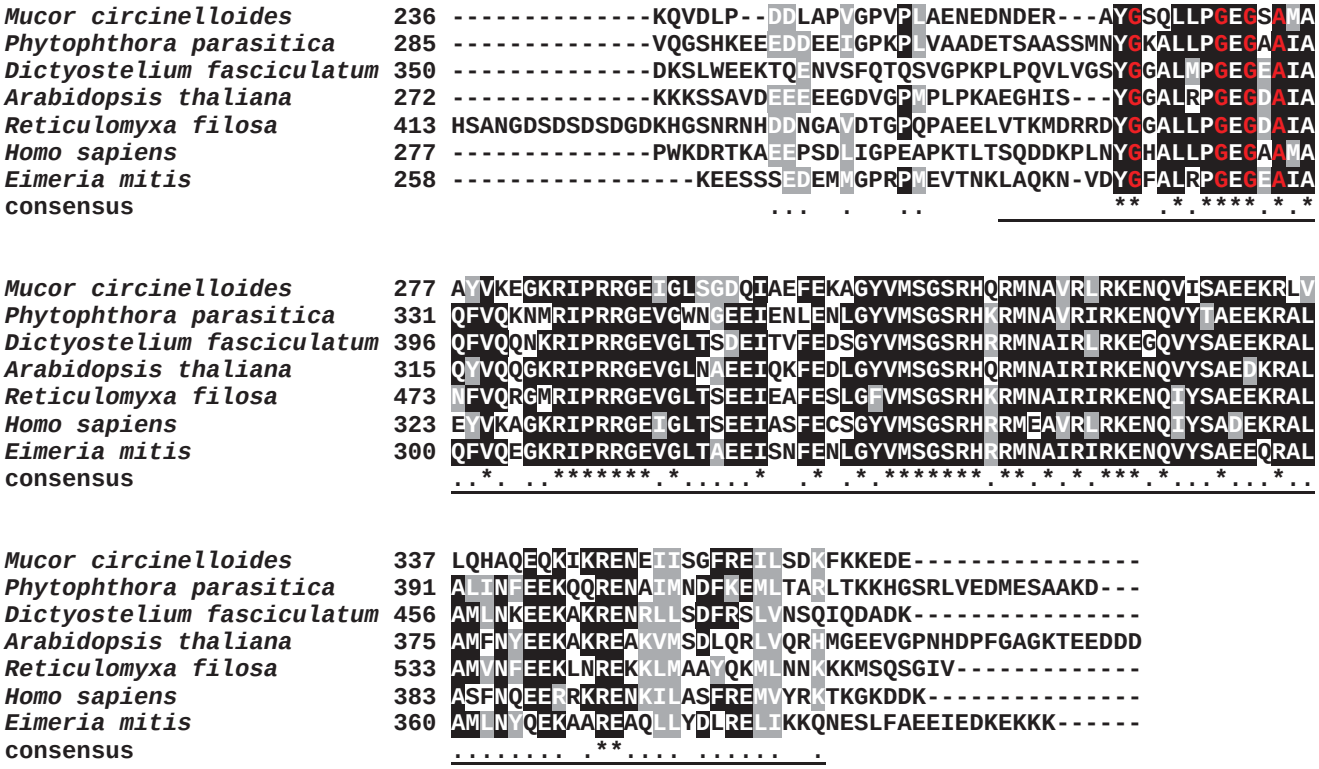

Supplemental Figure 3. Sequence conservation among eukaryotic NKAPs.
Sequence alignment of full-length putative MAS2 orthologs from *Mucor circinelloides* (representing Fungi), *Phytophthora parasitica* (Stramenopiles), *Dictyostelium fasciculatum* (Amoebozoa), *Arabidopsis thaliana* (Viridiplantae), *Reticulomyxa filosa* (Rhizaria), *Homo sapiens* (Holozoa), and *Eimeria mitis* (Alveolata). We found NKAP homologs in all of the eukaryotic supergroups except Excavata. Bacteria do not have NKAP homologs. Identical or similar residues shared by at least 50% of proteins are shaded black or gray, respectively. The order in which the sequences appear is determined by the guide tree (Higgins et al., 1992). Numbers indicate residue positions. The SynMuv domain (as described at NCBI) is indicated with a continuous black line under the consensus sequence shown at the bottom of the alignment. Amino acid substitutions caused by the *mas2* mutations are shown in red. Protein sequences were obtained using the BLASTP (Basic Local Alignment Search Tool) at NCBI (Altschul et al., 1990). This alignment and that of Figure S4 were obtained using ClustalW2 (Larkin et al., 2007) and shaded with Boxshade 3.21 (http://www.ch.embnet.org/software/BOX_form.html).

Supplemental Data. Sánchez-García et al. Plant Cell 2015 10.1105/tpc.15.00135

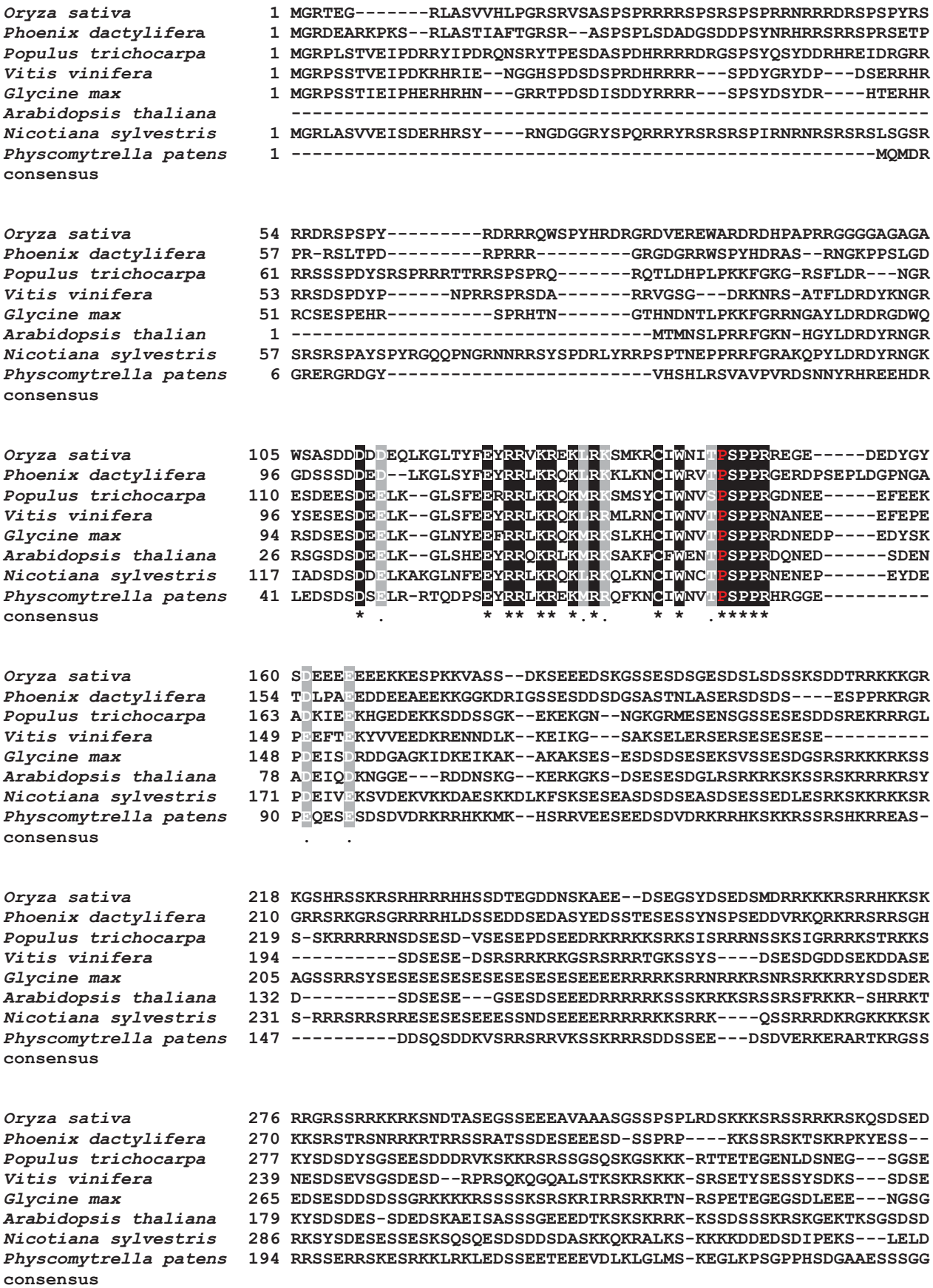

Supplemental Data. Sánchez-García et al. Plant Cell (2015) 10.1105/tpc.15.00135

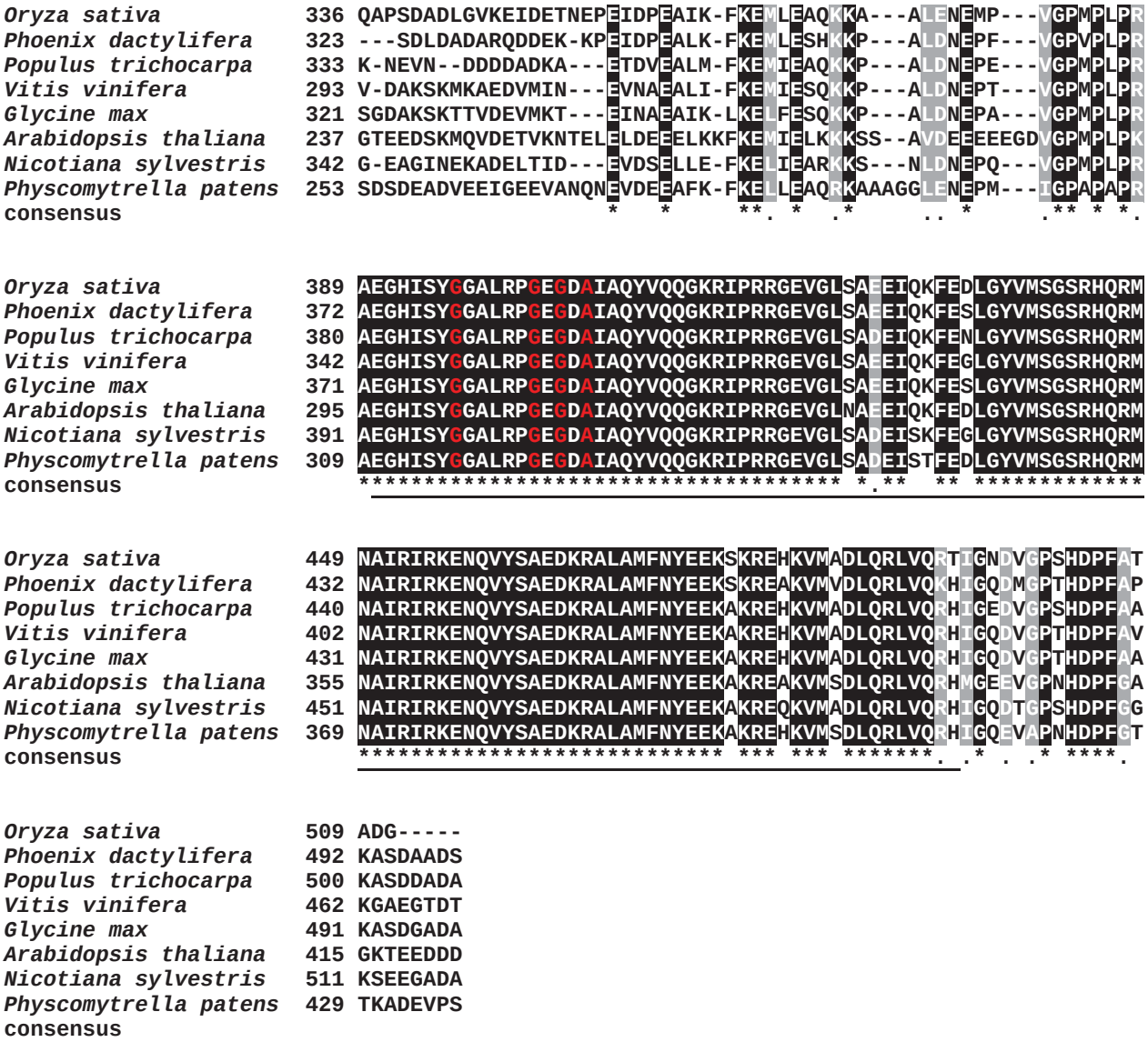

Supplemental Figure 4. Sequence conservation among plant NKAPs.
Sequence alignment of full-length putative MAS2 orthologs from different angiosperm lineages, as classified in Myburg et al. (2014), and mosses: *Oryza sativa* (representing Poales), *Phoenix dactylifera* (Arecales), *Populus trichocarpa* (Malpighiales), *Vitis vinifera* (Vitales), *Glycine max* (Fabids), *Arabidopsis thaliana* (Malvids), *Nicotiana sylvestris* (Asterids), and *Physcomitrella patens* (Bryophyte). Identical or similar residues across all of sequences are shaded in black and gray, respectively. Numbers indicates residues positions in each protein. The SynMuv domain, the amino acid changes and the consensus sequences are marked as in Figure S3.

Supplemental Data. Sánchez-García et al. Plant Cell (2015) 10.1105/tpc.15.00135

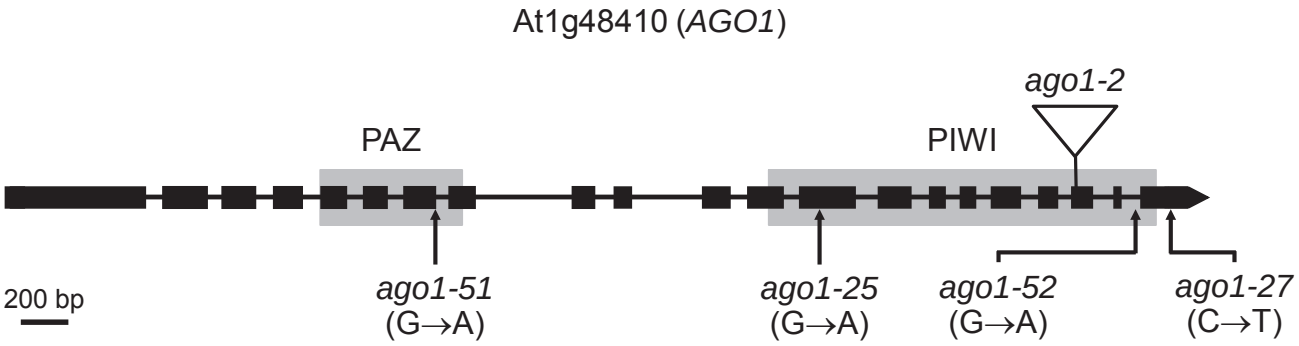

Supplemental Figure 5. *ago1* alleles used in this work.
Schematic representation of the *AGO1* gene, with the position and molecular nature of the mutations used in this work. Introns and exons are represented as black lines and boxes, respectively. The regions encoding the PAZ and PIWI domains of the AGO1 protein are shaded grey. The triangle indicates the T-DNA insertion carried by the *ago1-2* allele. The *ago1-51* mutation affects the PAZ domain of AGO1, and *ago1-25* and *ago1-52* affect the PIWI domain; *ago1-27* does not affect any known domain.

Supplemental Data. Sánchez-García et al. Plant Cell (2015) 10.1105/tpc.15.00135

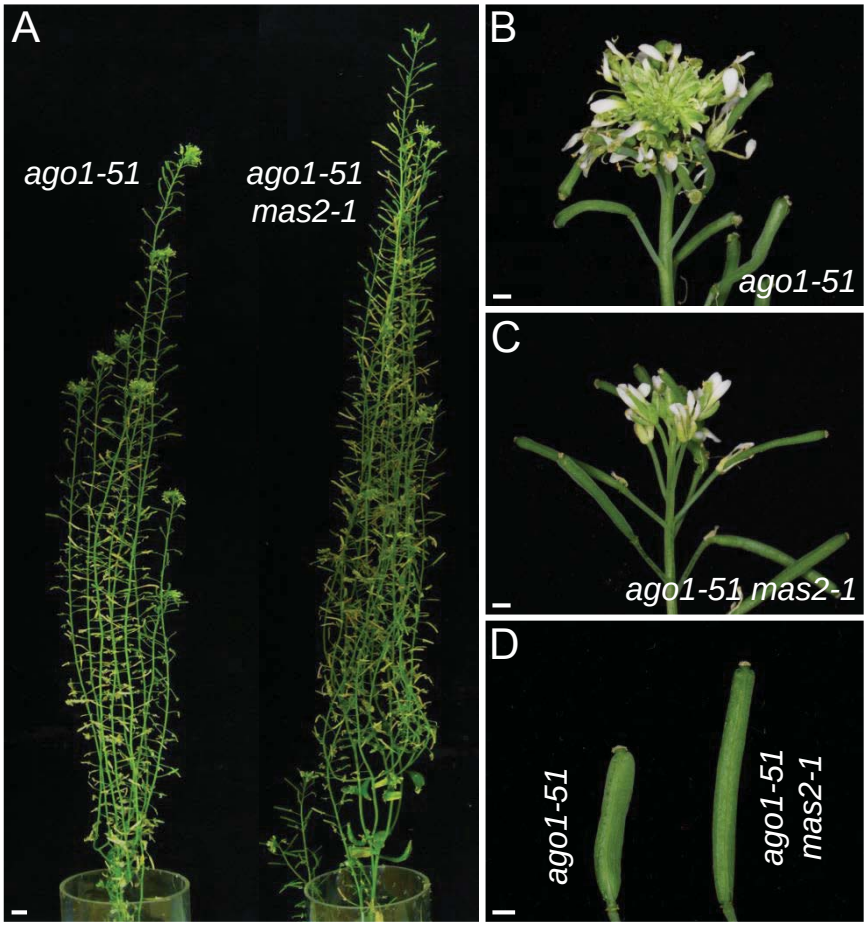

Supplemental Figure 6. Morphological phenotype of *ago1-51 mas2-1* adult plants.
(A) Adult *ago1-51* and *ago1-51 mas2-1* plants. (B, C) Inflorescences of (B) *ago1-51*, and (C) *ago1-51 mas2-1* plants. (D) Siliques of *ago1-51* and *ago1-51 mas2-1* plants. Pictures were taken at 75 das. Scale bars: (A) 1 cm, and (B-D) 1 mm.

Supplemental Data. Sánchez-García et al. Plant Cell (2015) 10.1105/tpc.15.00135

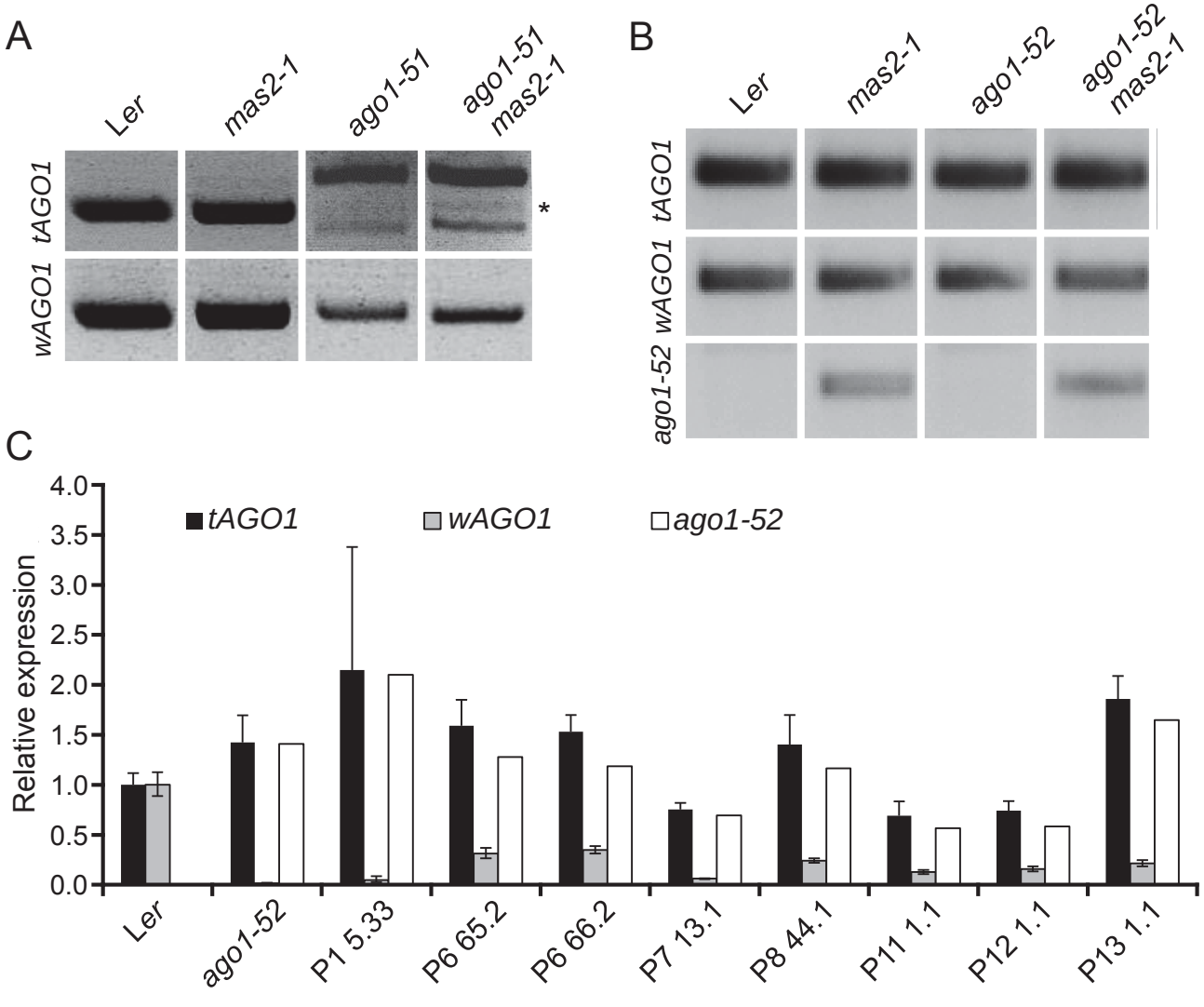

Supplemental Figure 7. Effects of the *mas2* mutations on the levels of *AGO1* splice variants. (A, B) RT-PCR analysis of RNA extracted from L*er*, *mas2-1*, *ago1-51*, *ago1-52, ago1-51 mas2-1* and *ago1-52 mas2-1* plants using primers (Table S2) designed to amplifiy (A) *tAGO1* or *wAGO1* mRNAs, and (B) *tAGO1*, *wAGO1* or *ago1-52* mRNAs. Asterisk indicates the *wAGO1* cDNA. (C) RT-qPCR analysis of the modification of the relative levels of *wAGO1* and *ago1-52* splice forms in the eight suppressor lines identified as described in Micol-Ponce et al. (2014), other than P2 11.1 (*ago1-52 mas2-1,* whose analysis is shown in Figure 4). Error bars represent standard deviations. RNA was extracted from plants collected at 15 das. Two biological replicas with three technical replicas each were performed.

Supplemental Data. Sánchez-García et al. Plant Cell (2015) 10.1105/tpc.15.00135

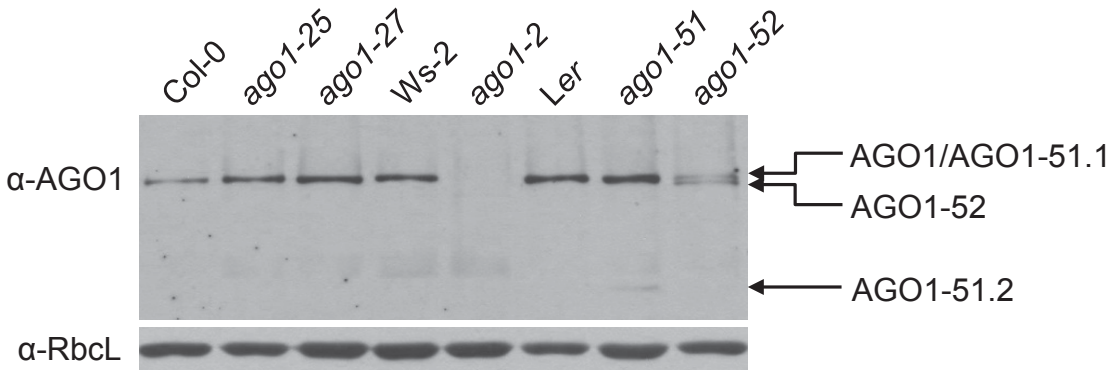

Supplemental Figure 8. Visualization of AGO1 protein isoforms in *ago1* mutants. Detection of AGO1 proteins by immunoblot using a primary antibody against AGO1 (α-AGO1) in protein extracts from *ago1-25* and *ago1-27* (in the Col-0 genetic background), *ago1-2* (Ws-2), and *ago1-51* and *ago1-52* (L*er*). Arrows indicate bands matching the expected size for the AGO1-51.1, AGO1-51.2, and AGO1-52 isoforms. The Rubisco (α-RbcL) large subunit was used as a loading control. Proteins were extracted from plants collected at 15 das.

Supplemental Data. Sánchez-García et al. Plant Cell (2015) 10.1105/tpc.15.00135

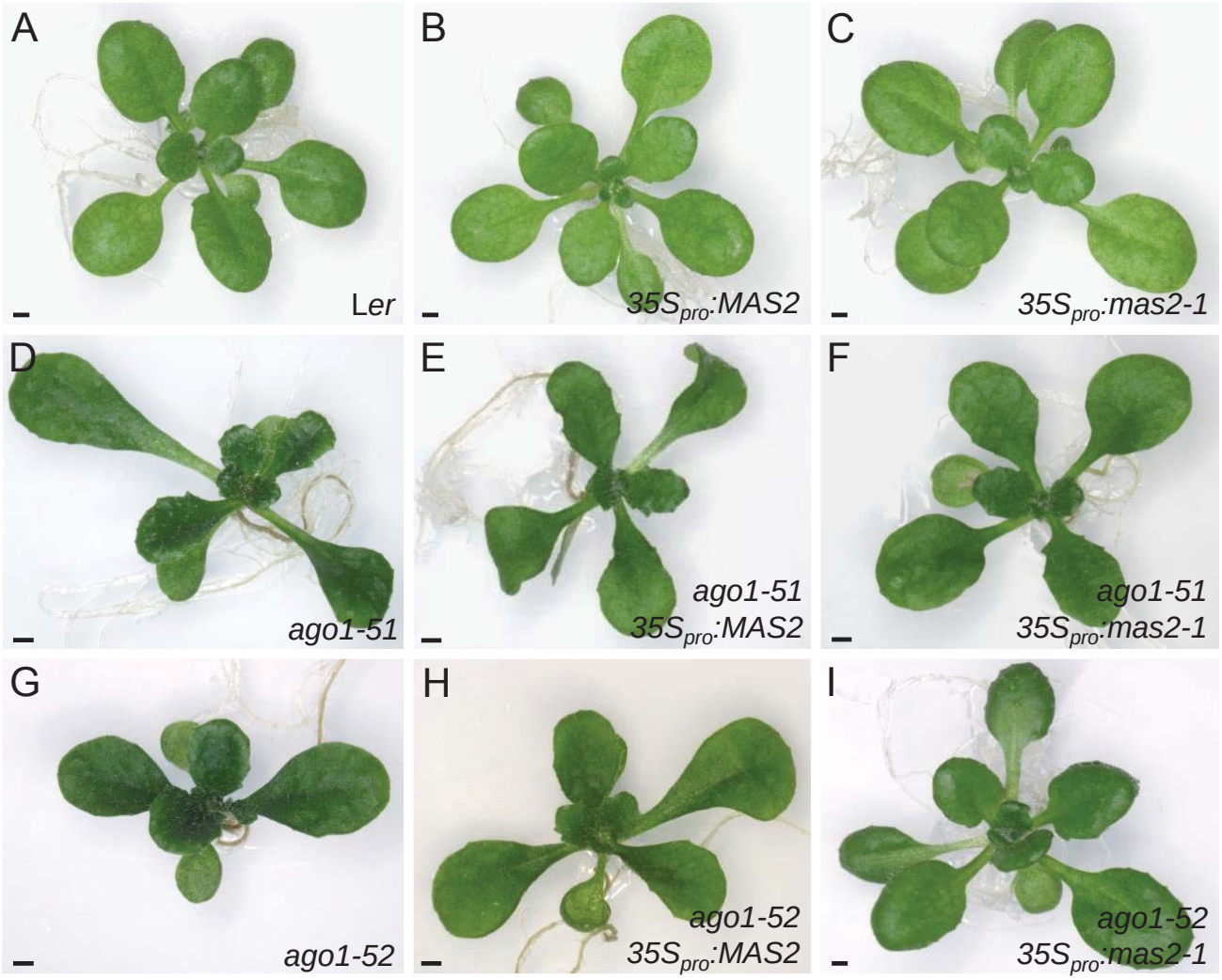

Supplemental Figure 9. Phenotypic effects of the overexpression of *MAS2* and *mas2-1* on the L*er*, *ago1-51* and *ago1-52* backgrounds at the rosette stage.
Rosettes of (A) L*er*, (B, C) *35S$_{pro}$:MAS2* and *35S$_{pro}$:mas2-1*, both in the L*er* background, (D) *ago1-51*, (E) *ago1-51 35S$_{pro}$:MAS2*, (F) *ago1-51 35S$_{pro}$:mas2-1*, (G) *ago1-52*, (H) *ago1-52 35S$_{pro}$:MAS2,* and (I) *ago1-52 35S$_{pro}$:mas2-1* plants. Pictures were taken at 21 das. Scale bars: 1 mm.

Supplemental Data. Sánchez-García et al. Plant Cell (2015) 10.1105/tpc.15.00135

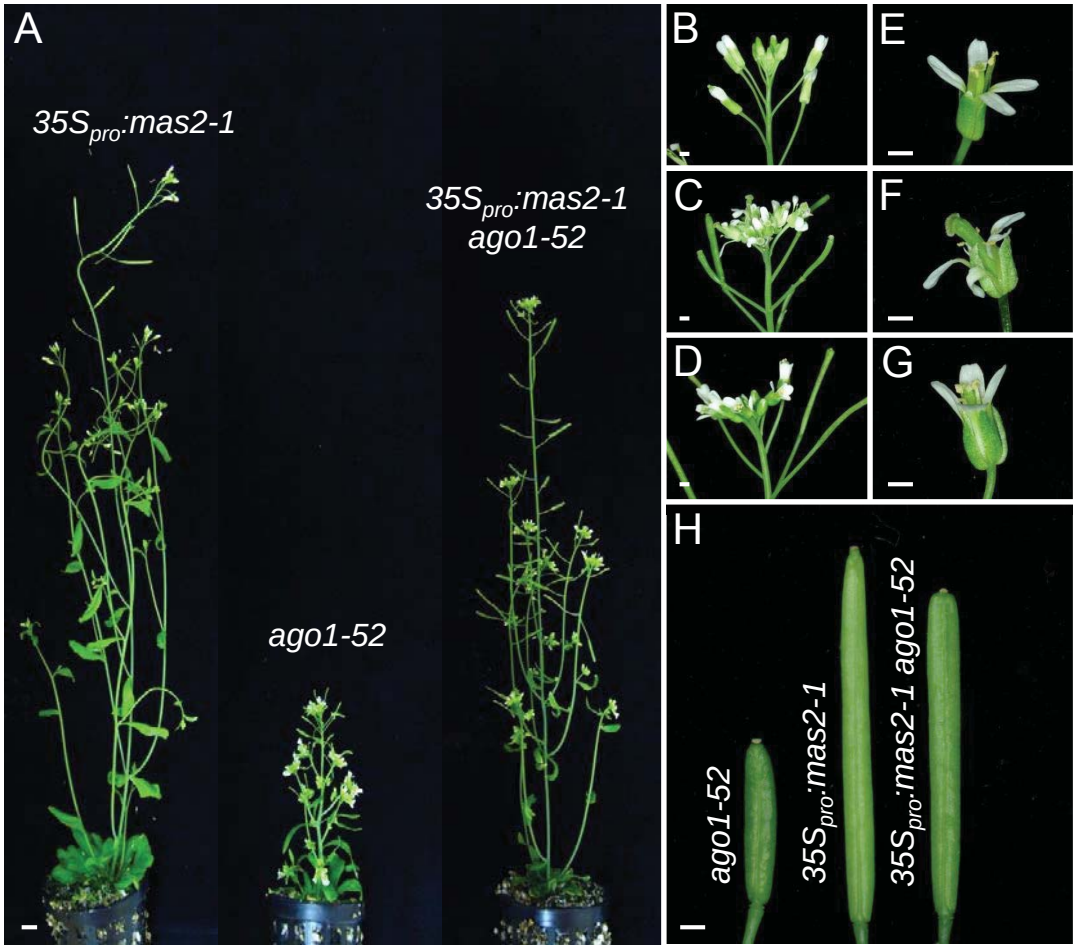

Supplemental Figure 10. Phenotypic effects of the overexpression of *mas2-1* on the *ago1-52* background in adult plants.
(A) Adult *35S$_{pro}$:mas2-1*, *ago1-52* and *35S$_{pro}$:mas2-1 ago1-52* plants. (B-G) Inflorescences and flowers of (B, E) *35S$_{pro}$:mas2-1,* (C, F) *ago1-52*, and (D, G) *35S$_{pro}$:mas2-1 ago1-52* plants. (H) *ago1-52*, *35S$_{pro}$:mas2-1* and *35S$_{pro}$:mas2-1 ago1-52* siliques. Pictures were taken at 48 das. Scale bars: (A) 1 cm, and (B-H) 1 mm.

Supplemental Data. Sánchez-García et al. Plant Cell (2015) 10.1105/tpc.15.00135

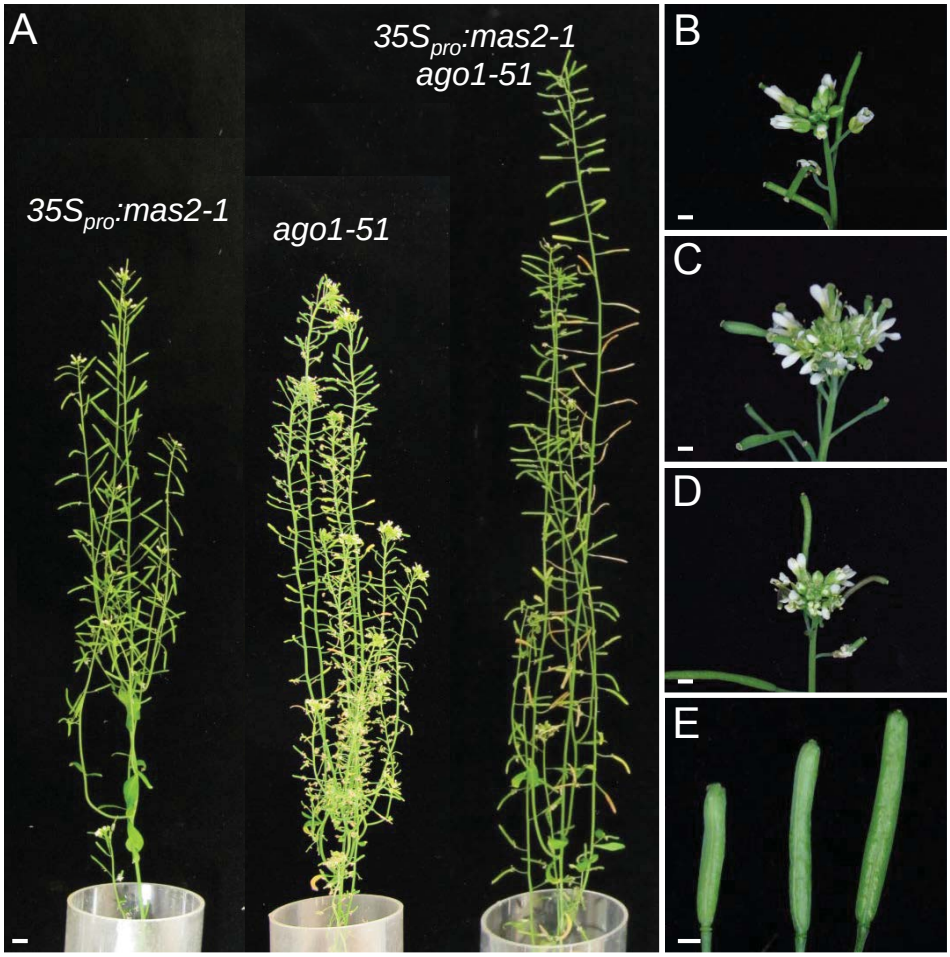

Supplemental Figure 11. Phenotypic effects of the overexpression of *mas2-1* on the *ago1-51* background in adult plants.
(A) Adult *35S$_{pro}$:mas2-1*, *ago1-51* and *35S$_{pro}$:mas2-1 ago1-51* plants. (B-D) Inflorescences of (B) *35S$_{pro}$:mas2-1,* (C) *ago1-51*, and (D) *35S$_{pro}$:mas2-1 ago1-51* plants. (E) From left to right: *ago1-51*, *35S$_{pro}$:mas2-1 ago1-51* and *35S$_{pro}$:mas2-1* siliques. Pictures were taken at 48 das. Scale bars: (A) 1 cm, and (B-E) 1 mm.

Supplemental Data. Sánchez-García et al. Plant Cell (2015) 10.1105/tpc.15.00135

A

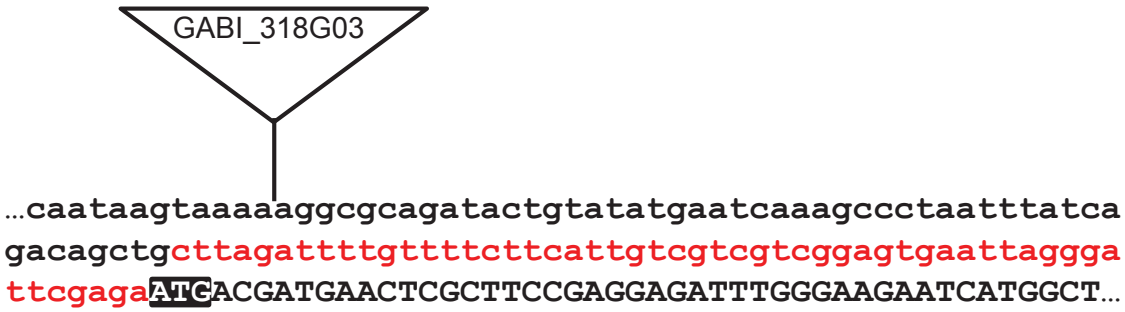

B

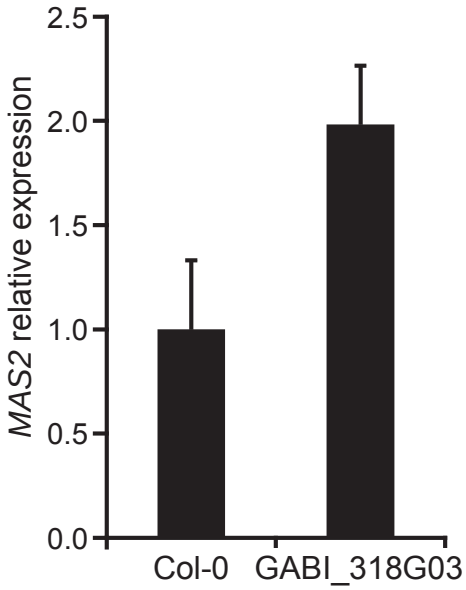

Supplemental Figure 12. Analysis of the of GABI_318G03 insertional line.
(A) The T-DNA insertion carried by the GABI_318G03 line in the putative promoter region of *MAS2* is represented by a triangle. Plants homozygous for this insertion were viable and phenotypically wild type. The T-DNA insertion is located 103 bp upstream of the start codon of *MAS2*, probably affecting its promoter region because its annotated leader is 53-nt long. Its position was verified by amplification with the MAS2_F2 + RB-pAC161, and LB-pAC161 + At4g02720_FR1 primer pairs (Table S2), followed of sequencing of the corresponding PCR products. The promoter region and the 5´UTR of *MAS2* are shown in black and red lowercase letters, respectively. The coding region is shown in black capital letters and its start codon is highlighted in bold. (B) RT-qPCR analysis of *MAS2* expression in Col-0 and homozygous GABI_318G03 plants, showing that the levels of *MAS2* transcripts were not reduced in this line. Error bars represent standard deviations. Three biological replicas with three technical replicas each were performed.

Supplemental Data. Sánchez-García et al. Plant Cell (2015) 10.1105/tpc.15.00135

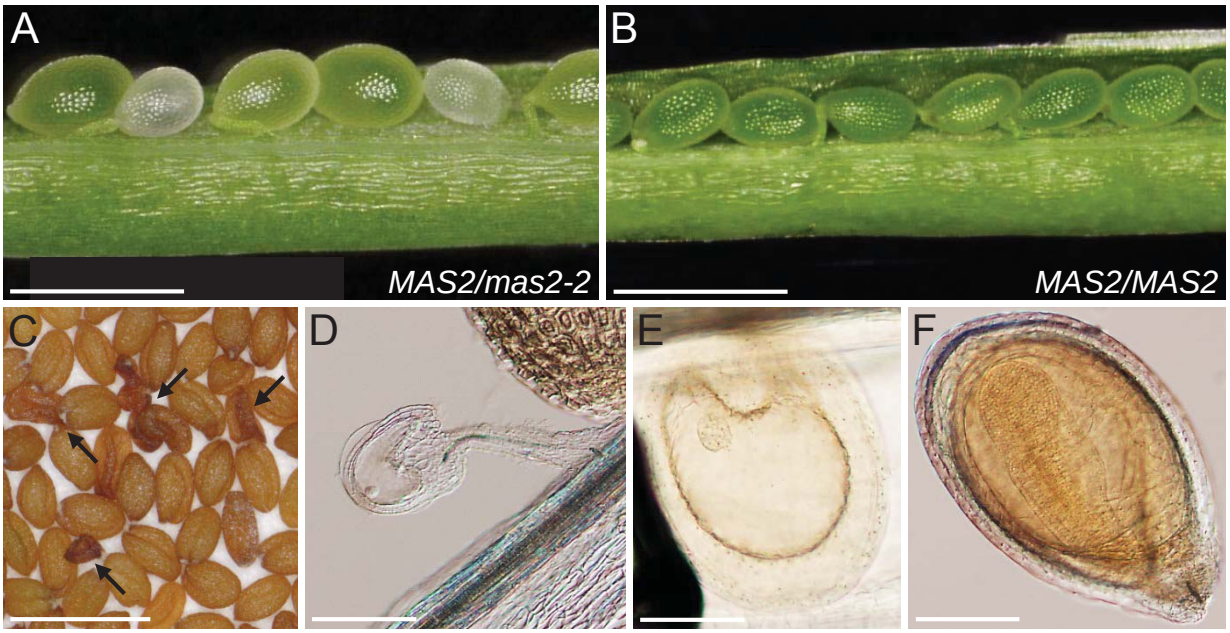

Supplemental Figure 13. Seeds and embryos of *MAS2/mas2-2* plants.
(A, B) Dissected siliques of (A) *MAS2/mas2-2,* and (B) Col-0 plants. (C) Mature seeds of *MAS2/mas2-2* plants. Arrows indicate wrinkled and abnormal seeds. (D-F) Confocal micrographs of (D) unfertilized or aborted ovules and (E, F) abnormal embryos arrested in the (E) globular and (F) linear-cotyledon stages found in the siliques of *MAS2/mas2-2* plants. Scale bars: (A-C) 1 mm, and (D-F) 200 µm.

Supplemental Data. Sánchez-García et al. Plant Cell (2015) 10.1105/tpc.15.00135

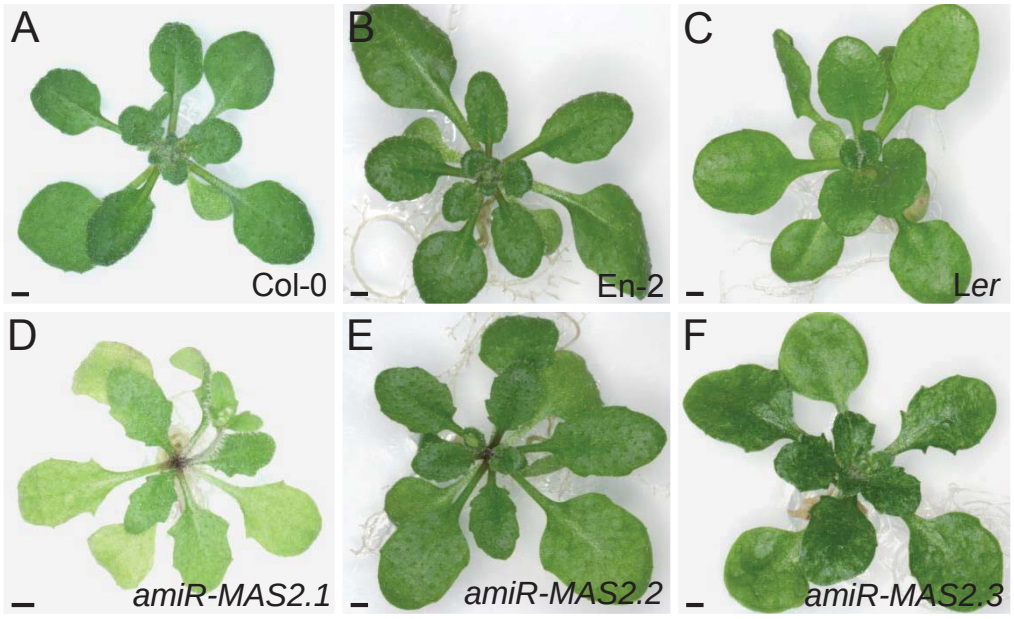

Supplemental Figure 14. Morphological phenotypes caused by the *amiR-MAS2* transgene in different genetic backgrounds.
Rosettes of (A) Col-0, (B) En-2, (C) L*er*, (D) *amiR-MAS2.1* (in a Col-0 background), (E) *amiR-MAS2.2* (En-2), and (F) *amiR-MAS2.3* (L*er*) plants. Pictures were taken at 28 das. Scale bars: 1 mm.

Supplemental Data. Sánchez-García et al. Plant Cell (2015) 10.1105/tpc.15.00135

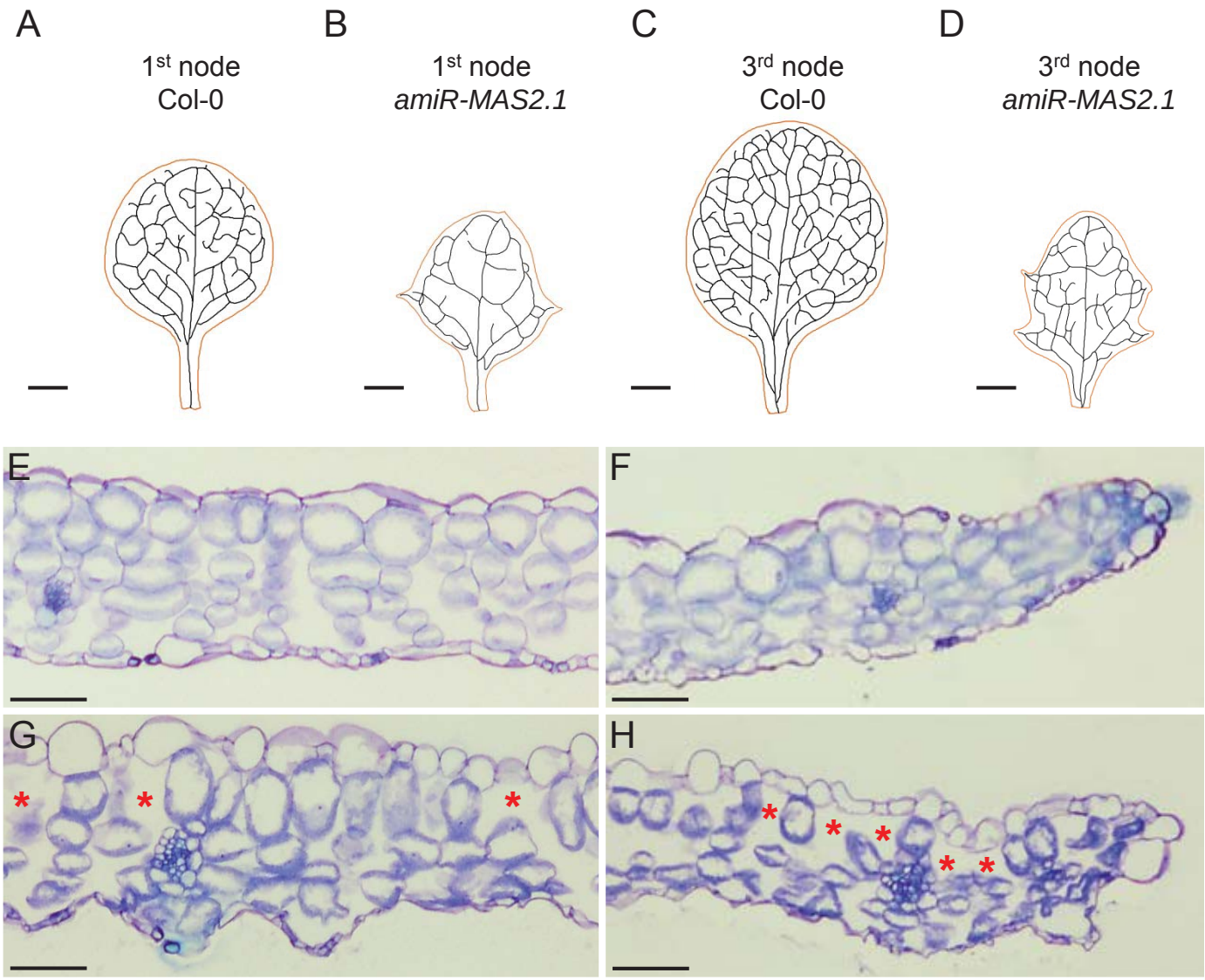

Supplemental Figure 15. Histology of *amiR-MAS2.1* leaves.
(A-D) Leaf venation pattern of *amiR-MAS2.1* plants. The leaf margin is shown in orange. Diagrams were drawn on micrographs taken from cleared (A, B) first- and (C, D) third-node leaves of (A, C) Col-0 and (B, D) *amiR-MAS2.1* plants. (E-H) Transverse sections of the (E, G) central and (F-H) marginal regions of third-node leaf lamina of (E, F) Col-0 and (G, H) *amiR-MAS2.1* plants. Asterisks highlight enlarged intercellular air spaces. Micrographs of central transects were taken midway between the primary vein and leaf margin. Plant material was collected at 21 das. Scale bars: (A-D) 1 mm, and (E-H) 50 µm.

Supplemental Data. Sánchez-García et al. Plant Cell (2015) 10.1105/tpc.15.00135

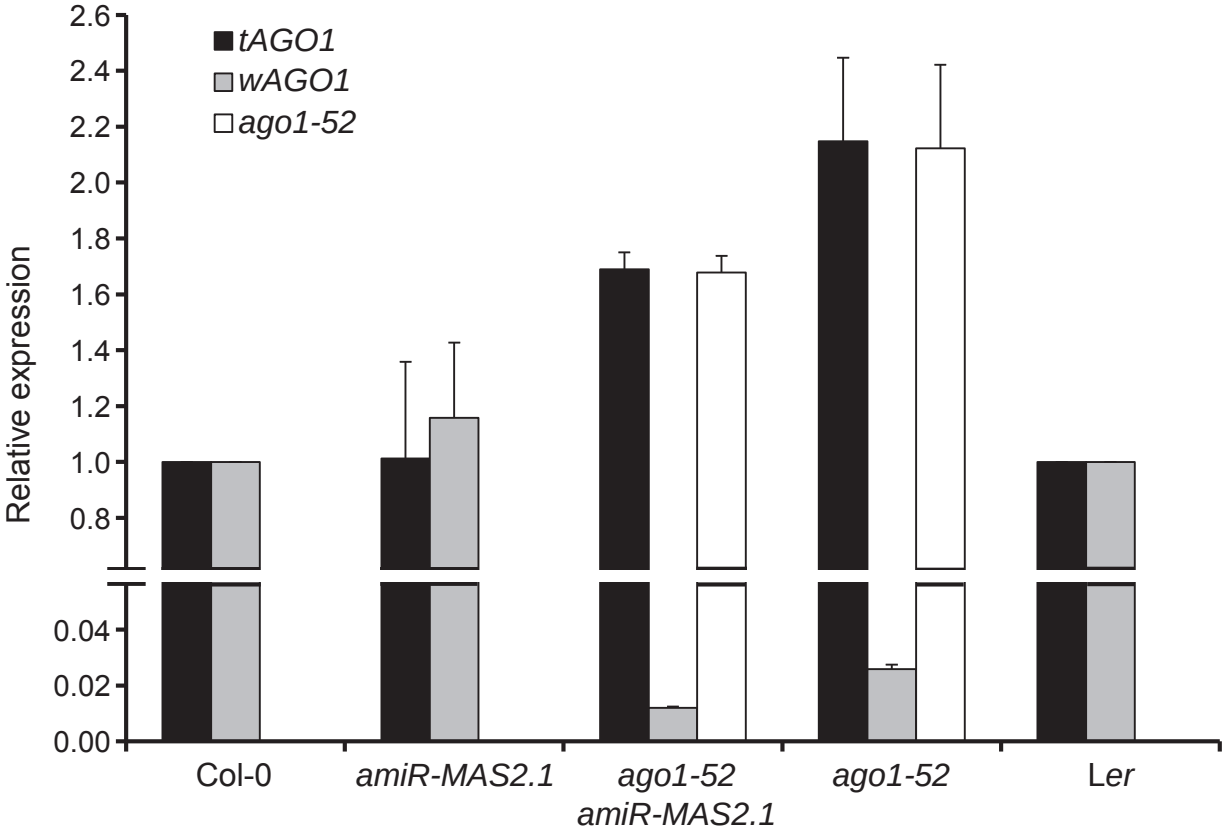

Supplemental Figure 16. Levels of the *AGO1* splice variants in *ago1-52 amiR-MAS2.1* plants.

RT-qPCR analysis of Col-0, *amiR.MAS2.1/amiR-MAS2.1, ago1-52/ago1-52; amiR-MAS2.1/amiR-MAS2.1*, *ago1-52/ago1-52*, and L*er* plants using specific primers to amplify cDNA from *tAGO1* (black bars), *wAGO1* (grey bars) and *ago1-52* (white bars) mRNAs. Error bars represent standard deviations. RNA was extracted from plants collected at 15 das. Two biological replicas with three technical replicas each were performed.

Supplemental Data. Sánchez-García et al. Plant Cell (2015) 10.1105/tpc.15.00135

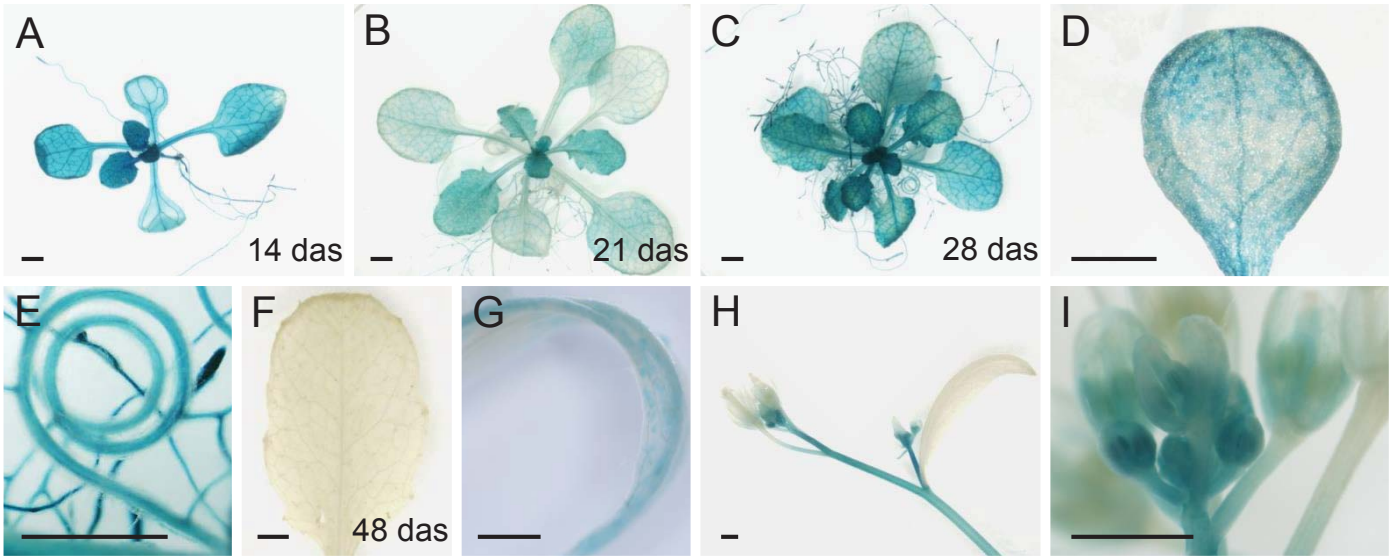

Supplemental Figure 17. Visualization of *MAS2*$_{pro}$*:GUS* activity in wild-type plants.
GUS staining of *MAS2*$_{pro}$*:GUS* transgenic plants in (A-C) rosettes collected (A) 14, (B) 21 and (C) 28 das, (D) a cotyledon, (E) roots, (F) a mature vegetative leaf (48 das), (G) an expanding cauline leaf, and (H) a shoot with a fully expanded cauline leaf and flower buds that are magnified in I. Scale bars: 1 mm.

Supplemental Data. Sánchez-García et al. Plant Cell (2015) 10.1105/tpc.15.00135

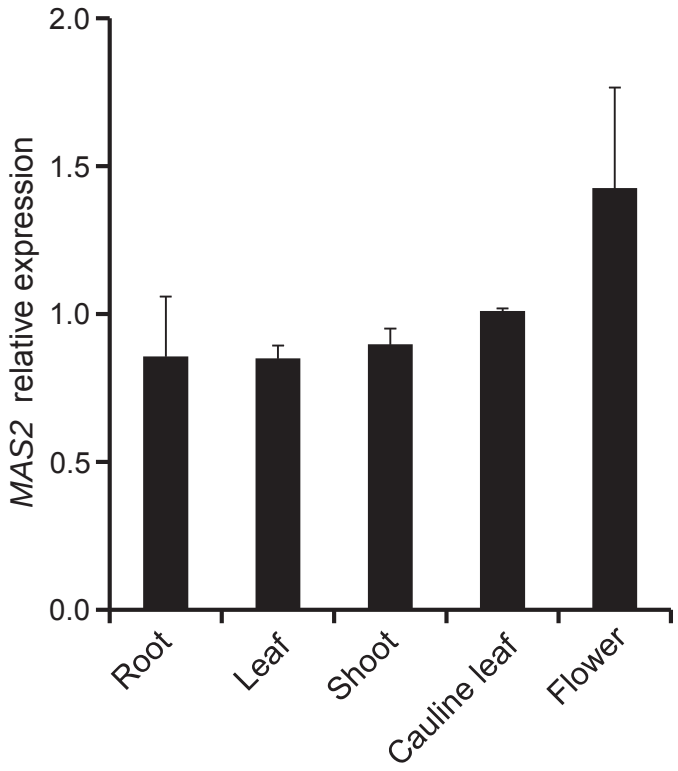

Supplemental Figure 18. Spatial pattern of expression of *MAS2*.
RT-qPCR analysis of *MAS2* expression in different tissues. Total RNA was isolated from the tissues indicated and used as a template. Error bars represent standard deviations. Two biological replicas with three technical replicas each were performed.

Supplemental Data. Sánchez-García et al. Plant Cell (2015) 10.1105/tpc.15.00135

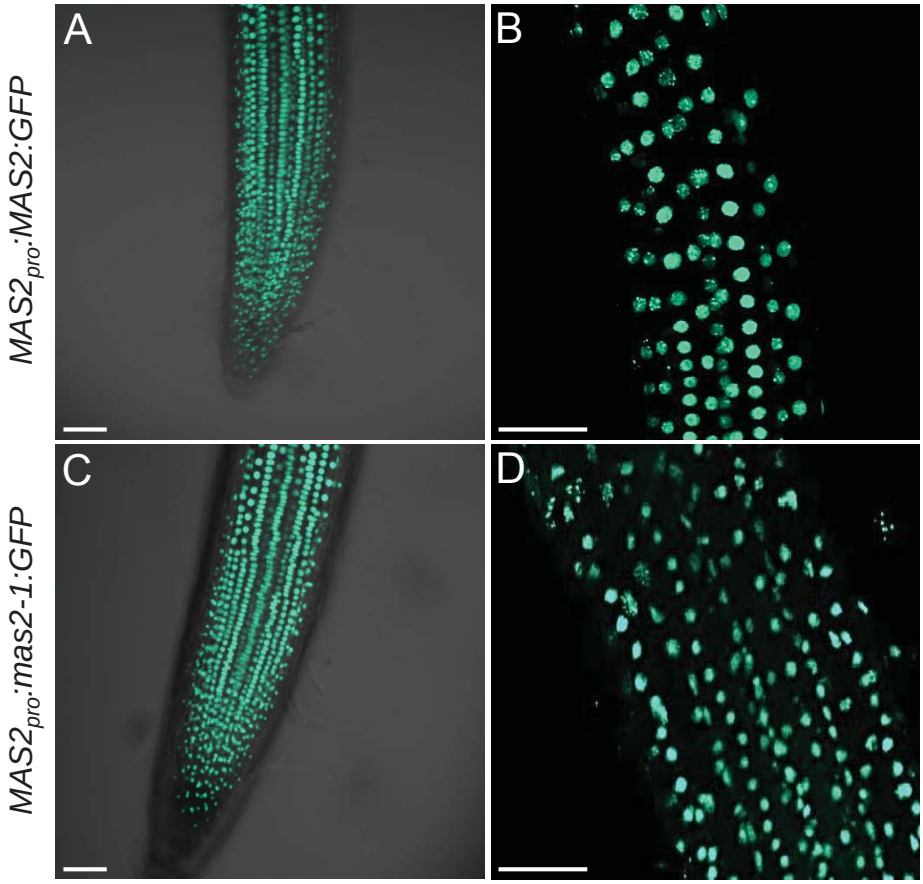

Supplemental Figure 19. Subcellular localization of the MAS2:GFP and MAS2-1:GFP proteins.

Confocal laser scanning microscopy of roots from plants carrying the (A, B) *MAS2$_{pro}$:MAS2:GFP*, and (C, D) *MAS2$_{pro}$:mas2-1:GFP* transgenes. The green signal corresponds to the fluorescent GFP emission in the root apex and root elongation zone (magnified in B, D). Scale bars: 50 µm.

Supplemental Data. Sánchez-García et al. Plant Cell (2015) 10.1105/tpc.15.00135

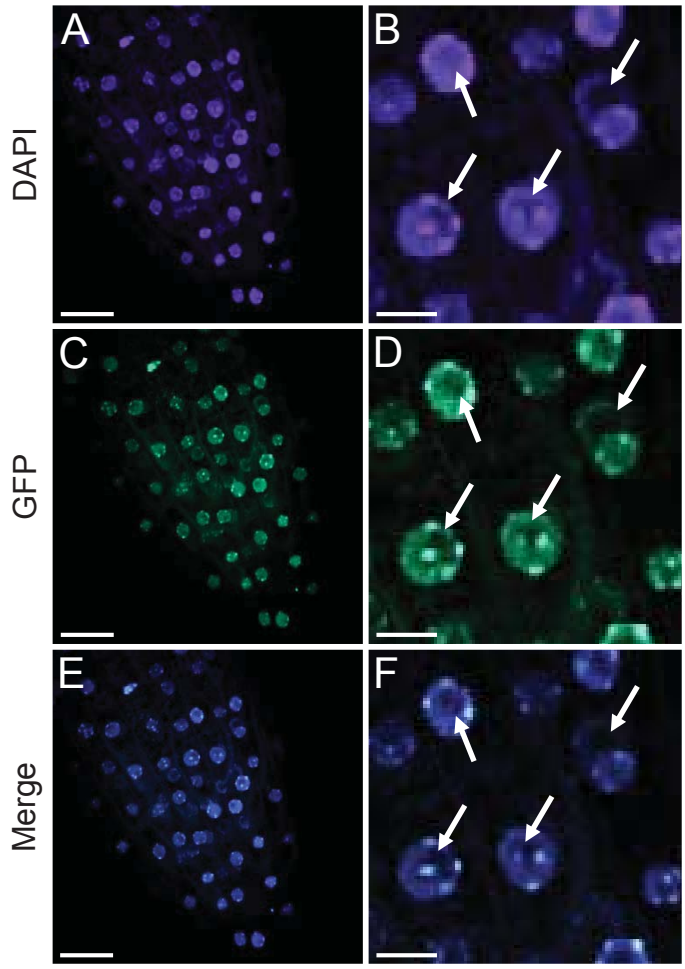

Supplemental Figure 20. Subcellular localization of the MAS2:GFP protein in cells of the root elongation zone from homozygous *35S$_{pro}$:MAS2:GFP* plants.
Fluorescence signals are shown from (A, B) DAPI, (C, D) GFP, and (E, F) their overlay. A, C and E images are magnified in B, D and F, respectively. Arrows indicate nucleoli. Scale bars: (A, C, E) 50 µm, and (B, D, F) 10 µm.

Supplemental Data. Sánchez-García et al. Plant Cell (2015) 10.1105/tpc.15.00135

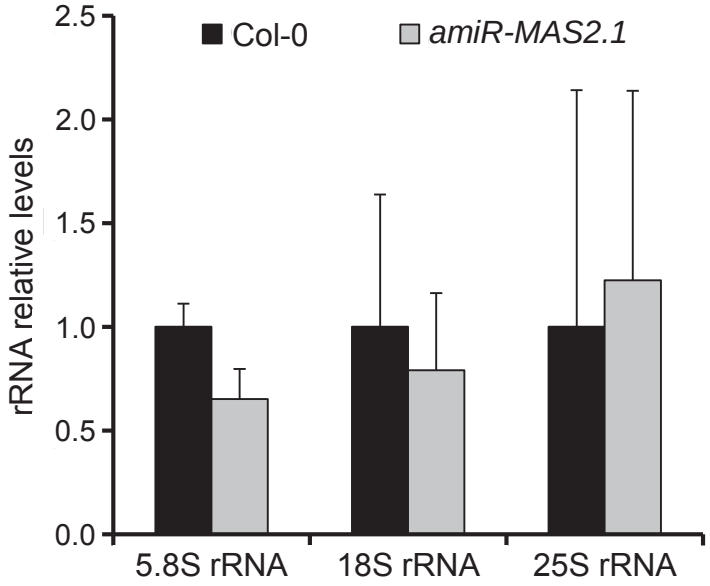

Supplemental Figure 21. Effects of *amiR-MAS2.1* on 45S rRNA processing.

Relative expression of mature rRNA products from the 45S rRNA processing in Col-0 and homozygous *amiR-MAS2.1* plants. rRNA levels were analyzed by RT-qPCR using the 5.8SrRNA_F + 5.8SrRNA_R, 18SrRNA_F + 18SrRNA_R and 25SrRNA_F + 25SrRNA_R primer pairs (Table S2). Relative expression levels of 5.8S, 18S and 25S rRNAs in *amiR-MAS2.1* plants were compared to the expression levels in Col-0 plants. Error bars represent standard deviations. Three biological replicas with three technical replicas each were performed.

Supplemental Table 1. Primer sets used for the fine mapping of *MAS2*

Marker		Locus	Oligonucleotide sequence (5´→3´)		PCR product size (bp)	
Name	Type		Forward primer	Reverse primer	L*er*	Col-0
CER466746	In/Del	AT4G00330-AT4G00335	CGGCGTTCAGTTATCCATTCC	GAACCAAAAATTGGAAACTAGTCG	349	369
CER451853	In/Del	AT4G01090-AT4G01100	GTAGATGTCGGACCACAGTTG	TCCCTAATTGATAAAAGGGCCC	218	246
CER448672	In/Del	AT4G01540	AACCCAGCAAGGATTTGCCTAG	AAATTCAGCACAATAGCCTACTC	277	289
CER457983	In/Del	AT4G02100-AT4G02110	CCGTCAAGCGACTAGTCTATT	ACAAATATCGAGAAACTAAAGCC	251	229
CER458010	In/Del	AT4G02710-AT4G02715	CATGATAACACAGGGCGTAATT	GACGAAAGTACCCTTGTATATG	179	212
CER460616	In/Del	AT4G03060-AT4G03063	GAGAATTGAAGACCAAACGCC	AGCGAGGCCGATGATTGTAC	342	386
nga12	SSLP	AT4G05520	AATGTTGTCCTCCCCTCCTC	CCTTGTAGATCTTCTGATGC*	252	262
nga1111	SSLP	AT4G09640	GGGTTCGGTTACAATCGTGT	AGTTCCAGATTGAGCTTTGAGC*	157	152
AthF28J12.3	SSLP	AT4G18500	GCTCCGCCGTTGGATTCTG	GCCTTTATCAATGGATGAGGAA*	257	265
nga1139	SSLP	AT4G34390	CTAGGCTCGGGTGAGTCAC	TTTTTCCTTGTGTTGCATTCC*	295	306

*Labelled with HEX (4, 7, 2', 4', 5', 7'-Hexachloro-6-carboxyfluorescein).

Supplemental Table 2. Other primer sets used in this work

Purpose	Oligonucleotide name(s)	Oligonucleotide sequence (5'→3')	
		Forward primer (F)	Reverse primer (R)
MAS2 sequencing	At4g02720_F1/R1	CAAAGCCCTAATTTATCAGACAG	TCAAGTTCTAGCTCAGTGTTCTT
	At4g02720_F2/R2	AGGCGGAAGAAATCTTCGGATT	GCAAGTAGCAAACAGCAGTATC
T-DNA insertion verification	Sail_LB1	GCCTTTTCAGAAATGGATAAATAGCCTTGCTTCC	
	Salk_LBb1	GCGTGGACCGCTTGCTGCAACT	
	Ds3_1	ACCCGACCGGATCGTATCGGT	
	LB-pAC161	ATATTGACCATCATACTCATTGC	
	RB-pAC161	GTGGATTTGATGTGATATCTCC	
Double mutant genotyping	At4g02720_F2/R2		
	AGO1_F1/R1	GGCTAATATGAGTCTTCTCTGC	CCATCCCTGTGCAGAATAACC[c]
	AGO1_F2/R2	TCTGCCACCCTACAGAGTTTG	GTCATAAAGATAGATAGAGGGTG[c]
	AGO1_F3/R3	ATCGACAGCCTTCATAGAGGC[c]	CTTGCATACCTGTGCAGCAAC
	AGO1_F4/R4	TTTACTGCAGATGGACTTCAATC	CAACTCAGCAGTAGAACATGAC
	HDA6_F/R	TCGATCGTTAGTTTAACATTCAG	ATCAGCGTCCTGTCTGTTTAA
	AtNUC-L1;PARL1_F/R	AGTTGCTGTCACCAAGAAG	TGGCCTACCATGGAATTCA
Overexpression	MAS2_F1/R1	*GGGGACAAGTTTGTACAAAAAAGCAGGCT*ATGACGATGAACTCGCTTCCGA[a]	*GGGGACCACTTTGTACAAGAAAGCTGGG*TCAATCATCATCTTCTTCAGTCTTTC[b]
	pMDC32_F1/R1	TTCATTTGGAGAGGACCTCG	GAAATTCGAGCTCCACCGCG
GUS assays	MAS2_F2/R2	*GGGGACAAGTTTGTACAAAAAAGCAGGC*CATTATCGTCCATGGCTGACAC[a]	*GGGGACCACTTTGTACAAGAAAGCTGGGT*CTCGAATCCCTAATTCACTCC[b]
	pMDC164_F1/R1	AAGACTGTAACCACGCGTCTG	TTGACTGCCTCTTCGCTGTAC
Subcellular localization	MAS2_F3/R3	*GGGGACAAGTTTGTACAAAAAAGCAGGC*CATTATCGTCCATGGCTGACAC[a]	*GGGGACCACTTTGTACAAGAAAGCTGGG*ATCATCATCTTCTTCAGTCTTTCC[b]
	MAS2_F4/R3	*GGGGACAAGTTTGTACAAAAAAGCAGGCT*ATGACGATGAACTCGCTTCCGA[a]	
	pMDC111R		TATGTTGCATCACCTTCACCCT
	pMDC85R		ATAATGATCAGCGAGTTGCAC
rDNA variant	p3/p4	GACAGACTTGTCCAAAACGCCCACC[d]	CTGGTCGAGGAATCCTGGACGATT[d]

Supplemental Table 2. Other primer sets used in this work

Purpose	Oligonucleotide name(s)	Oligonucleotide sequence (5'→3')	
		Forward primer (F)	Reverse primer (R)
expression			
45S pre-rRNA accumulation	+/-250-F and +/-250-R	CAAGCAAGCCCATTCTCCTC[e]	CAACTAGACCATGAAAATCC[e]
45S pre-rRNA processing	U1/U2	CGTAACGAAGATGTTCTTGGC[f]	ATGCGTCCCTTCCATAAGTC[f]
rDNA methylation	p2f/r	GCATGCAAAAAGAATTTTCAA[g]	CTGGAAAAAGGCAACAAAACC[g]
RT-PCR	AGO1_F3/R5		GAGGCTCGTATACTGCCTCC
RT-qPCR	At4g02720_F2/R1		
	AGO1_F5/R5	CTCCGGAAGTTACATCAAGGG	AAGATTGATTCTGAACTCCTTGG
	AGO1_F6/R6	GGCATGATAAAGGAGTTGCTCAT	CTGACTCCATCCCTGTAGAAGA
	AGO1_F4/R7		TAATATGCAGGGGGAACAATT
	AGO1_F7/R5	ACTACCATGCTTGCAAGTATGC	
	AGO1_F3/R3		
	AGO1_F4/R8		GATATTGTAGTTCCCCCTGC
	5.8SrRNA_F/R	ATCTCGGCTCTCGCATCGATG	CCCTCGGCCAGAAGGCTTGGGG
	18SrRNA_F/R	GGTGGTGGTGCATGGCCGTTCTT	GACGGGCGGTGTGTACAAAGGGC
	25SrRNA_F/R	GAACTTTGAAGGCCGAAGAG[h]	GACAGGGACAGTGGGAATCT[h]
	OTC_F/R	TGAAGGGACAAAGGTTGTGTATGTT[i]	CGCAGACAAAGTGGAATGGA[i]

[a-b]These oligonucleotides include at their 5´ ends [a]attB1 and [b]attB2 sequences (shown in italics).[c-i]Sequences of these oligonucleotides are as described in [c]Jover-Gil et al. (2012); [d]Pontvianne et al. (2010); [e]Earley et al. (2010); [f]Shi et al. (2005); [g]Harscoet et al. (2010); [h]Ren et al. (2011); and [i]Cnops et al. (2004).

Supplemental Table 3. Results of the Y2H screen using MAS2 as a bait

Prey identifier	Description: The activation domain (AD) is fused
1	in frame to the 178th aa of *Arabidopsis thaliana* CXIP4 (CAX INTERACTING PROTEIN 4); nucleic acid binding / zinc ion binding (CXIP4) (NM_128450)
2, 17	in frame to the 44th aa of *Arabidopsis thaliana* CXIP4 (CAX INTERACTING PROTEIN 4); nucleic acid binding / zinc ion binding (CXIP4) (NM_128450)
3-10	to *Arabidopsis thaliana* CXIP4 (CAX INTERACTING PROTEIN 4); nucleic acid binding / zinc ion binding (CXIP4) (NM_128450)
11	to the sequence encoding *Arabidopsis thaliana* CXIP4 (CAX INTERACTING PROTEIN 4); nucleic acid binding / zinc ion binding (CXIP4) which is followed by *Arabidopsis thaliana* ATPPC2 (PHOSPHOENOLPYRUVATE CARBOXYLASE 2); catalytic/ phosphoenolpyruvate carboxylase (ATPPC2) encoding sequence
12, 21	in frame to the 110th aa of *Arabidopsis thaliana* CXIP4 (CAX INTERACTING PROTEIN 4); nucleic acid binding / zinc ion binding (CXIP4) (NM_128450)
13	in frame to the 21st aa of *Arabidopsis thaliana* CXIP4 (CAX INTERACTING PROTEIN 4); nucleic acid binding / zinc ion binding (CXIP4) (NM_128450)
14	in frame to the 53rd aa of *Arabidopsis thaliana* CXIP4 (CAX INTERACTING PROTEIN 4); nucleic acid binding / zinc ion binding (CXIP4) (NM_128450)
15	to *Arabidopsis thaliana* CXIP4 (CAX INTERACTING PROTEIN 4); nucleic acid binding / zinc ion binding (CXIP4) (NM_128450).
16	to 5' UTR (untranslated region) of *Arabidopsis thaliana* CXIP4 (CAX INTERACTING PROTEIN 4); nucleic acid binding / zinc ion binding (CXIP4) mRNA at -6 nt (NM_128450)
18-20	to *Arabidopsis thaliana* CXIP4 (CAX INTERACTING PROTEIN 4); nucleic acid binding / zinc ion binding (CXIP4) (NM_128450)
22-23	to *Arabidopsis thaliana* CXIP4 (CAX INTERACTING PROTEIN 4); nucleic acid binding / zinc ion binding (CXIP4) (NM_128450)
24	in frame to the 617th aa of *Arabidopsis thaliana* SWAP (Suppressor-of-White-APricot)/surp domain-containing protein (AT5G55100) (NM_180863)
25, 29-31, 33, 34, 36	in frame to the 20th aa of *Arabidopsis thaliana* 40S ribosomal protein S24 (RPS24B) (AT5G28060) (NM_122689)
26, 42	to 5' UTR of *Arabidopsis thaliana* DEAD box RNA helicase, putative (AT1G20920) mRNA at -100 nt (NM_101945)
27	in frame to the 734th aa of *Arabidopsis thaliana* kinase interacting family protein (AT4G02710) (NM_116505)
28, 41	to 5' UTR of *Arabidopsis thaliana* unknown protein (AT2G44200) mRNA at -40 nt (NM_129984)
32, 37	in frame to the 4th aa of *Arabidopsis thaliana* endo/excinuclease amino terminal domain-containing protein (AT2G30350) (NM_128588)

Supplemental Table 3. Results of the Y2H screen using MAS2 as a bait

Prey identifier	Description: The activation domain (AD) is fused
35	in frame to the 6th aa of *Arabidopsis thaliana* NF-YC10 (NUCLEAR FACTOR Y, SUBUNIT C10); transcription factor (NF-YC10) (NM_100672)
38	to 5' UTR of *Arabidopsis thaliana* phototropic-responsive NPH3 family protein (AT5G47800) mRNA at -65 nt (NM_124154)
39	in frame to the 456th aa of *Arabidopsis thaliana* SWAP (Suppressor-of-White-APricot)/surp domain-containing protein (AT5G55100) (NM_124892)
40, 44	in frame to the 45th aa of *Arabidopsis thaliana* unknown protein (AT4G33690) (NM_119527)
43	to *Arabidopsis thaliana* DEAD box RNA helicase, putative (AT1G20920) (NM_101945)
45	in frame to the 3rd aa of *Arabidopsis thaliana* PPCK1 (PHOSPHOENOLPYRUVATE CARBOXYLASE KINASE); kinase/ protein serine/threonine kinase (PPCK1) (NM_100738)
46	in frame to the 143rd aa of *Arabidopsis thaliana* CXIP4 (CAX INTERACTING PROTEIN 4); nucleic acid binding / zinc ion binding (CXIP4) (NM_128450)
47, 48, 50	in frame to the 44th aa of *Arabidopsis thaliana* CXIP4 (CAX INTERACTING PROTEIN 4); nucleic acid binding / zinc ion binding (CXIP4) (NM_128450)
49	in frame to the 110th aa of *Arabidopsis thaliana* CXIP4 (CAX INTERACTING PROTEIN 4); nucleic acid binding / zinc ion binding (CXIP4) (NM_128450)
51-54	to *Arabidopsis thaliana* CXIP4 (CAX INTERACTING PROTEIN 4); nucleic acid binding / zinc ion binding (CXIP4) (NM_128450)
55	in frame to the 617th aa of *Arabidopsis thaliana* SWAP (Suppressor-of-White-APricot)/surp domain-containing protein (AT5G55100) (NM_180863)
56, 57	to 5' UTR (untranslated region) of *Arabidopsis thaliana* DEAD box RNA helicase, putative (AT1G20920) mRNA at -100 nt (NM_101945)
58, 59	in frame to the 20th aa of *Arabidopsis thaliana* 40S ribosomal protein S24 (RPS24B) (AT5G28060) (NM_122689)
60-65	to *Arabidopsis thaliana* 40S ribosomal protein S24 (RPS24B) (AT5G28060) (NM_122689)
66, 67	in frame to the 4th aa of *Arabidopsis thaliana* endo/excinuclease amino terminal domain-containing protein (AT2G30350) (NM_128588)
68-71	to *Arabidopsis thaliana* endo/excinuclease amino terminal domain-containing protein (AT2G30350) (NM_128588)
72	to 5' UTR of *Arabidopsis thaliana* unknown protein (AT2G40430) mRNA at -6 nt (NM_129603)
73	in frame to the 163rd aa of *Arabidopsis thaliana* myosin heavy chain-related (AT2G46250) (NM_130188)
74, 75	to *Arabidopsis thaliana* myosin heavy chain-related (AT2G46250) (NM_130188)

Supplemental Data. Sánchez-García et al. Plant Cell (2015) 10.1105/tpc.15.00135

Supplemental Table 3. Results of the Y2H screen using MAS2 as a bait

Prey identifier	Description: The activation domain (AD) is fused
76, 77	to 5' UTR of *Arabidopsis thaliana* unknown protein (AT2G44200) mRNA at -40 nt (NM_129984)
78	to 5' UTR of *Arabidopsis thaliana* unknown protein (AT5G38720) mRNA at -67nt (NM_123233)
79, 80	in frame to the 206th aa of *Arabidopsis thaliana* CXIP4 (CAX INTERACTING PROTEIN 4); nucleic acid binding / zinc ion binding (CXIP4) (NM_128450)
81, 82	out of frame to the 154th aa of *Arabidopsis thaliana* CXIP4 (CAX INTERACTING PROTEIN 4); nucleic acid binding / zinc ion binding (CXIP4) (NM_128450)
83-87	to *Arabidopsis thaliana* CXIP4 (CAX INTERACTING PROTEIN 4); nucleic acid binding / zinc ion binding (CXIP4) (NM_128450)
88	in frame to the 7th aa of *Arabidopsis thaliana* PPCK1 (PHOSPHOENOLPYRUVATE CARBOXYLASE KINASE); kinase/protein serine/threonine kinase (PPCK1) (NM_100738)
89, 90	to *Arabidopsis thaliana* PPCK1 (PHOSPHOENOLPYRUVATE CARBOXYLASE KINASE); kinase/ protein serine/threonine kinase (PPCK1) (NM_100738)
91	to the 456th aa of *Arabidopsis thaliana* SWAP (Suppressor-of-White-APricot)/surp domain-containing protein (AT5G55100) (NM_180863)

Supplemental Data. Sánchez-García et al. Plant Cell (2015) 10.1105/tpc.15.00135

SUPPLEMENTAL REFERENCES

Altschul, S.F., Gish, W., Miller, W., Myers, E.W., and Lipman, D.J. (1990). Basic local alignment search tool. J. Mol. Biol. **215**, 403-410.

Larkin, M.A., Blackshields, G., Brown, N.P., Chenna, R., McGettigan, P.A., McWilliam, H., Valentin, F., Wallace, I.M., Wilm, A., Lopez, R., Thompson, J.D., Gibson, T.J., and Higgins, D.G. (2007). Clustal W and Clustal X version 2.0. Bioinformatics **23**, 2947-2948.

Myburg, A.A., Grattapaglia, D., Tuskan, G.A., Hellsten, U., Hayes, R.D., Grimwood, J., Jenkins, J., Lindquist, E., Tice, H., Bauer, D., Goodstein, D.M., Dubchak, I., Poliakov, A., Mizrachi, E., Kullan, A.R., Hussey, S.G., Pinard, D., van der Merwe, K., Singh, P., van Jaarsveld, I., Silva-Junior, O.B., Togawa, R.C., Pappas, M.R., Faria, D.A., Sansaloni, C.P., Petroli, C.D., Yang, X., Ranjan, P., Tschaplinski, T.J., Ye, C.Y., Li, T., Sterck, L., Vanneste, K., Murat, F., Soler, M., Clemente, H.S., Saidi, N., Cassan-Wang, H., Dunand, C., Hefer, C.A., Bornberg-Bauer, E., Kersting, A.R., Vining, K., Amarasinghe, V., Ranik, M., Naithani, S., Elser, J., Boyd, A.E., Liston, A., Spatafora, J.W., Dharmwardhana, P., Raja, R., Sullivan, C., Romanel, E., Alves-Ferreira, M., Kulheim, C., Foley, W., Carocha, V., Paiva, J., Kudrna, D., Brommonschenkel, S.H., Pasquali, G., Byrne, M., Rigault, P., Tibbits, J., Spokevicius, A., Jones, R.C., Steane, D.A., Vaillancourt, R.E., Potts, B.M., Joubert, F., Barry, K., Pappas, G.J., Strauss, S.H., Jaiswal, P., Grima-Pettenati, J., Salse, J., Van de Peer, Y., Rokhsar, D.S., and Schmutz, J. (2014). The genome of *Eucalyptus grandis*. Nature **510**, 356-362.

The ribosomal biogenesis factor SMALL ORGAN 4 functions in 5.8S and 18S rRNA maturation in Arabidopsis

Rosa Micol-Ponce, Raquel Sarmiento-Mañús, and María Rosa Ponce

Instituto de Bioingeniería, Universidad Miguel Hernández, Campus de Elche, 03202 Elche, Alicante, Spain.

Running title: Arabidopsis SMO4 functions in 5.8S and 18S rRNA maturation

Corresponding author: María Rosa Ponce (mrponce@umh.es).

Character count, 50310; Word count (total), 8942; Word count excluding Title page, supporting information legends and References, 6988.
Word count breakdown: Title page, including Significance statement, 202; Significance statement, 74; Abstract, 236; Introduction, 680; Results, 2364; Discussion, 2016; Experimental procedures, 1106; Acknowledgements, Accession numbers, and Author contributions, 146; Tables, 0; Figure legends, 422; Supporting information legends, 180; References, 1572.

Figures: 4 Tables: 0 Supporting Figures: 11 Supporting Tables: 3 Supporting Datasets: 1

SIGNIFICANCE STATEMENT

Once thought by some to be a house-keeping function, ribosome biogenesis is now considered crucial for growth in multicellular eukaryotes, and is linked to human aging and diseases, including cancer. Hundreds of Arabidopsis genes are annotated as ribosome biogenesis factors (RBFs) based only on their evolutionary sequence conservation. Here, we provide experimental evidence for the role of Arabidopsis SMALL ORGAN 4 as a RBF involved in the maturation of 5.8S and 18S ribosomal RNAs.

ABSTRACT

Ribosome biogenesis is crucial for cellular metabolism and has important implications for disease and ageing. Nucleolar protein 53 (Nop53) and mRNA transport 4 (Mtr4) are ribosome biogenesis factors (RBFs) in yeast. Interaction between Nop53 and Mtr4 is required for the processing of 5.8S ribosomal RNA (rRNA) precursors. The conserved motifs that facilitate this interaction are also present in SMALL ORGAN 4 (SMO4) and MTR4, the Arabidopsis orthologs of Nop53 and Mtr4, respectively. Arabidopsis MORPHOLOGY OF ARGONAUTE1-52 SUPPRESSED 2 (MAS2) is required for 45S rDNA transcriptional regulation and 45S pre-rRNA processing. In a yeast two-hybrid screen, we found that SMO4 interacts with MAS2. In a genetic screen for Arabidopsis mutants with altered leaf shape, we identified *denticulata2* (*den2*), which resulted to be an allele of *SMO4*. We observed *SMO4* coexpression with numerous genes encoding demonstrated or predicted RBFs, including *MTR4*. Mutation of *SMO4* resulted in accumulation of 5.8S and 18S rRNA precursors that are present in trace amounts in wild type, and nucleolar retention of 25S and 18S, but not 5.8S rRNA species. Double mutant analysis revealed that *smo4-3* is epistatic to *mtr4-1* and synergistically interacts with *mas2-1* and alleles of *NUCLEOLIN1* (which encodes the NUC1 nucleolar RBF). These results show the role of SMO4 in ribosome biogenesis and confirm its interaction with MAS2. Comparable to its yeast and human orthologs, SMO4 participates in 5.8S rRNA maturation; however, in contrast, SMO4 also participates in 18S rRNA maturation.

INTRODUCTION

The eukaryotic 80S cytoplasmic ribosome was first described in the mid-1950s (Palade, 1955) and is now considered a paradigm of our understanding of complex molecular machines (Dinman, 2009). The structure and biogenesis of the 80S ribosome are similar in all eukaryotes. Furthermore, the ribosomal RNAs (rRNAs) and proteins (RPs) involved in these processes are highly conserved. The function of the 80S ribosome—messenger RNA (mRNA) translation—exhibits high-level evolutionary conservation similar to other essential cellular functions.

Approximately 80 RPs and four rRNAs form the 80S ribosome. These rRNAs are produced by processing of the primary transcripts of the repeated 5S rDNA and 47S, 45S, and 35S rDNA genes in animals, plants, and yeast, respectively. Processing of the 5S pre-rRNA primary transcript to produce the mature 5S rRNA is straightforward. By contrast, processing of the 47S/45S/35S pre-rRNA to produce the mature 5.8S and 18S rRNAs in all eukaryotes, the mature 25S rRNA in yeast and plants, and the mature 28S rRNA in animals is a complex, multistep process (Wilson and Doudna Cate, 2012). Biogenesis of the 80S ribosome in eukaryotes is best characterized in *Saccharomyces cerevisiae*. Indeed, the individual functions of not few plant and animal ribosome biogenesis factors (RBFs) and the interactions among them have been inferred based on their homology with putative yeast orthologs.

The exosome, an evolutionarily conserved complex in eukaryotes, has 3′→5′ exoribonuclease activity that is required for the metabolism of many RNA species, such as mRNAs, rRNAs, small nucleolar RNAs (snoRNAs), and small nuclear RNAs (snRNAs). For these RNA species, the exosome facilitates degradation, surveillance, precursor processing, and degradation of processing by-products (Kilchert *et al.*, 2016). In yeast, Nucleolar protein 53 (Nop53; Thomson and Tollervey, 2005) acts as an adaptor protein that targets the mRNA transport 4 (Mtr4) ATP-dependent RNA helicase (Kilchert *et al.*, 2016) to pre-ribosomal particles for exosome processing of the 3′ end of the 7S pre-rRNA, a 5.8S rRNA precursor (Figure S1; Thoms *et al.*, 2015). The loss of *Nop53* function causes severe growth effects and accumulation of 7S pre-rRNA and other 5.8S rRNA precursors (Granato *et al.*, 2005; Sydorskyy *et al.*, 2005; Thomson and Tollervey, 2005). Yeast Mtr4 is also essential and loss of Mtr4 function reduces 5.8S rRNA production (de la Cruz *et al.*, 1998). MTR4, the Arabidopsis ortholog of yeast Mtr4, is required for 18S and 5.8S rRNA maturation (Figure S2), and the Arabidopsis *mtr4* mutants accumulate 18S and 5.8S rRNA precursors (Lange *et al.*, 2011). The Arabidopsis ortholog of yeast *Nop53* is encoded by AT2G40430, which during the progress of this work was named *SMALL ORGAN 4* (*SMO4*) by Zhang *et al.* (2015).

SMO4 was characterized as a nuclear protein that affected cell proliferation (Zhang *et al.* (2015). A role for SMO4 in ribosome biogenesis has not been established to date.

In Arabidopsis, ARGONAUTE1 (AGO1) is the main ribonuclease that functions in post-transcriptional gene silencing (PTGS) pathways mediated by microRNAs (miRNAs) and other small RNAs (Baumberger and Baulcombe, 2005). In a suppressor screen performed following a second-site mutagenesis of the *ago1-52* hypomorphic and viable mutant, we isolated 22 extragenic suppressor mutations. Several of the suppressor mutations identified were alleles of AT4G02720, which we named *MORPHOLOGY OF ARGONAUTE1-52 SUPPRESSED 2* (*MAS2*; Micol-Ponce *et al.*, 2014). We found that MAS2 is an essential perinucleolar protein that colocalizes with 45S rDNA, negatively regulating 45S rDNA expression. We also found that MAS2 is required for 45S pre-rRNA processing. Subsequently, a yeast two-hybrid (Y2H) screen identified 14 MAS2 interactors (Sánchez-García *et al.*, 2015), which included SMO4.

Here, we studied the action and interactions of Arabidopsis SMO4 at the genetic, morphological, cytological, and molecular levels. We found that SMO4 localizes to both the nucleolus and nucleoplasm (similar to yeast Nop53), and observed its involvement in 5.8S rRNA maturation. However, in contrast to Nop53, we also found a role for SMO4 in 18S rRNA maturation. In addition, *smo4* alleles synergistically interact with the *mas2-1* allele, indicating a functional relationship between *MAS2* and *SMO4*. Our results thus show key roles for these RBFs in rRNA maturation and reveal intriguing differences between plants and other eukaryotes in this highly conserved process.

RESULTS

Nop53/GLTSCR2 family members possess a conserved motif of interaction with the Mtr4 exosome cofactor

The Nop53/GLTSCR2 protein family is conserved in all eukaryotes and includes yeast Nop53 and the human Glioma Tumor-Suppressor Candidate Region Gene 2 (GLTSCR2) nucleolar protein (Lee *et al.*, 2012), which is also known as GSCR2, p60, and PICT1 (Protein Interacting with Carboxyl Terminus 1′). The TAIR10 and Araport11 annotations of AT2G40430 (*SMO4*) describe the gene as encoding a homolog of yeast Nop53. Compared to human GLTSCR2, yeast Nop53 has 18.53% amino acid sequence identity and 30.76% similarity, and Arabidopsis SMO4 has 20.70% identity and 35.20% similarity, respectively. Yeast Nop53 and Arabidopsis SMO4 share 17.23% identity and 31.46% similarity. *SMO4* transcription generates three splice variants, which encode proteins with 442 (AT2G40430.1), 449 (AT2G40430.2), and 441 (AT2G40430.3) aa that differ from one another in the C-terminus.

In yeast, an N-terminal LFXφD arch interaction motif (AIM; X: any amino acid, φ: a hydrophobic amino acid) of Nop53 interacts with the arch domain of the Mtr4 exosome cofactor (Jackson *et al.*, 2010; Thoms *et al.*, 2015). The AIM in yeast Nop53, human GLTSCR2, and Arabidopsis SMO4 is well conserved, despite the above-mentioned relatively low identities shared between these proteins. The Arabidopsis SMO4 and yeast Nop53 AIM sequence is LFHVD, and the human GLTSCR2 AIM sequence is LFFVD (V: a hydrophobic residue; Figure S3). This motif is present in species representative of all the major plant clades, as is evident in a multiple alignment of putative plant Nop53 orthologs, where φ is V in all species except for *Glycine max*, where E, a charged residue, is present at this position (Figure S4). An arch domain is also present in Arabidopsis MTR4, which plays an important role in 5.8S rRNA maturation and degradation of the 5′-ETS of its precursors (Figure S2; Jackson *et al.*, 2010). The arch domain is well conserved in eukaryotic MTR4 orthologs from different kingdoms (Figure S5), in particular among representative plant species (Figure S6). However, the helicase domains of these orthologous proteins are conserved to a greater extent**.**

Novel alleles of *SMO4* confirm its non-essential role in Arabidopsis

In yeast, the lack of *Nop53* function is lethal or associated with significant growth defects (Granato *et al.*, 2005; Sydorskyy *et al.*, 2005; Thomson and Tollervey, 2005). The first identified *SMO4* mutant allele, *smo4-1*, was isolated because of its associated mutant phenotype: reduced plant size resulting from a delay in cell cycle progression during leaf development that ultimately reduced cell number (Zhang *et al.*, 2015). The *smo4-1* allele carries a 14-bp deletion in the 12th exon of *SMO4*, which is predicted to produce a

truncated protein 12 aa shorter than the wild-type version. We obtained publicly available lines carrying insertional mutant alleles of *SMO4*. These T-DNA insertions disrupted *SMO4* in its 14th exon (*smo4-2*; SALK_012561; Zhang *et al.*, 2015) and 12th intron (SALK_071764, referred to herein as *smo4-3*) (Figure 1a–d).

Under our growth conditions, the *smo4-2* and *smo4-3* mutants have very mild morphological phenotypes at 14 days after stratification (das), with mildly dentate and pointed rosette leaves, and mutant plants become near indistinguishable from wild type at bolting. The three *smo4* alleles described above are potentially hypomorphic based on their weak mutant phenotype and because the T-DNA insertions in *smo4-2* and *smo4-3* and the deletion mutation in *smo4-1* are located near the 3′ end of the AT2G40430 coding region (Figure 1a). Hence, we also included the GABI-082H04 line (herein referred to as *smo4-4*) in our analysis, which carries a *SMO4* allele with a T-DNA insertion disrupting the first exon (Figure 1a, e). Homozygous *smo4-2*, *smo4-3*, and *smo4-4* plants displayed indistinguishable phenotypes, suggesting that each mutant allele confers the same *SMO4* loss of function and are potentially null mutants.

In a large-scale EMS mutant screen performed in the laboratory of J.L. Micol, 58 *denticulata* (*den*) pointed-leaf mutants were isolated and found to fall into 17 complementation groups (Berná *et al.*, 1999). A single *den2* mutant allele was isolated and mapped at a low-resolution level to chromosome two (Robles and Micol, 2001). We delimited a candidate 3.8 Mb genomic region using iterative linkage analysis (Table S1) and performed whole-genome sequencing using DNA isolated from *den2* plants. This revealed a C→T base change in the 12th exon of AT2G40430, which is located in the candidate genomic region. This base change is predicted to cause a nonsense mutation (Arg372→STOP), producing a truncated protein that is 71 aa shorter than the wild-type protein (Figure 1a). A *smo4-3* × *den2* cross confirmed that these two mutants are allelic (Figure S7). The morphological phenotype of *den2* is more obvious than that of *smo4* plants (Figure 1f, g), which is potentially due to the L*er* genetic background of *den2*.

To verify that the *smo4* and *den2* mutant phenotypes were the result of a lack of SMO4 activity, we created $SMO4_{pro}$*:SMO4* construct, which was transferred into *smo4-2*, *smo4-3*, *den2*, Col-0, and L*er* plants. $SMO4_{pro}$*:SMO4* complemented the mutant phenotypes of *smo4* and *den2* (Figure 1h-j). We also created the and $35S_{pro}$*:SMO4* construct and no visible morphological effect was apparent when we transferred it into wild-type background. We concluded that *SMO4* is a single-copy yet non-essential gene, whose null mutation results in mild and transient growth effects.

SMO4 is located in both the nucleolus and nucleoplasm

In addition to 5.8S rRNA maturation (Figure S1), yeast Nop53 is required for the nuclear

export of the 60S pre-ribosomal particle, which matures in the cytoplasm into the 60S subunit of the 80S ribosome (Thomson and Tollervey, 2005). To perform this dual role in ribosome biogenesis, SMO4 should be located in both the nucleolus and the nucleoplasm. To test this hypothesis, we generated constructs containing SMO4:GFP translational fusion, with expression driven by the endogenous *SMO4* promoter. The *SMO4$_{pro}$:SMO4:GFP* construct produced a functional protein that complemented the mutant phenotype of *smo4-2*, *smo4-3*, and *den2* plants (Figure 1k–m).

Previously published results indicate that SMO4 is a nuclear protein (Zhang *et al.,* 2015), but its nucleolar and/or nucleoplasmic localization is not known. To visualize the nucleus, we stained the roots of Col-0 plants with Hoechst 33342, a dye that strongly binds double-stranded DNA but not RNA, which is the primary nucleic acid in the nucleolus. GFP fluorescence was detected in a diffuse pattern in both the nucleolus and the nucleoplasm (Figure 1n–p).

SMO4 is coexpressed with genes encoding nuclear proteins

To characterize the role that SMO4 plays in ribosome biogenesis, we analyzed the set of coregulated genes derived from microarray assays provided by the ATTED-II coexpression database. Out of 100 genes that displayed the highest level of coexpression with *SMO4*, 59 encoded nuclear proteins, and most of these are known or predicted to be RBFs of both subunits (Supporting Dataset 1). *RIBOSOMAL RNA-PROCESSING 7* (*RRP7*), which encodes another MAS2-interacting protein identified in our Y2H-based screen (Sánchez-García *et al.*, 2015; Micol-Ponce *et al.*, submitted), was ranked fourth highest among genes coexpressed with *SMO4*. The most represented genes among those coexpressed with *SMO4* were genes encoding components of the SSU processome, the large complex that initiates 45S pre-rRNA processing cotranscriptionally (Sloan *et al.*, 2014). We also identified *MTR4* and *XRN2* among genes coexpressed with *SMO4*, which were ranked 38th and 64th highest, respectively. As mentioned above, the Arabidopsis MTR4 helicase, like its Mtr4 yeast ortholog, associates with the nuclear exosome to process 5.8S rRNA precursors and rRNA maturation by-products (Lange *et al.*, 2011; Lange *et al.*, 2014). Arabidopsis XRN2 (EXORIBONUCLEASE2; yeast Xrn2 is also known as Ribonucleic acid trafficking 1, Rat1; Figure S1) is a 5′→3′ exoribonuclease that participates in the 5′-processing of 35S$_{A123B}$ pre-rRNA (Figure S2), and the degradation of precursors, intermediates, and by-products derived from pre-rRNA processing (Zakrzewska-Placzek *et al.*, 2010).

The combination of previously published results (Zhang *et al.*, 2015), data deposited at the Transcriptomic Variation Analysis (TraVA) Database (http://travadb.org/), and our observations of *SMO4* promoter activity using the *GUS*

reporter gene (data not shown) indicated that *SMO4* is expressed at different levels in all plant tissues studied. TraVA data on *MTR4* (Figure S8) and *XRN2* (Figure S9) also indicated generalized expression, as has been previously described (Lange *et al.*, 2011).

45S pre-rRNA processing is altered in the *smo4-2*, *smo4-3,* and *den2* mutants

Yeast *nop53* mutants accumulate 7S pre-rRNA and other 5.8S rRNA precursors (Granato *et al.*, 2005; Thomson and Tollervey, 2005), and Arabidopsis *mtr4* mutants accumulate 5.8S and 18S rRNA precursors (Lange *et al.*, 2011). To visualize the intermediates of 45S pre-rRNA processing in Arabidopsis (Figure S2), we performed a Northern blot analysis of RNA extracted from *smo4-2*, *smo4-3*, and *den2* plants using the previously described S7 and S9 probes (Lange *et al.*, 2011). The S7 and S9 probes are complementary to a segment of the ITS1 and ITS2, respectively (Figure 2a).

With the S9 probe, we detected accumulation of several intermediates in *smo4-2*, *smo4-3* and *den2* mutants: 27S ($27SA_2$/$27SA_3$ and/or 27SB) and 5.8S rRNA precursors, specifically the 7S, 5.8S+30, and 6S pre-rRNAs, (Figure 2b, c). Each of these pre-rRNA species was nearly or completely undetectable in L*er*, Col-0, and *smo4-3* $SMO4_{pro}$*:SMO4* plants (Figure 2b, c), with the exception of the 7S pre-rRNA, which was detected in all samples, and the 6S pre-rRNA, which was detected in *smo4-3* $SMO4_{pro}$*:SMO4*. We also detected a 5.8S rRNA precursor longer than the 7S species in *smo4-2* and *smo4-3* (Figure 2c and S2), which has been described previously in a study of the *xrn2 xrn3* double mutant as A3-C2 pre-rRNA (also called 5′-extended 7S pre-rRNA; Zakrzewska-Placzek *et al.*, 2010).

We did not observe substantial differences in 35S, 35S(P), 33S(P′) or 32S pre-rRNA levels between *smo4* and *den2* mutants and their wild types using the S7 or S9 probes (Figure 2b, d). However, strong accumulation of P-A_3 pre-rRNA, the first intermediate in the ITS1-first pathway (Figure S2), was detected in *smo4-2*, *smo4-3,* and *den2*, but not in *smo4-3* $SMO4_{pro}$*:SMO4* or the wild types using the S7 probe (Figure 2a, d). As previously reported (Lange *et al.*, 2011), we observed P′-A_3 pre-rRNA accumulation in the *mtr4-1* mutant, which was included as a control (Figure 2d). P-A3 is a precursor of P′-A_3, which is generated by cleavage at the P′ site of the P_1-A_3 pre-rRNA (Figure S2). In conclusion, both 5.8S and 18S rRNA maturation are perturbed in *smo4-2*, *smo4-3,* and *den2*. These effects are consistent with those in *mtr4-1*, in which 18S and 5.8S rRNA maturation are affected, as previously described (Figure 2c, d; Lange *et al.*, 2011; Lange *et al.*, 2014).

25S and 18S rRNA species accumulate in the nucleolus of *smo4-3* plants

Given that 45S pre-rRNA processing is defective in *smo4-2*, *smo4-3,* and *den2*, we further investigated whether any mature or precursor rRNA species accumulated in the nucleolus or the nucleoplasm in these mutant lines. We performed RNA fluorescence *in situ* hybridizations (RNA-FISH) using probes that hybridize with mature 5.8S, 18S, and 25S rRNAs, which also detect pre-rRNAs containing the 5.8S, 18S, and 25S coding sequences (Table S2). In wild-type plants, we detected 5.8S, 18S, and 25S species accumulating in the cytoplasm in a diffuse pattern, and some accumulation of 25S rRNA in the nucleolus. We also found 5.8S, 18S, and 25S species in the cytoplasm of *smo4-3* plants, as in the wild-type plants. In addition, we detected accumulation of 18S rRNA and high-level accumulation of 25S rRNA in the nucleolus of *smo4-3* (Figure 3a–d, h–k). Unexpectedly, no difference was observed between Col-0 and *smo4-3* plants regarding 5.8S rRNA subcellular distribution (Figure 3i–n).

smo4-3* is epistatic to *mtr4-1* and synergistically interacts with *mas2-1

The morphological phenotypes of *mtr4-1* and *smo4* plants are similar, although it is possible to distinguish between the two lines at early stages of vegetative development (Figure 1c, d, e, and 4a), which suggests that MTR4 and SMO4 participate in the same steps of 45S pre-rRNA processing. In addition, the *smo4-3 mtr4-1* double mutant is indistinguishable from the *smo4-3* single mutant (Figure 4b, f, g). The epistasis of *smo4-3* to *mtr4-1* suggests that SMO4 acts upstream MTR4 in the 5.8S and 18S rRNA maturation pathways, or that it plays alternate roles in rRNA biogenesis pathways.

To genetically confirm the Y2H-detected physical interaction of MAS2 with SMO4, we combined *smo4-3* with the *MAS2* allele *mas2-1*, the latter of which has a dominant suppressor effect on the mutant phenotype of *ago1-52* but lacks phenotypic effects *per se* (Figure 4c; Sánchez-García *et al.*, 2015). The *smo4-3 mas2-1* double mutant displayed a synergistic phenotype, with markedly dentate and pale vegetative leaves (Figure 4h).

Since *mas2* alleles appeared antimorphic, and null alleles of *MAS2* are lethal, we generated plants expressing *amiR-MAS2*, an artificial miRNA that reduces *MAS2* mRNA levels five-fold (Sánchez-García *et al.*, 2015). These plants, termed *amiR-MAS2.1*, possess a phenotype comparable to that of *mas2-1 smo4-3* double mutant plants. Despite their morphological aberrations, *smo4-3 mas2-1* double mutant plants, like *amiR-MAS2.1* plants, were viable and produced a small amount of seed.

smo4-3 synergistically interacts with alleles of *NUC1*

Arabidopsis has two paralogous genes encoding NUCLEOLIN proteins: *NUC1* and *NUC2*, which appear to act antagonistically in the control of 45S rDNA expression (Pontvianne *et al.*, 2007; Durut *et al.*, 2014) in the nucleolus. *NUC1* is expressed in all tissues and its mutations cause nucleolar disorganization, chromatin decondensation at the Nucleolar Organizer Regions, and 45S rDNA up-regulation. *NUC2* is expressed in *nuc1* but not in wild-type plants. *NUC1* was also identified based on its mutant phenotype of aberrations in leaf development and vein patterning. This phenotype was caused by *NUC1* null alleles termed *parallel1* (*parl1*), which cause accumulation of $35S_{A123B}$ pre-rRNA because of failure of cleavage at the P site (Petricka and Nelson, 2007; Pontvianne *et al.*, 2007) of the 5′-ETS of $35S_{A123B}$ pre-rRNA (Figure S2).

To determine if *NUC1* or *NUC2* are functionally related to *SMO4*, we obtained double mutant lines that combined *smo4-3* with either *parl1-2* or *nuc2-2*. The *smo4-3 parl1-2* double mutant exhibits a synergistic phenotype, characterized by narrow leaves and enhanced anthocyanin accumulation (Figure 4d, i). This result provides genetic evidence of a functional relationship between *SMO4* and *NUC1*. In contrast, the double mutant phenotype of *smo4-3 nuc2-2* plants was additive only (Figure 4e, j). The TraVA database confirmed that, as mentioned above, *NUC1* is expressed in most organs and developmental stages, in all of which *NUC2* mRNA is absent or present at a very low level, aside from in the anthers (Figures S11 and S12).

DISCUSSION

Evolutionary conservation and divergence of the SMO4 role in ribosome biogenesis

80S ribosome biogenesis is an essential and evolutionarily conserved process, which has diverged among fungi, plants, and animals. The extent of this conservation is proven by the existence of one or more Arabidopsis orthologs for 179 of the approximate 250 RBFs in yeast (Simm *et al.*, 2015). Evidence of the divergence in 80S ribosome biogenesis is provided by the observation that many human orthologs of yeast RBFs are involved in pre-rRNA processing but have evolved a different function, and that 74 human RBFs lack orthologs in yeast (Wild *et al.*, 2010; Tafforeau *et al.*, 2013).

Based on their homology with yeast and human proteomes, several hundred Arabidopsis proteins are annotated as encoding putative components of the ribosome biogenesis machinery, including RPs and RBFs. Mutants representing more than 20 affected RP-encoding genes have been isolated in screens for morphological aberrations or embryonic lethality (Byrne, 2009; Horiguchi *et al.*, 2011). A recent survey of plant RBFs studied at a mutational and molecular level detailed 28 individual proteins, all but one of which with a yeast ortholog. Aside from for two of these plant RBFs, gene mutations result in a developmental phenotype, and mutants in 16 of these RBF-encoding genes accumulate pre-rRNAs, which reveals that rRNA maturation is defective. The wild-type versions of 18 of these Arabidopsis RBF-encoding genes have been transferred into yeast strains that carry mutations causing absence or depletion of the corresponding RBF ortholog. Complementation of the yeast RBF mutant phenotype was observed with only eight of the 18 tested Arabidopsis RBF-encoding genes (Weis *et al.*, 2015).

Here, we report functional characterization of Arabidopsis *SMO4*, which encodes a Nop53/GLTSCR2 family protein with yeast and human orthologs that are proven RBFs. Our results provide experimental evidences for SMO4 function as an Arabidopsis RBF. Yeast *Nop53* is a single-copy, essential gene, as is expected from its key role in 5.8S rRNA maturation (Granato *et al.*, 2005). *SMO4* is also a single-copy gene in Arabidopsis, but it is not essential. Indeed, null alleles of Arabidopsis *SMO4* are associated with a mild morphological phenotype, characterized by an approximate 20% reduction in cell number and whole organ size in petals and vegetative leaves, as well as a reduction in root length (Zhang *et al.*, 2015), and which becomes less apparent in latter stages of plant development. The individual loss of a number of RBFs is lethal in *Saccharomyces cerevisiae*, but the same effect is not observed for some of their plant or animal orthologs. This may be due to the use of alternative pathways in Arabidopsis that circumvent

lethality following the loss of a single RBF. An alternative explanation is the assembly of aberrant, unprocessed rRNAs in ribosomal subunits to create translation-competent ribosomes. For example, *Escherichia coli* RNase III mutants accumulate unprocessed pre-rRNAs but are still viable because an alternative pathway for 16S rRNA maturation exists. In these mutants, an aberrant 23S pre-rRNA species retaining unprocessed extensions at its 5′ and 3′ ends can assemble into functional ribosomes (King *et al.*, 1984).

We found that a lack of *SMO4* function in *smo4-2*, *smo4-3*, and *den2* mutants causes accumulation of P-A_3, a 18S rRNA precursor that is absent or barely detected in the corresponding wild type. This observation implies that SMO4 is involved in 5.8S rRNA maturation, similarly to that described for yeast *nop53* mutants and for human HeLa cells with reduced *GLTSCR2* expression from RNA interference (Granato *et al.*, 2005; Thomson and Tollervey, 2005; Tafforeau *et al.*, 2013). It seems that the aberrant 5.8S rRNA precursor species detected here do not prevent the assembly and export of 60S pre-ribosomal particles to the cytoplasm, since we did not see accumulation of 5.8S rRNA in the nucleolus or nucleoplasm of *smo4-3* plants.

In conclusion, our description of the morphological, cytological, and molecular phenotypes caused by a *SMO4* lack of function sheds light on the role of SMO4 in ribosome biogenesis, specifically in the processing of 5.8S and 18S rRNA precursors. It can therefore be assumed that SMO4 acts as a RBF, notwithstanding that several Arabidopsis nucleolar proteins, including U3 snoRNP-associated factors but not SMO4, have been co-purified using a MTR4:GFP fusion protein. As mentioned above, many plant RBFs do not complement mutant yeast strains that lack the corresponding RBF ortholog (Weis *et al.*, 2015), one of which is *MTR4* (Lange *et al.*, 2014). It is thus unsurprising that Arabidopsis *SMO4* transferred into yeast did not complement a *Nop53* lack of function (Zhang *et al.*, 2015).

SMO4 is functionally related with *MTR4* and *NUC1*

We detected accumulation of several pre-rRNA intermediates in *smo4-2*, *smo4-3*, and *den2* compared to that in wild type (Col-0 and L*er*, respectively), namely the P-A_3, 7S, 5.8S+30, and 6S precursors. The 33S(P′), 32S, and 27SA_2 pre-rRNA species, which are absent from *smo4* mutants, are intermediates of the 5′-ETS-first pathway, but are not produced by the alternative ITS1-first pathway (Figure S2). This potentially indicates that, in the wild type, SMO4 promotes the use of the 5′-ETS-first pathway to separate the 40S and 60S pre-ribosomal particles. It appears that in *smo4* and *den2* plants, the ITS-first pathway is used and defective processing of the pre-rRNA intermediates lead to their accumulation (Figure S2). The bands visualized using the S9 probe were similar in size

and intensity in *smo4-3, smo4-2*, and *den2*, as well as in *mtr4-1* (Lange *et al.*, 2011), which was included as a control. These results suggest that SMO4 facilitates the exonucleolytic trimming of 5.8S rRNA precursors, comparable to what has been shown for yeast Mtr4, and Arabidopsis MTR4 in *mtr4* plants (Lange *et al.*, 2011).

Yeast Nop53 acts as an adaptor protein, interacting via its AIM with the arch domain of Mtr4 for exosome recruitment to rRNA precursors (Thoms *et al.*, 2015). Notwithstanding the low level of similarity observed between SMO4 and its yeast Nop53 and human GLTSCR2 orthologs, the AIM in these proteins is conserved like in comparable proteins in many other plant species. Conservation of the SMO4 AIM and the MTR4 arch domain in Arabidopsis and other plant species suggests that the mechanism of exosome recruitment to 45S pre-rRNA is also conserved. Taken together, these results and the similar morphological phenotypes of *mtr4-1*, *smo4-2*, *smo4-3*, and *den2* plants, as well as the epistasis of *smo4-3* to *mtr4-1*, indicate that MTR4 and SMO4 play roles in the same steps of the 18S and 5.8S rRNA maturation pathway, but that SMO4 acts upstream MTR4, as it has been shown in yeast.

We have found that SMO4 participates in the same steps than MTR4 in 5.8S rRNA biogenesis. However, SMO4 seems to act before MTR4 in the ITS1-first pathway that generates 18S rRNA (Figures 2 and S2). This is consistent with the epistasis of *smo4-3* to *mtr4-1* that we observed. The weak morphological phenotype of *smo4* mutants indicate that mature, functional 18S and 5.8S rRNAs are produced in these mutants by alternative pathways. We also conclude that accumulation of 5.8S and 18S rRNA precursors have no effect on viability or fertility, and only mildly affects development.

The synergistic phenotype of *smo4-3 parl1-2* serves as genetic evidence of the functional relationship between *SMO4* and *NUC1*. This result was expected, because both SMO4 and NUC1 are RBFs that participate in 45S pre-rRNA processing.

SMO4 is functionally related to *MAS2*

The number of proteins characterized to bind RNA or play roles in processes involving RNA molecules has been increasing over the last decades, together with the number of know RNA functions. Some of these proteins are known to play multiple roles in RNA metabolism pathways, of which many appear ancient. For example, metazoan NF-kappa B activating protein (NKAP) is a multifunctional factor involved in the regulation of diverse processes such as cellular differentiation, proliferation, and apoptosis. Human NKAP has been found bound to different spliceosomal complexes and to pre-mRNAs and spliced mRNAs, as well as associated with snRNAs, snoRNAs, rRNAs, and long intergenic noncoding RNAs (Burgute *et al.*, 2014).

Small RNAs are involved in PTGS pathways and epigenetic regulation of gene transcription. To further our understanding of AGO1 function, the main ribonuclease acting in PTGS pathways mediated by miRNAs, we performed a screen for suppressors of the morphological phenotype of the *ago1-52* hypomorphic and viable allele. One of the suppressor genes that we identified is *MAS2*, which encoded the Arabidopsis ortholog of human NKAP (Sánchez-García *et al.*, 2015). Comparable to NKAP, MAS2 is essential and multifunctional in that, among other processes including splicing, it participates in the control of 45S rDNA transcription, and 45S rRNA processing. In a search for physical interactors of MAS2, we identified SMO4.

The synergistic phenotype of the *smo4-3 mas2-1* double mutant and the similar phenotypes of *amiR-MAS2.1* and *smo4-3 mas2-1* plants confirm the physical interaction between SMO4 and MAS2 originally detected by Y2H. Taken together, these results indicate that SMO4 and MAS2 are functionally related. In addition, the similar phenotypes of *amiR-MAS2.1* and *smo4-3 mas2-1* suggest that MAS2 function requires SMO4. One possibility is that MAS2 acts downstream of SMO4 in 45S pre-rRNA processing. An alternate possibility is that SMO4, in addition to its role in rRNA biogenesis, participates together with MAS2 in the ribosome quality control (RQC) surveillance pathway, which enables the degradation of aberrantly spliced mRNAs or inhibits their export to the cytoplasm.

We have not found *in silico* yeast orthologs of Arabidopsis MAS2 or human NKAP. However, *Dictyostelium discoideum* has a NKAP ortholog that also, owing to its co-immunoprecipitation with several RPs and RNA-binding proteins, including RBFs such as bystin, appears to be a multifunctional protein functionally related to ribosome biogenesis (Burgute *et al.*, 2016). *Saccharomyces cerevisiae* possesses a bystin ortholog, namely Essential nuclear protein 1 (Enp1), which is required for efficient nuclear export of the pre-40S ribosomal particle (Seiser *et al.*, 2006). In *enp1* and *mtr4* yeast lines, mRNAs are retained within the nucleolus. Nuclear retention of mRNAs is also caused by mutations in genes involved in rRNA biogenesis or pre-mRNA splicing, RQC (including genes encoding components of the nuclear exosome), and mRNA nuclear export (Paul and Montpetit, 2016).

There are further examples of RBFs with roles in different RNA metabolism pathways. The DEAH box ATPase Prp43 is a yeast nucleolar protein that functions in both 18S rRNA maturation from its 20S pre-rRNA precursor and spliceosome disassembly (Combs *et al.*, 2006; Leeds *et al.*, 2006). The DEAD box, DEAH box, and SKI of helicases belong to the DExD/H family. Mtr4 is also a DExD/H family member, and it is a component of the TRAMP (Trf4/5-Air1/2-Mtr4 Polyadenylating) complex. The TRAMP complex has poly(A)polymerase activity, is associated with the nuclear

exosome, and is involved in the turnover and nuclear surveillance of intergenic transcripts and noncoding RNAs, including the degradation of aberrant mRNAs and tRNAs (Kilchert *et al.*, 2016). Mtr4 also has TRAMP-independent functions, including its above-mentioned role as an exosome cofactor, which, together with Nop53, is involved in processing of the 7S precursor of 5.8S rRNA. Also as mentioned above, the Arabidopsis XRN2 exoribonuclease is involved in 5′-processing of 5.8S pre-rRNAs (Zakrzewska-Placzek *et al.*, 2010). Together with its functionally redundant XRN3 paralog, XRN2 acts additionally as an endogenous suppressor in PTGS pathways that are mediated by AGO1. The loops that are formed in miRNA precursors are degraded by XRN2 and XRN3, preventing their inclusion in the PTGS pathway, and these precursors accumulate in *xrn2* and *xrn3* mutants (Gy *et al.*, 2007).

Nucleolar stress or ribosomal stress are terms used to describe any alteration of ribosome biogenesis or function that disrupts cell homeostasis (James *et al.*, 2014). Human p53 is a tumor suppressor that acts as a cellular stress sensor, triggering transient or permanent cell cycle arrest and apoptosis (Bieging *et al.*, 2014). GLTSCR2 (PICT1), the human ortholog of Arabidopsis SMO4, is a tumor suppressor factor that stabilizes p53, subsequently inhibiting cell cycle progression in response to nucleolar stress (Lee *et al.*, 2012). Although plants lack a p53 ortholog, it is possible that a member of the Nop53/GLTSCR2 family such as SMO4 participates in the response to nucleolar stress, which would be a further example of a protein acting in more than one RNA metabolism pathway.

EXPERIMENTAL PROCEDURES

Plant materials, growth conditions, and gene nomenclature

Arabidopsis thaliana (L) Heynh. Landsberg *erecta* (L*er)* and Columbia-0 (Col-0) wild-type accessions were initially obtained from the Nottingham Arabidopsis Stock Center (NASC; Nottingham, UK) and then propagated in our laboratory for further analysis. Seeds of the *smo4-2* (SALK_012561; Zhang *et al.*, 2015), *smo4-3* (SALK_071764; this work), *smo4-4* (GABI-082H04; this work), *parl1-2* (SALK_002764; Petricka and Nelson, 2007), and *mtr4-1* (GK_048G02; Lange *et al.*, 2011) lines were also provided by NASC. The *nuc2-2* (GABI_178D01; Durut *et al.*, 2014) seeds were provided by J. Saez-Vasquez. Each of the above mutants carries T-DNA insertions in the Col-0 genetic background. The *den2* and *mas2-1* mutants were isolated in the L*er* background following their generation using EMS mutagenesis in the laboratory of J.L. Micol (Berná *et al.*, 1999) and M.R. Ponce (Micol-Ponce *et al.*, 2014), respectively.

Seed sterilization and sowing, plant culture, and crosses were performed as previously described (Ponce *et al.*, 1998; Berná *et al.*, 1999). When required, culture media were supplemented with hygromycin (15 $\mu g \cdot mL^{-1}$). Since several synonyms have been used in the literature or databases for the AT1G48920 and AT3G18610 genes, we have used the *NUC1* and *NUC2* gene symbols, respectively, throughout this manuscript for the simplicity.

Molecular characterization of mutations

For identification of *den2*, a candidate interval of 3,827 kb was delimited by iterative linkage analysis as previously described (Ponce *et al.*, 1999; Ponce *et al.*, 2006) using PCR amplification and the polymorphic markers listed in Table S1. The *den2* point mutation was ultimately identified by whole-genome, next-generation sequencing, looking for the transitions typically caused by EMS (G→A or C→T) within the candidate interval. Only one EMS-type mutation (G→A) was found in a coding region and verified by Sanger sequencing. The raw data have been deposited in the Sequence Read Archive (SRA; https://www.ncbi.nlm.nih.gov/sra/) database with the SRP103180 accession number.

The presence of T-DNA insertions in the *SMO4*, *NUC1*, *NUC2*, and *MTR4* genes was verified by PCR using the primers shown in Table S3. Discrimination between the wild-type *MAS2* and mutant *mas2-1* alleles was carried out by PCR amplification followed by restriction digestion analysis, as described by Sánchez-García *et al.* (2015).

For next-generation sequencing, DNA was extracted using the DNeasy Plant Mini Kit (Qiagen, Hilden, Germany), and massively parallel sequenced using an Ion Proton platform, following the manufacturer's instructions (Applied Biosystems, now Thermo

Fisher Scientific, Waltham, Massachusetts, USA). The reads obtained were mapped to TAIR10 with Bowtie 2 (Langmead and Salzberg, 2012) and a list of the identified mutations was compiled using SHORE (http://1001genomes.org/software/shore; Schneeberger *et al.*, 2009). Sanger sequencing was performed with ABI PRISM BigDye Terminator Cycle Sequencing kits on an ABI PRISM 3130xl Genetic Analyzer (Applied Biosystems).

RNA isolation, reverse transcription and Northern blotting

RNA was extracted from the aerial tissue of 3 plants per genotype using the TRI RNA Isolation Reagent (Sigma-Aldrich; St. Louis, Missouri, USA). Since rRNA lacks introns and rDNA is present in hundreds of copies in the Arabidopsis genome, RNA used for RT-PCR analysis was treated prior to cDNA synthesis with a twice-repeated DNase treatment using 2 U of TURBO DNase (TURBO DNA-free Kit, Thermo Fisher Scientific) per microgram of RNA. Reverse-transcription was carried out using 2 μg of DNA-free RNA, random hexamers, and the Maxima Reverse Transcriptase system (Thermo Fisher Scientific) according to the manufacturer′s instructions.

For Northern blotting, 5′-DIG (digoxigenin) labeled S7 and S9 probes were obtained from Eurofins Genomics (Ebersberg, Germany). Three μg of total RNA was used per Northern blot, and samples were loaded into 1.2% (w/v) agarose/formaldehyde or 6% (w/v) polyacrylamide/8 M urea gels. The polyacrylamide gel was run for 1 h at 180 V in 0.5X TBE buffer. RNA was visualized following ethidium bromide staining, then transferred and cross-linked onto a Hybond N+ nylon membrane (Thermo Fisher Scientific). Hybridization and detection were performed as previously described (Alwine *et al.*, 1977; Alwine *et al.*, 1979): the membrane was pre-hybridized for 2 h at 65°C, and then hybridized overnight at 65°C with 149 ng·mL^{-1} of the probe. The membrane was incubated with 0.05 U·mL^{-1} α-DIG-AP Fab fragments antibody (Roche, Penzberg, Germany), washed, equilibrated in detection buffer and incubated with 25 mM CDP-Star (Roche) diluted 1:200 in detection buffer for 5 min in the dark. RNA bands were visualized after developing Lumi-film chemiluminescent films (Roche) exposed to the membrane for 20 min or overnight.

Construction of transgenes and transgenic lines

Constructs for Gateway cloning were generated and transferred into plants as described in Sánchez-García *et al.* (2015). We used the pGEM-T Easy221 entry vector, and the pMDC32, pMDC83, pMDC107, and pMDC164 destination vectors (Curtis and Grossniklaus, 2003). Inserts were generated by PCR using the primers with included *attB1* and *attB2* sequences as detailed in Table S3. Chemically competent *Escherichia*

coli DH5α cells were transformed by the heat-shock method with BP or LR Gateway cloning reaction products. *Agrobacterium tumefaciens* C58C1 cells carrying the pSOUP helper plasmid were transformed by electroporation.

To obtain the *$35S_{pro}$:SMO4* and *$35S_{pro}$:SMO4:GFP* overexpression constructs, the full-length coding sequence (stop codons were removed to obtain all GFP translational fusions) of *SMO4* was PCR amplified from Col-0. A 1,317-bp region upstream of the translation start codon of *SMO4* was PCR amplified and used as the promoter driving the *$SMO4_{pro}$:GUS* transgene. This same promoter region was present at one end of a 4,156-bp segment amplified to isolate the entire 2,839-bp *SMO4* transcription unit, which was used to create *$SMO4_{pro}$:SMO4* and *$SMO4_{pro}$:SMO4:GFP* constructs. The fidelity of all constructs was verified by Sanger sequencing before the constructs were transferred into plants via the floral dip method (Clough and Bent, 1998).

Histology and histochemical assays

All differential interference contrast, fluorescence, and confocal laser scanning microscopy images were generated using a Nikon D-Eclipse C1 confocal microscope, and digitally processed using the EZ-C1 operation software. *In situ* hybridizations of RNA were carried out as previously described by Parry *et al.* (2006), with some modifications. We analyzed approximately 100 cells in first- and second-node leaves from 10 plants of each genotype, which were collected 12 das and fixed in glass vials at 600 mbar for 25 min. Probes were synthetized by Eurofins MWG Company, by labeling oligonucleotides (Table S2) at their 5′ ends with 6-fluorescein (18S rRNA), Cy3 (25S rRNA), and DIG (5.8S rRNA). Probes were used in a 0.5 $\mu g \cdot mL^{-1}$ hybridization solution. Samples were mounted on slides with a drop of Vectashield antifade mounting medium (Vector Laboratories, Burlingame, California, USA) containing 10 $\mu g \cdot mL^{-1}$ of Hoechst 33342. Nuclear staining was performed as described by Díaz-Tielas *et al.* (2012). Visualization of SMO4 subcellular localization was performed in roots from plants of a Col-0 background that carried the *$SMO4_{pro}$:SMO4:GFP* or *$35S_{pro}$:SMO4:GFP* transgenes, with plant tissue collected at 10 das.

ACCESSION NUMBERS

Sequence data used in this study can be found in the TAIR and Araport databases associated with the following accession numbers: AT2G40430 (*SMO4*) and AT1G59760 (*MTR4*).

ACKNOWLEDGEMENTS

We thank J.M. Serrano-García, J. Castelló-Bañuls, M.J. Ñíguez-Gómez, and S.B. Ingham for their excellent technical assistance, and A. Toumi for her help in the preliminary analysis of *den2*. We also thank B. Scheres for the pGEM-T Easy221 vector, J. Saez-Vasquez for providing seeds of the *nuc2-2* mutant, and J.L. Micol for useful discussions, comments on the manuscript, providing the *den2* mutant, and the use of his facilities. This research was supported by grants from the Ministerio de Economía, Industria y Competitividad of Spain (BIO2014-56889-R) and the Generalitat Valenciana (PROMETEOII/2014/006) to M.R.P.

AUTHOR CONTRIBUTIONS

Conceptualization, Resources, Supervision and Funding Acquisition, M.R.P.; Methodology and Investigation, all authors; Writing – Original Draft, M.R.P. and R.M.-P.; Writing, Review & Editing, all authors.

FIGURE LEGENDS

Figure 1. *SMO4* gene structure; molecular features, rosette phenotype, and phenotypic rescue of *smo4* alleles; subnuclear localization of SMO4.

(a) Schematic representation of *SMO4* gene structure with the molecular features and positions of the mutant alleles included in this study. Filled and open boxes represent the exons, and the 5′- and 3′-UTRs, respectively. Lines between boxes represent introns, and triangles indicate T-DNA insertions. A red arrow indicates the position of the single-base substitution in *den2*. (b–g) Rosettes of (b) Col-0, (c) *smo4-2*, (d) *smo4-3*, (e) *smo4-4,* (f) L*er,* and (g) *den2* plants. (h–m) Transgenic complementation of the *smo4* and *den2* mutant phenotypes. Plants shown are homozygous for *smo4* alleles and the (h–j) $SMO4_{pro}$*:SMO4* or (k–m) $SMO4_{pro}$*:SMO4:GFP* transgenes. Pictures were taken 14 days after stratification. Scale bars: 3 mm. (n–p) Confocal laser scanning microscopy of roots from plants of a Col-0 background homozygous for the $SMO4_{pro}$*:SMO4:GFP* transgene. Fluorescence signals are of (n) Hoechst 33342, (o) GFP, and (p) their overlay.

Figure 2. Aberrant pre-rRNA processing in *smo4-2*, *smo4-3* and *den2* plants.

(a) Diagram modified from Hang *et al.* (2014) illustrating the pre-rRNA processing intermediates than can be detected in a Northern blot using the S9 and S7 probes. ETS: external transcribed spacer. ITS: internal transcribed spacer. (b–d) Northern blots. Total RNA was separated in (b, d) formaldehyde-agarose or (c) polyacrylamide-urea gels, transferred to a nylon membrane, and hybridized with the (b, c) S9 or (d) S7 probes. RNA was extracted from (b) L*er*, Col-0, *den2*, *smo4-2*, and *smo4-3* plants or (c, d) L*er*, Col-0, *den2*, *smo4-2*, *smo4-3*, *smo4-3* $SMO4_{pro}$*:SMO4*, and *mtr4-1* plants. EtBr: ethidium bromide stained gels, visualised before blotting, which serve as loading controls.

Figure 3. Subcellular localization of 18S, 25S, and 5.8S rRNA mature and precursor species in Col-0 and the *smo4-3* mutant.

Confocal laser scanning microscopy of palisade mesophyll cells in second- and third-node leaves from (a–g) Col-0 and (h–n) *smo4-3* plants. Fluorescence signals are of (a, e, h, l) Hoechst 33342, (b, i) 18S probe, (c, j) 25S probe, (f, m) 5.8S probe, and (d, g, k, n) their overlays. Scale bars: 10 μm.

Figure 4. Genetic interactions of *smo4-3* with *mtr4-1*, *mas2-1*, *parl1-2*, and *nuc2-2*.

(a) Rosette of Col-0. (b–f) Rosettes of (b) *mtr4-1*, (c) *mas2-1*, (d) *parl1-2*, (e) *nuc2-2*, and (f) *smo4-3* single mutant plants. (g–j) Rosettes of (g) *smo4-3 mtr4-1*, (h) *smo4-3 mas2-1*, (i) *smo4-3 parl1-2*, and (j) *smo4-3 nuc2-2* double mutant plants. Pictures were taken 21 days after stratification. Scale bars: 1 mm.

SUPPORTING INFORMATION LEGENDS

Figure S1. Overview of 35S pre-rRNA processing in yeast.

Figure S2. Overview of 45S pre-rRNA processing in Arabidopsis.

Figure S3. Sequence conservation of SMO4 orthologs in Arabidopsis, human, and yeast.

Figure S4. Sequence conservation among plant SMO4 orthologs.

Figure S5. Sequence conservation of MTR4 orthologs in Arabidopsis, human, and yeast.

Figure S6. Sequence conservation among plant MTR4 orthologs.

Figure S7. Allelism test of the *smo4-3* and *den2* mutants.

Figure S8. AT1G59760 (*MTR4*) expression profile in the organs and developmental stages shown, as obtained from the Transcriptome Variation Analysis (TraVA) database.

Figure S9. AT5G42540 (*XRN2*) expression profile in the organs and developmental stages shown, as obtained from the TraVA database.

Figure S10. AT1G48920 (*NUC1*) expression profile in the organs and developmental stages shown, as obtained from from the TraVA database.

Figure S11. AT3G18610 (*NUC2)* expression profile in the organs and developmental stages shown, as obtained from the TraVA database.

Table S1. Primer sets used for the fine mapping of *den2.*

Table S2. Fluorescent probes used in this work.

Table S3. Other primer sets used in this work.

Supporting Dataset 1. Top 100 ranking *SMO4* coexpressed genes, identified by ATTED-II.

REFERENCES

Alwine, J.C., Kemp, D.J., Parker, B.A., Reiser, J., Renart, J., Stark, G.R. and Wahl, G.M. (1979) Detection of specific RNAs or specific fragments of DNA by fractionation in gels and transfer to diazobenzyloxymethyl paper. *Methods in Enzymology* **68**, 220-242.

Alwine, J.C., Kemp, D.J. and Stark, G.R. (1977) Method for detection of specific RNAs in agarose gels by transfer to diazobenzyloxymethyl-paper and hybridization with DNA probes. *Proceedings of the National Academy of Sciences of the USA* **74**, 5350-5354.

Baumberger, N. and Baulcombe, D.C. (2005) Arabidopsis ARGONAUTE1 is an RNA Slicer that selectively recruits microRNAs and short interfering RNAs. *Proceedings of the National Academy of Sciences of the USA* **102**, 11928-11933.

Berná, G., Robles, P. and Micol, J.L. (1999) A mutational analysis of leaf morphogenesis in *Arabidopsis thaliana*. *Genetics* **152**, 729-742.

Bieging, K.T., Mello, S.S. and Attardi, L.D. (2014) Unravelling mechanisms of p53-mediated tumour suppression. *Nature Reviews Cancer* **14**, 359-370.

Burgute, B.D., Peche, V.S., Muller, R., Matthias, J., Gassen, B., Eichinger, L., Glockner, G. and Noegel, A.A. (2016) The C-Terminal SynMuv/DdDUF926 domain regulates the function of the N-Terminal domain of DdNKAP. *PLoS One* **11**, e0168617.

Burgute, B.D., Peche, V.S., Steckelberg, A.L., Glockner, G., Gassen, B., Gehring, N.H. and Noegel, A.A. (2014) NKAP is a novel RS-related protein that interacts with RNA and RNA binding proteins. *Nucleic Acids Research* **42**, 3177-3193.

Byrne, M.E. (2009) A role for the ribosome in development. *Trends in Plant Science* **14**, 512-519.

Clough, S.J. and Bent, A.F. (1998) Floral dip: a simplified method for *Agrobacterium*-mediated transformation of *Arabidopsis thaliana*. *Plant Journal* **16**, 735-743.

Combs, D.J., Nagel, R.J., Ares, M., Jr. and Stevens, S.W. (2006) Prp43p is a DEAH-box spliceosome disassembly factor essential for ribosome biogenesis. *Molecular and Cellular Biology* **26**, 523-534.

Curtis, M.D. and Grossniklaus, U. (2003) A gateway cloning vector set for high-throughput functional analysis of genes in planta. *Plant Physiology* **133**, 462-469.

de la Cruz, J., Kressler, D., Tollervey, D. and Linder, P. (1998) Dob1p (Mtr4p) is a putative ATP-dependent RNA helicase required for the 3' end formation of 5.8S rRNA in *Saccharomyces cerevisiae*. *EMBO Journal* **17**, 1128-1140.

Díaz-Tielas, C., Grana, E., Sotelo, T., Reigosa, M.J. and Sánchez-Moreiras, A.M. (2012) The natural compound trans-chalcone induces programmed cell death in *Arabidopsis thaliana* roots. *Plant, Cell and Environment* **35**, 1500-1517.

Dinman, J.D. (2009) The eukaryotic ribosome: current status and challenges. *Journal of Biological Chemistry* **284**, 11761-11765.

Durut, N., Abou-Ellail, M., Pontvianne, F., Das, S., Kojima, H., Ukai, S., de Bures, A., Comella, P., Nidelet, S., Rialle, S., Merret, R., Echeverria, M., Bouvet, P., Nakamura, K. and Saez-Vasquez, J. (2014) A duplicated *NUCLEOLIN* gene with antagonistic activity is required for chromatin organization of silent 45S rDNA in Arabidopsis. *Plant Cell* **26**, 1330-1344.

Granato, D.C., Gonzales, F.A., Luz, J.S., Cassiola, F., Machado-Santelli, G.M. and Oliveira, C.C. (2005) Nop53p, an essential nucleolar protein that interacts with Nop17p and Nip7p, is required for pre-rRNA processing in *Saccharomyces cerevisiae*. *FEBS Journal* **272**, 4450-4463.

Gy, I., Gasciolli, V., Lauressergues, D., Morel, J.B., Gombert, J., Proux, F., Proux, C., Vaucheret, H. and Mallory, A.C. (2007) Arabidopsis FIERY1, XRN2, and XRN3 are endogenous RNA silencing suppressors. *Plant Cell* **19**, 3451-3461.

Hang, R., Liu, C., Ahmad, A., Zhang, Y., Lu, F. and Cao, X. (2014) Arabidopsis protein arginine methyltransferase 3 is required for ribosome biogenesis by affecting precursor ribosomal RNA processing. *Proceedings of the National Academy of Sciences of the USA* **111**, 16190-19195.

Horiguchi, G., Mollá-Morales, A., Pérez-Pérez, J.M., Kojima, K., Robles, P., Ponce, M.R., Micol, J.L. and Tsukaya, H. (2011) Differential contributions of ribosomal protein genes to *Arabidopsis thaliana* leaf development. *Plant Journal* **65**, 724-736.

Jackson, R.N., Klauer, A.A., Hintze, B.J., Robinson, H., van Hoof, A. and Johnson, S.J. (2010) The crystal structure of Mtr4 reveals a novel arch domain required for rRNA processing. *EMBO Journal* **29**, 2205-2216.

James, A., Wang, Y., Raje, H., Rosby, R. and DiMario, P. (2014) Nucleolar stress with and without p53. *Nucleus* **5**, 402-426.

Kilchert, C., Wittmann, S. and Vasiljeva, L. (2016) The regulation and functions of the nuclear RNA exosome complex. *Nature Review Molecular Cell Biology* **17**, 227-239.

King, T.C., Sirdeshmukh, R. and Schlessinger, D. (1984) RNase III cleavage is obligate for maturation but not for function of *Escherichia coli* pre-23S rRNA. *Proceedings of the National Academy of Sciencias of the USA* **81**, 185-188.

Lange, H., Sement, F.M. and Gagliardi, D. (2011) MTR4, a putative RNA helicase and exosome co-factor, is required for proper rRNA biogenesis and development in *Arabidopsis thaliana*. *Plant Journal* **68**, 51-63.

Lange, H., Zuber, H., Sement, F.M., Chicher, J., Kuhn, L., Hammann, P., Brunaud, V., Berard, C., Bouteiller, N., Balzergue, S., Aubourg, S., Martin-Magniette, M.L., Vaucheret, H. and Gagliardi, D. (2014) The RNA helicases AtMTR4 and HEN2 target specific subsets of nuclear transcripts for degradation by the nuclear exosome in *Arabidopsis thaliana*. *PLoS Genetics* **10**, e1004564.

Langmead, B. and Salzberg, S.L. (2012) Fast gapped-read alignment with Bowtie 2. *Nature Methods* **9**, 357-359.

Lee, S., Kim, J.Y., Kim, Y.J., Seok, K.O., Kim, J.H., Chang, Y.J., Kang, H.Y. and Park, J.H. (2012) Nucleolar protein GLTSCR2 stabilizes p53 in response to ribosomal stresses. *Cell Death and Differentiation* **19**, 1613-1622.

Leeds, N.B., Small, E.C., Hiley, S.L., Hughes, T.R. and Staley, J.P. (2006) The splicing factor Prp43p, a DEAH box ATPase, functions in ribosome biogenesis. *Molecular and Cellular Biology* **26**, 513-522.

Micol-Ponce, R., Aguilera, V. and Ponce, M.R. (2014) A genetic screen for suppressors of a hypomorphic allele of Arabidopsis *ARGONAUTE1*. *Scientific Reports* **4**, 5533.

Palade, G.E. (1955) Studies on the endoplasmic reticulum. II. Simple dispositions in cells in situ. *Journal of Biophysical and Biochemical Cytology* **1**, 567-582.

Parry, G., Ward, S., Cernac, A., Dharmasiri, S. and Estelle, M. (2006) The Arabidopsis SUPPRESSOR OF AUXIN RESISTANCE proteins are nucleoporins with an important role in hormone signaling and development. *Plant Cell* **18**, 1590-1603.

Paul, B. and Montpetit, B. (2016) Altered RNA processing and export lead to retention of mRNAs near transcription sites and nuclear pore complexes or within the nucleolus. *Molecular Biology of the Cell* **27**, 2742-2756.

Petricka, J.J. and Nelson, T.M. (2007) Arabidopsis nucleolin affects plant development and patterning. *Plant Physiology* **144**, 173-186.

Ponce, M.R., Quesada, V. and Micol, J.L. (1998) Rapid discrimination of sequences flanking and within T-DNA insertions in the Arabidopsis genome. *Plant Journal* **14**, 497-501.

Ponce, M.R., Robles, P., Lozano, F.M., Brotons, M.A. and Micol, J.L. (2006) Low-resolution mapping of untagged mutations. *Methods in Molecular Biology* **323**, 105-113.

Ponce, M.R., Robles, P. and Micol, J.L. (1999) High-throughput genetic mapping in *Arabidopsis thaliana*. *Molecular and General Genetics* **261**, 408-415.

Pontvianne, F., Matia, I., Douet, J., Tourmente, S., Medina, F.J., Echeverria, M. and Saez-Vasquez, J. (2007) Characterization of *AtNUC-L1* reveals a central role of

nucleolin in nucleolus organization and silencing of *AtNUC-L2* gene in Arabidopsis. *Molecular Biology of the Cell* **18**, 369-379.

Robles, P. and Micol, J.L. (2001) Genome-wide linkage analysis of Arabidopsis genes required for leaf development. *Molecular Genetics and Genomics* **266**, 12-19.

Sánchez-García, A.B., Aguilera, V., Micol-Ponce, R., Jover-Gil, S. and Ponce, M.R. (2015) Arabidopsis *MAS2*, an essential gene that encodes a homolog of animal NF-kappa B activating protein, is involved in 45S ribosomal DNA silencing. *Plant Cell* **27**, 1999-2015.

Schneeberger, K., Ossowski, S., Lanz, C., Juul, T., Petersen, A.H., Nielsen, K.L., Jorgensen, J.E., Weigel, D. and Andersen, S.U. (2009) SHOREmap: simultaneous mapping and mutation identification by deep sequencing. *Nature Methods* **6**, 550-551.

Seiser, R.M., Sundberg, A.E., Wollam, B.J., Zobel-Thropp, P., Baldwin, K., Spector, M.D. and Lycan, D.E. (2006) Ltv1 is required for efficient nuclear export of the ribosomal small subunit in *Saccharomyces cerevisiae*. *Genetics* **174**, 679-691.

Simm, S., Fragkostefanakis, S., Paul, P., Keller, M., Einloft, J., Scharf, K.D. and Schleiff, E. (2015) Identification and expression analysis of ribosome biogenesis factor co-orthologs in *Solanum lycopersicum*. *Bioinformatics and Biology Insights* **9**, 1-17.

Sloan, K.E., Bohnsack, M.T., Schneider, C. and Watkins, N.J. (2014) The roles of SSU processome components and surveillance factors in the initial processing of human ribosomal RNA. *RNA* **20**, 540-550.

Sydorskyy, Y., Dilworth, D.J., Halloran, B., Yi, E.C., Makhnevych, T., Wozniak, R.W. and Aitchison, J.D. (2005) Nop53p is a novel nucleolar 60S ribosomal subunit biogenesis protein. *Biochemical Journal* **388**, 819-826.

Tafforeau, L., Zorbas, C., Langhendries, J.L., Mullineux, S.T., Stamatopoulou, V., Mullier, R., Wacheul, L. and Lafontaine, D.L. (2013) The complexity of human ribosome biogenesis revealed by systematic nucleolar screening of pre-rRNA processing factors. *Molecular Cell* **51**, 539-551.

Thoms, M., Thomson, E., Bassler, J., Gnadig, M., Griesel, S. and Hurt, E. (2015) The exosome is recruited to RNA substrates through specific adaptor proteins. *Cell* **162**, 1029-1038.

Thomson, E. and Tollervey, D. (2005) Nop53p is required for late 60S ribosome subunit maturation and nuclear export in yeast. *RNA* **11**, 1215-1224.

Weis, B.L., Kovacevic, J., Missbach, S. and Schleiff, E. (2015) Plant-specific features of ribosome biogenesis. *Trends in Plant Science* **20**, 729-740.

Wild, T., Horvath, P., Wyler, E., Widmann, B., Badertscher, L., Zemp, I., Kozak, K., Csucs, G., Lund, E. and Kutay, U. (2010) A protein inventory of human ribosome

biogenesis reveals an essential function of exportin 5 in 60S subunit export. *PLoS Biology* **8**, e1000522.

Wilson, D.N. and Doudna Cate, J.H. (2012) The structure and function of the eukaryotic ribosome. *Cold Spring Harbor Perspectives in Biology* **4**, a011536.

Zakrzewska-Placzek, M., Souret, F.F., Sobczyk, G.J., Green, P.J. and Kufel, J. (2010) *Arabidopsis thaliana* XRN2 is required for primary cleavage in the pre-ribosomal RNA. *Nucleic Acids Research* **38**, 4487-4502.

Zhang, X.R., Qin, Z., Zhang, X. and Hu, Y. (2015) Arabidopsis SMALL ORGAN 4, a homolog of yeast NOP53, regulates cell proliferation rate during organ growth. *Journal of Integrative Plant Biology* **57**, 810-818.

Micol-Ponce *et al*., Figure 1

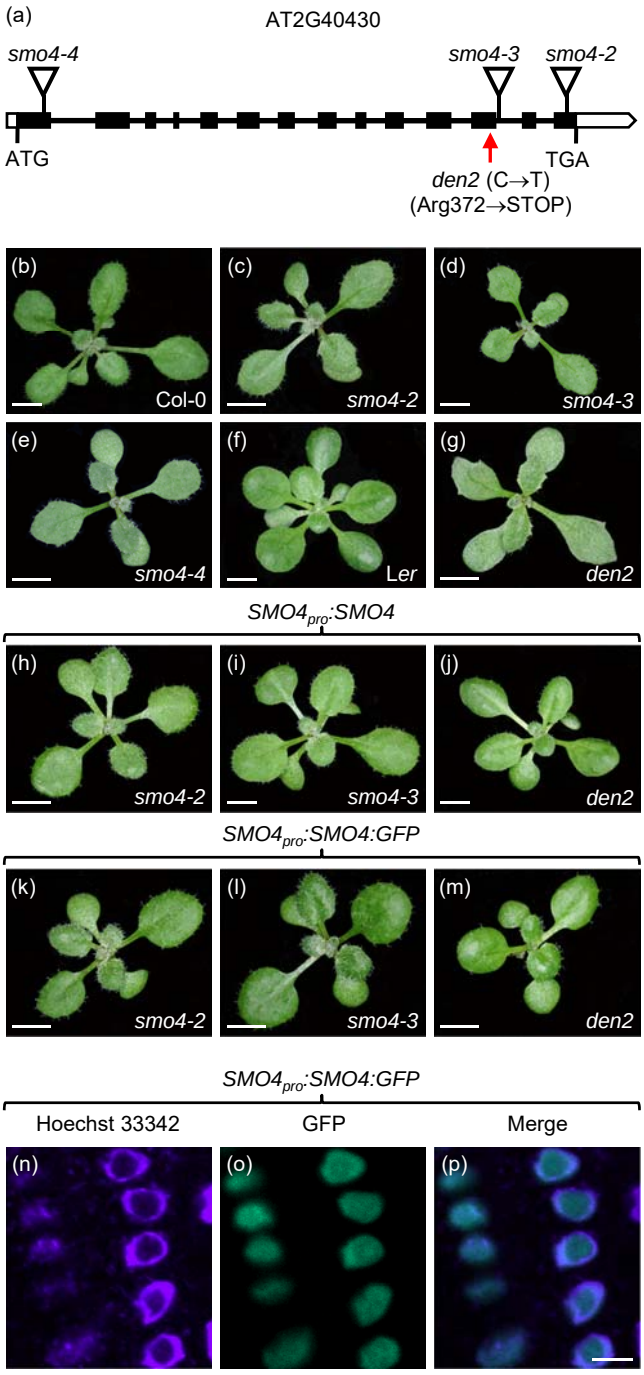

Micol-Ponce *et al*., Figure 2

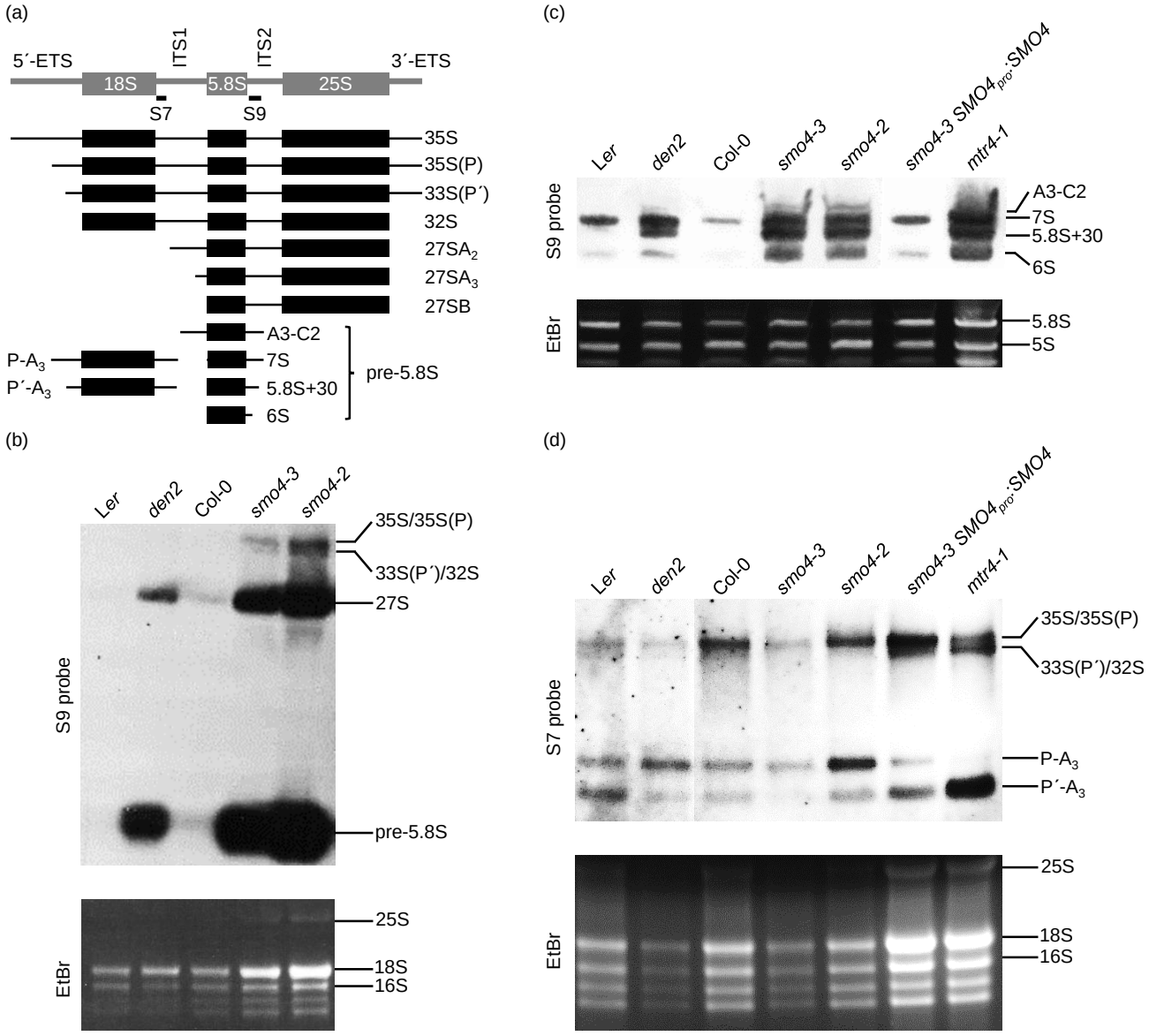

Micol-Ponce *et al*., Figure 3

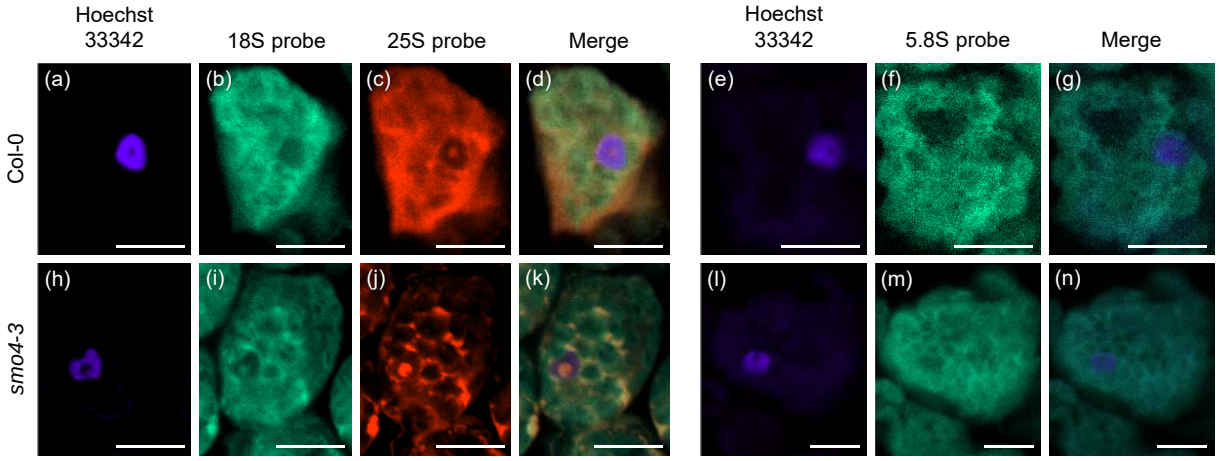

Micol-Ponce *et al*., Figure 4

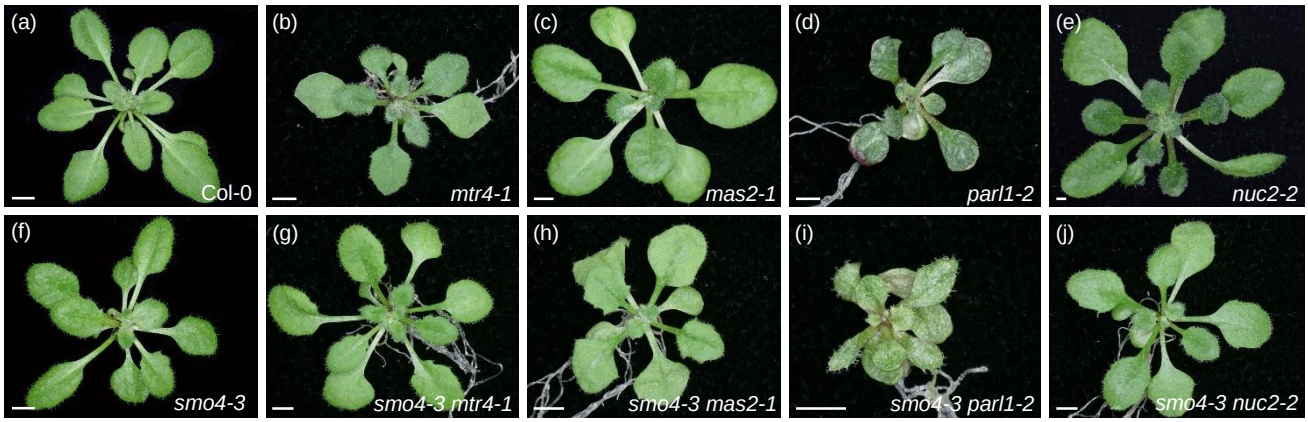

The ribosomal biogenesis factor SMALL ORGAN 4 functions in 5.8S and 18S rRNA maturation in Arabidopsis

Rosa Micol-Ponce, Raquel Sarmiento-Mañús, and María Rosa Ponce

Instituto de Bioingeniería, Universidad Miguel Hernández, Campus de Elche, 03202 Elche, Alicante, Spain.

Supporting Figures, Tables and References

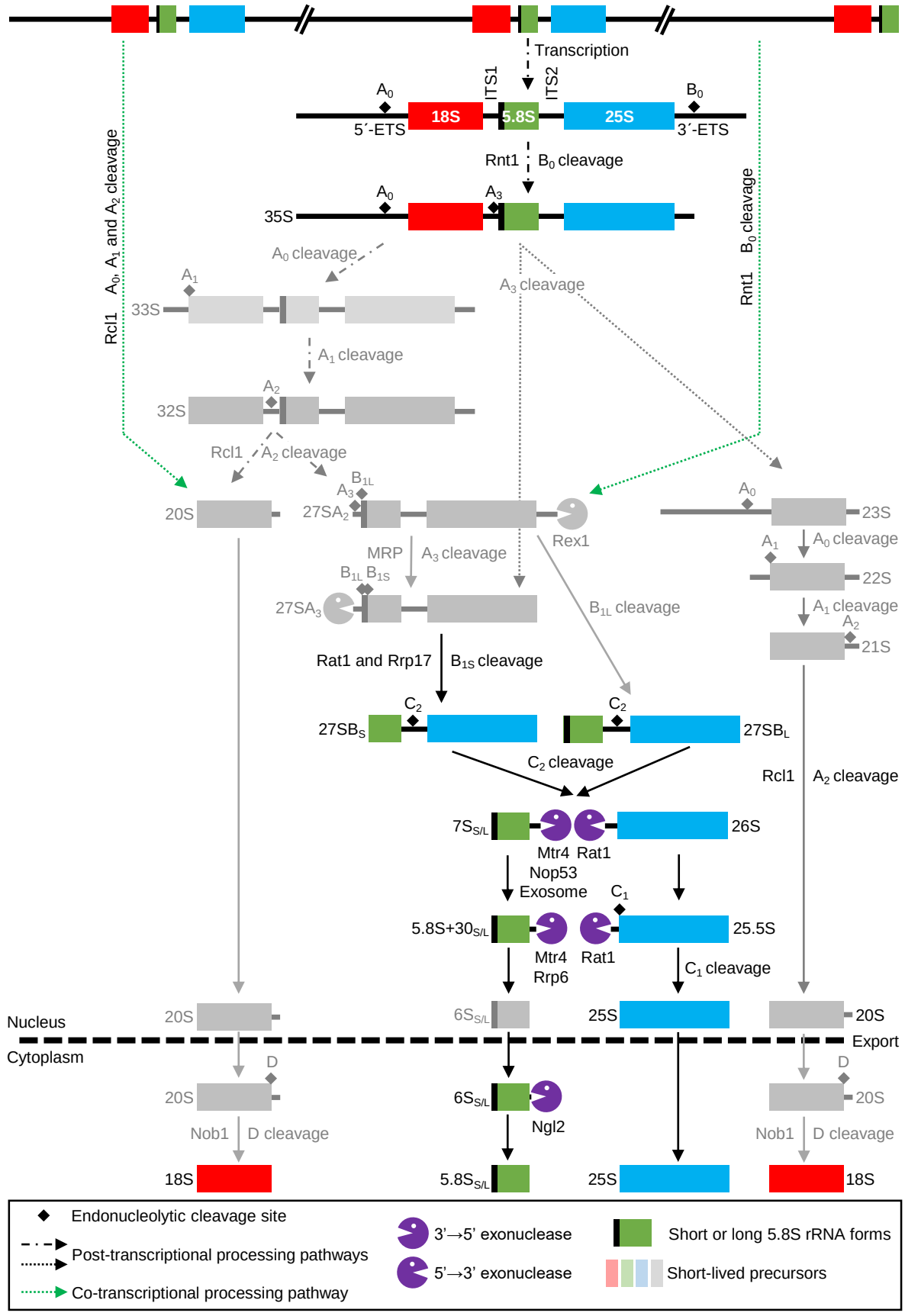

Figure S1. Overview of 35S pre-rRNA processing in yeast.
Most known endonucleolytic cleavages, exonucleolytic trimmings, and alternative pathways are shown. Only the elements relevant to this work are represented in color. ETS: external transcribed spacer. ITS: internal transcribed spacer. Modified from Henras *et al.* (2015) and Chaker-Margot *et al.* (2015).

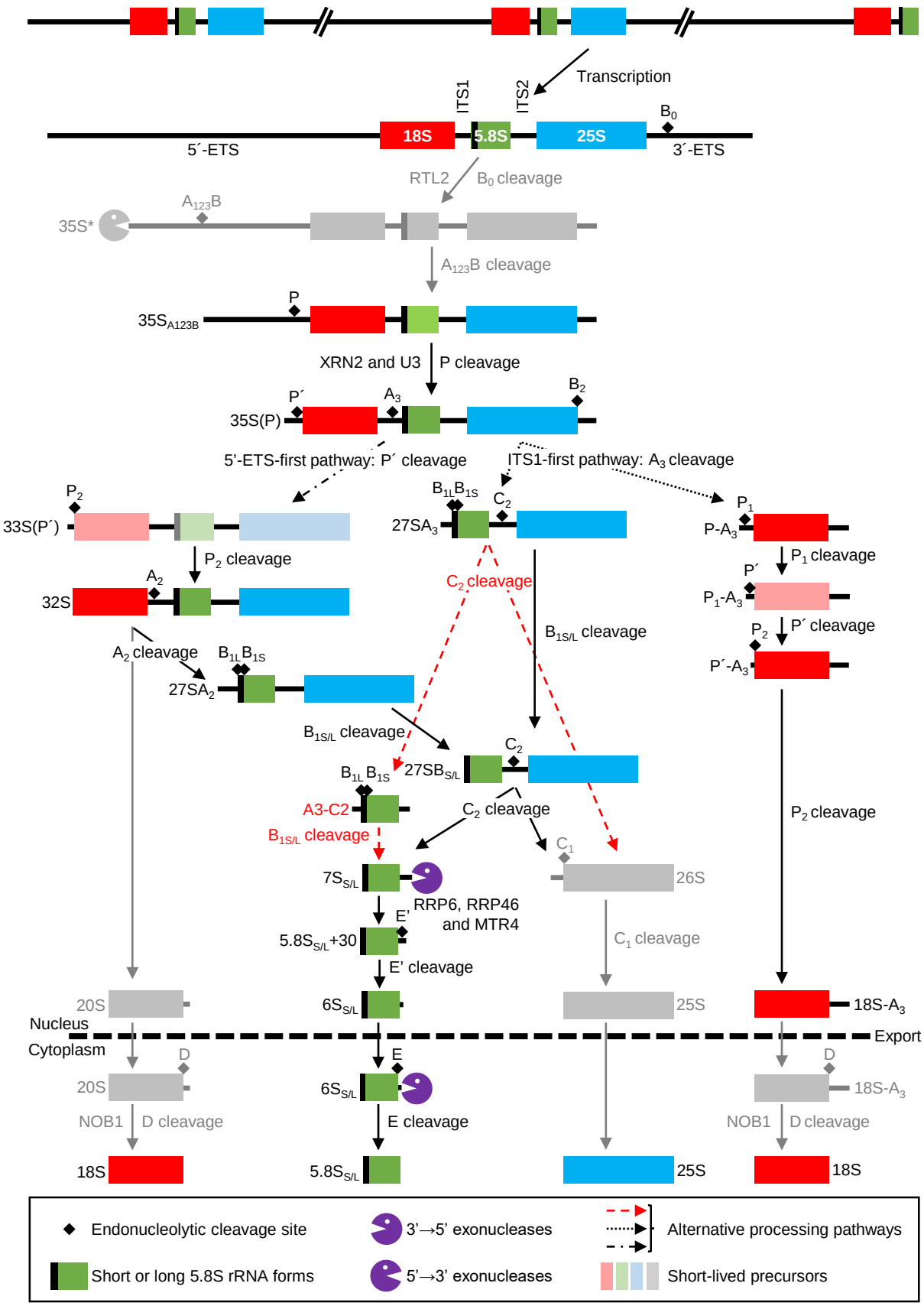

Figure S2. Overview of 45S pre-rRNA processing in Arabidopsis.
Most known endonucleolytic cleavages, exonucleolytic trimmings, and alternative pathways are shown. Only the elements relevant to this work are represented in color. We infer that the pathway represented in red is the most likely way to obtain the A3-C2 pre-rRNA, whose existence in Arabidopsis was published by Zakrzewska-Placzek *et al.* (2010). ETS: external transcribed spacer. ITS: internal transcribed spacer. Modified from Weis *et al.* (2015a) and Schillewaert *et al.* (2012)

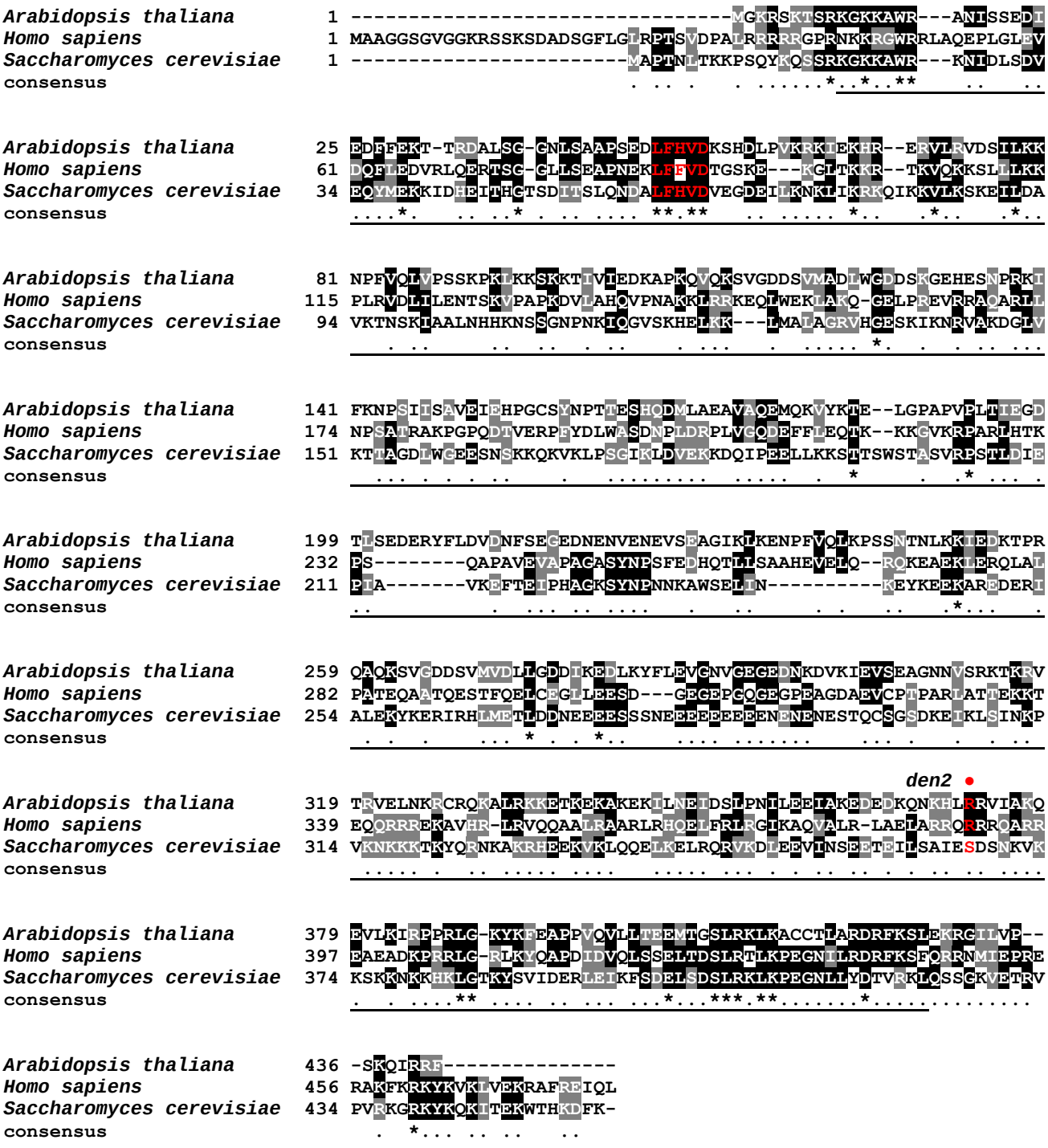

Figure S3. Sequence conservation of SMO4 orthologs in Arabidopsis, human, and yeast. Sequence alignment of the full-length SMO4 orthologs from *Homo sapiens* (GLTSCR2; GenBank accession number AAH06311), *Saccharomyces cerevisiae* (Nop53; KZV07369), and *Arabidopsis thaliana* (SMO4; NP_001078030), representing metazoans, yeast and plants, respectively. Identical and similar residues are shaded in black and gray, respectively. Numbers indicate residue positions. Asterisks and periods in the consensus indicate identical and conserved residues, respectively. For Arabidopsis, the AT2G40430.1 splice variant was used. Red letters highlight the consensus LFXφD motif (where X is any amino acid, and φ is a hydrophobic amino acid, which is Valine in the three proteins aligned), and the amino acid (red circle) that is replaced by a stop codon in the Arabidopsis *den2* allele that carries a nonsense mutation. The NOP53 domain is shown as a black line under the consensus, and was obtained from the HomoloGene database (https://www.ncbi.nlm.nih.gov/homologene). This alignment and those of Figures S4–S6 were generated using ClustalW2 (Larkin *et al.*, 2007) and shaded using Boxshade 3.21 (http://www.ch.embnet.org/software/BOX_form.html).

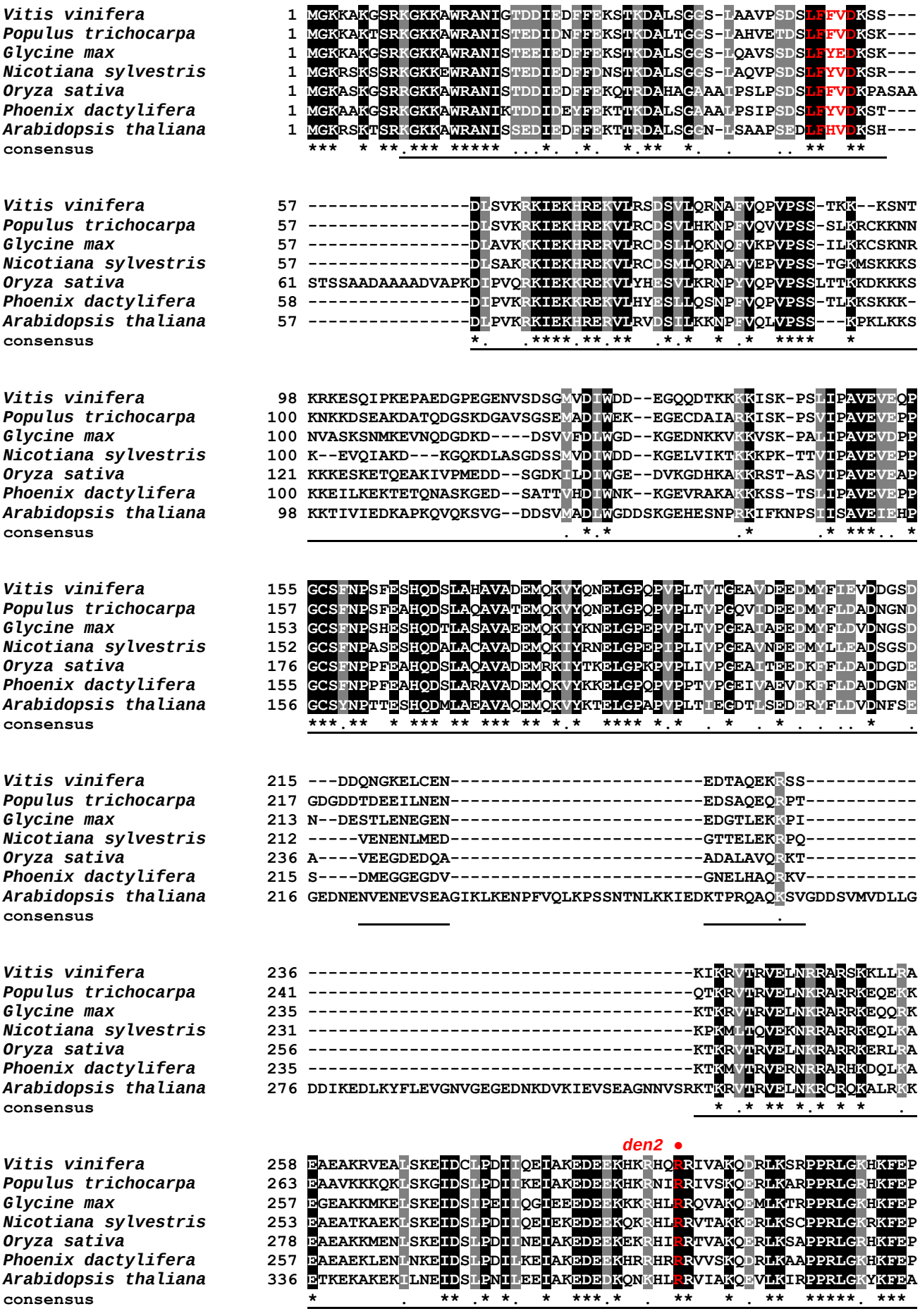
Vitis vinifera
Populus trichocarpa
Glycine max
Nicotiana sylvestris
Oryza sativa
Phoenix dactylifera
Arabidopsis thaliana
consensus
den2

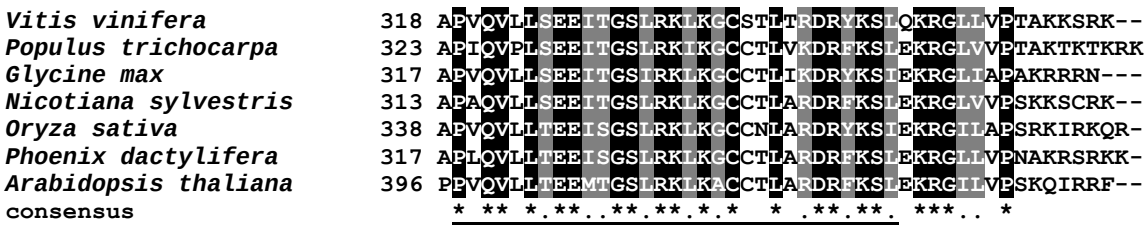

Figure S4. Sequence conservation among plant SMO4 orthologs.
Sequence alignment of full-length SMO4 orthologs from different angiosperm lineages, as classified in Myburg *et al.* (2014): *Vitis vinifera* XP_002278805 (representing Vitales), *Populus trichocarpa* XP_002311253 (Malpighiales), *Glycine max* NP_001241107 (Fabids), *Nicotiana sylvestris* XP_009803930 (Asterids), *Oryza sativa* XP_015637465 (Poales), *Phoenix dactylifera* XP_008813647 (Arecales), and *Arabidopsis thaliana* NP_001078030 (Malvids). Identical and similar residues across all sequences are shaded in black and gray, respectively. Numbers indicate residue positions. The NOP53 domain is shown as a black line under the consensus sequence. Red letters highlight the consensus LFXφD motif (AIM; where φ is a hydrophobic amino acid, which is Valine in all species except in *Glycine max*, in which it is Glutamic acid, a charged residue), and the conserved amino acid (red circle) that is replaced by a stop codon in the Arabidopsis *den2* allele that carries a nonsense mutation. Asterisks and periods in the consensus indicate identical and conserved residues, respectively.

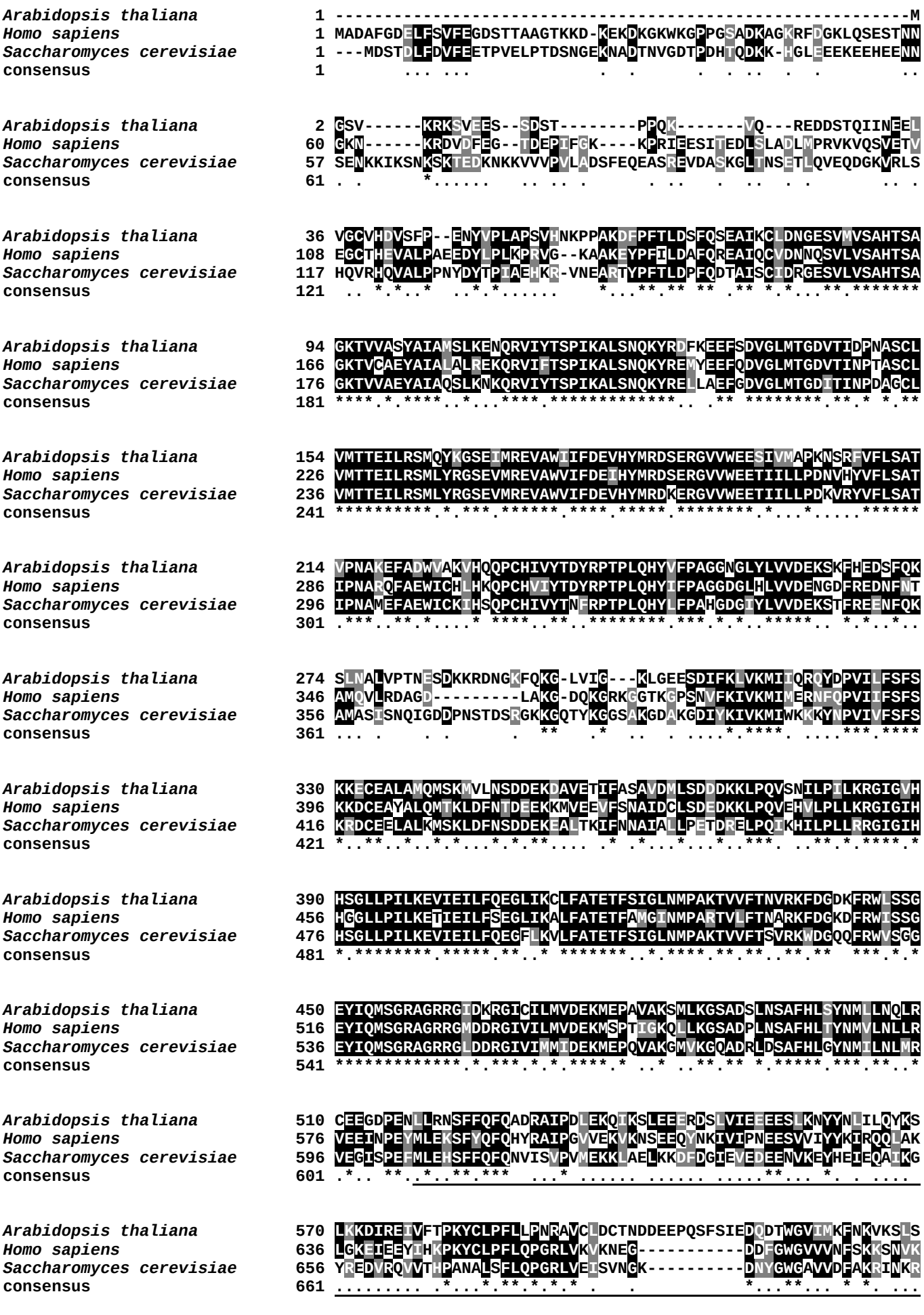
Arabidopsis thaliana
Homo sapiens
Saccharomyces cerevisiae
consensus

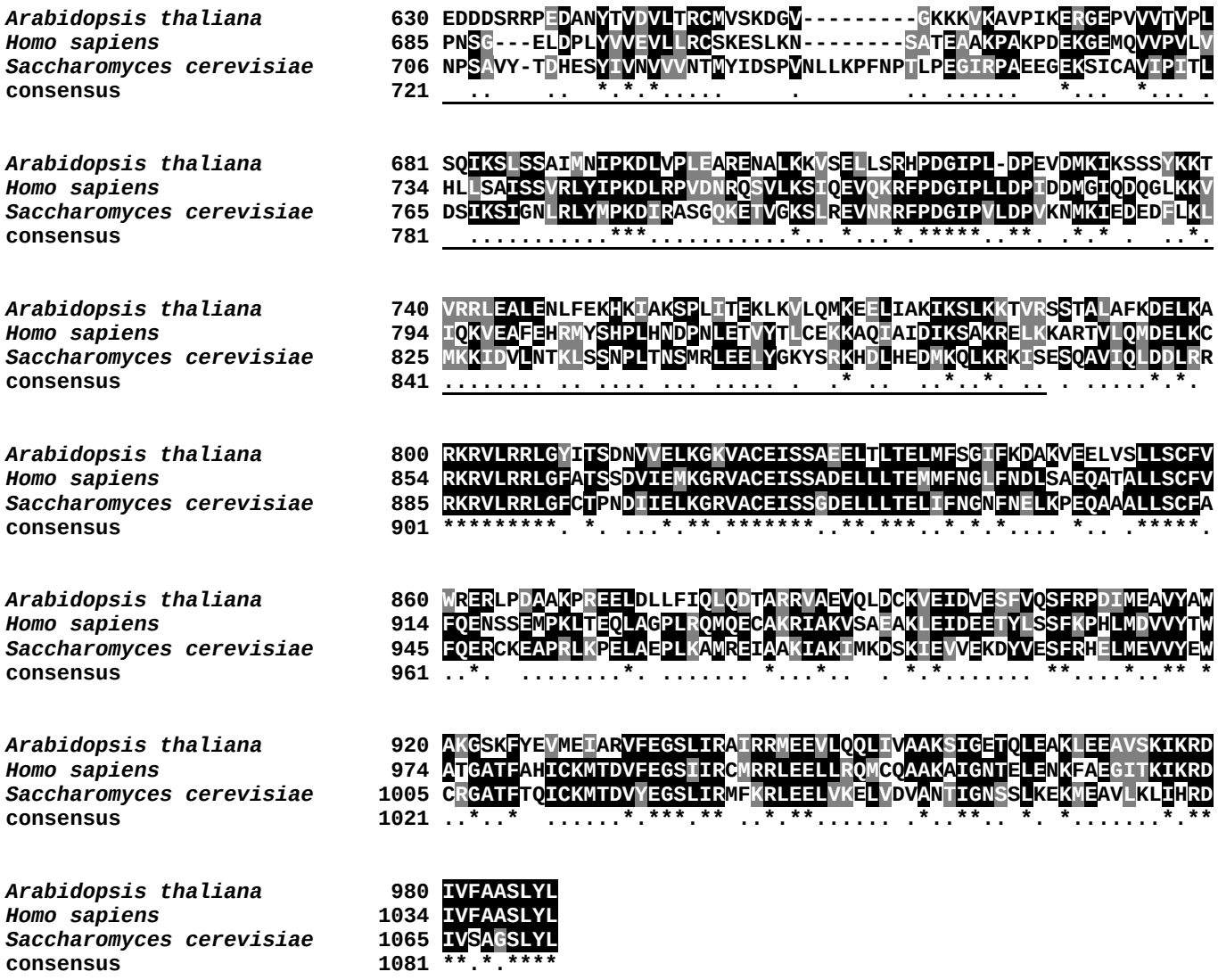

Figure S5. Sequence conservation of MTR4 orthologs in Arabidopsis, human, and yeast.
Sequence alignment of full-length MTR4 orthologs from *Homo sapiens* (GenBank accession number NP_056175), *Saccharomyces cerevisiae* (CAA89341), and *Arabidopsis thaliana* (OAP13689). Identical and similar residues across all sequences are shaded in black and gray, respectively. Numbers indicate residue positions. The arch domain, as defined in Jackson et al. (2010), is highlighted with a black line under the consensus. Asterisks and periods in the consensus indicate identical and conserved residues, respectively.

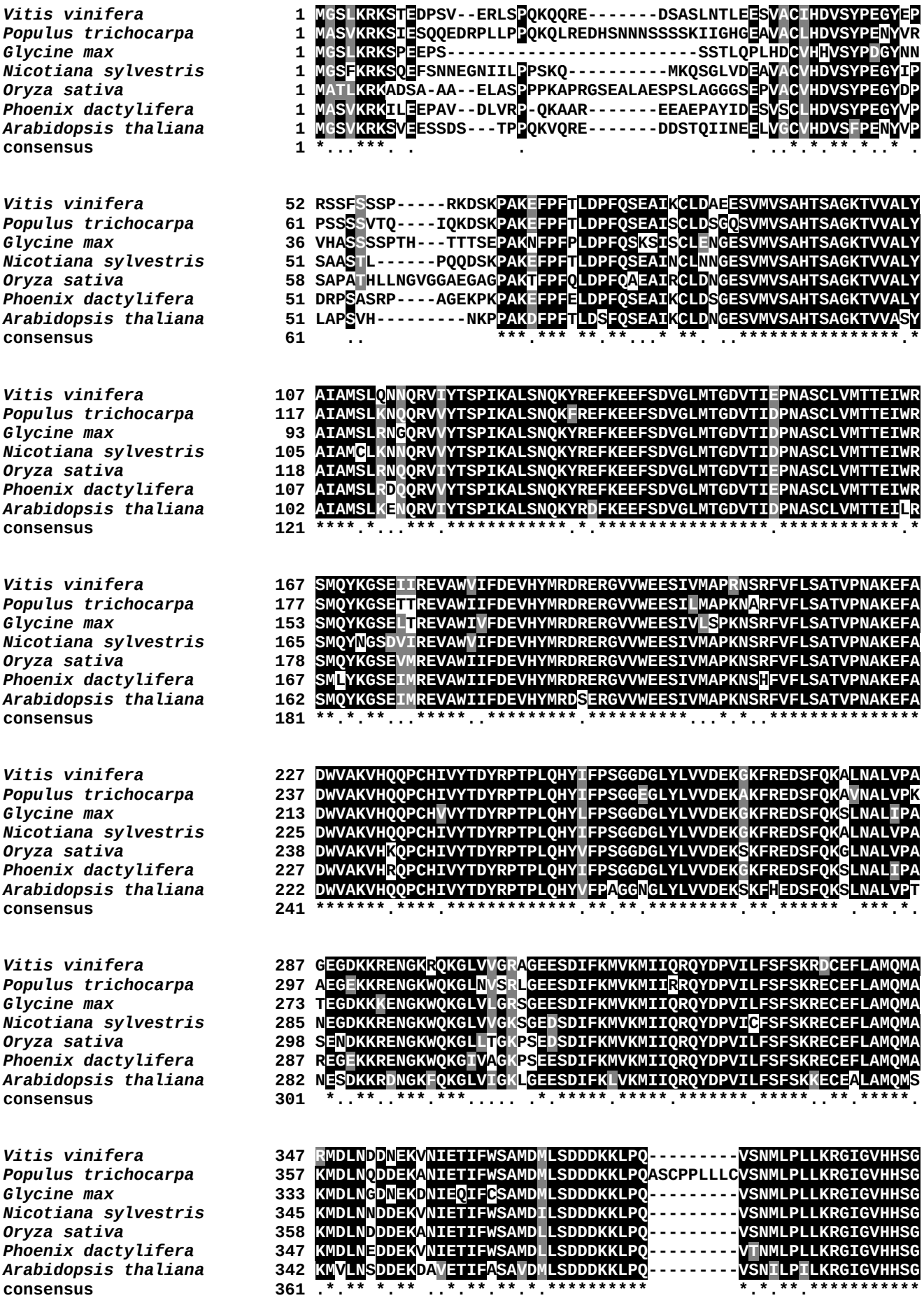
Vitis vinifera
Populus trichocarpa
Glycine max
Nicotiana sylvestris
Oryza sativa
Phoenix dactylifera
Arabidopsis thaliana
consensus

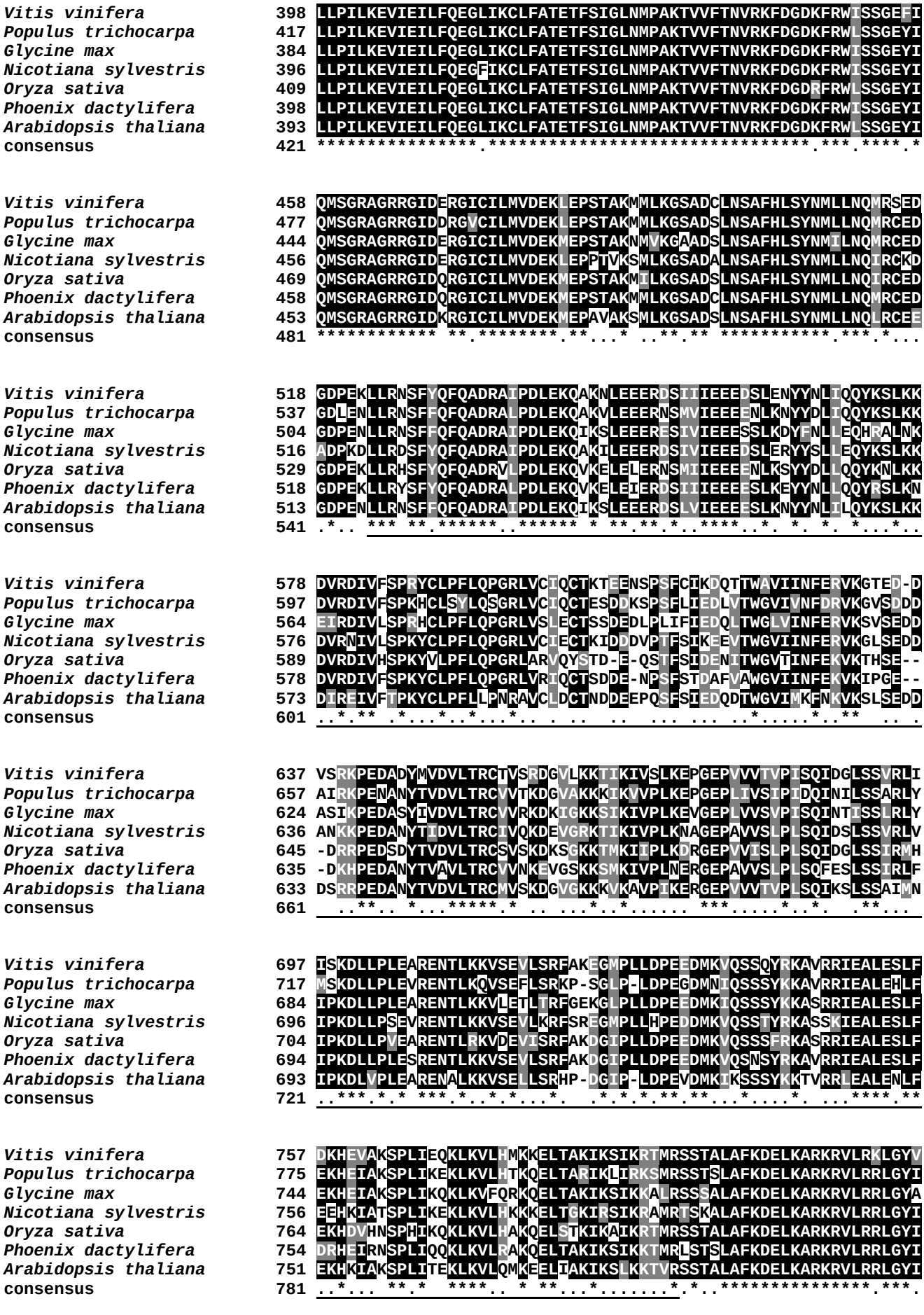
Vitis vinifera 398 LLPILKEVIEILFQEGLIKCLFATETFSIGLNMPAKTVVFTNVRKFDGDKFRWISSGEFI
Populus trichocarpa 417 LLPILKEVIEILFQEGLIKCLFATETFSIGLNMPAKTVVFTNVRKFDGDKFRWLSSGEYI
Glycine max 384 LLPILKEVIEILFQEGLIKCLFATETFSIGLNMPAKTVVFTNVRKFDGDKFRWISSGEYI
Nicotiana sylvestris 396 LLPILKEVIEILFQEGFIKCLFATETFSIGLNMPAKTVVFTNVRKFDGDKFRWISSGEYI
Oryza sativa 409 LLPILKEVIEILFQEGLIKCLFATETFSIGLNMPAKTVVFTNVRKFDGDRFRWLSSGEYI
Phoenix dactylifera 398 LLPILKEVIEILFQEGLIKCLFATETFSIGLNMPAKTVVFTNVRKFDGDKFRWISSGEYI
Arabidopsis thaliana 393 LLPILKEVIEILFQEGLIKCLFATETFSIGLNMPAKTVVFTNVRKFDGDKFRWLSSGEYI
consensus 421
Vitis vinifera 458 QMSGRAGRRGIDERGICILMVDEKLEPSTAKMMLKGSADCLNSAFHLSYNMLLNQMRSED
Populus trichocarpa 477 QMSGRAGRRGIDDRGVCILMVDEKLEPSTAKMMLKGSADSLNSAFHLSYNMLLNQMRCED
Glycine max 444 QMSGRAGRRGIDERGICILMVDEKMEPSTAKNMVKGAADSLNSAFHLSYNMILNQMRCED
Nicotiana sylvestris 456 QMSGRAGRRGIDERGICILMVDEKLEPPTVKSMLKGSADALNSAFHLSYNMLLNQIRCKD
Oryza sativa 469 QMSGRAGRRGIDQRGICILMVDEKMEPSTAKMILKGSADSLNSAFHLSYNMLLNQIRCED
Phoenix dactylifera 458 QMSGRAGRRGIDQRGICILMVDEKMEPSTAKMMLKGSADCLNSAFHLSYNMLLNQMRCED
Arabidopsis thaliana 453 QMSGRAGRRGIDKRGICILMVDEKMEPAVAKSMLKGSADSLNSAFHLSYNMLLNQLRCEE
consensus 481
Vitis vinifera 518 GDPEKLLRNSFYQFQADRAIPDLEKQAKNLEEERDSIIIEEEDSLENYYNLIQQYKSLKK
Populus trichocarpa 537 GDLENLLRNSFFQFQADRALPDLEKQAKVLEEERNSMVIEEEENLKNYYDLIQQYKSLKK
Glycine max 504 GDPENLLRNSFFQFQADRAIPDLEKQIKSLEEERESIVIEEESSLKDYFNLLEQHRALNK
Nicotiana sylvestris 516 ADPKDLLRDSFYQFQADRAIPDLEKQAKILEEERDSIVIEEEDSLERYYSLLEQYKSLKK
Oryza sativa 529 GDPEKLLRHSFYQFQADRVLPDLEKQVKELELERNSMIIEEEENLKSYYDLLQQYKNLKK
Phoenix dactylifera 518 GDPEKLLRYSFYQFQADRALPDLEKQVKELEIERDSIIIEEEESLKEYYNLLQQYRSLKN
Arabidopsis thaliana 513 GDPENLLRNSFFQFQADRAIPDLEKQIKSLEEERDSLVIEEEESLKNYYNLILQYKSLKK
consensus 541
Vitis vinifera 578 DVRDIVFSPRYCLPFLQPGRLVCIQCTKTEENSPSFCIKDQTTWAVIINFERVKGTED-D
Populus trichocarpa 597 DVRDIVFSPKHCLSYLQSGRLVCIQCTESDDKSPSFLIEDLVTWGVIVNFDRVKGVSDDD
Glycine max 564 EIRDIVLSPRHCLPFLQPGRLVSLECTSSDEDLPLIFIEDQLTWGLVINFERVKSVSEDD
Nicotiana sylvestris 576 DVRNIVLSPKYCLPFLQPGRLVCIECTKIDDDVPTFSIKEEVTWGVIINFERVKGLSEDD
Oryza sativa 589 DVRDIVHSPKYVLPFLQPGRLARVQYSTD-E-QSTFSIDENITWGVTINFEKVKTHSE--
Phoenix dactylifera 578 DVRDIVFSPKYCLPFLQPGRLVRIQCTSDDE-NPSFSTDAFVAWGVIINFEKVKIPGE--
Arabidopsis thaliana 573 DIREIVFTPKYCLPFLLPNRAVCLDCTNDDEEPQSFSIEDQDTWGVIMKFNKVKSLSEDD
consensus 601
Vitis vinifera 637 VSRKPEDADYMVDVLTRCTVSRDGVLKKTIKIVSLKEPGEPVVVTVPISQIDGLSSVRLI
Populus trichocarpa 657 AIRKPENANYTVDVLTRCVVTKDGVAKKKIKVVPLKEPGEPLIVSIPIDQINILSSARLY
Glycine max 624 ASIKPEDASYIVDVLTRCVVRKDKIGKKSIKIVPLKEVGEPLVVSVPISQINTISSLRLY
Nicotiana sylvestris 636 ANKKPEDANYTIDVLTRCIVQKDEVGRKTIKIVPLKNAGEPAVVSLPLSQIDSLSSVRLV
Oryza sativa 645 -DRRPEDSDYTVDVLTRCSVSKDKSGKKTMKIIPLKDRGEPVVISLPLSQIDGLSSIRMH
Phoenix dactylifera 635 -DKHPEDANYTVAVLTRCVVNKEVGSKKSMKIVPLNERGEPAVVSLPLSQFESLSSIRLF
Arabidopsis thaliana 633 DSRRPEDANYTVDVLTRCMVSKDGVGKKKVKAVPIKERGEPVVVTVPLSQIKSLSSAIMN
consensus 661
Vitis vinifera 697 ISKDLLPLEARENTLKKVSEVLSRFAKEGMPLLDPEEDMKVQSSQYRKAVRRIEALESLF
Populus trichocarpa 717 MSKDLLPLEVRENTLKQVSEFLSRKP-SGLP-LDPEGDMNIQSSSYKKAVRRIEALEHLF
Glycine max 684 IPKDLLPLEARENTLKKVLETLTRFGEKGLPLLDPEEDMKIQSSSYKKASRRIEALESLF
Nicotiana sylvestris 696 IPKDLLPSEVRENTLKKVSEVLKRFSREGMPLLHPEDDMKVQSSTYRKASSKIEALESLF
Oryza sativa 704 IPKDLLPVEARENTLRKVDEVISRFAKDGIPLLDPEEDMKVQSSSFRKASRRIEALESLF
Phoenix dactylifera 694 IPKDLLPLESRENTLKKVSEVLSRFAKDGIPLLDPEEDMKVQSNSYRKAVRRIEALESLF
Arabidopsis thaliana 693 IPKDLVPLEARENALKKVSELLSRHP-DGIP-LDPEVDMKIKSSSYKKTVRRLEALENLF
consensus 721
Vitis vinifera 757 DKHEVAKSPLIEQKLKVLHMKKELTAKIKSIKRTMRSSTALAFKDELKARKRVLRKLGYV
Populus trichocarpa 775 EKHEIAKSPLIKEKLKVLHTKQELTARIKLIRKSMRSSTSLAFKDELKARKRVLRRLGYI
Glycine max 744 EKHEIAKSPLIKQKLKVFQRKQELTAKIKSIKKALRSSSALAFKDELKARKRVLRRLGYA
Nicotiana sylvestris 756 EEHKIATSPLIKEKLKVLHKKKELTGKIRSIKRAMRTSKALAFKDELKARKRVLRRLGYI
Oryza sativa 764 EKHDVHNSPHIKQKLKVLHAKQELSTKIKAIKRTMRSSTALAFKDELKARKRVLRRLGYI
Phoenix dactylifera 754 DRHEIRNSPLIQQKLKVLRAKQELTAKIKSIKKTMRLSTSLAFKDELKARKRVLRRLGYI
Arabidopsis thaliana 751 EKHKIAKSPLITEKLKVLQMKEELIAKIKSLKKTVRSSTALAFKDELKARKRVLRRLGYI
consensus 781

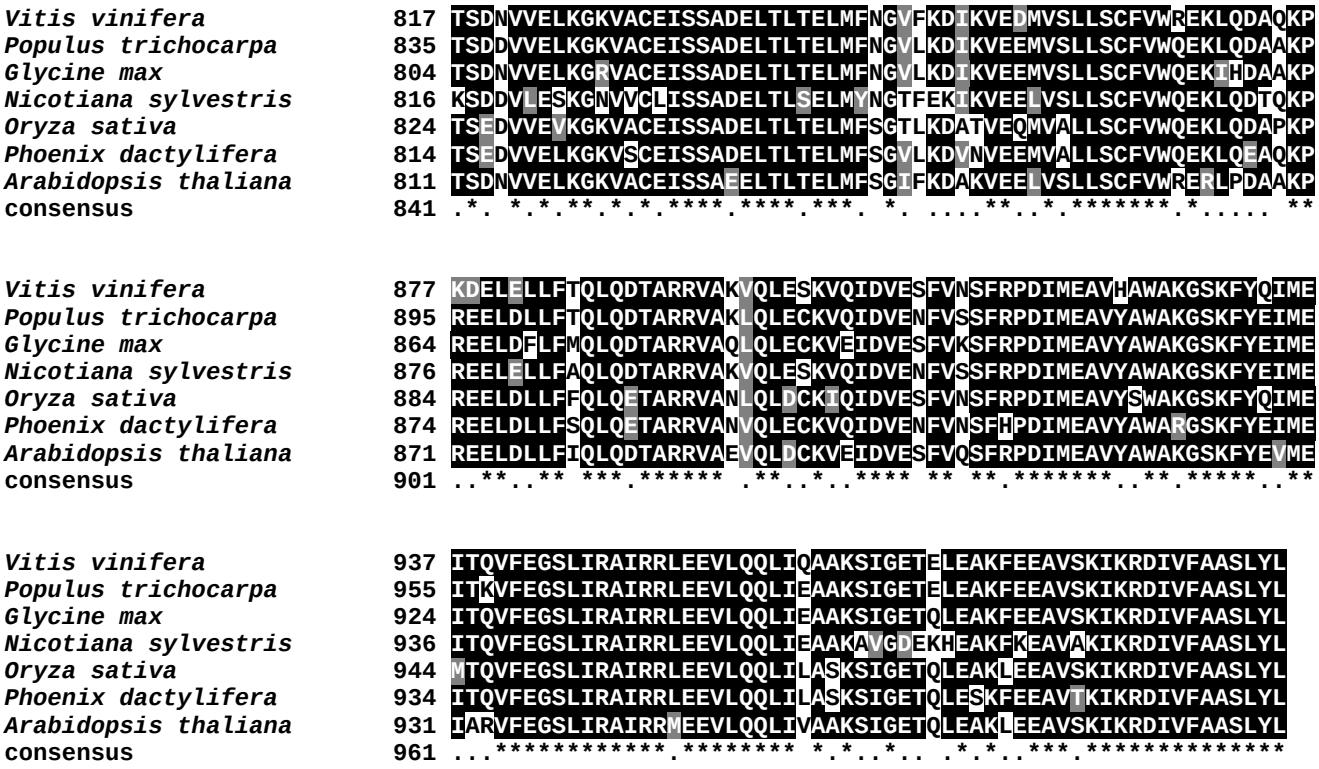

Figure S6. Sequence conservation among plant MTR4 orthologs.
Sequence alignment of full-length MTR4 orthologs from different angiosperm lineages, as classified in Myburg et al. (2014): *Vitis vinifera* XP_002273102 (representing Vitales), *Populus trichocarpa* XP_002328732 (Malpighiales), *Glycine max* XP_003532326 (Fabids), *Nicotiana sylvestris* XP_009771435 (Asterids), *Oryza sativa* XP_015620627 (Poales), *Phoenix dactylifera* XP_00880935 (Arecales), and *Arabidopsis thaliana* OAP13689 (Malvids). Identical and similar residues across all sequences are shaded in black and gray, respectively. Numbers indicate residue positions. The arch domain, as defined in Jackson *et al*. (2010), is highlighted with a black line under the consensus sequence. Asterisks and periods in the consensus indicate identical and conserved residues, respectively.

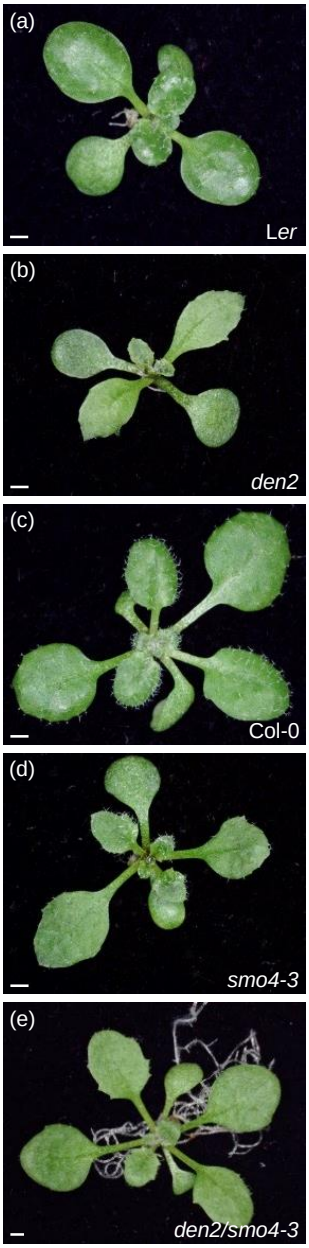

Figure S7. Allelism test of the *smo4-3* and *den2* mutants.
The genetic background of *den2* is L*er*, and that of *smo4-3* is Col-0. Pictures were taken at 14 (a–d) and 18 (e) days after stratification. Scale bars: 1 mm.

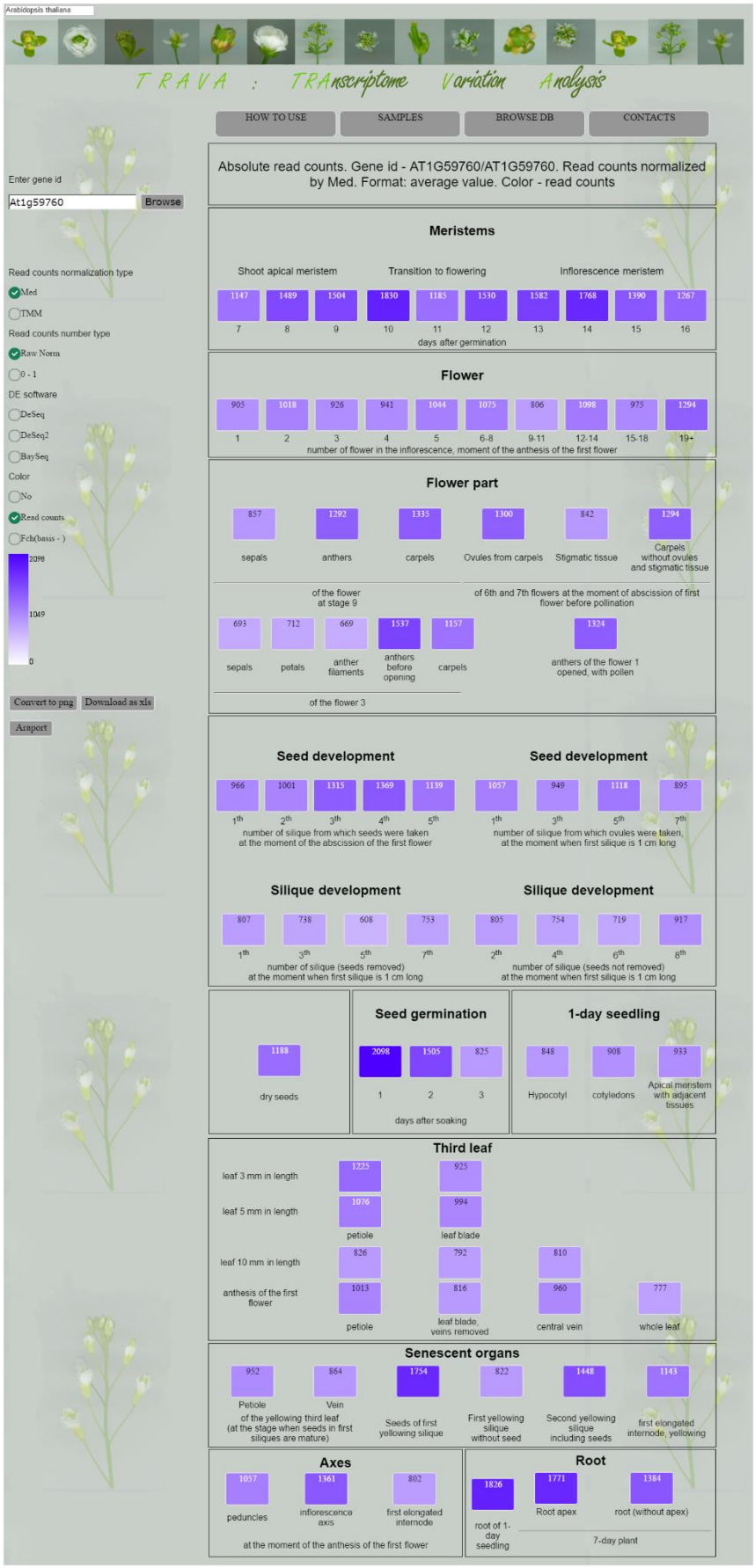

Figure S8. AT1G59760 (*MTR4*) expression profile in the organs and developmental stages shown, as obtained from the Transcriptome Variation Analysis (TraVA) database.

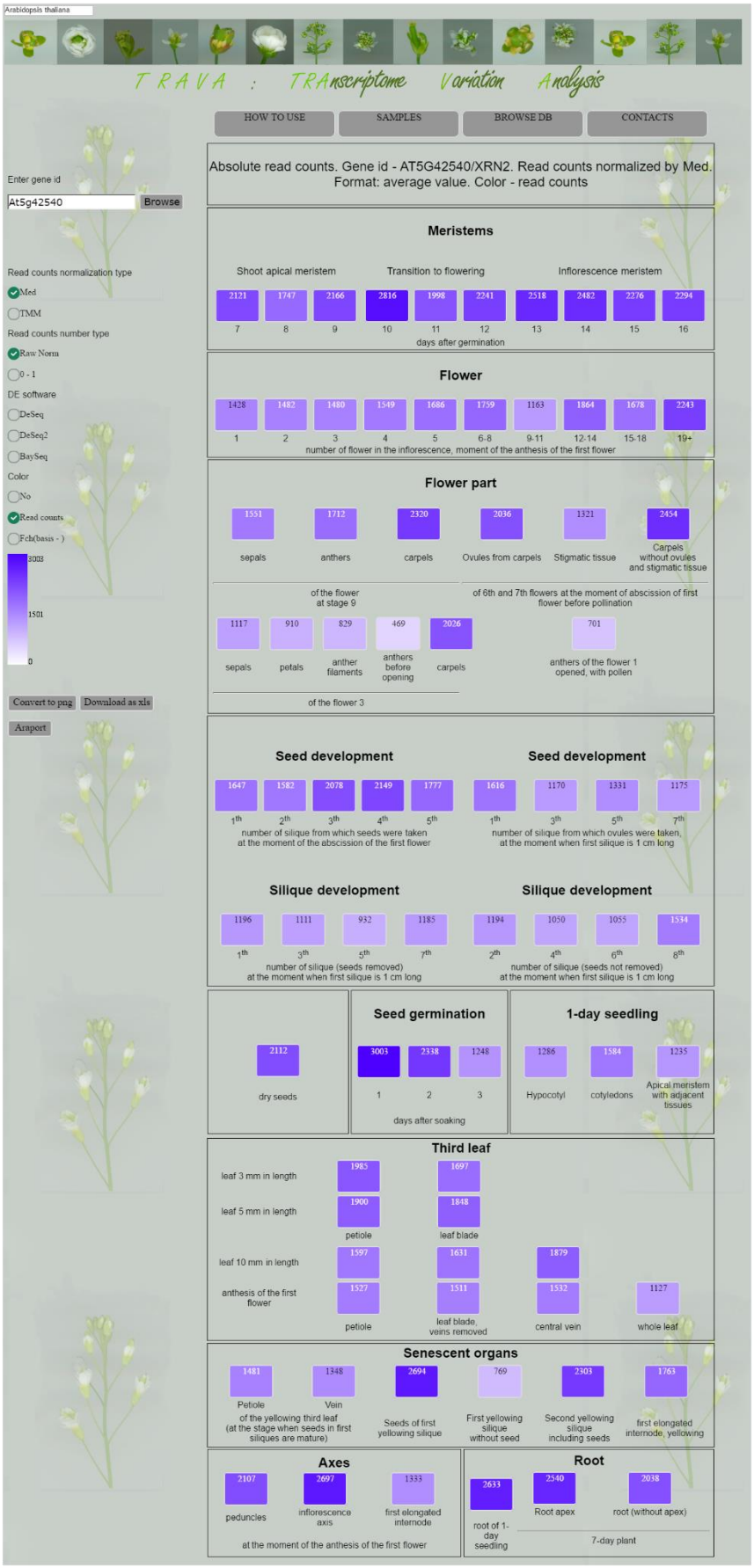

Figure S9. AT5G42540 (*XRN2*) expression profile in the organs and developmental stages shown, as obtained from the TraVA database.

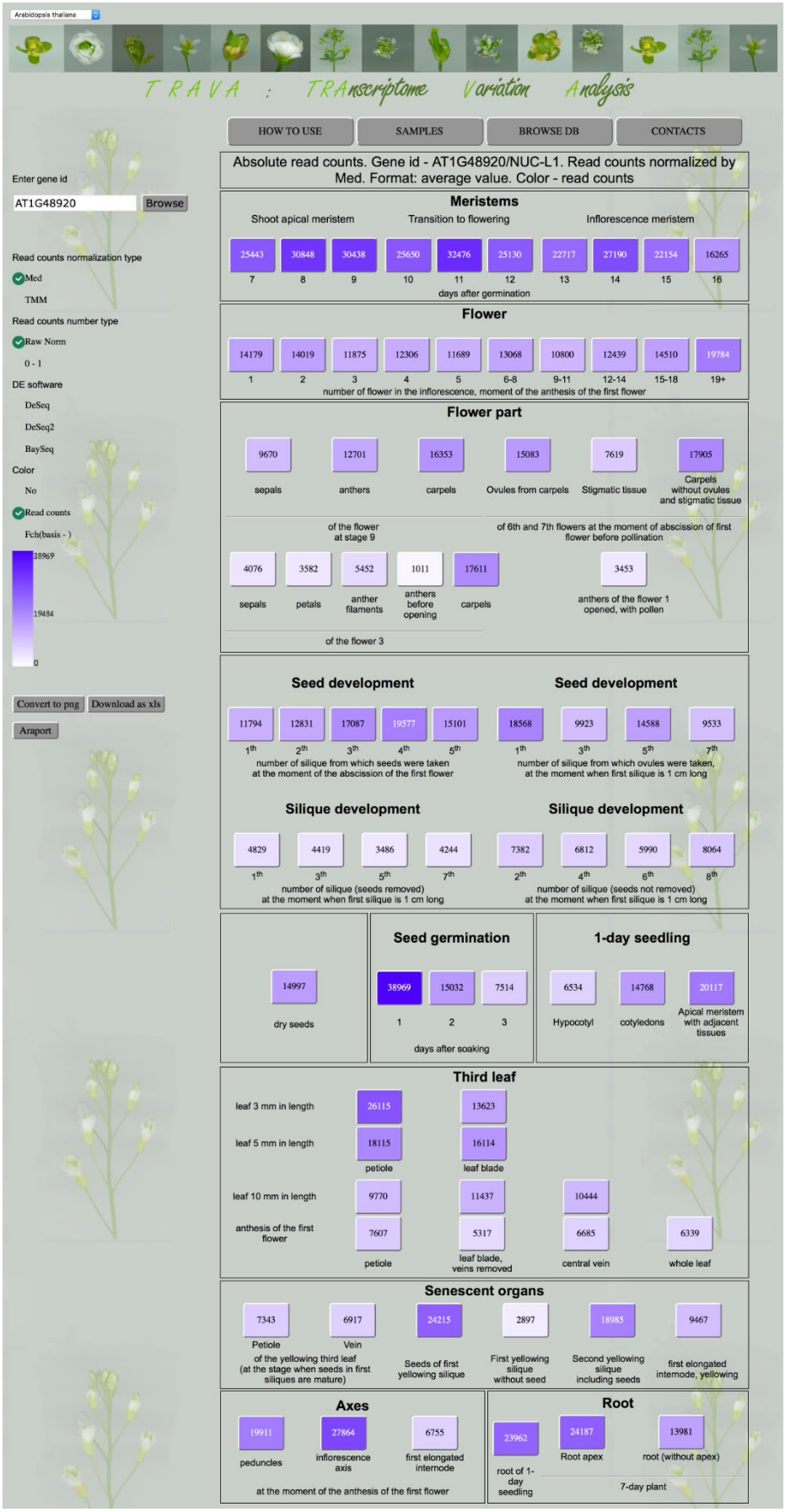

Figure S10. AT1G48920 (*NUC1*) expression profile in the organs and developmental stages shown, as obtained from the TraVA database.

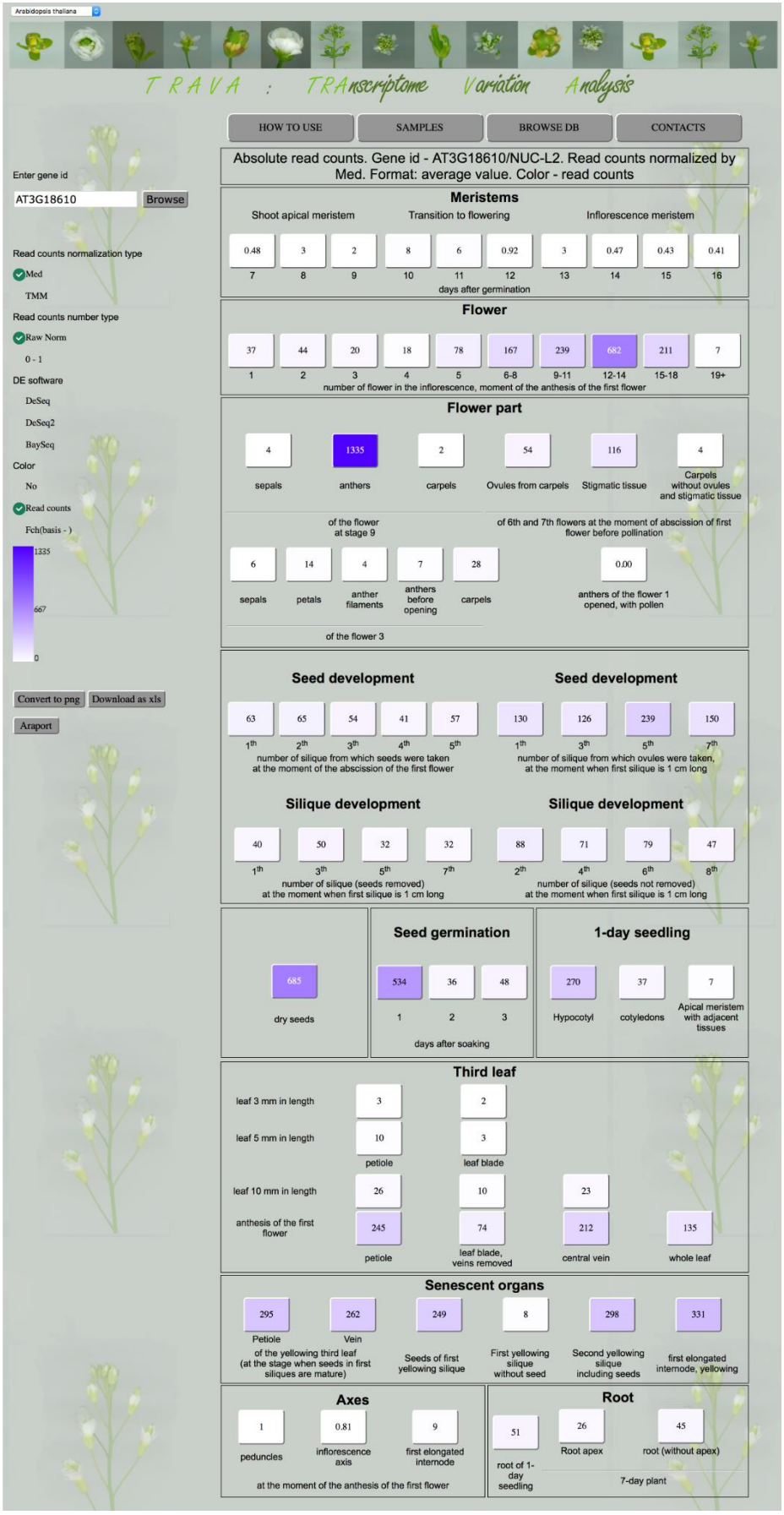

Figure S11. AT3G18610 (*NUC2*) expression profile in the organs and developmental stages shown, as obtained from the TraVA database.

Table S1. Primer sets used for the fine mapping of *den2*

Marker		Locus	Oligonucleotide sequence (5´→3´)		PCR product size (bp)	
Name	Type[a]		Forward primer	Reverse primer	L*er*	Col-0
CER449091	In/Del	AT2G34180-AT2G34185	AAAGAATAAAAGATCGATGT	CATTACACTACATATTCTGAATAG	162	188
nga168	SSLP	AT2G39010	CTACAGAGCTGTCATCGCTGA	GCCAACATTGTGTATCATCAATC[b]	385	401
CER452720	In/Del	AT2G44150-AT2G44160	CTGCAGGGGTTGGGGATTGA	GTAGTTAGACAACATGAGTTACA	225	254
CER448613	In/Del	AT2G46460	CAATTCTTTATTAGGTATCAGTGG	TTCGTCTATCTAACCTTAATGGG	419	953

[a]SSLP, simple sequence length polymorphism; In/Del, small insertion/deletion. [b]Labelled with HEX (4, 7, 2', 4', 5', 7'-Hexachloro-6-carboxyfluorescein).

Table S2. Fluorescent probes used in this work

Purpose	Oligonucleotide name	Oligonucleotide sequence (5'→3')
In situ hybridization	18S rRNA	TGTGAAACTGCGAATGGCTCATTAAATC[a]
	25S rRNA	GAAAGACTAATCGAACCATCTAGTAGCT[b]
	5.8S rRNA	CGTAGCGAAATGCGATAC[c]
Northern blots	S9[d]	AGGATGGTGAGGGACGACGATTT[c]
	S7[d]	GTCGTTCTGTTTTGGACAGGTATCGA[c]

[a-c]Oligonucleotides labeled with [a]FAM (6-Carboxyfluorescein), [b]CY3 (Cyanine 3) and [c]DIG (Digoxigenin). [d]Sequences taken from Lange *et al*. (2011).

Table S3. Other primer sets used in this work

Purpose		Oligonucleotide name(s)	Oligonucleotide sequence (5'→3')	
			Forward primer (F)	Reverse primer (R)
Genotyping of	*smo4-3*	NOP53_F1/R1	GTCTCGAACTTTTTCCTTGGG	AGTATTCCTCGCTTCTCGAGG
	smo4-2	NOP53_F2/R2	CAGAAGAGATGACTGGGTCAC	GATATATGAGTCGATTGAGACAG
	smo4-4	NOP53_F3/R3	ACATTAGCTCCGAGGACATTGA	GTCGGCCATTACAGAATCGTC
	den2	NOP53_F4[a]	CTTGCCCAACATCTTAGAAGAAA	
T-DNA insertion verification		Salk_LBb1[b]	GCGTGGACCGCTTGCTGCAACT	
		LB-pAC161[c]	ATATTGACCATCATACTCATTGC	
Double mutant genotyping		At4g02720_F2/R2[d]	AGGCGGAAGAAATCTTCGGATT	GCAAGTAGCAAACAGCAGTATC
		PARL1_F/R	AGTTGCTGTCACCAAGAAG	TGGCCTACCATGGAATTCA
		NUC2_F/R	CGACGATGGATCTTCTTCGGA	TGGTTTAGCATTCTTAACAACTG
		MTR4_F/R	TTTGTCAATACCTCGACGTCC	ATTGTCTGCGTACTGTGGGTC
Verification of inserts in destination vectors		pMDC32_F1/R1[d]	TTCATTTGGAGAGGACCTCG	GAAATTCGAGCTCCACCGCG
		M13_F/R	GTTGTAAAACGACGGCCAGTG	GGAAACAGCTATGACCATGAT
		pMDC111R[d]		TATGTTGCATCACCTTCACCCT
		pMDC85R[d]		ATAATGATCAGCGAGTTGCAC
Construction of transgenes	*35S$_{pro}$:SMO4*	NOP53-attB_F1/R1	*GGGGACAAGTTTGTACAAAAAAGCAGGCT*AT GGGGAAGAGGTCGAAAACA[e]	*GGGGACCACTTTGTACAAGAAAGCTGGGT*CT ATGAGTCATTGCCGTAAAA[e]
	SMO4$_{pro}$:SMO4	NOP53-attB_F2/R2	*GGGGACAAGTTTGTACAAAAAAGCAGGCT*GA TGGTCCTATGGAATCGTAA[e]	*GGGGACCACTTTGTACAAGAAAGCTGGGT*TG TTAGATGGTAGAGCTTGTG[e]
	35S$_{pro}$:SMO4:GFP	NOP53-attB_R3[f]		*GGGGACCACTTTGTACAAGAAAGCTGGGT*AT GAGTCATTGCCGTAAAAAA[e]

[a]The *den2* allele was genotyped using the NOP53_F4/R1 primer pair. [b-d]Sequences taken from [b]http://signal.salk.edu/tdnaprimers.2.html, [c]https://www.gabi-kat.de/faq/vector-a-primer-info.html, and [d]Sánchez-García *et al.* (2015). [e]The *attB* sequences are depicted in italics. [f]The *35S$_{pro}$:SMO4:GFP* and *SMO4$_{pro}$:SMO4:GFP* constructs were generated using the NOP53-attB_F1/R3 and NOP53-attB_F2/R3 primer pairs, respectively.

SUPPORTING REFERENCES

Aoki, Y., Okamura, Y., Tadaka, S., Kinoshita, K. and Obayashi, T. (2016) ATTED-II in 2016: A plant coexpression database towards lineage-specific coexpression. *Plant and Cell Physiology* **57**, e5.

Chaker-Margot, M., Barandun, J., Hunziker, M. and Klinge, S. (2017) Architecture of the yeast small subunit processome. *Science* **355**, aal1880.

Henras, A.K., Plisson-Chastang, C., O'Donohue, M.F., Chakraborty, A. and Gleizes, P.E. (2015) An overview of pre-ribosomal RNA processing in eukaryotes. *Wiley Interdisciplinary Reviews RNA* **6**, 225-242.

Jackson, R.N., Klauer, A.A., Hintze, B.J., Robinson, H., van Hoof, A. and Johnson, S.J. (2010) The crystal structure of Mtr4 reveals a novel arch domain required for rRNA processing. *EMBO Journal* **29**, 2205-2216.

Lange, H., Sement, F.M. and Gagliardi, D. (2011) MTR4, a putative RNA helicase and exosome co-factor, is required for proper rRNA biogenesis and development in *Arabidopsis thaliana*. *Plant Journal* **68**, 51-63.

Larkin, M.A., Blackshields, G., Brown, N.P., Chenna, R., McGettigan, P.A., McWilliam, H., Valentin, F., Wallace, I.M., Wilm, A., Lopez, R., Thompson, J.D., Gibson, T.J. and Higgins, D.G. (2007) Clustal W and Clustal X version 2.0. *Bioinformatics* **23**, 2947-2948.

Myburg, A.A., Grattapaglia, D., Tuskan, G.A., Hellsten, U., Hayes, R.D., Grimwood, J., Jenkins, J., Lindquist, E., Tice, H., Bauer, D., Goodstein, D.M., Dubchak, I., Poliakov, A., Mizrachi, E., Kullan, A.R., Hussey, S.G., Pinard, D., van der Merwe, K., Singh, P., van Jaarsveld, I., Silva-Junior, O.B., Togawa, R.C., Pappas, M.R., Faria, D.A., Sansaloni, C.P., Petroli, C.D., Yang, X., Ranjan, P., Tschaplinski, T.J., Ye, C.Y., Li, T., Sterck, L., Vanneste, K., Murat, F., Soler, M., Clemente, H.S., Saidi, N., Cassan-Wang, H., Dunand, C., Hefer, C.A., Bornberg-Bauer, E., Kersting, A.R., Vining, K., Amarasinghe, V., Ranik, M., Naithani, S., Elser, J., Boyd, A.E., Liston, A., Spatafora, J.W., Dharmwardhana, P., Raja, R., Sullivan, C., Romanel, E., Alves-Ferreira, M., Kulheim, C., Foley, W., Carocha, V., Paiva, J., Kudrna, D., Brommonschenkel, S.H., Pasquali, G., Byrne, M., Rigault, P., Tibbits, J., Spokevicius, A., Jones, R.C., Steane, D.A., Vaillancourt, R.E., Potts, B.M., Joubert, F., Barry, K., Pappas, G.J., Strauss, S.H., Jaiswal, P., Grima-Pettenati, J., Salse, J., Van de Peer, Y., Rokhsar, D.S. and Schmutz, J. (2014) The genome of *Eucalyptus grandis*. *Nature* **510**, 356-362.

Sánchez-García, A.B., Aguilera, V., Micol-Ponce, R., Jover-Gil, S. and Ponce, M.R. (2015) Arabidopsis *MAS2*, an essential gene that encodes a homolog of animal NF-kappa B activating protein, is involved in 45S ribosomal DNA silencing. *Plant Cell* **27**, 1999-2015.

Schillewaert, S., Wacheul, L., Lhomme, F. and Lafontaine, D.L. (2012) The evolutionarily conserved protein Las1 is required for pre-rRNA processing at both ends of ITS2. *Molecular and Cellular Biology* **32**, 430-444.

Weis, B.L., Kovacevic, J., Missbach, S. and Schleiff, E. (2015) Plant-specific features of ribosome biogenesis. *Trends in Plant Science* **20**, 729-740.

Zakrzewska-Placzek, M., Souret, F.F., Sobczyk, G.J., Green, P.J. and Kufel, J. (2010) *Arabidopsis thaliana* XRN2 is required for primary cleavage in the pre-ribosomal RNA. *Nucleic Acids Research* **38**, 4487-4502.

Supporting Dataset 1. Top 100 ranking genes coexpressed with *SMO4* , identified by ATTED-II

Supportability and Mutual Rank (MR) are used here as defined in Aoki et al. (2015).
Original short descriptions for genes were extended using the HomoloGene and Aramemnon databases.
Predictions of subcellular localizations in the Target column are shown as indicated in http://atted.jp/help/term.shtml#s

Rank	Locus	Short description	Supportability	MR	Target
0	At2g40430	SMO4, NOP53 homolog	☆☆	0.0	O,N
1	At5g67240	SDN3, small RNA degrading nuclease 3. Similar to human REXO4, 3'-5' exonuclease	☆☆	1.0	O,Y
2	At5g50310	Unknown protein, similar to KLHDC4	☆☆	1.7	O,N
3	At3g49990	Unknown protein	☆☆	2.6	O,N
4	**At5g38720**	**RRP7 homolog**	☆☆	3.2	O,N
5	At5g14440	SURF2, Surfeit locus protein 2	☆☆	5.0	O,N
6	At5g57120	Putative (yeast SRP40)-like protein of unknown function, with weak similarity to human Nucleolar phosphoprotein p130 (NOLC1)	☆☆	8.1	O,N
7	At4g02400	Putative (yeast UTP14)-like nucleolar component of U3 processome complex	☆☆☆	8.2	O,N
8	At2g21440	Similar to yeast NOP4, nucleolar protein required for pre-rRNA processing and accumulation of 60S ribosomal subunits. Nucleolar component of the spliceosomal small nuclear ribonucleoprotein (snRNP)complexes . It specifically associates with U1, U2, U4, U5, and U6 small nuclear RNAs (snRNAs), possibly coordinating their transition through the nucleolus.	☆☆	8.5	O,N
9	At5g08420	RNA-binding KH domain-containing protein	☆☆	8.9	O,N
10	At2g25670	Unknown protein	☆☆	9.5	O,N
11	At3g24080	Putative (yeast Kri1)-like protein, required for 40S ribosome biogenesis	☆☆	9.5	O,N
12	At5g22320	Leucine-rich repeat (LRR) family protein	☆☆	9.6	O,N
13	At1g80750	60S ribosomal protein L7 (RPL7A), similar to human ribosomal protein L7	☆☆☆	9.8	O,Y
14	At3g01160	Putative (yeast ESF1)-like pre-rRNA processing protein	☆☆	11.8	O,N
15	At1g13160	Putative SDA1-like protein of unknown function, required for actin cytoskeleton	☆☆☆	12.3	O,Y
16	At1g12270	Putative co-chaperone HOP1	☆	14.3	O,Y
17	At1g43860	Putative (yeast Sdo1)-like ribosome biogenesis factor	☆	14.6	M,C
18	At5g55920	OLI2. Similar to human Proliferation-associated nucleolar protein p120 and Saccharomyces cerevisiae Nucleolar protein NOP2	☆☆☆	14.8	M,N

19	At3g56510	Putative (yeast ESF12)-like U3 snoRNP-associated protein	☆☆	15.6	O,N
20	At5g05210	Surfeit locus 6, putative nucleolar matrix protein	☆☆	15.7	O,N
21	At5g06110	ZRF1b/GlsA2, putative ZRF-type J-protein co-chaperone	☆☆	15.7	O,Y
22	At3g62940	Similar to human OTUD6B, a member of the ovarian tumor domain (OTU)-containing subfamily of deubiquitinating enzymes	☆☆	16.7	O,N
23	At1g11240	Putative (yeast ESF1)-like pre-rRNA processing protein, required for 18S rRNA synthesis in Saccharomyces cerevisiae	☆☆	17.6	O,N
24	At1g72440	SWA2/EDA25, putative (yeast Noc1)-like protein associated with U3 processome complex	☆☆	18.9	S,N
25	At1g14610	VALRS, valyl-tRNA synthetase / valine--tRNA ligase	☆☆	19.4	M,C
26	At3g51270	Putative atypical Rio-type protein kinase	☆	19.6	O,Y
27	At2g37990	Ribosome biogenesis regulatory protein (RRS1) family protein	☆☆☆	21.4	O,N
28	At2g20280	C3H21, protein of unknown function, contains CCCH-type zinc ion binding domain	☆	23.2	O,N
29	At3g16840	RH13, Putative DEAD/DEAH-box-type helicase. Similar to yeast MAK5, involved in 60S subunit biogenesis	☆☆☆	23.2	O,N
30	At2g18220	Putative (yeast Noc2)-like protein	☆☆☆	24.8	O,N
31	At3g20430	Putative snRNA nuclear export protein	☆	24.9	O,N
32	At3g11710	KRS-1, lysyl-tRNA synthetase 1	☆☆	25.0	O,Y
33	At4g25730	Similar to yeast SPB1, 27S pre-rRNA (guanosine2922-2'-O)-methyltransferase. Required for 60S ribosomal subunit biogenesis in Saccharomyces cerevisiae	☆☆☆	25.2	O,
34	At5g12410	THUMP domain-containing protein	☆	25.4	O,Y
35	At1g31970	STRS1, DEA(D/H)-box RNA helicase family protein	☆☆	25.5	O,Y
36	At1g12650	Similar to yeast and human RRP36, involved in early cleavages of the pre-rRNA and production of the 40S ribosomal subunit	☆☆	25.7	O,N
37	At1g06720	Putative (yeast Bms1)-like protein of unknown function	☆☆☆	27.1	O,N
38	At1g59760	MTR4, RNA helicase, ATP-dependent, SK12/DOB1 protein	☆☆	27.6	O,N
39	At1g50920	Nog1-1, putative (yeast Nog1)-like nucleolar GTPase	☆☆	27.9	O,Y
40	At1g06670	NIH, DEIH-box RNA/DNA helicase	☆	28.2	O,P
41	At3g05060	NOP56-like pre RNA processing ribonucleoprotein, putative component of C/D snoRNP complex (AtNOP58-2/AtNOP5-2)	☆☆☆	28.8	O,Y
42	At1g72050	TFIIIa, putative RNA polymerase TFIIIa transcription factor	☆☆	29.0	O,N
43	At5g61770	PPAN, PETER PAN-like protein. Similar to human nucleolar PPAN and SSF1 and SSF2 rRNA-binding ribosome biosynthesis proteins of Saccharomyces cerevisiae	☆☆☆	30.7	O,N
44	At1g12830	Unknown protein	☆☆	31.5	O,N
45	At3g43590	Zinc knuckle (CCHC-type) family protein	☆☆	32.4	O,N

46	At5g61330	Unknown protein, contains weak similarity to Saccharomyces cerevisiae rRNA processing protein EBP2 (EBNA1-binding protein homolog) and human apoptosis antagonizing transcription factor AATF	☆☆	32.6	O,N
47	At2g28600	Putative DEAD/DEAH-box-type helicase	☆☆	33.6	O,N
48	At5g50840	Unknown protein	☆	34.6	O,N
49	At5g17930	Similar to human nucleolar NOM1, RNA export mediator	☆☆	34.6	O,N
50	At1g52380	NUP50 (Nucleoporin 50 kDa) protein	☆	34.9	O,N
51	At1g64880	Ribosomal protein S5 family protein	☆☆	38.8	M,M
52	At5g54910	RH32, putative DEAD/DEAH-box-type helicase	☆☆	39.2	O,Y
53	At4g19610	Similar to human RBM19 (RNA binding motif protein 19) and Saccharomyces cerevisiae MRD1, required for release of base-paired U3 snoRNA within the preribosomal complex (18S processing)	☆☆	39.5	O,N
54	At3g58660	Putative L1-type protein of large ribosomal subunit	☆☆☆	39.8	C,Y
55	At2g34357	Similar to human and yeast RRP12, ribosomal RNA processing 12 homolog, required for export of both ribosomal subunits	☆☆☆	40.7	O,N
56	At5g62440	Protein of unknown function (DUF3223)	☆☆	40.8	O,N
57	At1g53460	Unknown protein	☆	40.9	M,C
58	At1g02330	Similar to human C9orf78	☆	41.0	O,N
59	At5g57990	UBP23, ubiquitin-specific protease 23	☆☆	41.5	C,N
60	At5g58130	ROS3, REPRESSOR OF SILENCING 3, a RNA-binding protein required for DNA demethylation	☆☆	41.7	O,N
61	At3g22660	EBP2, putative rRNA processing protein involved in ribosome biogenesis	☆☆☆	41.7	O,N
62	At1g56110	NOP56, putative component of C/D snoRNP complex	☆☆☆	42.3	O,N
63	At4g26190	Haloacid dehalogenase-like hydrolase (HAD) superfamily protein	☆☆	42.6	O,N
64	At5g42540	XRN2, exoribonuclease 2, acts as a suppressor of posttranscriptional gene silencing. Probably involved in rRNA or snoRNA processing	☆☆	42.9	O,Y
65	At1g04190	TPR3, putative CC-TPR-type co-chaperone-like protein	☆	43.4	O,M
66	At3g57150	NAP57, putative TruB-type tRNA pseudouridine synthase of H/ACA ribonucleoprotein complex	☆☆	44.8	O,Y
67	At1g17130	Similar to cell cycle control protein cwf16 of Schizosaccharomyces pombe. Involved in mRNA splicing where it associates with cdc5 and the other cwf proteins as part of the spliceosome	☆	46.1	O,N
68	At2g40660	Nucleic acid-binding, OB-fold-like protein	☆	46.3	O,C
69	At1g69070	Putative (yeast UTP2/Nop14)-like nucleolar component of U3 processome complex	☆☆☆	47.3	O,Y
70	At1g52980	NUG2, putative (yeast NUG2)-like ribosome large subunit assembly factor	☆	47.4	O,N
71	At2g45520	Unknown protein	☆	47.8	M,N
72	At1g23280	MAK16. Required for the maturation of 25S and 5.8S rRNAs in the yeast Saccharomyces cerevisiae	☆☆	48.6	O,Y
73	At3g02760	Similar to human HisRS, Histidyl-tRNA synthetase	☆☆	49.2	C,C

74	At3g58840	PMD1, protein involved in peroxisomal and mitochondrial proliferation	☆☆	49.5	O,Y
75	At3g02950	THO7, putative component of THO/TREX RNA trafficking complex	☆	49.8	O,C
76	At1g79150	NOC3, putative (yeast Noc3)-like protein associated with U3 processome complex	☆☆☆	50.0	O,C
77	At1g79200	Putative SCI1-like kinase inhibitor	☆	50.4	O,N
78	At5g47680	TRM10, tRNA modification 10. putative tRNA (guanine-N(1)-)-methyltransferase	☆☆	51.2	O,N
79	At2g34900	(GTE1/IMB1), putative BET-type transcription factor	☆☆	51.6	O,C
80	At5g40530	Similar to human and yeast RNA processing 8, methyltransferase, involved in the modification of 25S rRNA	☆	52.5	O,N
81	At3g02220	Unknown protein with a conserved DUF2039 domain	☆☆	53.4	O,N
82	At5g10010	Unknown protein	☆	54.8	O,C
83	At4g28200	Similar to human and yeast UTP6, small subunit (SSU) processome component	☆☆	55.3	O,Y
84	At1g06530	PMD2, putative PMD1-like protein of unknown function	☆☆	55.7	O,
85	At1g55930	CBS domain-containing protein / transporter associated domain-containing protein	☆	55.9	C,P
86	At4g10760	MTA, putative MT-A70 subunit of S-adenosylmethionine-dependent methyltransferase	☆	57.5	O,Y
87	At3g57000	Putative Nep1-like methyltransferase involved in ribosome biogenesis	☆☆	57.8	O,Y
88	At3g11964	S1 RNA-binding domain-containing protein, similar to SP:Q05022 rRNA biogenesis protein RRP5 of Saccharomyces cerevisiae	☆☆☆	58.3	O,C
89	At4g25340	FKBP53, FK506 BINDING PROTEIN 53	☆☆	59.0	O,N
90	At5g16750	TOZ, TORMOZ. Putative (yeast UTP13)-like ribosome biogenesis factor of SSU processome	☆☆☆	59.4	M,C
91	At2g34750	RRN3b, putative TFIa/RRN3-type RNA polymerase I basal transcription factor	☆☆	59.9	O,Y_N
92	At1g28060	Putative PRP3-like pre-mRNA processing factor. Yeast PRP3 participates in pre-mRNA splicing and in nuclear mRNA export. May play a role in the assembly of the U4/U5/U6 tri-snRNP complex	☆☆	60.5	O,N
93	At3g10530	Putative (yeast UTP7)-like nucleolar component of U3 processome complex	☆☆☆	61.2	O,N
94	At2g47250	Similar to yeast Pre-mRNA splicing factor RNA helicase PRP43 and human DHX15	☆	62.5	O,Y
95	At3g56120	Putative TRMT5, tRNA methyltransferase 5	☆	64.4	O,Y
96	At4g01880	Similar to human and yeast TRM13, tRNA methyltransferase 13	☆	64.5	C,C
97	At4g38890	Similar to yeast DUS3, dihydrouridine synthase 3, required for dihydrouridine modification of tRNA	☆☆	64.9	O,N
98	At5g22650	HDT2, putative HD2-type histone deacetylase	☆☆☆	65.2	O,N
99	At2g28450	C3H24, contains CCCH-type zinc ion binding domain	☆☆	65.5	O,N
100	At2g43650	EMB2777, putative (yeast Sas10)-like protein of unknown function	☆☆	66.0	O,N

Arabidopsis RIBOSOMAL RNA PROCESSING 7 participates in 45S rDNA transcriptional regulation and 45S pre-rRNA processing

Rosa Micol-Ponce, Raquel Sarmiento-Mañús, Alejandro Ruiz-Bayón, and María Rosa Ponce

Instituto de Bioingeniería, Universidad Miguel Hernández, Campus de Elche, 03202 Elche, Alicante, Spain.

Running title: RRP7 acts in 45S pre-rRNA synthesis and processing

Corresponding author: María Rosa Ponce (telephone: +34 96 665 8503; fax: +34 96 665 8511; email: mrponce@umh.es).

The author responsible for distribution of materials integral to the findings presented in this article in accordance with the policy described in the Instructions for Authors (www.plantcell.org) is: María Rosa Ponce (mrponce@umh.es)

Character count: 83726. Word count (total): 14776.
Word count breakdown: Title page, 147; Summary, 219; Introduction, 921; Results, 4223; Discussion, 2911; Methods, 1419; Acknowledgements and author contributions, 115; Figure legends, 764; Supplemental Data, 261. References, 3828.

Figures: 9 Tables: 0 Supplemental Figures: 9 Supplemental Tables: 8 Supplemental Datasets: 1

ONE-SENTENCE SUMMARY

The ribosome biogenesis factor RIBOSOMAL RNA PROCESSING 7 participates in 45S rDNA transcriptional regulation and 45S pre-rRNA processing, interacts with MAS2, and likely functions in pre-mRNA splicing.

ABSTRACT

Ribosome biogenesis is a fundamental process that impacts growth and development in eukaryotes and is linked to human diseases and cancer. Arabidopsis MORPHOLOGY OF ARGONAUTE1-52 SUPPRESSED 2 (MAS2) participates in splicing and 45S ribosomal DNA (rDNA) expression. In a screen for MAS2 interactors, we identified RIBOSOMAL RNA PROCESSING 7 (RRP7), a putative ortholog of yeast Ribosomal RNA processing protein 7 (Rrp7), which is required for 18S ribosomal RNA (rRNA) maturation. Arabidopsis RRP7 localizes to the nucleolus and perinucleolar region, and lack of RRP7 function perturbs 18S rRNA maturation, causing nucleolar hypertrophy and retention of 18S rRNA precursors, and an increased 25S/18S rRNA ratio. The *rrp7* mutants exhibit slow growth, altered shoot phyllotaxy, aberrant venation in lateral organs, partial infertility, and abscisic acid hypersensitivity in seedlings. *RRP7* coexpresses with genes encoding ribosome biogenesis factors (RBFs), including SMALL ORGAN 4 (SMO4), which also interacts with MAS2 and participates in 5.8S and 18S rRNA maturation. Arabidopsis contains hundreds of 45S rDNA genes whose expression is epigenetically regulated and double mutant analysis revealed synergistic and epistatic interactions between *RRP7* alleles and alleles of *SMO4* and of various epigenetic regulators of 45S rDNA transcription. Our results unveil the evolutionarily conserved but divergent role of RRP7 as a RBF that participates in 45S rDNA transcriptional regulation and 45S pre-rRNA processing, interacts with MAS2, and might function in splicing.

INTRODUCTION

The ribosome, a molecular machine that originated 3–4 billion years ago, translates messenger RNAs (mRNAs) into proteins, a process universal to all life forms (Petrov et al., 2014). In Eukarya, cytoplasmic, mitochondrial, and chloroplast ribosomes are composed of a large subunit (LSU) and a small subunit (SSU), each consisting of 1–3 ribosomal RNAs (rRNAs) and tens of ribosomal proteins (RPs) (Wilson and Doudna Cate, 2012). For example, the eukaryotic cytoplasmic (80S) ribosome is composed of ~80 RPs and four rRNAs, which include one 28S/25S/23S rRNA (28S in metazoans, 25S in plants, or 23S in yeast), together with 18S, 5.8S, and 5S rRNAs.

The 28S/25S/23S, 18S, and 5.8S rRNAs are the final products of the transcription and complex processing of a single polycistronic precursor, the 47S/45S/35S pre-rRNA (Henras et al., 2015; Lafontaine, 2015). The 47S/45S/35S rDNA genes are transcribed by RNA polymerase I (RNA Pol I) in the nucleolus, resulting in a single 47S/45S/35S pre-rRNA, which undergoes chemical modifications, endonucleolytic cleavages, and exonucleolytic trimmings to render mature 28S/25S/23S, 18S, and 5.8S rRNAs (Supplemental Figures 1 and 2).

Biogenesis of the 80S ribosome begins with the transcription of the 47S/45S/35S rDNA genes and processing of the mature 28S/25S/23S, 18S, and 5.8S rRNAs. Next, the SSU and LSU are assembled in the nucleus and exported to the cytoplasm in almost completely mature form. The 40S subunit contains 18S rRNA and ~33 RPs, whereas the 60S subunit contains 28S/25S/23S, 5.8S, and 5S rRNAs and ~47 RPs (Weis et al., 2015). The final 80S ribosome is assembled in the cytoplasm from a 40S SSU and a 60S LSU.

Work on the yeast 80S ribosome has elucidated its composition, architecture, action, and the interactions of its components (Woolford and Baserga, 2013; Chaker-Margot et al., 2017). Much of the assembly and maturation of the yeast 40S ribosomal subunit is carried out by a large ribonucleoprotein complex termed the SSU processome or 90S pre-ribosomal particle (Phipps et al., 2011). The SSU processome is cotranscriptionally assembled during transcription of the 35S rDNA by the stepwise recruitment of ribosome biogenesis factors (RBFs). Many of these RBFs assemble as subcomplexes prior to their incorporation into the SSU processome. Some subcomplexes are small nucleolar ribonucleoprotein particles (snoRNPs) that include a snoRNA that is partially complementary to different regions of the 35S pre-rRNA. The snoRNAs guide site-specific cleavages, ribose 2′-O-methylation (box C/D family snoRNAs), and uridine-to-pseudouridine conversions (box H/ACA snoRNAs) (Kiss et al., 2002).

Examination of yeast snoRNPs has identified key factors in rRNA processing. Yeast U3 snoRNA is a conserved member of the box C/D family that plays a central role in SSU processome assembly and function (Hughes and Ares, 1991; Beltrame and Tollervey, 1992; 1995). RBFs identified based on their co-precipitation with U3 snoRNA are referred to as U-three proteins (Utps; Phipps et al., 2011). Together with U3 snoRNP, one subcomplex that joins the nascent SSU processome is UtpC, including the essential Ribosomal RNA-processing protein 7 (Rrp7), which is required for 18S rRNA maturation (Baudin-Baillieu et al., 1997; Krogan et al., 2004; Phipps et al., 2011), U3 snoRNA-associated protein 22 (Utp22), and the four subunits of Casein kinase 2 (CK2) (Krogan et al., 2004; Phipps et al., 2011). UtpC components also bind to the transcription factor Interact with Fork Head 1 (Ifh1) to form the CURI (CK2, Utp22, Rrp7, and Ifh1) complex, which does not belong to the SSU processome.

The CURI complex is thought to play a key role in coordinating the two parallel pathways required for ribosome biogenesis in yeast: (i) the transcription of rDNA and the processing of pre-rRNAs to produce mature rRNAs and (ii) the transcription of genes encoding RPs (Rudra et al., 2007). When 35S rDNA transcription is active, most Rrp7 and Utp22 molecules are engaged in processing 35S pre-RNAs and are not available to form CURI complexes, which in turn allows Ifh1 to bind Repressor/activator site binding protein 1 (Rap1) and the Fork Head-like 1 (Fhl1) transcription factor in the promoters of RP-encoding genes, thus activating their transcription. Conversely, when 35S rDNA transcription is less active, lfh1 contributes to the formation of CURI complexes, it does not bind Rap1 and Fhl1, and transcription of RP-encoding genes is not induced. Furthermore, the loss of Rrp7 function reduces 40S ribosomal subunit production and increases the expression of RP-encoding genes (Rudra et al., 2007).

The main Arabidopsis ribonuclease involved in post-transcriptional gene silencing pathways mediated by small RNAs, including microRNAs (miRNAs), is ARGONAUTE1 (AGO1; Baumberger and Baulcombe, 2005). We previously performed second-site mutagenesis of the *ago1-52* hypomorphic and viable mutant and isolated 22 extragenic suppressors; we named the corresponding genes *MORPHOLOGY OF ARGONAUTE1-52 SUPPRESSED* (*MAS*; Micol-Ponce et al., 2014). One of these genes, AT4G02720 (*MAS2*), encodes a perinucleolar protein that negatively regulates 45S rDNA expression (Sánchez-García et al., 2015). In a screen based on the yeast two-hybrid (Y2H) assay, we identified 14 interactors of MAS2, including three putative RBFs. For example, AT2G40430 encodes a putative RBF that interacts with MAS2 (Micol-Ponce et al., submitted), which during the progress of this work was named SMALL ORGAN4 (SMO4) by Zhang et al. (2015). AT5G38720, which encodes another MAS2 interactor, has not been studied in plants and is annotated to encode an ortholog of yeast

Rrp7. Here, we studied the action and interactions of AT5G38720, which we named *RRP7*. We obtained experimental evidence that Arabidopsis RRP7 is involved in 18S rRNA maturation, and that RRP7 is functionally related to MAS2 and SMO4, as well as NUCLEOLIN1 (NUC1) and HISTONE DEACETHYLASE6 (HDA6), which are epigenetic regulators of 45S rDNA transcription.

RESULTS

Arabidopsis RRP7 and its plant orthologs share an NTD but lack a CTD

AT5G38720, which we named *RRP7*, is annotated at TAIR10 and Araport11 as encoding a 306 amino-acid ortholog of yeast Rrp7. Both yeast Rrp7 and its human RRP7A ortholog are essential proteins required for 18S rRNA maturation (Baudin-Baillieu et al., 1997; Krogan et al., 2004; Phipps et al., 2011; Tafforeau et al., 2013). The identities and similarities among the full-length sequences of these three proteins are low: 20.89% and 35.44% (Arabidopsis RRP7 versus human RRP7A), 14.12% and 25.59% (Arabidopsis RRP7 versus yeast Rrp7), and 16.36% and 32.73% (human RRP7A versus yeast Rrp7), respectively.

Yeast Rrp7 has an N-terminal domain (NTD; amino acids 1–156) through which it dimerizes with Utp22 and a C-terminal domain (CTD; amino acids 190–297) with RNA-binding capability that is required for its association with the central domain of the 18S rRNA coding sequence of the 35S pre-rRNA; deletion of either NTD or CTD is lethal (Lin et al., 2013). Alignment of yeast Rrp7 with its human and Arabidopsis orthologs indicates that only the region containing the CTD is conserved to some extent (Supplemental Figure 3). According to HomoloGene, RRP7 proteins share an RRP7_like conserved domain occupying their C-terminal half, which includes the CTD defined by Lin et al. (2013). The RRP7_like domain of Arabidopsis RRP7 (135 aa) shares an identity and similarity of 31.65% and 52.52%, respectively, with its human ortholog (130 aa) and 23.61% and 38.89%, respectively, with that of yeast (128 aa). The amino acid sequence identity and similarity between the RRP7_like domain of human RRP7A and that of yeast Rrp7 are 21.92% and 43.15%, respectively.

As expected, the level of conservation among plant RRP7 orthologs is higher than that shared with RRP7 orthologs from other kingdoms, considering both their full-length sequences and the RRP7_like domain only (Supplemental Figure 4; Supplemental Tables 1 and 2). For the full-length plant RRP7 orthologs, the lowest identity and similarity were 29.24% and 37.59% (for *Glycine max* versus *Oryza sativa*) and the highest were 48.18% and 58.18% (for *Populus trichocarpa* versus *Vitis vinifera*), respectively. For the RRP7_like domains of plant RRP7 orthologs, the lowest identity and similarity were 62.96% and 78.52% (for *Arabidopsis thaliana* versus *Populus trichocarpa*) and the highest were 81.34% and 92.54% (for *Phoenix dactylifera* versus *Vitis vinifera*), respectively.

RRP7 plays several roles in Arabidopsis development

We obtained two publicly available lines carrying T-DNA insertions disrupting AT5G38720, SAIL_628_F08 and WISCDSLOX461-464C16, which we named *rrp7-1*

and *rrp7-2*, respectively (Figure 1A). Plants homozygous for these mutations were viable and indistinguishable, and they exhibited slow growth and pointed leaves (Figure 1B-J). This leaf phenotype is characteristic of mutations in genes encoding RPs (Van Lijsebettens et al., 1994; Horiguchi et al., 2011; Weis et al., 2015) and is similar (although a bit more severe) to that caused by null alleles of *NUCLEOLIN1* (*NUC1*). NUC1 is nucleolar protein involved in transcriptional regulation of 45S rDNA and 45S pre-rRNA processing (Petricka and Nelson, 2007; Pontvianne et al., 2007).

To confirm that the phenotype of *rrp7* mutants is caused by the absence of AT5G38720 activity, we constructed *RRP7*$_{pro}$*:RRP7* and *35S*$_{pro}$*:RRP7* transgenes and transferred them into *rrp7* plants, which fully complemented the mutant phenotypes (Figure 1K-M). These transgenes had no visible phenotypic effect when transferred in the wild-type Col-0 or L*er* genetic backgrounds.

The *rrp7* mutants exhibited two or three cauline leaves emerging from each axil (Figure 2A, B). Despite their delayed growth, the *rrp7* mutants reached a final stature similar to that of wild type (Figure 2C). Siliques of these plants contained many unfertilized ovules and only produced ~10% viable seeds compared to Col-0 (Figure 2D-G). Flowering occurred earlier in Col-0 than in *rrp7*, which also developed an increased number of vegetative leaves before bolting (Figure 2H, I), suggesting that the late flowering of the mutants is not simply a consequence of slow growth.

Arabidopsis *NUC1* is also referred to as *PARALLEL1* (*PARL1*) because null *parl1* mutants exhibit parallel veins in their cotyledons, vegetative leaves, sepals, and petals, a pattern never observed in wild-type plants (Petricka and Nelson, 2007). We found that *rrp7-1* cotyledons, first- and third-node leaves, and petals also exhibited aberrant venation patterns (Figure 3). The cotyledons of *rrp7-1* have two areoles (closed loops) instead of four (as in Col-0), whereas *parl1-2* cotyledons lack areoles. First- and third-node *rrp7-1* leaves, collected 21 days after stratification (das), exhibited a reduced number of venation branching points. The basal region of the lamina of *rrp7-1* leaves has parallel veins (Figure 3J, K). In Col-0, petal veins form some areoles (Figure 3D), which are absent from *rrp7-1* and *parl1-2* (Figure 3H, L). Morphometric analysis of leaf venation parameters commonly used to describe vascular pattern complexity (Supplemental Table 3) confirmed that vein patterning in leaves is more defective in *rrp7-1* than in *parl1-2.*

RRP7 is coexpressed with genes encoding known or predicted nucleolar RBFs

Ribosome biogenesis in yeast requires several snoRNAs and more than 250 RBFs, including endoribonucleases, exoribonucleases, RNA helicases, and assembly factors (Fromont-Racine et al., 2003). To obtain further information about the steps of ribosome

biogenesis in which RRP7 might participate, we analyzed the coregulated genes in microarray assays provided by the ATTED-II coexpression database (see Methods).

Fifty-eight of the top-100 ranking genes coexpressed with *RRP7* were predicted to be nuclear, many of which encode nucleolar proteins known or assumed to be RBFs (Supplemental Dataset 1A). *SMALL ORGAN4* (*SMO4*), which encodes another MAS2 interactor that we identified in a Y2H-based screen (Sánchez-García et al., 2015), was third on the list. *SMO4* encodes the Arabidopsis ortholog of yeast Nucleolar protein 53 (Nop53; Thomson and Tollervey, 2005) and human Glioma Tumor-Suppressor Candidate Region Gene 2 (GLTSCR2; Lee et al., 2012), which are demonstrated RBFs. *RRP7* held the fourth position among the top-100 ranking genes coexpressed with *SMO4* (Micol-Ponce et al., submitted). Comparison of the top-100 genes coexpressed with either *RRP7* (this work) or *SMO4* (Micol-Ponce *et al*., submitted) revealed 55 common genes (Supplemental Dataset 1B). The most highly represented group among this common set includes genes encoding RBFs known or predicted to be integrated in the SSU processome (Sloan et al., 2014). The correlation coefficient of the coexpression between *RRP7* and *SMO4* was 0.802, as determined using the Coexpression viewer tool of ATTED-II.

We also identified the top-100 genes that are coexpressed with *MAS2* (Supplemental Dataset 1C), which mainly encode putative splicing factors, epigenetic factors, and components of ubiquitination complexes, but only a few RBFs. Only four genes are common to the top-100 sets of genes coexpressed with *MAS2*, *SMO4*, and *RRP7*, two of which encode RBFs (Supplemental Dataset 1F). The top-100 genes that are coexpressed with *MAS2* and *SMO4* include seven additional genes, two of which are related to splicing (Supplemental Dataset 1G).

RRP7 expression is widespread, and its promoter shares regulatory elements with *SMO4* and *MAS2*

According to the eFP browser and the TraVA databases (see Methods), *RRP7* and *SMO4* are expressed in all organs and at all developmental stages, with maximum expression at the beginning of seed germination. In addition, *SMO4* expression levels are 3- to 4-fold higher than those of *RRP7* in most cases. We constructed transgenes with the *GUS* reporter gene driven by the *SMO4* or *RRP7* promoter. The $SMO4_{pro}$*:GUS* transgene was expressed in all tissues examined, but to a lesser extent in flowers and siliques, in agreement with previous results (Zhang et al., 2015). We detected less GUS staining in all tissues of $RRP7_{pro}$*:GUS* plants, whose flowers and siliques showed no GUS activity (Supplemental Figure 5), probably because the GUS assay is much less sensitive than microarray and RNA-seq analyses.

We also analyzed the *SMO4*, *RRP7*, and *MAS2* promoters using the PLACE and Athena databases (see Methods; Supplemental Figure 6). We found two identical GGCCCATTA motifs in the *SMO4* promoter at –52 to –44 and –82 to –74 bp from its transcription start site (TSS; +1 position). These motifs correspond to the UP1ATMSD (GGCCCAWWW, where W is A or T) element, which also appears twice in the *MAS2* promoter, once (GGCCCAATA) at –65 to –57 and once (inverted) at –82 to –77 (TATTGGGCC). Enrichment of the UP1ATMSD motif has been found in the promoters of genes upregulated after main stem decapitation in Arabidopsis (Tatematsu et al., 2005). The TELOBOXATEEF1AA1 motif (AAACCCTAA) was found at the –20 to –12 position in the *RRP7* promoter. The TELOBOXATEEF1AA1 motif is a longer version of the UP2ATMSD (AAACCCTA) and Telo-box (Short interstitial telomere) motifs (AAACCCWA; where W is A or T). The UP1ATMSD and UP2ATMSD motifs are enriched among genes encoding RPs (Ma et al., 2012). The 7-bp Telo-box sequence is identical to the repeat units of plant telomeres and has been preferentially found in 5´ flanking regions of Arabidopsis and rice genes encoding components of the ribosome biogenesis machinery, including RPs, snoRNAs, and RBFs (Tremousaygue et al., 1999; Gaspin et al., 2010). These results reinforce the hypothesis of a functional relationship among *SMO4*, *RRP7*, and *MAS2* and their activity in ribosome biogenesis.

PropSearch analyses suggest that RRP7, SMO4, and MAS2 are functionally related

As mentioned above, the full-length sequence identity of RRP7 and its human and yeast orthologs is low. Even when considering only the RRP7_like domain, identity between Arabidopsis RRP7 and yeast Rrp7 is only 23.61%. Indeed, no plant homolog of yeast Rrp7 or human RRP7A was found in the HomoloGene database. To further explore the roles of RRP7 and SMO4, as well as their functional relationship with MAS2, we searched for their putative homologs with PropSearch (see Methods and Supplemental Tables 4-6, which include the full names of all proteins identified). This program and associated database have been used as an alternative to alignment programs such as BLASTP, which fail to detect homology when sequence identity falls below 25%.

The most highly ranked putative homolog of RRP7 (Supplemental Table 4) is *Drosophila melanogaster* Surf6, a nucleolar protein (Magoulas et al., 1998; Romanova et al., 2006) whose yeast ortholog is Rrp14, which ranked 17th and is assumed to form a complex with the Ssf1, Ssf2, Rrp15, and Unhealthy ribosome biogenesis 1 (Urb1) nucleolar factors; this complex participates in the biogenesis of the 60S ribosomal subunit (Krogan et al., 2006). Mouse Surf6 is ranked 5th; its partial loss-of-function reduces 18S rRNA levels (Romanova et al., 2006). Although human Surf6 did not appear on any of the lists, it is associated with nucleolin and with Upstream-binding factor 1

(UBF1), a component of the pre-initiation complex that mediates the recruitment of RNA pol I to the 47S rDNA promoter (Kordyukova et al., 2014).

Seven of the 20 factors found to be related to Arabidopsis SMO4 by PropSearch analysis (Supplemental Table 5) are involved in ribosome biogenesis, and four are involved in pre-mRNA splicing. Seven of the 20 are *Saccharomyces cerevisiae* proteins, including Ssf1 and Ssf2, which ranked 2nd and 3rd, respectively; these redundant nucleolar factors prevent premature processing of 27SA$_2$ pre-rRNA (Supplemental Figure 1), and their individual depletion results in the loss of 25S and 5.8S mature rRNAs (Fatica et al., 2002). Rnt1, ranking 13th, is involved in the processing of 35S pre-rRNA (cleavage of the B$_0$ site of the 3´-ETS) and other RNA species (Bernstein et al., 2012). Rnp24, which ranked 15th, is the *Schizosaccharomyces pombe* ortholog of *Saccharomyces cerevisiae* Nop13, a nuclear exosome cofactor (Milligan et al., 2008). Both Rnt1 and the exosome function in 35S pre-RNA processing (Supplemental Figure 1). *Xenopus laevis* LAA, which ranked 18th, participates in the translational control of mRNAs encoding RPs (Pellizzoni et al., 1996). Cus1 ranked 6th and is required for the assembly of U2 snRNP into the spliceosome (Wells et al., 1996).

None of the factors identified in our PropSearch analyses appears on all three lists (Supplemental Tables 4-6), but several from the RRP7 and MAS2 lists are identical or orthologs (Supplemental Table 7), including five of the above-mentioned animal SURF6 proteins, *Caenorhabditis elegans* ccdc-55, and Arabidopsis U1-70K and RSP41. ccdc-55 is required for larval development (Kovacevic et al., 2012) and its human ortholog, Nuclear speckle splicing regulatory protein 1 (NSRP1), binds SRSF1 and SRSF2, two members of the serine (S)/arginine (R)-rich (SR) family of splicing factors (Kim et al., 2016). Arabidopsis U1-70K is involved in 5´ splice site selection of pre-mRNAs (Rosbash and Séraphin, 1991; Golovkin and Reddy, 1996). Arabidopsis RSP41 is not only required for splicing but also for miRNA biogenesis (Chen et al., 2013; Chen et al., 2015b). Human MPP8 ranked 18th on the RRP7 list and 3rd on the MAS2 list. MPP8 is a component of the HUSH (Human Silencing Hub) repressive complex, which is required for transcriptional silencing of endogenous and viral genes at heterochromatic loci marked by H3K9me3 (Tchasovnikarova et al., 2015). Yeast Spt2 ranked 11th and is a histone chaperone that facilities 35S rDNA transcription (Winston et al., 1984). Yeast Spt2 and human SPT2 are involved in the recycling of H3/H4 tetramers during transcription by RNA pol II and in the suppression of spurious transcription from within coding regions (Chen et al., 2015a). Chicken SPT2 accumulates at the nucleolus and binds RNA pol I (Osakabe et al., 2013).

These results further support the hypothesis of a functional link among SMO4, RRP7, and MAS2, which appear to be related to ribosome biogenesis and pre-mRNA

splicing. In particular, RRP7 and MAS2 appear to function in the control of transcription. Indeed, we previously demonstrated that MAS2 functions in ribosome biogenesis and splicing (Sánchez-García et al., 2015).

RRP7 and *SMO4* regulate the expression of 45S rDNA variants

Four different variants (*VARs*) exist among the hundreds of copies of the 45S rDNA gene in Arabidopsis. These *VARs* differ in their 3′-EST sequences and their temporal and spatial expression patterns, as observed in wild-type accessions (Figure 4A, B; Pontvianne et al., 2010). The number of genomic copies of each variant does not appear to be related to their expression levels. Indeed, *VAR1* is the most abundant 45S rDNA variant in Col-0, but it is only expressed during seed germination; this accession contains few copies of *VAR2*, but they are highly expressed.

We analyzed the abundance of each *VAR* and their expression levels in the *smo4-3* and *rrp7-1* mutants. We amplified the 3´-ETS of 45S rDNA, which contains the polymorphic sequences, by PCR using the p3/p4 primer pair (Figure 4; Supplemental Table 7) and measured its corresponding transcript levels by RT-PCR (Pontvianne et al., 2010) of RNA extracted from plants collected 14 das. There was no difference in the genomic content of each *VAR* among the mutants and wild type. We did not detect *VAR1* expression in Col-0, and *VAR2* was much more highly expressed than *VAR3* and *VAR4*, which were expressed at similar levels (Figure 4; Pontvianne et al., 2010). However, heterochronic expression of *VAR1* was detected in *smo4-2* and *rrp7-1*, and increased expression of *VAR2* and *VAR3* was detected in *smo4-2* at the same ratio as that of Col-0. *VAR3* expression levels were higher in *rrp7-1* than in Col-0. These results suggest that SMO4 and RRP7 participate in the control of 45S rDNA expression and are required for the negative regulation of *VAR1*.

RRP7 is epistatic to *SMO4* and synergistically interacts with *MAS2*, *NUC1*, and *HDA6*

To genetically confirm the physical interaction of RRP7 with MAS2 detected in our previous Y2H screen, we obtained double mutant combinations of *rrp7-1* with a viable *MAS2* allele, *mas2-1*, which acts as a dominant suppressor of *ago1-52*, and lacks phenotypic effects *per se*, in a wild-type genetic background (Sánchez-García et al., 2015). The *rrp7-1 mas2-1* double mutant displayed a synergistic phenotype, with very dwarf rosettes and narrow, pointed cotyledons and leaves (Figure 5A, F, and Supplemental Figure 7). Despite their strong morphological aberrations, *rrp7-1 mas2-1* double mutant plants completed their life cycles and produced some seeds.

The physical interaction of SMO4 and RRP7 with MAS2 (Sánchez-García et al., 2015), the coexpression of *RRP7* and *SMO4*, the regulatory elements shared by their promoters, the many genes coexpressed with both genes, and the synergistic phenotypes of the *rrp7-1 mas2-1* (this work) and *smo4-3 mas2-1* (Micol-Ponce et al., submitted) double mutants prompted us to obtain the *rrp7-1 smo4-3* double mutant, which was morphologically indistinguishable from the *rrp7-1* single mutant (Figure 5B, G and Supplemental Figure 7). The epistasis of *rrp7-1* to *smo4-3* suggests that RRP7 acts first in a pathway in which SMO4 is also involved.

The above-mentioned temporal expression pattern of *VAR1* is modified by mutant alleles of *HISTONE DEACETYLASE6* (*HDA6*), *NUC1*, and *NUC2* (Petricka and Nelson, 2007; Pontvianne et al., 2010; Layat et al., 2012; Durut et al., 2014). To determine if any of these genes interact with *RRP7*, we obtained double mutant combinations of *rrp7-1* with *parl1-2*, *nuc2-2*, or *hda6-7.* The *rrp7-1 parl1-2* plants exhibited very short roots and small rosettes with narrow leaves that accumulated anthocyanins (Figure 5C, H). Rosettes of *rrp7-1 nuc2-2* plants were morphologically similar to those of *rrp7-1* but larger, with pale leaves (Figure 5D, and Supplemental Figure 7). Although *hda6-7* plants were barely distinguishable from wild type (Figure 5E and Supplemental Figure 7), *rrp7-1 hda6-7* plants displayed the most extreme phenotype among the double mutants obtained, with very dwarf rosettes. Unexpectedly, flowering was earlier in *rrp7-1 hda6-7* than in *rrp7-1* or *hda6-7*, both of which are late-flowering mutants. Only some plants produced seeds, most of which (83.33%) failed to germinate (Figure 5E, J and Supplemental Figure 7). These synergistic phenotypes reveal a functional relationship of *RRP7* with *NUC1* and *HDA6*.

RRP7 is a nucleolar and perinucleolar protein

To visualize the subcellular localization of RRP7, we generated translational fusions of RRP7 and GFP (green fluorescent protein) under the control of the *RRP7* endogenous promoter or the *35S* promoter. The *RRP7:GFP* fusions were functional, as shown by full complementation of the mutant phenotype of *rrp7* plants (Figure 1G). To visualize GFP fluorescence, we used roots of Col-0 plants stained with Hoechst 33342. This dye strongly binds double-stranded DNA and counterstains the nucleus, not staining the nucleolus, which mainly contains RNA. As expected, GFP fluorescence was detected in the nucleoli using both the *35S$_{pro}$:RRP7:GFP* and *RRP7$_{pro}$:RRP7:GFP* transgenes. The GFP signal was broader than the nucleolus and slightly overlapped with the DAPI-stained region (Figure 6A-C).

To determine if RRP7 is exclusively nucleolar, we carried out a fluorescent immunoassay using an antibody against fibrillarin, a conserved nucleolar

methyltransferase that directs 2´-O-ribose methylation of pre-rRNAs, a commonly used nucleolar marker. RRP7 and fibrillarin partially colocalized, since the GFP signal occupied a larger portion of the nucleolus than fibrillarin (Figure 6D-G). A small portion of the GFP signal clearly colocalized with DAPI at the nucleolar periphery.

18S rRNA maturation is impaired in the *rrp7* mutants

In yeast, *rrp7* null mutations cause lethality, and *rrp7* conditional alleles reduce mature 18S rRNA and 40S ribosomal subunit production. In these mutants, the depletion of 18S rRNA levels appears to be due to the inhibition of cleavage at the A_2 site in 32S pre-rRNA (Supplemental Figure 1), which leads to a loss of $27SA_2$ and 20S pre-rRNAs (Baudin-Baillieu et al., 1997). In addition, yeast Rrp7 coimmunoprecipitates with 90S pre-ribosomes containing 35S or 23S pre-rRNAs (Lin et al., 2013). The yeast SSU processome synthesizes 18S rRNA via cotranscriptional cleavage at the A_0, A_1, and A_2 sites of 35S pre-rRNA, generating $27SA_2$ and 20S pre-rRNAs. By contrast, 23S pre-rRNA, which includes most of the 5´-ETS, results from endonucleolytic cleavage at the A_3 site of 35S pre-rRNA prior to cleavage at the A_0, A_1, and A_2 sites via an alternative pathway (Supplemental Figure 1; Granneman and Baserga, 2004; Chaker-Margot et al., 2017).

To determine if RRP7 plays a role in Arabidopsis 45S pre-rRNA processing, we performed RNA gel blot analyses of RNA extracted from *rrp7* plants hybridized with the S9 and p42-p43 probes (Lange et al., 2011), which respectively bind ITS2 and ITS1 (Figure 7A; Supplemental Figure 2). Using the S9 probe, we found that the *rrp7-1* and *rrp7-2* mutants accumulated 35S(P) precursor and had much higher levels of 27S pre-rRNAs ($27SA_2$, $27SA_3$ and/or 27SB) than wild type. When we used the p42-p43 probe, bands corresponding to the 35S(P) and 33S(P´)/32S pre-rRNAs were visible in Col-0, *parl1-2*, and *rrp7-1 RRP7*$_{pro}$*:RRP7*, whereas in *rrp7-1*, *rrp7-2*, and *rrp7-1 smo4-3* plants, 35S(P) pre-rRNA accumulated but 33S(P´)/32S pre-rRNAs were not detected (Figure 7C). Since we did not detect the $27SA_2$ intermediate using the p42-p43 probe, we reasoned that the accumulation of the 27S precursor shown with the S9 probe corresponds to $27SA_3$ and/or 27SB pre-rRNAs.

When we used the p42-p43 probe, we also found strong accumulation of P-A_3 pre-rRNA (Figure 7C), which is an intermediate of the ITS1-first pathway for 18S rRNA maturation (Supplemental Figure 2). We also analyzed the processing of 45S pre-rRNA in the epistatic *rrp7-1 smo4-3* double mutant, which exhibited the molecular defects of both *rrp7-1* and *smo4-3*. These results indicate that the strong accumulation of 5.8S rRNA precursors observed in *smo4* mutants (Micol-Ponce et al., submitted) contributes little to the double mutant morphological phenotype.

As mentioned in the Introduction, Rrp7 is thought to coordinate RP and mature rRNA production in yeast, and Rudra et al. (2007) proposed that Ifh1 is required for such coordination. In agreement with this model, depletion of Rrp7 causes the overexpression of genes encoding RPs of both subunits. To determine if this model applies to plants, we performed a BLASP search, which failed to identify an Arabidopsis ortholog of yeast Ifh1. In addition, the NTD of yeast Rrp7, which is required for its dimerization with Utp22, appears to be absent from Arabidopsis RRP7 and its plant orthologs. We then performed RT-qPCR to analyze the expression of two genes (AT3G62870 and AT5G28060) encoding RPs of different subunits (RPL7aB and RPS24B, respectively), together with AT3G55620, encoding the translation initiation factor eIF6A, whose ortholog in yeast, Translation initiation factor 6 (Tif6), is required for 60S ribosomal subunit biogenesis (Basu et al., 2001). Of the two eIF6 co-orthologs in the Arabidopsis genome, eIF6A is the most highly expressed gene (Guo et al., 2011). All of the genes examined were slightly upregulated in the *rrp7-1* mutant compared to wild type (Supplemental Figure 8).

18S rRNA species accumulate in *rrp7* nucleoli

We examined the rRNA profiles of the *rrp7* mutants using an Agilent 2100 Bioanalyzer, as previously utilized in a functional analysis of putative RBFs in human HeLa cells (Tafforeau et al., 2013). The 25S/18S mature rRNA ratios were 2.00 ± 0.00 in the *rrp7* mutants and 1.23 ± 0.06 in the wild type (Supplemental Figure 9). Taken together, these results indicate that RRP7 is required for the synthesis and/or stabilization of mature 18S rRNA species. In addition, the rRNA ratios in *rrp7* are reminiscent of the reduced 23S/18S ratio observed in yeast *rrp7* conditional mutants by Baudin-Baillieu et al. (1997).

Since the above results suggest that 45S pre-rRNA processing is defective in the *rrp7* mutants, we carried out RNA fluorescence *in situ* hybridization (RNA-FISH), using probes that detect mature 25S, 18S, or 5.8S rRNAs and their respective precursors. No alteration in the subnuclear localization of 25S or 5.8S rRNAs was detected (Figure 8C, J, E-G, L-N), but hypertrophy and 18S rRNA accumulation were observed in the nucleolus of the *rrp7-1* mutant (Figure 8B, I). To quantify the size of the nucleolus, we simultaneously stained cells with DAPI and Acridine orange, which emits green or red fluorescence depending on whether it is bound to DNA or RNA, respectively. The ratio of nucleolus size to whole cell size was significantly higher in *rrp7-1* plants than in wild type (Figure 8O). These results indicate that 18S rRNA processing is impaired in *rrp7-1* plants, which in turn causes nucleolar hypertrophy and hinders the assembly of 40S pre-ribosomal particles and their export to the cytoplasm.

Loss of function of *RRP7* or *MAS2,* but not *SMO4*, causes abscisic acid hypersensitivity during seedling establishment

The role of abscisic acid (ABA) in the inhibition of seed germination under adverse conditions is well known (Lopez-Molina et al., 2001). Mutations in genes involved in several aspects of mRNA metabolism, such as pre-mRNA maturation and mRNA degradation, export, or translation cause hypersensitivity to ABA (Kuhn et al., 2008). To determine whether *smo4-2*, *rrp7-1*, *parl1-2*, and *amiR-MAS2.1* plants exhibit ABA hypersensitivity, we sowed seeds of these lines on ABA-supplemented medium. As controls, we used *abscisic acid deficient1-104* (*aba1-104*) and *abscisic acid insensitive4-2* (*abi4-2*) seeds, which are hypersensitive and insensitive to ABA, respectively (Quesada et al., 2000).

As expected, the germination rates of these seeds did not differ: all seeds germinated like their respective wild types (data not shown). However, the seedling establishment rates clearly differed among lines (Figure 9). Whereas almost all Col-0 seedlings exhibited expanded cotyledons on 0.5 μM ABA, only 3.4 ± 3.9% of *rrp7-1* seedlings did so, and no expanded cotyledons were detected at higher ABA concentrations; the values for *parl1-2* were 45.8 ± 7.7% at 0.5 μM, 14.8 ± 4.2% at 1.5 μM (50.4 ± 4.7% of Col-0), and 0.2 ± 0.7% at 3 μM ABA (10.4 ± 2.4% of Col-0). The *amiR-MAS2.1* plants were more sensitive to ABA than Col-0 at all concentrations tested, but to a lesser extent than *parl1-2* and *rrp7-1*. No significant differences were detected between *smo4-2* and Col-0.

DISCUSSION

In silico analyses support the evolutionary conservation of RRP7 as an RBF

Essential cellular functions, such as the translation of mRNA into protein, are evolutionarily conserved. The 80S ribosome is the molecular machine that performs protein synthesis in the cytoplasm in Eukarya; its mature structure is very similar in all organisms studied, although its biogenesis in fungi, plants, and metazoans exhibits both evolutionary conservation and diversification (Tafforeau et al., 2013; Woolford and Baserga, 2013).

A number of RBFs have been extensively studied in yeast and some in human and/or mouse cells, and comparative analyses have provided examples of both conservation and divergence. However, only a few RBFs have been experimentally studied in plants (Weis et al., 2015). For example, both yeast Rrp7 and human RRP7A share an NTD and a CTD, only the latter being conserved (to some extent) in Arabidopsis RRP7. These findings suggest that the ability of Rrp7 to bind pre-rRNAs within pre-ribosomal particles is conserved in RRP7 and RRP7A, but dimerization with an Utp22 ortholog is conserved only in RRP7A. Indeed, mammalian Utp22 orthologs exist (Utama et al., 2002), including mouse Nucleolar RNA-associated protein (Nrap) and human Nucleolar protein 6 (NOL6), whose interaction with RRP7A was demonstrated by affinity-purification mass spectrometry, although a role for NTD in such dimerization is yet to be demonstrated (Huttlin et al., 2015).

According to HomoloGene, AT1G63810 encodes the Arabidopsis ortholog of Utp22. This gene has not been studied and is annotated as encoding a nucleolar protein in Araport11 and as Nrap-like in the ARAMEMNON database. This protein shares 31.3% identity with yeast Utp22 and 33.8% with NOL6 and Nrap. Since Arabidopsis RRP7 lacks a NTD, it likely does not interact with the AT1G63810 gene product, unless they dimerize in a way substantially different from that of RRP7A with NOL6 (and Rrp7 with Utp22). Since we found increased expression of some RP-encoding genes in the *rrp7-1* mutant, it remains possible that RRP7 helps coordinate the production of the protein and RNA components of the ribosome through a mechanism not requiring an interaction between RRP7 and the Arabidopsis ortholog of Utp22.

We identified the RRP7 (this work) and SMO4 (Micol-Ponce et al., submitted) RBFs in a Y2H screen for interactors of MAS2, the Arabidopsis ortholog of human NKAP (Sánchez-García et al., 2015). Our *in silico* analyses strongly suggested that these three genes are functionally related and that they act in more than one RNA metabolism pathway, in particular, in rRNA maturation and pre-mRNA splicing. In ATTED-II analyses, *SMO4* ranked high among the genes most highly coexpressed with *RRP7*, and vice versa. *MAS2* was absent from the top-100 list of genes most highly coexpressed with

SMO4 or *RRP7*, and vice versa. Many genes that are coexpressed with *RRP7* and *SMO4* encode demonstrated or putative RBFs. Genes coexpressed with *RRP7* but not with *SMO4* encode orthologs of known or putative components of the yeast SSU processome, including homologs of Rrp4, Rrp45, and Rrp46, components of the yeast nuclear exosome. These results suggest the existence of an unexpected relationship between RRP7 and the exosome, given that no link between its yeast or metazoan orthologs and the exosome has been proposed. The 3′→5′ exonuclease activity of the exosome is required for rRNA maturation as well as processing, turnover, and surveillance of other normal and aberrant RNA species (Januszyk et al., 2015).

MAS2, *SMO4*, and *RRP7* appear to be expressed in all tissues and developmental stages, particularly in actively dividing cells (Sánchez-García et al., 2015; Zhang et al., 2015; Micol-Ponce et al., submitted; this work). *Cis* regulatory elements usually map within the −1,000 to +200 bp (including introns) regions of Arabidopsis gene promoters relative to the TSS, with a peak at −50 bp (Yu et al., 2016). Indeed, we identified known regulatory elements within the −85 to −1 bp upstream regions of the *MAS2*, *SMO4*, and *RRP7* promoters. These elements are shared by many genes related to the translational machinery, providing additional support for the assignment of MAS2, SMO4, and RRP7 to the functional class of proteins related to the translational apparatus.

Among the 20 proteins most closely related to RRP7 identified by PropSearch analysis, 18 are eukaryotic, four are related to pre-mRNA splicing, and 11 are RBFs. These RBFs include the hypothetical Mtr4 ortholog of *Schizosaccharomyces pombe,* the *Drosophila melanogaster* ortholog of yeast Nop53, Arabidopsis SMO4, and six orthologs of SURF6. RBFs and splicing factors were also found in the lists of proteins related to SMO4 and MAS2. We detected major overlap between the RRP7 and MAS2 lists due to the presence of five SURF6 orthologs in both lists. This overlap also includes human MPP8, a factor involved in the control of 45S rDNA transcription. Together with the physical (Sánchez-García et al., 2015) and genetic (this work) interaction of RRP7 with MAS2, these results suggest that RRP7 functions in splicing, 45S rDNA transcriptional regulation, and 45S pre-rRNA processing.

PropSearch is a bioinformatic tool based on protein sequence distance (defined as the weighted sum of differences in compositional properties) rather than sequence alignment. These properties include singlet and doublet amino acid composition, molecular weight, and isoelectric point, among others. PropSearch was created to identify remote homologs of a query amino acid sequence by scanning a database of preprocessed protein sequences (Hobohm and Sander, 1995). We used this tool and found the results to be surprisingly consistent: together with obvious false positives,

proteins with an evident functional relationship emerged. However, instead of being distant members of the same family as the protein used as a query sequence, more than a few of the proteins identified appeared to be components of the same molecular machinery, without any apparent ancestral relationship. Nevertheless, only 20 RBF lineages are thought to have existed in the last eukaryotic common ancestor (Ebersberger et al., 2014), which further diverged during the divergence of eukaryotes by gene duplication, innovation, and loss (Feng et al., 2013). Under this assumption, our PropSearch results appear to expose just the ancient common origin of several groups of RBFs, such as those to which SMO4 and RRP7 belong, and of nuclear factors that function in splicing, such as MAS2, which in turn appears to be more closely related to RRP7 than to SMO4.

Loss of *RRP7* function causes pleiotropic developmental effects, but not lethality

Most yeast, human, and Arabidopsis genes encoding RBFs are single-copy genes. Their null alleles, however, are lethal in yeast and human or mouse cells, but not in Arabidopsis; this is the case for *RRP7* and *SMO4*. By contrast, the absence of MAS2 or any other NKAP is lethal in all species studied to date. A plausible explanation for the viability and mild phenotypes of the *rrp7* and *smo4* mutants is that yeast does not use alternative pre-rRNA processing pathways or uses these pathways to a lesser extent than Arabidopsis. Therefore, in null alleles of yeast *Rrp7*, the levels of translation-competent ribosomes are below the threshold for lethality, but this is not the case for Arabidopsis *rrp7* null alleles. Other examples include Arabidopsis *mtr4* and *smo4* null alleles, which are viable and their phenotypes are mild, whereas their mammalian and yeast equivalents are lethal. Accumulation of pre-rRNAs would occur as a consequence of *rrp7*, *mtr4*, and *smo4* mutations, but the levels of mature rRNAs would be sufficient for viability owing to the pre-rRNA processing alternative pathway(s). Some other Arabidopsis genes encoding RBFs mentioned in this work have a redundant paralog, such as *NUC1* and *XRN2*, which easily explains their mild phenotypes; the severe phenotypes of the *nuc1 nuc2* and *xrn2 xrn3* double mutants confirm this explanation. By contrast, null alleles of the genes encoding other Arabidopsis RBFs, such as orthologs of yeast Rrp5, Periodic tryptophan protein 2 (Pwp2), Nin one binding protein 1 (Nob1; Supplemental Figure 1), Essential nuclear protein 1 (Enp1), and Nucleolar complex protein 4 (Noc4) cause lethality in Arabidopsis, as do null alleles of their orthologs in yeast (Missbach et al., 2013).

Although *RRP7* is not essential, it appears to play important roles in physiology and development, as shown by the pleiotropic phenotype of the *rrp7* mutants, which exhibit delayed growth, altered phyllotaxy, late flowering, partial infertility, and

hypersensitivity to exogenous ABA at the seedling establishment stage. A deficiency in mature ribosome levels might explain these phenotypes, although it is not clear why a general reduction in mRNA translation causes specific defects in processes as diverse and specific as phyllotaxy regulation, flowering time control, embryogenesis, lateral organ venation patterning (or provascular cell differentiation), and ABA perception.

The absence of RRP7 or NUC1 or the depletion of MAS2 (but not the absence of SMO4) caused ABA hypersensitivity at the seedling establishment stage. The strongest effect was observed in *rrp7* plants and the weakest was observed in *amiRMAS2.1* plants. These results suggest that *RRP7*, *NUC1*, and *MAS2* contribute (to different extents) to the negative regulation of ABA responses. RECEPTOR FOR ACTIVATED C KINASE1 (RACK1) and eIF6 are also required for normal ribosome production and negatively regulate ABA responses in Arabidopsis; *rack1* mutants are hypersensitive to ABA (Guo and Chen, 2008; Guo et al., 2009). In addition to its known role as a seed germination inhibitor under adverse conditions, ABA appears to play a role in the control of ribosome biogenesis. During germination, chromatin is decondensed at nucleolar organizer regions, acetylation of the 45S rDNA promoter increases, and its transcription is induced, but the opposite process occurs in plants grown in the presence of ABA (Zhang et al., 2012). ABA also induces the expression of *DEAD-BOX ATP-DEPENDENT RNA HELICASE57* (*RH57*), whose product is involved in 45S pre-RNA processing; the *rh57-1* null mutant is hypersensitive to ABA (Hsu et al., 2014). In addition, Arabidopsis NUC1 is likely a substrate of SUCROSE NONFERMENTING 1 (SNF1)-RELATED PROTEIN KINASE 2 (SNRK2) in response to ABA (Umezawa et al., 2013; Wang et al., 2013). The *auxin gene expression1-5* (*axe1-5)* allele of the *HDA6* gene also causes hypersensitivity to ABA (Chen et al., 2010). Notably, we found a synergistic phenotype in the *rrp7-1 hda6-7* double mutant, indicating a genetic interaction between *RRP7* and *HDA6*.

RRP7 is a nucleolar and perinucleolar protein required for 18S rRNA maturation and 45S rDNA transcriptional regulation

A recent analysis of the nuclear proteome of Arabidopsis identified 1,602 proteins in the nucleolar fraction and 2,544 in the nuclear fraction, 1,429 of which overlapped; RRP7 was detected in both fractions (Palm et al., 2016). Consistent with these findings, we found that RRP7 mainly localized to the nucleolus but also to the perinucleolar region, which might correspond to the perinucleolar compartment in human cells; this dynamic structure is enriched in RNA-binding proteins, including RNA pol III, nucleolin, and factors involved in the control of alternative splicing (Pollock and Huang, 2010). The only overlapping subnuclear localization of the RRP7 and MAS2 interacting proteins is the perinucleolar compartment, which is consistent with a role for RRP7 in splicing, as

mentioned above.

We found that RRP7 is involved in 18S rRNA maturation and that 18S rRNA precursors accumulate in *rrp7* mutants. In particular, we detected the accumulation of 35S(P), 27SB and/or $27SA_3$ rRNAs, which is an intermediate specie of the ITS1-first pathway. This result suggests that RRP7 promotes the use of the 5´-ETS-first pathway. RRP7 would be involved in cleaving ITS1 using the 5´-ETS-first alternative pathway (Supplemental Figure 2). The inability of *rrp7* mutants to use both pathways to produce mature 18S RNA would reduce its concentration and consequently, the number of 40S pre-ribosomal particles able to assemble into mature 80S ribosomes. Under this model, *rrp7* cells would have an excess of 60S subunits compared to 40S subunits, which would explain their increased 25S/18S rRNA ratio, in turn leading to a deficiency in mature ribosomes, thereby causing delayed growth. In addition, the nucleolus is enlarged in *rrp7* cells, likely due to the accumulation of 18S rRNA species, which we detected by RNA-FISH. Enlarged nucleoli have been observed in other mutants affected in genes encoding RBFs, such as *arabidopsis pumilio23-1* (*apum23-1*). In *apum23-1* plants, 18S and 5.8S rRNA precursors accumulate, but their mature rRNAs do not, indicating that, like RRP7, APUM23 is involved in 35S pre-rRNA processing and/or the degradation of pre-rRNA processing byproducts (Abbasi et al., 2010).

As mentioned in the Introduction, the loss of function of yeast Rrp7 reduces 18S rRNA production, which in turn induces the expression of RP-encoding genes and causes a deficiency in the formation of 40S ribosomal subunits (Rudra et al., 2007). In agreement with the indirect role of Rrp7 in coordinating rDNA transcription and pre-rRNA processing with the transcription of genes encoding RPs, our RT-qPCR analysis revealed increased levels of mRNA from genes encoding RPs in the *rrp7* mutants. In addition, *in silico* analysis revealed putative Arabidopsis orthologs of the Utp22 and CK2 members of the CURI complex, but not of Ifh1, suggesting that Arabidopsis lacks a CURI complex. However, we cannot exclude the possibility that RRP7 forms part of another complex that coordinates the pathways for the biogenesis of rRNA and RP ribosome components.

RRP7 is functionally related to *SMO4*, *MAS2*, *HDA6*, and *NUC1*

Several of our *in silico* and experimental results suggest that *RRP7* and *MAS2* are functionally related. In addition, the synergistic phenotypes of *rrp7-1 parl1-2* and *rrp7-1 mas2-1* are very similar, indicating that *RRP7* genetically interacts with *NUC1* and *MAS2*. The extremely severe phenotype of *rrp7-1 hda6-7* suggests a closer relationship of *RRP7* with *HDA6*. *MAS2* participates in the control of 45S rDNA expression, as well as splicing (Sánchez-García et al., 2015). *NUC1* is involved in the regulation of 45S rDNA

expression and 45S pre-rRNA processing (Petricka and Nelson, 2007; Pontvianne et al., 2007). *HDA6* participates in several epigenetic processes, including 45S rDNA, transgene, and transposon silencing (Aufsatz et al., 2002; Probst et al., 2004; Earley et al., 2010), but it has not been associated with 45S pre-rRNA processing. The link between MAS2, NUC1, and HDA6 is their participation in the control of 45S rDNA transcription, a process that might involve RRP7. This genetic evidence reinforces the notion that RRP7 is involved in 45S rDNA transcriptional regulation. Indeed, we detected heterochronic activation of the *VAR1* 45S rDNA variant in the *rrp7* mutants. We cannot rule out the possibility that this is an indirect effect caused by impaired 45S pre-rRNA processing if 45S rDNA transcription is subjected to negative feedback self-regulation. On the other hand, deregulation of 45S rDNA transcription does not appear to contribute to the phenotype of *rrp7*, because in *hda6* and *smo4* plants, *VAR1* is also heterochronically misexpressed and their developmental phenotypes are very mild (Pontvianne et al., 2010; Micol-Ponce et al., submitted). Furthermore, in *nuc1* and *hda6* mutants, *VAR1* misexpression is correlated with rDNA chromatin decondensation in the nucleolar organizer region (Earley et al., 2010; Pontvianne et al., 2010), which we did not observe in the *rrp7* mutants.

The additive phenotype of *rrp7-1 nuc2-2* plants was expected, given that *NUC2* expression is almost undetectable in wild-type plants and that this gene is thought to play a marginal role in ribosome biogenesis compared with *NUC1* (Durut et al., 2014).

RRP7 acts in different RNA metabolism pathways

The information available for yeast Rrp7 includes its subcellular localization and its structure, as determined based on X-ray crystallography and nuclear magnetic resonance spectroscopy data. The function of yeast *Rrp7* has been deduced based on the effects of its deletion, conditional depletion, and site-directed mutagenesis on growth and molecular phenotypes, including the accumulation of pre-rRNAs in *rrp7* mutants (Lin et al., 2013).

By contrast, little is known about mammalian *Rrp7a*, a single-copy gene that has also been named *Gastric cancer antigen Zg14*, since it was identified in a search for human immunogenic proteins for gastric cancer that resulted in the isolation of 14 distinct serum-reactive antigens (Line et al., 2002). *Rrp7a* was annotated in large-scale cDNA sequencing projects (Kawai et al., 2001; Okazaki et al., 2002). According to HomoloGene, the human RRP7A protein shares 83.9% identity and 91.8% similarity with its mouse Rrp7a ortholog. Mouse *Rrp7a* is expressed in preimplantation embryos and is required for the morula-to-blastocyst transition, as shown by the lethality caused by its knockdown by microinjection of double-stranded RNA in zygotes (Maserati et al., 2014).

Surprisingly, Rrp7a is found throughout the cytoplasm but not in the nucleus of 8-cell blastomeres, which prompted the authors to suggest that this protein is a structural component of the ribosome. More recently, however, human RRP7A has been identified as a member of the nucleolar proteome of HeLa cells, and its depletion by siRNAs caused a reduction in the levels of 21S and 18S-E pre-rRNAs (Tafforeau et al., 2013).

One finding of the current study is that RRP7 is an Arabidopsis RBF that might also participate in splicing, together with MAS2. Indeed, many other proteins participate in more than one RNA metabolism pathway, such as ribosome biogenesis and splicing. For example, the yeast DEAH box ATPase pre-mRNA processing factor 43 (Prp43) is a nucleolar protein with a dual role in spliceosome disassembly and 45S pre-rRNA processing (Combs et al., 2006; Leeds et al., 2006).

Our results might shed light on the activity of the mammalian orthologs of Arabidopsis RRP7, given the scarcity of information available. Our findings demonstrate that RRP7 acts as a plant RBF, and they increase our understanding of the conservation and diversification of RRP7 function among eukaryotes. Our work also provides a deeper understanding of the relationship between MAS2 and other nuclear factors, in particular, providing bioinformatic and genetic confirmation of its demonstrated physical interaction with RRP7. Further research is needed to verify and detail the different roles played by RRP7 in Arabidopsis RNA metabolism, such as 45S rDNA transcriptional regulation, 18S rRNA biogenesis, and pre-mRNA splicing.

METHODS

Plant material and growth conditions

The *Arabidopsis thaliana* (L) Heynh. Columbia-0 (Col-0) wild-type accession was initially obtained from the Nottingham Arabidopsis Stock Center (NASC; Nottingham, UK) and propagated at our laboratory for further analysis. Seeds of the *rrp7-1* (SAIL_628_F08), *rrp7-2* (WISCDSLOX461-464C16), *parl1-2* (SALK_002764; Petricka and Nelson, 2007), *mtr4-1* (GK_048G02; Lange et al., 2011), and *hda6-7* (also named *rts1-1*; Aufsatz et al., 2002) mutants were also provided by NASC. The *nuc2-2* (GABI_178D01; Durut et al., 2014) seeds were provided by J. Saez-Vasquez. All T-DNA insertional mutants were in the Col-0 background. Plant culture, seed sterilization, and sowing were performed as previously described (Ponce et al., 1998; Berná et al., 1999).

Culture medium was supplemented, when required, with hygromycin (15 $\mu g \cdot mL^{-1}$). ABA sensitivity assays were conducted with three plates per genotype, each sown with 50 mutant and 50 wild-type seeds, and were repeated three times. For these ABA assays, the medium was supplemented with 0, 0.5, 1.5, and 3 µM ABA, and non-germinated seeds, seeds exhibiting aborted germination, and seedlings with expanded, green cotyledons were scored 10 das. The scores of each line were obtained after calculating the percentages of germinated seedlings on supplemented medium versus the same line on non-supplemented medium.

Gene nomenclature, accession numbers, and genotyping

RRP7 can be found under accession number AT5G38720 at TAIR (http://arabidopsis.org) and Araport (http://araport.org). *NUC1* is the name used for AT1G48920 and *NUC2* is used for AT3G18610: these genes were given several different names in the literature. The presence of T-DNA insertions in the genes was verified by PCR using the primers shown in Supplemental Table 8. Discrimination between the wild-type *MAS2* and mutant *mas2-1* alleles was carried out as described in Sánchez-García et al. (2015).

RNA isolation, quantification, reverse transcription, and RNA gel blot analysis

Experiments were repeated twice, each with three different biological replicates. Total RNA was isolated from three rosettes per genotype with TRI RNA Isolation Reagent (Sigma-Aldrich; St. Louis, Missouri, USA). RNA samples were treated with DNase (twice; 2 U of TURBO DNase [TURBO DNA-free Kit, Thermo Fisher Scientific, Waltham, MA, USA] per microgram of RNA) or not depending of their use for RT-qPCR or RNA gel blots, respectively. Quantification of mature rRNA species was performed in an Agilent 2100 Bioanalyzer (Agilent Technologies, Santa Clara, CA, USA) using the sizing

software, chips, and protocols provided by the manufacturer.

For RT-PCR analysis, reverse-transcription was carried out using random hexamers, 2 µg of DNA-free RNA, and Maxima Reverse Transcriptase (Thermo Fisher Scientific, Waltham, MA, USA) following the manufacturer's instructions. A Step-One Real-Time PCR System (Applied Biosystems) was used for qPCR amplifications, which were performed with three biological and three technical replicates and the *ACTIN2* (*ACT2*) housekeeping gene as an internal control.

RNA gel blot analysis was performed with digoxigenin (DIG) labeled probes; S9 is a 5´-DIG labeled oligonucleotide (Eurofins Genomics), and the p42-p43 probe was synthetized by PCR using DIG-11-dUTP (Roche). Primers for the synthesis of both probes (Supplemental Table 8) were described in Lange et al. (2011). RNA gel blot analysis of 3 µg total RNA samples was performed in 1.2% (w/v) agarose/formaldehyde or 6% polyacrylamide/8 M urea gels. The RNA was visualized and transferred/cross-linked to a Hybond N+ nylon membrane (Thermo Fisher Scientific). Electrophoresis, hybridization, and detection were performed as previously described (Jover-Gil et al., 2014). In brief, the membrane was prehybridized for 2 h at 65°C and hybridized overnight at 65°C with 149 ng·mL^{-1} of probe. No blocking agent was added to the hybridization solution. The membrane was incubated with 0.05 U·mL^{-1} of Fab fragments from an anti-digoxin antibody from sheep, conjugated with alkaline phosphatase (α-DIG-AP, Fab fragments; Roche), washed twice, equilibrated in detection buffer, and incubated with 25 mM CDP-Star (Roche) diluted 1:200 in detection buffer for 5 min in the dark. Visualization of RNA bands was performed after developing Lumi-film chemiluminescent films (Roche) exposed to the membrane for 20 min or overnight.

Construction of transgenic lines

Transgenic plants were obtained as described in Sánchez-García et al. (2015). The transgenes were obtained using the pGEM-T Easy221 entry vector and the pMDC32, pMD164, pMDC83, and pMDC107 destination vectors (Curtis and Grossniklaus, 2003). To construct the *35S$_{pro}$:SMO4*, *35S$_{pro}$:SMO4:GFP*, *35S$_{pro}$:RRP7*, and *35S$_{pro}$:RRP7:GFP* overexpression transgenes, the full-length coding sequences (stop codons were removed to obtain the GFP translational fusions) of *SMO4* or *RRP7* were PCR amplified from Col-0. DNA regions 1,317-bp and 1,026-bp upstream of the translation start codon of *SMO4* and *RRP7*, respectively, were PCR amplified and used as promoters to drive the *SMO4$_{pro}$:GUS*, *SMO4$_{pro}$:SMO4:GFP*, *RRP7$_{pro}$:GUS*, and *RRP7$_{pro}$:RRP7:GFP* constructs. All constructs were sequence verified before being transferred into plants. Primers used to obtain these constructs and for Sanger sequencing are described in Supplemental Table 8. Sanger sequencing was performed with ABI PRISM BigDye

Terminator Cycle Sequencing kits on an ABI PRISM 3130xl Genetic Analyzer (Applied Biosystems [now Thermo Fisher Scientific], Waltham, MA, USA).

Morphometry, histology, histochemical assays, and *in situ* hybridization

A Nikon D-Eclipse C1 confocal microscope was used for microscopy. Micrographs were digitally processed using EZ-C1 operation software. To investigate venation pattern morphometry, cotyledons, leaves, and petals were collected, cleared, and mounted on slides, and the corresponding micrographs taken and converted into diagrams as previously described (Candela et al., 1999; Robles et al., 2010; Jover-Gil et al., 2012). For leaf venation morphometry, phenoVein software (http://www.plant-image-analysis.org/) was used. GUS assays were performed as described by Robles et al. (2010): GUS activity was analyzed in plants homozygous for the *GUS* transgene, taking photographs from three plants from each of three independent lines per genotype.

Visualization of SMO4 and RRP7 subcellular localization was performed in roots from $RRP7_{pro}$*:RRP7:GFP* or $35S_{pro}$*:RRP7:GFP* transgenic plants collected 10 das. For immunolocalization with fibrillarin, $RRP7_{pro}$*:RRP7:GFP* seedlings were collected at 10 das and squashed on slides in a mix of PBS 1x and 4% paraformaldehyde. Immunodetection of fibrillarin was performed using the mouse monoclonal Anti-Fibrillarin antibody [38F3] (Abcam, Cambridge, UK), followed by detection with TRITC (Tetramethylrhodamine-5-isothiocyanate)-conjugated anti-mouse IgG secondary antibody (Sigma-Aldrich, St. Louis, MO, USA). Nuclei were stained as previously described (Díaz-Tielas et al., 2012) with Hoechst 33342 and mounting medium (Vectashield, Vector Laboratories, Burlingame, CA, USA).

In situ hybridizations of RNA were carried out as described in Parry et al. (2006), with some modifications, as described in Micol-Ponce et al. (submitted). Probes were obtained using the labeled oligonucleotides shown in Supplemental Table 8. Approximately 100 cells from first- and second-node leaves from 10 plants per genotype were analyzed.

Bioinformatic and statistical analyses

BLASTP searches were performed against the sequences for all organisms at the National Center for Biotechnology Information BLASTP server (NCBI; https://blast.ncbi.nlm.nih.gov/Blast.cgi; Altschul et al., 1997) using the NCBI non-redundant database with default settings. Alignments were obtained with ClustalW (http://www.ebi.ac.uk/Tools/msa/clustalo/; Larkin et al., 2007) and shaded with BOXSHADE3.21 (http://www.ch.embnet.org/software/BOX_form.html). Pair-wise identity and similarity percentages were calculated from the alignments using the Ident

and Sim feature of the Sequence Manipulation Suite (http://www.bioinformatics.org/sms2/ident_sim.html; Stothard, 2000).

Sets of coregulated genes in microarray assays were identified in the ATTED-II (*Arabidopsis thaliana trans*-factor and *cis*-element database; http://atted.jp/; Aoki et al., 2016) coexpression database. The ARAMEMNON (http://aramemnon.uni-koeln.de/; Schwacke et al., 2003) and HomoloGene (https://www.ncbi.nlm.nih.gov/homologene) databases were used to obtain the functional descriptions of genes that were incomplete or absent from ATTED-II.

For promoter analysis, the Scan tool of the PLACE (Plant *cis*-acting regulatory DNA elements; http://www.dna.affrc.go.jp/PLACE; Higo et al., 1998; Higo et al., 1999) and Athena (http://bioinformatics1.smb.wsu.edu/cgi-bin/Athena/cgi/home.pl; O'Connor et al., 2005) databases were used. The original PLACE website is no longer available, but its dataset of regulatory motifs can be accessed at http://togodb.biosciencedbc.jp/togodb/view/place_main#en.

Spatiotemporal gene expression patterns were obtained from the TraVA (Transcriptome Variation Analysis) database (http://travadb.org/; Klepikova et al., 2016) based on RNA-seq data. For TraVA output visualization, the Raw Norm option was chosen for read counts number type, and default values were chosen for all other options.

Putative homologs of RRP7, SMO4, and MAS2 were detected with PropSearch (http://abcis.cbs.cnrs.fr/propsearch/; Hobohm and Sander, 1995) using a preprocessed database. PropSearch is based on amino acid composition rather than amino acid sequence. The PropSearch algorithm weights 144 properties from the query sequence, including average charge and hydrophobicity and the content of small and large residues. A query vector is obtained that allows the Euclidian distance between the query and database sequences to be calculated.

To compare the mutant, transgenic, and wild-type lines, statistical analyses were performed as described in Robles et al. (2010). The Mann-Whitney *U*-test ($n \leq 10$) or Student's *t*-test ($n > 10$) was used, depending on the number of samples.

ACKNOWLEDGMENTS

We thank J.M. Serrano-García, J. Castelló-Bañuls, M.J. Ñíguez-Gómez and S.B. Ingham for their excellent technical assistance, and F.J. Medina for his help and advice with fibrillarin immunolocalization. We also thank J. Saez-Vasquez for providing seeds of the *nuc2-2* mutant, B. Scheres for the pGEM-T Easy221 vector, and J.L. Micol for useful discussions, comments on the manuscript, and the use of his facilities. This research was supported by grants from the Ministerio de Economía, Industria y Competitividad of Spain (BIO2014-56889-R) and the Generalitat Valenciana (PROMETEOII/2014/006) to M.R.P.

AUTHOR CONTRIBUTIONS

Conceptualization, Resources, Supervision, and Funding Acquisition, M.R.P.; Methodology, M.R.P., R.M.-P., and R.S.-M; Investigation, all authors; Writing of Original Draft, M.R.P. and R.M.-P.; Writing, Reviewing, and Editing, all authors.

FIGURE LEGENDS

Figure 1. Structure of *RRP7* and the molecular nature, rosette phenotype, and transgene-mediated complementation of its mutant alleles.

(A) Schematic representation of *RRP7*, including the positions and molecular nature of the *rrp7* mutations. Black boxes represent coding exons, and open boxes represent the 5´- and 3´-UTRs. Lines between boxes represent introns, and triangles represent T-DNA insertions. (B-J) Rosettes of Col-0 (B, E, H), *rrp7-1* (C, F, I), and *rrp7-2* (D, G, J). Photographs were taken at 7 (B-D), 14 (E-G), and 21 (H-J) days after stratification (das). (K-M) Rosettes of *rrp7-1* $RRP7_{pro}$*:RRP7* (K), *rrp7-2* $RRP7_{pro}$*:RRP7* (L), and *rrp7-2* $RRP7_{pro}$*:RRP7:GFP* (M) plants; the photographs were taken at 14 das. All plants were homozygous for the mutations and transgenes shown. Scale bars: 1 mm.

Figure 2. Pleiotropic morphological phenotype of *rrp7* plants.

(A, B) Presence of three cauline leaves in the axils of *rrp7* mutant stems. (C) Adult Col-0 and *rrp7-1* plants. (D–F) Dissected siliques from Col-0 (D), *rrp7-1* (E), and *rrp7-2* (F) plants. Red arrows indicate aborted ovules. Photographs were taken at 60 das. (G) Fertility of *rrp7* plants, expressed as the number of seeds per silique. Seeds from 10 siliques collected from five plants per genotype were counted. (H) Flowering time (number of days from stratification to bolting) in the *rrp7* mutants. (I) Number of rosette leaves that developed before bolting in *rrp7* plants. Error bars indicate standard deviations. Asterisks indicate values significantly different from the corresponding wild type in a Student's *t*-test (***$P < 0.001$). Scale bars: 3 cm (C), and 1 mm (D–F).

Figure 3. Aberrant venation patterns in *parl1-2* and *rrp7-1* cotyledons, vegetative leaves, and petals.

Diagrams were drawn from micrographs taken from cotyledons (A, E, I), first-node leaves (B, F, J), third-node leaves (C, G, K), and petals (D, H, L). Cotyledons and leaves were collected at 21 das, and petals were collected at 63 das, from Col-0 (A–D), *parl1-2* (E–H) and *rrp7-1* (I–L). The leaf margin is shown in orange. Scale bars: 1 mm.

Figure 4. 45S rDNA *VAR* expression in *smo4-3* and *rrp7-1*.

(A, B) Schematic representation of 45S pre-rRNA (A) and its 3´-ETS polymorphic region (B). (C, D) PCR analysis of the relative abundance of 45S rDNA variants in reverse transcribed, complementary DNA (C), and genomic DNA (D) from Col-0, *smo4-3*, and *rrp7-1* plants. The p3 and p4 primers (not drawn to scale) shown in (A) and (B) were used (Supplemental Table 8).

Figure 5. Genetic interactions of *rrp7-1* with *mas2-1*, *smo4-3*, *parl1-2*, *nuc2-2*, and *hda6-7*. Rosettes of *mas2-1* (A), *smo4-3* (B), *parl1-2* (C), *nuc2-2* (D), *hda6-7* (E), *rrp7-1 mas2-1* (F), *rrp7-1 smo4-3* (G), *rrp7-1 parl1-2* (H), *rrp7-1 nuc2-2* (I), and *rrp7-1 hda6-7* (J) plants. Photographs were taken at 14 das. Scale bars: 1 mm.

Figure 6. Subcellular localization of RRP7.
(A-C) Confocal laser-scanning micrographs of roots from plants homozygous for the *RRP7$_{pro}$:RRP7:GFP* transgene. Fluorescence signals correspond to Hoechst 33342 (A), GFP (B), and their overlay (C). (D-G) Immunolocalization of fibrillarin in plants homozygous for the *RRP7$_{pro}$:RRP7:GFP* transgene. Fluorescence signals correspond to DAPI and the secondary antibody for fibrillarin detection (D), DAPI and GFP (E), and their overlay (F, G). Scale bars: 10 µm.

Figure 7. Processing of 45S pre-rRNA in *rrp7* and *parl1-2*.
(A) Diagram illustrating the pre-rRNA processing intermediates than can be detected in an RNA gel blot using the p42-p43 and S9 probes. Modified from Hang et al. (2014). 5´-ETS and 3´-ETS, external transcribed spacers. ITS1 and ITS2, internal transcribed spacers. (B, C) RNA gel blots. Total RNA was separated in formaldehyde-agarose (B) or formaldehyde-polyacrylamide (C) gels, transferred to a nylon membrane, and hybridized with the S9 (B) and p42-p43 (C) probes. RNA was extracted from Col-0, *smo4-2*, *smo4-3*, *rrp7-1*, *rrp7-2*, *rrp7-1 RRP7$_{pro}$:RRP7*, *rrp7-1 smo4-3*, and *parl1-2* plants. EtBr: photographs of ethidium bromide-stained gels taken before blotting, which served as loading controls.

Figure 8. Subcellular localization of 25S, 18S, and 5.8S rRNA species in *rrp7-1* plants.
Fluorescence signals correspond to Hoechst 33342 (A, H, O, R), 18S probe (B, I), 25S probe (C, J), 5.8S probe (F, M), Acridine orange (P, S), and their overlay (D, K, G, N, O, T). Scale bars: 10 µm.

Figure 9. Effect of exogenous ABA on *rrp7-1*, *smo4-3*, *parl1-2*, and *amiR-MAS2.1* plants.
Percentage of seedlings grown in medium supplemented with different concentrations of ABA that displayed green, fully expanded cotyledons, scored at 10 das. The *abi4-2* and *aba1-104* mutants were used as controls. Error bars indicate standard deviation. Asterisks indicate values significantly different from the corresponding wild type in a Student's *t*-test (*$P < 0.05$, and **$P < 0.01$). The genetic background of *abi4-2* and *aba1-104* is Col-5, and that of all other mutants is Col-0.

SUPPLEMENTAL DATA

Supplemental Figure 1. Overview of 35S pre-rRNA processing in yeast.

Supplemental Figure 2. Overview of 45S pre-rRNA processing in Arabidopsis.

Supplemental Figure 3. Sequence conservation among human, yeast, and Arabidopsis RRP7 orthologs.

Supplemental Figure 4. Sequence conservation among plant RRP7 orthologs.

Supplemental Figure 5. Spatial expression pattern of *RRP7*.

Supplemental Figure 6. Translational apparatus-related motifs found in the *MAS2*, *SMO4*, and *RRP7* promoters.

Supplemental Figure 7. Genetic interactions of *rrp7-1* with *mas2-1*, *smo4-3*, *parl1-2*, *nuc2-2*, and *hda6-7*, as observed in plants at 14 das in plates and 31 das in pots.

Supplemental Figure 8. Expression of *RPL7AB*, *RPS24B*, and *eiF6a* in Col-0 and *rrp7-1* plants.

Supplemental Figure 9. Agilent 2100 Bioanalyzer electropherogram profiles of total RNA samples extracted from Col-0, *rrp7-1*, and *rrp7-1 RRP7*$_{pro}$*:RRP7* plants collected at 15 das.

Supplemental Table 1. Identity and similarity among full-length representative plant RRP7 orthologs.

Supplemental Table 2. Identity and similarity among the RRP7-like domains of representative plant RRP7 orthologs.

Supplemental Table 3. Morphometry of leaf venation in *rrp7-1* and *parl1-2*.

Supplemental Table 4. Putative homologs of Arabidopsis RRP7 identified by PropSearch analysis.

Supplemental Table 5. Putative homologs of Arabidopsis SMO4 identified by PropSearch analysis.

Supplemental Table 6. Putative homologs of Arabidopsis MAS2 identified by PropSearch analysis.

Supplemental Table 7. Identical or closely related putative homologs of Arabidopsis MAS2 and RRP7 identified by PropSearch analyses.

Supplemental Table 8. Oligonucleotides used in this work.

Supplemental Data Set 1. Top-100 ranking genes coexpressed with *RRP7* and *MAS2*, identified by ATTED-II.

REFERENCES

Abbasi, N., Kim, H.B., Park, N.I., Kim, H.S., Kim, Y.K., Park, Y.I., and Choi, S.B. (2010). APUM23, a nucleolar Puf domain protein, is involved in pre-ribosomal RNA processing and normal growth patterning in Arabidopsis. Plant J. **64,** 960-976.

Altschul, S.F., Madden, T.L., Schaffer, A.A., Zhang, J., Zhang, Z., Miller, W., and Lipman, D.J. (1997). Gapped BLAST and PSI-BLAST: a new generation of protein database search programs. Nucleic Acids Res. **25,** 3389-3402.

Aoki, Y., Okamura, Y., Tadaka, S., Kinoshita, K., and Obayashi, T. (2016). ATTED-II in 2016: A plant coexpression database towards lineage-specific coexpression. Plant Cell Physiol. **57,** e5.

Aufsatz, W., Mette, M.F., van der Winden, J., Matzke, M., and Matzke, A.J. (2002). HDA6, a putative histone deacetylase needed to enhance DNA methylation induced by double-stranded RNA. EMBO J. **21,** 6832-6841.

Basu, U., Si, K., Warner, J.R., and Maitra, U. (2001). The *Saccharomyces cerevisiae TIF6* gene encoding translation initiation factor 6 is required for 60S ribosomal subunit biogenesis. Mol. Cell. Biol. **21,** 1453-1462.

Baudin-Baillieu, A., Tollervey, D., Cullin, C., and Lacroute, F. (1997). Functional analysis of Rrp7p, an essential yeast protein involved in pre-rRNA processing and ribosome assembly. Mol. Cell. Biol. **17,** 5023-5032.

Baumberger, N., and Baulcombe, D.C. (2005). Arabidopsis ARGONAUTE1 is an RNA Slicer that selectively recruits microRNAs and short interfering RNAs. Proc. Natl. Acad. Sci. USA **102,** 11928-11933.

Beltrame, M., and Tollervey, D. (1992). Identification and functional analysis of two U3 binding sites on yeast pre-ribosomal RNA. EMBO J. **11,** 1531-1542.

Beltrame, M., and Tollervey, D. (1995). Base pairing between U3 and the pre-ribosomal RNA is required for 18S rRNA synthesis. EMBO J. **14,** 4350-4356.

Berná, G., Robles, P., and Micol, J.L. (1999). A mutational analysis of leaf morphogenesis in *Arabidopsis thaliana*. Genetics **152,** 729-742.

Bernstein, D.A., Vyas, V.K., and Fink, G.R. (2012). Genes come and go: the evolutionarily plastic path of budding yeast RNase III enzymes. RNA Biol. **9,** 1123-1128.

Candela, H., Martínez-Laborda, A., and Micol, J.L. (1999). Venation pattern formation in *Arabidopsis thaliana* vegetative leaves. Dev. Biol. **205,** 205-216.

Chaker-Margot, M., Barandun, J., Hunziker, M., and Klinge, S. (2017). Architecture of the yeast small subunit processome. Science **355,** aal1880.

Chen, L.T., Luo, M., Wang, Y.Y., and Wu, K. (2010). Involvement of *Arabidopsis* histone deacetylase HDA6 in ABA and salt stress response. J. Exp. Bot. **61,** 3345-3353.

Chen, S., Rufiange, A., Huang, H., Rajashankar, K.R., Nourani, A., and Patel, D.J. (2015a). Structure-function studies of histone H3/H4 tetramer maintenance during transcription by chaperone Spt2. Genes Dev. **29,** 1326-1340.

Chen, T., Cui, P., and Xiong, L. (2015b). The RNA-binding protein HOS5 and serine/arginine-rich proteins RS40 and RS41 participate in miRNA biogenesis in Arabidopsis. Nucleic Acids Res. **43,** 8283-8298.

Chen, T., Cui, P., Chen, H., Ali, S., Zhang, S., and Xiong, L. (2013). A KH-domain RNA-binding protein interacts with FIERY2/CTD phosphatase-like 1 and splicing factors and is important for pre-mRNA splicing in Arabidopsis. PLoS Genet. **9,** e1003875.

Curtis, M.D., and Grossniklaus, U. (2003). A gateway cloning vector set for high-throughput functional analysis of genes in planta. Plant Physiol. **133,** 462-469.

Díaz-Tielas, C., Grana, E., Sotelo, T., Reigosa, M.J., and Sánchez-Moreiras, A.M. (2012). The natural compound trans-chalcone induces programmed cell death in *Arabidopsis thaliana* roots. Plant Cell Environ. **35,** 1500-1517.

Durut, N., Abou-Ellail, M., Pontvianne, F., Das, S., Kojima, H., Ukai, S., de Bures, A., Comella, P., Nidelet, S., Rialle, S., Merret, R., Echeverria, M., Bouvet, P., Nakamura, K., and Saez-Vasquez, J. (2014). A duplicated *NUCLEOLIN* gene with antagonistic activity is required for chromatin organization of silent 45S rDNA in Arabidopsis. Plant Cell **26,** 1330-1344.

Earley, K., Smith, M., Weber, R., Gregory, B., and Poethig, R.S. (2010). An endogenous F-box protein regulates ARGONAUTE1 in *Arabidopsis thaliana*. Silence **1,** 15.

Ebersberger, I., Simm, S., Leisegang, M.S., Schmitzberger, P., Mirus, O., von Haeseler, A., Bohnsack, M.T., and Schleiff, E. (2014). The evolution of the ribosome biogenesis pathway from a yeast perspective. Nucleic Acids Res. **42,** 1509-1523.

Fatica, A., Cronshaw, A.D., Dlakic, M., and Tollervey, D. (2002). Ssf1p prevents premature processing of an early pre-60S ribosomal particle. Mol. Cell **9,** 341-351.

Feng, J.M., Tian, H.F., and Wen, J.F. (2013). Origin and evolution of the eukaryotic SSU processome revealed by a comprehensive genomic analysis and implications for the origin of the nucleolus. Genome Biol Evol **5,** 2255-2267.

Fromont-Racine, M., Senger, B., Saveanu, C., and Fasiolo, F. (2003). Ribosome assembly in eukaryotes. Gene **313,** 17-42.

Gaspin, C., Rami, J.F., and Lescure, B. (2010). Distribution of short interstitial telomere motifs in two plant genomes: putative origin and function. BMC Plant Biol. **10,** 283.

Golovkin, M., and Reddy, A.S. (1996). Structure and expression of a plant U1 snRNP 70K gene: alternative splicing of U1 snRNP 70K pre-mRNAs produces two different transcripts. Plant Cell **8,** 1421-1435.

Granneman, S., and Baserga, S.J. (2004). Ribosome biogenesis: of knobs and RNA processing. Exp. Cell Res. **296,** 43-50.

Guo, J., and Chen, J.G. (2008). RACK1 genes regulate plant development with unequal genetic redundancy in Arabidopsis. BMC Plant Biol. **8,** 108.

Guo, J., Wang, J., Xi, L., Huang, W.D., Liang, J., and Chen, J.G. (2009). RACK1 is a negative regulator of ABA responses in Arabidopsis. J. Exp. Bot. **60,** 3819-3833.

Guo, J., Wang, S., Valerius, O., Hall, H., Zeng, Q., Li, J.F., Weston, D.J., Ellis, B.E., and Chen, J.G. (2011). Involvement of Arabidopsis RACK1 in protein translation and its regulation by abscisic acid. Plant Physiol. **155,** 370-383.

Hang, R., Liu, C., Ahmad, A., Zhang, Y., Lu, F., and Cao, X. (2014). Arabidopsis protein arginine methyltransferase 3 is required for ribosome biogenesis by affecting precursor ribosomal RNA processing. Proc. Natl. Acad. Sci. USA **111,** 16190-19195.

Henras, A.K., Plisson-Chastang, C., O'Donohue, M.F., Chakraborty, A., and Gleizes, P.E. (2015). An overview of pre-ribosomal RNA processing in eukaryotes. Wiley Interdiscip. Rev. RNA **6,** 225-242.

Higo, K., Ugawa, Y., Iwamoto, M., and Higo, H. (1998). PLACE: a database of plant cis-acting regulatory DNA elements. Nucleic Acids Res. **26,** 358-359.

Higo, K., Ugawa, Y., Iwamoto, M., and Korenaga, T. (1999). Plant cis-acting regulatory DNA elements (PLACE) database: 1999. Nucleic Acids Res. **27,** 297-300.

Hobohm, U., and Sander, C. (1995). A sequence property approach to searching protein databases. J. Mol. Biol. **251,** 390-399.

Horiguchi, G., Mollá-Morales, A., Pérez-Pérez, J.M., Kojima, K., Robles, P., Ponce, M.R., Micol, J.L., and Tsukaya, H. (2011). Differential contributions of ribosomal protein genes to *Arabidopsis thaliana* leaf development. Plant J. **65,** 724-736.

Hsu, Y.F., Chen, Y.C., Hsiao, Y.C., Wang, B.J., Lin, S.Y., Cheng, W.H., Jauh, G.Y., Harada, J.J., and Wang, C.S. (2014). AtRH57, a DEAD-box RNA helicase, is involved in feedback inhibition of glucose-mediated abscisic acid accumulation during seedling development and additively affects pre-ribosomal RNA processing with high glucose. Plant J. **77,** 119-135.

Hughes, J.M., and Ares, M., Jr. (1991). Depletion of U3 small nucleolar RNA inhibits cleavage in the 5' external transcribed spacer of yeast pre-ribosomal RNA and impairs formation of 18S ribosomal RNA. EMBO J. **10,** 4231-4239.

Huttlin, E.L., Ting, L., Bruckner, R.J., Gebreab, F., Gygi, M.P., Szpyt, J., Tam, S., Zarraga, G., Colby, G., Baltier, K., Dong, R., Guarani, V., Vaites, L.P., Ordureau, A., Rad, R., Erickson, B.K., Wuhr, M., Chick, J., Zhai, B., Kolippakkam, D., Mintseris, J., Obar, R.A., Harris, T., Artavanis-Tsakonas, S., Sowa, M.E., De Camilli, P., Paulo, J.A., Harper, J.W., and Gygi, S.P. (2015). The BioPlex Network: A systematic exploration of the human interactome. Cell **162,** 425-440.

Januszyk, M., Rennert, R.C., Sorkin, M., Maan, Z.N., Wong, L.K., Whittam, A.J., Whitmore, A., Duscher, D., and Gurtner, G.C. (2015). Evaluating the effect of cell culture on gene expression in primary tissue samples using microfluidic-based single cell transcriptional analysis. Microarrays **4,** 540-550.

Jover-Gil, S., Paz-Ares, J., Micol, J.L., and Ponce, M.R. (2014). Multi-gene silencing in Arabidopsis: a collection of artificial microRNAs targeting groups of paralogs encoding transcription factors. Plant J. **80,** 149-160.

Jover-Gil, S., Candela, H., Robles, P., Aguilera, V., Barrero, J.M., Micol, J.L., and Ponce, M.R. (2012). The microRNA pathway genes *AGO1, HEN1* and *HYL1* participate in leaf proximal-distal, venation and stomatal patterning in Arabidopsis. Plant Cell Physiol. **53,** 1322-1333.

Kawai, J., Shinagawa, A., Shibata, K., Yoshino, M., Itoh, M., Ishii, Y., Arakawa, T., Hara, A., Fukunishi, Y., Konno, H., Adachi, J., Fukuda, S., Aizawa, K., Izawa, M., Nishi, K., Kiyosawa, H., Kondo, S., Yamanaka, I., Saito, T., Okazaki, Y., Gojobori, T., Bono, H., Kasukawa, T., Saito, R., Kadota, K., Matsuda, H., Ashburner, M., Batalov, S., Casavant, T., Fleischmann, W., Gaasterland, T., Gissi, C., King, B., Kochiwa, H., Kuehl, P., Lewis, S., Matsuo, Y., Nikaido, I., Pesole, G., Quackenbush, J., Schriml, L.M., Staubli, F., Suzuki, R., Tomita, M., Wagner, L., Washio, T., Sakai, K., Okido, T., Furuno, M., Aono, H., Baldarelli, R., Barsh, G., Blake, J., Boffelli, D., Bojunga, N., Carninci, P., de Bonaldo, M.F., Brownstein, M.J., Bult, C., Fletcher, C., Fujita, M., Gariboldi, M., Gustincich, S., Hill, D., Hofmann, M., Hume, D.A., Kamiya, M., Lee, N.H., Lyons, P., Marchionni, L., Mashima, J., Mazzarelli, J., Mombaerts, P., Nordone, P., Ring, B., Ringwald, M., Rodriguez, I., Sakamoto, N., Sasaki, H., Sato, K., Schonbach, C., Seya, T., Shibata, Y., Storch, K.F., Suzuki, H., Toyo-oka, K., Wang, K.H., Weitz, C., Whittaker, C., Wilming, L., Wynshaw-Boris, A., Yoshida, K., Hasegawa, Y., Kawaji, H., Kohtsuki, S., Hayashizaki, Y., Riken Genome Exploration Research Group Phase II Team, and the Fantom Consortium. (2001). Functional annotation of a full-length mouse cDNA collection. Nature **409,** 685-690.

Kim, C.H., Kim, Y.D., Choi, E.K., Kim, H.R., Na, B.R., Im, S.H., and Jun, C.D. (2016). Nuclear speckle-related protein 70 binds to serine/arginine-rich splicing factors 1 and

2 via an arginine/rerine-like region and counteracts their alternative splicing activity. J. Biol. Chem. **291,** 6169-6181.

Kiss, A.M., Jady, B.E., Darzacq, X., Verheggen, C., Bertrand, E., and Kiss, T. (2002). A Cajal body-specific pseudouridylation guide RNA is composed of two box H/ACA snoRNA-like domains. Nucleic Acids Res. **30,** 4643-4649.

Klepikova, A.V., Kasianov, A.S., Gerasimov, E.S., Logacheva, M.D., and Penin, A.A. (2016). A high resolution map of the *Arabidopsis thaliana* developmental transcriptome based on RNA-seq profiling. Plant J. **88,** 1058-1070.

Kordyukova, M.Y., Polzikov, M.A., Shishova, K.V., and Zatsepina, O.V. (2014). Functional significance of the human nucleolar protein SURF6, the key member of the SURF6 protein family in eukaryotes. Russ. J. Bioorg. Chem. **455,** 65-67.

Kovacevic, I., Ho, R., and Cram, E.J. (2012). CCDC-55 is required for larval development and distal tip cell migration in *Caenorhabditis elegans*. Mechanisms of Development **128,** 548-559.

Krogan, N.J., Peng, W.T., Cagney, G., Robinson, M.D., Haw, R., Zhong, G., Guo, X., Zhang, X., Canadien, V., Richards, D.P., Beattie, B.K., Lalev, A., Zhang, W., Davierwala, A.P., Mnaimneh, S., Starostine, A., Tikuisis, A.P., Grigull, J., Datta, N., Bray, J.E., Hughes, T.R., Emili, A., and Greenblatt, J.F. (2004). High-definition macromolecular composition of yeast RNA-processing complexes. Mol. Cell **13,** 225-239.

Krogan, N.J., Cagney, G., Yu, H., Zhong, G., Guo, X., Ignatchenko, A., Li, J., Pu, S., Datta, N., Tikuisis, A.P., Punna, T., Peregrin-Alvarez, J.M., Shales, M., Zhang, X., Davey, M., Robinson, M.D., Paccanaro, A., Bray, J.E., Sheung, A., Beattie, B., Richards, D.P., Canadien, V., Lalev, A., Mena, F., Wong, P., Starostine, A., Canete, M.M., Vlasblom, J., Wu, S., Orsi, C., Collins, S.R., Chandran, S., Haw, R., Rilstone, J.J., Gandi, K., Thompson, N.J., Musso, G., St Onge, P., Ghanny, S., Lam, M.H., Butland, G., Altaf-Ul, A.M., Kanaya, S., Shilatifard, A., O'Shea, E., Weissman, J.S., Ingles, C.J., Hughes, T.R., Parkinson, J., Gerstein, M., Wodak, S.J., Emili, A., and Greenblatt, J.F. (2006). Global landscape of protein complexes in the yeast *Saccharomyces cerevisiae*. Nature **440,** 637-643.

Kuhn, J.M., Hugouvieux, V., and Schroeder, J.I. (2008). mRNA cap binding proteins: effects on abscisic acid signal transduction, mRNA processing, and microarray analyses. Curr. Top. Microbiol. Immunol. **326,** 139-150.

Lafontaine, D.L. (2015). Noncoding RNAs in eukaryotic ribosome biogenesis and function. Nat. Struct. Mol. Biol. **22,** 11-19.

Lange, H., Sement, F.M., and Gagliardi, D. (2011). MTR4, a putative RNA helicase and exosome co-factor, is required for proper rRNA biogenesis and development in *Arabidopsis thaliana*. Plant J. **68,** 51-63.

Larkin, M.A., Blackshields, G., Brown, N.P., Chenna, R., McGettigan, P.A., McWilliam, H., Valentin, F., Wallace, I.M., Wilm, A., Lopez, R., Thompson, J.D., Gibson, T.J., and Higgins, D.G. (2007). Clustal W and Clustal X version 2.0. Bioinformatics **23,** 2947-2948.

Layat, E., Saez-Vasquez, J., and Tourmente, S. (2012). Regulation of Pol I-transcribed 45S rDNA and Pol III-transcribed 5S rDNA in Arabidopsis. Plant Cell Physiol. **53,** 267-276.

Lee, S., Kim, J.Y., Kim, Y.J., Seok, K.O., Kim, J.H., Chang, Y.J., Kang, H.Y., and Park, J.H. (2012). Nucleolar protein GLTSCR2 stabilizes p53 in response to ribosomal stresses. Cell Death Differ. **19,** 1613-1622.

Lin, J., Lu, J., Feng, Y., Sun, M., and Ye, K. (2013). An RNA-binding complex involved in ribosome biogenesis contains a protein with homology to tRNA CCA-adding enzyme. PLoS Biol. **11,** e1001669.

Line, A., Stengrevics, A., Slucka, Z., Li, G., Jankevics, E., and Rees, R.C. (2002). Serological identification and expression analysis of gastric cancer-associated genes. Br. J. Cancer **86,** 1824-1830.

Lopez-Molina, L., Mongrand, S., and Chua, N.H. (2001). A postgermination developmental arrest checkpoint is mediated by abscisic acid and requires the ABI5 transcription factor in Arabidopsis. Proc. Natl. Acad. Sci. USA **98,** 4782-4787.

Ma, S., Bachan, S., Porto, M., Bohnert, H.J., Snyder, M., and Dinesh-Kumar, S.P. (2012). Discovery of stress responsive DNA regulatory motifs in Arabidopsis. PLoS One **7,** e43198.

Magoulas, C., Zatsepina, O.V., Jordan, P.W., Jordan, E.G., and Fried, M. (1998). The SURF-6 protein is a component of the nucleolar matrix and has a high binding capacity for nucleic acids in vitro. Eur. J. Cell Biol. **75,** 174-183.

Maserati, M., Dai, X., Walentuk, M., and Mager, J. (2014). Identification of four genes required for mammalian blastocyst formation. Zygote **22,** 331-339.

Micol-Ponce, R., Aguilera, V., and Ponce, M.R. (2014). A genetic screen for suppressors of a hypomorphic allele of Arabidopsis *ARGONAUTE1*. Sci. Rep. **4,** 5533.

Milligan, L., Decourty, L., Saveanu, C., Rappsilber, J., Ceulemans, H., Jacquier, A., and Tollervey, D. (2008). A yeast exosome cofactor, Mpp6, functions in RNA surveillance and in the degradation of noncoding RNA transcripts. Mol. Cel. Biol. **28,** 5446-5457.

Missbach, S., Weis, B.L., Martin, R., Simm, S., Bohnsack, M.T., and Schleiff, E. (2013). 40S ribosome biogenesis co-factors are essential for gametophyte and embryo development. PLoS One **8,** e54084.

O'Connor, T.R., Dyreson, C., and Wyrick, J.J. (2005). Athena: a resource for rapid visualization and systematic analysis of Arabidopsis promoter sequences. Bioinformatics **21,** 4411-4413.

Okazaki, Y., Furuno, M., Kasukawa, T., Adachi, J., Bono, H., Kondo, S., Nikaido, I., Osato, N., Saito, R., Suzuki, H., Yamanaka, I., Kiyosawa, H., Yagi, K., Tomaru, Y., Hasegawa, Y., Nogami, A., Schonbach, C., Gojobori, T., Baldarelli, R., Hill, D.P., Bult, C., Hume, D.A., Quackenbush, J., Schriml, L.M., Kanapin, A., Matsuda, H., Batalov, S., Beisel, K.W., Blake, J.A., Bradt, D., Brusic, V., Chothia, C., Corbani, L.E., Cousins, S., Dalla, E., Dragani, T.A., Fletcher, C.F., Forrest, A., Frazer, K.S., Gaasterland, T., Gariboldi, M., Gissi, C., Godzik, A., Gough, J., Grimmond, S., Gustincich, S., Hirokawa, N., Jackson, I.J., Jarvis, E.D., Kanai, A., Kawaji, H., Kawasawa, Y., Kedzierski, R.M., King, B.L., Konagaya, A., Kurochkin, I.V., Lee, Y., Lenhard, B., Lyons, P.A., Maglott, D.R., Maltais, L., Marchionni, L., McKenzie, L., Miki, H., Nagashima, T., Numata, K., Okido, T., Pavan, W.J., Pertea, G., Pesole, G., Petrovsky, N., Pillai, R., Pontius, J.U., Qi, D., Ramachandran, S., Ravasi, T., Reed, J.C., Reed, D.J., Reid, J., Ring, B.Z., Ringwald, M., Sandelin, A., Schneider, C., Semple, C.A., Setou, M., Shimada, K., Sultana, R., Takenaka, Y., Taylor, M.S., Teasdale, R.D., Tomita, M., Verardo, R., Wagner, L., Wahlestedt, C., Wang, Y., Watanabe, Y., Wells, C., Wilming, L.G., Wynshaw-Boris, A., Yanagisawa, M., Yang, I., Yang, L., Yuan, Z., Zavolan, M., Zhu, Y., Zimmer, A., Carninci, P., Hayatsu, N., Hirozane-Kishikawa, T., Konno, H., Nakamura, M., Sakazume, N., Sato, K., Shiraki, T., Waki, K., Kawai, J., Aizawa, K., Arakawa, T., Fukuda, S., Hara, A., Hashizume, W., Imotani, K., Ishii, Y., Itoh, M., Kagawa, I., Miyazaki, A., Sakai, K., Sasaki, D., Shibata, K., Shinagawa, A., Yasunishi, A., Yoshino, M., Waterston, R., Lander, E.S., Rogers, J., Birney, E., Hayashizaki, Y., Consortium, F., I, R.G.E.R.G.P., and Team, I.I. (2002). Analysis of the mouse transcriptome based on functional annotation of 60,770 full-length cDNAs. Nature **420,** 563-573.

Osakabe, A., Tachiwana, H., Takaku, M., Hori, T., Obuse, C., Kimura, H., Fukagawa, T., and Kurumizaka, H. (2013). Vertebrate Spt2 is a novel nucleolar histone chaperone that assists in ribosomal DNA transcription. J. Cell Sci. **126,** 1323-1332.

Palm, D., Simm, S., Darm, K., Weis, B.L., Ruprecht, M., Schleiff, E., and Scharf, C. (2016). Proteome distribution between nucleoplasm and nucleolus and its relation to ribosome biogenesis in *Arabidopsis thaliana*. RNA Biol. **13,** 441-454.

Parry, G., Ward, S., Cernac, A., Dharmasiri, S., and Estelle, M. (2006). The Arabidopsis SUPPRESSOR OF AUXIN RESISTANCE proteins are nucleoporins with an important role in hormone signaling and development. Plant Cell **18,** 1590-1603.

Pellizzoni, L., Cardinali, B., Lin-Marq, N., Mercanti, D., and Pierandrei-Amaldi, P. (1996). A *Xenopus laevis* homologue of the La autoantigen binds the pyrimidine tract of the 5' UTR of ribosomal protein mRNAs in vitro: implication of a protein factor in complex formation. J. Mol. Biol. **259,** 904-915.

Petricka, J.J., and Nelson, T.M. (2007). Arabidopsis nucleolin affects plant development and patterning. Plant Physiol. **144,** 173-186.

Petrov, A.S., Bernier, C.R., Hsiao, C., Norris, A.M., Kovacs, N.A., Waterbury, C.C., Stepanov, V.G., Harvey, S.C., Fox, G.E., Wartell, R.M., Hud, N.V., and Williams, L.D. (2014). Evolution of the ribosome at atomic resolution. Proc. Natl. Acad. Sci. USA **111,** 10251-10256.

Phipps, K.R., Charette, J., and Baserga, S.J. (2011). The small subunit processome in ribosome biogenesis-progress and prospects. Wiley Interdisciplinary Reviews: RNA **2,** 1-21.

Ponce, M.R., Quesada, V., and Micol, J.L. (1998). Rapid discrimination of sequences flanking and within T-DNA insertions in the Arabidopsis genome. Plant J. **14,** 497-501.

Pontvianne, F., Matia, I., Douet, J., Tourmente, S., Medina, F.J., Echeverria, M., and Saez-Vasquez, J. (2007). Characterization of *AtNUC-L1* reveals a central role of nucleolin in nucleolus organization and silencing of *AtNUC-L2* gene in Arabidopsis. Mol. Biol. Cell **18,** 369-379.

Pontvianne, F., Abou-Ellail, M., Douet, J., Comella, P., Matia, I., Chandrasekhara, C., Debures, A., Blevins, T., Cooke, R., Medina, F.J., Tourmente, S., Pikaard, C.S., and Saez-Vasquez, J. (2010). Nucleolin is required for DNA methylation state and the expression of rRNA gene variants in *Arabidopsis thaliana*. PLoS Genet. **6,** e1001225.

Probst, A.V., Fagard, M., Proux, F., Mourrain, P., Boutet, S., Earley, K., Lawrence, R.J., Pikaard, C.S., Murfett, J., Furner, I., Vaucheret, H., and Mittelsten Scheid, O. (2004). Arabidopsis histone deacetylase HDA6 is required for maintenance of transcriptional gene silencing and determines nuclear organization of rDNA repeats. Plant Cell **16,** 1021-1034.

Quesada, V., Ponce, M.R., and Micol, J.L. (2000). Genetic analysis of salt-tolerant mutants in *Arabidopsis thaliana*. Genetics **154,** 421-436.

Robles, P., Fleury, D., Candela, H., Cnops, G., Alonso-Peral, M.M., Anami, S., Falcone, A., Caldana, C., Willmitzer, L., Ponce, M.R., Van Lijsebettens, M., and

Micol, J.L. (2010). The *RON1/FRY1/SAL1* gene is required for leaf morphogenesis and venation patterning in Arabidopsis. Plant Physiol. **152,** 1357-1372.

Romanova, L.G., Anger, M., Zatsepina, O.V., and Schultz, R.M. (2006). Implication of nucleolar protein SURF6 in ribosome biogenesis and preimplantation mouse development. Biol. Reprod. **75,** 690-696.

Rosbash, M., and Séraphin, B. (1991). Who's on first? The U1 snRNP-5' splice site interaction and splicing. Trends Biochem. Sci. **16,** 187-190.

Rudra, D., Mallick, J., Zhao, Y., and Warner, J.R. (2007). Potential interface between ribosomal protein production and pre-rRNA processing. Mol. Cell. Biol. **27,** 4815-4824.

Sánchez-García, A.B., Aguilera, V., Micol-Ponce, R., Jover-Gil, S., and Ponce, M.R. (2015). Arabidopsis *MAS2*, an essential gene that encodes a homolog of animal NF-kappa B activating protein, is involved in 45S ribosomal DNA silencing. Plant Cell **27,** 1999-2015.

Schwacke, R., Schneider, A., van der Graaff, E., Fischer, K., Catoni, E., Desimone, M., Frommer, W.B., Flugge, U.I., and Kunze, R. (2003). ARAMEMNON, a novel database for Arabidopsis integral membrane proteins. Plant Physiol. **131,** 16-26.

Sloan, K.E., Bohnsack, M.T., Schneider, C., and Watkins, N.J. (2014). The roles of SSU processome components and surveillance factors in the initial processing of human ribosomal RNA. RNA **20,** 540-550.

Stothard, P. (2000). The sequence manipulation suite: JavaScript programs for analyzing and formatting protein and DNA sequences. BioTechniques **28,** 1102, 1104.

Tafforeau, L., Zorbas, C., Langhendries, J.L., Mullineux, S.T., Stamatopoulou, V., Mullier, R., Wacheul, L., and Lafontaine, D.L. (2013). The complexity of human ribosome biogenesis revealed by systematic nucleolar screening of pre-rRNA processing factors. Mol. Cell **51,** 539-551.

Tatematsu, K., Ward, S., Leyser, O., Kamiya, Y., and Nambara, E. (2005). Identification of cis-elements that regulate gene expression during initiation of axillary bud outgrowth in Arabidopsis. Plant Physiol. **138,** 757-766.

Tchasovnikarova, I.A., Timms, R.T., Matheson, N.J., Wals, K., Antrobus, R., Gottgens, B., Dougan, G., Dawson, M.A., and Lehner, P.J. (2015). Epigenetic silencing by the HUSH complex mediates position-effect variegation in human cells. Science **348,** 1481-1485.

Thomson, E., and Tollervey, D. (2005). Nop53p is required for late 60S ribosome subunit maturation and nuclear export in yeast. RNA **11,** 1215-1224.

Tremousaygue, D., Manevski, A., Bardet, C., Lescure, N., and Lescure, B. (1999). Plant interstitial telomere motifs participate in the control of gene expression in root meristems. Plant J. **20,** 553-561.

Umezawa, T., Sugiyama, N., Takahashi, F., Anderson, J.C., Ishihama, Y., Peck, S.C., and Shinozaki, K. (2013). Genetics and phosphoproteomics reveal a protein phosphorylation network in the abscisic acid signaling pathway in *Arabidopsis thaliana*. Science Signaling **6,** rs8.

Utama, B., Kennedy, D., Ru, K., and Mattick, J.S. (2002). Isolation and characterization of a new nucleolar protein, Nrap, that is conserved from yeast to humans. Genes Cells **7,** 115-132.

Van Lijsebettens, M., Vanderhaeghen, R., De Block, M., Bauw, G., Villarroel, R., and Van Montagu, M. (1994). An S18 ribosomal protein gene copy at the Arabidopsis *PFL* locus affects plant development by its specific expression in meristems. EMBO J. **13,** 3378-3388.

Wang, P., Xue, L., Batelli, G., Lee, S., Hou, Y.J., Van Oosten, M.J., Zhang, H., Tao, W.A., and Zhu, J.K. (2013). Quantitative phosphoproteomics identifies SnRK2 protein kinase substrates and reveals the effectors of abscisic acid action. Proc. Natl. Acad. Sci. USA **110,** 11205-11210.

Weis, B.L., Kovacevic, J., Missbach, S., and Schleiff, E. (2015). Plant-specific features of ribosome biogenesis. Trends Plant Sci. **20,** 729-740.

Wells, S.E., Neville, M., Haynes, M., Wang, J., Igel, H., and Ares, M., Jr. (1996). CUS1, a suppressor of cold-sensitive U2 snRNA mutations, is a novel yeast splicing factor homologous to human SAP 145. Genes Dev. **10,** 220-232.

Wilson, D.N., and Doudna Cate, J.H. (2012). The structure and function of the eukaryotic ribosome. Cold Spring Harb. Perspect. Biol. **4,** a011536.

Winston, F., Chaleff, D.T., Valent, B., and Fink, G.R. (1984). Mutations affecting Ty-mediated expression of the *HIS4* gene of *Saccharomyces cerevisiae*. Genetics **107,** 179-197.

Woolford, J.L., Jr., and Baserga, S.J. (2013). Ribosome biogenesis in the yeast *Saccharomyces cerevisiae*. Genetics **195,** 643-681.

Yu, C.P., Lin, J.J., and Li, W.H. (2016). Positional distribution of transcription factor binding sites in *Arabidopsis thaliana*. Sci. Rep. **6,** 25164.

Zhang, L., Hu, Y., Yan, S., Li, H., He, S., Huang, M., and Li, L. (2012). ABA-mediated inhibition of seed germination is associated with ribosomal DNA chromatin condensation, decreased transcription, and ribosomal RNA gene hypoacetylation. Plant Mol Biol **79,** 285-293.

Zhang, X.R., Qin, Z., Zhang, X., and Hu, Y. (2015). Arabidopsis SMALL ORGAN 4, a homolog of yeast NOP53, regulates cell proliferation rate during organ growth. J. Integr. Plant Biol. **57,** 810-818.

Micol-Ponce *et al*., Figure 1

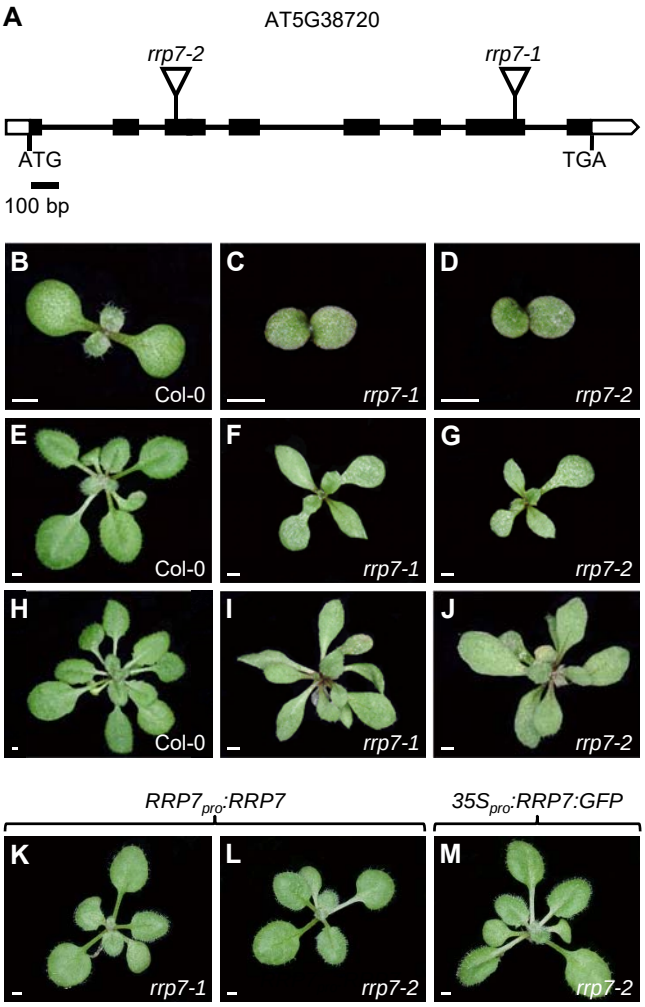

Micol-Ponce *et al.*, Figure 2

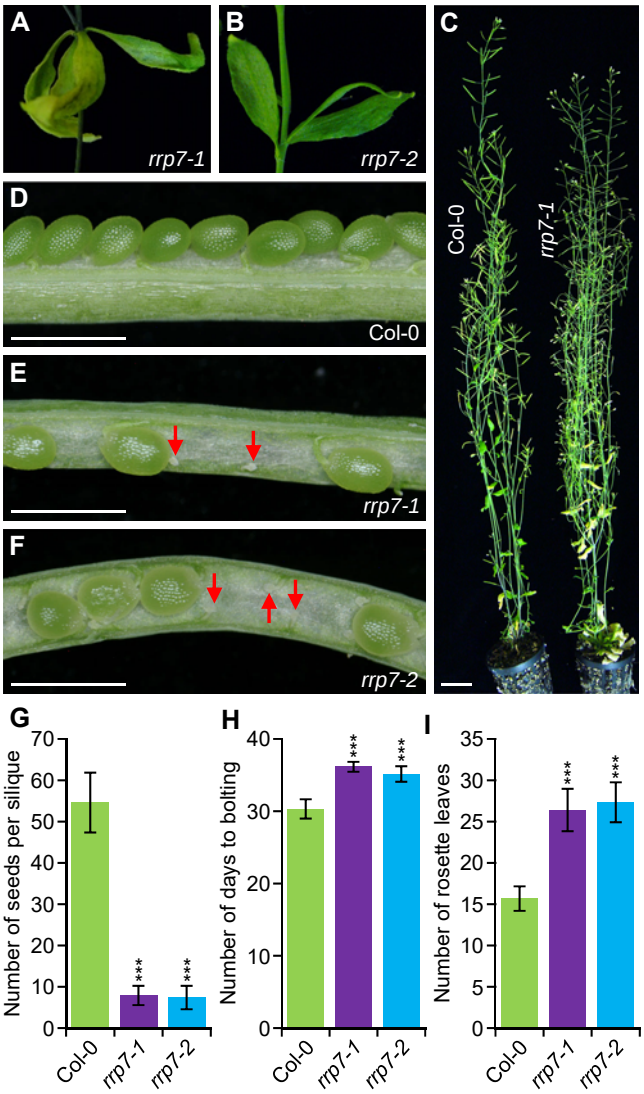

Micol-Ponce *et al.*, Figure 3

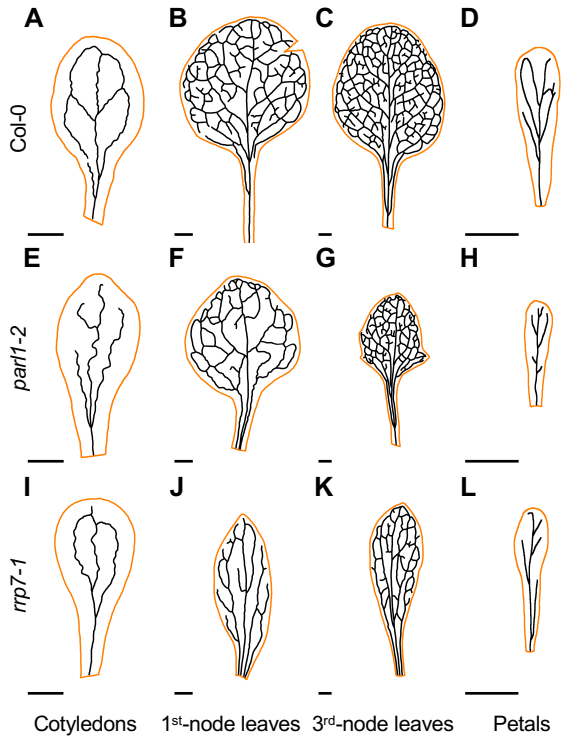

Micol-Ponce *et al*., Figure 4

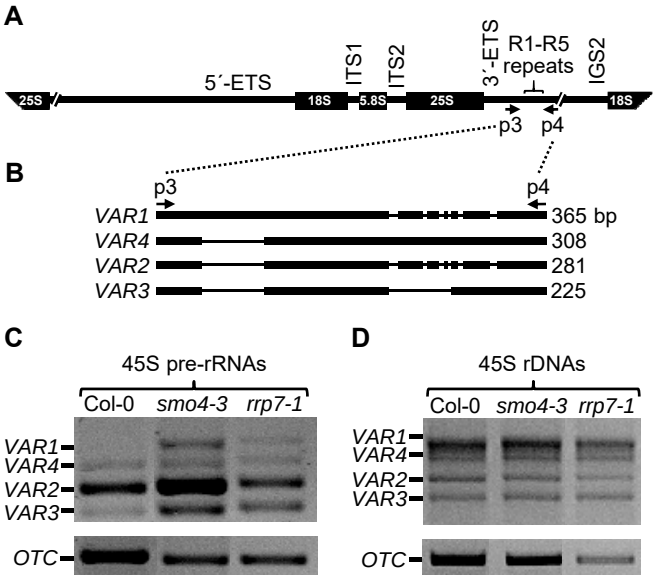

Micol-Ponce *et al.*, Figure 5

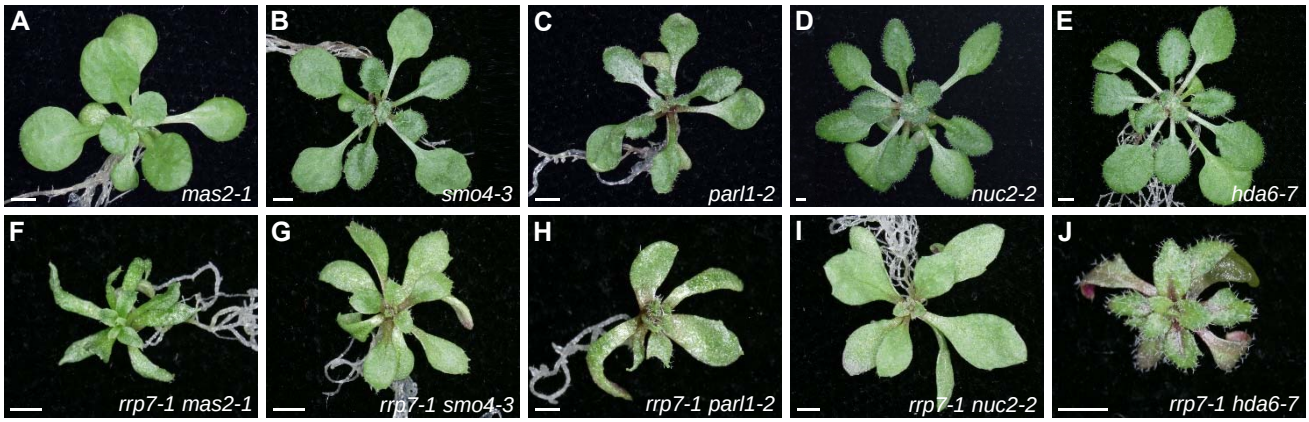

Micol-Ponce *et al.*, Figure 6

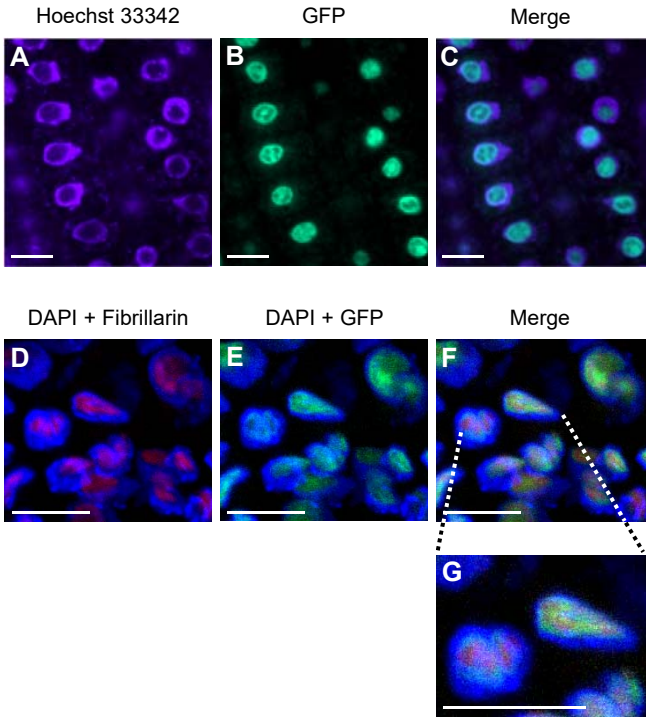

Micol-Ponce *et al*., Figure 7

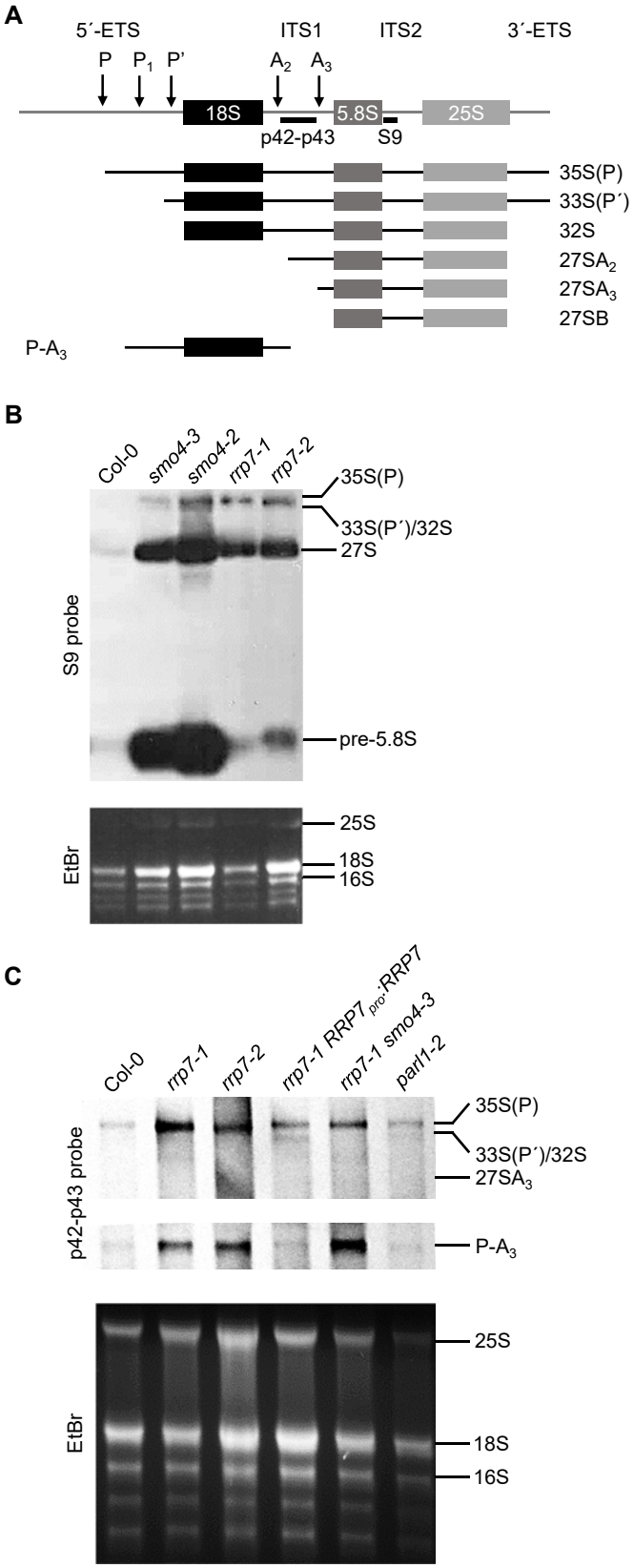

Micol-Ponce *et al.*, Figure 8

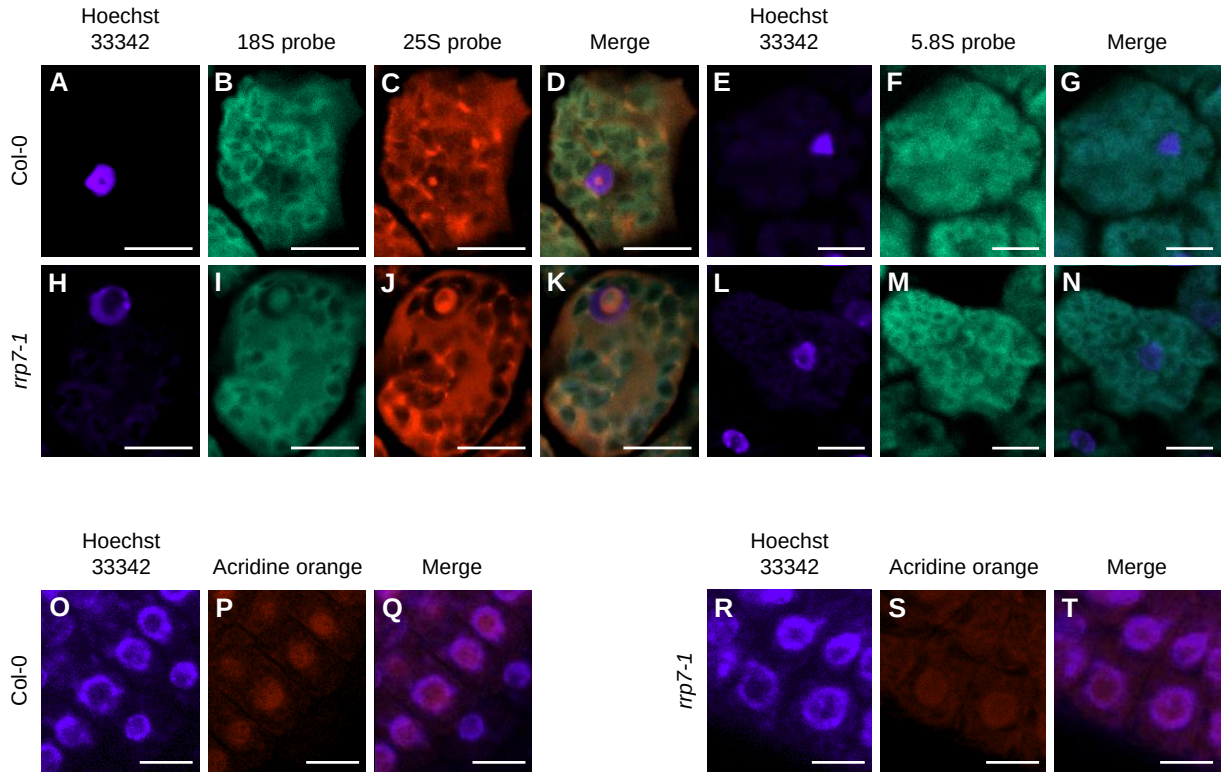

Micol-Ponce *et al.*, Figure 9

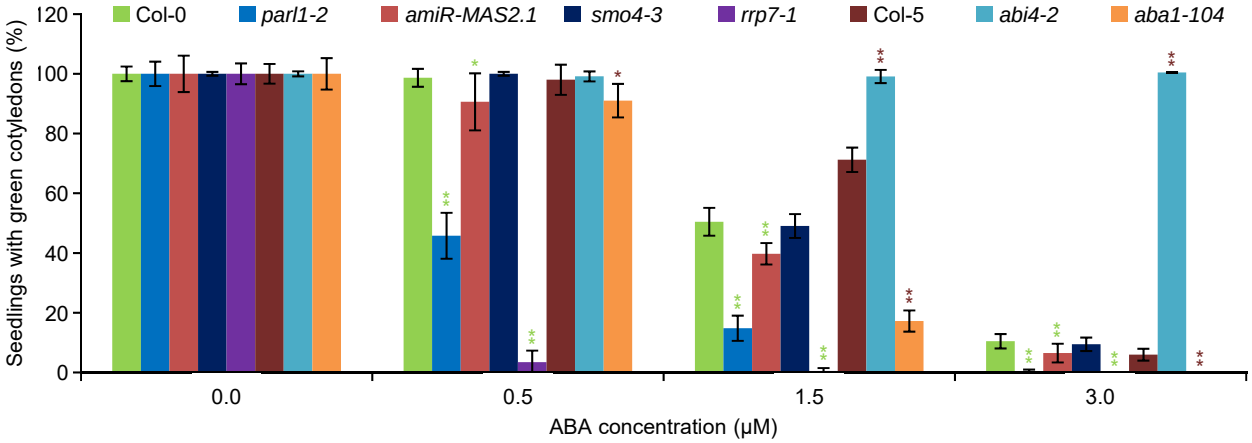

Arabidopsis RIBOSOMAL RNA PROCESSING 7 participates in 45S rDNA transcriptional regulation and 45S pre-rRNA processing

Rosa Micol-Ponce, Raquel Sarmiento-Mañús, Alejandro Ruiz-Bayón and María Rosa Ponce

Instituto de Bioingeniería, Universidad Miguel Hernández, Campus de Elche, 03202 Elche, Alicante, Spain.

Supplemental Figures, Tables and References

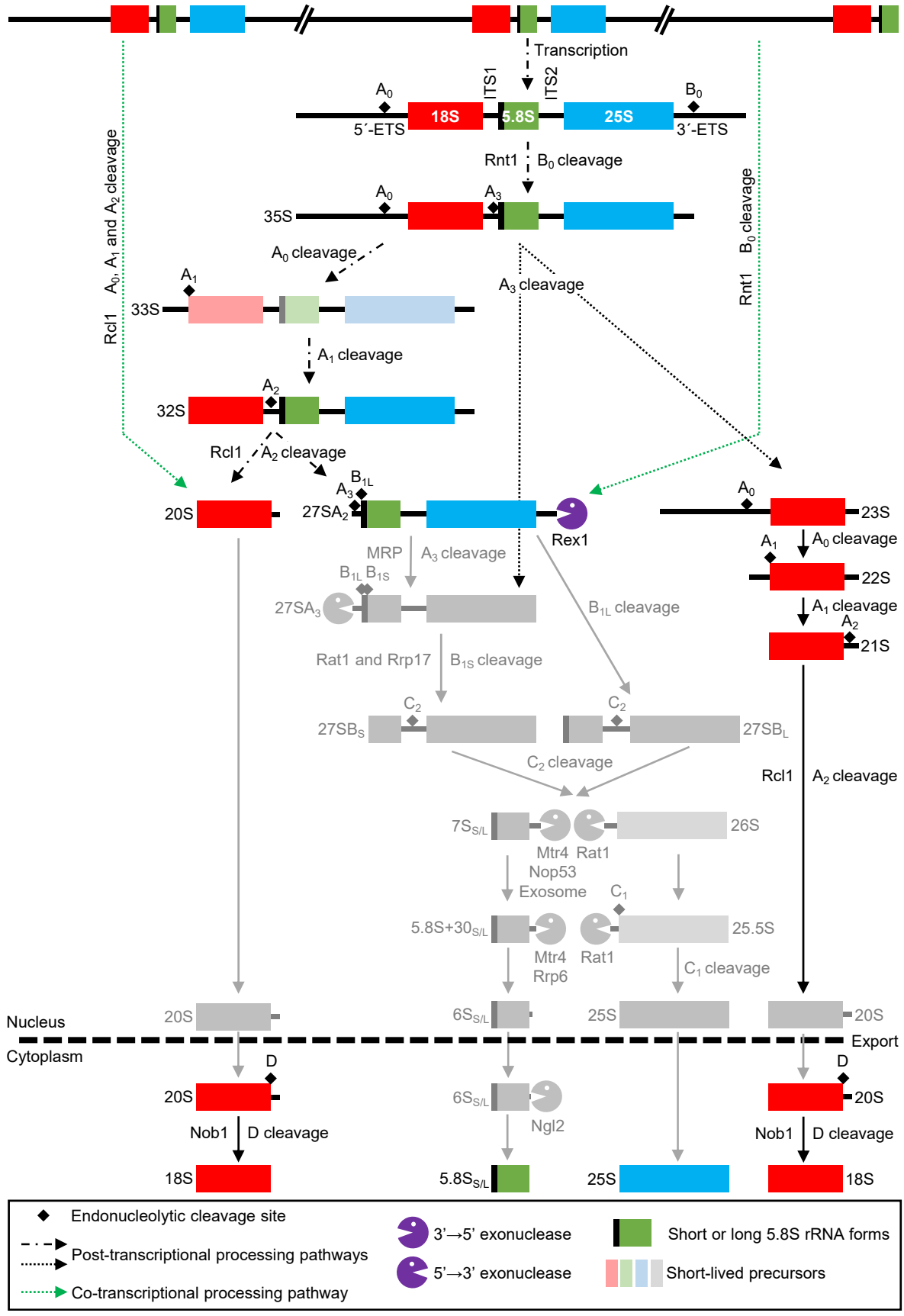

Supplemental Figure 1. Overview of 35S pre-rRNA processing in yeast.
Most known endonucleolytic cleavages, exonucleolytic trimmings, and alternative pathways are shown. Only the elements relevant to this work are represented in color. ETS: external transcribed spacer. ITS: internal transcribed spacer. Modified from Henras et al. (2015) and Chaker-Margot et al. (2015).

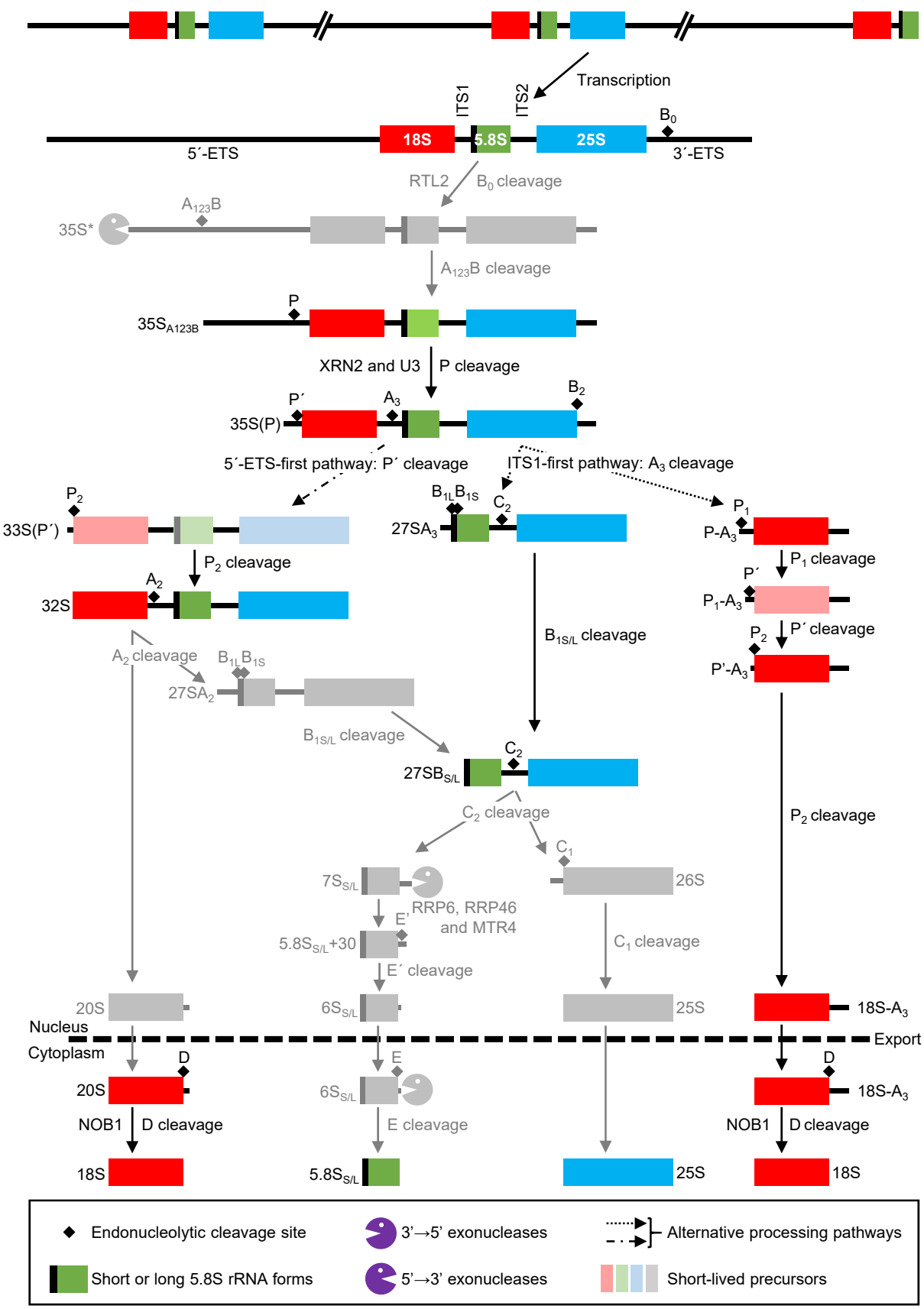

Supplemental Figure 2. Overview of 45S pre-rRNA processing in Arabidopsis.
Most known endonucleolytic cleavages, exonucleolytic trimmings, and alternative pathways are shown. Only the elements relevant to this work are represented in color. ETS: external transcribed spacer. ITS: internal transcribed spacer. Modified from Weis et al. (2015a) and Schillewaert et al. (2012).

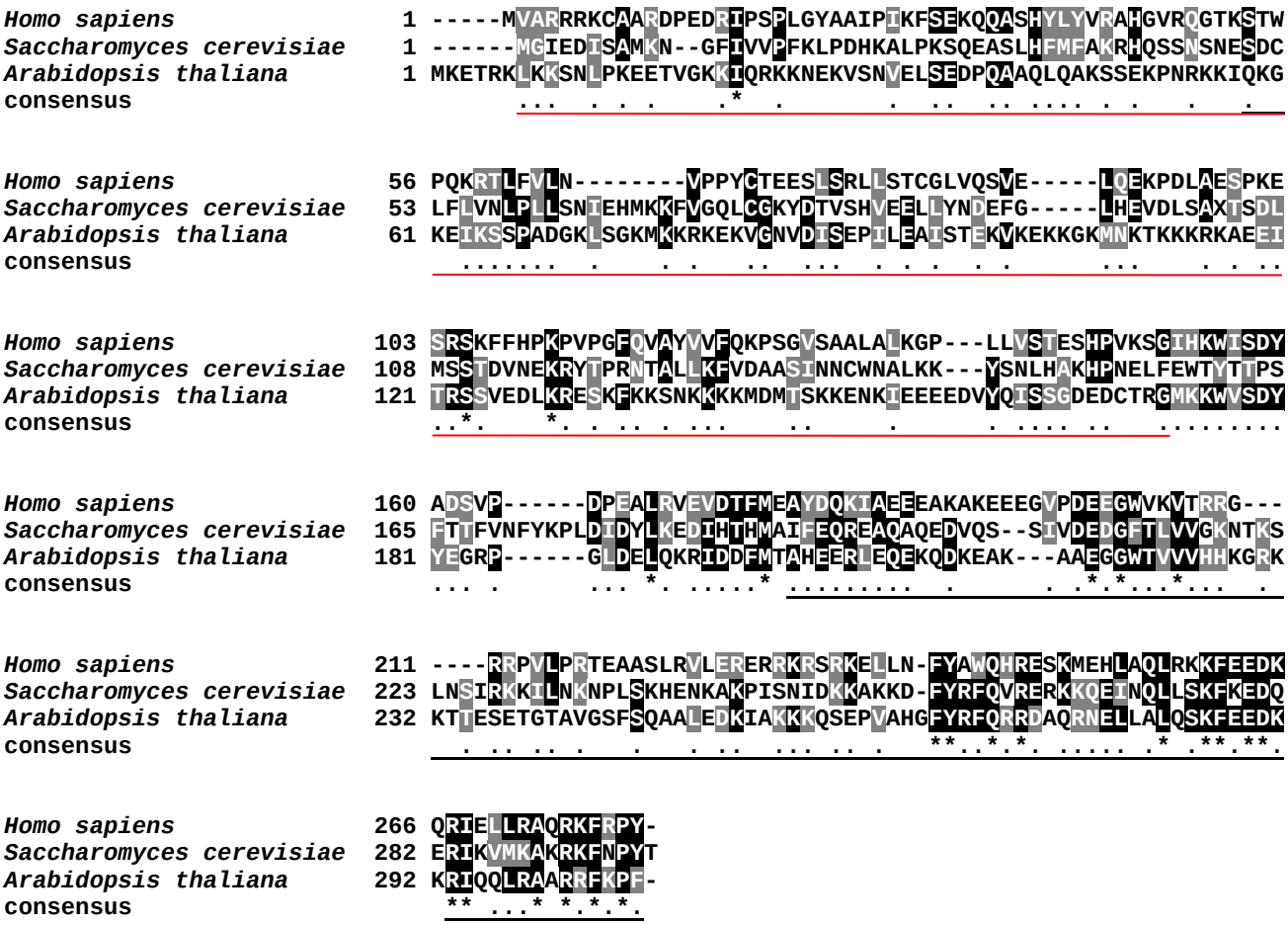

Supplemental Figure 3. Sequence conservation among human, yeast, and Arabidopsis RRP7 orthologs.

Sequence alignment of full-length RRP7 orthologs from *Homo sapiens* (RRP7A; GenBank accession number NP_056518), *Saccharomyces cerevisiae* (Rrp7; NP_009899) and *Arabidopsis thaliana* (RRP7; NP_198688), representing metazoans, yeast, and plants, respectively. Identical and similar residues are shaded in black or gray, respectively. Asterisks and periods indicate identical and conserved residues, respectively. Numbers indicate residue positions. The NTD and CTD domains, as defined for yeast NP_009899 by Lin et al. (2013), have been highlighted with red and black lines, respectively, under the consensus sequence. This alignment and that of Supplemental Figure 4 were obtained using ClustalW2 (Larkin et al., 2007) and shaded with Boxshade 3.21 (http://www.ch.embnet.org/software/BOX_form.html).

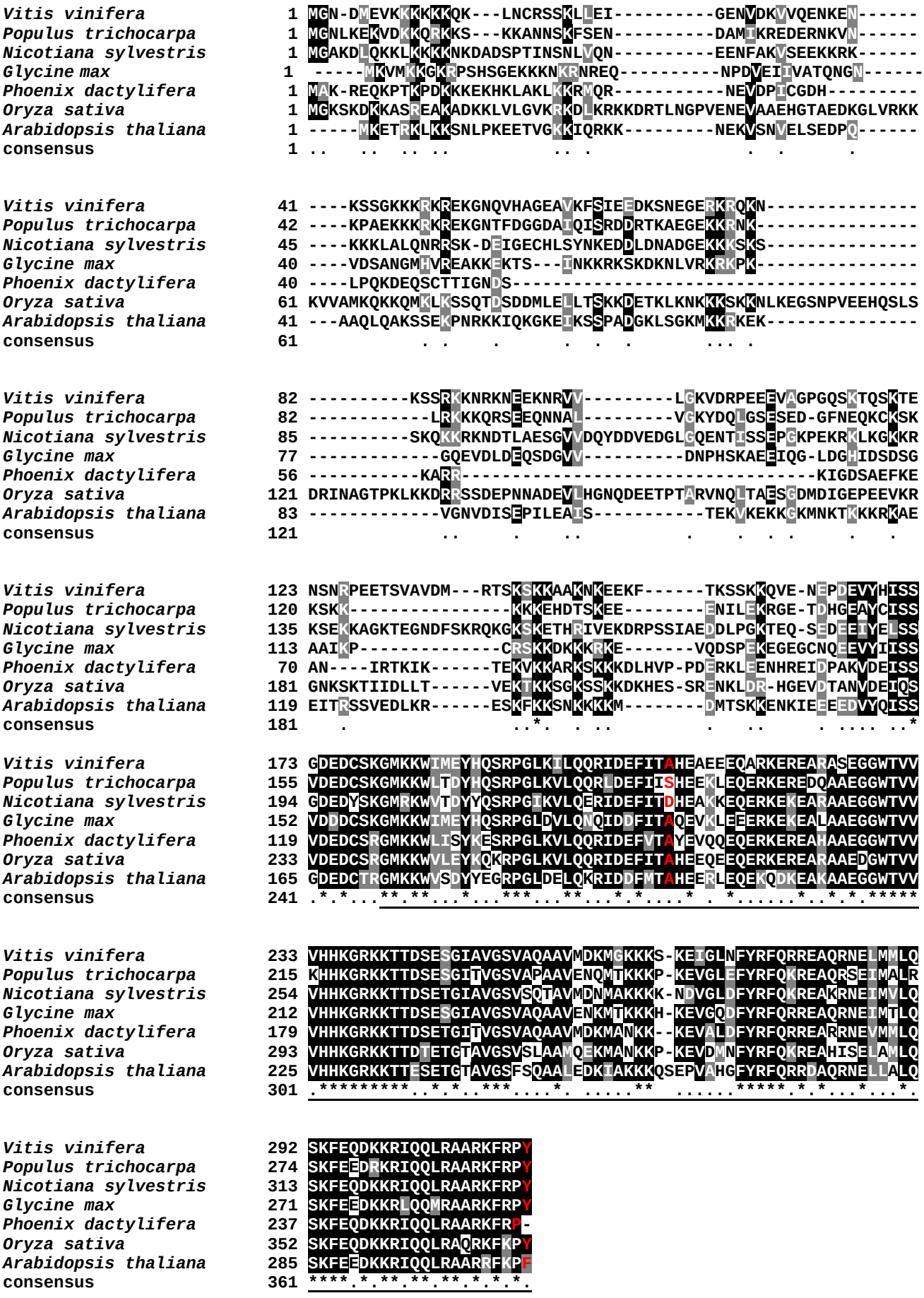
Vitis vinifera
Populus trichocarpa
Nicotiana sylvestris
Glycine max
Phoenix dactylifera
Oryza sativa
Arabidopsis thaliana
consensus

Supplemental Figure 4. Sequence conservation among plant RRP7 orthologs.
Sequence alignment of full-length RRP7 orthologs from different angiosperm lineages, as classified in Myburg et al. (2014): *Vitis vinifera* XP_010660530 (repressing Vitales), *Populus trichocarpa* XP_002305975 (Malpighiales), *Nicotiana sylvestris* XP_009764776 (Asterids), *Glycine max* XP_003529364 (Fabids), *Phoenix dactylifera* XP_008784326 (Arecales), *Oryza sativa* XP_015625591 (Poales), and *Arabidopsis thaliana* NP_198688 (Malvids). For *Vitis vinifera*, *Phoenix dactylifera*, *Gycine max*, *Nicotiana sylvestris,* and *Oryza sativa* RRP7 orthologs, the isoform with a higher number of amino acids was chosen for the aligment. Identical and similar residues across all sequences are shaded in black and gray, respectively. Asterisks and periods indicate identical and conserved residues, respectively. Numbers indicate residue positions. The RRP7_like (NCBI cd12932) conserved domain is underlined. Residues in red letters are the ends of the CTD.

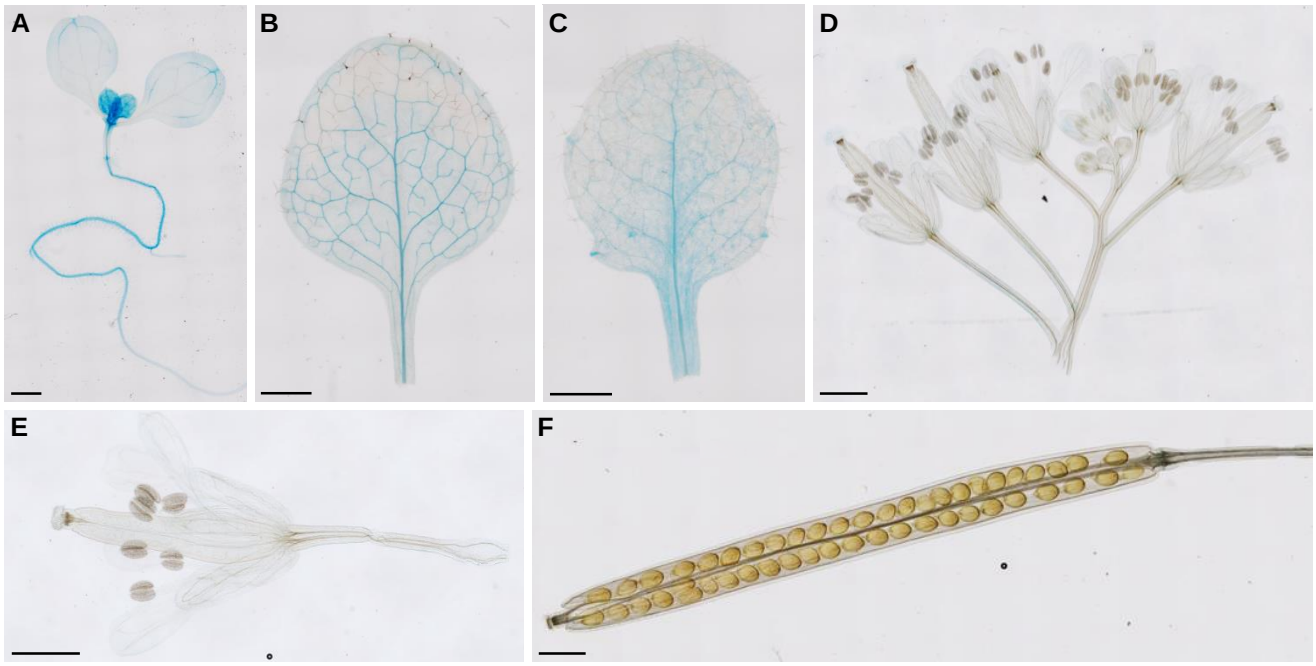

Supplemental Figure 5. Spatial expression pattern of *RRP7*.
GUS staining in seedlings (A), first-node leaves (B), third-node leaves (C), inflorescences (D), flowers (E), and siliques (F) from of *RRP7*$_{pro}$*:GUS* transgenic plants. Plant material was collected 7 (A), 14 (B, C) and 50 (D-F) das. Scale bars: 1 mm.

MAS2 promoter (137 bp upstream from the transcription start site)

GCCGAAACGGCGACAGAGACACGGCGGACATGGAGAGACTTGCCATctgaagacgacgataaggatagag
gactcgattgactctaattaaaatgtggggtgctttgtgtaaaatcaaaacatgattttcagtggtgaat
UP1ATMSD UP1ATMSD
aatgataaatattgggccctattcgttaaggggcccaataagtaaaaaggcgcagatactgtatatgaatca
aagccctaatttatcagacagctgcttagattttgttttcttcattgtcgtcgtcggagtgaattaggga
ttcgagaATGACGATGAACTCGCTTCCGAGGAGATTTGGGAAGAATCATGGCTATTTGGATCGAGATTAT

SMO4 promoter (500 bp upstream from the transcription start site)

tataaccaaaacttatttgttggaatcccacaaaaatgggagagaactcacgttaacaaaatatatgctc
aagtttaacatattgatcaatgttgtttatttacattagaatcagacgatgtccgattttccgtaatgat
caatgttatcacttcaatttttttatttcactaacatgtaagacatgataacattttatactgtgttaat
ctttttatgataaaatttagttttatgtacttgatttttttattttttatttactaaatactttgatg
gtttttctgtgagtatgaaaaagtgttattgttgcaaaatgaaaaaaagtagtatataaccaagaaaaaa
UP1ATMSD
aaacaaaactaaatatatgtggaaaggaaaatgaatgtacgtacgtcgtaggaattaaaaagtatatggg
UP1ATMSD
cccattaagaggaaatggagaaacgtaaggcccattatgtttctctctaagccctacccctagtgtgtgt
cctcttcttcaatcatcatcttttcgataccgaagcagcaaccttcgcgccgccgagagataacgagaaa
aaATGGGGAAGAGGTCGAAAACATCAAGGAAAGGGAAAAAAGCATGGAGGGCTAACATTAGCTCCGAGGA

RRP7 promoter (500 bp upstream from the transcription start site)

cagagaaagctcagagattacctgagtggttatcgctgatttcaataacccagaatcaactttgtgtttc
agaatatttttccagtttcctttcaatactgttgcacagatgctttgtgcaatcaaagcttctcgatttg
ctgacaacaaattcaccattgttgttcctcaagtgttgtaggagtaacagagaagagcaacggcgataaa
gagaaggcctaaaccggtttgaatttctccagtagatgaaccagaccagattatttaccaattaaccgat
aaaggactgaattcaaaaccggaagcgaatcgattgttttggaatatccgggaaacggcccgagagaaaa
tacgtaataaatcgaactgaacccaattttagaccggtttagtcaagaatacgtatatgtcctctcgtgt
TELOBOXATEEF1AA1
tgctgatattaacaactttacccttgtatctgtttcagtccaaaacctcacaaaaagcaaaaaccctaat
ttacatggtcgtggcctgactaatccctaatttttccgagagcgtcgacgccgacaatcgccgacagagt
ttttgcttctcacgcgatagaaagaagATGAAGGAGACGAGAAAGCTGAAGAAGAGTAATCTCCCTAAAG

Supplemental Figure 6. Translation-apparatus-related motifs in the promoters of *MAS2*, *SMO4* and *RRP7*.
Two UP1ATMSD (GGCCCAWWW, where W is A or T) and TELO-box (AAACCCTAA) motifs are highlighted in white letters and shaded in blue. The transcription units and the coding regions—in capital letters—are written in red letters. Start codons are highlighted in white letters and shaded in black. The sequence of AT4G02725, the gene adjacent to *MAS2* (AT4G02720), is shown in green letters.

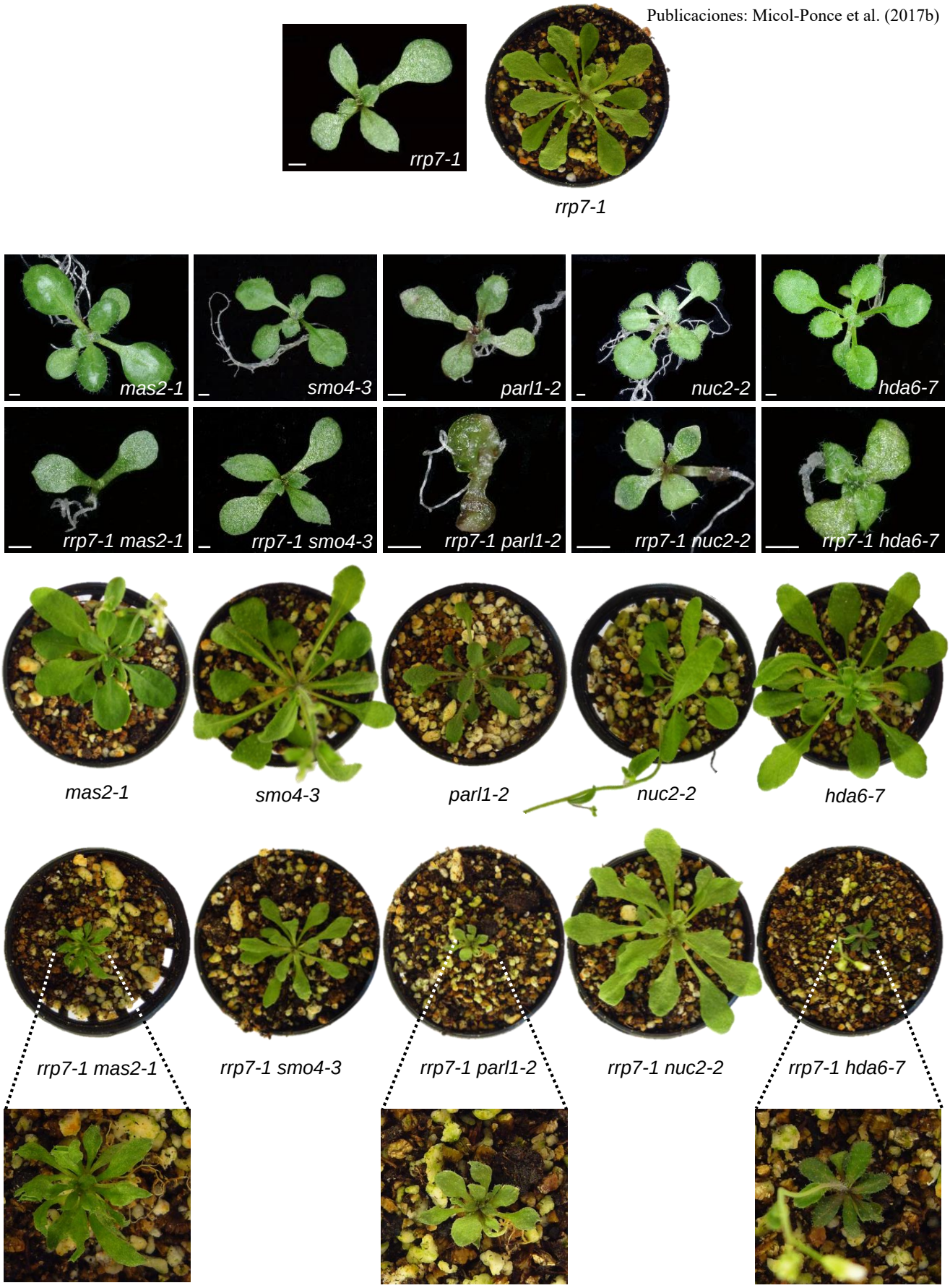

Supplemental Figure 7. Genetic interactions of *rrp7-1* with *mas2-1*, *smo4-3*, *parl1-2*, *nuc2-2*, and *hda6-7*. Pictures with a black background were taken from plants grown on plates 14 days after stratification (das). Plants that are displayed in pots were grown on plates for 14 das and transferred into pots, and the pictures were taken 17 days later. The three smaller plants are shown at higher magnification in the bottom row. Scale bars indicate 1 mm.

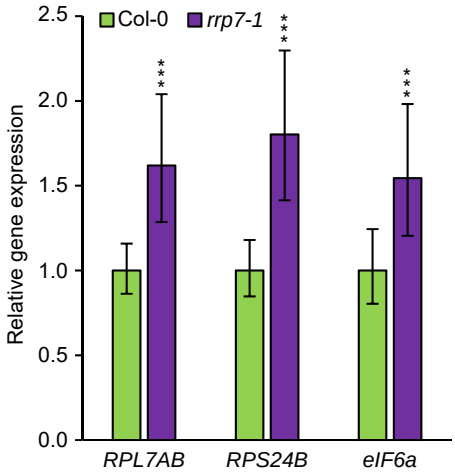

Supplemental Figure 8. Relative expression of *RPL7AB*, *RPS24B* and *eiF6a* in Col-0 and *rrp7-1* plants.

RNA for RT-qPCR analyses was extracted from three groups of three plants collected 14 das. Error bars indicate $2^{-(\Delta\Delta C_T)\pm SD}$ (SD: standard deviation). Asterisks indicate values significantly different from Col-0 in a Mann-Whitney *U*-test (***$P < 0.001$; n = 9).

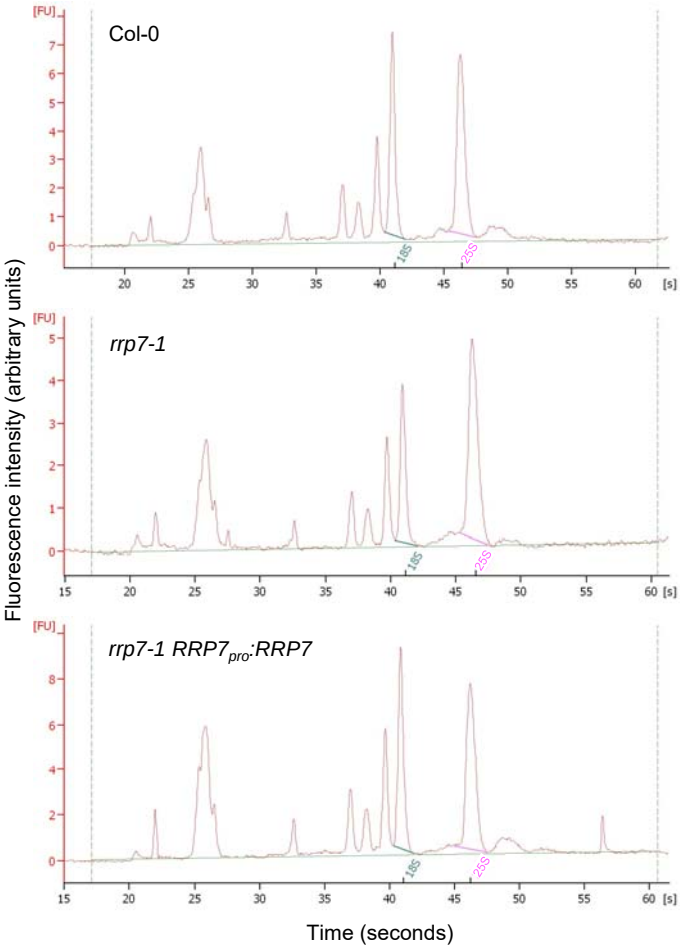

Supplemental Figure 9. Agilent 2100 Bioanalyzer electropherogram profiles of total RNA samples extracted from Col-0, *rrp7-1* and *rrp7-1 RRP7*$_{pro}$*:RRP7* plants, collected 15 das.

Supplemental Table 1. Identity and similarity among full-length representative plant RRP7 orthologs

	Arabidopsis thaliana	*Glycine max*	*Populus trichocarpa*	*Nicotiana sylvestris*	*Vitis vinifera*	*Phoenix dactylifera*	*Oryza sativa*
Arabidopsis thaliana		49.70	44.99	47.93	48.85	45.57	40.35
Glycine max	37.50		50.00	47.91	52.65	47.92	37.59
Populus trichocarpa	34.10	41.62		53.13	58.18	46.25	46.98
Nicotiana sylvestris	35.81	37.60	41.76		54.78	45.83	45.75
Vitis vinifera	37.64	42.65	48.18	44.66		48.45	48.57
Phoenix dactylifera	36.71	39.30	38.75	37.50	40.99		45.41
Oryza sativa	31.68	29.24	35.43	35.25	39.22	38.92	

Values correspond to percent identity (lower triangle) and similarity (upper triangle) between members of each pair, calculated as described in Methods. Orthologous RRP7 proteins are those described in the legend of Supplemental Figure 4.

Supplemental Table 2. Identity and similarity among the RRP7_like domains of representative plant RRP7 orthologs

	Arabidopsis thaliana	*Glycine max*	*Populus trichocarpa*	*Nicotiana sylvestris*	*Vitis vinifera*	*Phoenix dactylifera*	*Oryza sativa*
Arabidopsis thaliana		81.48	78.52	83.70	80.74	77.78	79.26
Glycine max	68.15		85.82	86.57	89.55	87.31	80.60
Populus trichocarpa	62.96	77.61		85.82	85.07	83.58	80.60
Nicotiana sylvestris	68.15	75.37	75.37		89.55	88.81	82.09
Vitis vinifera	66.67	80.60	76.87	79.10		92.54	85.07
Phoenix dactylifera	67.41	76.12	74.63	78.36	81.34		85.82
Oryza sativa	66.67	68.66	70.90	73.13	76.87	76.12	

Values correspond to percent identity (lower triangle) and similarity (upper triangle) between members of each pair, calculated as described in Methods. Orthologous RRP7 proteins are those described in the legend of Supplemental Figure 4.

Supplemental Table 3. Morphometry of leaf venation in the *rrp7-1* and *parl1-2* mutants

	First-node leaf			Third-node leaf		
Variable	Col-0	*parl1-2*	*rrp7-1*	Col-0	*parl1-2*	*rrp7-1*
Lamina area (mm^2)	36.8 ± 11.8	24.1 ± 7.6**	19.7 ± 4.3**	61.5 ± 24.9	27.2 ± 7.3**	26.1 ± 5.2**
Lamina length/width	1.1 ± 0.1	1.1 ± 0.2	2.3 ± 0.3**	1.2 ± 0.1	1.2 ± 0.1	1.9 ± 0.3**
Venation length (mm)	95.8 ± 25.0	59.1 ± 13.8**	45.9 ± 9.4**	178.5 ± 58.7	74.6 ± 21.4**	64.8 ± 10.8**
Venation density ($mm \cdot mm^{-2}$)	2.7 ± 0.4	2.5 ± 0.3	2.3 ± 0.2*	3.0 ± 0.6	2.8 ± 0.5	2.5 ± 0.1**
Branching points	113.7 ± 35.4	64.5 ± 13.4**	25.3 ± 9.1**	247.1 ± 64.5	90.9 ± 46.0**	54.9 ± 12.6**
Branching points per mm^2	3.2 ± 1.2	2.8 ± 0.8	1.3 ± 0.3**	4.5 ± 1.9	3.4 ± 1.3	2.1 ± 0.4**
Free-ending veins	34.2 ± 9.9	20.2 ± 4.8**	11.7 ± 3.2**	64.3 ± 18.1	21.9 ± 6.1**	16.7 ± 4.3**
Free-ending veins per mm^2	1.0 ± 0.3	0.9 ± 0.4	0.6 ± 0.2**	1.1 ± 0.4	0.8 ± 0.2*	0.7 ± 0.2**

Percentages ± standard deviation are shown. Asterisks indicate values significantly different from the wild-type Col-0 in a Student's *t*-test (*$P < 0.05$, and **$P < 0.01$).

Supplemental Table 4. Putative homologs of Arabidopsis RRP7 identified in a PropSearch analysis

Rank	ID	Organism	Distance	Description	Function
1	SURF6	*Drosophila melanogaster*	8.62	Surfeit locus protein 6 homolog	Ribosome biogenesis
2	ccdc-55	*Caenorhabditis elegans*	8.99	Nuclear speckle splicing regulatory protein 1	Pre-mRNA splicing
3	YKI2	*Caenorhabditis elegans*	9.11	Similar to *S. cerevisiae* RRP14	Ribosome biogenesis
4	SURF6	*Fugu rubripes*	9.16	Surfeit locus protein 6 homolog	Ribosome biogenesis
5	SURF6	*Mus musculus*	9.24	Surfeit locus protein 6 homolog	Ribosome biogenesis
6	B0361.2	*Caenorhabditis elegans*	9.36	CWF19-like protein 2 homolog	Pre-mRNA splicing
7	SURF6	*Caenorhabditis elegans*	9.90	Surfeit locus protein 6 homolog	Ribosome biogenesis
8	UTP11	*Caenorhabditis elegans*	9.96	UTP11, putative U3-associated protein 11	Ribosome biogenesis
9	RLX3	*Staphylococcus aureus*	10.38	RLX protein	Conjugation
10	SURF6	*Xenopus laevis*	10.40	Surfeit locus protein 6 homolog	Ribosome biogenesis
11	SPT2	*Saccharomyces cerevisiae*	10.53	Suppressor of Ty's 2	Nucleolar histone chaperone
12	C17H9.05	*Schizosaccharomyces pombe*	10.62	Hypothetical Mtr4 ortholog	Exosome cofactor, ribosome biogenesis
13	U1-70K	*Arabidopsis thaliana*	10.63	U1 small nuclear ribonucleoprotein 70 kDa	Pre-mRNA splicing
14	M21	*Streptococcus pyogenes*	10.73	M protein, serotype 2.1 precursor	Virulence
15	RSP41	*Arabidopsis thaliana*	10.86	Arginine/serine-rich splicing factor RSP41	Pre-mRNA splicing
16	CG1785	*Drosophila melanogaster*	10.87	NOP53 ortholog	Ribosome biogenesis
17	RRP14	*Saccharomyces cerevisiae*	11.08	Ribosomal RNA-processing protein 14	Ribosome biogenesis
18	MPP8	*Homo sapiens*	11.11	M-phase phosphoprotein 8 (MPHOSPH8)	Transcriptional silencing
19	ESF2	*Saccharomyces cerevisiae*	11.13	pre-rRNA-processing protein ESF2	Ribosome biogenesis
20	RS40	*Arabidopsis thaliana*	11.15	Arginine/serine-rich splicing factor RSP40	Pre-mRNA splicing

RRP7 is not included in the PropSearch preprocessed database, which is based on Uniprot registers.

Supplemental Table 5. Putative homologs of Arabidopsis SMO4 identified in a PropSearch analysis

Rank	ID	Organism	Distance	Description	Function
1	GSR2*	*Arabidopsis thaliana*	2.22	At2g40430	Cell proliferation
2	SSF2	*Saccharomyces cerevisiae*	6.19	Suppressor of ste4 (Four) 2	Ribosome biogenesis
3	SSF1	*Saccharomyces cerevisiae*	6.22	Suppressor of ste4 (Four) 1	Ribosome biogenesis
4	NOP13	*Saccharomyces cerevisiae*	6.58	Nucleolar protein 13	Ribosome biogenesis
5	RPSD	*Mycoplasma pneumoniae*	6.67	RNA polymerase sigma factor rpoD	RNA transcription in bacteria
6	CUS1	*Saccharomyces cerevisiae*	6.99	Cold sensitive U2 snRNA suppressor	Pre-mRNA splicing
7	YLF3	*Caenorhabditis elegans*	7.10	Hypothetical protein C40H1.3	Unknown
8	RPSD	*Mycobacterium genitalium*	7.11	RNA polymerase sigma factor rpoD	RNA transcription in bacteria
9	YOTA	*Caenorhabditis elegans*	7.13	ZK632.11, PSP_pro-rich protein family	Spliceosome associated protein
10	YM17	*Caenorhabditis elegans*	7.27	Hypothetical protein F55H2.7	Unknown
11	MYSQ	*Drosophila melanogaster*	7.69	Paramyosin	Motor protein
12	YRL4	*Caenorhabditis elegans*	7.76	R03D7.4, Elongin-A	General transcription elongation factor for RNA pol II
13	RNT1	*Saccharomyces cerevisiae*	7.77	Ribonuclease III	Ribosome biogenesis
14	YM63	*Saccharomyces cerevisiae*	7.84	Hypothetical protein	Unknown
15	RNP24	*Schizosaccharomyces pombe*	8.04	NOP13 homolog	Ribosome biogenesis
16	T2FB	*Saccharomyces cerevisiae*	8.05	Transcription initiation factor IIF beta	RNA pol II transcription preinitiation complex
17	NEK2	*Homo sapiens*	8.06	NIMA-related kinase 2	Cytokinesis
18	LAA	*Xenopus laevis*	8.09	Lupus LA protein homolog A	Translational control of mRNAs encoding RPs
19	SEP7	*Mus musculus*	8.15	Septin 7	Cytokinesis
20	PRP3	*Schizosaccharomyces pombe*	8.20	Pre-mRNA processing protein	Pre-mRNA splicing and in nuclear mRNA export

*SMO4 is included in the PropSearch preprocessed database, which is based on Uniprot registers. However, SMO4 appears in the Uniprot database as UniProtKB - O22892 (GSR2_ARATH), and is annotated as “Uncharacterized protein At2g40430”. In addition, the first 14 versions of the GSR2_ARATH register included a protein sequence of 416 aa, which was later substituted by other with 442 aa. The sequence of SMO4 in the PropSearch preprocessed database is that of 416 aa, which would yield a distance value of 0.0 if PropSearch is queried with an identical sequence. This table shows a distance value of 2.2 because the query was performed with the currently available SMO4 sequence of 442 aa, which cannot completely match a sequence of 416 aa.

Supplemental Table 6. Putative homologs of Arabidopsis MAS2 identified in a PropSearch analysis

Rank	ID	Organism	Distance	Description	Function
1	BUD13	*Caenorhabditis elegans*	6.96	BUD13-like protein	Pre-mRNA splicing
2	ccdc-55	*Caenorhabditis elegans*	7.84	Nuclear speckle splicing regulatory protein 1	Pre-mRNA splicing
3	MPP8	*Homo sapiens*	9.44	M-phase phosphoprotein 8 (MPHOSPH8)	Transcriptional silencing
4	SURF6	*Caenorhabditis elegans*	9.55	Surfeit locus protein 6 homolog	Ribosome biogenesis
5	CYP8	*Caenorhabditis elegans*	9.65	Cyclophilin-8	Protein folding
6	U1-70K	*Arabidopsis thaliana*	9.70	U1 small nuclear ribonucleoprotein 70 kDa	Pre-mRNA splicing
7	RSP41	*Arabidopsis thaliana*	10.26	Arginine/serine-rich splicing factor RSP41	Pre-mRNA splicing
8	CYL1	*Homo sapiens*	10.53	Cylicin I	Cytoskeletal protein
9	TRDN	*Oryctolagus cuniculus*	10.76	Triadin	Muscle contraction
10	TRDN	*Homo sapiens*	11.01	Triadin	Muscle contraction
11	RSP40	*Arabidopsis thaliana*	11.09	Arginine/serine-rich splicing factor RSP40	Pre-mRNA splicing
12	SURF6	*Mus musculus*	11.15	Surfeit locus protein 6 homolog	Ribosome biogenesis
13	CYL1	*Bos taurus*	11.37	Cylicin I	Cytoskeletal protein
14	SURF6	*Drosophila melanogaster*	11.44	Surfeit locus protein 6 homolog	Ribosome biogenesis
15	SURF6	*Xenopus laevis*	11.48	Surfeit locus protein 6 homolog	Ribosome biogenesis
16	M21	*Streptococcus pyogenes*	11.52	M protein, serotype 2.1 precursor	Virulence
17	RLX3	*Staphylococcus aureus*	11.72	RLX protein	Conjugation
18	RRP14	*Saccharomyces cerevisiae*	11.80	Ribosomal RNA-processing protein 14	Ribosome biogenesis
19	DEK	*Homo sapiens*	11.82	DEK protein	Pre-mRNA splicing
20	CG1785	*Drosophila melanogaster*	11.82	Nop53 ortholog	Ribosome biogenesis

MAS2 is not included in the PropSearch preprocessed database, which is based on Uniprot registers.

Supplemental Table 7. Identical or closely related putative homologs of Arabidopsis MAS2 and RRP7 found in PropSearch analyses

Protein	Organism	MAS2 homologs		RRP7 homologs		Function
		Rank	Distance	Rank	Distance	
ccdc-55	*Caenorhabditis elegans*	2	7.84	2	8.99	Pre-mRNA splicing
MPP8	*Homo sapiens*	3	9.44	18	11.11	Transcriptional silencing
SURF6	*Caenorhabditis elegans*	4	9.55	7	9.90	Ribosome biogenesis
U1-70K	*Arabidopsis thaliana*	6	9.70	13	10.61	Pre-mRNA splicing
RSP41	*Arabidopsis thaliana*	7	10.26	15	10.86	Pre-mRNA splicing
SURF6	*Mus musculus*	12	11.15	5	9.24	Ribosome biogenesis
SURF6	*Drosophila melanogaster*	14	11.44	1	8.62	Ribosome biogenesis
SURF6	*Xenopus laevis*	15	11.48	10	10.10	Ribosome biogenesis
SURF6	*Fugu rubripes*			4	9.16	Ribosome biogenesis
M21	*Streptococcus pyogenes*	16	11.52	14	10.72	Virulence
RLX3	*Staphylococcus aureus*	17	11.72	9	10.38	Conjugation

Supplemental Table 8. Oligonucleotides used in this work

Purpose		Oligonucleotide name(s)	Oligonucleotide sequence (5'→3')	
			Forward primer (F)	Reverse primer (R)
Genotyping of	*smo4-3*	NOP53_F1/R1[a]	GTCTCGAACTTTTTCCTTGGG	AGTATTCCTCGCTTCTCGAGG
	rrp7-1	RRP7_F1/R1	CTCATGAAGAACGCCTTGAAC	GTGGAGATCGTGGAGATGAAG
	rrp7-2	RRP7_F2/R2	ATGAAGGAGACGAGAAAGCTG	TGTGCAATCCTCATCGCCTGA
T-DNA insertion verification		Sail_LB1[b]	GCCTTTTCAGAAATGGATAAATAGCCTTGCTTCC	
		Salk_LBb1[c]	GCGTGGACCGCTTGCTGCAACT	
		WiscdDsloxp745[d]	AACGTCCGCAATGTGTTATTAAGTTGTC	
Double mutant genotyping		At4g02720_F2/R2[e]	AGGCGGAAGAAATCTTCGGATT	GCAAGTAGCAAACAGCAGTATC
		HDA6-7_F/R	TTTCTCAGGCATTGTTGACACAA	TATGAGCCATACGGATCCGGT
		PARL1_F/R	AGTTGCTGTCACCAAGAAG	TGGCCTACCATGGAATTCA
		NUC2_F/R	CGACGATGGATCTTCTTCGGA	TGGTTTAGCATTCTTAACAACTG
Verification of inserts in destination vectors		pMDC32_F1/R1[e]	TTCATTTGGAGAGGACCTCG	GAAATTCGAGCTCCACCGCG
		M13_F/R	GTTGTAAAACGACGGCCAGTG	GGAAACAGCTATGACCATGAT
		pMDC111R[e]		TATGTTGCATCACCTTCACCCT
		pMDC85R[e]		ATAATGATCAGCGAGTTGCAC
		pMDC164_F1/R1[e]	AAGACTGTAACCACGCGTCTG	TTGACTGCCTCTTCGCTGTAC
45S rDNA variant expression		p3/p4[f]	GACAGACTTGTCCAAAACGCCCACC	CTGGTCGAGGAATCCTGGACGATT
		OTC_F/R[g]	TGAAGGGACAAAGGTTGTGTATGTT	CGCAGACAAGTGGAATGGA
Probes for	RNA gel blots	S7[h]	GTCGTTCTGTTTTGGACAGGTATCGA	
		P42F/P43R[i]	GCCGGTTTCTTAGCCGATTCCTTGC	CACTTTTCGTGCCGGGGTTTTGTG
	in situ hybridization	18S rRNA[j]	FAM-TGTGAAACTGCGAATGGCTCATTAAATC	
		25S rRNA[k]	CY3-GAAAGACTAATCGAACCATCTAGTAGCT	
		5.8S rRNA[l]	DIG-CGTAGCGAAATGCGATAC	

[a-i]Sequences taken from [a]Micol-Ponce et al. (submitted), [b]http://signal.salk.edu/tdnaprimers.2.html, [c]https://www.gabi-kat.de/faq/vector-a-primer-info.html, [d]Woody et al. (2007), [e]Sánchez-García et al. (2015), [f]Pontvianne et al. (2010), [g]Shi et al. (2005), [h]Lange et al. (2011), and [i]Weis et al. (2015b). [j-l]Oligonucleotides labeled with [j]FAM (6-Carboxyfluorescein), [k]CY3 (Cyanine 3), and [l]DIG (Digoxigenin).

Supplemental Table 8 (continued). Oligonucleotides used in this work

Purpose		Oligonucleotide name(s)	Oligonucleotide sequence (5'→3')[m]	
			Forward primer (F)	Reverse primer (R)
Construction of transgenes	*35S$_{pro}$:RRP7*	RRP7-attB_F1/R1	*GGGGACAAGTTTGTACAAAAAAGCAGGCT*TGATGAAGGAGACGAGAAAGCTG	*GGGGACCACTTTGTACAAGAAAGCTGGGT*TTTAGAAAGGCTTAAACCTACGAG
	RRP7$_{pro}$:RRP7	RRP7-attB_F2/R2	*GGGGACAAGTTTGTACAAAAAAGCAGGCT*CAACACCTAACTTAACCATCTTC	*GGGGACCACTTTGTACAAGAAAGCTGGGT*TGTGTCAATCAGAGAATGCATCAG
	35S$_{pro}$:RRP7:GFP	RRP7-attB_R3[n]		*GGGGACCACTTTGTACAAGAAAGCTGGGT*AGAAAGGCTTAAACCTACGAG
	RRP7$_{pro}$:GUS	RRP7-attB_ R4[o]		*GGGGACCACTTTGTACAAGAAAGCTGGGT*CTTCTTTCTATCGCGTGAGAA
	SMO4$_{pro}$:GUS	NOP53-attB_F2/R4	*GGGGACAAGTTTGTACAAAAAAGCAGGCT*CAACACCTAACTTAACCATCTTC	*GGGGACCACTTTGTACAAGAAAGCTGGGT*TTTTCTCGTTATCTCTCGGC

[m]The *attB* sequences are shown in italics. [n-p]The [n]*35S$_{pro}$:RRP7:GFP* and [o]*RRP7$_{pro}$:GUS* constructs were obtained with the [n]RRP7-attB_F1/R3 and [o]RRP7-attB_F2/R4 primer pairs.

SUPPLEMENTAL REFERENCES

Aoki, Y., Okamura, Y., Tadaka, S., Kinoshita, K., and Obayashi, T. (2016). ATTED-II in 2016: A plant coexpression database towards lineage-specific coexpression. Plant Cell Physiol. **57,** e5.

Chaker-Margot, M., Barandun, J., Hunziker, M., and Klinge, S. (2017). Architecture of the yeast small subunit processome. Science **355,** aal1880.

Henras, A.K., Plisson-Chastang, C., O'Donohue, M.F., Chakraborty, A., and Gleizes, P.E. (2015). An overview of pre-ribosomal RNA processing in eukaryotes. Wiley Interdiscip. Rev. RNA **6,** 225-242.

Lange, H., Sement, F.M., and Gagliardi, D. (2011). MTR4, a putative RNA helicase and exosome co-factor, is required for proper rRNA biogenesis and development in *Arabidopsis thaliana*. Plant J. **68,** 51-63.

Larkin, M.A., Blackshields, G., Brown, N.P., Chenna, R., McGettigan, P.A., McWilliam, H., Valentin, F., Wallace, I.M., Wilm, A., Lopez, R., Thompson, J.D., Gibson, T.J., and Higgins, D.G. (2007). Clustal W and Clustal X version 2.0. Bioinformatics **23,** 2947-2948.

Lin, J., Lu, J., Feng, Y., Sun, M., and Ye, K. (2013). An RNA-binding complex involved in ribosome biogenesis contains a protein with homology to tRNA CCA-adding enzyme. PLoS Biol. **11,** e1001669.

Myburg, A.A., Grattapaglia, D., Tuskan, G.A., Hellsten, U., Hayes, R.D., Grimwood, J., Jenkins, J., Lindquist, E., Tice, H., Bauer, D., Goodstein, D.M., Dubchak, I., Poliakov, A., Mizrachi, E., Kullan, A.R., Hussey, S.G., Pinard, D., van der Merwe, K., Singh, P., van Jaarsveld, I., Silva-Junior, O.B., Togawa, R.C., Pappas, M.R., Faria, D.A., Sansaloni, C.P., Petroli, C.D., Yang, X., Ranjan, P., Tschaplinski, T.J., Ye, C.Y., Li, T., Sterck, L., Vanneste, K., Murat, F., Soler, M., Clemente, H.S., Saidi, N., Cassan-Wang, H., Dunand, C., Hefer, C.A., Bornberg-Bauer, E., Kersting, A.R., Vining, K., Amarasinghe, V., Ranik, M., Naithani, S., Elser, J., Boyd, A.E., Liston, A., Spatafora, J.W., Dharmwardhana, P., Raja, R., Sullivan, C., Romanel, E., Alves-Ferreira, M., Kulheim, C., Foley, W., Carocha, V., Paiva, J., Kudrna, D., Brommonschenkel, S.H., Pasquali, G., Byrne, M., Rigault, P., Tibbits, J., Spokevicius, A., Jones, R.C., Steane, D.A., Vaillancourt, R.E., Potts, B.M., Joubert, F., Barry, K., Pappas, G.J., Strauss, S.H., Jaiswal, P., Grima-Pettenati, J., Salse, J., Van de Peer, Y., Rokhsar, D.S., and Schmutz, J. (2014). The genome of *Eucalyptus grandis*. Nature **510,** 356-362.

Pontvianne, F., Abou-Ellail, M., Douet, J., Comella, P., Matia, I., Chandrasekhara, C., Debures, A., Blevins, T., Cooke, R., Medina, F.J., Tourmente, S., Pikaard, C.S., and Saez-Vasquez, J. (2010). Nucleolin is required for DNA methylation state and the expression of rRNA gene variants in *Arabidopsis thaliana*. PLoS Genet. **6,** e1001225.

Sánchez-García, A.B., Aguilera, V., Micol-Ponce, R., Jover-Gil, S., and Ponce, M.R. (2015). Arabidopsis *MAS2*, an essential gene that encodes a homolog of animal NF-kappa B activating protein, is involved in 45S ribosomal DNA silencing. Plant Cell **27,** 1999-2015.

Schillewaert, S., Wacheul, L., Lhomme, F., and Lafontaine, D.L. (2012). The evolutionarily conserved protein Las1 is required for pre-rRNA processing at both ends of ITS2. Mol. Cell. Biol. **32,** 430-444.

Shi, D.Q., Liu, J., Xiang, Y.H., Ye, D., Sundaresan, V., and Yang, W.C. (2005). SLOW WALKER1, essential for gametogenesis in Arabidopsis, encodes a WD40 protein involved in 18S ribosomal RNA biogenesis. Plant Cell **17,** 2340-2354.

Weis, B.L., Kovacevic, J., Missbach, S., and Schleiff, E. (2015a). Plant-specific features of ribosome biogenesis. Trends Plant Sci. **20,** 729-740.

Weis, B.L., Palm, D., Missbach, S., Bohnsack, M.T., and Schleiff, E. (2015b). atBRX1-1 and atBRX1-2 are involved in an alternative rRNA processing pathway in *Arabidopsis thaliana*. RNA **21,** 415-425.

Woody, S.T., Austin-Phillips, S., Amasino, R.M., and Krysan, P.J. (2007). The WiscDsLox T-DNA collection: an arabidopsis community resource generated by using an improved high-throughput T-DNA sequencing pipeline. J. Plant Res. **120,** 157-165.

Zakrzewska-Placzek, M., Souret, F.F., Sobczyk, G.J., Green, P.J., and Kufel, J. (2010). *Arabidopsis thaliana* XRN2 is required for primary cleavage in the pre-ribosomal RNA. Nucleic Acids Res. **38,** 4487-4502.

Supplemental Dataset 1. Top 100 ranking genes coexpressed with *RRP7* or *MAS2* , identified by ATTED-II

Supplemental Dataset 1A. Genes coexpressed with *RRP7*

Supportability and Mutual Rank (MR) are used here as defined in Aoki et al. (2015).
Original short descriptions for genes were extended using the HomoloGene and Aramemnon databases.
Predictions of subcellular localizations in the Target column are shown as indicated in http://atted.jp/help/term.shtml#s

Rank	Locus	Short description	Supportability	MR	Target
0	At5g38720	RRP7 homolog	☆☆	0.0	O,N
1	At3g01160	Putative (yeast ESF1)-like pre-rRNA processing protein	☆☆	2.2	O,N
2	At2g19385	Putative (mammal LYAR)-like nucleolar protein of unknown function	☆☆	2.8	O,N
3	**At2g40430**	**NOP53 homolog (SMO4)**	**☆☆**	**3.2**	**O,N**
4	At2g18220	Putative (yeast Noc2)-like protein	☆☆☆	4.7	O,N
5	At4g25340	FK506 BINDING PROTEIN 53	☆☆	7.2	O,N
6	At5g54910	RH32, putative DEAD/DEAH-box-type helicase	☆☆	7.5	O,Y
7	At4g02400	Putative (yeast UTP14)-like nucleolar component of U3 processome complex	☆☆☆	7.8	O,N
8	At3g62940	Similar to human OTUD6B, a member of the ovarian tumor domain (OTU)-containing subfamily of deubiquitinating enzymes	☆☆	9.2	O,N
9	At3g10530	Putative (yeast UTP7)-like nucleolar component of U3 processome complex	☆☆☆	9.5	O,N
10	At1g80750	60S ribosomal protein L7 (RPL7A), similar to human ribosomal protein L7	☆☆☆	10.2	O,Y
11	At3g12340	FKBP-type peptidyl-prolyl isomerase (AtFKBP43)	☆☆	10.7	O,N
12	At3g13940	Subunit of TFIf-type RNA polymerase I basal transcription factor (AtC49)	☆☆	14.3	O,Y
13	At5g57120	Putative (yeast SRP40)-like protein of unknown function, with weak similarity to human Nucleolar phosphoprotein p130 (NOLC1)	☆☆	14.4	O,N
14	At3g20430	Putative snRNA nuclear export protein	☆	15.1	O,N
15	At3g49990	Unknown protein	☆☆	15.5	O,N
16	At3g57000	Putative Nep1-like methyltransferase involved in ribosome biogenesis	☆☆	15.9	O,Y
17	At5g55920	OLI2. Similar to human Proliferation-associated nucleolar protein p120 and Saccharomyces cerevisiae Nucleolar protein NOP2	☆☆☆	16.0	M,N
18	At2g37990	Ribosome biogenesis regulatory protein (RRS1) family protein	☆☆☆	16.4	O,N
19	At3g55510	Putative (yeast Noc2)-like protein required for flower development, REBELOTE (AtRBL)	☆☆☆	17.6	O,C
20	At5g62440	Protein of unknown function (DUF3223)	☆☆	17.9	O,N

21	At3g15080	Similar to human REX4 homolog, 3,-5, exonuclease. Rex4 is involved in processing of ITS1 in Saccharomyces cerevisiae pre-rRNA	☆☆	18.0	C,N
22	At5g40530	Similar to human and yeast RNA processing 8, methyltransferase, involved in the modification of 25S rRNA	☆	18.5	O,N
23	At4g05410	Putative (yeast Rrp9)-like nucleolar component of U3 processome complex (AtYAO1)	☆☆	20.1	O,N
24	At1g79150	NOC3, putative (yeast Noc3)-like protein associated with U3 processome complex	☆☆☆	20.5	O,C
25	At5g50840	Unknown protein	☆	20.7	O,N
26	At5g17930	Similar to human nucleolar NOM1, RNA export mediator	☆☆	20.9	O,N
27	At5g22320	Leucine-rich repeat (LRR) family protein	☆☆	21.3	O,N
28	At5g67240	SDN3, small RNA degrading nuclease 3. Similar to human REXO4, 3'-5' exonuclease	☆☆	21.9	O,Y
29	At3g05060	NOP56-like pre RNA processing ribonucleoprotein, putative component of C/D snoRNP complex (AtNOP58-2/AtNOP5-2)	☆☆☆	22.6	O,Y
30	At3g16810	PUM24, protein of unknown function, contains pumilio/Puf RNA-binding domain	☆☆☆	23.7	O,N
31	At5g61330	Unknown protein, contains weak similarity to Saccharomyces cerevisiae rRNA processing protein EBP2 (EBNA1-binding protein homolog) and human apoptosis antagonizing transcription factor AATF	☆☆	23.8	O,N
32	At1g12830	Unknown protein	☆☆	24.7	O,N
33	At5g15750	Putative (yeast Imp3)-like nucleolar component of U3 processome complex	☆☆	27.5	O,Y
34	At2g34570	MEE21, putative (yeast Fcf1)-like pre-rRNA processing protein	☆☆	27.7	M,M
35	At5g61770	PPAN, PETER PAN-like protein. Similar to human nucleolar PPAN and SSF1 and SSF2 rRNA-binding ribosome biosynthesis proteins of Saccharomyces cerevisiae	☆☆☆	27.9	O,N
36	At1g13160	Putative SDA1-like protein of unknown function, required for actin cytoskeleton	☆☆☆	28.0	O,Y
37	At2g31725	DUF842	☆☆	28.1	O,C
38	At5g52380	VASCULAR-RELATED NAC-DOMAIN 6	☆☆	28.5	O,N
39	At1g03360	Putative (yeast Rrp4)-like component of exosome complex	☆☆	29.9	M,C
40	At3g16840	RH13, Putative DEAD/DEAH-box-type helicase. Similar to yeast MAK5, involved in 60S subunit biogenesis	☆☆☆	30.2	O,N
41	At3g21540	Putative (yeast UTP12)-like nucleolar component of U3 processome complex	☆☆☆	32.6	O,Y
42	At3g22660	EBP2, putative rRNA processing protein involved in ribosome biogenesis	☆☆☆	33.0	O,N
43	At4g25730	Similar to yeast SPB1, 27S pre-rRNA (guanosine2922-2'-O)-methyltransferase. Required for 60S ribosomal subunit biogenesis in Saccharomyces cerevisiae	☆☆☆	33.2	O,
44	At5g05210	SURF6, Surfeit locus 6, putative nucleolar matrix protein	☆☆	33.8	O,N
45	At2g21440	Similar to yeast NOP4, nucleolar protein required for pre-rRNA processing and accumulation of 60S ribosomal subunits	☆☆	34.6	O,N
46	At1g43860	Putative (yeast Sdo1)-like ribosome biogenesis factor. Control translational activation of ribosomes		35.2	M,C
47	At2g34780	MEE22, unknown protein	☆☆	35.4	O,N
48	At2g45730	Putative (yeast TRM6)-like component of TRM61-TRM6 tRNA adenine-methyltransferase complex	☆☆	35.8	O,Y
49	At1g06720	Putative (yeast Bms1)-like protein of unknown function	☆☆☆	35.9	O,N

50	At1g69070	Putative (yeast UTP2/Nop14)-like nucleolar component of U3 processome complex	☆☆☆	36.3	O,Y
51	At3g60360	UTP11/EDA14, putative (yeast UTP11)-like nucleolar component of U3 processome complex	☆☆☆	36.5	O,N
52	At1g30960	ERA2/ERG, putative (bacteria Era)-like GTPase	☆☆	36.7	M,C
53	At1g12650	Similar to RRP36 exosome nuclease subunit	☆☆	37.4	O,N
54	At3g58660	Putative L1-type protein of large ribosomal subunit	☆☆☆	37.4	C,Y
55	At1g80270	PPR596, protein of unknown function with pentatricopeptide (PPR) repeats	☆☆☆	38.4	M,M
56	At2g18330	Putative AAA-type ATPase associated with unknown cellular activities	☆☆	38.4	C,C
57	At5g50310	Unknown protein, similar to KLHDC4	☆☆	38.6	O,N
58	At3g12270	PRMT3, putative ribosomal protein methyltransferase	☆☆	39.2	O,Y
59	At5g51130	Similar to human MEPCE, methylphosphate capping enzyme. Human MePCE is involved in stabilizing 7SK snRNA and facilitating the assembly of 7SK snRNP	☆	39.2	O,N
60	At3g23620	Similar to RPF2, ribosome production factor 2 homolog (Saccharomyces cerevisiae). Assembly factors Rpf2 recruit 5S rRNA and ribosomal proteins rpL5 and rpL11 into nascent ribosomes	☆☆☆	39.5	O,N
61	At1g52930	Similar to BRX1, biogenesis of ribosomes, homolog (Saccharomyces cerevisiae). 60S ribosomal subunit assembly in Saccharomyces cerevisiae.	☆☆☆	39.7	O,N
62	At2g34260	Similar to human WDR55, WD repeat domain 55. Defects in nucleolar WDR55 cause aberrant accumulation of rRNA intermediates and cell cycle arrest	☆☆☆	40.6	O,Y
63	At4g37090	Unknown protein	☆☆	40.6	O,N
64	At5g14440	SURF2, Surfeit locus protein 2	☆☆	40.7	O,N
65	At5g50315	Mutator-like transposaseMuDR family		40.8	
66	At3g56120	Putative TRMT5, tRNA methyltransferase 5	☆	41.4	O,Y
67	At5g66540	Putative (yeast Mpp10)-like nucleolar component of U3 processome complex	☆☆☆	41.5	O,Y
68	At5g18440	NUFIP, putative (human NUFIP1)-like protein, controls biogenesis of snoRNPs and scaRNPs	☆☆	41.6	M,N
69	At4g01990	Protein of unknown function, contains pentatricopeptide (PPR) repeats	☆☆	42.3	M,M
70	At1g23280	MAK16, required for the maturation of 25S and 5.8S rRNAs in the yeast Saccharomyces cerevisiae	☆☆	42.6	O,Y
71	At1g60850	RPAC42, putative component of DNA-dependent RNA polymerase I complex	☆☆☆	42.8	O,Y
72	At3g58840	PMD1, protein involved in peroxisomal and mitochondrial proliferation	☆☆	43.4	O,Y
73	At1g56110	NOP56, putative component of C/D snoRNP complex	☆☆☆	43.6	O,N
74	At1g13030	Unknown protein	☆☆	44.0	O,N
75	At1g72440	SWA2/EDA25, putative (yeast Noc1)-like protein associated with U3 processome complex	☆☆	44.1	S,N
76	At3g61620	RRP41, putative (yeast Rrp46)-like PH-type ribonuclease of exosome complex	☆☆	44.7	O,Y
77	At1g11240	Putative (yeast ESF1)-like pre-rRNA processing protein, required for 18S rRNA synthesis in Saccharomyces cerevisiae	☆☆	44.8	O,N
78	At5g57280	RID2, putative methyltransferase involved in pre-rRNA processing. Similar to yeast BUD23 and human WBSCR22 (Williams Beuren syndrome chromosome region 22)	☆☆	45.0	O,N

79	At1g72050	TFIIIa, putative RNA polymerase TFIIIa transcription factor	☆☆	45.2	O,N
80	At5g27395	Tim44, mitochondrial inner membrane translocase complex	☆☆	45.6	M,M
81	At5g65900	RH27, putative DEAD/DEAH-box-type helicase. Similar to yeast Has1p and human DDX18. Has1p is required for snoRNA release from pre-rRNA and 40S ribosomal subunit biogenesis	☆☆	45.6	O,N
82	At2g34357	Similar to human and yeast RRP12, ribosomal RNA processing 12 homolog, required for export of both ribosomal subunits	☆☆☆	45.8	O,N
83	At3g24080	Putative (yeast Kri1)-like protein, required for 40S ribosome biogenesis	☆☆	46.5	O,N
84	At5g19300	Unknown protein. Similar to human C9orf114 (chromosome 9 open reading frame 114)	☆☆	46.5	O,Y
85	At5g16750	TOZ, TORMOZ. Putative (yeast UTP13)-like ribosome biogenesis factor of SSU processome	☆☆☆	48.0	M,C
86	At1g06380	Putative L1-type protein of large ribosomal subunit	☆☆	49.6	C,C
87	At3g57150	NAP57, putative TruB-type tRNA pseudouridine synthase of H/ACA ribonucleoprotein complex	☆☆	50.2	O,Y
88	At1g04190	TPR3, putative CC-TPR-type co-chaperone-like protein	☆	51.0	O,M
89	At1g13120	GLE1, putative scaffold nucleoporin of outer ring of nuclear pore complex	☆	53.3	O,Y
90	At5g14050	Similar to human and yeast UTP18 small subunit (SSU) processome component	☆☆☆	53.3	O,N
91	At3g11964	S1 RNA-binding domain-containing protein, similar to SP:Q05022 rRNA biogenesis protein RRP5 of Saccharomyces cerevisiae	☆☆☆	53.7	O,C
92	At5g12220	Putative Las1-like protein	☆☆	53.9	O,N
93	At3g02320	Similar to human and yeast TRMT1, RNA methyltransferase 1	☆☆	53.9	O,N
94	At2g40360	Similar to human BOP1 and yeast ERB1, required for maturation of the 25S and 5.8S ribosomal RNAs	☆☆☆	54.0	O,N
95	At1g08580	Unknown protein	☆☆	55,1	O,N
96	At2g44510	Similar to protein-transporting protein BCP1 of Saccharomyces cerevisiae, involved in ribosomal large subunit export from nucleus	☆☆	55,2	M,M
97	At1g76120	Similar to human and yeast PUS1, pseudouridylate synthase 1. Pus1p exhibits a dual substrate specificity for U2 snRNA and tRNA.	☆	55,7	O,Y
98	At3g56510	Putative (yeast ESF12)-like U3 snoRNP-associated protein	☆☆	56	O,N
99	At2g25355	Similar to human EXOSC3, exosome component 3 and yeast exosome subunit Rrp40	☆☆	56,5	O,N
100	At4g38890	Similar to yeast DUS3, dihydrouridine synthase 3, required for dihydrouridine modification of tRNA	☆☆	56,5	O,N

Supplemental Dataset 1. Top 100 ranking genes coexpressed with *RRP7* or *MAS2* , identified by ATTED-II

Supplemental Dataset 1B. Genes coexpressed with *RRP7* and *SMO4*

Locus	Short description
At1g04190	TPR3, putative CC-TPR-type co-chaperone-like protein
At1g06720	Putative (yeast Bms1)-like protein of unknown function
At1g11240	Putative (yeast ESF1)-like pre-rRNA processing protein, required for 18S rRNA synthesis in Saccharomyces cerevisiae
At1g12650	Similar to yeast and human RRP36, involved in early cleavages of the pre-rRNA and production of the 40S ribosomal subunit
At1g12830	Unknown protein
At1g13160	Putative SDA1-like protein of unknown function, required for actin cytoskeleton
At1g23280	MAK16, required for the maturation of 25S and 5.8S rRNAs in the yeast Saccharomyces cerevisiae
At1g56110	NOP56, putative component of C/D snoRNP complex
At1g69070	Putative (yeast UTP2/Nop14)-like nucleolar component of U3 processome complex
At1g72050	TFIIIa, putative RNA polymerase TFIIIa transcription factor
At1g72440	SWA2/EDA25, putative (yeast Noc1)-like protein associated with U3 processome complex
At1g79150	NOC3, putative (yeast Noc3)-like protein associated with U3 processome complex
At1g80750	60S ribosomal protein L7 (RPL7A), similar to human ribosomal protein L7
At2g18220	Putative (yeast Noc2)-like protein
At2g21440	Similar to yeast NOP4, nucleolar protein required for pre-rRNA processing and accumulation of 60S ribosomal subunits
At2g34357	Similar to human and yeast RRP12, ribosomal RNA processing 12 homolog, required for export of both ribosomal subunits
At2g37990	Ribosome biogenesis regulatory protein (RRS1) family protein
At2g40430	NOP53 homolog
At3g01160	Putative (yeast ESF1)-like pre-rRNA processing protein
At3g05060	NOP56-like pre RNA processing ribonucleoprotein, putative component of C/D snoRNP complex (AtNOP58-2/AtNOP5-2)
At3g10530	Putative (yeast UTP7)-like nucleolar component of U3 processome complex
At3g11964	S1 RNA-binding domain-containing protein, similar to SP:Q05022 rRNA biogenesis protein RRP5 of Saccharomyces cerevisiae
At3g16840	RH13, Putative DEAD/DEAH-box-type helicase. Similar to yeast MAK5, involved in 60S subunit biogenesis
At3g20430	Putative snRNA nuclear export protein
At3g22660	EBP2, putative rRNA processing protein involved in ribosome biogenesis
At3g24080	Putative (yeast Kri1)-like protein, required for 40S ribosome biogenesis
At3g49990	Unkown protein
At3g56120	Putative TRMT5, tRNA methyltransferase 5

At3g56510	Putative (yeast ESF12)-like U3 snoRNP-associated protein
At3g57000	Putative Nep1-like methyltransferase involved in ribosome biogenesis
At3g57150	NAP57, putative TruB-type tRNA pseudouridine synthase of H/ACA ribonucleoprotein complex
At3g58660	Putative L1-type protein of large ribosomal subunit
At3g58840	PMD1, protein involved in peroxisomal and mitochondrial proliferation
At4g02400	Putative (yeast UTP14)-like nucleolar component of U3 processome complex
At4g25340	FK506 BINDING PROTEIN 53
At4g25730	Similar to yeast SPB1, 27S pre-rRNA (guanosine2922-2'-O)-methyltransferase. Required for 60S ribosomal subunit biogenesis in Saccharomyces cerevisiae
At4g38890	Similar to yeast DUS3, dihydrouridine synthase 3, required for dihydrouridine modification of tRNA
At5g05210	SURF6, Surfeit locus 6, putative nucleolar matrix protein
At5g14440	SURF2, Surfeit locus protein 2
At5g16750	TOZ, TORMOZ. Putative (yeast UTP13)-like ribosome biogenesis factor of SSU processome
At5g17930	Similar to human nucleolar NOM1, RNA export mediator
At5g22320	Leucine-rich repeat (LRR) family protein
At5g38720	**RRP7 homolog**
At5g40530	Similar to human and yeast RNA processing 8, methyltransferase, involved in the modification of 25S rRNA
At5g50310	Unknown protein, similar to KLHDC4
At5g50840	Unknown protein
At5g54910	RH32, putative DEAD/DEAH-box-type helicase
At5g55920	OLI2. Similar to human Proliferation-associated nucleolar protein p120 and Saccharomyces cerevisiae Nucleolar protein NOP2
At5g57120	Putative (yeast SRP40)-like protein of unknown function, with weak similarity to human Nucleolar phosphoprotein p130 (NOLC1)
At5g61330	Unknown protein, contains weak similarity to Saccharomyces cerevisiae rRNA processing protein EBP2 (EBNA1-binding protein homolog) and human apoptosis antagonizing transcription factor AATF
At5g61770	PPAN, PETER PAN-like protein. Similar to human nucleolar PPAN and SSF1 and SSF2 rRNA-binding ribosome biosynthesis proteins of Saccharomyces cerevisiae
At5g62440	Protein of unknown function (DUF3223)
At5g67240	SDN3 small RNA degrading nuclease 3. Similar to human REXO4, 3'-5' exonuclease

Supplemental Dataset 1. Top 100 ranking genes coexpressed with *RRP7* or *MAS2* , identified by ATTED-II

Supplemental Dataset 1C. Genes coexpressed with *MAS2*

Supportability and Mutual Rank (MR) are used here as defined in Aoki et al. (2015).
Original short descriptions for genes were extended using the HomoloGene and Aramemnon databases.
Predictions of subcellular localizations in the Target column are shown as indicated in http://atted.jp/help/term.shtml#s

Rank	Locus	Short description	Supportability	MR	Target
0	At4g02720	MAS2	☆	0.0	M,N
1	At3g54540	GCN4, general control non-repressible 4. Similar to human ABCF1, ATP-binding cassette, sub-family F (GCN20), member 1. ABCF1 is s a critical protein that associates with viral double-stranded DNA, and promotes translation initiation in mammalian cells	☆	1.4	O,N
2	At5g41770	CRN1cMAC10, putative associated component of spliceosome-associated MAC complex. Similar to yeast cwf4 and human CRNKL1, crooked neck pre-mRNA splicing factor 1	☆	2.0	O,Y
3	At2g26990	FUS12/CSN2, putative subunit 2-like component of COP9 signalosome complex. putative subunit 2-like component of COP9 signalosome complex,	☆	3.5	O,Y
4	At3g06400	CHR11, putative ATP-dependent chromatin remodeling factor. Similar to yeast ISW1 and human SMARCA5 (SWI/SNF related, matrix associated, actin dependent regulator of chromatin, subfamily a, member 5) . Isw1 acts independently of the Isw1a and Isw1b complexes in regulating transcriptional silencing at the ribosomal DNA locus in Saccharomyces cerevisiae	☆☆	6.7	O,Y
5	At4g10710	SPT16, putative (yeast SPT16)-like component of FACT histone chaperone complex. Rpd3- and spt16-mediated nucleosome assembly and transcriptional regulation on yeast ribosomal DNA genes	☆☆	7.1	O,Y
6	At1g15340	MBD10, putative mediator of chromatin cytosine methylation, required for nucleolar dominance	☆	7.1	O,N
7	At3g26560	Similar to human DHX8/HRH1 and yeast PRP22. HRH1, facilitates nuclear export of spliced mRNA by releasing the RNA from the spliceosome	☆	7.9	O,Y
8	At2g16860	Putative SYF2-type pre-mRNA splicing factor	☆☆	8.0	O,N
9	At1g03910	CACTIN, an essential nuclear protein in Arabidopsis and may be associated with the spliceosome	☆☆	8.4	C,N
10	At5g55300	TOP1ALPHA/MGO1, putative Topo-Ib monomeric DNA topoisomerase. Similar to human and yeast TOP1. DNA topoisomerase I alpha (Promotes Transcriptional Silencing of Transposable Elements through DNA Methylation and Histone Lysine 9 Dimethylation in Arabidopsis).	☆☆	9.8	O,N
11	At1g65660	SMP1, similar to human an yeast SLU7 splicing factor. Pre-mRNA splicing Prp18-interacting factor	☆☆	10.5	O,N
12	At1g80930	MIF4G domain-containing protein/MA3 domain-containing protein. Similar to human and yeast cwf22 that connects pre-mRNA splicing and exon junction complex assembly	☆☆	11.2	O,N
13	At1g16210	Protein of unknown function (DUF1014)	☆	11.8	O,N

14	At1g31870	Similar to yeast BUD13, integranting of the pre-mRNA retention and splicing complex	☆☆	11.8	O,N
15	At3g12140	EML1, putative EMSY-type protein of unknown function. EMSY-like genes are required for full RPP7-mediated race-specific immunity and basal defense in Arabidopsis	☆	12.6	O,G
16	At5g49930	EMB1441, putative (bacteria FbpA)-like protein of unknown function	☆☆	13.5	O,Y
17	At2g39260	UPF2, putative peripheral component of mRNA quality control exon junction complex	☆☆	13.9	O,N
18	At4g37120	SMP2, similar to human an yeast SLU7 splicing factor. Pre-mRNA splicing Prp18-interacting factor	☆☆	14.0	O,N
19	At5g53800	Unknown protein	☆☆	14.4	O,N
20	At1g02330	Similar to humanC90rf78, chromosome 9 open reading frame 78	☆	15.8	O,N
21	At1g48900	SRP-54C, SRP54-type protein subunit of signal recognition particle	☆	15.9	O,Y
22	At4g21710	RPB2, putative component of DNA-dependent RNA polymerase II complex	☆☆	16.9	O,N
23	At1g17070	STIPL1, spliceosomal timekeeper locus1	☆	17.0	O,V
24	At1g06530	PMD2, putative PMD1-like protein of unknown function	☆☆	17.0	O,
25	At5g25070	Unknown protein	☆	17.3	O,Y
26	At3g54190	Transducin/WD40 repeat-like superfamily protein		17.6	C,C
27	At2g20280	C3H21, protein of unknown function, contains CCCH-type zinc ion binding domain	☆	19.0	O,N
28	At5g16780	Putative (yeast SART-1)-like component of U4/U6 x U5 tri-snRNP complex	☆☆	19.4	O,N
29	At1g76810	Putative type 2 translation initiation factor eIF-2	☆☆	19.6	O,Y
30	At4g11160	Similar to MTIF2, mitochondrial translational initiation factor 2	☆	20.1	C,C
31	At3g22220	Unknown protein	☆	20.4	O,N
32	At3g59990	MAP2B, putative methionine aminopeptidase	☆	21.4	O,N
33	At3g09850	Unknown protein, contains single-stranded nucleic acid binding domain. Similar to tuftelin interacting protein 11, a splicing factor involved in spliceosome disassembly	☆	21.6	C,N
34	At3g22170	FHY3, FAR-RED ELONGATED HYPOCOTYLS 3. Component of PHYA signaling network	☆	21.6	O,N
35	At4g31880	PDS5c, putative cell cycle cohesin cofactor	☆☆	23.0	O,N
36	At1g55460	Kin17, similar to human KIN (antigenic determinant of recA protein)	☆☆	23.4	O,N
37	At5g44080	bZIP13, putative bZIP-type transcription factor	☆	23.6	C,N
38	At5g49880	MAD1, putative Mad1-like core mitotic spindle checkpoint protein. Mitosis-specific regulation of nuclear transport by the spindle assembly checkpoint protein Mad1p.	☆	25.1	M,C
39	At1g09770	CDC5/AtMAC1, putative core component of spliceosome-associated MAC complex	☆☆☆	25.3	O,Y
40	At3g18790	MAC8/ISY1, putative associated component of spliceosome-associated MAC complex	☆☆	26.1	O,N
41	At2g16640	TOC132, GTP-binding chloroplast protein import receptor	☆	26.5	O,N
42	At3g53110	LOS4, putative DEAD/DEAH-box-type helicase involved in export of poly A RNA	☆	27.7	O,Y
43	At2g33730	RH21, putative DEAD/DEAH-box-type helicase. Similar to human DDX23 and yeast prp28 (U5 snRNP-associated protein Prp28)	☆	29.7	O,Y
44	At5g13970	Unknown protein	☆	30.1	S,N

45	At5g52040	RS41, putative non-snRNP SR-type splicing factor	☆☆	31.3	O,N
46	At5g65260	PABN1, putative component of mRNA polyadenylation complex	☆	31.9	O,N
47	At1g26830	CUL3A, cullin component of SCF-type ubiquitin-protein ligase complex	☆☆	32.2	O,Y
48	At5g67250	VFB4/SKIP2, ubiquitin-protein ligase, F-box family/subfamily C	☆	32.3	O,Y
49	At3g18640	C3H38, protein of unknown function, contains CCCH-type zinc ion binding domain. Zinc finger C-x8-C-x5-C-x3-H type family protein.	☆	32.4	O,N
50	At5g65720	NIFS1, putative cysteine desulfurase of ISC-type iron-sulfur-cluster assembly	☆	32.7	M,Y
51	At1g74250	DNAJ heat shock N-terminal domain-containing protein	☆☆	33.5	O,N
52	At4g05420	DDB1A, putative ubiquitin ligase E3 of COP10-DDB1-DET1 (CDD) ubiquitylation complex	☆	34.7	O,Y
53	At3g24490	Putative Trihelix-type transcription factor Myb/SANT-like	☆	35.1	O,N
54	At1g69670	CUL3B, cullin component of SCF-type ubiquitin-protein ligase complex	☆	35.2	O,Y
55	At1g32130	IWS1, putative component of RNA polymerase II complex	☆☆	35.8	O,N
56	At2g27285	DUF2040. Coiled-coil domain-containing protein 55 (DUF2040).	☆☆	36.0	M,C
57	At3g19760	EIF4A-III/HNI9, putative component of RNA polymerase II complex	☆	36.4	O,Y
58	At3g02760	Putative aminoacyl-tRNA synthetase	☆☆	36.5	C,C
59	At5g62390	BAG7, BAG-type chaperone regulator	☆	36.9	O,Y
60	At5g16260	ELF9, RNA binding protein, targeting SOC1 transcript. Similar to yeast U2 snRNP-associated protein Uap2	☆	37.4	O,N
61	At5g46070	Similar to human guanylate binding protein 1, actin cytoskeleton remodeling factor	☆☆	37.5	M,Y
62	At5g37380	Chaperone DnaJ-domain superfamily protein	☆	37.8	O,N
63	At5g55310	TOP1BETA, DNA topoisomerase 1 beta	☆☆	37.9	O,N
64	At1g03350	Protein of unknown function, contains BSD-type domain	☆	37.9	O,N
65	At4g32620	Enhancer of polycomb-like transcription factor protein	☆☆	38.9	O,N
66	At1g15200	Putative (mammal pinin)-like protein of unknown function	☆☆	39.2	O,N
67	At1g28060	Putative PRP3-like pre-mRNA processing factor. Yeas PRP3 participates in pre-mRNA splicing and in nuclear mRNA export	☆☆	40.0	O,N
68	At5g05210	Surfeit locus protein 6, nucleolar matrix protein-related	☆☆	41.3	O,N
69	At1g17130	Similar to cell cycle control protein cwf16 of Schizosaccharomyces pomb, which is involved in mRNA splicing where it associates with cdc5 and the other cwf proteins as part of the spliceosome	☆	45.7	O,N
70	At4g08310	Protein of unknown function, contains histone chaperone domain CHZ	☆☆	46.0	O,N
71	At3g11910	UBP13, ubiquitin-specific protease 13	☆☆	48.2	O,Y
72	At1g50660	Unknown protein	☆	49.6	C,N

73	At4g11420	TIF3A1, eukaryotic translation initiation factor 3A. EIF3A is required for several steps in the initiation of protein synthesis. The eIF-3 complex associates with the 40S ribosome and facilitates the recruitment of eIF-1, eIF-1A, eIF-2:GTP:methionyl-tRNAi and eIF-5 to form the 43S pre-initiation complex (43S PIC). The eIF-3 complex stimulates mRNA recruitment to the 43S PIC and scanning of the mRNA for AUG recognition. The eIF-3 complex is also required for disassembly and recycling of post-termination ribosomal complexes and subsequently prevents premature joining of the 40S and 60S ribosomal subunits prior to initiation	☆☆	51.4	O,Y
74	At5g65770	LINC4, little nuclei4. Putative lamin-like protein involved in nucleus organization	☆☆	52.4	C,C
75	At5g20170	MED17, (yeast MED17)-like component of Mediator transcriptional regulatory complex	☆	52.6	O,N
76	At1g67230	LINC1, little nuclei1. Putative lamin-like protein involved in nucleus organization	☆☆	55.5	M,C
77	At3g07740	HXA2/ADA2a, putative component of SAGA transcription regulation complex. Similar to yeast ADA2a that interacts with histone acetyltransferase GCN5 homolog and CBF1	☆	56.5	O,C
78	At5g28740	MAC9/SYF1, putative associated component of spliceosome-associated MAC complex	☆	58.2	O,Y
79	At5g50310	Protein of unknown function, similar to human KLHDC4 (kelch domain containing 4)	☆☆	58.6	O,N
80	At1g79940	ERDJ2A, DnaJ / Sec63 Brl domains-containing protein. Putative Sec63 component of Sec translocation system	☆☆	59.6	S,P
81	At1g20960	EMB1507, similar to human SNRNP200 and yeast BRR2 required for RNA unwinding in U4/U6 snRNPs	☆☆	60.1	M,Y
82	At3g58840	PMD1, protein involved in peroxisomal and mitochondrial proliferation	☆☆	60.2	O,Y
83	At1g71080	RNA polymerase II transcription elongation factor		60.7	O,N
84	At3g56150	TIF3C1, putative subunit eIF3c of eukaryotic translation initiation factor 3 complex	☆☆	60.7	O,N
85	At1g05150	Putative N-acetyl glucosamine transferase	☆	60.8	O,C
86	At2g14120	DRP3B/ADL2b, dynamin-like organelle fission mediator	☆	60.9	C,N
87	At5g55670	RNA-binding protein. Weak similarity to human CPSF6 (cleavage and polyadenylation specific factor 6)	☆	61.5	O,N
88	At5g53440	Unknown protein	☆☆	61.5	O,N
89	At5g47680	TRM10, tRNA modification 10. Putative tRNA (guanine-N(1)-)-methyltransferase	☆☆	61.5	O,N
90	At2g32260	CCT1, phosphorylcholine cytidylyltransferase	☆	61.5	O,Y
91	At5g13020	EML3, putative EMSY-type protein of unknown function	☆	63.4	O,N
92	At4g27120	Protein of unknown function, contains DDRGK motif	☆	64.0	S,P
93	At1g50200	ALATS, Alanyl-tRNA synthetase	☆☆	64.7	C,C
94	At1g61040	VIP5, VERNALIZATION INDEPENDENCE 5. Encodes a yeast Paf1C subunit homolog required for the expression of the MADS box gene FLC and other members of the FLC/MAF MADS-box gene family	☆	65.5	C,N
95	At4g36690	U2AF65A, U2 snRNP auxilliary factor, large subunit, splicing factor	☆☆	66.7	O,N
96	At2g02570	Putative (animal SPF30)-like protein of unknown function	☆	67.1	O,N
97	At5g06910	J6, putative Hsp40/DnaJ-type molecular chaperone		67.5	O,N
98	At5g04240	ELF6/PKDM9b, EARLY FLOWERING 6, putative JmjC-type histone demethylase	☆☆	68.2	O,C
99	At2g17410	Unknown protein. Weak similarity to human ARID2, a chromatin remodeling protein	☆	68.5	O,N

100	At1g43860	Similar to yeast guanine nucleotide exchange factor SDO1 and human SBDS (Shwachman-Bodian-Diamond syndrome), mediates translational activation of ribosomes in yeast	☆	68.9	M,C

Supplemental Dataset 1. Top 100 ranking genes coexpressed with *RRP7* or *MAS2* , identified by ATTED-II

Supplemental Dataset 1D. Genes coexpressed with *SMO4* but not with *RRP7*

Locus	Short description
At1g02330	Similar to human C9orf78
At1g06530	PMD2, putative PMD1-like protein of unknown function
At1g06670	NIH, DEIH-box RNA/DNA helicase
At1g12270	Putative co-chaperone HOP1
At1g14610	VALRS, valyl-tRNA synthetase
At1g17130	Similar to cell cycle control protein cwf16 of Schizosaccharomyces pombe. Involved in mRNA splicing where it associates with cdc5 and the other cwf proteins as part of the spliceosome
At1g28060	Putative PRP3-like pre-mRNA processing factor. Yeas PRP3 participates in pre-mRNA splicing and in nuclear mRNA export
At1g31970	STRS1, DEA(D/H)-box RNA helicase family protein
At1g43860	Putative (yeast Sdo1)-like ribosome biogenesis factor
At1g50920	Nog1-1, putative (yeast Nog1)-like nucleolar GTPase
At1g52380	NUP50 (Nucleoporin 50 kDa) protein
At1g52980	NUG2, putative (yeast NUG2)-like ribosome large subunit assembly factor
At1g53460	Unknown protein
At1g55930	CBS domain-containing protein / transporter associated domain-containing protein
At1g59760	MTR4, RNA helicase, ATP-dependent, SK12/DOB1 protein
At1g64880	Ribosomal protein S5 family protein
At1g79200	Putative SCI1-like kinase inhibitor
At2g20280	Zinc finger (CCCH-type) family protein, contains Pfam domain, PF00642: Zinc finger C-x8-C-x5-C-x3-H type (and similar)
At2g25670	Unknown protein
At2g28450	C3H24, contains CCCH-type zinc ion binding domain
At2g28600	Putative DEAD/DEAH-box-type helicase
At2g34750	RRN3b, putative TFIa/RRN3-type RNA polymerase I basal transcription factor
At2g34900	(GTE1/IMB1), putative BET-type transcription factor
At2g40660	Nucleic acid-binding, OB-fold-like protein
At2g43650	EMB2777, putative (yeast Sas10)-like protein of unknown function
At2g45520	Unknown protein
At2g47250	Similar to yeast Pre-mRNA splicing factor RNA helicase PRP43 and human DHX15
At3g02220	Unknown protein with a conserved DUF2039 domain

At3g02760	Similar to human HisRS, Histidyl-tRNA synthetase
At3g02950	THO7, putative component of THO/TREX RNA trafficking complex
At3g11710	KRS-1, lysyl-tRNA synthetase 1
At3g11964	S1 RNA-binding domain-containing protein, similar to SP:Q05022 rRNA biogenesis protein RRP5 of Saccharomyces cerevisiae
At3g43590	Zinc knuckle (CCHC-type) family protein
At3g51270	Putative atypical Rio-type protein kinase
At3g57000	Putative Nep1-like methyltransferase involved in ribosome biogenesis
At3g62940	Similar to human OTUD6B, a member of the ovarian tumor domain (OTU)-containing subfamily of deubiquitinating enzymes
At4g01880	Similar to human and yeast TRM13, tRNA methyltransferase 13
At4g10760	MTA, putative MT-A70 subunit of S-adenosylmethionine-dependent methyltransferase
At4g19610	Similar to human RBM19 (RNA binding motif protein 19) and Saccharomyces cerevisiae MRD1, required for release of base-paired U3 snoRNA within the preribosomal complex (18S processing)
At4g26190	Haloacid dehalogenase-like hydrolase (HAD) superfamily protein
At4g28200	Similar to human and yeast UTP6, small subunit (SSU) processome component
At5g06110	ZRF1b/GlsA2, putative ZRF-type J-protein co-chaperone
At5g08420	RNA-binding KH domain-containing protein
At5g10010	Unknown protein
At5g12410	THUMP domain-containing protein
At5g22650	HDT2, putative HD2-type histone deacetylase
At5g42540	XRN2, exoribonuclease 2, acts as a suppressor of posttranscriptional gene silencing. Probably involved in rRNA or snoRNA processing
At5g47680	TRM10, tRNA modification 10. putative tRNA (guanine-N(1)-)-methyltransferase
At5g57990	UBP23, ubiquitin-specific protease 23
At5g58130	ROS3, REPRESSOR OF SILENCING 3, a RNA-binding protein required for DNA demethylation

Supplemental Dataset 1. Top 100 ranking genes coexpressed with *RRP7* or *MAS2* , identified by ATTED-II

Supplemental Dataset 1E. Genes coexpressed with *RRP7* but not with *SMO4*

Locus	Short description
At1g03360	Putative (yeast Rrp4)-like component of exosome complex
At1g06380	Putative L1-type protein of large ribosomal subunit
At1g08580	Unknown protein
At1g12830	Unknown protein
At1g13030	Unknown protein
At1g13120	GLE1, putative scaffold nucleoporin of outer ring of nuclear pore complex Similar to human GLE1, RNA export mediatorRequired for poly(A)+ RNA export
At1g30960	ERA2/ERG, putative (bacteria Era)-like GTPase
At1g43860	Putative (yeast Sdo1)-like ribosome biogenesis factor. Control translational activation of ribosomes
At1g52930	Similar to BRX1, biogenesis of ribosomes, homolog (S. cerevisiae). 60S ribosomal subunit assembly in Saccharomyces cerevisiae
At1g60850	RPAC42, putative component of DNA-dependent RNA polymerase I complex
At1g72440	SWA2/EDA25, putative (yeast Noc1)-like protein associated with U3 processome complex
At1g76120	Similar to human and yeast PUS1, pseudouridylate synthase 1. Pus1p exhibits a dual substrate specificity for U2 snRNA and tRNA
At1g79150	NOC3, putative (yeast Noc3)-like protein associated with U3 processome complex
At1g80270	PPR596, protein of unknown function with pentatricopeptide (PPR) repeats
At2g18330	Putative AAA-type ATPase associated with unknown cellular activities
At2g19385	Putative (mammal LYAR)-like nucleolar protein of unknown function.
At2g25355	Similar to human EXOSC3, exosome component 3 and yeast exosome subunit Rrp40 (predicted)
At2g31725	DUF842
At2g34260	Similar to human WDR55, WD repeat domain 55. Defects in nucleolar WDR55 cause aberrant accumulation of rRNA intermediates and cell cycle arrest
At2g34570	MEE21, putative (yeast Fcf1)-like pre-rRNA processing protein
At2g34780	MEE22, unknown protein
At2g37990	Ribosome biogenesis regulatory protein (RRS1) family protein
At2g40360	Similar to human BOP1 and yeast ERB1, required for maturation of the 25S and 5.8S ribosomal RNAs
At2g44510	Similar to protein-transporting protein BCP1 of S. cerevisiae, involved in ribosomal large subunit export from nucleus
At2g45730	Putative (yeast TRM6)-like component of TRM61-TRM6 tRNA adenine-methyltransferase complex

At3g02320	Similar to human and yeast TRMT1, RNA methyltransferase 1
At3g12270	PRMT3, putative ribosomal protein methyltransferase
At3g12340	FKBP-type peptidyl-prolyl isomerase (AtFKBP43)
At3g13940	Subunit of TFIf-type RNA polymerase I basal transcription factor (AtC49)
At3g15080	Similar to human REX4 homolog, 3,-5, exonuclease. Rex4 is involved in processing of ITS1 in Saccharomyces cerevisiae pre-rRNA.
At3g16810	PUM24, protein of unknown function, contains pumilio/Puf RNA-binding domain
At3g21540	Putative (yeast UTP12)-like nucleolar component of U3 processome complex
At3g23620	Similar to RPF2, ribosome production factor 2 homolog (S. cerevisiae). Assembly factors Rpf2 recruit 5S rRNA and ribosomal proteins rpL5 and rpL11 into nascent ribosomes
At3g55510	Putative (yeast Noc2)-like protein required for flower development, REBELOTE (AtRBL)
At3g60360	UTP11/EDA14, putative (yeast UTP11)-like nucleolar component of U3 processome complex
At3g61620	RRP41, putative (yeast Rrp46)-like PH-type ribonuclease of exosome complex
At3g62940	Similar to human OTUD6B, a member of the ovarian tumor domain (OTU)-containing subfamily of deubiquitinating enzymes
At4g01990	Protein of unknown function, contains pentatricopeptide (PPR) repeats
At4g05410	Putative (yeast Rrp9)-like nucleolar component of U3 processome complex (AtYAO1)
At4g37090	Unknown protein
At5g12220	Putative Las1-like protein
At5g14050	Similar to human and yeast UTP18 small subunit (SSU) processome component
At5g15750	Putative (yeast Imp3)-like nucleolar component of U3 processome complex
At5g17930	Similar to human nucleolar NOM1, RNA export mediator
At5g18440	NUFIP, putative (human NUFIP1)-like protein, controls biogenesis of snoRNPs and scaRNPs
At5g19300	Unknown protein. Similar to human C9orf114 (chromosome 9 open reading frame 114)
At5g27395	Tim44, Mitochondrial inner membrane translocase complex, subunit Tim44-related protein
At5g50315	Mutator-like transposaseMuDR family
At5g51130	Similar to human MEPCE, methylphosphate capping enzyme. Human MePCE is involved in stabilizing 7SK snRNA and facilitating the assembly of 7SK snRNP
At5g52380	VASCULAR-RELATED NAC-DOMAIN 6
At5g57280	RID2, putative methyltransferase involved in pre-rRNA processing. Similar to yeast BUD23 and human WBSCR22 (Williams Beuren syndrome chromosome region 22)
At5g65900	RH27, putative DEAD/DEAH-box-type helicase. Similar to yeast Has1p and human DDX18. Has1p is required for snoRNA release from pre-rRNA and 40S ribosomal subunit biogenesis
At5g66540	Putative (yeast Mpp10)-like nucleolar component of U3 processome complex

Supplemental Dataset 1. Top 100 ranking genes coexpressed with *RRP7* or *MAS2* , identified by ATTED-II

Supplemental Dataset 1F. Genes coexpressed with *SMO4* and *MAS2*

Locus	Short description
At1g02330	Similar to human C9orf78
At1g06530	PMD2, putative PMD1-like protein of unknown function
At1g17130	Similar to cell cycle control protein cwf16 of Schizosaccharomyces pombe. Involved in mRNA splicing where it associates with cdc5 and the other cwf proteins as part of the spliceosome
At1g28060	Putative PRP3-like pre-mRNA processing factor. Yeas PRP3 participates in pre-mRNA splicing and in nuclear mRNA export. May play a role in the assembly of the U4/U5/U6 tri-snRNP complex
At1g43860	Putative (yeast Sdo1)-like ribosome biogenesis factor. Involved in the biogenesis of the 60S ribosomal subunit and translational activation of ribosomes. Together with the EF-2-like GTPase RIA1, may trigger the GTP-dependent release of TIF6 from 60S pre-ribosomes in the cytoplasm, thereby activating ribosomes for translation competence by allowing 80S ribosome assembly and facilitating TIF6 recycling to the nucleus, where it is required for 60S rRNA processing and nuclear export
At2g20280	C3H21, protein of unknown function, contains CCCH-type zinc ion binding domain
At3g02760	Similar to human HisRS, Histidyl-tRNA synthetase
At3g58840	PMD1, protein involved in peroxisomal and mitochondrial proliferation
At5g05210	Surfeit locus 6, putative nucleolar matrix protein. Human surfeit 6 is a component of the nucleolar matrix and may represent a nucleolar constitutive protein involved in ribosomal biosynthesis or assembly
At5g47680	TRM10, tRNA modification 10. putative tRNA (guanine-N(1)-)-methyltransferase
At5g50310	Unknown protein, similar to human KLHDC4

Supplemental Dataset 1. Top 100 ranking genes coexpressed with *RRP7* or *MAS2* , identified by ATTED-II

Supplemental Dataset 1G. Genes coexpressed with *RRP7* , *SMO4* and *MAS2*

Locus	Short description
At1g43860	Putative (yeast Sdo1)-like ribosome biogenesis factor. Involved in the biogenesis of the 60S ribosomal subunit and translational activation of ribosomes. Together with the EF-2-like GTPase RIA1, may trigger the GTP-dependent release of TIF6 from 60S pre-ribosomes in the cytoplasm, thereby activating ribosomes for translation competence by allowing 80S ribosome assembly and facilitating TIF6 recycling to the nucleus, where it is required for 60S rRNA processing and nuclear expor
At3g58840	PMD1, protein involved in peroxisomal and mitochondrial proliferation
At5g05210	Surfeit locus 6, putative nucleolar matrix protein. Human surfeit 6 is a component of the nucleolar matrix and may represent a nucleolar constitutive protein involved in ribosomal biosynthesis or assembly
At5g50310	Unknown protein, similar to KLHDC4

VI.- ANEXO:
COMUNICACIONES A CONGRESOS

A search for mutations suppressing the morphological phenotype of *argonaute1*

Verónica Aguilera, Patricia Quinto, Rosa Micol-Ponce, José Luis Micol, María Rosa Ponce

División de Genética and Instituto de Bioingeniería, Universidad Miguel Hernández, Campus de Elche, 03202 Elche, Spain

ARGONAUTE (AGO) proteins are key components of the RNA-Induced Silencing Complex (RISC) that act in the microRNA pathway. In *Arabidopsis thaliana*, the *ago1* loss-of-function mutant alleles of the *AGO1* gene disturb many developmental processes and often cause lethality or sterility.

With a view to identify novel genes involved in microRNA-guided gene silencing, we mutagenized seeds of the viable and fertile *ago1-52* line, already isolated in our laboratory. We have screened 36,810 M_2 seeds, identifying 17 lines in which the morphological phenotype caused by *ago1-52* is partially or almost completely suppressed. We are positionally cloning these suppressor mutations.

2009

20th International Conference on Arabidopsis Research

Edimburgo, Reino Unido.

Póster

A search for mutations suppressing the morphological phenotype of an *argonaute1* allele

V. Aguilera, P. Quinto, R. Micol-Ponce, J.L. Micol and M.R. Ponce

División de Genética and Instituto de Bioingeniería, Universidad Miguel Hernández, Campus de Elche, 03202 Elche, Alicante, Spain.

vaguilera@umh.es mrponce@umh.es http://genetica.umh.es

We have taken a genetic and molecular approach to the identification of new elements of the miRNA pathway that participate in the control of plant development. In Arabidopsis, the main component of the miRNA-mediated silencing complex (RISC) is encoded by the *ARGONAUTE1* (*AGO1*) gene, whose *ago1* mutant alleles perturb many developmental processes and often cause lethality or sterility[1-3].

We isolated *ago1-51* and *ago1-52*, two viable and moderately fertile mutants, and obtained their double mutant combinations with alleles of other miRNA machinery genes, and of some miRNA target genes. All the double mutants displayed synergistic phenotypes, as expected from the functional relationship among the genes involved[4]. By means of a microarray analysis, we found that in the *ago1-52* mutant, as well as in other three non-allelic miRNA machinery mutants already isolated in our laboratory, the mRNAs of known miRNA targets were accumulated. Taken together, theses results prompted us to mutagenize with ethyl metanosulphonate (EMS) the *ago1-52* line in order to identify second-site mutations modifying the Ago1-52 phenotype.

After screening 36,810 M_2 seeds, we identified 4,189 putative double mutants (Table 1), most of which were sterile and displayed a mutant phenotype stronger than that of *ago1-52*. Only 302 M_2 putative double mutants were viable and fertile, 21 of which displayed partial suppression of the Ago1-52 phenotype. Four of them exhibited only weak suppression and were discarded. Some of the remaining 17 were not easily distinguishable from the L*er* wild type (Fig. 1). Plant body architecture and other morphological traits of the Ago1-52 phenotype became normalized in most of these lines putatively carrying suppressor mutations (Fig. 2). We backcrossed to L*er* the above mentioned 17 lines, with the purpose of determining the mode of inheritance of their new mutations and found that most of them did not exhibit a mutant phenotype *per se*, in an *AGO1/AGO1* background.

We initiated the positional cloning of these suppressor mutations, by crossing M_3 plants to Col-0 and *ago1-27*[5], a line carrying a fertile *ago1* allele in a Col-0 background. P1 5.33, P2 11.1, P7 26.1, P8 14.1 and P8 25.1 are some of these double mutants, whose characterization (Fig. 2) and positional cloning (Fig. 3) is in progress.

Tabla 1.- Putative double mutants isolated in our screening

	M_2			M_3
	Lethal	Esterile	Fertile	
Total	3,366	521	302	92
Extremed Ago1-52 phenotype	23	67	42	11
Partially supressed Ago1-52 phenotype	29	91	93	21
Synergistic	3,130	3	0	0
Other mutant phenotypes	184	360	167	60

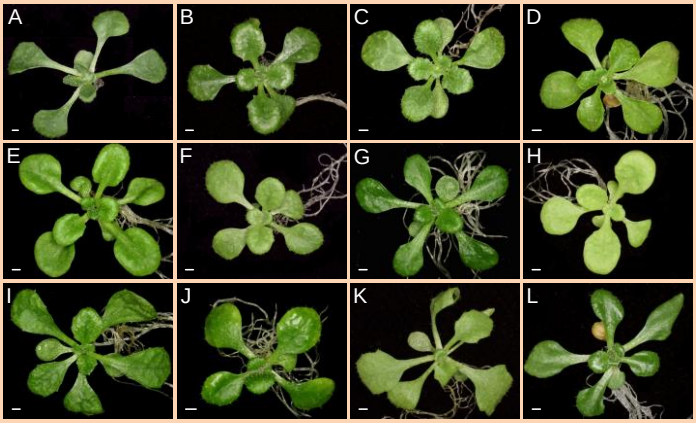

Figure 1.- Rosettes of some putative double mutants that exhibit partial suppression of the Ago1-52 phenotype. (A) P1 3.1, (B) P4 22.2, (C) P5 11.1, (D) P6 65.2, (E) P6 66.2, (F) P7 13.1, (G) P7 22.1, (H) P7 23.1, (I) P7 24.1, (J) P7 49.1, (K) P8 4.1 y (L) P8 44.1. Pictures were taken 21 days after stratification. Scale bars: 1 mm.

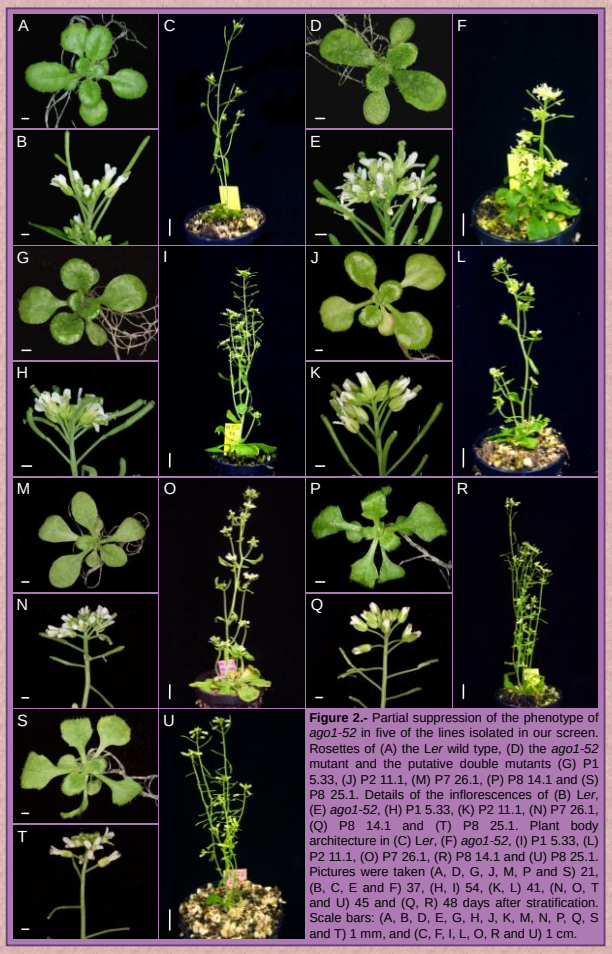

Figure 2.- Partial suppression of the phenotype of *ago1-52* in five of the lines isolated in our screen. Rosettes of (A) the L*er* wild type, (D) the *ago1-52* mutant and the putative double mutants (G) P1 5.33, (J) P2 11.1, (M) P7 26.1, (P) P8 14.1 and (S) P8 25.1. Details of the inflorescences of (B) L*er*, (E) *ago1-52*, (H) P1 5.33, (K) P2 11.1, (N) P7 26.1, (Q) P8 14.1 and (T) P8 25.1. Plant body architecture in (C) L*er*, (F) *ago1-52*, (I) P1 5.33, (L) P2 11.1, (O) P7 26.1, (R) P8 14.1 and (U) P8 25.1. Pictures were taken (A, D, G, J, M, P and S) 21, (B, C, E and F) 37, (H, I) 54, (K, L) 41, (N, O, T and U) 45 and (Q, R) 48 days after stratification. Scale bars: (A, B, D, E, G, H, J, K, M, N, P, Q, S and T) 1 mm, and (C, F, I, L, O, R and U) 1 cm.

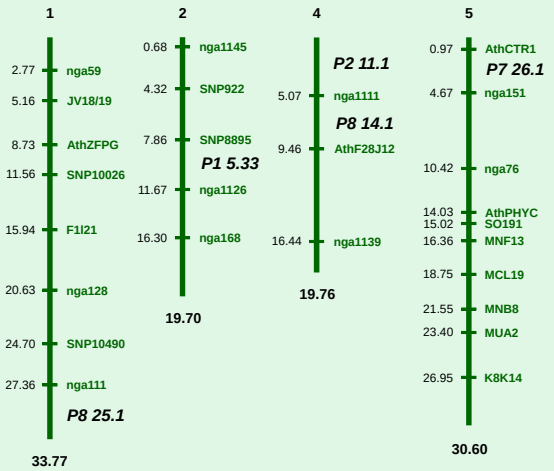

Figure 3.- *Arabidopsis thaliana* physical map with indication of the approximate positions of five of the supressor mutations whose characterization is in progress. Low-resolution mapping was performed as described in reference 7. All figures indicate Mb, the only exceptions being chromosome numbers. Chromosome 3 has been deliberately excluded.

MATERIALS AND METHODS

Plants were grown at 20±1°C and 60-70% relative humidity, under constant fluorescent light (5.000 lux)[6].

ACKNOWLEDGMENTS

The *ago1-27* line was kindly provided by H. Vaucheret. This work was supported by grants (BMC2003-09763, BIO2007-67920 and BIO2008-01900 to M.R. Ponce) and a fellowship (to V. Aguilera) from the Ministerio de Ciencia e Innovación of Spain.

REFERENCES

1.- Bohmert, K., Camus, I., Bellini, C., Bouchez, D., Caboche, M., and Benning, C. (1998). *EMBO J.* **17,** 170-180.
2.- Baumbenger, N., and Baulcombe, D.C. (2005). *Proc. Natl. Acad. Sci. USA* **102,** 11928-11933.
3.- Qi, Y., Denli, M., and Hannon, G. J. (2005). *Mol. Cell* **19,** 421-428.
4.- Jover-Gil, S., Candela, H., and Ponce, M.R. (2005). *Int. J. Dev. Biol.* **49,** 733-744.
5.- Morel, J.B., Godon, C., Mourrain, P., Béclin, C., Boutet, S., Feuerbach, F., Proux, F., and Vaucheret, H. (2002). *Plant Cell* **14,** 629-639.
6.- Ponce, M.R., Quesada, V., and Micol, J.L. (1998). *Plant J.* **14,** 497-501.
7.- Ponce, M.R., Robles, P., Lozano, F.M., Brotóns, M.A., and Micol, J.L. (2006). *Methods Mol. Biol.* **323,** 105-113.

Búsqueda de supresores del fenotipo morfológico de un mutante *ago1*

Aguilera V., Quinto P., Micol-Ponce R., Micol J.L., Ponce M.R.

División de Genética e Instituto de Bioingeniería, Universidad Miguel Hernández, Campus de Elche, 03202 Elche, Alicante

En la planta modelo *Arabidopsis thaliana* el principal componente de los complejos del silenciamiento génico mediado por los microARN (RISC) es la proteína AGO1 (ARGONAUTE1), cuya insuficiencia de función perturba muchos procesos de desarrollo y suele causar esterilidad o letalidad. Hemos aislado el mutante *ago1-52*, que es viable, relativamente fértil y portador de un alelo del gen *AGO1*. Con el objetivo de identificar nuevos genes implicados en la ruta del silenciamiento génico mediado por los microARN, hemos mutagenizado semillas M_1 de *ago1-52* con metanosulfonato de etilo. Hemos sometido a escrutinio 36.810 semillas M_2, identificando 17 líneas en las que el fenotipo morfológico de *ago1-52* se suprime total o parcialmente. Estamos caracterizando estas líneas y clonando posicionalmente los genes supresores.

2009

XXXVII Congreso de la Sociedad Española de Genética

Torremolinos

Póster

Búsqueda de supresores del fenotipo morfológico de un mutante *ago1*

V. Aguilera, P. Quinto, R. Micol-Ponce, J.L. Micol y M.R. Ponce

División de Genética e Instituto de Bioingeniería, Universidad Miguel Hernández, Campus de Elche, 03202 Elche, Alicante.

mrponce@umh.es http://genetica.umh.es

El principal componente de los complejos (RISC) del silenciamiento génico mediado por los microARN (miARN) en la planta modelo *Arabidopsis thaliana* es la proteína AGO1 (ARGONAUTE1)[1], cuya insuficiencia de función perturba muchos procesos de desarrollo y suele causar esterilidad o letalidad. Hemos aislado el mutante *ago1-52* (Fig. 1), que es portador de un alelo hipomorfo del gen *AGO1* que elimina 55 aa del extremo carboxilo de la proteína AGO1, causa un fenotipo morfológico débil aunque inequívocamente distinguible del silvestre, y reduce sólo parcialmente la viabilidad y la fertilidad.

Hemos supuesto que una búsqueda de modificadores del fenotipo de una estirpe *ago1* viable y fértil podría ayudarnos a identificar nuevos elementos de la ruta de los miARN. La mutagénesis con EMS de unas 60.000 semillas M_1 *ago1-52* resultó fructífera, ya que sometimos a escrutinio 36.810 semillas de su progenie M_2 e identificamos 4.189 presuntos dobles mutantes en los que el fenotipo Ago1-52 se debilitaba o acentuaba, o manifestaban rasgos inesperados (Tabla 1). 3.133 de ellos resultaron estériles o letales y mostraron un fenotipo muy severo y similar al de los dobles mutantes previamente obtenidos combinando alelos de genes de la maquinaria de los miARN. Sólo 302 de las plantas M_2 seleccionadas resultaron viables y fértiles, de las que 92 transmitieron su fenotipo a su descendencia M_3 con penetrancia completa y expresividad poco variable. El mayor número de dobles mutantes M_2 viables y fértiles se encontró en la clase en la que el fenotipo Ago1-52 se suprimió parcialmente (Figs. 2 y 3).

Nos hemos centrado en el estudio de las 17 líneas que mostraron mayor supresión, a cuyas mutaciones hemos denominado *mas* (*morphology of argonaute1-52 suppressed*). El análisis iterativo del ligamiento a marcadores moleculares, realizado genotipando plantas F_2 de la poblaciones cartográficas obtenidas cruzando los dobles mutantes por Col-0 y *ago1-27*[2] nos ha permitido definir intervalos candidatos de 42 genes para la mutación *mas1-1*, 39 para *mas2-1*, y 94 para *mas3-1* (180, 158 y 396 kb, respectivamente).

Tabla 1.- Presuntos dobles mutantes identificados tras la mutagénesis de *ago1-52* con EMS

	M_2			M_3
	Letales	Estériles	Fértiles	
Total	3.366	521	302	92
Fenotipo Ago1-52 extremo	23	67	42	11
Fenotipo Ago1-52 débil	29	91	93	21
Sinergia	3.130	3	0	0
Otros fenotipos mutantes	184	360	167	60

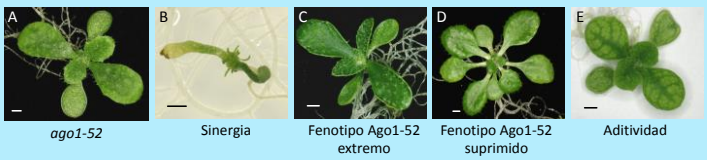

Figura 1.- Rosetas de (A) *ago1-52* y de plantas representativas de las clases fenotípicas que hemos establecido en las generaciones (B) M_2 y (C-E) M_3 para nuestros presuntos dobles mutantes. Las fotografías se tomaron 21 días después de la estratificación. Las barras de escala indican 1 mm.

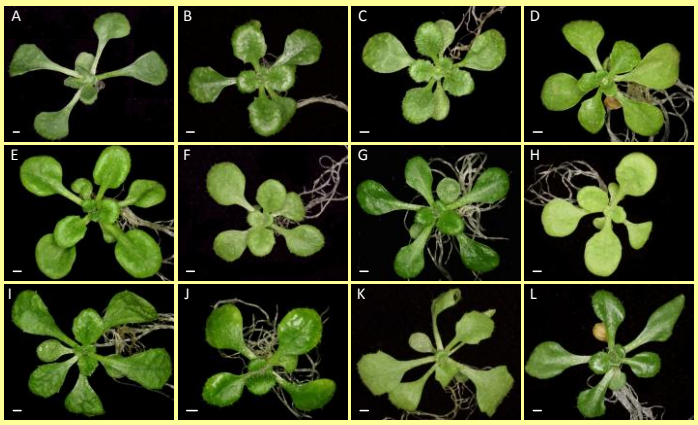

Figura 2.- Rosetas de algunos de los presuntos dobles mutantes que exhiben supresión parcial del fenotipo Ago1-52. (A) P1 3.1, (B) P4 22.2, (C) P5 11.1, (D) P6 65.2, (E) P6 66.2, (F) P7 13.1, (G) P7 22.1, (H) P7 23.1, (I) P7 24.1, (J) P7 49.1, (K) P8 4.1 y (L) P8 44.1. Las fotografías se tomaron 21 días después de la estratificación. Las barras de escala indican 1 mm.

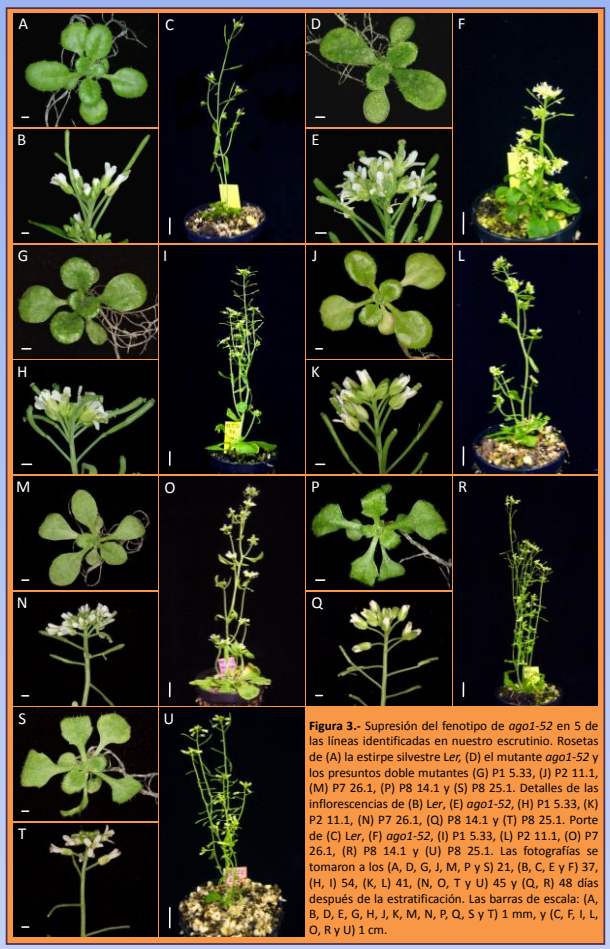

Figura 3.- Supresión del fenotipo de *ago1-52* en 5 de las líneas identificadas en nuestro escrutinio. Rosetas de (A) la estirpe silvestre *Ler*, (D) el mutante *ago1-52* y los presuntos doble mutantes (G) P1 5.33, (J) P2 11.1, (M) P7 26.1, (P) P8 14.1 y (S) P8 25.1. Detalles de las inflorescencias de (B) *Ler*, (E) *ago1-52*, (H) P1 5.33, (K) P2 11.1, (N) P7 26.1, (Q) P8 14.1 y (T) P8 25.1. Porte de (C) *Ler*, (F) *ago1-52*, (I) P1 5.33, (L) P2 11.1, (O) P7 26.1, (R) P8 14.1 y (U) P8 25.1. Las fotografías se tomaron a los (A, D, G, J, M, P y S) 21, (B, C, E y F) 37, (H, I) 54, (K, L) 41, (N, O, T y U) 45 y (Q, R) 48 días después de la estratificación. Las barras de escala: (A, B, D, E, G, H, J, K, M, N, P, Q, S y T) 1 mm, y (C, F, I, L, O, R y U) 1 cm.

Figura 4.- Mapa físico de 4 de los 5 cromosomas de *Arabidopsis thaliana* en el que se indican las posiciones de los cinco genes supresores que estamos analizando. Las líneas P1.5.33, P2.11.1, P.8.14.1, P7.26.1 y P8.25.1 son portadoras de las mutaciones *mas1-1*, *mas2-1*, *mas3-1*, *mas4-1* y *mas5-1*, respectivamente. La cartografía se realizó según se describe en la referencia 3. Todas los números indican Mb, excepto de los que aparecen sobre los cromosomas. Se ha omitido deliberadamente el cromosoma 3.

AGRADECIMIENTOS

La línea *ago1-27* fue donada por H. Vaucheret. Este trabajo ha sido financiado por el Ministerio de Ciencia e Innovación (proyectos BMC2003-09763, BIO2007-67920 y BIO2008-01900, concedidos a M.R. Ponce, y una beca FPU a V. Aguilera).

REFERENCIAS

1.- Bohmert, K., Camus, I., Bellini, C., Bouchez, D., Caboche, M., y Benning, C. (1998). *EMBO J.* **17,** 170-180.
2.- Morel, J.B., Godon, C., Mourrain, P., Béclin, C., Boutet, S., Feuerbach, F., Proux, F., y Vaucheret, H. (2002). *Plant Cell* **14,** 629-639.
3.- Ponce, M.R., Robles, P., Lozano, F.M., Brotóns, M.A., y Micol, J.L. (2006). *Methods Mol. Biol.* **323,** 105-113.

MATERIALES Y MÉTODOS

Los cultivos se realizaron a 20±1°C y 60-70% de humedad relativa, bajo iluminación continua (7.000 lx)[2].

A search for mutations that suppress the morphological phenotype of an *argonaute1* allele

Aguilera, V., Quinto, P., Micol-Ponce, R., Ece, S., Albolafio, S., Jover-Gil, S., Micol, J.L., and Ponce, M.R.

División de Genética and Instituto de Bioingeniería, Universidad Miguel Hernández, Campus de Elche, 03202 Elche, Alicante, Spain

The main component of the miRNA-mediated silencing complex (RISC) is encoded by the *ARGONAUTE1* (*AGO1*) gene in the model plant *Arabidopsis thaliana*. Mutant *ago1* alleles alter leaf morphogenesis and many other developmental processes, often causing lethality or sterility.

With a view to identify novel genes involved in miRNA-guided gene silencing, we have mutagenized seeds of the viable and fertile *ago1-52* line, which had been isolated in our laboratory. In a screening of 36,810 M_2 seeds, we have identified 17 lines in which the phenotype of *ago1-52* is partially or almost completely suppressed. We are positionally cloning these suppressor mutations.

2009

Plant Growth Biology and Modeling Workshop

Elche

Póster

A search for mutations that suppress the morphological phenotype of an *argonaute1* allele

Aguilera, V., Quinto, P., Micol-Ponce, R., Ece, S., Albolafio, S., Jover-Gil, S., Micol, J. L., and Ponce, M. R.

División de Genética and Instituto de Bioingeniería, Universidad Miguel Hernández, Campus de Elche, 03202 Elche, Alicante, Spain.

mrponce@umh.es http://genetica.umh.es

We have taken a genetic and molecular approach to the identification of new elements of the miRNA pathway that participate in the control of plant development. In Arabidopsis, the main component of the miRNA-mediated silencing complex (RISC) is encoded by the *ARGONAUTE1* (*AGO1)* gene, whose *ago1* mutant alleles perturb many developmental processes and often cause lethality or sterility[1-3].

We isolated *ago1-51* and *ago1-52*, two viable and moderately fertile mutants, and obtained their double mutant combinations with alleles of other miRNA machinery genes, and of some miRNA target genes. All the double mutants displayed synergistic phenotypes, as expected from the functional relationship among the genes involved[4]. By means of a microarray analysis, we found that in the *ago1-52* mutant, as well as in other three non-allelic miRNA machinery mutants already isolated in our laboratory, the mRNAs of known miRNA targets were accumulated. Taken together, theses results prompted us to mutagenize with ethyl metanosulphonate (EMS) the *ago1-52* line in order to identify second-site mutations modifying the Ago1-52 phenotype.

After screening 36,810 M_2 seeds, we identified 4,189 putative double mutants (Table 1), most of which were sterile and displayed a mutant phenotype stronger than that of *ago1-52*. Only 302 M_2 putative double mutants were viable and fertile, 21 of which displayed partial suppression of the Ago1-52 phenotype. Four of them exhibited only weak suppression and were discarded. Some of the remaining 17 were not easily distinguishable from the L*er* wild type (Fig. 1). Plant body architecture and other morphological traits of the Ago1-52 phenotype became normalized in most of these lines putatively carrying suppressor mutations (Fig. 2). We have named *mas* (*morphology of argonaute1-52 suppressed*) to these suppressor mutations.

We backcrossed to L*er* the above mentioned 17 lines, with the purpose of determining the mode of inheritance of their new mutations and found that most of them did not exhibit a mutant phenotype *per se*, in an *AGO1/AGO1* background.

We initiated the positional cloning of the *MAS* genes, by crossing M_3 plants to Col-0 and *ago1-27*[5], a line carrying a fertile *ago1* allele in a Col-0 background. P1.3.1, P1 5.33, P2 11.1, P7 26.1, P7.49.1, P8 14.1, and P8 25.1 are some of these double mutants, whose characterization (Fig. 1 and 2) and positional cloning (Fig. 3) is in progress.

Tabla 1.- Putative double mutants isolated in our screening

	M_2			M_3
	Lethal	Esterile	Fertile	
Total	3,366	521	302	92
Extremed Ago1-52 phenotype	23	67	42	11
Partially supressed Ago1-52 phenotype	29	91	93	21
Synergistic	3,130	3	0	0
Other mutant phenotypes	184	360	167	60

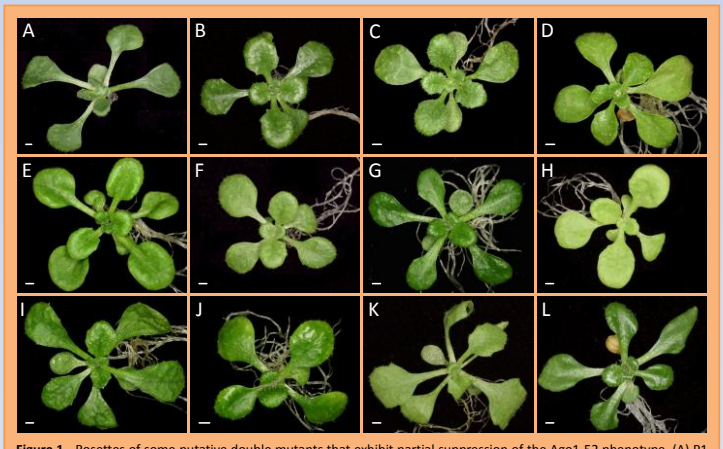

Figure 1.- Rosettes of some putative double mutants that exhibit partial suppression of the Ago1-52 phenotype. (A) P1 3.1, (B) P4 22.2, (C) P5 11.1, (D) P6 65.2, (E) P6 66.2, (F) P7 13.1, (G) P7 22.1, (H) P7 23.1, (I) P7 24.1, (J) P7 49.1, (K) P8 4.1 y (L) P8 44.1. Pictures were taken 21 days after stratification. Scale bars: 1 mm.

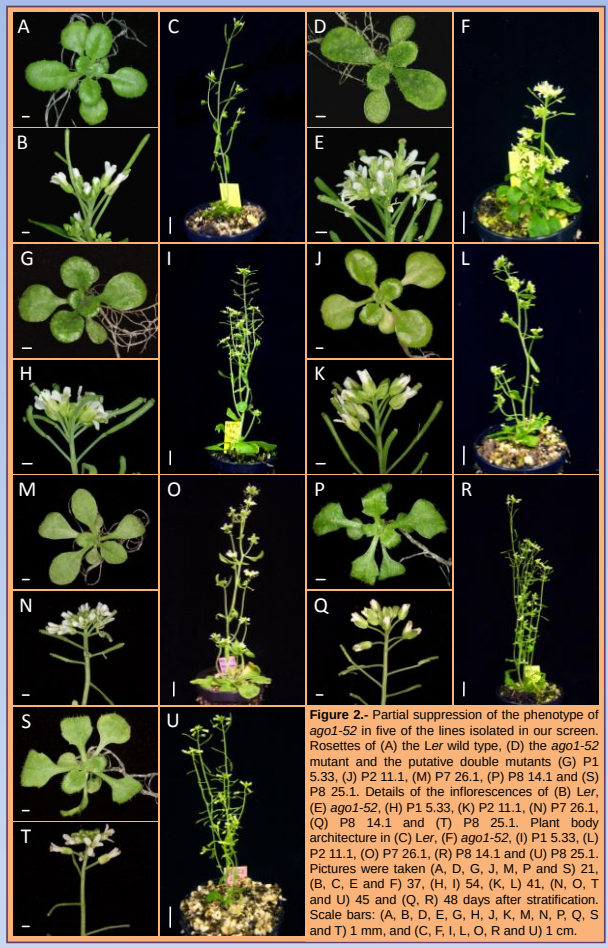

Figure 2.- Partial suppression of the phenotype of *ago1-52* in five of the lines isolated in our screen. Rosettes of (A) the L*er* wild type, (D) the *ago1-52* mutant and the putative double mutants (G) P1 5.33, (J) P2 11.1, (M) P7 26.1, (P) P8 14.1 and (S) P8 25.1. Details of the inflorescences of (B) L*er*, (E) *ago1-52*, (H) P1 5.33, (K) P2 11.1, (N) P7 26.1, (Q) P8 14.1 and (T) P8 25.1. Plant body architecture in (C) L*er*, (F) *ago1-52*, (I) P1 5.33, (L) P2 11.1, (O) P7 26.1, (R) P8 14.1 and (U) P8 25.1. Pictures were taken (A, D, G, J, M, P and S) 21, (B, C, E and F) 37, (H, I) 54, (K, L) 41, (N, O, T and U) 45 and (Q, R) 48 days after stratification. Scale bars: (A, B, D, E, G, H, J, K, M, N, P, Q, S and T) 1 mm, and (C, F, I, L, O, R and U) 1 cm.

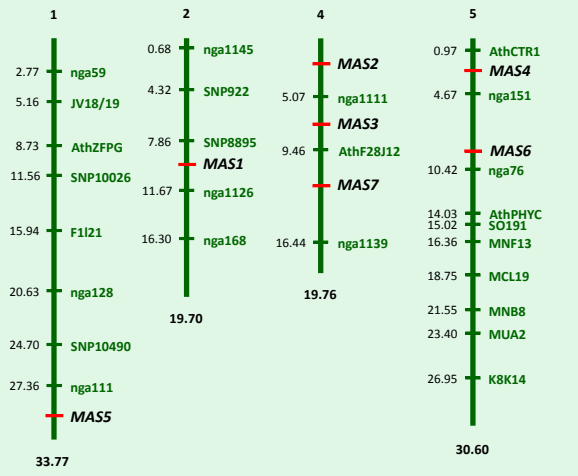

Figure 3.- *Arabidopsis thaliana* physical map with indication of the approximate positions of seven of the *MAS* genes whose characterization is in progress. The P1.5.33, P2.11.1, P8.14.1, P7.26.1, P8.25.1, P8.49.1 and P1.3.1 lines carry the *mas1-mas7* mutations, respectively. Low-resolution mapping was performed as described in reference 7. All figures indicate Mb, the only exceptions being chromosome numbers. Chromosome 3 has been deliberately left out of the figure for simplicity.

METHODS

Plants were grown at 20±1°C and 60-70% relative humidity, under constant fluorescent light (5,000 lux)[6].

ACKNOWLEDGMENTS

The *ago1-27* line was kindly provided by H. Vaucheret. This work was supported by grants (BMC2003-09763, BIO2007-67920 and BIO2008-01900 to M.R. Ponce) and a fellowship (to V. Aguilera) from the Ministerio de Ciencia e Innovación of Spain.

REFERENCES

1.- Bohmert, K., Camus, I., Bellini, C., Bouchez, D., Caboche, M., and Benning, C. (1998). *EMBO J.* **17,** 170-180.
2.- Baumbenger, N., and Baulcombe, D.C. (2005). *Proc. Natl. Acad. Sci. USA* **102,** 11928-11933.
3.- Qi, Y., Denli, M., and Hannon, G. J. (2005). *Mol. Cell* **19,** 421-428.
4.- Jover-Gil, S., Candela, H., and Ponce, M.R. (2005). *Int. J. Dev. Biol.* **49,** 733-744.
5.- Morel, J.B., Godon, C., Mourrain, P., Béclin, C., Boutet, S., Feuerbach, F., Proux, F., and Vaucheret, H. (2002). *Plant Cell* **14,** 629-639.
6.- Ponce, M.R., Quesada, V., and Micol, J.L. (1998). *Plant J.* **14,** 497-501.
7.- Ponce, M.R., Robles, P., Lozano, F.M., Brotóns, M.A., and Micol, J.L. (2006). *Methods Mol. Biol.* **323,** 105-113.

Genetic and molecular analysis of the Arabidopsis *MAS* genes

Sánchez-García, A.B., Jover-Gil, S., Aguilera, V., Quinto, P., Micol-Ponce, R., Micol, J.L., and Ponce, M.R.

Instituto de Bioingeniería, Universidad Miguel Hernández, Campus de Elche, 03202 Elche, Alicante, Spain

The Arabidopsis ARGONAUTE1 (AGO1) protein is the core component of the RNA-induced silencing complex (RISC) that mediates the regulation of gene expression by microRNAs (miRNAs). The *ago1* loss-of-function alleles of the *AGO1* gene alter many developmental processes and often cause lethality or sterility. With a view to identify novel genes involved in miRNA-guided gene silencing, we mutagenized with EMS seeds of the viable and fertile *ago1-52* mutant, which had been isolated in our laboratory. We screened 36,810 M_2 seeds and identified 17 lines in which the phenotype caused by *ago1-52* is from partially to almost completely suppressed. We have already mapped five of the suppressor mutations, which we named *mas* (*morphology of argonaute1-52 suppressed*), and have positionally cloned three of them. We will present our results on the genetic and molecular characterization of the *MAS* genes.

2010

XVII Congress of the Federation of European Societies of Plant Biology

Valencia

Póster

Genetic and molecular analysis of the Arabidopsis *MAS* genes

A.B. Sánchez-García, S. Jover-Gil, V. Aguilera, P. Quinto, R. Micol-Ponce, J.L. Micol and M.R. Ponce

Instituto de Bioingeniería, Universidad Miguel Hernández, Campus de Elche, 03202 Elche, Alicante, Spain.

mrponce@umh.es genetica.umh.es

In *Arabidopsis thaliana*, the core component of the miRNA mediated silencing complex (RISC) is encoded by the *ARGONAUTE1* (*AGO1*) gene, whose *ago1* loss-of-function mutant alleles disturb many developmental processes and often cause lethality or sterility[1-3]. With a view to identify novel genes involved in miRNA-guided gene silencing, we mutagenized with EMS M_1 seeds of the viable and fertile *ago1-52* line, which had been isolated in our laboratory[4]. After screening 36,810 M_2 seeds, we identified 4,189 putative double mutants (Table 1), most of which were sterile and displayed a mutant phenotype stronger than that of *ago1-52*. Only 302 M_2 putative double mutants were viable and fertile, 21 of which displayed partial suppression of the Ago1-52 phenotype. Four of them exhibited only weak suppression and were discarded. Some of the remaining 17 were not easily distinguishable from the L*er* wild type. Plant body architecture and other morphological traits of the Ago1-52 phenotype became normalized in most of these lines carrying suppressor mutations (Fig. 1).

We have mapped so far seven of these suppressor mutations, which we named *mas* (*morphology of argonaute1-52 suppressed*), and positionally cloned three of them (Fig. 2). Positional cloning of the *mas2-1* mutation allowed us to determine that *MAS2* is a single-copy gene encoding a protein of unknown function, conserved among plants and animals. *mas2-1* seems to be a gain-of-function allele and carries a point mutation that causes no visible phenotype in *mas2-1/mas2-1;AGO1/AGO1* plants. We identified a line carrying a T-DNA insertion in the *MAS2* gene, which we named *mas2-2*. *MAS2* seems to be an essential gene as suggested by lethality of *mas2-2/mas2-2* embryos (Fig. 3).

Constitutive expression of *MAS2* had no phenotypic effects in a wild-type background but suppressed the mutant phenotype in a*go1-52* and *hen1-13* plants (Fig. 3). This observation confirms the gain of function of *MAS2* is able to suppress the phenotypes of loss-of-function mutations affecting the *AGO1* and *HEN1* genes, which participate in the miRNA and short interfering RNA (siRNA) pathways. We have also obtained transgenic plants overexpressing *mas2-1* in a wild-type background, which show a wild-type phenotype.

Another approach taken to determine the function of *MAS2* was the generation of transgenic plants carrying a construct for the expression of an artificial miRNA (amiRNA) designed to target *MAS2* mRNA. These transgenic plants rendered a phenotype of serrated leaves that exhibited premature senescence (Fig. 3), suggesting that *MAS2* might be involved in senescence or cell death pathways in Arabidopsis.

Table 1.- Putative double mutants isolated in our screening

	M_2			M_3
	Lethal	Esterile	Fertile	
Total	3,366	521	302	92
Extremed Ago1-52 phenotype	23	67	42	11
Partially supressed Ago1-52 phenotype	29	91	93	21
Synergistic	3,130	3	0	0
Other mutant phenotypes	184	360	167	60

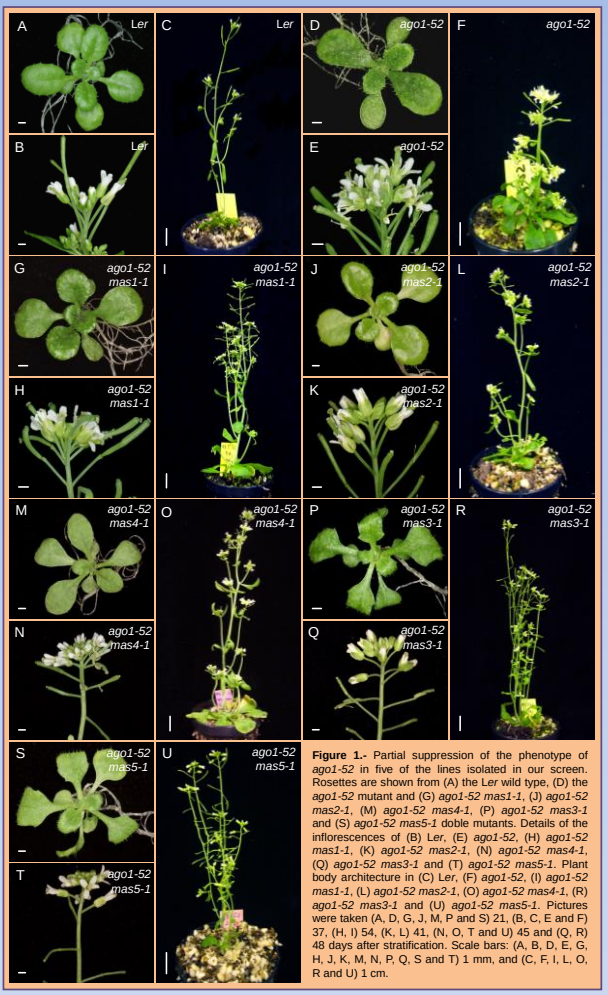

Figure 1.- Partial suppression of the phenotype of *ago1-52* in five of the lines isolated in our screen. Rosettes are shown from (A) the L*er* wild type, (D) the *ago1-52* mutant and (G) *ago1-52 mas1-1*, (J) *ago1-52 mas2-1*, (M) *ago1-52 mas4-1*, (P) *ago1-52 mas3-1* and (S) *ago1-52 mas5-1* doble mutants. Details of the inflorescences of (B) L*er*, (E) *ago1-52*, (H) *ago1-52 mas1-1*, (K) *ago1-52 mas2-1*, (N) *ago1-52 mas4-1*, (Q) *ago1-52 mas3-1* and (T) *ago1-52 mas5-1*. Plant body architecture in (C) L*er*, (F) *ago1-52*, (I) *ago1-52 mas1-1*, (L) *ago1-52 mas2-1*, (O) *ago1-52 mas4-1*, (R) *ago1-52 mas3-1* and (U) *ago1-52 mas5-1*. Pictures were taken (A, D, G, J, M, P and S) 21, (B, C, E and F) 37, (H, I) 54, (K, L) 41, (N, O, T and U) 45 and (Q, R) 48 days after stratification. Scale bars: (A, B, D, E, G, H, J, K, M, N, P, Q, S and T) 1 mm, and (C, F, I, L, O, R and U) 1 cm.

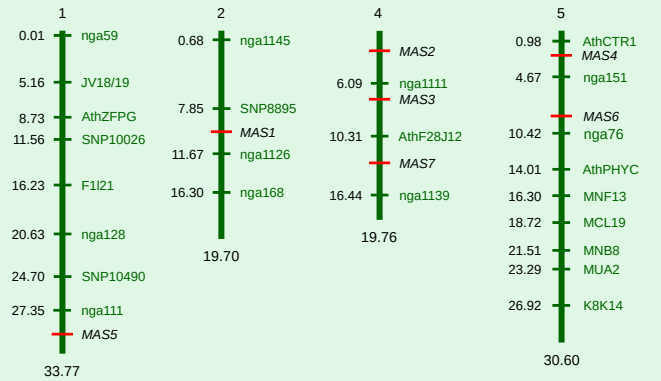

Figure 2.- *Arabidopsis thaliana* physical map with indication of the approximate positions of seven of the *MAS* genes whose characterization is in progress. Low-resolution mapping was performed as described in reference 6. All figures indicate Mb, the only exceptions being chromosome numbers. Chromosome 3 has been deliberately left out of the figure for simplicity.

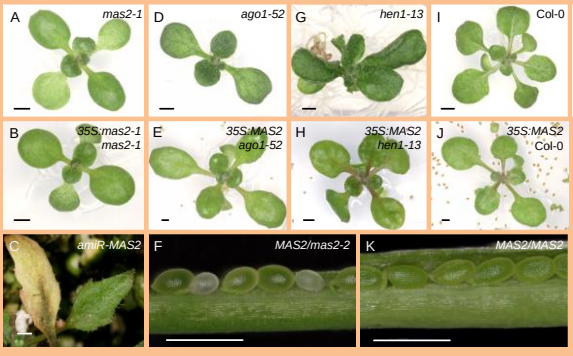

Figure 3.- Rosettes of (A) the *mas2-1* mutant, (B) a L*er* plant carrying a *35S:mas2-1* transgene, (D) the *ago1-52* mutant, (E) an *ago1-52* plant carrying a *35S:MAS2* transgene, (G) the *hen1-13* mutant, (H) a *hen1-13* plant carrying a *35S:MAS2* transgen, (I) the wild type Col-0 and (J) a Col-0 plant carrying a *35S:MAS2* trangene. (C) Details of the leaves of a transgenic plant expressing an amiRNA designed against *MAS2* in a Col-0 background. (F) Seeds of *MAS2/mas2-2* and (K) *MAS2/MAS2* plants. Pictures were taken at (A, B, D, E, G, H, I, J) 15, (F, K) 28 and (C) 45 days after stratification. Scale bars: 1 mm.

REFERENCES

1.- Bohmert, K., Camus, I., Bellini, C., Bouchez, D., Caboche, M., and Benning, C. (1998). *EMBO J.* **17,** 170-180.
2.- Baumbenger, N., and Baulcombe, D.C. (2005). *Proc. Natl. Acad. Sci. USA* **102,** 11928-11933.
3.- Qi, Y., Denli, M., and Hannon, G.J. (2005). *Mol. Cell* **19,** 421-428.
4.- Jover-Gil, S., Candela, H., and Ponce, M.R. (2005). *Int. J. Dev. Biol*. **49,** 733-744.
5.- Ponce, M.R., Quesada, V., and Micol, J.L. (1998). *Plant J.* **14,** 497-501.
6.- Ponce, M.R., Robles, P., Lozano, F.M., Brotóns, M.A., and Micol, J.L. (2006). *Methods Mol. Biol.* **323,** 105-113.

METHODS

Plants were grown at 20±1°C and 60-70% relative humidity, under constant fluorescent light (5,000 lux)[5].

ACKNOWLEDGMENTS

Research in the laboratory of M.R.P. is supported by grants from the Ministerio de Ciencia e Innovación of Spain (BIO2008-01900) and the Generalitat Valenciana (PROMETEO/2009/112 and ACOMP/2009/049). A.B.S.G. holds a fellowship from the Generalitat Valenciana.

Análisis genético y molecular de los genes *MAS* de *Arabidopsis thaliana*

Sánchez-García A.B., Jover-Gil, S., Aguilera V., Quinto P., Micol-Ponce R., Micol J.L., y Ponce, M.R.

Instituto de Bioingeniería, Universidad Miguel Hernández, Campus de Elche, 03202 Elche, Alicante

En *Arabidopsis thaliana*, el principal componente de los complejos del silenciamiento génico inducido por ARN (RISC) es la proteína AGO1 (ARGONAUTE1), cuya insuficiencia de función perturba numerosos procesos de desarrollo y suele causar esterilidad o letalidad. Hemos aislado el mutante *ago1-52*, que es viable, relativamente fértil y portador de un alelo hipomorfo del gen *AGO1*. Con el objetivo de identificar nuevos genes implicados en la ruta del silenciamiento génico mediado por los microARN, hemos mutagenizado semillas de *ago1-52* con metanosulfonato de etilo. Hemos sometido a escrutinio 36.810 semillas M_2, identificando 17 líneas en las que el fenotipo morfológico de *ago1-52* se suprime total o parcialmente. Hemos cartografiado hasta el momento 5 mutaciones supresoras y clonado tres de ellas, que hemos denominado *mas* (*morphology of argonaute1-52 suppressed*). Estamos obteniendo construcciones para la sobreexpresión de los alelos mutantes y silvestres de los genes *MAS*, así como para visualizar sus patrones de expresión espacial y temporal, y para determinar la localización subcelular de las proteínas MAS. También estamos intentando desentrañar los mecanismos moleculares por los cuales *mas1-1*, *mas2-1* y *mas3-1* suprimen el fenotipo morfológico de *ago1-52.*

2010

X Reunión de Biología Molecular de Plantas

Valencia

Póster

Análisis genético y molecular de los genes *MAS* de *Arabidopsis thaliana*

A.B. Sánchez-García, S. Jover-Gil, V. Aguilera, P. Quinto, R. Micol-Ponce, J.L. Micol y M.R. Ponce

Instituto de Bioingeniería, Universidad Miguel Hernández, Campus de Elche, 03202 Elche, Alicante.
mrponce@umh.es genetica.umh.es

En *Arabidopsis thaliana*, el principal componente de los complejos de silenciamiento génico mediado por los microARN (RISC) es la proteína AGO1 (ARGONAUTE1), cuya insuficiencia de función perturba numerosos procesos de desarrollo y suele causar esterilidad o letalidad[1-3]. Con el objetivo de identificar nuevos genes implicados en el silenciamiento génico mediado por los miARN, hemos mutagenizado con EMS semillas M_1 de *ago1-52*, un mutante aislado anteriormente en nuestro laboratorio[4].

Tras el escrutinio de 36.810 semillas M_2, identificamos 4.189 presuntos dobles mutantes (Tabla 1), muchos de los cuales fueron estériles y mostraron un fenotipo Ago1-52 extremo. Sólo 302 presuntos dobles mutantes M_2 fueron fértiles y viables, y 21 de ellos mostraron una supresión parcial del fenotipo Ago1-52. Entre estos 21 mutantes, 4 presentaron una supresión muy débil y fueron descartados. Las 17 líneas restantes mostraron un fenotipo muy similar al de la estirpe silvestre L*er*. El porte y otros rasgos morfológicos del fenotipo Ago1-52 se normalizaron en la mayoría de estas líneas (Fig. 1).

Hemos cartografiado hasta el momento siete de estas mutaciones supresoras, a las que hemos llamado *mas* (*morphology of argonaute1-52 suppressed*), y hemos clonado tres de ellas (Fig. 2). La clonación posicional de la mutación *mas2-1* nos ha permitido determinar que *MAS2* es un gen de copia única, que codifica una proteína de función desconocida y que está conservada en animales y plantas. Nuestros resultados sugieren que *mas2-1* es un alelo de ganancia de función, que contiene una mutación puntual que no causa un fenotipo visible en las plantas *mas2-1/mas2-1;AGO1/AGO1*. Hemos identificado una línea portadora de una inserción de ADN-T en el gen *MAS2* y la hemos llamado *mas2-2*. *MAS2* parece ser un gen esencial, ya que los embriones *mas2-2/mas2-2* sufren letalidad (Fig. 3).

La expresión constitutiva de *MAS2* no causa efectos fenotípicos en un fondo silvestre pero es capaz de suprimir el fenotipo mutante de las plantas *ago1-52* y *hen1-13* (Fig. 3). Estas observaciones confirman que *mas2-1* es un alelo hipermorfo, capaz de suprimir los fenotipos de la insuficiencia de función de los genes *AGO1* y *HEN1*, que participan en las rutas de los miARN y los ARN cortos interfentes (siARN). La sobreexpresión de *mas2-1* en un fondo silvestre no tiene efectos fenotípicos.

Otra aproximación llevada a cabo para determinar la función de *MAS2* ha sido la generación de plantas transgénicas portadoras de una construcción que contenía un miARN artificial (amiARN) diseñado contra el ARNm de *MAS2*. La expresión de este amiARN en plantas transgénicas causa un fenotipo de hojas aserradas, que muestran una senescencia prematura (Fig. 3), lo que sugiere que *MAS2* podría estar implicado en la senescencia o la muerte celular en Arabidopsis.

Tabla 1.- Presuntos dobles mutantes identificados tras la mutagénesis de *ago1-52* con EMS

	M_2			M_3
	Letal	Estériles	Fértiles	
Total	3.366	521	302	92
Fenotipo Ago1-52 extremo	23	67	42	11
Fenotipo Ago1-52 débil	29	91	93	21
Sinergia	3.130	3	0	0
Otros fenotipos mutantes	184	360	167	60

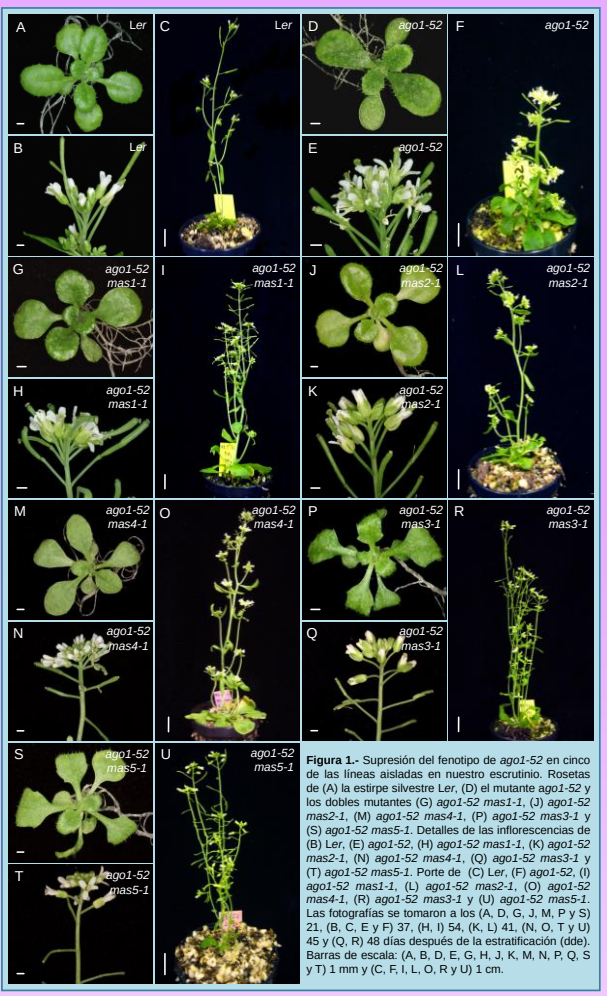

Figura 1.- Supresión del fenotipo de *ago1-52* en cinco de las líneas aisladas en nuestro escrutinio. Rosetas de (A) la estirpe silvestre L*er*, (D) el mutante *ago1-52* y los dobles mutantes (G) *ago1-52 mas1-1*, (J) *ago1-52 mas2-1*, (M) *ago1-52 mas4-1*, (P) *ago1-52 mas3-1* y (S) *ago1-52 mas5-1*. Detalles de las inflorescencias de (B) L*er*, (E) *ago1-52*, (H) *ago1-52 mas1-1*, (K) *ago1-52 mas2-1*, (N) *ago1-52 mas4-1*, (Q) *ago1-52 mas3-1* y (T) *ago1-52 mas5-1*. Porte de (C) L*er*, (F) *ago1-52*, (I) *ago1-52 mas1-1*, (L) *ago1-52 mas2-1*, (O) *ago1-52 mas4-1*, (R) *ago1-52 mas3-1* y (U) *ago1-52 mas5-1*. Las fotografías se tomaron a los (A, D, G, J, M, P y S) 21, (B, C, E y F) 37, (H, I) 54, (K, L) 41, (N, O, T y U) 45 y (Q, R) 48 días después de la estratificación (dde). Barras de escala: (A, B, D, E, G, H, J, K, M, N, P, Q, S y T) 1 mm y (C, F, I, L, O, R y U) 1 cm.

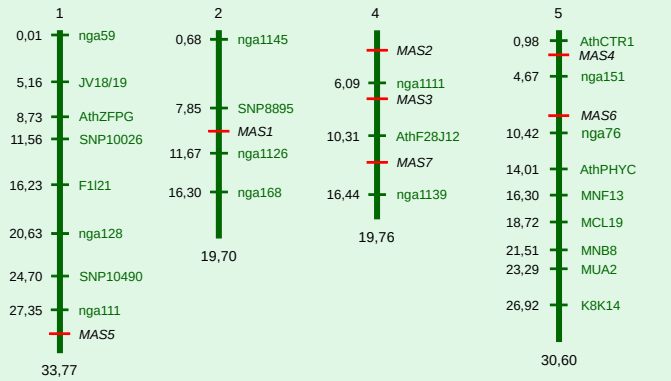

Figura 2.- Mapa físico de 4 de los 5 cromosomas de *Arabidopsis thaliana* en el que se indican las posiciones de los siete genes supresores que estamos analizando. La cartografía se realizó según se describe en la referencia 6. Todos los números indican Mb, excepto los que aparecen sobre los cromosomas. Se ha omitido deliberadamente el cromosoma 3.

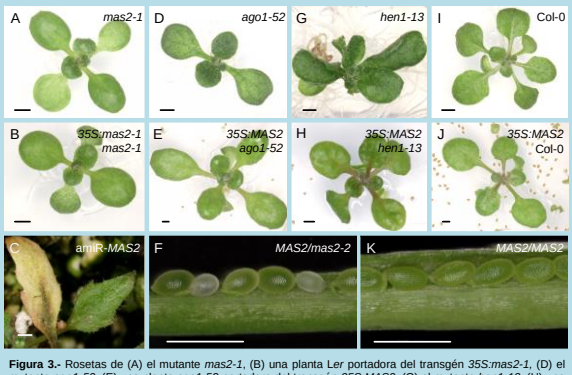

Figura 3.- Rosetas de (A) el mutante *mas2-1*, (B) una planta L*er* portadora del transgén *35S:mas2-1*, (D) el mutante *ago1-52*, (E) una planta ago1-52 portadora del transgén *35S:MAS2*, (G) el mutante *hen1-13*, (H) una planta *hen1-13* portadora del transgén *35S:MAS2*, (I) la estirpe silvestre Col-0 y (J) una planta Col-0 portadora del transgén *35S:MAS2*. (C) Detalles de las hojas de una planta transgénica que expresa un amiARN diseñado contra *MAS2*. (F) Silicuas inmaduras de plantas *MAS2/mas2-2* (obsérvese la letalidad embrionaria) y (K) *MAS2/MAS2*. Las fotos se tomaron (A, B, D, E, G, H, I, J) 15, (F, K) 28 y (C) 45 dde. Barras de escala: 1 mm.

BIBLIOGRAFÍA

1.- Bohmert, K., Camus, I., Bellini, C., Bouchez, D., Caboche, M., y Benning, C. (1998). *EMBO J.* **17,** 170-180.
2.- Baumbenger, N., y Baulcombe, D.C. (2005). *Proc. Natl. Acad. Sci. USA* **102,** 11928-11933.
3.- Qi, Y., Denli, M., y Hannon, G.J. (2005). *Mol. Cell* **19,** 421-428.
4.- Jover-Gil, S., Candela, H., y Ponce, M.R. (2005). *Int. J. Dev. Biol.* **49,** 733-744.
5.- Ponce, M.R., Quesada, V., y Micol, J.L. (1998). *Plant J.* **14,** 497-501.
6.- Ponce, M.R., Robles, P., Lozano, F.M., Brotóns, M.A., y Micol, J.L. (2006). *Methods Mol. Biol.* **323,** 105-113.

MATERIALES Y MÉTODOS

Los cultivos se realizaron a 20±1°C y 60-70% de humedad relativa, bajo iluminación continua (5,000 lux)[5].

AGRADECIMIENTOS

El trabajo en el laboratorio de M.R.P. ha sido financiado por el Ministerio de Ciencia e Innovación (proyecto BIO2008-01900) y por la Generalitat Valenciana (proyectos PROMETEO/2009/112 y ACOMP/2009/049). A.B.S.G. disfruta de una beca concedida por la Generalitat Valenciana.

The Arabidopsis *MAS* genes

Sánchez-García, A.B., Jover-Gil, S., Aguilera, V., Quinto, P., Micol-Ponce, R., Micol, J.L., and Ponce, M.R.

Instituto de Bioingeniería, Universidad Miguel Hernández, Campus de Elche, 03202 Elche, Alicante, Spain

In *Arabidopsis thaliana*, the core component of the miRNA mediated silencing complex (RISC) is encoded by the *ARGONAUTE1* (*AGO1*) gene, whose *ago1* loss-of-function mutant alleles disturb many developmental processes and often cause lethality or sterility. With a view to identify novel genes involved in miRNA-guided gene silencing, we mutagenized with EMS seeds of the viable and fertile *ago1-52* line, which had been isolated in our laboratory. After screening 36,810 M_2 seeds, we identified 4,189 putative double mutants, most of which were sterile and displayed a mutant phenotype stronger than that of *ago1-52*. Only 302 M_2 putative double mutants were viable and fertile, 21 of which displayed partial suppression of the Ago1-52 phenotype. Four of them exhibited only weak suppression and were discarded. Some of the remaining 17 were not easily distinguishable from the L*er* wild type. Plant body architecture and other morphological traits of the Ago1-52 phenotype became normalized in most of these lines carrying suppressor mutations.

We have mapped so far seven of these suppressor mutations, which we named *mas* (*morphology of argonaute1-52 suppressed*), and positionally cloned three of them. Positional cloning of the *mas2-1* mutation allowed us to determine that *MAS2* is a single-copy gene encoding a protein of unknown function, conserved among plants and animals. *mas2-1* seems to be a gain-of-function allele and carries a point mutation that causes no visible phenotype in *mas2-1/mas2-1;AGO1/AGO1* plants. We identified a line carrying a T-DNA insertion in the *MAS2* gene, which we named *mas2-2*. *MAS2* seems to be an essential gene as suggested by lethality of *mas2-2/mas2-2* embryos.

Constitutive expression of *MAS2* had no phenotypic effects in a wild-type background but suppressed the mutant phenotype in *ago1-52* and *hen1-13* plants. This observation confirms that the gain of function of *MAS2* is able to suppress the phenotypes of loss-of-function mutations affecting the *AGO1* and *HEN1* genes, which participate in the miRNA and short interfering RNA (siRNA) pathways. We have also obtained transgenic plants overexpressing *mas2-1* in a wild-type background, which show a wild-type phenotype.

Another approach taken to determine the function of *MAS2* was the generation of transgenic plants carrying a construct for the expression of an artificial miRNA (amiRNA) designed to target *MAS2* mRNA. These transgenic plants rendered a phenotype of serrated leaves that exhibited premature senescence, suggesting that *MAS2* might be involved in senescence or cell death pathways in Arabidopsis.

2010

Plant Biology 2010

Montreal

Póster

The Arabidopsis *MAS* genes

A.B. Sánchez-García, S. Jover-Gil, V. Aguilera, P. Quinto, R. Micol-Ponce, J.L. Micol and M.R. Ponce

Instituto de Bioingeniería, Universidad Miguel Hernández, Campus de Elche, 03202 Elche, Alicante, Spain.

mrponce@umh.es genetica.umh.es

In *Arabidopsis thaliana*, the core component of the miRNA mediated silencing complex (RISC) is encoded by the *ARGONAUTE1* (*AGO1*) gene, whose *ago1* loss-of-function mutant alleles disturb many developmental processes and often cause lethality or sterility[1-3]. With a view to identify novel genes involved in miRNA-guided gene silencing, we mutagenized with EMS M_1 seeds of the viable and fertile *ago1-52* line, which had been isolated in our laboratory[4]. After screening 36,810 M_2 seeds, we identified 4,189 putative double mutants (Table 1), most of which were sterile and displayed a mutant phenotype stronger than that of *ago1-52*. Only 302 M_2 putative double mutants were viable and fertile, 21 of which displayed partial suppression of the Ago1-52 phenotype. Four of them exhibited only weak suppression and were discarded. Some of the remaining 17 were not easily distinguishable from the L*er* wild type. Plant body architecture and other morphological traits of the Ago1-52 phenotype became normalized in most of these lines carrying suppressor mutations (Fig. 1).

We have mapped so far seven of these suppressor mutations, which we named *mas* (*morphology of argonaute1-52 suppressed*), and positionally cloned three of them (Fig. 2). Positional cloning of the *mas2-1* mutation allowed us to determine that *MAS2* is a single-copy gene encoding a protein of unknown function, conserved among plants and animals. *mas2-1* seems to be a gain-of-function allele and carries a point mutation that causes no visible phenotype in *mas2-1/mas2-1;AGO1/AGO1* plants. We identified a line carrying a T-DNA insertion in the *MAS2* gene, which we named *mas2-2*. *MAS2* seems to be an essential gene as suggested by lethality of *mas2-2/mas2-2* embryos (Fig. 3).

Constitutive expression of *MAS2* had no phenotypic effects in a wild-type background but suppressed the mutant phenotype in a*go1-52* and *hen1-13* plants (Fig. 3). This observation confirms the gain of function of *MAS2* is able to suppress the phenotypes of loss-of-function mutations affecting the *AGO1* and *HEN1* genes, which participate in the miRNA and short interfering RNA (siRNA) pathways. We have also obtained transgenic plants overexpressing *mas2-1* in a wild-type background, which show a wild-type phenotype.

Another approach taken to determine the function of *MAS2* was the generation of transgenic plants carrying a construct for the expression of an artificial miRNA (amiRNA) designed to target *MAS2* mRNA. These transgenic plants rendered a phenotype of serrated leaves that exhibited premature senescence (Fig. 3), suggesting that *MAS2* might be involved in senescence or cell death pathways in Arabidopsis.

Table 1.- Putative double mutants isolated in our screening

	M_2			M_3
	Lethal	Esterile	Fertile	
Total	3,366	521	302	92
Extremed Ago1-52 phenotype	23	67	42	11
Partially supressed Ago1-52 phenotype	29	91	93	21
Synergistic	3,130	3	0	0
Other mutant phenotypes	184	360	167	60

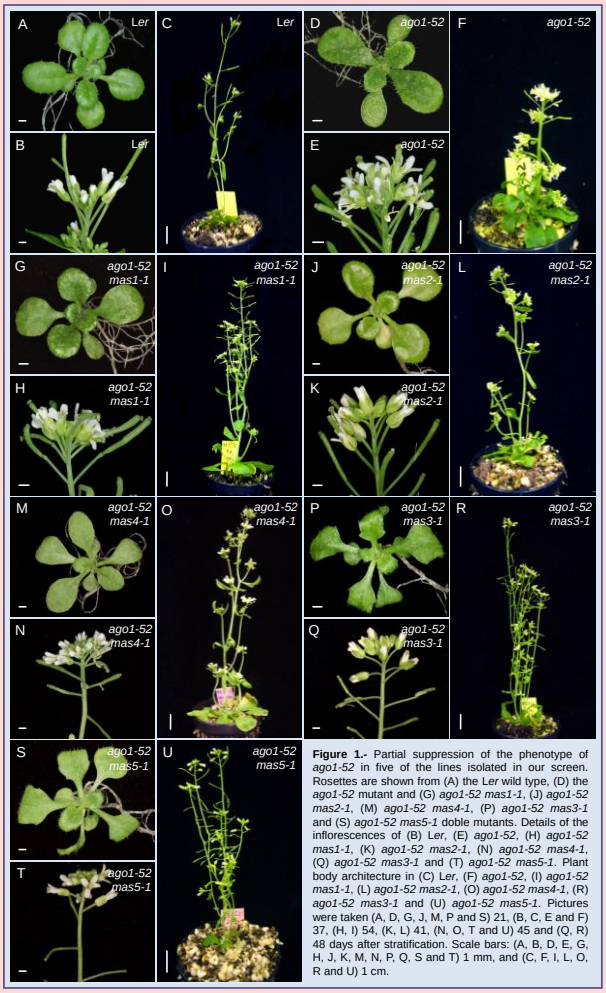

Figure 1.- Partial suppression of the phenotype of *ago1-52* in five of the lines isolated in our screen. Rosettes are shown from (A) the L*er* wild type, (D) the *ago1-52* mutant and (G) *ago1-52 mas1-1*, (J) *ago1-52 mas2-1*, (M) *ago1-52 mas4-1*, (P) *ago1-52 mas3-1* and (S) *ago1-52 mas5-1* doble mutants. Details of the inflorescences of (B) L*er*, (E) *ago1-52*, (H) *ago1-52 mas1-1*, (K) *ago1-52 mas2-1*, (N) *ago1-52 mas4-1*, (Q) *ago1-52 mas3-1* and (T) *ago1-52 mas5-1*. Plant body architecture in (C) L*er*, (F) *ago1-52*, (I) *ago1-52 mas1-1*, (L) *ago1-52 mas2-1*, (O) *ago1-52 mas4-1*, (R) *ago1-52 mas3-1* and (U) *ago1-52 mas5-1*. Pictures were taken (A, D, G, J, M, P and S) 21, (B, C, E and F) 37, (H, I) 54, (K, L) 41, (N, O, T and U) 45 and (Q, R) 48 days after stratification. Scale bars: (A, B, D, E, G, H, J, K, M, N, P, Q, S and T) 1 mm, and (C, F, I, L, O, R and U) 1 cm.

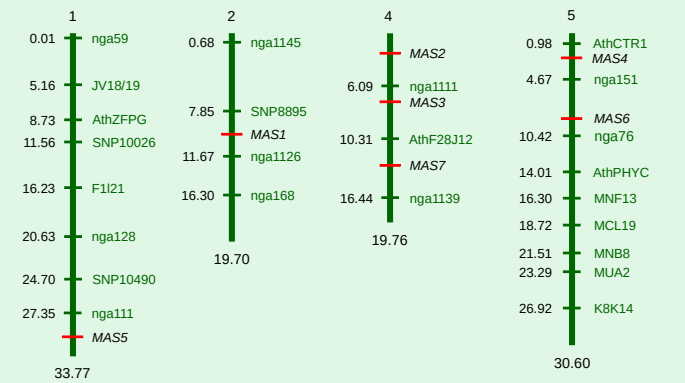

Figure 2.- *Arabidopsis thaliana* physical map with indication of the approximate positions of seven of the *MAS* genes whose characterization is in progress. Low-resolution mapping was performed as described in reference 6. All figures indicate Mb, the only exceptions being chromosome numbers. Chromosome 3 has been deliberately left out of the figure for simplicity.

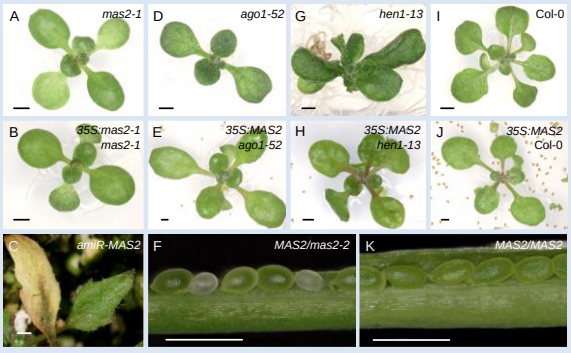

Figure 3.- Rosettes of (A) the *mas2-1* mutant, (B) a L*er* plant carrying a *35S:mas2-1* transgene, (D) the *ago1-52* mutant, (E) an *ago1-52* plant carrying a *35S:MAS2* transgene, (G) the *hen1-13* mutant, (H) a *hen1-13* plant carrying a *35S:MAS2* transgen, (I) the wild type Col-0 and (J) a Col-0 plant carrying a *35S:MAS2* trangene. (C) Details of the leaves of a transgenic plant expressing an amiRNA designed against *MAS2* in a Col-0 background. (F) Seeds of *MAS2/mas2-2* and (K) *MAS2/MAS2* plants. Pictures were taken at (A, B, D, E, G, H, I, J) 15, (F, K) 28 and (C) 45 days after stratification. Scale bars: 1 mm.

REFERENCES

1.- Bohmert, K., Camus, I., Bellini, C., Bouchez, D., Caboche, M., and Benning, C. (1998). *EMBO J.* **17,** 170-180.
2.- Baumbenger, N., and Baulcombe, D.C. (2005). *Proc. Natl. Acad. Sci. USA* **102,** 11928-11933.
3.- Qi, Y., Denli, M., and Hannon, G.J. (2005). *Mol. Cell* **19,** 421-428.
4.- Jover-Gil, S., Candela, H., and Ponce, M.R. (2005). *Int. J. Dev. Biol.* **49,** 733-744.
5.- Ponce, M.R., Quesada, V., and Micol, J.L. (1998). *Plant J.* **14,** 497-501.
6.- Ponce, M.R., Robles, P., Lozano, F.M., Brotóns, M.A., and Micol, J.L. (2006). *Methods Mol. Biol.* **323,** 105-113.

METHODS

Plants were grown at 20±1°C and 60-70% relative humidity, under constant fluorescent light (5,000 lux)[5].

ACKNOWLEDGMENTS

Research in the laboratory of M.R.P. is supported by grants from the Ministerio de Ciencia e Innovación of Spain (BIO2008-01900) and the Generalitat Valenciana (PROMETEO/2009/112 and ACOMP/2009/049). A.B.S.G. holds a fellowship from the Generalitat Valenciana.

Characterization of the Arabidopsis *MAS5* gene

Micol-Ponce, R., Aguilera, V., Parres-Molina, L., Micol, J.L., and Ponce M.R.

Instituto de Bioingeniería, Universidad Miguel Hernández, Campus de Elche, 03202 Elche, Alicante, Spain

We screened 37.000 M_2 seeds derived from a second-site mutagenesis of the *ago1-52* line, which carries a hypomorphic and viable recessive allele of the *ARGONAUTE1* (*AGO1*) gene of *Arabidopsis thaliana* in a L*er* genetic background. We isolated in this way 17 mutants exhibiting suppression of the morphological phenotype of *ago1-52*, which we named *mas* (*morphology of argonaute1-52 suppressed*).

For the positional cloning of the *mas5-1* mutation, we first obtained F_2 mapping populations by crossing the *ago1-52 mas5-1* double mutant either to *ago1-25* or *ago1-27* single mutants, both of which carry a hypomorphic allele of *AGO1* in a Col-0 genetic background. Iterative linkage analysis to molecular markers allowed us to define a 445 kb candidate interval encompassing 122 genes. In silico analyses of these genes and the subsequent sequencing of some of them allowed us to identify a G to A transition —that would result in the substitution of a lysine by glutamic acid— in a gene involved in an essential step in the maturation of pre-mRNA.

Whereas null alleles of *MAS5* are embryonic lethal, our results suggest that *mas5-1* is a dominant allele, probably of gain of function. We will continue our molecular and genetic characterization of *MAS5* to unravel its functional relationship with *AGO1*.

2011

Plant Growth Biology and Modeling 2011

Elche

Póster

Characterization of the Arabidopsis *MAS5* gene

Micol-Ponce, R., Aguilera, V., Parres-Molina, L., Micol, J.L., and Ponce, M.R.

Instituto de Bioingeniería, Universidad Miguel Hernández, Campus de Elche, 03202 Elche, Alicante, Spain

rmicol@umh.es mrponce@umh.es http:\\genetica.umh.es

We screened 37.000 M_2 seeds derived from a second-site mutagenesis of the *ago1-52* line[1], which carries a hypomorphic and viable recessive allele of the *ARGONAUTE1* (*AGO1*)[2] gene of *Arabidopsis thaliana* in a L*er* genetic background. We isolated in this way 17 mutants exhibiting suppression of the morphological phenotype of *ago1-52*. We have named *mas* (*morphology of argonaute1-52 suppressed*) to the suppressor mutations. *MAS5* is the mutated gene in the P8 25.1 line (Fig. 1) and *mas5-1* its mutant allele.

For the positional cloning of the *mas5-1* mutation, we first obtained F_2 mapping populations by crossing the *ago1-52 mas5-1* double mutant either to *ago1-25* or *ago1-27* single mutants, both of which carrying hypomorphic alleles of *AGO1,* in a Col-0 genetic background[3]. Iterative linkage analysis to molecular markers allowed us to define a 445 kb candidate interval encompassing 122 genes. In silico analyses of these genes (Fig. 2) and the subsequent sequencing of some of them allowed us to identify in AT1G80070 a G to A transition —that would result in the substitution of a lysine by glutamic acid— in a highly conserved region of the protein (Fig. 3 and 4). MAS5 encodes a PRP8 factor (pre-mRNA processing factor 8), a large protein (2,359 aa in Arabidopsis) highly conserved in eukaryotes, which is a central component of the spliceosome (Fig. 5).

Whereas null alleles of *MAS5* are embryonic lethal [the gene is also known as *SUS2* (*ABNORMAL SUSPENSOR 2*), *EMB14* (*EMBRYO DEFECTIVE 14*), *EMB33* and *EMB177*], our results suggest that *mas5-1* is a dominant allele, probably of gain of function (Fig. 6). We will continue our molecular and genetic characterization of *MAS5* to unravel its functional relationship with *AGO1*.

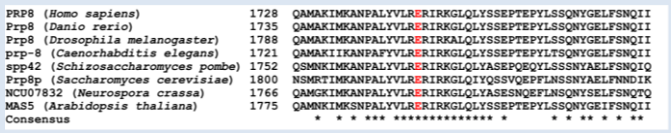

PRP8 (*Homo sapiens*)	1728	QAMAKIMKANPALYVLRERIRKGLQLYSSEPTEPYLSSQNYGELFSNQII
Prp8 (*Danio rerio*)	1735	QAMAKIMKANPALYVLRERIRKGLQLYSSEPTEPYLSSQNYGELFSNQII
Prp8 (*Drosophila melanogaster*)	1788	QAMAKIMKANPALYVLRERIRKALQLYSSEPTEPYLSSQNYGELFSNQII
prp-8 (*Caenorhabditis elegans*)	1721	QAMAKIIKANPAFYVLRERIRKGLQLYSSEPTEPYLTSQNYGELFSNQII
spp42 (*Schizosaccharomyces pombe*)	1752	QSMNKIMKANPALYVLRERIRKGLQLYASEPQEQYLSSSNYAELFSNQIQ
Prp8p (*Saccharomyces cerevisiae*)	1800	NSMRTIMKANPALYVLRERIRKGLQIYQSSVQEPFLNSSNYAELFNNDIK
NCU07832 (*Neurospora crassa*)	1766	QAMGKIMKANPALYVLRERIRKGLQLYASESNQEFLNSQNYSELFSNQTQ
MAS5 (*Arabidopsis thaliana*)	1775	QAMNKIMKSNPALYVLRERIRKGLQLYSSEPTEPYLSSQNYGEIFSNQII
Consensus		* * * *** ************** * * ** * * **

Figure 4.- Partial alignment of PRP8 proteins. Only the region around the amino acid changed by the *mas5-1* mutation (in red) is shown. Numbers correspond to amino acid positions in the corresponding orthologous proteins. Sequences were obtained from NCBI (http://www.ncbi.nlm.nih.gov) and aligned with the CLUSTALW2 program (http://www.ebi.ac.uk/Tools/msa/clustalw2/). Asterisks indicate conserved residues in all aligned proteins.

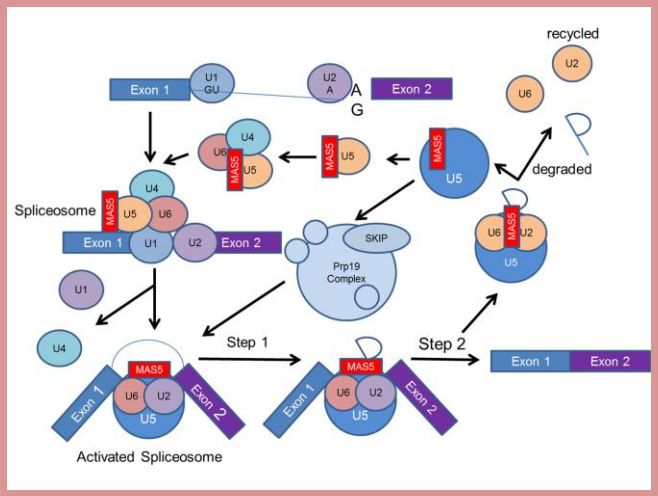

Figure 5.- Assembly and recycling of major spliceosome components. PRP8 appears here as MAS5. U1-U6 are small nuclear RNA–protein (snRNP) complexes formed by small nuclear RNAs (snRNAs) and proteins. Spliceosome is formed stepwise, through several "presplicing complexes". Splicing involves two trans-esterification reactions that require PRP8. Following completion of the splicing reaction, spliceosome components are recycled and the intron is degraded. Adapted from Grainger and Beggs (2005).

Figure 1.- Some phenotypic traits of the P8 25.1 (*ago1-52 mas5-1*) line. (A-C) Inflorescences and (E-G) rosettes of (A, E) L*er*, (B, F) P8 25.1 and (C, G) *ago1-52*. (D) From left to right, adult plants of L*er*, P8 25.1 and *ago1-52*. Pictures were taken (A-D) 54 and (E-G) 21 days afeter stratification (das). Scale bars: (A-C, E-G) 1 mm and (D) 1 cm.

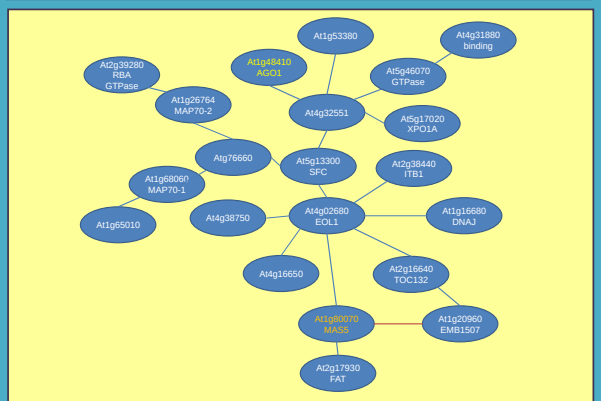

Figure 2.- Coexpressed gene network for *AGO1* and *MAS5*. Thick lines indicate higher coexpression than thin. Orange lines indicate conserved coexpression between Arabidopsis and at least one of three mammalian species (human, mouse and rat)[1]. Redrawn from from the output of ATTED[4] (at http://atted.jp/gmap/).

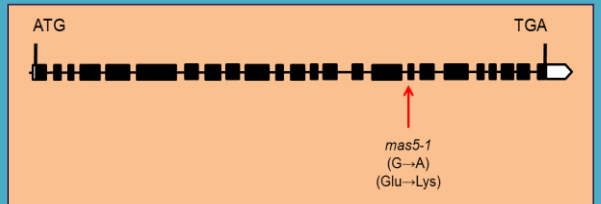

Figure 3.- Schematic representation of the *MAS5* gene. Exons and introns are depicted as black boxes and lines, respectively. White boxes indicate 5´and 3´UTRs. The predicted translation start (ATG) and stop (TAA) codons are indicated. A red arrow marks the position of the point mutation in the *mas5-1* allele, and the predicted amino acid substitution in the MAS5 protein.

Figure 6.- Dominance of the suppresor effect of *mas5-1* on *ago1-52*. Rosettes are shown from (A) *ago1-52/ago1-52;MAS5/MAS5*, (B) *ago1-52/ago1-52; MAS5/mas5-1* and (C) *ago1-52/ago1-52;mas5-1/mas5-1* plants. Pictures were taken 17 das.

METHODS

Plant growth and low resolution mapping were performed as described in refs. 6 and 7, respectively.

.

REFERENCES

1.- Jover-Gil, S., Candela, H., and Ponce, M.R. (2005). *Int. J. Dev. Biol.* **49**, 733-744.
2.- Bohmert, K., Camus, I., Bellini, C., Bouchez, D., Caboche, M., and Benning, C. (1998). *EMBO J.* **17,** 170-180.
3.- Morel, J.B., Godon, C., Mourrain, P., Béclin, C., Boutet, S., Feuerbach, F., Proux, F., and Vaucheret, H. (2002). *Plant Cell* **14**, 629-639.
4.- Obayashi T, Nishida K, Kasahara K, and Kinoshita K. (2011). Plant Cell Phys. 52, 213-219.
5.- Grainger, R.J., and Beggs, J.D. (2005). *RNA* **11,** 533-537.
6.- Ponce, M.R., Quesada, V., and Micol, J.L. (1998). Plant J. 14, 497-501.
7.- Ponce, M.R., Robles, P., Lozano, F.M., Brotóns, M.A., and Micol, J.L. (2006). *Methods Mol. Biol.* **323,** 105-113.

ACKNOWLEDGEMENTS

ago1-25 and *ago1-27* lines were a gift from H. Vaucheret. Research in the laboratory of M.R.P. is supported by grants from the Ministerio de Ciencia e Innovación of Spain (BIO2008-01900) and the Generalitat Valenciana (PROMETEO/2009/112 and ACOMP/2009/049).

Genetic and molecular analysis of the *MAS2* gene of *Arabidopsis thaliana*

Sánchez-García, A.B., Jover-Gil, S., Aguilera, V., Micol-Ponce, R., Kahveci, Z., Olechwier, A.M., Micol, J.L. and Ponce, M.R.

Instituto de Bioingeniería, Universidad Miguel Hernández, Campus de Elche, 03202 Elche, Alicante, Spain

In eukaryotes, small non-coding RNAs mediate transcriptional and post-transcriptional gene silencing by binding to ARGONAUTE (AGO) proteins to form RNA-Induced Silencing Complexes (RISCs). AGO1 is the main component of the miRNA pathway in Arabidopsis. We had previously isolated *ago1-52*, a hypomorphic allele of *AGO1*. We isolated suppressor mutations that were named *mas* (*morphology of argonaute1-52 suppressed*) after an EMS second-site mutagenesis of *ago1-52* plants.

Positional cloning of the *MAS2* gene revealed that it is a single copy Arabidopsis gene that encodes a protein of unknown function and conserved among plants and animals. The *mas2-1* point mutation causes an alanine-to-threonine substitution at a highly conserved position of the MAS2 protein and has no visible phenotype by its own. A T-DNA insertion that disrupts *MAS2* (*mas2-2*) causes embryonic lethality. We are obtaining transgenic plants expressing an artificial microRNA targeting *MAS2*.

Overexpression of the wild-type allele of *MAS2* in an *ago1-52* background suppressed the mutant phenotype of *ago1-52*. We have also obtained constructs that showed the ubiquitous expression of *MAS2* and the nuclear localization of its protein product, as already known for its animal´s orthologs.

2011

Plant Growth Biology and Modelling 2011

Elche

Póster

Genetic and molecular analysis of the *MAS2* gene of *Arabidopsis thaliana*

Sánchez-García, A.B., Jover-Gil, S., Aguilera, V., Micol-Ponce, R., Kahveci, Z., Olechwier, A.M., Micol, J.L., and Ponce, M.R.

Instituto de Bioingeniería, Universidad Miguel Hernández, Campus de Elche, 03202 Elche, Alicante, Spain
ana.sanchezg@umh.es mrponce@umh.es http://genetica.umh.es

In eukaryotes, small non-coding RNAs mediate transcriptional and post-transcriptional gene silencing by binding to ARGONAUTE (AGO) proteins to form RNA-Induced Silencing Complexes (RISCs). AGO1 is the main component of the microRNA pathway in Arabidopsis, which also participates in other small interfering RNA-mediated pathways.

Aiming to identify novel genes functionally related to *AGO1*, we performed a screen for suppressors of the phenotype of *ago1-52*, a hypomorphic allele of *AGO1* previously isolated in our laboratory[1]. We have named *mas* (*morphology of argonaute1-52 suppressed*) the suppressor mutations isolated after an EMS second-site mutagenesis of *ago1-52* plants, *MAS2* to the mutated gene in the P2 11.1 line (Fig. 1) and *mas2-1* to its mutant allele.

Positional cloning of the *MAS2* gene (Fig. 2A) revealed that it is a single copy Arabidopsis gene that encodes a protein of unknown function and conserved among plants and animals. The *mas2-1* point mutation causes an alanine-to-threonine substitution at a highly conserved position of the MAS2 protein (Fig. 2B) and has an almost wild-type phenotype, consisting of wider apexes of the fruits and more roundish leaves than those of the wild type (Fig. 3A-G).

We identified a T-DNA insertion that disrupts *MAS2*, which was named *mas2-2* (Fig. 2B). This insertional allele causes embryonic lethality (Fig. 3H-N), which suggests that *MAS2* is essential during embryogenesis.

We obtained transgenic plants expressing an artificial microRNA targeting *MAS2*, which allow us to study different degrees of loss of function of the *MAS2* gene throughout the plant life cycle (Fig. 4).

We also obtained constructs that showed the ubiquitous expression of *MAS2* (Fig. 5A-I) and the nuclear localization of the MAS2 protein (Fig. 5J-L), as already known for its animal´s orthologs.

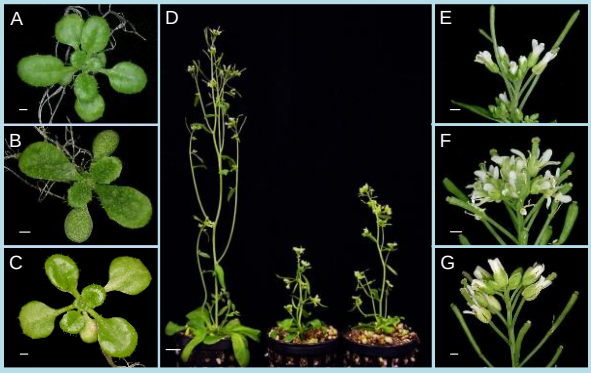

Figure 1.- Some phenotypic traits of the P2 11.1 (*ago1-52 mas2-1*) line. (A-C) Rosettes of (A) *Ler*, (B) *ago1-52* and (C) P2 11.1. (D) From left to right, adult plants of *Ler*, *ago1-52* and P2 11.1. (E-G) Inflorescences of (E) *Ler*, (F) *ago1-52* and (G) P2 11.1. Pictures were taken (A-C) 21 and (D-G) 43 days after stratification (das). Scale bars: (A-C, E-G) 1 mm and (D) 1 cm.

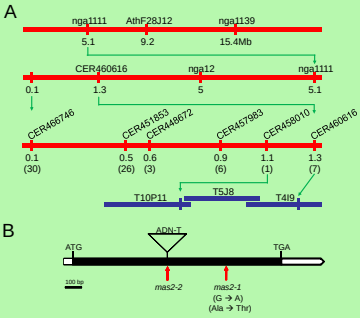

Figure 2.- Positional cloning of the *MAS2* gene. (A) Red bars represent chromosome 2 segments, and blue bars indicate BAC clones that contain the candidate region for the *MAS2* gene. The number of informative recombinants for each marker is shown between brackets. Low resolution mapping indicated that *MAS2* is flanked by the CER458010 and CER460616 markers. (B) *MAS2* gene sequencing in double mutants revealed the presence of a G→A transition that causes an aminoacid change (alanine-to-threonine) in a highly conserved region of the MAS2 protein. Low resolution mapping was performed as described in Ponce *et al.* (2006).

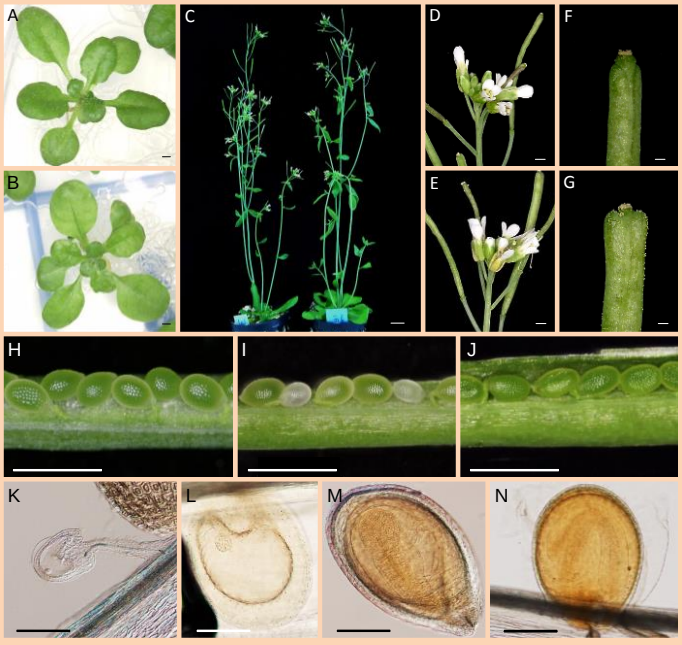

Figure 3.- (A, B) Rosettes of (A) *Ler* and (B) *mas2-1*. (C) From left to right, plants of *Ler* and *mas2-1* collected at 45 das. (D, E) Inflorescences of (D) *Ler* and (E) *mas2-1*. (F, G) Siliques of (F) *Ler* and (G) *mas2-1*. (H-J) Seeds of (H) *mas2-1*, (I) *mas2-2* and (J) *Ler*. (K) Unfertilized ovule in a *MAS2*/*mas2-2* plant. (L-N) Embryos of *MAS2*/*mas2-2* plants in (L) globular, (M) globular-heart and (N) mature stages. Scale bars: (A, B, n D-J) 1 mm, (C) 1 cm and (K-N) 200 µm.

Figura 4.- Transgenic T_2 plants carrying a *35S:amiR-MAS2* construct. Individuals were classified according to the severity of their phenotype in (A) wild type, (B) mutant and (C) mutant with a extreme phenotype. (D-F) Detail of (D, E) leaves of (D) a wild-type and (E) a mutant plant, and (F) a dissected fruit of a mutant displaying the same phenotype as in B. Red arrows indicate seeds with arrested embryo development and unfertilized ovules. Pictures were taken (A-E) 21 and (F) 54 das. Scale bars: 1 mm.

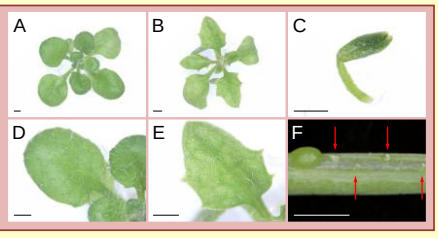

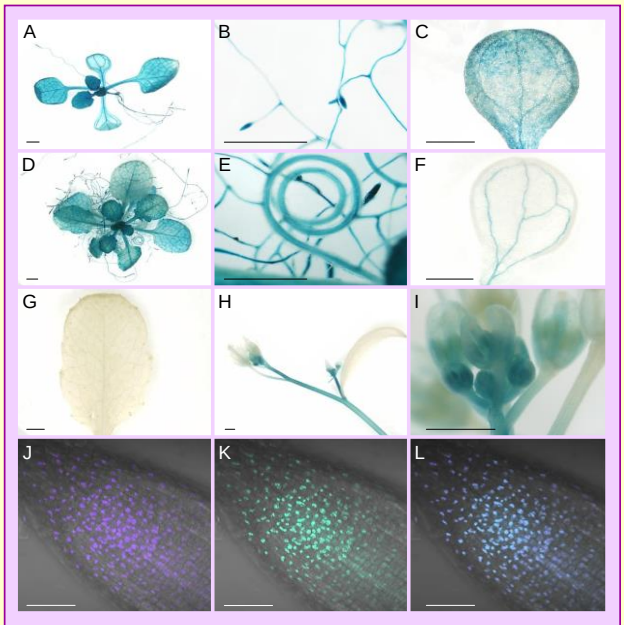

Figure 5.- Expression analysis of the *MAS2* gene. (A-I) Detection of β-glucuronidase activity in T_2 plants carrying a $MAS2_{pro}$:*GUS* construct. (A, D) Rosettes, (B, E) roots and (C, F) cotyledons of (A-C) 15 and (D-F) of plants collected at 28 das. (G) Leaf, (H) shoot and (I) inflorescence of a 48-das plant. (J-L) Subcellular localization of the MAS2 protein. (J) Detection of the fluorescent emission of DAPI (4',6-diamidino-2-phenylindole), (K) GFP and (L) their overlay in roots of transgenic plants expressing a *MAS2-GFP* construct. Scale bars: (A-I) 1 mm and (J-L) 50 µm.

REFERENCES

1.- Jover-Gil, S., Candela, H., and Ponce, M.R. (2005). *Int. J. Dev. Biol.* **49,** 733-744.
2.- Ponce, M.R., Robles, P., Lozano, F.M., Brotóns, M.A., and Micol, J.L. (2006). *Methods Mol. Biol.* **323**, 105-113.
3.- Ponce, M.R., Quesada, V., and Micol, J.L. (1998). *Plant J.* **14,** 497-501.

METHODS

Plants were grown as described in ref. 3.

ACKNOWLEDGEMENTS

Research in the laboratory of M.R.P. is supported by grants from the Ministerio de Ciencia e Innovación of Spain (BIO2008-01900) and the Generalitat Valenciana (PROMETEO/2009/112 and ACOMP/2009/049).

A search for mutations suppressing the morphological phenotype of an *argonaute1* allele

Aguilera, V., Micol-Ponce, R., Sánchez-García, A.B., Jover-Gil, S., Ere, Z., Isbilir, A., Erbasi, N., Micol, J.L. and Ponce, M.R.

Instituto de Bioingeniería, Universidad Miguel Hernández, Campus de Elche, 03202 Elche, Alicante, Spain.

In *Arabidopsis thaliana*, the main component of the miRNA mediated silencing complex (RISC) is encoded by the *ARGONAUTE1* gene, whose *ago1* mutant alleles disturb many developmental processes and often cause lethality or sterility. With a view to identify genes functionally related to *AGO1*, we mutagenized with EMS seeds of the *ago1-52* mutant, which is moderately fertile and was isolated in our laboratory. The *ago1-52* recessive allele carries a G→A mutation that causes missplicing of an *AGO1* intron, which in turn partially deletes the PIWI domain of the AGO1 protein. We have screened ≈ 60.000 M_2 seeds, identifying 26 lines in which the phenotype caused by *ago1-52* is partially or almost completely supressed. We named these suppressor mutations *mas* (*morphology of argonaute1-52 suppressed*). All the putative *ago1-52 mas* double mutants were confirmed not to be revertants or pseudorevertants. We have mapped so far six of the suppressor genes (*MAS1-MAS6*), and positionally cloned four of them (*MAS1*, *MAS2*, *MAS3* and *MAS5*). The aberrant splicing of *AGO1* transcripts shown by the *ago1-52* single mutant was also observed in its double mutant combinations with *mas1-1*, *mas2-1*, *mas3-1* and *mas5-1*. We will present in this meeting the results of our screenings as well as the genetic and molecular characterization of the *MAS2* and *MAS5* genes.

2011

Plant Growth Biology and Modelling 2011

Elche

Póster

A search for mutations suppressing the morphological phenotype of an *argonaute1* allele

Aguilera, V., Micol-Ponce, R., Sánchez-García, A.B., Jover-Gil, S., Eren, Z., Isbilir, A., Erbasi, N., Micol, J.L., and Ponce, M.R.

Instituto de Bioingeniería, Universidad Miguel Hernández, Campus de Elche, 03202 Elche, Alicante, Spain
mrponce@umh.es http://genetica.umh.es

In *Arabidopsis thaliana*, the core component of the miRNA mediated silencing complex (RISC) is encoded by the *ARGONAUTE1* (*AGO1*) gene, whose loss-of-function disturbs many developmental processes and often causes lethality or sterility[1].

With a view to identify genes functionally related to *AGO1*, we mutagenized with EMS seeds of the *ago1-52* mutant, which is moderately fertile and was isolated in our laboratory[2]. The *ago1-52* recessive allele carries a G→A mutation that causes missplicing of an *AGO1* intron, which in turn partially deletes the PIWI domain of the AGO1 protein (Fig. 1).

We have screened ≈ 60.000 M_2 seeds, identifying 26 lines, 17 in a first round (Fig. 2) and 9 in a second round (Fig. 3), in which the phenotype caused by *ago1-52* is partially or almost completely suppressed. We named these suppressor mutations *mas* (*morphology of argonaute1-52 suppressed*). All the putative *ago1-52 mas* double mutants were confirmed not to be revertants or pseudorevertants.

We have mapped so far seven of the suppressor genes (*MAS1*-*MAS7*; Fig. 4), and positionally cloned four of them (*MAS1*, *MAS2*, *MAS3* and *MAS5*). The aberrant splicing of *AGO1* transcripts shown by the *ago1-52* single mutant was also observed in its double mutant combinations with *mas1-1*, *mas2-1*, *mas3-1* and *mas5-1* (Fig. 5). We present the genetic and molecular characterization of the *MAS2* and *MAS5* genes in two other posters.

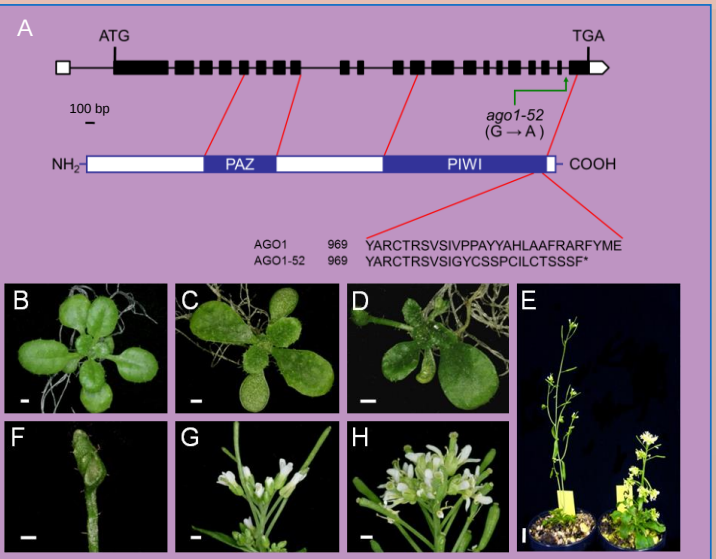

Figure 1.- Molecular nature and pleiotropic phenotypic effects of the *ago1-52* mutation. (A) *AGO1* gene and protein structures. (A) The green arrow indicates the position of the *ago1-52* mutation, which generates a premature stop codon in the PIWI domain. Exons are represented by boxes, and introns as lines between boxes. White boxes indicate the 5' and 3' UTR. An asterisk indicates a premature stop codon. (B-D) Rosettes of (B) *Ler* and (C, D) *ago1-52*. (D, F) A radialized leaf is shown in D, and magnified in F. (E) *Ler* (left) and *ago1-52* plants (right). (G, H) Terminal inflorescence of (G) *Ler* and (H) *ago1-52*. Pictures were taken 21 (A-F) and 54 (G-H) days after stratification (das). Scale bars represent (B-D, F-H) 1 mm and (E) 1 cm.

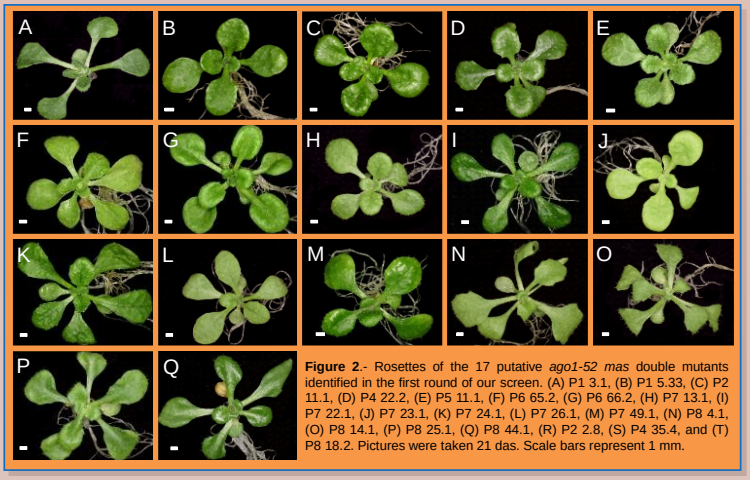

Figure 2.- Rosettes of the 17 putative *ago1-52 mas* double mutants identified in the first round of our screen. (A) P1 3.1, (B) P1 5.33, (C) P2 11.1, (D) P4 22.2, (E) P5 11.1, (F) P6 65.2, (G) P6 66.2, (H) P7 13.1, (I) P7 22.1, (J) P7 23.1, (K) P7 24.1, (L) P7 26.1, (M) P7 49.1, (N) P8 4.1, (O) P8 14.1, (P) P8 25.1, (Q) P8 44.1, (R) P2 2.8, (S) P4 35.4, and (T) P8 18.2. Pictures were taken 21 das. Scale bars represent 1 mm.

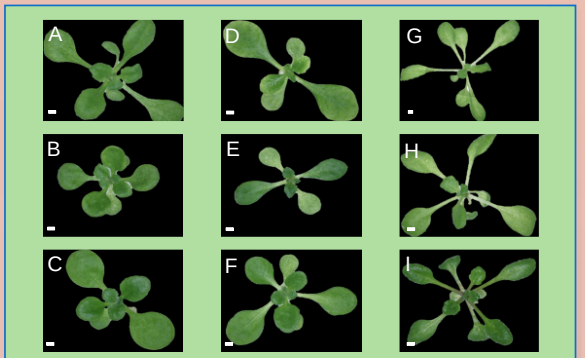

Figure 3.- Putative *ago1-52 mas* double mutants identified in the second round of our screen. Rosettes of the 9 lines displaying a higher suppression are shown: (A) P9 3.3, (B) P11 1.1, (C) P12 1.1, (D) P12 1.2, (E) P12 3.1, (F) P13 1.1, (G) P13 1.2, (H) P15 6.2 and (I) P15 8.1. Pictures were taken at 17 das. Scale bars represent 1 mm.

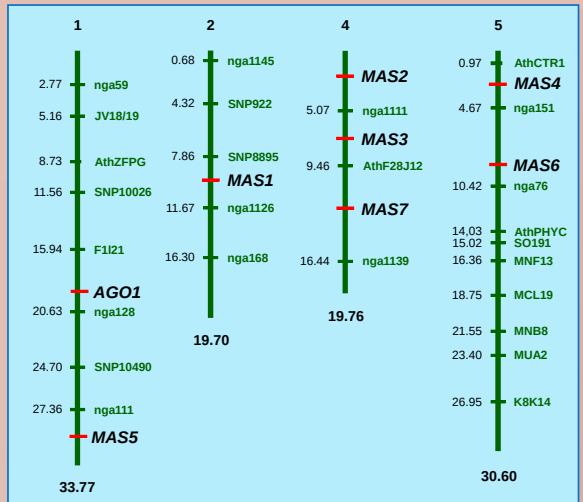

Figure 4.- *Arabidopsis thaliana* physical map with indication of the approximate positions of seven of the *MAS* genes whose characterization is in progress and that of *AGO1*. Lines P1 5.33, P2 11.1, P8 14.1, P7 26.1, P8 25.1, P7 49.1 and P7 13.1 carry the *mas1-1*, *mas2-1*, *mas3-1*, *mas4-1*, *mas5-1*, *mas6-1* and *mas7-1* mutations, respectively. Low-resolution mapping was performed as described in Ponce *et al.* (2006). All figures indicate Mb, the only exceptions being chromosome numbers. Chromosome 3 has been deliberately left out of the figure for simplicity.

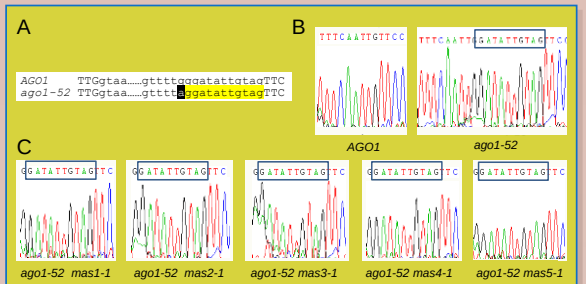

Figure 5.- Sequencing of the *AGO1* region in *ago1-52 mas* double mutant cDNAs indicates that the *mas* mutations do not modify the missplicing caused by *ago1-52*. (A) Partial sequence of *AGO1* gene in *Ler* and *ago1-52*, whose mutation is highlighted with a white letter on a black background. Exons and introns are represented by upper and lower case, respectively. Some intron nucleotides have been substituted by a dotted line. Nucleotides highlighted in yellow in (A) and within blue boxes in (B) and (C) represent the nucleotides from the 20th intron of the *AGO1* gene that are present in the mature mRNA of *ago1-52* and the *ago1-52 mas* double mutants shown.

METHODS

Plants were grown as described in ref. 4.

REFERENCES

1.- Bohmert, K., *et al.* (1998). *EMBO J.* **17,** 170-180.
2.- Jover-Gil, S., Candela, H., and Ponce, M.R. (2005). *Int. J. Dev. Biol.* **49**, 733-744.
3.- Ponce, M.R., *et al.* (2006). *Methods Mol. Biol.* **323,** 105-113.
4.- Ponce, M.R., Quesada, V., and Micol, J.L. (1998). *Plant J.* **14**, 497-501.

ACKNOWLEDGEMENTS

Research in the laboratory of M.R.P. is supported by grants from the Ministerio de Ciencia e Innovación of Spain (BIO2008-01900) and the Generalitat Valenciana (PROMETEO/2009/112 and ACOMP/2009/049).

Caracterización funcional del gen *MAS5* de *Arabidopsis thaliana*

Micol-Ponce R, Aguilera, V, Micol JL y Ponce MR

Instituto de Bioingeniería, Universidad Miguel Hernández, Campus de Elche, 03202 Elche, Alicante

Un escrutinio de unas 37.000 semillas M_2 derivadas de una mutagénesis de la estirpe *ago1-52*, portadora de un alelo hipomorfo y viable del gen *ARGONAUTE 1* (*AGO1*) de *Arabidopsis thaliana* nos permitió identificar 17 mutaciones supresoras de su fenotipo morfológico, a las que denominamos *mas* (*morphology of argonaute1-52 suppressed*).

Hemos llevado a cabo la clonación posicional de *MAS5*. Para ello, obtuvimos poblaciones cartográficas F_2 cruzando los dobles mutantes *ago1-52 mas5-1* por *ago1-25* y *ago1-27*, dos estirpes portadoras de alelos hipomorfos de *AGO1*, obtenidas a partir de la estirpe silvestre Col-0, que es polimórfica con respecto a L*er*, de la que procede *ago1-52*. El análisis iterativo del ligamiento a marcadores moleculares permitió definir un intervalo candidato de 445 kb, en el telómero inferior del cromosoma 1. El análisis *in silico* de los 73 genes candidatos y la posterior secuenciación de algunos de ellos nos permitió identificar una transición de G a A en el decimoctavo exón de *MAS5*, que se traduciría en un cambio de ácido glutámico por lisina. *MAS5* parece ser un elemento clave de la maquinaria del *splicing*, que se encuentra muy conservado en los eucariotas.

Los alelos nulos de *MAS5* son letales embrionarios. *MAS5* cuenta con un parálogo en Arabidopsis, que también estamos estudiando. La supresión que *mas5-1* ejerce sobre *ago1-52* no es específica de alelo, ya que también se manifiesta sobre *ago1-25* y *ago1-27*. Hemos iniciado la caracterización genética y molecular de MAS5 para desentrañar su función y su relación con la ruta de los miARN.

2011

XXXVIII Congreso de la Sociedad Española de Genética

Murcia

Póster

Caracterización funcional del gen *MAS5* de *Arabidopsis thaliana*

Micol-Ponce, R., Aguilera, V., Micol, J.L., y Ponce, M.R.

Instituto de Bioingeniería, Universidad Miguel Hernández, Campus de Elche, 03202 Elche, Alicante.

rmicol@umh.es mrponce@umh.es genetica.umh.es

El escrutinio de unas 37.000 semillas M_2 derivadas de una mutagénesis de la estirpe *ago1-52*[1], portadora de un alelo hipomorfo del gen *ARGONAUTE1* (*AGO1*)[2] de *Arabidopsis thaliana*, nos permitió identificar 17 mutaciones supresoras de su fenotipo morfológico. Hemos denominado *mas* (*morphology of argonaute1-52 suppressed*) a estas mutaciones, y *mas5-1* a la de la línea P8 25.1 (Fig. 1).

Con el fin de clonar posicionalmente el gen *MAS5*, cruzamos el doble mutante *ago1-52 mas5-1* por *ago1-25* y *ago1-27*, dos estirpes portadoras de alelos hipomorfos de *AGO1*, obtenidas a partir del tipo silvestre Col-0[3], que es polimórfico con respecto a L*er*, del que procede *ago1-52*. El análisis iterativo del ligamiento a marcadores moleculares en la F_2 de estos cruzamientos permitió definir un intervalo candidato de 445 kb, en el telómero inferior del cromosoma 1. El análisis *in silico* de los 73 genes candidatos (Fig. 2) y la posterior secuenciación de algunos de ellos nos permitió identificar una transición G→A en el decimoctavo exón del gen At1g80070, que se traduciría en un cambio de ácido glutámico por lisina en su producto proteico, PRP8 (Fig. 3). MAS5/PRP8 parece ser un elemento clave de la maquinaria del *splicing*, que se encuentra muy conservado en los eucariotas (Fig. 4 y 5).

Hemos iniciado la caracterización genética y molecular de *MAS5* para desentrañar su relación funcional con *AGO1*. Hemos comprobado que *mas5-1* es dominante en su efecto supresor sobre *ago1-52* (Fig. 6) y que no normaliza el *splicing* aberrante que esta última causa. Sus alelos nulos son letales embrionarios.

```
PRP8 (Homo sapiens)                1728  QAMAKIMKANPALYVLRERIRKGLQLYSSEPTEPYLSSQNYGELFSNQII
Prp8 (Danio rerio)                 1735  QAMAKIMKANPALYVLRERIRKGLQLYSSEPTEPYLSSQNYGELFSNQII
Prp8 (Drosophila melanogaster)     1788  QAMAKIMKANPALYVLRERIRKALQLYSSEPTEPYLSSQNYGELFSNQII
prp-8 (Caenorhabditis elegans)     1721  QAMAKIIKANPAFYVLRERIRKGLQLYSSEPTEPYLTSQNYGELFSNQII
spp42 (Schizosaccharomyces pombe)  1752  QSMNKIMKANPALYVLRERIRKGLQLYASEPQEQYLSSSNYAELFSNQIQ
Prp8p (Saccharomyces cerevisiae)   1800  NSMRTIMKANPALYVLRERIRKGLQIYQSSVQEPFLNSSNYAELFNNDIK
NCU07832 (Neurospora crassa)       1766  QAMGKIMKANPALYVLRERIRKGLQLYASESNQEFLNSQNYSELFSNQTQ
MAS5 (Arabidopsis thaliana)        1775  QAMNKIMKSNPALYVLRERIRKGLQLYSSEPTEPYLSSQNYGEIFSNQII
Consenso                                 * * * *** ************** *       * * ** * * **
```

Figura 4.- Alineamiento múltiple de parte de la secuencia de las proteínas PRP8. Se muestra únicamente la región adyacente al aminoácido modificado por la mutación *mas5-1*, que se ha coloreado en rojo. Las secuencias se obtuvieron del NCBI (http://www.ncbi.nlm.nih.gov) y se alinearon con el programa CLUSTALW2 (http://www.ebi.ac.uk/Tools/msa/clustalw2/). Los números indican las posiciones en las respectivas secuencias proteicas, y los asteriscos, los aminoácidos conservados en todas las especies representadas en el alineamiento.

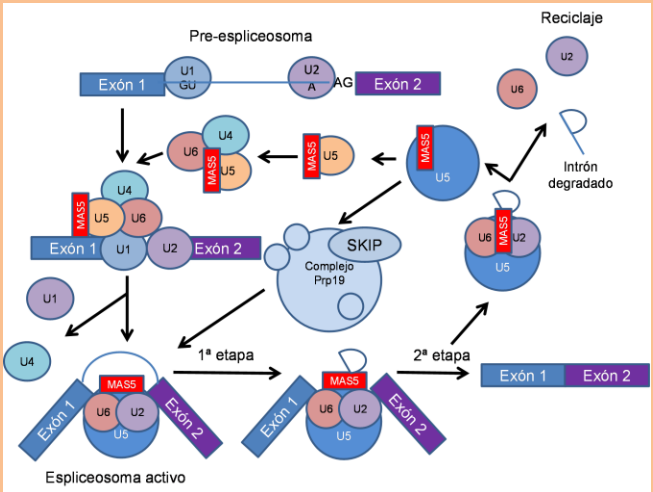

Figura 5.-Ensamblaje y reciclaje de los componentes del espliceosoma. U1-U6 son complejos de pequeños ARN nucleares y proteínas (snRNP). U1 y U2 se unen a las secuencias donantes y al punto de ramificación del *splicing*, en el intrón, para formar el pre-espliceosoma. Su unión al complejo integrado por U4, U5, U6 y PRP8 genera el espliceosoma, que se activa al disociarse U1, U4 y U5. PRP8 se requiere en las dos etapas del *splicing*. Finalizado el proceso, algunos de los componentes del espliceosoma se reciclan y el intrón se degrada. Esquema adaptado a partir de Grainger y Beggs (2005), en el que se ha sustituido PRP8 por MAS5.

Figura 1.- Algunos rasgos fenotípicos de la línea P8 25.1 (*ago1-52 mas5-1*). (A-C) Inflorescencias terminales y (E-G) rosetas de (A, E) L*er*, (B, F) P8 25.1 y (C, G) *ago1-52*. (D) De izquierda a derecha, plantas adultas de L*er*, P8 25.1 y *ago1-52*. Las fotografías fueron tomadas (A-D) 54 y (E-G) 21 días después de la estratificación (dde). Las barras de escala indican (A-C, E-G) 1 mm y (D) 1 cm.

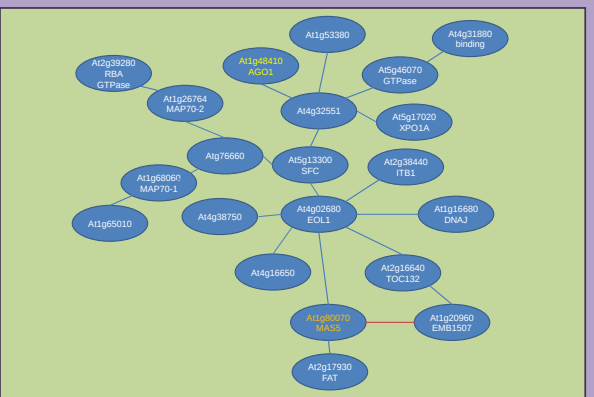

Figura 2.- Red de coexpresión de *AGO1* y *MAS5*. La longitud de las líneas no es informativa, aunque sí lo es su color y grosor. La línea roja representa una coexpresión conservada entre las plantas y los mamíferos, teniendo en cuenta los resultados de micromatrices de la rata, el ratón, las plantas y humanas. Los trazos mas gruesos indican un nivel de coexpresión mayor que los más finos, según se describe en Obayashi *et al.* (2011). Redibujado a partir del análisis de coexpresión realizado en la base de datos ATTED-II (http://atted.jp).

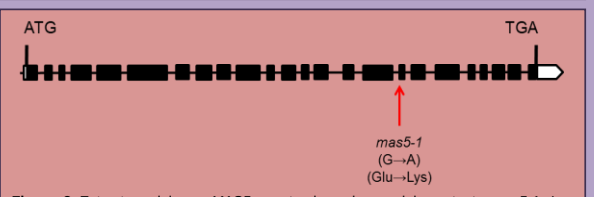

Figura 3.-Estructura del gen *MAS5* y naturaleza de su alelo mutante *mas5-1*. Los rectángulos negros representan a los exones, y las líneas que los separan, a los intrones. Se indican en blanco las regiones del gen correspondientes al líder y el trailer de su ARNm. La flecha roja señala la posición de la mutación puntual *mas5-1*, así como el cambio que presuntamente causa en la proteína.

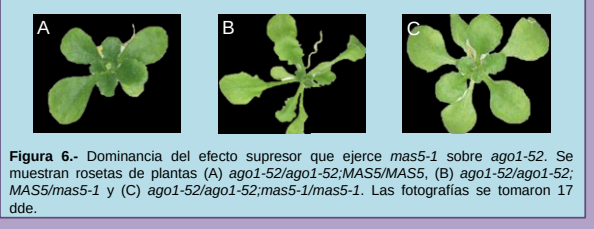

Figura 6.- Dominancia del efecto supresor que ejerce *mas5-1* sobre *ago1-52*. Se muestran rosetas de plantas (A) *ago1-52/ago1-52;MAS5/MAS5*, (B) *ago1-52/ago1-52; MAS5/mas5-1* y (C) *ago1-52/ago1-52;mas5-1/mas5-1*. Las fotografías se tomaron 17 dde.

MATERIALES Y MÉTODOS

Los cultivos se realizaron a 20±1°C y 60-70% de humedad relativa, bajo iluminación continua (5.500 lx)[5]. La cartografía génica se realizo según se describe en la referencia 6.

REFERENCIAS

1.- Jover-Gil, S., Candela, H., y Ponce, M.R. (2005). *Int. J. Dev. Biol.* **49**, 733-744.
2.- Bohmert, K., Camus, I., Bellini, C., Bouchez, D., Caboche, M., y Benning, C. (1998). *EMBO J.* **17,** 170-180.
3.- Morel, J.B., Godon, C., Mourrain, P., Béclin, C., Boutet, S., Feuerbach, F., Proux, F., y Vaucheret, H. (2002). *Plant Cell* **14**, 629-639.
4.- Grainger, R.J., y Beggs, J.D. (2005). *RNA* **11,** 533-537.
5.- Obayashi T, Nishida K, Kasahara K, Kinoshita K. (2011). *Plant Cell Phys.* **52**, 213-219.
6.- Ponce, M.R., Robles, P., Lozano, F.M., Brotóns, M.A., y Micol, J.L. (2006). *Methods Mol. Biol.* **323,** 105-113.

AGRADECIMIENTOS

Las líneas *ago1-25* y *ago1-27* fueron donadas por H. Vaucheret. Este trabajo ha sido financiado por el Ministerio de Ciencia e Innovación (proyecto BIO2008-01900) y por la Generalitat Valenciana (PROMETEO/2009/112 y ACOMP/2009/049), concedidos a M.R. Ponce. R.M.P. disfruta de un contrato de la Comisión Europea.

Análisis genético y molecular del gen *MAS2* de *Arabidopsis thaliana*

Sánchez-García AB, Jover-Gil S, Aguilera V, Micol-Ponce R, Kahveci Z, Micol JL, y Ponce MR

Instituto de Bioingeniería, Universidad Miguel Hernández, Campus de Elche, 03202 Elche, Alicante.

El silenciamiento génico postranscripcional mediado por pequeños ARN no codificantes tiene lugar en los eucariotas en complejos denominados RISC (*RNA-Induced Silencing Complexes*), cuyo componente principal es un miembro de la familia ARGONAUTE (AGO). En Arabidopsis existen 10 proteínas AGO, siendo AGO1 la más implicada en la regulación génica mediada por los microARN (miARN). AGO1 también participa en rutas mediadas por otros pequeños ARN interferentes (siARN).

Pretendemos identificar nuevos genes implicados en las rutas de silenciamiento génico en las que participa AGO1. Hemos llevado a cabo con este fin una búsqueda de supresores del fenotipo morfológico de *ago1-52*, una estirpe portadora de un alelo hipomorfo de *AGO1* anteriormente aislada en nuestro laboratorio. Hemos denominando *mas* (*morphology of argonaute1-52 suppressed*) a las mutaciones supresoras que hemos identificado tras la mutagénesis de *ago1-52* con EMS.

La clonación posicional de *mas2-1* nos ha permitido determinar que *MAS2* es un gen de copia única en Arabidopsis, que codifica una proteína de función desconocida, presente tanto en los animales como en las plantas. La mutación puntual *mas2-1* causa un cambio de alanina por treonina en una posición muy conservada de la proteína MAS2.

Hemos obtenido una inserción de ADN-T que interrumpe el único exón de *MAS2*, a la que hemos denominado *mas2-2*. Su letalidad recesiva indica que *MAS2* es un gen esencial durante la embriogénesis. Hemos generado un microARN artificial para silenciar *MAS2,* con el objetivo de estudiar los fenotipos de su insuficiencia parcial de función a lo largo de todo el ciclo de vida de la planta.

Hemos sobreexpresado el alelo silvestre del gen *MAS2* en los mutantes *ago1-52* y *hen1-13*. Este último es portador de un alelo posiblemente nulo del gen *HUA ENHANCER1* (*HEN1*), que codifica una metilasa que estabiliza los miARN y siARN. En ambos casos se suprimieron los fenotipos mutantes. Hemos obtenido además construcciones que nos han permitido establecer que el gen *MAS2* se expresa ubicuamente y que su producto proteico es nuclear, tal como ocurre con sus ortólogos animales.

2011
XXXVIII Congreso de la Sociedad Española de Genética
Murcia
Póster (Premio al mejor póster del congreso)

Análisis genético y molecular del gen *MAS2* de *Arabidopsis thaliana*

Sánchez-García, A.B., Jover-Gil, S., Aguilera, V., Micol-Ponce, R., Kahveci, Z., Micol, J.L., y Ponce, M.R.

Instituto de Bioingeniería, Universidad Miguel Hernández, Campus de Elche, 03202 Elche, Alicante.
ana.sanchezg@umh.es mrponce@umh.es http://genetica.umh.es

El silenciamiento génico postranscripcional mediado por pequeños ARN no codificantes tiene lugar en los eucariotas en complejos denominados RISC (*RNA-Induced Silencing Complexes*), cuyo componente principal es un miembro de la familia ARGONAUTE (AGO). En Arabidopsis existen 10 proteínas AGO, siendo AGO1 la más implicada en la regulación génica mediada por los microARN (miARN). AGO1 también participa en rutas mediadas por otros pequeños ARN interferentes.

Pretendemos identificar nuevos genes relacionados funcionalmente con *AGO1*. Hemos llevado a cabo con este fin una búsqueda de supresores del fenotipo morfológico de *ago1-52*, una estirpe portadora de un alelo hipomorfo de *AGO1* anteriormente aislada en nuestro laboratorio[1]. Hemos denominado *mas* (*morphology of argonaute1-52 suppressed*) a las mutaciones supresoras que hemos identificado tras la mutagénesis de *ago1-52* con EMS, *MAS2* al gen mutado en la línea P2 11.1 (Fig. 1) y *mas2-1* a su alelo mutante.

La clonación posicional de *mas2-1* (Fig. 2A) nos ha permitido determinar que *MAS2* es un gen de copia única en Arabidopsis, que codifica una proteína de función desconocida, presente tanto en los animales como en las plantas. La mutación puntual *mas2-1* causa un cambio de alanina por treonina en una posición muy conservada de la proteína (Fig. 2B). Sin embargo, las plantas *mas2-1* son prácticamente silvestres (Fig. 3A-G).

Hemos obtenido una inserción de ADN-T que interrumpe el único exón de *MAS2*, a la que hemos denominado *mas2-2* (Fig. 2B). La letalidad recesiva que muestra este alelo (Fig. 3H-N) indica que *MAS2* es un gen esencial durante la embriogénesis.

También hemos generado diferentes construcciones que nos han permitido establecer que el gen *MAS2* se expresa ubicuamente (Fig. 4A-I) y que su producto proteico es nuclear (Fig. 4J-L), tal como ocurre con sus ortólogos animales.

La generación de un microARN artificial para silenciar *MAS2* nos está permitiendo estudiar los efectos de la insuficiencia parcial de función de este gen a lo largo de todo el ciclo de vida de la planta (Fig. 5).

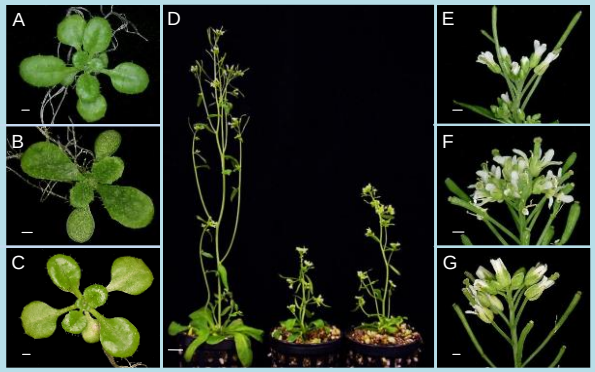

Figura 1.- Algunos rasgos fenotípicos de la línea P2 11.1 (*ago1-52 mas2-1*). (A-C) Rosetas de (A) Ler, (B) *ago1-52* y (C) P2 11.1. (D) De izquierda a derecha, plantas adultas de Ler, *ago1-52* y P2 11.1. (E-G) Inflorescencias terminales de (E) Ler, (F) *ago1-52* y (G) P2 11.1. Las fotografías fueron tomadas (A-C) 21 y (D-G) 43 días después de la estratificación (dde). Las barras de escala indican (A-C, E-G) 1 mm y (D) 1 cm.

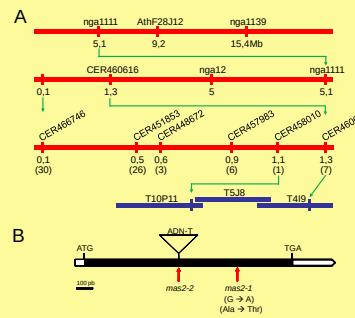

Figura 2.- Clonación posicional del gen *MAS2*. (A) Las barras rojas representan segmentos del cromosoma 2, y las azules, los clones BAC que incluyen el intervalo candidato a contener el gen *MAS2*. Se indica entre paréntesis el número de individuos recombinantes informativos obtenidos para cada marcador. La cartografía de baja resolución indicó que *MAS2* se localiza entre los marcadores CER458010 y CER460616. (B) La secuenciación del gen *MAS2* en los individuos dobles mutantes reveló la presencia de una transición G→A que se traduce en un cambio de aminoácido (alanina por treonina) en una región muy conservada de la proteína MAS2. La cartografía se realizó tal como se detalla en Ponce *et al.* (2006).

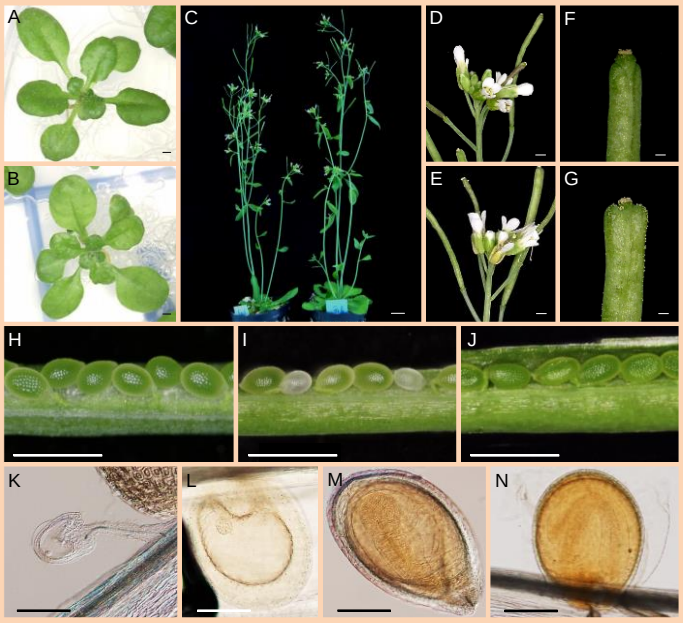

Figura 3.- Rasgos fenotípicos de los mutantes *mas2-1*. (A, B) Rosetas de (A) Ler y (B) *mas2-1*. (C) De izquierda a derecha, plantas adultas de Ler y *mas2-1*. (D, E) Inflorescencias de (D) Ler y (E) *mas2-1*. (F, G) Silicuas de (F) Ler y (G) *mas2-1*. (H-J) Semillas de (H) *mas2-1*, (I) *mas2-2* y (J) Ler. (K) Óvulo sin fecundar. (L-N) Embriones resultantes de la autofecundación de plantas *MAS2/mas2-2* en estadio (L) globular, (M) globular-corazón y (N) maduro. Las barras de escala indican (A, B y D-J) 1 mm, (C) 1 cm y (K-N) 200 µm.

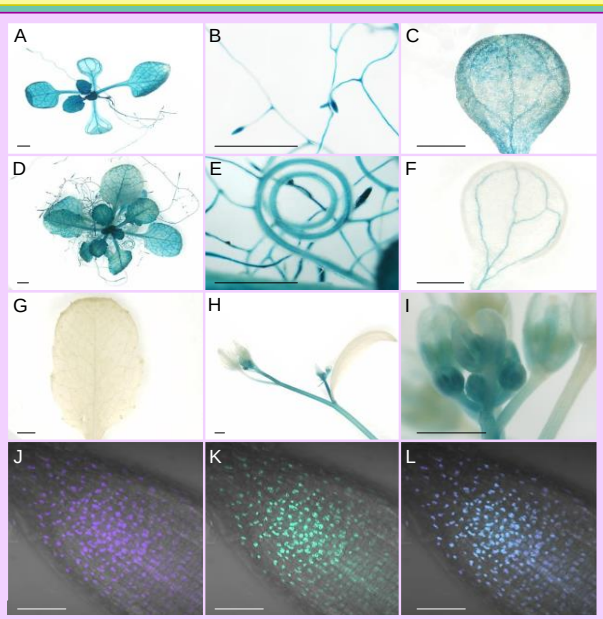

Figura 4.- Análisis de la expresión de *MAS2*. (A-I) Detección de la actividad β-glucuronidasa en plantas T_2 portadoras de la construcción $MAS2_{pro}$:*GUS*. (A, D) Rosetas, (B, E) raíces y (C, F) cotiledones de plantas recolectadas (A-C) 15 y (D-F) 28 dde. (G) Hoja vegetativa del tercer nudo, (H) tallo e (I) inflorescencia apical del tallo de 48 dde. (J-L) Localización subcelular de la proteína MAS2. (J) Detección de la emisión de fluorescencia del DAPI (4',6-diamidino-2-phenylindole), (K) GFP y (L) DAPI y GFP solapadas con la emisión de luz transmitida en raíces de plantas T_3 portadoras de la construcción *MAS2-GFP* en homocigosis. Las barras de escala indican (A-I) 1 mm y (J-L) 50 µm.

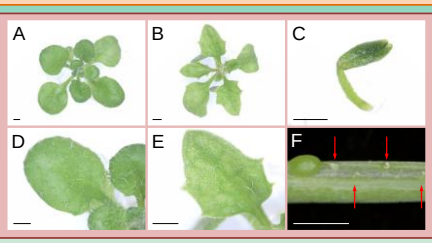

Figura 5.- Plantas transgénicas T_2 portadoras de la construcción *35S:amiR-MAS2*. Los individuos se clasificaron según la severidad de su fenotipo en (A) Silvestre, (B) Mutante y (C) Mutante extremo. (D-F) Detalle de (D, E) hojas de individuos con fenotipo (D) Silvestre y (E) Mutante, y (F) de un fruto de un individuo Mutante, como en B. Las flechas rojas señalan semillas en las que el desarrollo del embrión se interrumpió y óvulos sin fecundar. Las barras de escala indican 1 mm. Las fotografías se tomaron 21 (A-E) y 54 (F) dde.

BIBLIOGRAFÍA

1.- Jover-Gil, S., Candela, H., y Ponce, M.R. (2005). *Int. J. Dev. Biol.* **49,** 733-744.
2.- Ponce, M.R., Robles, P., Lozano, F.M., Brotóns, M.A., y Micol, J.L. (2006). *Methods Mol. Biol.* **323**, 105-113.

AGRADECIMIENTOS

La investigación en el laboratorio de M.R.P. ha sido financiada por el Ministerio de Ciencia e Innovación (BIO2008-01900) y por la Generalitat Valenciana (PROMETEO/2009/112 y ACOMP/2009/049). A.B.S.G. disfruta de un contrato predoctoral de la Generalitat Valenciana.

Análisis genético y molecular del gen *MAS5* de Arabidopsis

Micol-Ponce, R., Aguilera, V., Micol, J.L., y Ponce, M.R.

Instituto de Bioingeniería, Universidad Miguel Hernández, Campus de Elche, 03202 Elche, Alicante.

El silenciamiento génico postranscripcional mediado por pequeños ARN no codificantes tiene lugar en los eucariotas en complejos denominados RISC (RNA-Induced Silencing Complexes), cuyo componente principal es un miembro de la familia ARGONAUTE (AGO). AGO1, una de las 10 proteínas AGO de Arabidopsis, juega un papel central en la ruta de los microARN y también participa en las de silenciamiento mediadas por pequeños ARN interferentes. Con el objetivo de caracterizar las funciones del gen *AGO1*, hemos llevado a cabo una búsqueda de mutaciones supresoras del fenotipo morfológico de uno de sus alelos hipomorfos, *ago1-52*, a las que hemos denominado *mas* (*morphology of argonaute1-52 suppressed*).

Hemos clonado posicionalmente el gen *MAS5*. Para ello, obtuvimos poblaciones cartográficas F_2 cruzando los dobles mutantes *ago1-52 mas5-1* por *ago1-25* y *ago1-27*, dos estirpes portadoras de alelos hipomorfos de *AGO1*, obtenidas a partir de la estirpe silvestre Col-0, que es polimórfica con respecto a L*er*, de la que procede *ago1-52*. El análisis iterativo del ligamiento a marcadores moleculares nos permitió definir un intervalo candidato de 445 kb, en el telómero inferior del cromosoma 1. El análisis *in silico* de los 73 genes candidatos y la posterior secuenciación de algunos de ellos reveló una transición G→A en el decimoctavo exón de *MAS5*, que se traduciría en un cambio de ácido glutámico por lisina. Hemos encontrado en nuestra colección de supresores otros 5 alelos de *MAS5*, pertenecientes a dos grupos parentales diferentes, todos ellos portadores de la misma mutación que *mas5-1*. Los alelos nulos de *MAS5* son letales embrionarios. La proteína MAS5 parece ser un elemento clave de la maquinaria del *splicing*, que se encuentra muy conservado entre los eucariotas. El gen *MAS5* cuenta con un parálogo en Arabidopsis, que también estamos estudiando.

2012

XI Reunión de Biología Molecular de Plantas

Segovia

Póster

Análisis genético y molecular del gen *MAS5* de *Arabidopsis thaliana*

Micol-Ponce, R., Aguilera, V., Micol, J.L., y Ponce, M.R.

Instituto de Bioingeniería, Universidad Miguel Hernández, Campus de Elche, 03202 Elche, Alicante.
rmicol@umh.es mrponce@umh.es genetica.umh.es

El escrutinio de unas 60.000 semillas M_2 derivadas de una mutagénesis de la estirpe *ago1-52*[1], portadora de un alelo hipomorfo del gen *ARGONAUTE1* (*AGO1*)[2] de *Arabidopsis thaliana*, nos permitió identificar 23 mutaciones supresoras de su fenotipo morfológico. Hemos denominado *mas* (*morphology of argonaute1-52 suppressed*) a estas mutaciones, y *mas5-1* a la de la línea P8 25.1 (Fig. 1).

Con el fin de clonar posicionalmente el gen *MAS5*, cruzamos el doble mutante *ago1-52 mas5-1* por *ago1-25* y *ago1-27*, dos estirpes portadoras de alelos hipomorfos de *AGO1*, obtenidas a partir del tipo silvestre Col-0[3], que es polimórfico con respecto a L*er*, del que procede *ago1-52*. El análisis iterativo del ligamiento a marcadores moleculares en la F_2 de estos cruzamientos permitió definir un intervalo candidato de 445 kb, en el telómero inferior del cromosoma 1. El análisis *in silico* de los 73 genes candidatos y la posterior secuenciación de algunos de ellos reveló una transición G→A en el decimoctavo exón del gen At1g80070, que se traduciría en un cambio de ácido glutámico por lisina en su producto proteico, PRP8 (Fig. 2). MAS5/PRP8 parece ser un elemento clave de la maquinaria del *splicing*, que se encuentra muy conservado en los eucariotas (Fig. 3 y 4). Hemos encontrado en nuestra colección de supresores otros 5 alelos de *MAS5*, pertenecientes a dos grupos parentales diferentes, todos ellos portadores de la misma mutación que *mas5-1*.

Hemos iniciado la caracterización genética y molecular de *MAS5* para desentrañar su relación funcional con *AGO1*. Hemos comprobado que *mas5-1* es dominante en su efecto supresor sobre *ago1-52* (Fig. 5) y que no normaliza el *splicing* aberrante que esta última causa (Fig. 6). Sus alelos nulos son letales embrionarios.

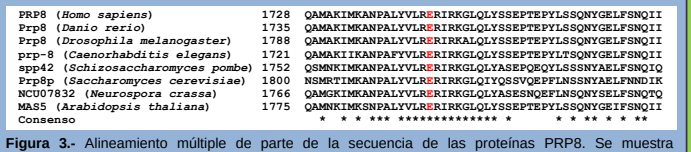

PRP8 (*Homo sapiens*)	1728	QAMAKIMKANPALYVLRERIRKGLQLYSSEPTEPYLSSQNYGELFSNQII
Prp8 (*Danio rerio*)	1735	QAMAKIMKANPALYVLRERIRKGLQLYSSEPTEPYLSSQNYGELFSNQII
Prp8 (*Drosophila melanogaster*)	1788	QAMAKIMKANPALYVLRERIRKALQLYSSEPTEPYLSSQNYGELFSNQII
prp-8 (*Caenorhabditis elegans*)	1721	QAMAKIIKANPAFYVLRERIRKGLQLYSSEPTEPYLTSQNYGELFSNQII
spp42 (*Schizosaccharomyces pombe*)	1752	QSMNKIMKANPALYVLRERIRKGLQLYASEPQEQYLSSSNYAELFSNQIQ
Prp8p (*Saccharomyces cerevisiae*)	1800	NSMRTIMKANPALYVLRERIRKGLQIYQSSVQEPFLNSSNYAELFNNDIK
NCU07832 (*Neurospora crassa*)	1766	QAMGKIMKANPALYVLRERIRKGLQLYASESNQEFLNSQNYSELFSNQTQ
MAS5 (*Arabidopsis thaliana*)	1775	QAMNKIMKSNPALYVLRERIRKGLQLYSSEPTEPYLSSQNYGEIFSNQII
Consenso		* * * *** ************** * * * ** * * **

Figura 3.- Alineamiento múltiple de parte de la secuencia de las proteínas PRP8. Se muestra únicamente la región adyacente al aminoácido modificado por la mutación *mas5-1*, que se ha coloreado en rojo. Las secuencias se obtuvieron del NCBI (http://www.ncbi.nlm.nih.gov) y se alinearon con el programa CLUSTALW2 (http://www.ebi.ac.uk/Tools/msa/clustalw2/). Los números indican las posiciones en las respectivas secuencias proteicas, y los asteriscos, los aminoácidos conservados en todas las especies representadas en el alineamiento.

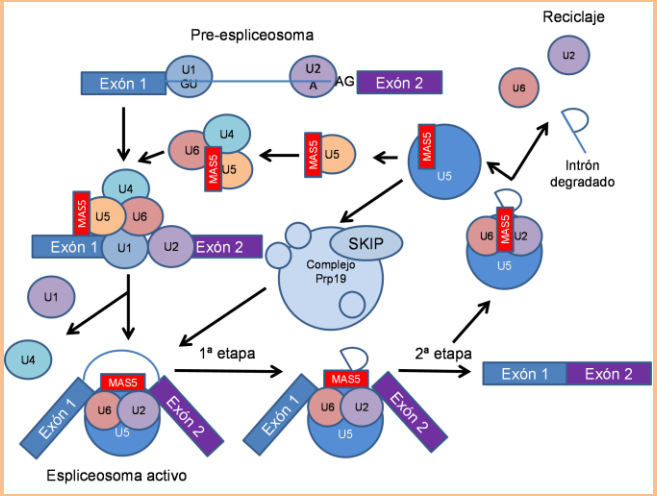

Figura 4.- Ensamblaje y reciclaje de los componentes del espliceosoma. U1-U6 son complejos de pequeños ARN nucleares y proteínas (snRNP). U1 y U2 se unen a las secuencias donantes y al punto de ramificación del *splicing*, en el intrón, para formar el pre-espliceosoma. Su unión al complejo integrado por U4, U5, U6 y PRP8 genera el espliceosoma, que se activa al disociarse U1, U4 y U5. PRP8 se requiere en las dos etapas del *splicing*. Finalizado el proceso, algunos de los componentes del espliceosoma se reciclan y el intrón se degrada. Esquema adaptado a partir de Grainger y Beggs (2005), en el que se ha sustituido PRP8 por MAS5.

MATERIALES Y MÉTODOS

Los cultivos se realizaron a 20±1°C y 60-70% de humedad relativa, bajo iluminación continua (5.500 lx)[5]. La cartografía génica se realizo según se describe en la referencia 6.

AGRADECIMIENTOS

Las líneas de *ago1-25* y *ago1-27* fueron donadas por H. Vaucheret. La investigación en el laboratorio de M.R.P. ha sido financiada por el Ministerio de Ciencia e Innovación (proyecto BIO2008-01900) y la Generalitat Valenciana (PROMETEO/2009/112 y ACOMP/2009/049). R.M.P. disfruta de un contrato de la Comisión Europea.

Figura 1.- Algunos rasgos fenotípicos de la línea P8 25.1 (*ago1-52 mas5-1*). (A-C) Inflorescencias terminales y (E-G) rosetas de (A, E) L*er*, (B, F) P8 25.1 y (C, G) *ago1-52*. (D) De izquierda a derecha, plantas adultas de L*er*, P8 25.1 y *ago1-52*. Las fotografías fueron tomadas (A-D) 54 y (E-G) 21 días después de la estratificación (dde). Las barras de escala indican (A-C, E-G) 1 mm y (D) 1 cm.

Figura 2.- Estructura del gen *MAS5* y naturaleza de su alelo mutante *mas5-1*. Los rectángulos negros representan a los exones, y las líneas que los separan, a los intrones. Se indican en blanco las regiones del gen correspondientes al líder y el trailer de su ARNm. La flecha roja señala la posición de la mutación puntual *mas5-1*, así como el cambio que presuntamente causa en la proteína MAS5.

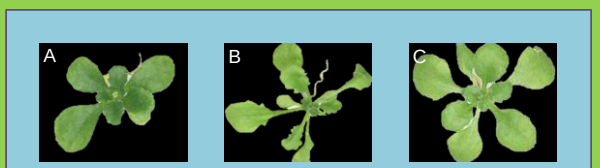

Figura 5.- Dominancia del efecto supresor que ejerce *mas5-1* sobre *ago1-52*. Se muestran rosetas de plantas (A) *ago1-52/ago1-52;MAS5/MAS5*, (B) *ago1-52/ago1-52; MAS5/mas5-1* y (C) *ago1-52/ago1-52;mas5-1/mas5-1*. Las fotografías se tomaron 17 dde.

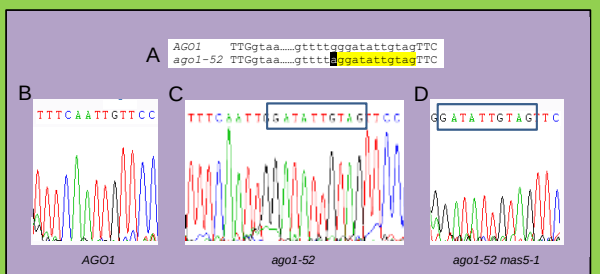

Figura 6.- Demostración de la ausencia de efectos de las mutaciones *mas* sobre el *splicing* de *ago1-52*. (A) Secuencia parcial del gen *AGO1* en L*er* y *ago1-52*, cuya mutación se destaca con una letra blanca sobre fondo negro. La secuencia de los exones e intrones se indica con letras mayúsculas y minúsculas, respectivamente. Algunos nucleótidos del intrón se han sustituido por puntos suspensivos. Se destacan en amarillo los nucleótidos del vigésimo intrón del gen *AGO1* que forman parte del ARNm maduro de *ago1-52* y de los dobles mutantes cuyo ADNc se ha secuenciado, que se han recuadrado en los electroferogramas de (B) L*er* (*AGO1*), (C) *ago1-52*, y (D) el doble mutante *ago1-52 mas5-1*.

REFERENCIAS

1.- Jover-Gil, S., Candela, H., y Ponce, M.R. (2005). *Int. J. Dev. Biol.* **49**, 733-744.
2.- Bohmert, K., Camus, I., Bellini, C., Bouchez, D., Caboche, M., y Benning, C. (1998). *EMBO J.* **17**, 170-180.
3.- Morel, J.B., Godon, C., Mourrain, P., Béclin, C., Boutet, S., Feuerbach, F., Proux, F., y Vaucheret, H. (2002). *Plant Cell* **14**, 629-639.
4.- Grainger, R.J., y Beggs, J.D. (2005). *RNA* **11,** 533-537.
5.- Obayashi T, Nishida K, Kasahara K, Kinoshita K. (2011). *Plant Cell Phys.* **52**, 213-219.
6.- Ponce, M.R., Robles, P., Lozano, F.M., Brotóns, M.A., y Micol, J.L. (2006). *Methods Mol. Biol.* **323,** 105-113.

Análisis genético y molecular del gen *MAS2* de *Arabidopsis thaliana*

Sánchez-García A.B., Jover-Gil S., Micol-Ponce R., Aguilera V., Micol J.L., y Ponce M.R.

Instituto de Bioingeniería, Universidad Miguel Hernández, Campus de Elche, 03202 Elche, Alicante.

La insuficiencia de función de la proteína ARGONAUTE1 (AGO1), un elemento clave de la ruta de los microARN, perturba numerosos procesos de desarrollo y suele causar esterilidad o letalidad. Con el fin de identificar nuevos genes implicados en las rutas de silenciamiento génico en las que participa AGO1, hemos llevado a cabo una búsqueda de supresores del fenotipo morfológico de *ago1-52*, un alelo hipomorfo de *AGO1*, a los que hemos denominando *mas* (*morphology of argonaute1-52 suppressed*).

La mutación *mas2-1* suprime totalmente el fenotipo de *ago1-52*, pero carece de fenotipo por sí misma. Su clonación posicional nos ha permitido establecer que *MAS2* es un gen de copia única en Arabidopsis, que codifica una proteína de función desconocida, presente tanto en los animales como en las plantas. *mas2-1* manifiesta un efecto supresor dominante, y causa un cambio de alanina por treonina en una posición muy conservada de la proteína MAS2. Hemos identificado entre nuestros supresores 10 alelos adicionales de *MAS2*, 9 de los cuales son portadores de cambios puntuales en una región muy conservada de *MAS2*, de solo 13 pb, todos los cuales causan presuntamente sustituciones de aminoácidos.

La letalidad embrionaria de *mas2-2*, un alelo insercional de *MAS2*, indica que este gen es esencial durante la embriogénesis. Hemos generado un microARN artificial para silenciar *MAS2,* con el objetivo de estudiar los efectos de su insuficiencia de función parcial. Hemos obtenido transgenes que nos han permitido establecer que el gen *MAS2* se expresa en todos los tejidos y órganos estudiados, que su expresión constitutiva suprime el fenotipo de *ago1-52*, y que su producto proteico es nuclear, tal como ocurre con sus ortólogos animales. Hemos demostrado mediante hibridación *in situ* la colocalización de MAS2 y los ADNr 45S, en los organizadores nucleolares.

2012

XI Reunión de Biología Molecular de Plantas

Segovia

Póster

Análisis genético y molecular del gen *MAS2* de *Arabidopsis thaliana*

Sánchez-García, A.B., Jover-Gil, S., Micol-Ponce, R., Aguilera, V., Micol, J.L., y Ponce, M.R.

Instituto de Bioingeniería, Universidad Miguel Hernández, Campus de Elche, 03202 Elche, Alicante.
ana.sanchezg@umh.es mrponce@umh.es http://genetica.umh.es

La insuficiencia de función de la proteína ARGONAUTE1 (AGO1), un elemento clave de la ruta de los microARN, perturba numerosos procesos de desarrollo y suele causar esterilidad o letalidad. Con el fin de identificar nuevos genes implicados en las rutas de silenciamiento génico en las que participa AGO1, hemos llevado a cabo una búsqueda de supresores del fenotipo morfológico de *ago1-52*, un alelo hipomorfo de *AGO1* aislado anteriormente en nuestro laboratorio[1], a los que hemos denominando *mas* (*morphology of argonaute1-52 suppressed*).

La mutación *mas2-1* suprime en gran medida el fenotipo de *ago1-52* (Fig. 1). Su clonación posicional (Fig. 2A) nos ha permitido establecer que *MAS2* es un gen de copia única en Arabidopsis y que codifica una proteína de función desconocida, presente tanto en los animales como en las plantas. *mas2-1* manifiesta un efecto supresor dominante, y causa un cambio de alanina por treonina en una posición muy conservada de la proteína MAS2 (Fig. 2B). Hemos identificado entre nuestras 23 líneas supresoras 10 alelos adicionales de *MAS2*, 9 de los cuales son portadores de cambios puntuales en una región muy estrecha, de solo 13 pb, y que causan sustituciones de aminoácidos muy conservados entre la proteína MAS2 y sus ortólogas.

La letalidad embrionaria de *mas2-2*, un alelo insercional de *MAS2* (Fig. 2B), revela su papel esencial durante la embriogénesis (Fig. 3A-F). Hemos generado un microARN artificial para silenciar *MAS2* (*amiR-MAS2*) (Fig. 3G-I), con el objetivo de estudiar los efectos de su insuficiencia de función parcial. Hemos obtenido transgenes que nos han permitido establecer que el gen *MAS2* se expresa en todos los tejidos y órganos estudiados (Fig. 4A-I), que su expresión constitutiva suprime el fenotipo de *ago1-52*, y que su producto proteico es nuclear (Fig. 5A-D), tal como ocurre con sus ortólogos animales. Hemos demostrado mediante hibridación *in situ* la colocalización de MAS2 y los ADNr 45S, en los organizadores nucleolares (Fig. 5A-D).

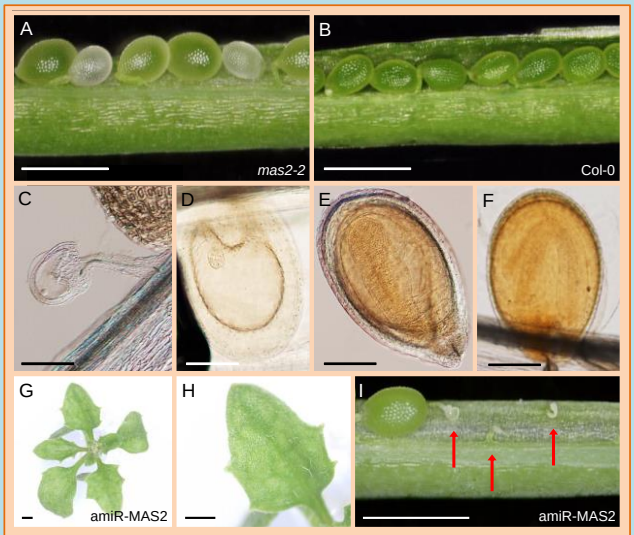

Figura 3.- Algunos rasgos fenotípicos del mutante *mas2-2* y la línea transgénica amiR-MAS2. (A, B) Silicuas inmaduras de (A) *mas2-2* y (B) Col-0. (C) Óvulo sin fecundar. (D-F) Embriones resultantes de la autofecundación de plantas *MAS2/mas2-2* en estadio (D) globular, (E) globular-corazón y (F) maduro. (G) Roseta de una planta transgénica T_3 amiR-MAS2, fotografiada 21 dde. (H) Hoja vegetativa del tercer nudo y (I) silicua inmadura de la planta representada en G. Las flechas rojas señalan semillas abortivas y óvulos sin fecundar. Las barras de escala indican (A, B e I) 1 cm, (C-F) 200 µm y (G, H) 1 mm.

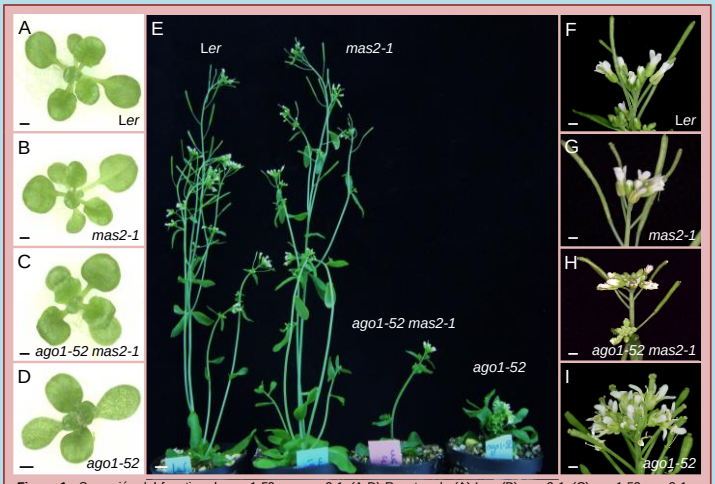

Figura 1.- Supresión del fenotipo de *ago1-52* por *mas2-1*. (A-D) Rosetas de (A) Ler, (B) *mas2-1*, (C) *ago1-52 mas2-1* y (D) *ago1-52*. (E) De izquierda a derecha, plantas adultas de Ler, *mas2-1*, *ago1-52 mas2-1* y *ago1-52*. (F-I) Inflorescencias terminales de (F) Ler, (G) *mas2-1*, (H) *mas2-1 ago1-52* y (I) *ago1-52*. Las fotografías fueron tomadas (A-D) 15 y (E) 43 días después de la estratificación (dde). Las barras de escala indican (A-D, F-I) 1 mm y (E) 1 cm.

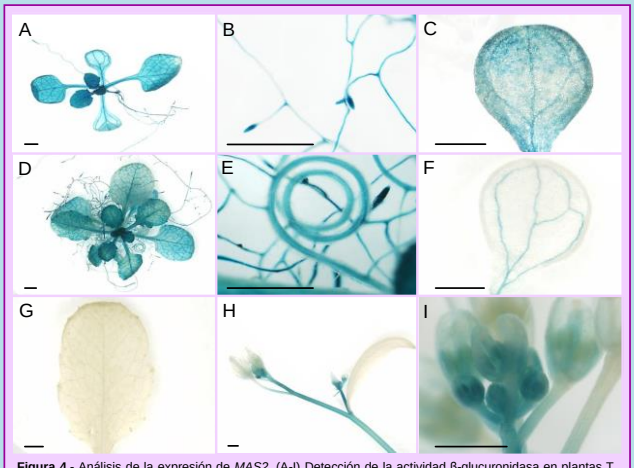

Figura 4.- Análisis de la expresión de *MAS2*. (A-I) Detección de la actividad β-glucuronidasa en plantas T_2 portadoras de la construcción $MAS2_{pro}$:*GUS*. (A, D) Rosetas, (B, E) raíces y (C, F) cotiledones de plantas recolectadas (A-C) 15 y (D-F) 28 dde. (G) Hoja vegetativa del tercer nudo, (H) tallo e (I) inflorescencia apical del tallo, recolectados 48 dde. Las barras de escala indican 1 mm.

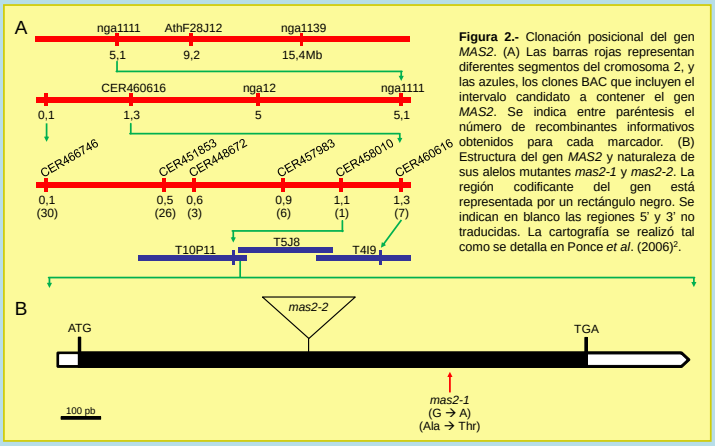

Figura 2.- Clonación posicional del gen *MAS2*. (A) Las barras rojas representan diferentes segmentos del cromosoma 2, y las azules, los clones BAC que incluyen el intervalo candidato a contener el gen *MAS2*. Se indica entre paréntesis el número de recombinantes informativos obtenidos para cada marcador. (B) Estructura del gen *MAS2* y naturaleza de sus alelos mutantes *mas2-1* y *mas2-2*. La región codificante del gen está representada por un rectángulo negro. Se indican en blanco las regiones 5' y 3' no traducidas. La cartografía se realizó tal como se detalla en Ponce *et al*. (2006)[2].

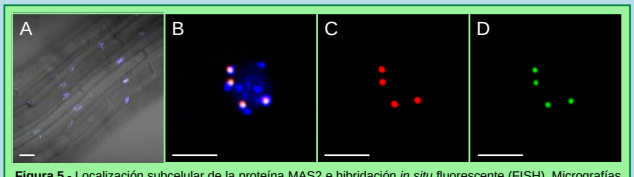

Figura 5.- Localización subcelular de la proteína MAS2 e hibridación *in situ* fluorescente (FISH). Micrografías confocales de (A) la raíz y (B-D) un núcleo en profase mitótica de una planta en la que se expresa el transgén *35S:MAS2:GFP*. (A) Superposición de la emisión fluorescente de la GFP (verde) y del DAPI (4',6-diamidino-2-fenilindol) (azul) con la imagen de la raíz en campo claro. (B-D) Emisión fluorescente de (B) la sonda pTa71 (detección de los ADNr 45S, Sánchez-Morán *et al*., 2001)[4] (rojo), la GFP (verde) y el DAPI (azul) solapadas, (C) la sonda pTa71 y (D) la GFP. Las barras de escala indican 50 µm.

AGRADECIMIENTOS

La investigación en el laboratorio de M.R.P. ha sido financiada por el Ministerio de Ciencia e Innovación (BIO2008-01900) y la Generalitat Valenciana (PROMETEO/2009/112). A.B.S.G. disfruta de un contrato predoctoral de la Generalitat Valenciana.

MÉTODOS

Las plantas fueron cultivadas tal como se describe en la referencia 3, a 20±1ºC y a 60-70% de humedad relativa e iluminación continua (5.000 lx). El medio de cultivo para la selección de plantas transgénicas fue suplementado con 25 µg/ml de higromicina.

BIBLIOGRAFÍA

1.- Jover-Gil, S., Candela, H., y Ponce, M.R. (2005). *Int. J. Dev. Biol.* **49,** 733-744.
2.- Ponce, M.R., Robles, P., Lozano, F.M., Brotóns, M.A., y Micol, J.L. (2006). *Methods Mol. Biol.* **323**, 105-113.
3.- Ponce, M.R., Quesada, V., y Micol, J.L. (1998). *Plant J.* **14**, 497-501.
4.- Sánchez-Morán, E., Armstrong, S.J., Santos, J.L., Franklin, F.C.H., y Jones, G.H. (2001). *Chromosome Research* **9**, 121-128.

Characterization of the Arabidopsis *MAS5* gene

Micol-Ponce, R., García-Asencio, F., Aguilera, V., Micol J.L., and Ponce, M.R.

Instituto de Bioingeniería, Universidad Miguel Hernández de Elche, 03202 Elche, Alicante

We screened 37.000 M_2 seeds derived from a second-site mutagenesis of the *ago1-52* mutant, which carries a hypomorphic and viable recessive allele of the *ARGONAUTE1* (*AGO1*) Arabidopsis gene in a L*er* genetic background. We isolated in this way 17 mutants exhibiting suppression of the morphological phenotype of *ago1-52*, which we termed *mas* (*morphology of argonaute1-52 suppressed*). Presence of the *ago1-52* mutation was sequence verified in all these double mutants. For the positional cloning of the *mas5-1* mutation, we first obtained F_2 mapping populations by crossing the *ago1-52 mas5-1* double mutant to the *ago1-25* and *ago1-27* single mutants, both of which carry a hypomorphic allele of *AGO1* in a Col-0 genetic background. Iterative linkage analysis to molecular markers allowed us to define a 445 kb candidate interval encompassing 122 genes. *In silico* analyses of these genes and the subsequent sequencing of some of them allowed us to identify a G to A transition —that would result in the lysine to glutamic acid substitution— in a conserved gene known to participate in pre-mRNA maturation. We isolated 7 suppressor lines carrying mutations in *MAS5*, belonging to three different parental groups. Four of these suppressors carry the *mas5-1* allele. The *mas5-2* (isolated twice) and *mas5-3* alleles are also transitions causing amino acid substitutions, arginine to lysine in *mas5-2*, and arginine to threonine in *mas5-3*.

2013

Society for Experimental Biology Annual Meeting

Valencia

Póster y comunicación oral

Characterization of the Arabidopsis *MAS5* gene

Micol-Ponce, R., García-Asencio, F., Aguilera, V.[1], Micol, J.L., and Ponce, M.R.

Instituto de Bioingeniería, Universidad Miguel Hernández, Campus de Elche, 03202 Elche, Alicante, Spain.

rmicol@umh.es mrponce@umh.es genetica.umh.es

[1]Current address: Departamento de Genética Molecular de Plantas, Centro Nacional de Biotecnología, Consejo Superior de Investigaciones Científicas, 28049 Madrid, Spain.

We screened 37,000 M_2 seeds derived from a second-site mutagenesis of the *ago1-52* mutant, which carries a hypomorphic and viable recessive allele of the *ARGONAUTE1* (*AGO1*) Arabidopsis gene in a *Ler* genetic background. We isolated in this way 17 mutants exhibiting suppression of the morphological phenotype of *ago1-52*, which we termed *mas* (*morphology of argonaute1-52 suppressed*). Presence of the *ago1-52* mutation was sequence verified in all these double mutants. We dubbed *mas5-1* the mutation carried by the P8 25.1 line (Fig. 1).

For the positional cloning of the *mas5-1* mutation, we first obtained F_2 mapping populations by crossing the *ago1-52 mas5-1* double mutant to the *ago1-25* and *ago1-27* single mutants, both of which carry a hypomorphic allele of *AGO1* in a Col-0 genetic background. Iterative linkage analysis to molecular markers allowed us to define a 445-kb candidate interval encompassing 122 genes. *In silico* analyses of these genes and the subsequent sequencing of some of them allowed us to identify a G→A transition —that would result in a Glu→Lys substitution— in the endonuclease domain of the very large and conserved Pre-mRNA-processing-splicing factor 8 (PRP8), which plays a key role in the activation of the spliceosome (Fig. 2-4).

Whereas null alleles of *MAS5* are embryonic lethal [the gene is also known as *SUS2* (*ABNORMAL SUSPENSOR 2*), *EMB14* (*EMBRYO DEFECTIVE 14*) and *EMB33* and *EMB177*], our results suggest that *mas5-1* is a dominant allele, probably of gain of function (Fig. 5). It seems that *mas5-1* does not normalize the aberrant *splicing* caused by *ago1-52* (Fig. 6).

After the identification of the *mas5-1* mutation, we isolated 6 additional suppressor lines carrying mutations in *MAS5*, belonging to three different parental groups. Three of these suppressors carry the *mas5-1* allele. The *mas5-2* (isolated twice) and *mas5-3* alleles are also transitions, causing amino acid substitutions: Arg→Lys in *mas5-2*, and Thr→Ile in *mas5-3* (Fig. 2).

Further research will be required to understand the molecular nature of the suppression of *ago1-52* by the *mas5-1* alleles and the role of MAS5 in the miRNA pathway.

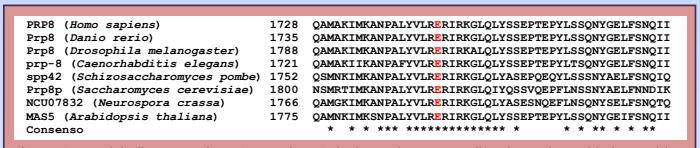

PRP8 (*Homo sapiens*)	1728	QAMAKIMKANPALYVLRERIRKGLQLYSSEPTEPYLSSQNYGELFSNQII
Prp8 (*Danio rerio*)	1735	QAMAKIMKANPALYVLRERIRKGLQLYSSEPTEPYLSSQNYGELFSNQII
Prp8 (*Drosophila melanogaster*)	1788	QAMAKIMKANPALYVLRERIRKALQLYSSEPTEPYLSSQNYGELFSNQII
prp-8 (*Caenorhabditis elegans*)	1721	QAMAKIIKANPAFYVLRERIRKGLQLYSSEPTEPYLTSQNYGELFSNQII
spp42 (*Schizosaccharomyces pombe*)	1752	QSMNKIMKANPALYVLRERIRKGLQLYASEPQEQYLSSSNYAELFSNQIQ
Prp8p (*Saccharomyces cerevisiae*)	1800	NSMRTIMKANPALYVLRERIRKGLQIYQSSVQEPFLNSSNYAELFNNDIK
NCU07832 (*Neurospora crassa*)	1766	QAMGKIMKANPALYVLRERIRKGLQLYASESNQEFLNSQNYSELFSNQTQ
MAS5 (*Arabidopsis thaliana*)	1775	QAMNKIMKSNPALYVLRERIRKGLQLYSSEPTEPYLSSQNYGEIFSNQII
Consenso		* * * *** ********** * * ** * * **

Figure 3.- Partial alignment of PRP8 proteins. Only the region surrounding the amino acid changed by the *mas5-1* mutation (in red) is shown. Numbers indicate amino acid residues. Sequences were obtained from NCBI (http://www.ncbi.nlm.nih.gov) and aligned with the CLUSTALW2 program (http://www.ebi.ac.uk/Tools/msa/clustalw2/). Asterisks indicate residues conserved in all aligned proteins.

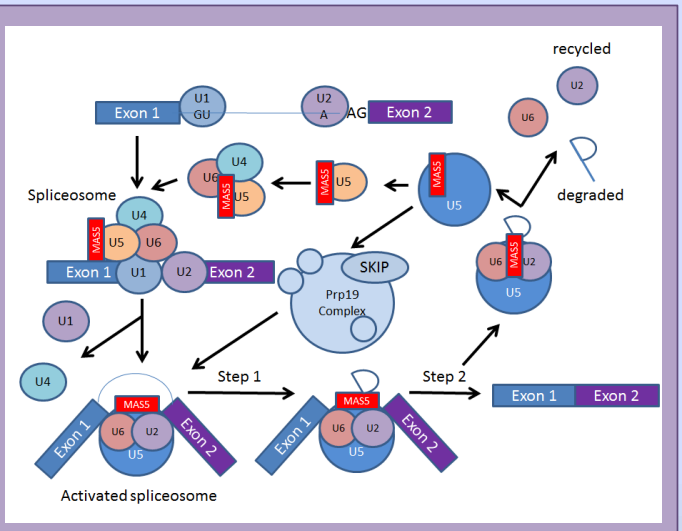

Figure 4- Assembly and recycling of major spliceosome components. PRP8 appears here as MAS5. U1-U6 are small nuclear RNA–protein (snRNP) complexes formed by small nuclear RNAs (snRNAs) and proteins. The spliceosome is formed stepwise, through several presplicing complexes. Splicing involves two trans-esterification reactions that require PRP8. Following completion of the splicing reaction, spliceosome components are recycled and the intron is degraded. Adapted from Grainger and Beggs (2005).

ACKNOWLEDGEMENTS

The *ago1-25* and *ago1-27* mutants were a gift from H. Vaucheret. Research in the laboratory of M.R.P. is supported by grants from the Ministerio de Ciencia e Innovación of Spain (BIO2008-01900) and the Generalitat Valenciana (PROMETEO/2009/112).

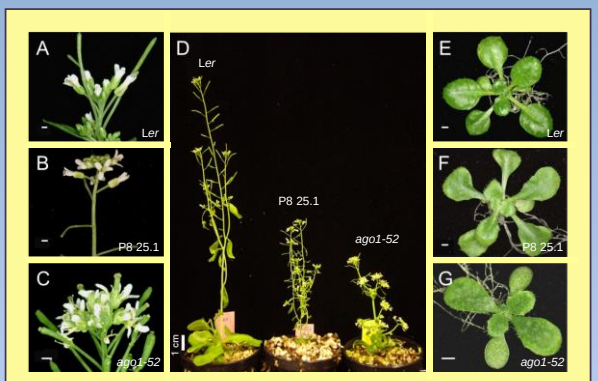

Figure 1.- Some phenotypic traits of the P8 25.1 (*ago1-52 mas5-1*) line. (A-C) Inflorescences and (E-G) rosettes of (A, E) *Ler*, (B, F) P8 25.1 and (C, G) *ago1-52*. (D) *Ler*, P8 25.1 and *ago1-52* adult plants. Pictures were taken (A-D) 54 and (E-G) 21 days after stratification (das). Scale bars: (A-C, E-G) 1 mm and (D) 1 cm.

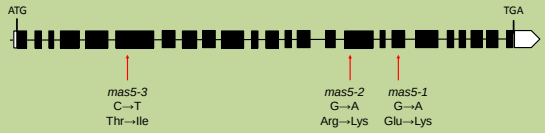

Figure 2.- Structure and mutant alleles of the *MAS5* gene. Exons and introns are depicted as black boxes and lines, respectively. White boxes indicate 5´- and 3´-UTRs. The predicted translation start (ATG) and stop (TAA) codons are indicated. Red arrows mark the positions of the point mutations in the *mas5* alleles, and the predicted amino acid substitutions in the MAS5 protein.

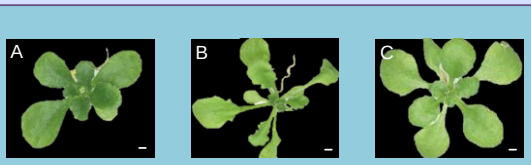

Figure 5.- Dominance of the suppresor effect of *mas5-1* on *ago1-52*. Rosettes are shown from (A) *ago1-52/ago1-52;MAS5/MAS5*, (B) *ago1-52/ago1-52;MAS5/mas5-1* and (C) *ago1-52/ago1-52;mas5-1/mas5-1* plants. Pictures were taken 17 das. Scale base: 1 mm.

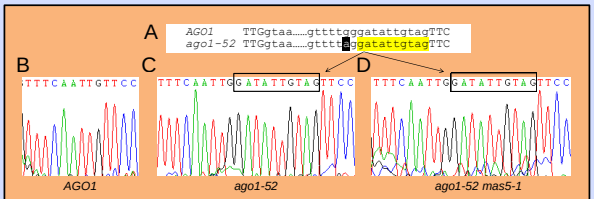

Figure 6.- The aberrant splicing of *ago1-52* seems not to be modified in the *ago1-52 mas5-1* double mutant. (A) Partial sequence of the wild type *AGO1* (*Ler*) and the mutant *ago1-52* alleles. Exons are shown in uppercase and introns in lowercase letters. The nucleotide mutated in *ago1-52* is shaded black.The nucleotides highlighted in yellow are present in the mature mRNA of the *ago1-52* single mutant and the *ago1-52 mas* double mutants but not in the wild type are (B) absent from the mature mRNA, but present in (C) the *ago1-52* single mutant and (D) the *ago1-52 mas5-1* double mutant.

METHODS

Plant culture and low resolution mapping were performed as described in refs. 6 and 7, respectively.

REFERENCES

1.- Jover-Gil, S., Candela, H., and Ponce, M.R. (2005). *Int. J. Dev. Biol.* **49**, 733-744.
2.- Bohmert, K., Camus, I., Bellini, C., Bouchez, D., Caboche, M., and Benning, C. (1998). *EMBO J.* **17**, 170-180.
3.- Morel, J.B., Godon, C., Mourrain, P., Béclin, C., Boutet, S., Feuerbach, F., Proux, F., and Vaucheret, H. (2002). *Plant Cell* **14**, 629-639.
4.- Grainger, R.J., and Beggs, J.D. (2005). *RNA* **11,** 533-537.
5.- Obayashi T, Nishida K, Kasahara K, Kinoshita K. (2011). *Plant Cell Phys.* **52**, 213-219.
6.- Ponce, M.R., Quesada, V., and Micol, J.L. (1998). *Plant J.* **14**, 497-501.
7.- Ponce, M.R., Robles, P., Lozano, F.M., Brotóns, M.A., y Micol, J.L. (2006). *Methods Mol. Biol.* **323,** 105-113.

Genetic and molecular analysis of the Arabidopsis *MAS2* gene

Sánchez-García, A.B., Aguilera, V, Micol-Ponce, R., Jover-Gil, S., Candela-Noguera, V., Micol, J.L. and Ponce, M.R.

Instituto de Bioingeniería, Universidad Miguel Hernández de Elche, 03202 Elche, Alicante

In eukaryotes, small non-coding RNAs mediate transcriptional and post-transcriptional gene silencing by binding to ARGONAUTE (AGO) proteins to form RNA-Induced Silencing Complexes (RISCs). In order to study the action and interactions of AGO1 —a key component of the miRNA pathway in Arabidopsis— we first isolated ago1 hypomorphic alleles of the *AGO1* gene. A second-site mutagenesis screen for suppressors of *ago1-52* allowed us to isolate a number of *mas* (*morphology of argonaute1-52 suppressed*) mutants. We identified in this way 11 alleles of the gene that we termed *MAS2*, which was positionally cloned and found to encode a protein of unknown function conserved among plants and animals. A total of 9 of these alleles cause amino acid substitutions mapping within a 13-bp highly conserved region and have no visible phenotype on their own. A T-DNA insertion that disrupts *MAS2* (*mas2-2*), however, causes embryonic lethality. In addition, we obtained transgenic plants expressing an artificial microRNA targeting *MAS2*. The pleiotropic phenotype of these transgenic plants indicates essential roles for *MAS2* in many developmental stages. We have also shown that *MAS2* is broadly expressed and the nuclear localization of its protein product, as already known for its animal orthologs. *In situ* hybridization (FISH) allowed us to demonstrate that MAS2 co-localizes with 45S rDNA.

2013

Society for Experimental Biology Annual Meeting

Valencia

Póster y comunicación oral

Genetic and molecular analysis of the Arabidopsis *MAS2* gene

Sánchez-García, A.B., Aguilera, V., Micol-Ponce, R., Jover-Gil, S., Candela-Noguera, V., Micol, J.L., and Ponce, M.R.

Instituto de Bioingeniería, Universidad Miguel Hernández, Campus de Elche, 03202 Elche, Alicante, Spain.
ana.sanchezg@umh.es mrponce@umh.es http://genetica.umh.es

In eukaryotes, small non-coding RNAs mediate transcriptional and post-transcriptional gene silencing by binding to ARGONAUTE (AGO) proteins to form RNA-Induced Silencing Complexes (RISCs). In order to study the action and interactions of AGO1 —a key component of the miRNA pathway in Arabidopsis— we first isolated *ago1* hypomorphic alleles of the *AGO1* gene[1,2]. A second-site mutagenesis screen for suppressors of *ago1-52* allowed us to isolate 23 *mas* (*morphology of argonaute1-52 suppressed*) mutants (Fig. 1). We identified in this way 10 alleles of the gene that we termed *MAS2*, which was positionally cloned (Fig. 2) and found to encode a protein of unknown function conserved among plants and animals. A total of 9 of these alleles contain a mutation which causes amino acid substitutions in a highly conserved region of the MAS2 protein. A T-DNA insertional allele of *MAS2* (*mas2-2*) causes embryonic lethality (Fig. 2B and Fig. 3).

In addition, we obtained transgenic plants expressing an artificial microRNA targeting *MAS2* (*2x35S$_{pro}$:amiR-MAS2*)[5]. The pleiotropic phenotype of these transgenic plants indicate essential roles for *MAS2* in several developmental processes (Fig. 4). We have also shown that *MAS2* is broadly expressed and the nuclear localization of its protein product, as already known for its animal orthologs (Fig. 5A-G). Fluorescent *in situ* hybridization (FISH) allowed us to demonstrate that MAS2 co-localizes with 45S rDNA (Fig. 5H-K).

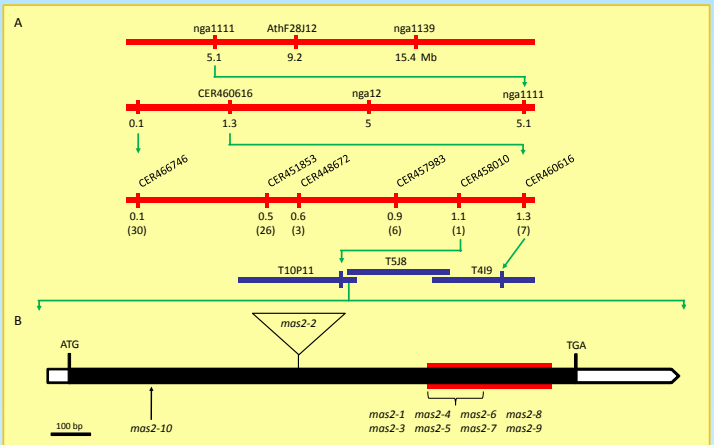

Figure 2.- Positional cloning of the *MAS2* gene. (A) Red bars represent chromosome 2 segments, and blue bars indicate BAC clones that contain the candidate region for the *MAS2* gene. The number of informative recombinants for each marker is shown between brackets. (B) *MAS2* gene structure with indication of the nature and position of the *mas* mutations. The red box indicates the region that encodes the single domain of the MAS protein, which is highly conserved in plants and animals. Low resolution mapping was performed as previosuly described[3].

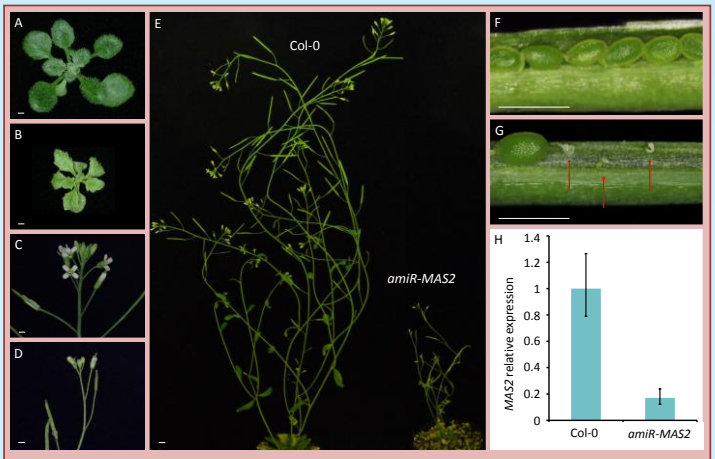

Figure 4.- Phenotypes caused by the *2x35Spro:amiR-MAS2* transgene. (A, B) Rosettes of (A) Col-0 and (B) *amiR-MAS2*. (C, D) Inflorescences of (C) Col-0 and (D) *amiR-MAS2*. (E) Col-0 and *amiR-MAS2* adult plants. (F, G) Seeds of (F) Col-0 and (G) *amiR-MAS2*. Red arrows indicate aborted ovules and embryos arrested in early stages of development. (H) Expression of *MAS2* in Col-0 and *amiR-MAS2* plants. Pictures were taken (A, B) 21 and (E) 48 das. Scale bars: (A-D, F, G) 1 mm and (E) 1 cm.

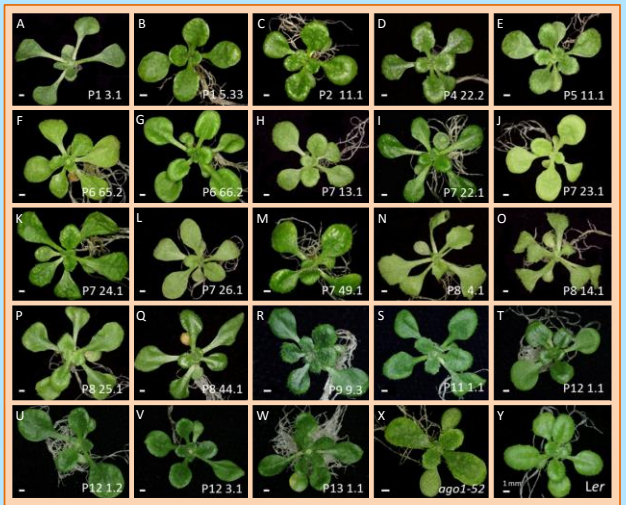

Figure 1.- (A-W) *ago1-52 mas* double mutants, (X) the *ago1-52* single mutant, and (Y) the *Ler* wild type. Plants shown in A-C, F-H, Q, S, T and W carry *mas2* alleles. Pictures were taken 21 days after stratification (das). Scale bars: 1 mm.

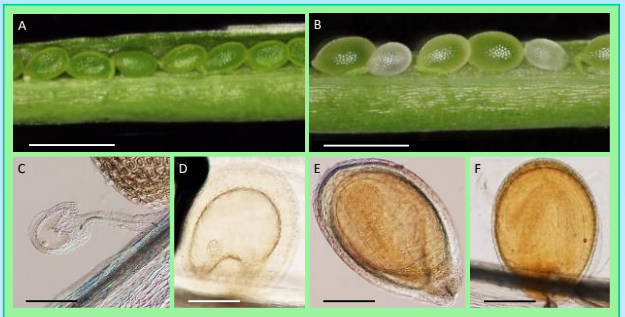

Figure 3.- (A, B) Seeds of dissected siliques from (A) Col-0 and (B) *MAS2/mas2-2* plants. (C) Aborted ovule in a *MAS2/mas2-2* plant. (D-F) Embryos from *MAS2/mas2-2* siliques. (D, E) Abnormal embryos arrested in the (D) globular and (E) globular-heart stages. (F) Phenotypically wild type mature embryo. Scale bars: (A, B) 1 mm and (C-F) 200 µm.

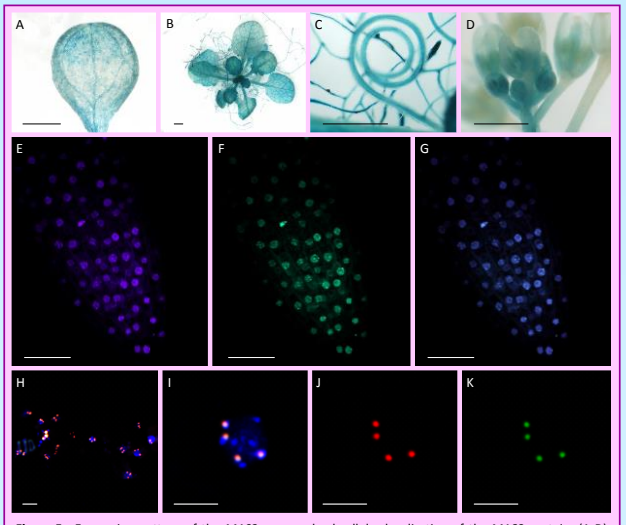

Figure 5.- Expression pattern of the *MAS2* gene and subcellular localization of the MAS2 protein. (A-D) Detection of β-glucuronidase activity in T_2 plants carrying a *MAS2$_{pro}$:GUS* transgene: (A) Cotyledon, (B) rosette, (C) roots and (D) inflorescence. (E-K) MAS2 subcellular localization. (E) Detection of the fluorescent emission of DAPI (4',6-diamidino-2-phenylindole), (F) GFP and (G) their overlay in roots of transgenic plants expressing a *2x35S$_{pro}$:MAS2:GFP* transgene. (H-K) Fluorescent *in situ* hibridization (FISH). (H, I) Overlay of DAPI, MAS2:GFP and a 45S rDNA probe (pTa71)[4], (H) several nuclei and (I) magnification of a mitotic prophase nucleus. (J-K) Fluorescent emission of (J) pTa71 probe and (K) MAS2-GFP shown in I. Scale bars: (A-D) 1 mm, (E-G, I-K) 50 µm, and (H) 25 µm.

REFERENCES

1.- Jover-Gil, S., Candela, H., and Ponce, M.R. (2005). *Int. J. Dev. Biol.* **49,** 733-744.
2.- Jover-Gil, S., Candela, H., Robles, P., Aguilera, V., Barrero, J.M., Micol, J.L., and Ponce, M.R. (2012). *Plant Cell Physiol.* **53**,1322-1333.
3.- Ponce, M.R., Robles, P., Lozano, F.M., Brotóns, M.A., and Micol, J.L. (2006). *Methods Mol. Biol.* **323**, 105-113.
4.- Sánchez-Morán, E., Armstrong, S.J., Santos, J.L., Franklin, F.C.H., y Jones, G.H. (2001). *Chromosome Res.* **9**, 121-128.
5.- Jover-Gil, S., Paz-Ares, J., Micol, J.L., and Ponce, M.R. (2013). Submitted.

ACKNOWLEDGEMENTS

Research in the laboratory of M.R.P. is supported by grants from the Ministerio de Economía y Competitividad of Spain (BIO2008-01900) and the Generalitat Valenciana (PROMETEO/2009/112).

Dominant alleles of the gene encoding the core spliceosome component PRP8 suppress the phenotype of *ago1-52*

Micol-Ponce, R., Ruiz-Bayón, A., and Ponce, M.R.

Instituto de Bioingeniería, Universidad Miguel Hernández, Campus de Elche, 03202 Elche, Alicante, Spain

We screened 67,500 M_2 seeds derived from a second-site mutagenesis of the *ago1-52* mutant, which carries a hypomorphic and viable recessive allele of the *ARGONAUTE1* (*AGO1*) Arabidopsis gene in a L*er* genetic background. We isolated in this way 23 mutants exhibiting suppression of the morphological phenotype of *ago1-52*, which we termed *mas* (*morphology of argonaute1-52 suppressed*). Presence of the *ago1-52* mutation was sequence verified in all these double mutants, all but one of which were shown to carry extragenic suppressors.

For the positional cloning of the *mas5-1* mutation, we first obtained F_2 mapping populations by crossing the *ago1-52 mas5-1* double mutant to the *ago1-25* and *ago1-27* single mutants, both of which carry a hypomorphic allele of *AGO1* in a Col-0 genetic background. Iterative linkage analysis to molecular markers allowed us to define a 445 kb candidate interval encompassing 122 genes. *In silico* analyses of these genes and the subsequent sequencing of some of them allowed us to identify a G to A transition —that would result in the acid glutamic to lysine substitution— in the gene encoding the pre-mRNA processing factor 8 (PRP8), one of the most highly conserved nuclear proteins that plays a key role in the catalytic core of the spliceosome.

We isolated 8 suppressor lines carrying alleles of *MAS5*, which belong to three different parental groups. Five of these suppressors carry the *mas5-1* allele. The *mas5-2* (isolated twice) and the *mas5-3* mutations are also transitions causing amino acid substitutions: arginine to threonine and threonine to isoleucine, respectively.

2014

XII Reunión de Biología Molecular de Plantas

Cartagena

Póster

Dominant alleles of the gene encoding the core spliceosome component PRP8 suppress the phenotype of *ago1-52*

Micol-Ponce, R., Ruiz-Bayón, A., and Ponce, M.R.

Instituto de Bioingeniería, Universidad Miguel Hernández, Campus de Elche, 03202 Elche, Alicante, Spain.

rmicol@umh.es mrponce@umh.es http://genetica.umh.es

We screened 67,500 M_2 seeds derived from a second-site mutagenesis of the *ago1-52* mutant[1], which carries a hypomorphic and viable recessive allele of the *ARGONAUTE1* (*AGO1*)[2] Arabidopsis gene in a L*er* genetic background. We isolated in this way 23 mutants exhibiting suppression of the morphological phenotype of *ago1-52*, which we termed *mas* (*morphology of argonaute1-52 suppressed*). Presence of the *ago1-52* mutation was sequence verified in all these double mutants, all but one of which were shown to carry extragenic suppressors.

For the positional cloning of the *mas5-1* mutation, we first obtained F_2 mapping populations by crossing the *ago1-52 mas5-1* double mutant (Fig. 1) to the *ago1-25* and *ago1-27* single mutants, both of which carry a hypomorphic allele of *AGO1* in a Col-0 genetic background[3]. Iterative linkage analysis to molecular markers allowed us to define a 445-kb candidate interval encompassing 122 genes. *In silico* analyses of these genes and the subsequent sequencing of some of them allowed us to identify a G to A transition —that would result in a glutamic acid to lysine substitution— in the gene encoding the pre-mRNA processing factor 8 (PRP8), one of the most highly conserved nuclear proteins that play a key role in the catalytic core of the spliceosome (Fig. 2-4).

Whereas null alleles of *MAS5* are embryonic lethal [the gene is also known as *SUS2* (*ABNORMAL SUSPENSOR 2*), *EMB14* (*EMBRYO DEFECTIVE 14*) and *EMB33* and *EMB177*], our results suggest that *mas5-1* is a dominant allele, probably of gain of function (Fig. 5). It seems that *mas5-1* does not normalize the aberrant *splicing* caused by *ago1-52* (Fig. 6).

We isolated 8 suppressor lines carrying alleles of *MAS5*, which belong to three different parental groups. Five of these suppressors carry the *mas5-1* allele. The *mas5-2* (isolated twice) and *mas5-3* mutations are also transitions causing amino acid substitutions: arginine to threonine and threonine to isoleucine, respectively (Fig. 2).

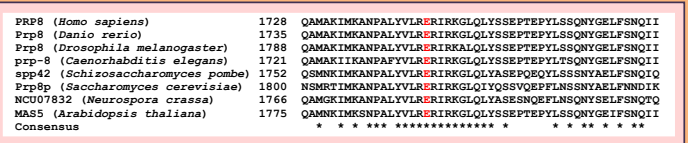

```
PRP8 (Homo sapiens)              1728  QAMAKIMKANPALYVLRERIRKGLQLYSSEPTEPYLSSQNYGELFSNQII
Prp8 (Danio rerio)               1735  QAMAKIMKANPALYVLRERIRKGLQLYSSEPTEPYLSSQNYGELFSNQII
Prp8 (Drosophila melanogaster)   1788  QAMAKIMKANPALYVLRERIRKALQLYSSEPTEPYLSSQNYGELFSNQII
prp-8 (Caenorhabditis elegans)   1721  QAMAKIIKANPAFYVLRERIRKGLQLYSSEPTEPYLTSQNYGELFSNQII
spp42 (Schizosaccharomyces pombe) 1752  QSMNKIMKANPALYVLRERIRKGLQLYASEPQEQYLSSSNYAELFSNQIQ
Prp8p (Saccharomyces carevisiae) 1800  NSMRTIMKANPALYVLRERIRKGLQIYQSSVQEPFLNSSNYAELFNNDIK
NCU07832 (Neurospora crassa)     1766  QAMGKIMKANPALYVLRERIRKGLQLYASESNQEFLNSQNYSELFSNQTQ
MAS5 (Arabidopsis thaliana)      1775  QAMNKIMKSNPALYVLRERIRKGLQLYSSEPTEPYLSSQNYGEIFSNQII
Consensus                              *  * * *** ************** *      * * ** * * **
```

Figure 3.- Partial alignment of PRP8 proteins. Only the region surrounding the amino acid changed by the *mas5-1* mutation (in red) is shown. Numbers indicate amino acid residues. Sequences were obtained from NCBI (http://www.ncbi.nlm.nih.gov) and aligned with the CLUSTALW2 program (http://www.ebi.ac.uk/Tools/msa/clustalw2/). Asterisks indicate residues conserved in all aligned proteins.

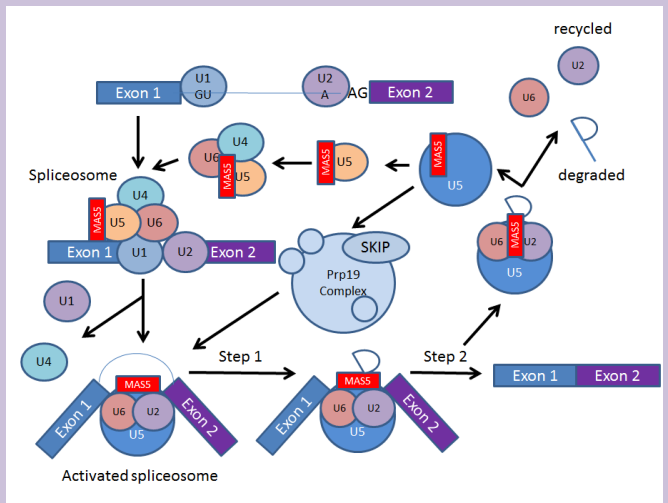

Figure 4- Assembly and recycling of major spliceosome components. PRP8 appears here as MAS5. U1-U6 are small nuclear RNA–protein (snRNP) complexes formed by small nuclear RNAs (snRNAs) and proteins. The spliceosome is formed stepwise, through several presplicing complexes. Splicing involves two trans-esterification reactions that require PRP8. Following completion of the splicing reaction, spliceosome components are recycled and the intron is degraded. Adapted from Grainger and Beggs (2005)[4].

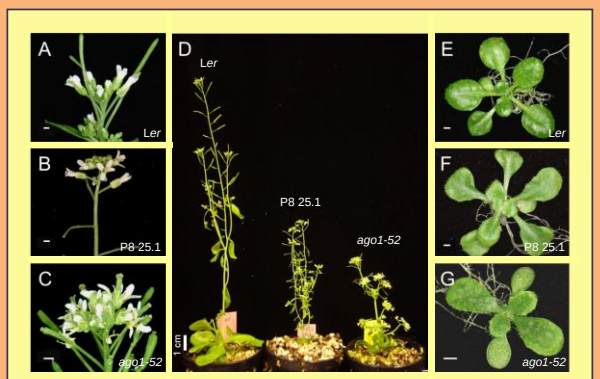

Figure 1.- Some phenotypic traits of the P8 25.1 (*ago1-52 mas5-1*) line. (A-C) Inflorescences and (E-G) rosettes of (A, E) L*er*, (B, F) P8 25.1 and (C, G) *ago1-52*. (D) L*er*, P8 25.1 and *ago1-52* adult plants. Pictures were taken (A-D) 54 and (E-G) 21 days after stratification (das). Scale bars: (A-C, E-G) 1 mm and (D) 1 cm.

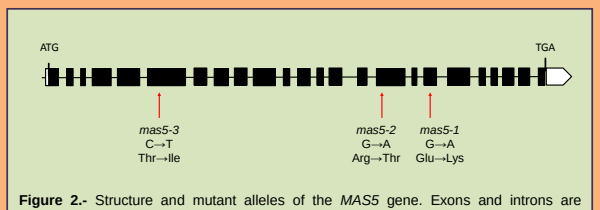

Figure 2.- Structure and mutant alleles of the *MAS5* gene. Exons and introns are depicted as black boxes and lines, respectively. White boxes indicate 5´- and 3´-UTRs. The predicted translation start (ATG) and stop (TAA) codons are indicated. Red arrows mark the positions of the point mutations in the *mas5* alleles, and the predicted amino acid substitutions in the MAS5 protein.

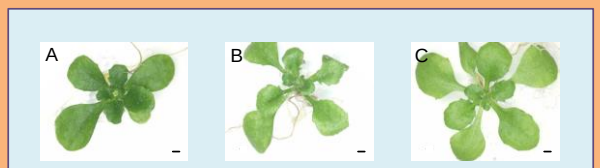

Figure 5.- Dominance of the suppresor effect of *mas5-1* on *ago1-52*. Rosettes are shown from (A) *ago1-52/ago1-52;MAS5/MAS5*, (B) *ago1-52/ago1-52;MAS5/mas5-1* and (C) *ago1-52/ago1-52;mas5-1/mas5-1* plants. Pictures were taken 17 das. Scale bar: 1 mm.

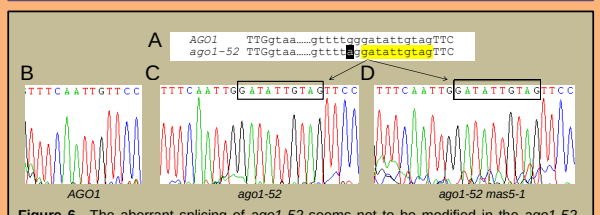

Figure 6.- The aberrant splicing of *ago1-52* seems not to be modified in the *ago1-52 mas5-1* double mutant. (A) Partial sequence of the wild type *AGO1* (L*er*) and the mutant *ago1-52* alleles. Exons are shown in uppercase and introns in lowercase letters. The nucleotide mutated in *ago1-52* is shaded black.The nucleotides highlighted in yellow are present in the mature mRNA of the *ago1-52* single mutant and the *ago1-52 mas* double mutants but not in the wild type are (B) absent from the mature mRNA, but present in (C) the *ago1-52* single mutant and (D) the *ago1-52 mas5-1* double mutant.

METHODS

Plant culture and low resolution mapping were performed as described in refs. 5 and 6, respectively.

ACKNOWLEDGEMENTS

The *ago1-25* and *ago1-27* mutants were a gift from H. Vaucheret. Research in the laboratory of M.R.P. is supported by grants from the Ministerio de Ciencia e Innovación of Spain (BIO2008-01900) and the Generalitat Valenciana (PROMETEO/2009/112).

REFERENCES

1.- Jover-Gil, S., Candela, H., and Ponce, M.R. (2005). *Int. J. Dev. Biol*. **49**, 733-744.
2.- Bohmert, K., Camus, I., Bellini, C., Bouchez, D., Caboche, M., and Benning, C. (1998). *EMBO J.* **17**, 170-180.
3.- Morel, J.B., Godon, C., Mourrain, P., Béclin, C., Boutet, S., Feuerbach, F., Proux, F., and Vaucheret, H. (2002). *Plant Cell* **14**, 629-639.
4.- Grainger, R.J., and Beggs, J.D. (2005). *RNA* **11,** 533-537.
5.- Ponce, M.R., Quesada, V., and Micol, J.L. (1998). *Plant J.* **14**, 497-501.
6.- Ponce, M.R., Robles, P., Lozano, F.M., Brotóns, M.A., y Micol, J.L. (2006). *Methods Mol. Biol.* **323,** 105-113.

MAS2, the Arabidopsis ortholog of human NKAP, regulates 45S rDNA transcription

Sánchez-García, A.B., Micol-Ponce, R., Jover-Gil, S., Nikolaeva-Koleva, M. and Ponce, M.R.

Instituto de Bioingeniería, Universidad Miguel Hernández, Campus de Elche, 03202 Elche, Alicante, Spain

We performed a second-site mutagenesis screen for extragenic suppressors of the morphological phenotype of *ago1-52* in Arabidopsis. A total of 23 *mas* (*morphology of argonaute1-52 suppressed*) lines were isolated, which exhibited suppression at a different extent. We identified in this way 10 alleles of the gene that we termed *MAS2*, which was positionally cloned and found to encode the human NKAP ortholog, a highly conserved eukaryotic protein involved in transcriptional repression. Nine of these *mas2* alleles cause amino acid substitutions, map within a 13-bp highly conserved region and cause no visible phenotype on their own. Two T-DNA insertions that disrupt *MAS2* (*mas2-2* and *mas2-3*), however, cause embryonic lethality. We also obtained transgenic plants expressing an artificial microRNA targeting *MAS2* (*amiR-MAS2*); the pleiotropic phenotype of these plants indicate essential roles for *MAS2* in many developmental stages. We have also shown that *MAS2* is broadly expressed and the nuclear localization of its protein product, as already known for its animal orthologs. We demonstrated by *in situ* hybridization (FISH) that MAS2 co-localizes with 45S rDNA in wild-type plants. The molecular and genetic analysis of *amiR-MAS2* plants allowed us to uncover a role for MAS2 in the control of 45S rDNA transcription.

2014

XII Reunión de Biología Molecular de Plantas

Cartagena

Póster

MAS2, the Arabidopsis ortholog of human NKAP, regulates 45S rDNA transcription

Ana Belén Sánchez-García, Rosa Micol-Ponce, Sara Jover-Gil, Magdalena Nikolaeva-Koleva, and María Rosa Ponce

Instituto de Bioingeniería, Universidad Miguel Hernández, Campus de Elche, 03202 Elche, Alicante, Spain.

mrponce@umh.es http://genetics.umh.es

We performed a second-site mutagenesis screen for extragenic suppressors of the morphological phenotype of *ago1-52* in Arabidopsis[1]. A total of 23 *mas* (*morphology of argonaute1-52 suppressed*) lines were isolated, which exhibited suppression at a different extent[2]. We identified in this way 10 alleles of the gene that we termed *MAS2* (Fig. 1), which was positionally cloned and found to encode the human NKAP ortholog, a highly conserved eukaryotic protein involved in transcriptional repression. Nine of these *mas2* alleles cause amino acid substitutions, map within a 32-bp highly conserved region and cause no visible phenotype on their own (Fig. 2). Two T-DNA insertions that disrupt *MAS2* (*mas2-2* and *mas2-3*), however, cause embryonic lethality (Fig. 2 and 3).

We also obtained transgenic plants expressing an artificial microRNA targeting *MAS2* (*amiR-MAS2*)[4]; the pleiotropic phenotype of these plants indicate essential roles for *MAS2* in many developmental stages (Fig. 4). We have also shown that MAS2 is a nuclear protein, as already known for its animal orthologs (Fig. 5A-C).

We probed that MAS2 co-localizes with 45S rDNA (Fig. 5D-G). Further, *mas2-1* and *amiR-MAS2.1* plants interacted with mutant alleles of the *NUCLEOLIN-LIKE PROTEIN1* (*AtNUC-L1*) and *HISTONE DEACETYLASE6* (*HDA6*) genes, which are involved in transcriptional regulation of 45S rDNA (Figure 6A-J). We found that *amiR-MAS2.1* plants are deficient in cytosine methylation at the 45S rDNA promoter (Figure 6K).

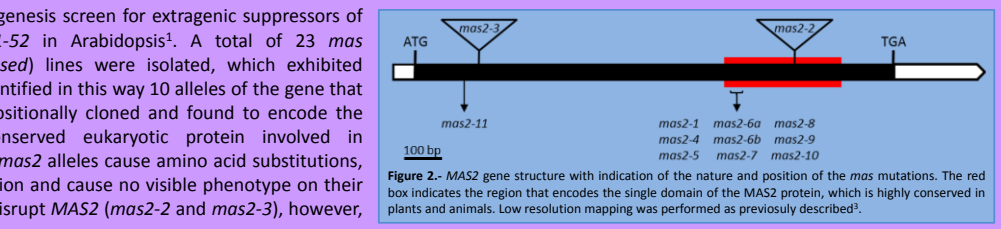

Figure 2.- *MAS2* gene structure with indication of the nature and position of the *mas* mutations. The red box indicates the region that encodes the single domain of the MAS2 protein, which is highly conserved in plants and animals. Low resolution mapping was performed as previosuly described[3].

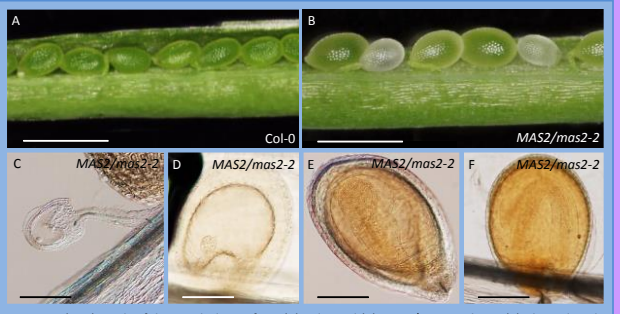

Figure 3.- (A, B) Seeds of dissected siliques from (A) Col-0 and (B) *MAS2/mas2-2* plants. (C) Aborted ovule in a *MAS2/mas2-2* plant. (D-F) Embryos from *MAS2/mas2-2* siliques. (D, E) Abnormal embryos arrested in the (D) globular and (E) globular-heart stages. (F) Phenotypically wild type mature embryo. Scale bars: (A, B) 1 mm and (C-F) 200 µm.

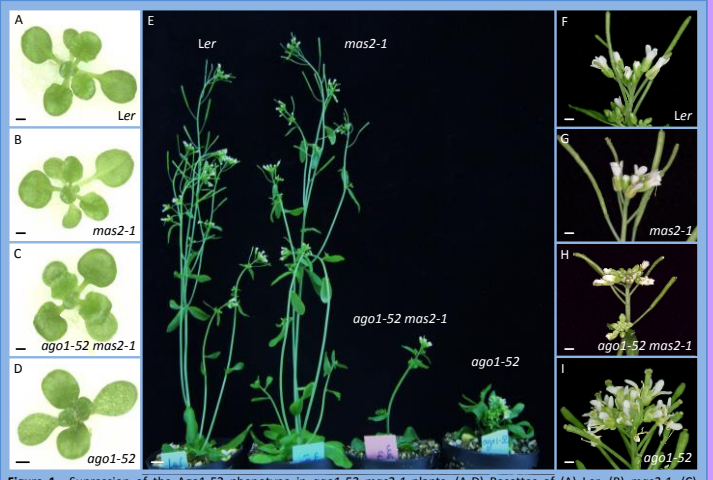

Figure 1.- Supression of the Ago1-52 phenotype in *ago1-52 mas2-1* plants. (A-D) Rosettes of (A) L*er*, (B) *mas2-1*, (C) *ago1-52 mas2-1* and (D) *ago1-52*. (E) Adult L*er*, *mas2-1*, *ago1-52 mas2-1* and *ago1-52* plants. (F-I) Terminal region of the inflorescences of (F) L*er*, (G) *mas2-1*, (H) *mas2-1 ago1-52* and (I) *ago1-52*. Pictures were taken (A-D) 15 and (E) 43 days after stratification (das). Scale bars: (A-D, F-I) 1 mm and (E) 1 cm.

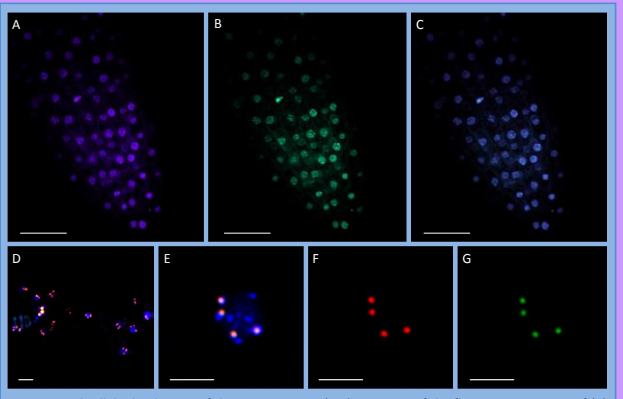

Figure 5.- Subcellular localization of the MAS2 protein. (A-C) Detection of the fluorescent emission of (A) DAPI (4',6-diamidino-2-phenylindole), (B) GFP and (C) their overlay in roots of transgenic plants expressing a *2x35S$_{pro}$:MAS2:GFP* transgene. (D-G) Fluorescent *in situ* hibridization (FISH): (D, E) Overlay of DAPI, MAS2:GFP and a 45S rDNA probe (pTa71), (D) several nuclei and (E) magnification of a mitotic prophase nucleus. (F-G) Fluorescent emission of (F) pTa71 probe and (G) MAS2-GFP. Scale bars: (A-C, E-G) 50 µm, and (D) 25 µm.

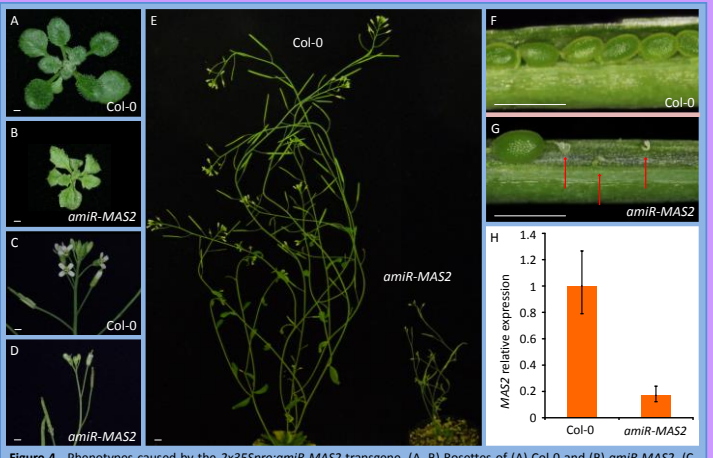

Figure 4.- Phenotypes caused by the *2x35Spro:amiR-MAS2* transgene. (A, B) Rosettes of (A) Col-0 and (B) *amiR-MAS2*. (C, D) Terminal region of the inflorescences of (C) Col-0 and (D) *amiR-MAS2*. (E) Col-0 and *amiR-MAS2* adult plants. (F, G) Dissected siliques of (F) Col-0 and (G) *amiR-MAS2*. Red arrows indicate aborted ovules and embryos arrested in early stages of development. (H) Expression of *MAS2* in Col-0 and *amiR-MAS2* plants. Pictures were taken (A, B) 21 and (E) 48 das. Scale bars: (A-D, F, G) 1 mm and (E) 1 cm.

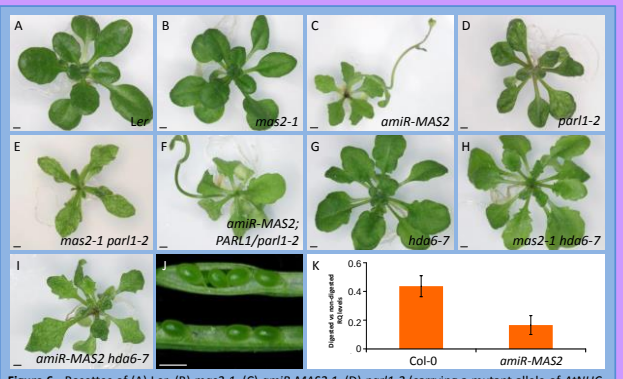

Figure 6.- Rosettes of (A) L*er*, (B) *mas2-1*, (C) *amiR-MAS2.1*, (D) *parl1-2* (carrying a mutant allele of *AtNUC-L1*), (E) *mas2-1 parl1-2*, (F) *amiR-MAS2;PARL1/parl1-2*, (G) *hda6-7*, (H) *mas2-1 hda6-7* and (I) *amiR-MAS2 hda6-7*. (J) Dissected siliques of *amiR-MAS2;PARL1/parl1-2* plants. No *amiR-MAS2;parl1-2/parl1-2* plants were identified after genotyping 84 plants of different F_2 and F_3 families. (K) Quantification of DNA methylation levels of the 45S rDNA gene promoter in Col-0 and *amiR-MAS2.1* plants. The DNA methylation status was analyzed by qPCR, using genomic DNA that was digested or not with the methylation-sensitive *Hpa*II endonuclease, which digests only non-methylated CCGG sequences. Bars represent the ratio between digested and undigested amplification levels. Scale bars: (A-I) 1 mm and (J) 0.5 mm.

REFERENCES

1.- Jover-Gil, S., Candela, H., Robles, P., Aguilera, V., Barrero, J.M., Micol, J.L., and Ponce, M.R. (2012). The microRNA pathway genes *AGO1*, *HEN1* and *HYL1* participate in leaf proximal-distal, venation and stomatal patterning in Arabidopsis. *Plant Cell Physiol.* **53**,1322-1333.

2.- Micol-Ponce, R., Aguilera, V., and Ponce, M.R. (2014). A genetic screen for suppressors of a hypomorphic allele of Arabidopsis *ARGONAUTE1*. Submitted.

3.- Ponce, M.R., Robles, P., Lozano, F.M., Brotóns, M.A., and Micol, J.L. (2006). Low-resolution mapping of untagged mutations. *Methods Mol. Biol.* **323**, 105-113.

4.- Jover-Gil, S., Paz-Ares, J., Micol, J.L., and Ponce, M.R. (2014). Multi-gene silencing in Arabidopsis: a collection of artificial microRNAs targeting groups of paralogs encoding transcription factors. Submitted.

ACKNOWLEDGEMENTS

Research in the laboratory of M.R.P. is supported by grants from the Ministerio de Economía y Competitividad of Spain (BIO2008-01900) and the Generalitat Valenciana (PROMETEO/2009/112).

Ribosome biogenesis requires RRP7 and NOP53 in Arabidopsis

Rosa Micol-Ponce, Alejandro Ruiz-Bayón, Noemi Castroviejo-Jiménez and María Rosa Ponce

Instituto de Bioingeniería, Universidad Miguel Hernández, Campus de Elche, 03202 Elche, Alicante, Spain

We identified *mas2* (*morphology of argonaute1-52 suppressed 2*) alleles as informational suppressors of *ago1-52*, a hypomorphic allele of *AGO1*. The *MAS2* gene was positionally cloned and found to encode the Arabidopsis ortholog of NKAP (NF-kappa B activating protein), a conserved protein involved in transcriptional repression in animals. A yeast two hybrid assay with MAS2 as a bait identified 14 interactors, two of which are the putative orthologues of proteins known to participate in ribosome biogenesis in *Saccharomyces cerevisiae*: Ribosomal RNA Processing Protein 7 (RRP7) and Nucleolar Protein 53 (NOP53).

The Arabidopsis *rrp7-1* and *nop53-1* insertional mutants exhibit pointed and reticulated leaves, which are traits shared by many mutants defective in ribosome biogenesis. We obtained transgenic plants expressing the NOP53:GFP and RRP7:GFP translational fusions and found that both are nuclear proteins. We also obtained double mutant combinations of *nop53-1* or *rrp7-1* and loss-of-function alleles of genes required for ribosome biogenesis and the microRNA pathway; the phenotypes of most of these double mutants resulted to be synergistic.

2015

26th International Conference on Arabidopsis Research

París

Póster

Ribosome biogenesis requires RRP7 and NOP53 in Arabidopsis

Rosa Micol-Ponce, Alejandro Ruiz-Bayón, Noemi Castroviejo-Jiménez and María Rosa Ponce

Instituto de Bioingeniería, Universidad Miguel Hernández, Campus de Elche, 03202 Elche, Alicante, Spain.

rmicol@umh.es mrponce@umh.es http://genetica.umh.es

We identified *mas2* (*morphology of argonaute1-52 suppressed 2*) alleles[1] as informational suppressors of *ago1-52*[2], a hypomorphic allele of *AGO1*. The *MAS2* gene was positionally cloned and found to encode the Arabidopsis ortholog of NKAP (NF-kappa B activating protein), a conserved protein involved in transcriptional repression in animals[3]. A yeast two hybrid assay with MAS2 as a bait identified 14 interactors, two of which are the putative orthologues of proteins known to participate in ribosome biogenesis in *Saccharomyces cerevisiae*: Ribosomal RNA Processing Protein 7 (RRP7) and Nucleolar Protein 53 (NOP53).

The Arabidopsis *rrp7* and *nop53* insertional mutants exhibit pointed and reticulated leaves (Fig. 1), which are traits shared by many mutants defective in ribosome biogenesis[4]. We obtained transgenic plants expressing the $NOP53_{pro}$*:NOP53:GFP* and $RRP7_{pro}$*:RRP7:GFP* translational fusions and found that both seem to be nucleolar proteins (Fig. 3). Inmunofluorescence assays against fibrillarin, which is a nucleolar marker, allowed us to confirm that NOP53 and RRP7 colocalizes at the nucleolus (Fig. 4). We also obtained double mutant combinations of *nop53-1* or *rrp7-1* and loss-of-function alleles of genes required for ribosome biogenesis and the microRNA pathway (Fig. 5); the phenotypes of most of these double mutants resulted to be synergistic.

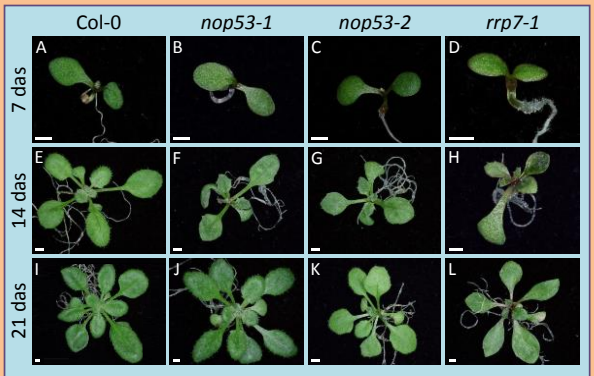

Figure 1.- Some phenotypic traits of the *nop53-1*, *nop53-2* and *rrp7-1* lines. Rosettes from (A, E, I) Col-0, (B, F, J) *nop53-1*, (C, G, K) *nop53-2* and (D, H, L) *rrp7-1* plants are shown. Pictures were taken (A-D) 7, (E-H) 14 and (I-L) 21 days after stratification (das). Scale bars: 1 mm.

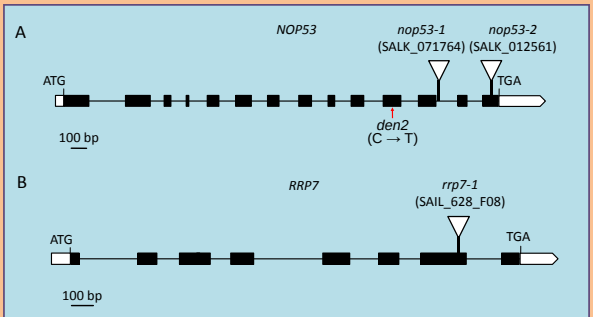

Figure 2.- Structure and mutant alleles of the *NOP53* and *RRP7* genes. Exons and introns are depicted as black boxes and lines, respectively. White boxes indicate 5´- and 3´-UTRs. The predicted translation start lines, (ATG) and stop (TGA) codons are indicated. Red arrows mark the positions of the point mutation in the *den2* allele.

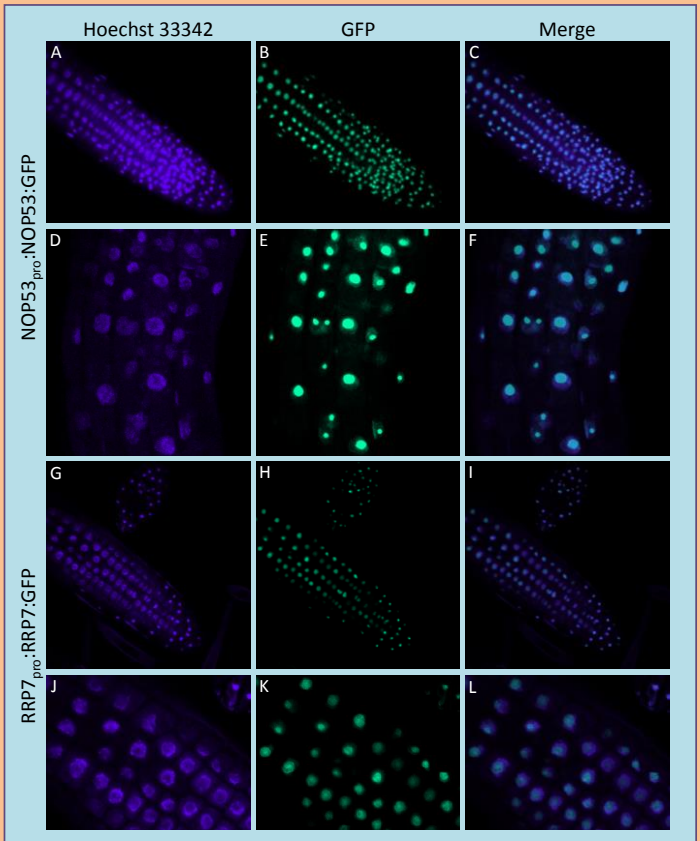

Figure 3.- Nuclear localization of NOP53 and RRP7. (A-L) Detection of the fluorescent emission of (A, D, G, J) Hoechst 33342, (B, E, H, K) GFP and (C, F, I, L) their overlay, in roots of transgenic plants expressing the (A-F) $NOP53_{pro}$*:NOP53:GFP* and (G-L) $RRP7_{pro}$*:RRP7:GFP* transgenes.

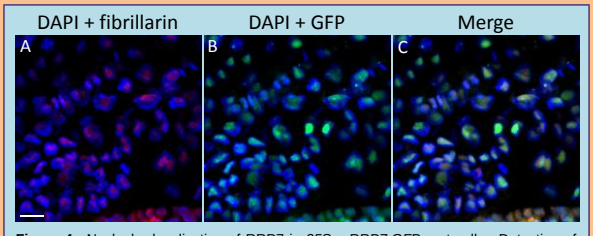

Figure 4.- Nucleolar localization of RRP7 in $35S_{pro}$*:RRP7:GFP* root cells. Detection of the fluorescent emission of (A) DAPI (4',6-diamidino-2-phenylindole) and the TRITC (Tetramethylrhodamineisothiocyanate) conjugated anti-mouse IgG secondary antibody used to detect fribrillarin, (B) DAPI and GFP, and (C) their overlay. Scale bar: 10 µm.

Figure 5.- Genetic interactions of *nop53-1* and *rrp7-1* with *ago1-52*. Rosettes from the (A) *nop53-1*, (B) *rrp7-1* and (C) *ago1-52* single mutants, and the (D) *nop53-1 ago1-52* and (E) *rrp7-1 ago1-52* double mutants. Pictures were taken (A, D) 21 and (B, C, E) 23 das. Scale bars: 1 mm.

REFERENCES

1.- Jover-Gil, S., Candela, H., Robles, P., Aguilera, V., Barrero, J.M., Micol, J.L., and Ponce, M.R. (2012). The microRNA pathway genes *AGO1*, *HEN1* and *HYL1* participate in leaf proximal-distal, venation and stomatal patterning in Arabidopsis. *Plant Cell Physiol.* **53**,1322-1333.

2.- Micol-Ponce, R., Aguilera, V., and Ponce, M.R. (2014). A genetic screen for suppressors of a hypomorphic allele of Arabidopsis *ARGONAUTE1*. *Scientific Reports* **4,** 5533.

3.- Sánchez-García, A.B., Aguilera, V., Micol-Ponce, R., Jover-Gil, S., and Ponce, M.R. (2015). Arabidopsis *MAS2*, an essential gene that encodes a homolog of animal NF-kappa B Activating Protein, is involved in 45S ribosomal DNA silencing. *Plant Cell*, in press.

4.-Van Lijsebettens, M., Vanderhaeghen, R., De Block, M., Bauw, G., Villarroel, R., and Van Montagu, M. (1994). An S18 ribosomal protein gene copy at the Arabidopsis PFL locus affects plant development by its specific expression in meristems. *EMBO J.* **13,** 3378-3388.

ACKNOWLEDGEMENTS

We would like to thank F.J. Medina for his help and advice on immunofluorescence assays, Research in the laboratory of M.R.P. is supported by grants from the Ministerio de Economía y Competitividad of Spain (BIO2008-01900 and BIO2014-56889-R) and the Generalitat Valenciana (PROMETEO/2009/112 and PROMETEOII/2014/006).

MAS2, the Arabidopsis ortholog of human NKAP, regulates 45S rDNA transcription

Ana Belén Sánchez-García, Rosa Micol-Ponce, Sara Jover-Gil and María Rosa Ponce

Instituto de Bioingeniería, Universidad Miguel Hernández, Campus de Elche, 03202 Elche, Alicante, Spain

We conducted a screen for suppressors of *Arabidopsis thaliana ago1-52*, a hypomorphic allele of *AGO1* (*ARGONAUTE1*), a key gene in microRNA pathways. We identified nine extragenic suppressors as alleles of *MORPHOLOGY OF AGO1-52 SUPPRESSED 2* (*MAS2*). Positional cloning showed that *MAS2* encodes the putative ortholog of NKAP (NF-kappa B activating protein), a conserved eukaryotic protein involved in transcriptional repression and splicing in animals. The *mas2* mutations behave as informational suppressors of *ago1* alleles that cause missplicing. *MAS2* is a single-copy gene whose insertional alleles are embryonic lethal. The artificial microRNA *amiR-MAS2* partially repressed *MAS2* and synergistically interacted with a loss-of-function allele of *AtNuc-L1*, which encodes NUCLEOLIN1, which affects epigenetic control of 45S rDNA expression. 45S rDNA promoters were hypomethylated in *amiR-MAS2* plants, indicating that MAS2 negatively regulates 45S rDNA expression. In yeast two-hybrid assays, MAS2 interacted with splicing and ribosome biogenesis proteins, and fluorescence *in situ* hybridization showed that MAS2 co-localized with 45S rDNA at the Nucleolar Organizer Regions. Our results thus reveal a key player in the regulation of rRNA synthesis in plants.

2015

26th International Conference on Arabidopsis Research

París

Póster

MAS2, the Arabidopsis ortholog of human NKAP, regulates 45S rDNA transcription

Ana Belén Sánchez-García, Rosa Micol-Ponce, Sara Jover-Gil, and María Rosa Ponce

Instituto de Bioingeniería, Universidad Miguel Hernández, Campus de Elche, 03202 Elche, Alicante, Spain.
mrponce@umh.es http://genetics.umh.es

Synthesis of rRNAs consumes most of the transcriptional activity of eukaryotic cells, but its regulation remains largely unclear in plants. We conducted a screen for EMS-induced suppressors of *ago1-52*[1,2], a hypomorphic allele of *AGO1* (*ARGONAUTE1*), a key gene in microRNA pathways (Fig. 1). We identified nine extragenic suppressors as alleles of *MAS2* (*MORPHOLOGY OF AGO1-52 SUPPRESSED2;* Fig. 2). *MAS2* encodes the putative ortholog of NKAP (NF-kappa B activating protein), which is involved in transcriptional repression and splicing in animals. The *mas2* point mutations behave as informational suppressors of *ago1* alleles that cause missplicing. *MAS2* is a single-copy gene whose insertional alleles are embryonic lethal (Fig. 3). In yeast two-hybrid assays, MAS2 interacted with splicing and ribosome biogenesis proteins, and fluorescence *in situ* hybridization showed that MAS2 co-localizes with the 45S rDNA at the NORs (Fig. 4). The artificial microRNA *amiR-MAS2.1* partially repressed *MAS2* (Fig. 5), synergistically interacted with *Atnuc-L1* mutations, and caused hypomethylation of 45S rDNA promoters as well as partial NOR decondensation (Fig. 6), indicating that MAS2 negatively regulates 45S rDNA expression. Our results thus reveal a key player in the regulation of rRNA synthesis in plants.

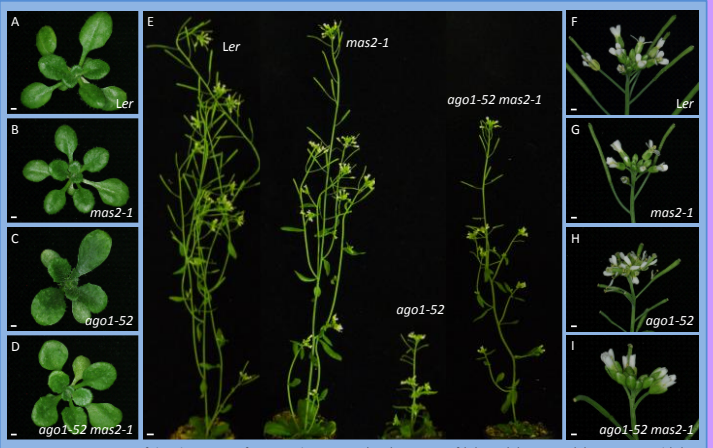

Figure 1.- Suppression of the phenotype of *ago1-52* by *mas2-1*. (A-D) Rosettes of (A) *Ler*, (B) *mas2-1*, (C) *ago1-52*, and (D) *ago1-52 mas2-1* plants. (E) adult plants of *Ler*, *mas2-1*, *ago1-52*, and *ago1-52 mas2-1*. (F-I) Inflorescences of (F) *Ler*, (G) *mas2-1*, (H) *ago1-52*, and (I) *ago1-52 mas2-1* plants. Pictures were taken at (A-D) 21 and (E) 48 days after stratification (das). Scale bars: (A-D and F-I) 1 mm, and (E) 1 cm.

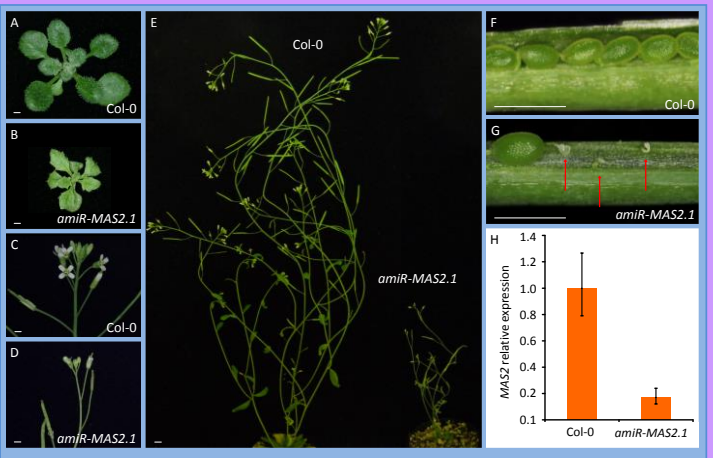

Figure 5.- Phenotypic effects of the *amiR-MAS2.1* transgene in the Col-0 background. (A, B) Rosettes of (A) Col-0 and (B) *amiR-MAS2.1* (in the Col-0 background) plants. (C, D) Inflorescences of (C) Col-0 and (D) *amiR-MAS2.1* plants. (E) Adult Col-0 and *amiR-MAS2.1* plants. (F, G) Dissected siliques from (F) Col-0 and (G) *amiR-MAS2.1* plants. Red arrows indicate unfertilized ovules and aborted seeds. (H) *MAS2* expression levels in Col-0 and *amiR-MAS2.1* plants. Pictures were taken at 21 (A, B) and 48 (C-G) das. Scale bars: (A-D, F, G) 1 mm and (E) 1 cm.

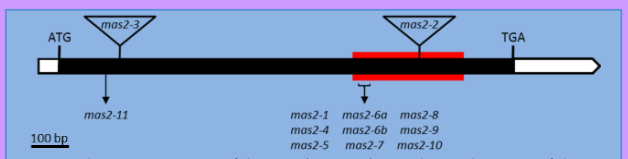

Figure 2.- Schematic representation of the *MAS2* (At4g02720) gene, showing the position of the *mas2* mutant alleles. Open and black boxes represent untranslated and coding regions, respectively. The region encoding the SynMuv domain, which is highly conserved in eukaryotes, is shown in red. Triangles indicate T-DNA insertions. Low resolution mapping was performed as previously described[2].

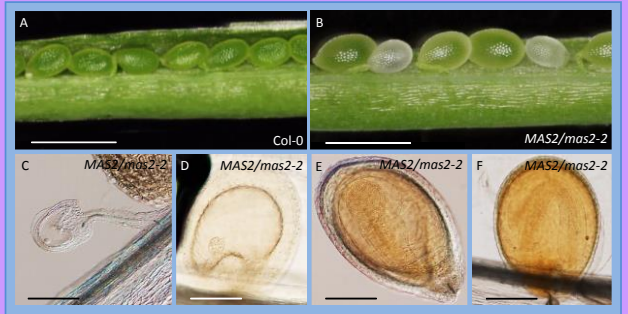

Figure 3.- (A, B) Seeds of dissected siliques from (A) Col-0 and (B) *MAS2/mas2-2* plants. (C) Aborted ovule in a *MAS2/mas2-2* plant. (D-F) Embryos from *MAS2/mas2-2* siliques: (D, E) Abnormal embryos arrested in the (D) globular and (E) globular-heart stages; (F) Phenotypically wild type mature embryo. Scale bars: (A, B) 1 mm and (C-F) 200 µm.

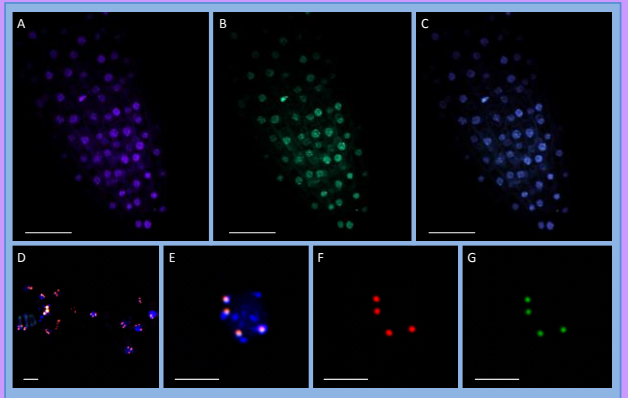

Figure 4.- Subcellular localization of the MAS2 protein. (A-C) Detection of the fluorescent emission of (A) DAPI (4',6-diamidino-2-phenylindole), (B) GFP and (C) their overlay in roots of transgenic plants expressing a *2x35S$_{pro}$:MAS2:GFP* transgene. (D-G) Fluorescent *in situ* hibridization (FISH): (D, E) Overlay of DAPI, MAS2:GFP and a 45S rDNA probe (pTa71), (D) several nuclei and (E) magnification of a mitotic prophase nucleus. (F-G) Fluorescent emission of (F) pTa71 probe and (G) MAS2-GFP. Scale bars: (A-C, E-G) 50 µm, and (D) 25 µm.

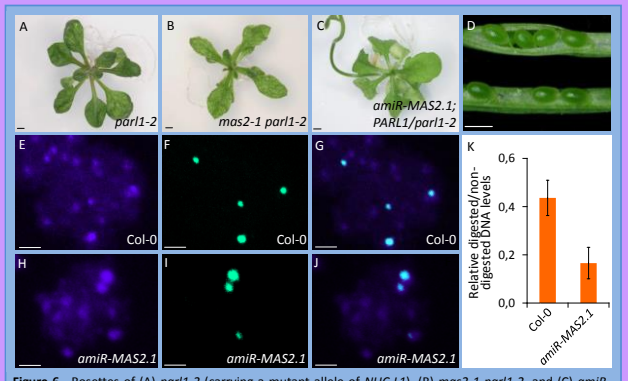

Figure 6.- Rosettes of (A) *parl1-2* (carrying a mutant allele of *NUC-L1*), (B) *mas2-1 parl1-2*, and (C) *amiR-MAS2;PARL1/parl1-2*. (D) Dissected siliques of *amiR-MAS2.1;PARL1/parl1-2* plants. No *amiR-MAS2.1;parl1-2/parl1-2* plants were identified after genotyping 84 plants of different F_2 and F_3 families. (E-J) FISH assay: Representative mitotic prophase nuclei from (E-G) Col-0, and (H-J) *amiR-MAS2.1* cells. Fluorescent emissions are: (E, H) DAPI, (F, I) hybridized 45S rDNA probe, and (G, J) their overlay. (K) Quantification of DNA methylation levels of the 45S rDNA gene promoter in Col-0 and *amiR-MAS2.1* plants. The DNA methylation status was analyzed by qPCR, using genomic DNA that was digested or not with the *Hpa*II endonuclease, which digests only non-methylated CCGG sequences. Bars represent the ratio between digested and undigested amplification levels. Scale bars: (A-C) 1 mm, (D) 0.5 mm and (E-J) 2.5 µm.

REFERENCES

1.- Jover-Gil, S., Candela, H., Robles, P., Aguilera, V., Barrero, J.M., Micol, J.L., and Ponce, M.R. (2012). The microRNA pathway genes *AGO1*, *HEN1* and *HYL1* participate in leaf proximal-distal, venation and stomatal patterning in Arabidopsis. *Plant Cell Physiol.* **53**,1322-1333.

2.- Micol-Ponce, R., Aguilera, V., and Ponce, M.R. (2014). A genetic screen for suppressors of a hypomorphic allele of Arabidopsis *ARGONAUTE1*. *Scientific Reports* **4**, 5533.

3.- Jover-Gil, S., Paz-Ares, J., Micol, J.L., and Ponce, M.R. (2014). Multi-gene silencing in Arabidopsis: a collection of artificial microRNAs targeting groups of paralogs encoding transcription factors. *Plant J.* **80**, 149-160.

ACKNOWLEDGEMENTS

Research in the laboratory of M.R.P. is supported by grants from the Ministerio de Economía y Competitividad of Spain (BIO2008-01900 and BIO2014-56889-R) and the Generalitat Valenciana (PROMETEO/2009/112 and PROMETEOII/2014/006).

RRP7 y NOP53 participan en la biogénesis del ribosoma en *Arabidopsis*

Rosa Micol-Ponce, Alejandro Ruiz-Bayón, Samuel Lup, Maria Rosa Ponce

Instituto de Bioingeniería, Universidad Miguel Hernández, Campus de Elche, 03202 Elche, Alicante

La proteína AGO1 (ARGONAUTE1) es un elemento central de la ruta de los microARN en *Arabidopsis*. Hemos mutagenizado el mutante *ago1-52*, portador de un alelo hipomorfo del gen *AGO1*, encontrando 22 supresores de su fenotipo, a los que hemos denominado *mas* (*morphology of argonaute1-52 suppressed*). Nueve de estos supresores extragénicos son alelos del gen *MAS2*, cuya clonación posicional ha revelado que codifica el ortólogo de la NKAP (NF-kappa B activating protein) humana, una proteína multifuncional muy conservada entre los eucariotas, que en los animales participa en la represión de la transcripción y en otros procesos. Hemos utilizado MAS2 como cebo en escrutinios de doble hibrido de levadura, identificando 14 presas; dos de estos presuntos interactores de MAS2 son ortólogos de proteínas necesarias para la biogénesis del ribosoma en *Saccharomyces cerevisiae*: Ribosomal RNA Processing Protein 7 (RRP7) y Nucleolar Protein 53 (NOP53).

Hemos identificado dos mutantes insercionales de *Arabidopsis rrp7* y *nop53*, cuyas hojas son reticuladas, indentadas y apuntadas, rasgos típicos de la insuficiencia de función de las proteínas ribosómicas. Hemos obtenido plantas transgénicas en las que se expresan las proteínas de fusión RRP7:GFP y NOP53:GFP, que han resultado ser nucleolares. Hemos obtenido combinaciones dobles mutantes de *rrp7-1* o *nop53-1* y alelos de insuficiencia de función de genes implicados en la biogénesis del ribosoma o en la maquinaria de los microARN. Hemos encontrado fenotipos sinérgicos en muchos de estos dobles mutantes, que sugieren que las funciones de los genes mutados están relacionadas. Nuestros resultados indican que la biogénesis del ribosoma y la ruta de los microARN están relacionadas en *Arabidopsis.*

2015

XL Congreso de la Sociedad Española de Genética

Córdoba

Póster

RRP7 y NOP53 participan en la biogénesis del ribosoma en Arabidopsis

Rosa Micol-Ponce, Alejandro Ruiz-Bayón, Samuel Lup y María Rosa Ponce

Instituto de Bioingeniería, Universidad Miguel Hernández, Campus de Elche, 03202 Elche, Alicante.

rmicol@umh.es mrponce@umh.es http://genetica.umh.es

La proteína AGO1 (ARGONAUTE1) es un elemento central de la ruta de los microARN en *Arabidopsis*. Hemos mutagenizado el mutante *ago1-52*, portador de un alelo hipomorfo del gen *AGO1*, encontrando 22 supresores de su fenotipo, a los que hemos denominado *mas* (*morphology of argonaute1-52 suppressed*)[1]. Nueve de estos supresores extragénicos son alelos del gen *MAS2*[2], cuya clonación posicional ha revelado que codifica el ortólogo de la NKAP (NF-kappa B activating protein) humana, una proteína multifuncional muy conservada entre los eucariotas, que en los animales participa en la represión de la transcripción y en otros procesos[3]. Hemos utilizado MAS2 como cebo en escrutinios de doble hibrido de levadura, identificando 14 presas; dos de estos presuntos interactores de MAS2 son ortólogos de proteínas necesarias para la biogénesis del ribosoma en *Saccharomyces cerevisiae*: Ribosomal RNA Processing Protein 7 (RRP7) y Nucleolar Protein 53 (NOP53).

Hemos identificado dos mutantes insercionales de Arabidopsis, *rrp7* y *nop53*, cuyas hojas son reticuladas, indentadas y apuntadas (Figuras 1 y 2), rasgos típicos de la insuficiencia de función de las proteínas ribosómicas[4]. Hemos obtenido plantas transgénicas en las que se expresan las proteínas de fusión RRP7:GFP y NOP53:GFP, que han resultado ser nucleolares (Figuras 3 y 4). Hemos obtenido combinaciones dobles mutantes de *rrp7-1* o *nop53-1* y alelos de insuficiencia de función de genes implicados en la biogénesis del ribosoma o en la ruta de los microARN (Figura 5). Hemos encontrado fenotipos sinérgicos en muchos de estos dobles mutantes, que sugieren que las funciones de los genes mutados están relacionadas.

rrp7-1, *nop53-1* y los mutantes de la ruta de los microARN que hemos estudiado son hipersensibles a la zeocina y la anisomicina, dos compuestos que causan estrés nucleolar (Figura 6); la zeocina inhibe la traducción y la anisomicina provoca rupturas en la doble cadena de ADN. Nuestros resultados indican que la biogénesis del ribosoma y la ruta de los microARN están relacionadas en Arabidopsis.

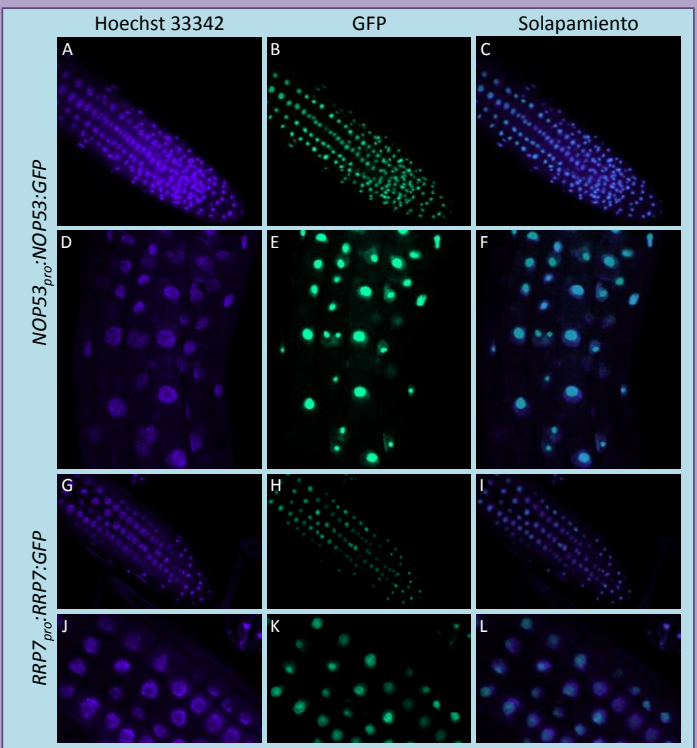

Figura 3.- Localización nuclear de las proteínas NOP53 y RRP7. Se muestra la emisión fluorescente (A, D, G, J) del agente de tinción Hoechst 33342, (B, E, H, K) de la GFP y (C, F, I, L) su solapamiento, en raíces de plantas en las que se expresan los transgenes (A-F) $NOP53_{pro}$:*NOP53:GFP* y (G-L) $RRP7_{pro}$:*RRP7:GFP*.

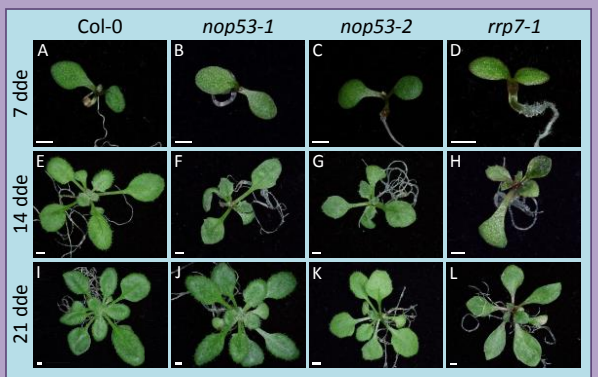

Figura 1.- Fenotipo vegetativo de los mutantes *nop53-1*, *nop53-2* y *rrp7-1*. Se muestran rosetas (A, E, I) del tipo silvestre Col-0 y de los mutantes (B, F, J) *nop53-1*, (C, G, K) *nop53-2* y (D, H, L) *rrp7-1*. Las imágenes fueron tomadas (A-D) 7, (E-H) 14 y (I-L) 21 días después de la estratificación (dde). Las barras de escala indican 1 mm.

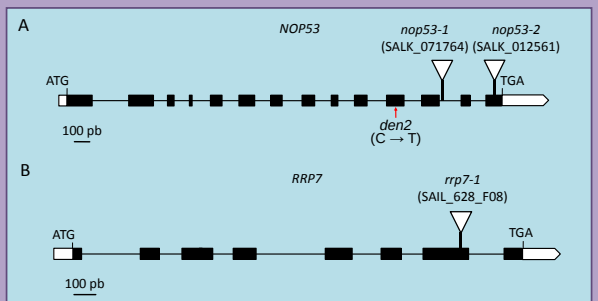

Figura 2.- Estructura de los genes *NOP53* y *RRP7* y de sus alelos mutantes. Las líneas representan a los intrones, y los rectángulos, a los exones (se destacan en blanco sus segmentos no traducidos). Los triángulos indican inserciones de AND-T. La flecha roja indica la posición de la mutación puntual del alelo *denticulata2* (*den2*), que se indujo mediante tratamiento con metanosulfonato de etilo.

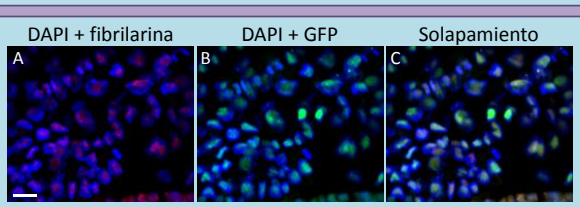

Figura 4.- Localización nucleolar de la proteína RRP7 en células de la raíz de plantas $35S_{pro}$:*RRP7:GFP*. Se muestra la emisión fluorescente (A) del DAPI (4',6-diamidino-2-fenilindol) y el TRITC (isotiocianato de tetrametilrodamina) conjugado con un anticuerpo secundario a fin de detectar la fibrilarina (una proteína nucleolar), (B) del DAPI y la GFP, y (C) su solapamiento. Las barras de escala indican 10 µm.

Figura 5.- Interacciones genéticas de *nop53-1* y *rrp7-1* con *ago1-52*. Se muestran rosetas de los mutantes simples (A) *nop53-1*, (B) *rrp7-1* y (C) *ago1-52*, y de los dobles mutantes (D) *nop53-1 ago1-52* y (E) *rrp7-1 ago1-52*. Las imágenes se tomaron (A, D) 21 y (B, C, E) 23 dde. Las barras de escala indican 1 mm.

Figura 6.- Efectos de la anisomicina (5 µM) y la zeocina (10 µM) sobre el desarrollo radicular de los mutantes *rrp7-1*, *nop53-1* y *ago1-25*. Se destacan con asteriscos los valores que resultaron significativamente distintos del silvestre tras aplicar el estadístico *t* de Student ($P < 0,01$; n = 15).

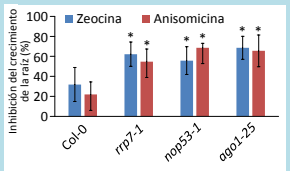

REFERENCIAS

1.- Jover-Gil, S., Candela, H., Robles, P., Aguilera, V., Barrero, J.M., Micol, J.L., y Ponce, M.R. (2012). The microRNA pathway genes *AGO1*, *HEN1* and *HYL1* participate in leaf proximal-distal, venation and stomatal patterning in Arabidopsis. *Plant Cell Physiol.* **53**, 1322-1333.

2.- Micol-Ponce, R., Aguilera, V., y Ponce, M.R. (2014). A genetic screen for suppressors of a hypomorphic allele of Arabidopsis *ARGONAUTE1*. *Sci. Rep.* **4,** 5533.

3.- Sánchez-García, A.B., Aguilera, V., Micol-Ponce, R., Jover-Gil, S., y Ponce, M.R. (2015). Arabidopsis *MAS2*, an essential gene that encodes a homolog of animal NF-kappa B Activating Protein, is involved in 45S ribosomal DNA silencing. *Plant Cell* **27,** 1999-2015.

4.- Van Lijsebettens, M., Vanderhaeghen, R., De Block, M., Bauw, G., Villarroel, R., y Van Montagu, M. (1994). An S18 ribosomal protein gene copy at the Arabidopsis *PFL* locus affects plant development by its specific expression in meristems. *EMBO J.* **13,** 3378-3388.

AGRADECIMIENTOS

Agradecemos a F.J. Medina su ayuda en los ensayos de inmunofluorescencia. La investigación en el laboratorio de M.R.P. ha sido financiada por el Ministerio de Economía y Competitividad (BIO2008-01900 y BIO2014-56889-R) y la Generalitat Valenciana (PROMETEOII/2014/006).

Arabidopsis MAS2 interactors identified in a yeast two-hybrid screen

Alejandro Ruiz Bayón, Raquel Sarmiento Mañús, Rosa Micol-Ponce, María Rosa Ponce

Instituto de Bioingeniería, Universidad Miguel Hernández, Campus de Elche, 03202 Elche, Spain

Arabidopsis *MAS2* is an essential gene that encodes a homolog of animal NF-kappa B Activating Protein and seems to be a key player in the regulation of rRNA synthesis in plants[1]. Fluorescence *in situ* hybridization showed that MAS2 colocalizes with the 45S rDNA in the nucleolar organizer regions. To better understand the function of MAS2, we screened for interactors in a yeast two-hybrid (Y2H) assay. Two Arabidopsis cDNA libraries obtained from whole Arabidopsis plants, totalling 21 million prey clones, were used in the screening. The bait contained the full-length coding region of *MAS2*. The screen identified 91 prey clones, representing 14 different genes, and these clones were confirmed by directed Y2H assays.

The most represented interactor in the Y2H-based screen, in 23 of the 55 clones, was CAX INTERACTING PROTEIN4 (CXIP4), a protein of unknown function that was previously identified as interacting with the high-affinity vacuolar calcium antiporter CAX1 and found in the nucleus and cytoplasm[2]. CXIP4 occurs exclusively in plants and 30 amino acids of its N-terminal region show 70% similarity to the mammalian splicing factor SREK1-interacting protein 1. Three MAS2 interactors were related to ribosome biogenesis, including RPS24B, the second most represented interactor, which is one of the two Arabidopsis S24-type proteins in the 40S ribosomal subunit.

CXIP4 is encoded by AT2G28910, a plant-specific, single-copy gene. The CXIP4 N-terminal region contains a conserved CysX2CysX4HisX4Cys (CCHC)-type zinc finger domain, termed a zinc knuckle. Selfing of plants heterozygous for the *cxip4-1* insertional allele did not produce homozygous mutant progeny, the only exception being a few extremely dwarf, morphologically aberrant escapers, whose growth arrested several days after germination. We constructed two artificial microRNAs designed to target *CXIP4*, to circumvent the lethality associated with the lack of *CXIP4* function. Additional transgenes were obtained to complement the mutant phenotype of homozygous *cxip4-1* plants, and to visualize the spatial pattern of expression of *CXIP4* and the subcellular localization of the CXIP4 protein. We are also studying the genetic interactions of *CXIP4* and *RPS24B*, with a

particular focus on *MAS2* viable alleles and alleles of genes encoding components of the microRNA pathway.

1. Sánchez-García, A.B., Aguilera, V., Micol-Ponce, R., Jover-Gil, S., and Ponce, M.R. (2015). *Plant Cell* 27, 1999-2015.
2. Cheng, N.H., Liu, J.Z., Nelson, R.S., and Hirschi, K.D. (2004). *FEBS Letters* 559, 99-106.

2016

XIII Reunión de Biología Molecular de Plantas

Oviedo

Póster

Arabidopsis MAS2 interactors identified in a yeast two-hybrid screen

Alejandro Ruiz-Bayón, Raquel Sarmiento-Mañús, Rosa Micol-Ponce and María Rosa Ponce

Instituto de Bioingeniería, Universidad Miguel Hernández, Campus de Elche, 03202 Elche, Alicante, Spain.

alejandro.ruizb@umh.es mrponce@umh.es http://genetica.umh.es

Arabidopsis *MAS2* is an essential gene that encodes a homolog of animal NF-kappa B Activating Protein and seems to be a key player in the regulation of rRNA synthesis in plants[1]. Fluorescence *in situ* hybridization showed that MAS2 colocalizes with the 45S rDNA in the nucleolar organizer regions. To better understand the function of MAS2, we screened for interactors in a yeast two-hybrid (Y2H) assay. Two Arabidopsis cDNA libraries obtained from whole Arabidopsis plants, totalling 21 million prey clones, were used in the screening. The bait contained the full-length coding region of *MAS2*. The screen identified 91 prey clones, representing 14 different genes, and these clones were confirmed by directed Y2H assays.

The most represented interactor in the Y2H-based screen, in 23 of the 55 positive clones, was CAX INTERACTING PROTEIN4 (CXIP4), a protein of unknown function that was previously identified as interacting with the high-affinity vacuolar calcium antiporter CAX1 and found in the nucleus and cytoplasm[2]. CXIP4 occurs exclusively in plants (Figure 1) and 30 amino acids of its N-terminal region show 70% similarity to the mammalian splicing factor SREK1-interacting protein 1. Three MAS2 interactors were related to ribosome biogenesis, including RPS24B, the second most represented interactor (14 clones), which is one of the two Arabidopsis S24-type proteins in the 40S ribosomal subunit.

CXIP4 is encoded by AT2G28910, a plant-specific[3], single-copy gene (Figure 2). The CXIP4 N-terminal region contains a conserved CysX2CysX4HisX4Cys (CCHC)-type zinc finger domain, termed a zinc knuckle. Selfing of plants heterozygous for the *cxip4-1* insertional allele did not produce homozygous mutant progeny, the only exception being a few extremely dwarf, morphologically aberrant escapers, whose growth arrested several days after germination (Figure 3). We constructed two artificial microRNAs[4] designed to target *CXIP4*, to circumvent the lethality associated with the lack of *CXIP4* function (Figure 4). Additional transgenes were obtained to complement the mutant phenotype of homozygous *cxip4-1* plants, and to visualize the spatial pattern of expression of *CXIP4* and the subcellular localization of the CXIP4 protein. We are also studying the genetic interactions of *CXIP4* and *RPS24B*, with a particular focus on *MAS2* viable alleles and alleles of genes encoding components of the microRNA pathway.

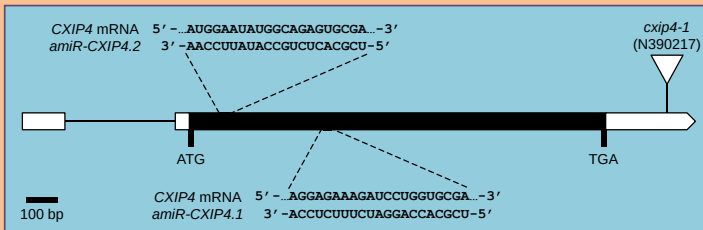

Figure 2.- Structure of the *CXIP4* gene. Introns and exons are represented as black lines and boxes, respectively. Untranslated and coding regions are shown in white and black, respectively. The triangle indicates the T-DNA insertion carried by the *cxip4-1* lethal allele. amiRNA sequences and the sequences and positions of their mRNA targets are shown. The translation start (ATG) and stop (TGA) codons are also shown.

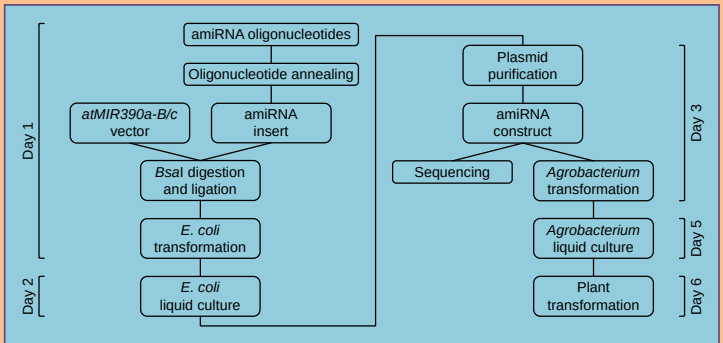

Figure 4.- Workflow for amiRNA construction and cloning. Boxes represent steps of the process. Time planning is shown at both sides. Taken from Carbonell *et al.* (2014) with small modifications.

ACKNOWLEDGEMENTS

Research in the laboratory of M.R.P. is supported by grants from the Ministerio de Economía y Competitividad of Spain (BIO2014-56889-R) and the Generalitat Valenciana (PROMETEOII/2014/006).

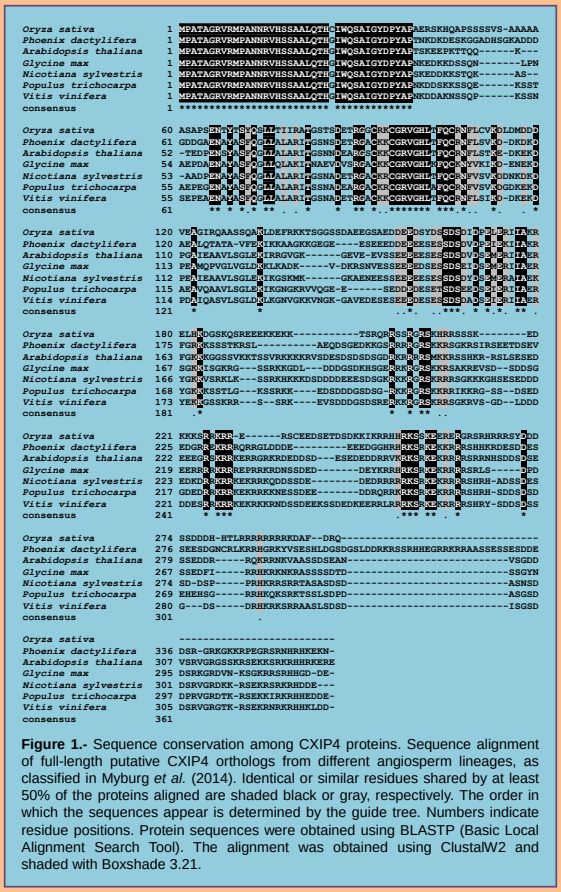

Figure 1.- Sequence conservation among CXIP4 proteins. Sequence alignment of full-length putative CXIP4 orthologs from different angiosperm lineages, as classified in Myburg *et al.* (2014). Identical or similar residues shared by at least 50% of the proteins aligned are shaded black or gray, respectively. The order in which the sequences appear is determined by the guide tree. Numbers indicate residue positions. Protein sequences were obtained using BLASTP (Basic Local Alignment Search Tool). The alignment was obtained using ClustalW2 and shaded with Boxshade 3.21.

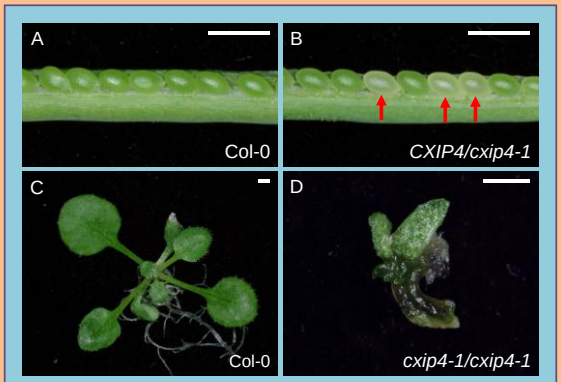

Figure 3.- Phenotypic effects of *CXIP4* loss of function. (A, B) Dissected immature siliques from (A) Col-0 and (B) *CXIP4/cxip4-1* plants. Red arrows indicate aborted seeds. (C, D) Two-week old rosettes from (C) Col-0 and (D) a *cxip4-1/cxip4-1* escaper. Scale bars indicate 1 mm.

REFERENCES

1.- Sánchez-García, A.B., Aguilera, V., Micol-Ponce, R., Jover-Gil, S., and Ponce, M.R. (2015). *Plant Cell* **27**, 1999-2015.

2.- Cheng, N.H., Liu, J.Z., Nelson, R.S., and Hirschi, K.D. (2004). *FEBS Letters* **559**, 99-106.

3.- Myburg *et al.* (2014). *Nature* **510**, 356-362.

4.- Carbonell, A., Takeda, A., Fahlgren, N., Johnson, S.C., Cuperus, J.T., y Carrington, J.C. (2014). *Plant Physiology* **165**, 15-29.

The microRNA pathway regulates cuticle formation

Raquel Sarmiento Mañús, Sara Jover-Gil, Rosa Micol-Ponce, María Rosa Ponce

Instituto de Bioingeniería, Universidad Miguel Hernández, Campus de Elche, 03202 Elche, Spain

Genes encoding components of RNA metabolism often cause pleiotropic phenotypes when mutated, probably because their products have many targets. Pleiotropy is also exhibited by mutants affected in components of gene silencing pathways mediated by small RNAs[1]. For example, mutations in genes encoding components of the microRNA (miRNA)-silencing pathway often show drought resistance and hypersensitivity to abscisic acid (ABA); the processes underlying these mutant traits are unknown. Indeed, we found increased tolerance to water deprivation, as well as hypersensitivity to salt and ABA, in seven mutants carrying loss-of-function alleles of genes that encode components of the miRNA machinery, six of which had been isolated in our laboratory[2]: *dcl1-9* (*dicer-like1-9*), *hyl1-11* (*hyponastic leaves1-11*), *hyl1-12*, *hen1-13* (*hua enhancer1-13*), *hst-21* (*hasty-21*), *ago1-51* (*argonaute1-51*) and *ago1-52*. DCL1 and HYL1 participate in miRNA biogenesis, HEN1 in miRNA stabilization, and HST in miRNA nuclear export. AGO1 is the core component of the miRNA-induced silencing complex.

The aerial surfaces of land plants are covered by the cuticle, a hydrophobic layer composed of cutin and cuticular waxes, which acts as a protective barrier. We hypothesized that the mutants mentioned above have a less-permeable cuticle than that of wild-type plants, conferring drought resistance and hypersensitivity to salt and ABA. Indeed, we found that the *dcl1*, *hyl1*, *hen1*, *hst*, and *ago1* mutants studied exhibit reduced water loss and cuticle permeability, which might be caused by the increased epicuticular wax deposition that we also observed. At least one mutant, *hst-21,* has a thicker cuticle than that of the wild type.

WAX INDUCER1 (*WIN1*), also named *SHINE1* (*SHN1*), encodes an ethylene-responsive transcription factor whose overexpression triggers the induction of several genes of the wax biosynthesis pathway*,* leading to an increase of epidermal cutin and wax accumulation[3]. Plants over-expressing *SHN1* are drought-tolerant. We found the transcription factor *SHN1* upregulated in all the mutants studied, except *ago1-51* and *ago1-52*. Mis-regulation of *SHN1* could explain the decrease in permeability and water loss shown

by the mutants. These results suggest that the microRNA pathway is involved in the regulation of waxes and cutin production mediated by *SHN1*.

1. Jover-Gil, S., Candela, H., and Ponce, M.R. (2005). *International Journal of Developmental Biology* 49, 733-744.
2. Jover-Gil, S., Candela, H., Robles, P., Aguilera, V., Barrero, J.M., Micol, J.L., and Ponce, M.R. (2012). *Plant and Cell Physiology* 53, 1322-1333.
3. Aharoni, A., Dixit, S., Jetter R, Thoenes, E., van Arkel, G., and Pereira, A. (2004). *Plant Cell* 16, 2463-2480

2016
XIII Reunión de Biología Molecular de Plantas
Oviedo
Póster

The microRNA pathway regulates cuticle formation

Raquel Sarmiento-Mañús, Sara Jover-Gil, Rosa Micol-Ponce and María Rosa Ponce

Instituto de Bioingeniería, Universidad Miguel Hernández, Campus de Elche, 03202 Elche, Alicante, Spain.

rsarmiento@umh.es mrponce@umh.es http://genetica.umh.es

Genes encoding components of RNA metabolism patways often cause pleiotropic phenotypes when mutated, probably because their products have many targets. Pleiotropy is also exhibited by mutants affected in components of gene silencing pathways mediated by small RNAs[1]. For example, mutations in genes encoding components of the microRNA (miRNA)-silencing pathway often show drought resistance and hypersensitivity to abscisic acid (ABA); the processes underlying these mutant traits are unknown. Indeed, we found increased tolerance to water deprivation (Fig. 1), as well as hypersensitivity to salt and ABA in seven mutants carrying loss-of-function alleles of genes that encode components of the miRNA machinery, six of which had been isolated in our laboratory[2]: *dcl1-9* (*dicer-like1-9*), *hyl1-11* (*hyponastic leaves1-11*),*hyl1-12*, *hen1-13* (*hua enhancer1-13*), *hst-21* (*hasty-21*), *ago1-51* (*argonaute1-51*) and *ago1-52*. DCL1 and HYL1 participate in miRNA biogenesis, HEN1 in miRNA stabilization, and HST in miRNA nuclear export. AGO1 is the core component of the miRNA-induced silencing complex.

The aerial surfaces of land plants are covered by the cuticle, a hydrophobic layer composed of cutin and cuticular waxes, which acts as a protective barrier. We hypothesized that the mutants mentioned above have a less-permeable cuticle than that of wild-type plants, conferring drought resistance and hypersensitivity to salt and ABA. Indeed, we found that the *dcl1*, *hyl1*, *hen1*, *hst*, and *ago1* mutants studied exhibit reduced water loss and cuticle permeability (Fig. 2), which might be caused by the increased epicuticular wax deposition that we also observed (Fig. 3). At least one mutant, *hst-21,* has a cuticle thicker than that of the wild type (Fig. 4).

The *SHN* genes constitute a clade inside the AP2/EREBP plant transcription factor family whose overexpression results in aberrant plant surfaces[3]. Overexpression of the *SHN*, confer drought tolerance and activate wax biosynthesis, although cuticle permeability is increased[3]. We found the *SHN3* gene upregulated in all the mutants studied, exceptions being *ago1-51* and *ago1-52*, and *SHN1* is only overexpressed in *hyl1* mutants (Fig. 5). Overexpression of *SHN1* and *SHN3* may explain the tolerance to water deficiency exhibited by the mutants studied. These results suggest that the microRNA pathway is involved in the regulation of waxes and cutin production mediated by *SHN* genes.

ACKNOWLEDGEMENTS

Research in the laboratory of M.R.P. is supported by grants from the Ministerio de Economía y Competitividad of Spain (BIO2014-56889-R) and the Generalitat Valenciana (PROMETEOII/2014/006).

REFERENCES

1.- Jover-Gil, S., Candela, H., and Ponce, M.R. (2005). *International Journal of Developmental Biology* **49**, 733-744.

2.- Jover-Gil, S., Candela, H., Robles, P., Aguilera, V., Barrero, J.M., Micol, J.L., and Ponce, M.R. (2012). *Plant and Cell Physiology* **53**, 1322-1333.

3.- Aharoni, A., Dixit, S., Jetter R, Thoenes, E., van Arkel, G., and Pereira, A. (2004). *Plant Cell* **16**, 2463-2480.

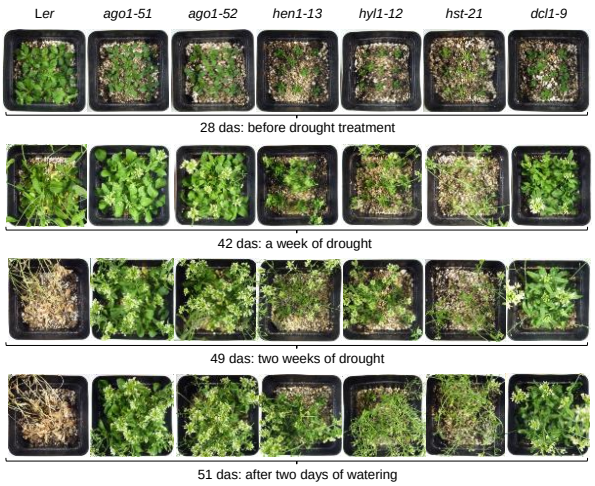

Figure 1.- Drought tolerance in the *ago1-51*, *ago1-52*, *hen1-13*, *hyl1-12*, *hst-21* and *dcl1-9* mutants. After a week of drought the wild-type L*er* and the mutants are still green, but after two weeks of drought only the mutants keep being green. L*er* is unable to recover from the drought effects even after rehydration. das: days after stratification.

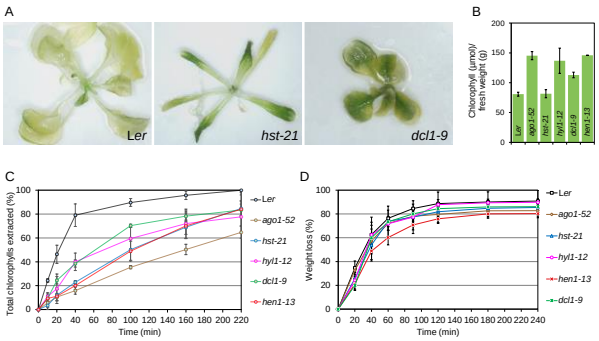

Figure 2.- Reduced cuticle permeability in *hst-21*, *hen1-13*, *dcl1-9*, *hyl1-11*, *hyl1-12*, *ago1-51* and *ago1-52* mutants. (A) Rosettes after a 24-h immersion in 80% ethanol. (B) Total chlorophyll content. (C) Chlorophyll extraction rate expressed as percentage of total chlorophyll extracted after 24 h. (D) Percentage of weight loss. The data represent means ± standard deviation of three replicates. All experiments were performed on plants collected 28 das.

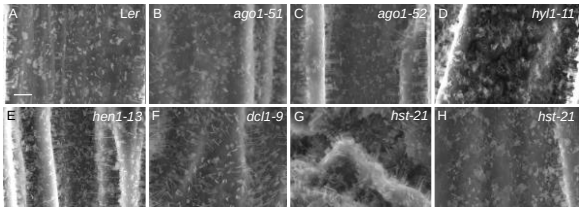

Figure 3.- Scanning electron micrographs of L*er*, *ago1-51*, *ago1-52*, *hyl1-11*, *hen1-13*, *hst-21* and *dcl1-9* stems. Increased presence of wax crystals is shown in (G, H) *hst-21*, (D) *hyl1-11*, (E) *hen1-13* and (F) *dcl1-9* mutant stems. Scale bar: 5 µm.

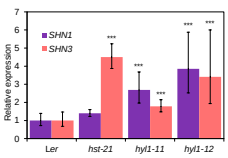

Figure 5.- RT-qPCR of *SHN1* and *SHN3* expression in the *hst-21*, *hyl1-11* and *hyl1-12* mutants and the L*er* wild type. Plants were collected at the same developmental stage, after bolting: 28 (L*er*), 25 (*hst-21*), and 29 (*hyl1-11* and *hyl1-12*) das. Expression data were obtained from three different biological replicates. Asterisks indicate values significantly different from L*er* in a Mann-Whitney *U* test (***) $p < 0.001$.

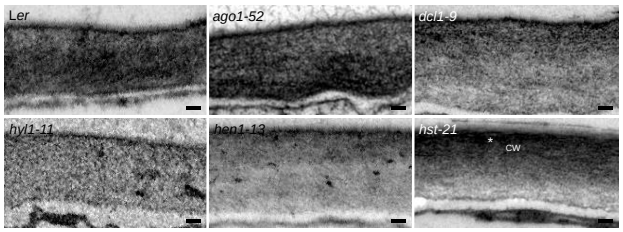

Figure 4.- Transmission electron micrographs of the adaxial cuticle of L*er*, *ago1-52*, *hyl1-11*, *hen1-13*, *hst-21* and *dcl1-9* leaves. The cuticle of *hst-21* is thicker than that of L*er*. The asterisk indicates the cuticular layer. CW: cell wall. Scale bars:100 nm.

Transcriptional regulation of the Arabidopsis *ARGONAUTE1* gene

Adrián Cabezas-Fuster, Rosa Micol-Ponce, Raquel Sarmiento-Mañús, María Rosa Ponce

Instituto de Bioingeniería, Universidad Miguel Hernández, Campus de Elche, 03202 Elche, Spain

The Arabidopsis ARGONAUTE1 (AGO1) ribonuclease is the main effector of posttranscriptional gene silencing pathways that are mediated by small interfering RNAs, including microRNAs (miRNAs)[1]. Also, a miRNA targets *AGO1* transcripts. Hypomorphic *ago1* alleles disrupt many developmental pathways and responses to biotic and abiotic stress factors; null *ago1* alleles are lethal. Expression of *AGO1* is widespread and virtually constitutive under normal conditions; also *AGO1* expression increases under certain environmental conditions, such as viral infection. We have a wealth of information on the mechanisms by which *AGO1* post-transcriptionally regulates expression of other genes, but we lack information on the transcriptional regulation of *AGO1* itself.

To analyse the transcriptional regulation of *AGO1*, we generated an $AGO1_{pro}$*:GUS* transcriptional fusion, which carries a putative full-length *AGO1* promoter. Plants homozygous for the $AGO1_{pro}$*:GUS* transgene were grown on media with different concentrations of NaCl, abscisic acid (ABA), or sucrose, or exposed to different light intensities and dark periods. ABA treatments and dark exposure significantly altered GUS activity, but sucrose and NaCl did not affect GUS activity.

Among other subcellular locations, Arabidopsis AGO1 occurs in the endoplasmic reticulum, where it represses translation of target mRNAs[2]. An *in silico* analysis of the promoter of *AGO1* allowed us to identify two regulatory elements associated with the unfolded protein response (UPR) in the endoplasmic reticulum, which we also found in the promoters of the *AGO1* orthologs of rice and *Brassica rapa*; these sequences seem to be relevant for the regulation of *AGO1* expression.

To identify the key regulatory *AGO1* promoter sequences, we constructed four transcriptional *GUS* fusions driven by different segments of the *AGO1* promoter, lacking one or both UPR elements. We are examining these fragments by mobility shift assays with nuclear protein extracts. In addition, we are analysing the effects of each mutant promoter variant on the expression of the *GUS* reporter gene in plants grown in the different culture conditions mentioned above, and in the presence of tunicamycin or dithiothreitol, which induce UPR.

1. Kidner, C.A., and Martienssen, R.A. (2005). *Current Opinion in Plant Biology* 8, 38-44.
2. Li, S., Liu, L., Zhuang ,X., Yu, Y., Liu, X., Cui, X., Ji, L., Pan, Z., Cao, X., Mo, B., Zhang, F., Raikhel, N., Jiang, L., and Chen, X. (2013). *Cell* 153, 562-574.

2016

XIII Reunión de Biología Molecular de Plantas

Oviedo

Póster

Transcriptional regulation of the Arabidopsis *ARGONAUTE1* gene

Adrián Cabezas-Fuster, Rosa Micol-Ponce, Raquel Sarmiento-Mañús and María Rosa Ponce

Instituto de Bioingeniería, Universidad Miguel Hernández, Campus de Elche, 03202 Elche, Alicante, Spain

acabezas@umh.es mrponce@umh.es http://genetics.umh.es

The Arabidopsis ARGONAUTE1 (AGO1) ribonuclease is the main effector of posttranscriptional gene silencing pathways that are mediated by small interfering RNAs, including microRNAs (miRNAs)[1]. Also, a miRNA targets *AGO1* transcripts. Hypomorphic *ago1* alleles disrupt many developmental pathways and responses to biotic and abiotic stress factors; null *ago1* alleles are lethal. Expression of *AGO1* is widespread and virtually constitutive under normal conditions; also *AGO1* expression increases under certain environmental conditions, such as viral infection. We have a wealth of information on the mechanisms by which *AGO1* post-transcriptionally regulates expression of other genes, but we lack information on the transcriptional regulation of *AGO1* itself.

Among other subcellular locations, Arabidopsis AGO1 occurs in the endoplasmic reticulum, where it represses translation of target mRNAs[2]. An *in silico* analysis of the promoter of *AGO1* allowed us to identify two regulatory elements associated with the unfolded protein response (UPR) in the endoplasmic reticulum (Fig. 1), which we also found in the promoters of the *AGO1* orthologs of rice and *Brassica rapa* (Fig. 2); these sequences seem to be relevant for the regulation of *AGO1* expression.

To analyse the transcriptional regulation of *AGO1*, we generated an $AGO1_{pro}$*:GUS* transcriptional fusion, which carries a putative full-length *AGO1* promoter (Fig. 3). To identify the key regulatory *AGO1* promoter sequences, we constructed four transcriptional *GUS* fusions driven by different segments of the *AGO1* promoter, lacking one or both UPR elements (Fig. 3).

Plants homozygous for the $AGO1_{pro}$*#1:GUS* transgene (Fig. 4) were grown on media with different concentrations of NaCl, abscisic acid (ABA), or sucrose, or exposed to different light intensities and dark periods. Dark exposure (Fig. 5) and ABA treatments (Fig. 6) significantly altered GUS activity, but sucrose and NaCl did not affect GUS activity. We are examining $AGO1_{pro}$ fragments by mobility shift assays with nuclear protein extracts. In addition, we are analysing quantitatively the effects of each mutant promoter variant on the expression of the *GUS* reporter gene in plants grown in the different culture conditions mentioned above, and in the presence of tunicamycin or dithiothreitol, which induce UPR.

perfect HSE

aacgacaaaaatgtttttcgtcttgttgttttcgagaagcttctttttccggattaaaaaaa
cattatgcaattccacgtcatcagcgcattacatacaatgaaagactacacacgaccttgg

UPRE2AT

UPRMOTIFIIAR

gtcagcattccaaagaccccaaccctgactcgccacgtcgacatatgccagctattaatgaa
gagggtaattccgtaacttactctaaccacagaacccttgaatttaaagtgtagcaGTAAA
ATCTCATTTCTTTGAGTTATCTCGTTTGTTCGGAGTTAGAGAGAGAGAGAAAGATATAGAG
AGAACACAGAGAGGCGAGAGCGACGTAGGGTTGGTGTTTCGTACGGATTTTCTCGGTCAAT
CTTAGTTTCTCCGGCGAGAGATTGCTTTTCAGgtaaaaatggcggcggttttggtgtttgt
tcttcacttaatctgtgttcgatctgcgtatgaactcgatttttccactcgattgggtgga
tccgcttcgttttggtgttatggttcactgatagtgttgtatgtttagttgatctttgcga
tttcggatctattagcttcgtagctgttttggtgtgtgtgttcgtcttcgaagatatttag
gttttttttttttgttgcttcaaatttcttactgtttcgtgcttgttttcttacttcgttt
tctgtttaggtctttgattgtttcttactaggttttctatgtttgctttgggctgttgaat
ttggtttctatctctctagctaatcactggttttcgtgcttctgagtcgtttgtttttga
agctagttagggttttcttctgttgcttctatatttcgatagttttgtgcttgttttcaat
gtttgcttcttattttcaaggataatttttaaaatgacccactgtttttgggtggttgtgtt
attttcacagGAATCATCGATGGTGAGAA

Figure 1.- Regulatory sequences identified in the promoter of the *AGO1* gene. The perfect HSE, UPRE2AT and UPRMOTIFIIAT elements and the translation initiation codon are highlighted in red, green, yellow and black, respectively. Exonic sequences are shown in capital letters. The untranslated 5' region is shown in red. The regions conserved in Arabidopsis and *Brassica rapa* are underlined in red.

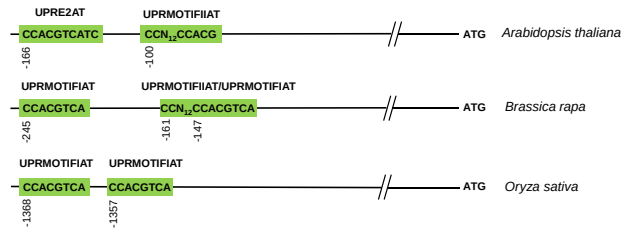

Figure 2.- Conservation of UPR-related regulatory elements across plant *AGO1* promoters. Two or three UPR-related elements are found in the putative promoters of the *Arabidopsis thaliana*, *Brassica rapa* and *Oryza sativa AGO1* orthologs. Numbers indicate the distance, in nucleotides, to the transcriptional start site (not drawn to scale).

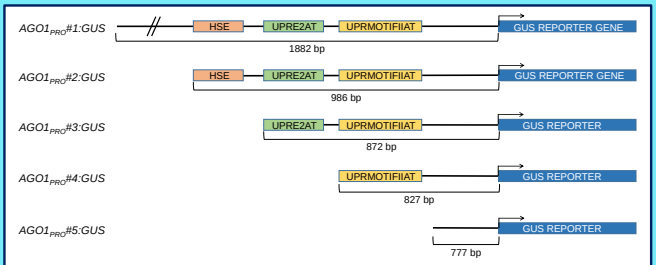

Figure 3.- $AGO1_{pro}$*:GUS* transcriptional fusions constructed in this work (not drawn to scale). $AGO1_{pro}$*#1:GUS* includes the full-length *AGO1* promoter. One, two or three regulatory elements are deleted in the remaining constructs.

Figure 4.- $AGO1_{PRO}$*#1:GUS* activity in a wild-type Col-0 background. GUS staining is shown of (A) a Col-0 wild-type seedling, and (B) a seedling and (C) a rosette of plants homozygous for $AGO1_{pro}$*#1:GUS*. Plants were collected (A, B) 7 and (C) 23 days after stratification (das). Scale bars: 1 mm

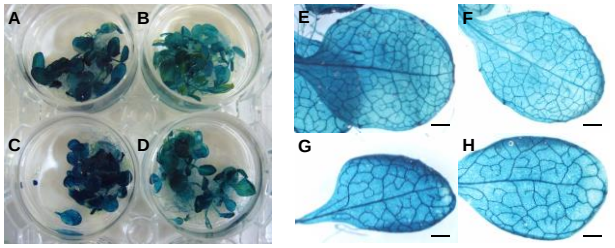

Figure 5.- $AGO1_{pro}$*#1:GUS* expression in Col-0 plants homozygous for $AGO1_{pro}$*#1:GUS*, exposed or not to darkness and sucrose. Plants were grown for 21 days in solid GM medium, and then 6 hours in liquid medium with or without light. Solid and liquid media were supplemented or not with 29 mM sucrose. (A-D) Rosettes and (E-F) leaves from plants (A, C, E, G) exposed or (B, D, F, H) not to darkness, and (A, B, E, F) without or (C, D, G, H) with sucrose. Exposure to darkness increased GUS staining. Scale bars: 1 mm.

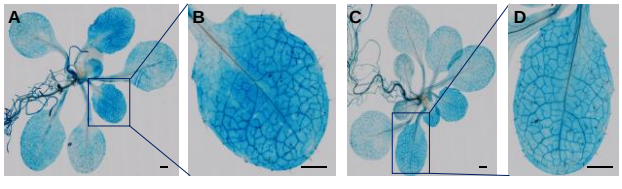

Figure 6.- Effects of ABA on $AGO1_{pro}$*#1:GUS* expression. (A, C) Rosettes and (B, D) vegetative leaves from plants grown in medium (A, B) not supplemented or (C, D) supplemented with 0.1 mM ABA. GUS staining was higher in plants grown in the absence of exogenous ABA. Plants were homozygous for $AGO1_{pro}$*#1:GUS* in the Col-0 genetic background, and were collected 21 das. Scale bars: 1 mm

REFERENCES

1. Kidner, C.A., and Martienssen, R.A. (2005). *Current Opinion in Plant Biology* **8**, 38-44.
2. Li, S., Liu, L., Zhuang ,X., Yu, Y., Liu, X., Cui, X., Ji, L., Pan, Z., Cao, X., Mo, B., Zhang, F., Raikhel, N., Jiang, L., and Chen, X. (2013). *Cell* **153**, 562-574.

ACKNOWLEDGMENTS

Research in the laboratory of M.R.P. is supported by grants from the Ministerio de Economía y Competitividad of Spain (BIO2014-56889-R) and the Generalitat Valenciana (PROMETEOII/2014/006).

Ribosome biogenesis requires RRP7 and NOP53 in Arabidopsis

Rosa Micol-Ponce, Raquel Sarmiento-Mañús, Alejandro Ruiz-Bayón, Sara Fontcuberta-Cervera, Jorge Ruiz-Ramírez, María Rosa Ponce

Instituto de Bioingeniería, Universidad Miguel Hernández, Campus de Elche, 03202 Elche, Spain

We identified *mas2* (*morphology of argonaute1-52 suppressed2*) alleles as informational suppressors of *ago1-52*, a hypomorphic allele of Arabidopsis *AGO1* (*ARGONAUTE1*)[1]. Positional cloning and sequence analysis showed that *MAS2* encodes the Arabidopsis ortholog of NKAP (NF-kappa B activating protein)[2], a protein conserved in most eukaryotes and involved in transcriptional repression in animals. A yeast two-hybrid assay with MAS2 as bait identified 14 interactors, including two putative orthologues of proteins that participate in ribosome biogenesis in *Saccharomyces cerevisiae*: Ribosomal RNA Processing Protein 7 (RRP7) and Nucleolar Protein 53 (NOP53). Ribosome biogenesis requires stoichiometric amounts of ribosomal proteins and ribosomal RNAs (rRNAs). Although rRNA biogenesis consumes most of the transcriptional activity of eukaryotic cells, its regulation remains largely unclear in plants.

We obtained *rrp7-1*, *rrp7-2*, *nop53-1*, and *nop53-2* insertional mutants from public collections; these mutants exhibited pointed and reticulate leaves, similar to many mutants defective in ribosome biogenesis. We constructed $NOP53_{pro}$*:NOP53:GFP* and $RRP7_{pro}$*:RRP7:GFP* translational fusions; examination of transgenic plants showed that RRP7 is nucleolar, and NOP53 both nucleolar and nucleoplasmic.

The yeast orthologs of NOP53 and RRP7 participate in the control of 45S rDNA transcription and transcript processing, processes that we found to be defective in Arabidopsis *nop53* and *rrp7* mutants. All *rrp7* and *nop53* mutations synergistically interacted in double mutants with *parallel1* (*parl1*), a loss-of-function allele of Arabidopsis *NUCL1* isolated in a screen for mutants with altered venation patterning[3]. *NUCL1* encodes the nucleolar protein NUCLEOLIN1, which participates in the epigenetic control of 45S rDNA expression[4]. Morphometry of the vasculature of cotyledons, leaves, and petals showed strong reductions in venation length, density and number of bifurcations in *rrp7-1* and *parl1* mutants, but not in *nop53-1*. Since altered abscisic acid (ABA) responses have been described for several mutations in genes involved in different pathways of RNA metabolism, seeds of *rrp7-1*, *nop53-1* and *parl-1* were sown in medium supplemented with 3 µm ABA.

Their germination rates were undistinguishable from wild type, but *rrp7-1* and *parl1* showed a strongly reduced cotyledon expansion and greening.

We also found synergistic phenotypes in double mutant combinations of *nop53* or *rrp7* with mutations in genes encoding microRNA machinery components. Taken together, our results suggest a functional relationship between the miRNA pathway and ribosome biogenesis.

1. Micol-Ponce, R., Aguilera, V., and Ponce, M.R. (2014). *Scientific Reports* 4, 5533.
2. Sánchez-García, A.B., Aguilera, V., Micol-Ponce, R., Jover-Gil, S., and Ponce, M.R. (2015). *Plant Cell* 27, 1999-2015.
3. Petricka, J.J., and Nelson, T.M. (2007). *Plant Physiology* 144, 173-186.
4. Pontvianne, F., Matía, I., Douet, J., Tourmente, S., Medina, F.J., Echeverria, M., and Saez-Vasquez J. (2007) *Molecular Biology of the Cell* 18, 369-379.

2016
XIII Reunión de Biología Molecular de Plantas
Oviedo
Póster

Ribosome biogenesis requires RRP7 and NOP53 in Arabidopsis

Rosa Micol-Ponce, Raquel Sarmiento-Mañús, Alejandro Ruiz-Bayón, Sara Fontcuberta-Cervera, Jorge Ruiz-Ramírez and María Rosa Ponce

Instituto de Bioingeniería, Universidad Miguel Hernández, Campus de Elche, 03202 Elche, Alicante, Spain.

rmicol@umh.es mrponce@umh.es http://genetica.umh.es

We identified *mas2* (*morphology of argonaute1-52 suppressed2*) alleles as informational suppressors of *ago1-52*, a hypomorphic allele of Arabidopsis *AGO1* (*ARGONAUTE1*)[1]. Positional cloning and sequence analysis showed that *MAS2* encodes the Arabidopsis ortholog of NKAP (NF-kappa B activating protein)[2], a protein conserved in most eukaryotes and involved in transcriptional repression in animals. A yeast two-hybrid assay with MAS2 as bait identified 14 interactors, including two putative orthologues of proteins that participate in ribosome biogenesis in *Saccharomyces cerevisiae*: Ribosomal RNA Processing Protein 7 (RRP7) and Nucleolar Protein 53 (NOP53). Ribosome biogenesis requires stoichiometric amounts of ribosomal proteins and ribosomal RNAs (rRNAs). Although rRNA biogenesis consumes most of the transcriptional activity of eukaryotic cells, its regulation remains largely unclear in plants.

We obtained *rrp7-1*, *rrp7-2*, *nop53-1*, and *nop53-2* insertional mutants from public collections; these mutants exhibited pointed and reticulate leaves, similar to many mutants defective in ribosome biogenesis (Figs. 1 and 2). We constructed *NOP53*$_{pro}$*:NOP53:GFP* and *RRP7*$_{pro}$*:RRP7:GFP* translational fusions; examination of transgenic plants showed that RRP7 is nucleolar, and NOP53 both nucleolar and nucleoplasmic (Figs. 3 and 4).

The yeast orthologs of NOP53 and RRP7 participate in the control of 45S rDNA transcription and transcript processing, processes that we found to be defective in Arabidopsis *nop53* and *rrp7* mutants. All *rrp7* and *nop53* mutations synergistically interacted in double mutants with *parallel1* (*parl1*), a loss-of-function allele of Arabidopsis *NUCL1* isolated in a screen for mutants with altered venation patterning[3]. *NUCL1* encodes the nucleolar protein NUCLEOLIN1, which participates in the epigenetic control of 45S rDNA expression[4]. Morphometry of the vasculature of cotyledons, leaves, and petals showed strong reductions in venation length, density and number of bifurcations in *rrp7-1* and *parl1* mutants, but not in *nop53-1*. Since altered abscisic acid (ABA) responses have been described for several mutations in genes involved in different pathways of RNA metabolism, seeds of *rrp7-1*, *nop53-1* and *parl-1* were sown in medium supplemented with ABA (Fig. 5). Their germination rates were undistinguishable from wild type, but *rrp7-1* and *parl1* showed strongly reduced cotyledon expansion and greening.

We found synergistic phenotypes in double mutant combinations of *nop53* or *rrp7* with mutations in genes encoding microRNA machinery components (Fig. 6). We also observed that NOP53 is required for proper rRNA biogenesis as shown by accumulation of 5.8S precursor molecules in *nop53* mutants (Fig. 7). Taken together, our results suggest a functional relationship between the miRNA pathway and ribosome biogenesis.

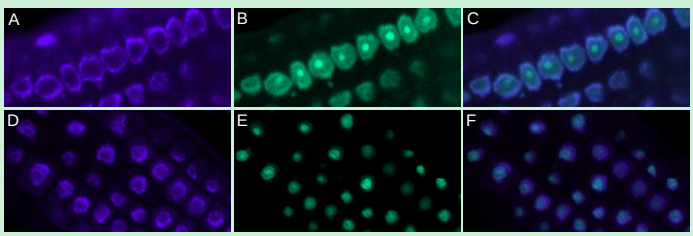

Figure 3.- Nuclear localization of NOP53 and RRP7. (A-L) Detection of the fluorescent emission of (A, D, G, J) DAPI (4',6-diamidino-2-phenylindole), (B, E, H, K) GFP, and (C, F, I, L) their overlay, in roots of transgenic plants expressing the (A-F) *NOP53*$_{pro}$*:NOP53:GFP* and (G-L) *RRP7*$_{pro}$*:RRP7:GFP* transgenes.

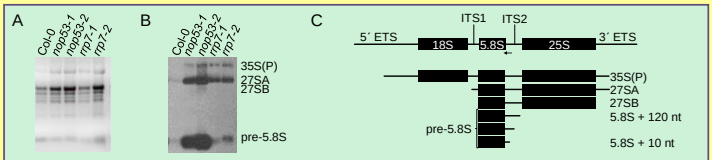

Figure 7.- Accumulation of unprocessed 5.8S rRNA in *nop53* mutants. (A) Total RNA isolated from the Col-0 wild type and the *nop53* and *rrp7* mutants, and (B) Northern analysis of 5.8S rRNA precursors. (C) Diagram illustrating the processing intermediates detected. Horizontal arrow indicate the position of the probe. ETS and ITS: external and internal transcribed spacers, respectively.

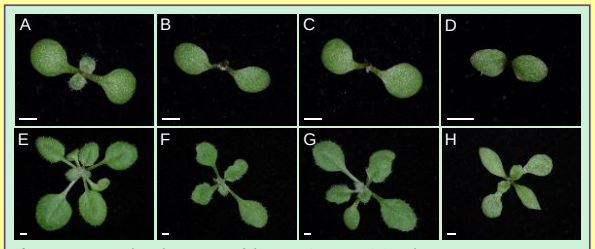

Figure 1.- Vegetative phenotypes of the *nop53-1*, *nop53-2* and *rrp7-1* mutants. Rosettes from (A, E) Col-0, (B, F) *nop53-1*, (C, G) *nop53-2*, and (D, H) *rrp7-1* plants are shown. All mutants are homozygous for the mutations indicated. Pictures were taken (A-D) 7 and (E-H) 14 days after stratification (das). Scale bars: 1 mm.

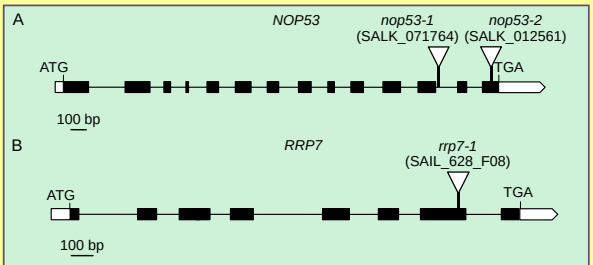

Figure 2.- Structure and mutant alleles of the *NOP53* and *RRP7* genes. Exons and introns are depicted as black boxes and lines, respectively. White boxes indicate 5´- and 3´-UTRs. The predicted translation start (ATG) and stop (TGA) codons are indicated.

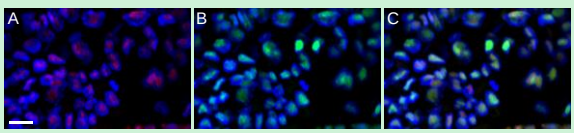

Figure 4.- Nucleolar localization of RRP7 in *35S*$_{pro}$*:RRP7:GFP* root cells. Detection of the fluorescent emission of (A) DAPI and the TRITC (tetramethylrhodamineisothiocyanate) conjugated anti-mouse IgG secondary antibody used to detect fribrillarin, (B) DAPI and GFP, and (C) their overlay. Scale bar: 10 µm.

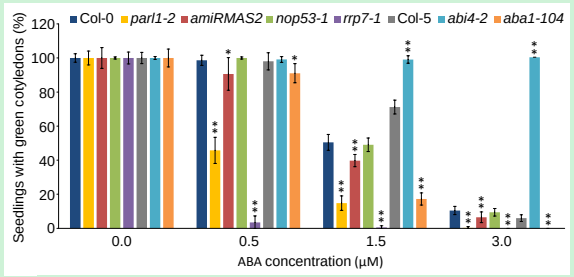

Figure 5.- Effects of ABA on *rrp7-1* and *nop53-1* seedling establishment and post-germination growth. Percentage of seedlings grown in media supplemented with different ABA concentrations that displayed green, fully expanded cotyledons, scored 10 das. Error bars indicate standard deviation. Asterisks indicate significant differences between a mutant and its wild type in Student's *t*-tests (*p<0.05 and **p<0.01).

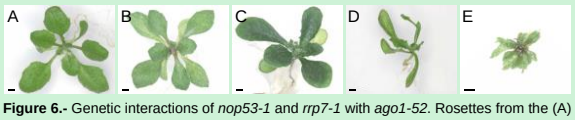

Figure 6.- Genetic interactions of *nop53-1* and *rrp7-1* with *ago1-52*. Rosettes from the (A) *nop53-1*, (B) *rrp7-1* and (C) *ago1-52* single mutants, and the (D) *nop53-1 ago1-52* and (E) *rrp7-1 ago1-52* double mutants. Pictures were taken (A, D) 21 and (B, C, E) 23 das. Scale bars: 1 mm.

REFERENCES

1.- Micol-Ponce, R., Aguilera, V., and Ponce, M.R. (2014). *Scientific Reports* **4**, 5533.
2.- Sánchez-García, A.B., Aguilera, V., Micol-Ponce, R., Jover-Gil, S., and Ponce, M.R. (2015). *Plant Cell* **27**, 1999-2015.
3.- Petricka, J.J., and Nelson, T.M. (2007). *Plant Physiology* **144**, 173-186.
4.- Pontvianne, F., Matía, I., Doue,t J., Tourmente, S., Medina, F.J., Echeverria, M., and Sáez-Vásquez, J. (2007). *Molecular Biology of the Cell* **18**, 369-379.

ACKNOWLEDGEMENTS

Research in the laboratory of M.R.P. is supported by grants from the Ministerio de Economía y Competitividad of Spain (BIO2014-56889-R) and the Generalitat Valenciana (PROMETEOII/2014/006).

NOP53 and RRP7 participate in the control of 45S rDNA transcription and pre-rRNA processing

Rosa Micol-Ponce, Raquel Sarmiento-Mañús, Alejandro Ruiz-Bayón and María Rosa Ponce

Instituto de Bioingeniería, Universidad Miguel Hernández, Campus de Elche, 03202 Elche, Spain

We identified *mas2* (*morphology of argonaute1-52 suppressed2*) alleles as informational suppressors of *ago1-52*, a hypomorphic allele of Arabidopsis *AGO1* (*ARGONAUTE1*) [1]. Positional cloning and sequence analysis showed that *MAS2* encodes the Arabidopsis ortholog of NKAP (NF-kappa B activating protein) [2], a protein conserved in most eukaryotes and involved in transcriptional repression in animals. A yeast two-hybrid assay with MAS2 as bait identified 14 interactors, including two putative orthologues of proteins that participate in ribosome biogenesis in *Saccharomyces cerevisiae*: Ribosomal RNA Processing Protein 7 (RRP7) and Nucleolar Protein 53 (NOP53). Ribosome biogenesis requires stoichiometric amounts of ribosomal proteins and ribosomal RNAs (rRNAs). Although rRNA biogenesis consumes most of the transcriptional activity of eukaryotic cells, its regulation remains largely unclear in plants.

We obtained *rrp7-1*, *rrp7-2*, *nop53-1*, and *nop53-2* insertional mutants from public collections; these mutants exhibited pointed and reticulate leaves, similar to many mutants defective in ribosome biogenesis. We constructed $NOP53_{pro}$*:NOP53:GFP* and $RRP7_{pro}$*:RRP7:GFP* translational fusions; examination of transgenic plants showed that RRP7 is nucleolar, and NOP53 both nucleolar and nucleoplasmic.

The yeast orthologs of NOP53 and RRP7 participate in the control of 45S rDNA transcription and transcript processing, processes that we found to be defective in Arabidopsis *nop53* and *rrp7* mutants. All *rrp7* and *nop53* mutations synergistically interacted in double mutants with *parallel1* (*parl1*), a loss-of-function allele of Arabidopsis *NUCL1* isolated in a screen for mutants with altered venation patterning [3]. *NUCL1* encodes the nucleolar protein NUCLEOLIN1, which participates in the epigenetic control of 45S rDNA expression [4]. Morphometry of the vasculature of cotyledons, leaves, and petals showed strong reductions in venation length, density and number of bifurcations in *rrp7-1* and *parl1* mutants, but not in *nop53-1*. Since altered abscisic acid (ABA) responses have been described for several mutations in genes involved in different pathways of RNA metabolism,

seeds of *rrp7-1*, *nop53-1* and *parl-1* were sown in medium supplemented with 3 µm ABA. Their germination rates were undistinguishable from wild type, but *rrp7-1* and *parl1* showed a strongly reduced cotyledon expansion and greening.

We also found synergistic phenotypes in double mutant combinations of *nop53* or *rrp7* with mutations in genes encoding microRNA machinery components. Taken together, our results suggest a functional relationship between the miRNA pathway and ribosome biogenesis.

1. Micol-Ponce, R., Aguilera, V., and Ponce, M.R. (2014). *Scientific Reports* 4, 5533.
2. Sánchez-García, A.B., Aguilera, V., Micol-Ponce, R., Jover-Gil, S., and Ponce, M.R. (2015). *Plant Cell* 27, 1999-2015.
3. Petricka, J.J., and Nelson, T.M. (2007). *Plant Physiology* 144, 173-186.
4. Pontvianne, F., Matía, I., Douet, J., Tourmente, S., Medina, F.J., Echeverria, M., and Saez-Vasquez J. (2007) *Molecular Biology of the Cell* 18, 369-379.

2016

27th International Conference on Arabidopsis Research

GyeongJu, Corea del Sur

Póster

NOP53 and RRP7 participate in the control of 45S rDNA transcription and pre-rRNA processing

Rosa Micol-Ponce, Raquel Sarmiento-Mañús, Alejandro Ruiz-Bayón and María Rosa Ponce

Instituto de Bioingeniería, Universidad Miguel Hernández, Campus de Elche, 03202 Elche, Alicante, Spain.

rmicol@umh.es mrponce@umh.es http://genetica.umh.es

We identified *mas2* (*morphology of argonaute1-52 suppressed2*) alleles as informational suppressors of *ago1-52*, a hypomorphic allele of Arabidopsis *AGO1* (*ARGONAUTE1*)[1]. Positional cloning and sequence analysis showed that *MAS2* encodes the Arabidopsis ortholog of NKAP (NF-kappa B activating protein)[2], a protein conserved in most eukaryotes and involved in transcriptional repression in animals. A yeast two-hybrid assay with MAS2 as bait identified 14 interactors, including two putative orthologues of proteins that participate in ribosome biogenesis in *Saccharomyces cerevisiae*: Ribosomal RNA Processing Protein 7 (RRP7) and Nucleolar Protein 53 (NOP53). Ribosome biogenesis requires stoichiometric amounts of ribosomal proteins and ribosomal RNAs (rRNAs). Although rRNA biogenesis consumes most of the transcriptional activity of eukaryotic cells, its regulation remains largely unclear in plants.

We obtained *rrp7-1*, *rrp7-2*, *nop53-1*, and *nop53-2* insertional mutants from public collections; these mutants exhibited pointed and reticulate leaves, similar to many mutants defective in ribosome biogenesis (Figs. 1 and 2). We constructed $NOP53_{pro}$*:NOP53:GFP* and $RRP7_{pro}$*:RRP7:GFP* translational fusions; examination of transgenic plants showed that RRP7 is nucleolar, and NOP53 both nucleolar and nucleoplasmic (Figs. 3 and 4).

The yeast orthologs of NOP53 and RRP7 participate in the control of 45S rDNA transcription and transcript processing, processes that we found to be defective in Arabidopsis *nop53* and *rrp7* mutants. All *rrp7* and *nop53* mutations synergistically interacted in double mutants with *parallel1* (*parl1*), a loss-of-function allele of Arabidopsis *NUCL1* isolated in a screen for mutants with altered venation patterning[3]. *NUCL1* encodes the nucleolar protein NUCLEOLIN1, which participates in the epigenetic control of 45S rDNA expression[4]. Morphometry of the vasculature of cotyledons, leaves, and petals showed strong reductions in venation length, density and number of bifurcations in *rrp7-1* and *parl1* mutants, but not in *nop53-1*. Since altered abscisic acid (ABA) responses have been described for several mutations in genes involved in different pathways of RNA metabolism, seeds of *rrp7-1*, *nop53-1* and *parl-1* were sown in medium supplemented with ABA (Fig. 5). Their germination rates were undistinguishable from wild type, but *rrp7-1* and *parl1* showed strongly reduced cotyledon expansion and greening.

We found synergistic phenotypes in double mutant combinations of *nop53* or *rrp7* with mutations in genes encoding microRNA machinery components (Fig. 6). We also observed that NOP53 is required for proper rRNA biogenesis as shown by accumulation of 5.8S precursor molecules in *nop53* mutants (Fig. 7). Taken together, our results suggest a functional relationship between the miRNA pathway and ribosome biogenesis.

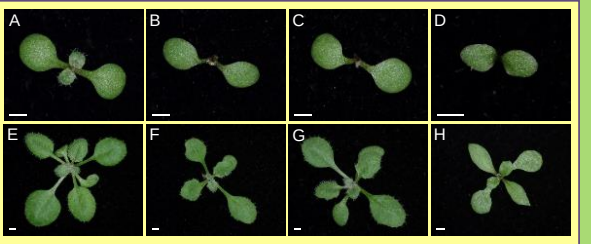

Figure 1.- Vegetative phenotypes of the *nop53-1*, *nop53-2* and *rrp7-1* mutants. Rosettes from (A, E) Col-0, (B, F) *nop53-1*, (C, G) *nop53-2*, and (D, H) *rrp7-1* plants are shown. All mutants are homozygous for the mutations indicated. Pictures were taken (A-D) 7 and (E-H) 14 days after stratification (das). Scale bars: 1 mm.

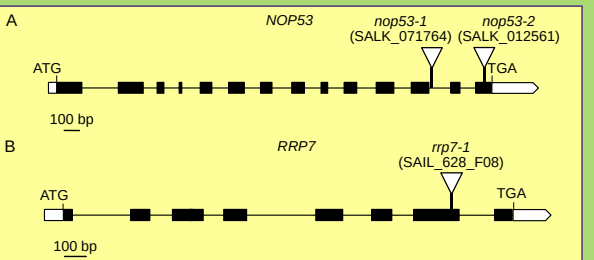

Figure 2.- Structure and mutant alleles of the *NOP53* and *RRP7* genes. Exons and introns are depicted as black boxes and lines, respectively. White boxes indicate 5´- and 3´-UTRs. The predicted translation start (ATG) and stop (TGA) codons are indicated.

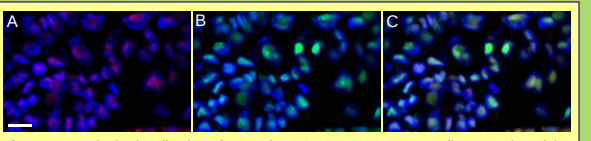

Figure 4.- Nucleolar localization of RRP7 in $35S_{pro}$*:RRP7:GFP* root cells. Detection of the fluorescent emission of (A) DAPI and the TRITC (tetramethylrhodamineisothiocyanate) conjugated anti-mouse IgG secondary antibody used to detect fribrillarin, (B) DAPI and GFP, and (C) their overlay. Scale bar: 10 µm.

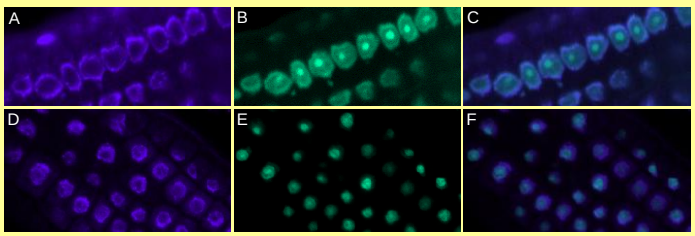

Figure 3.- Nuclear localization of NOP53 and RRP7. (A-L) Detection of the fluorescent emission of (A, D, G, J) DAPI (4',6-diamidino-2-phenylindole), (B, E, H, K) GFP, and (C, F, I, L) their overlay, in roots of transgenic plants expressing the (A-C) $NOP53_{pro}$*:NOP53:GFP* and (D-F) $RRP7_{pro}$*:RRP7:GFP* transgenes.

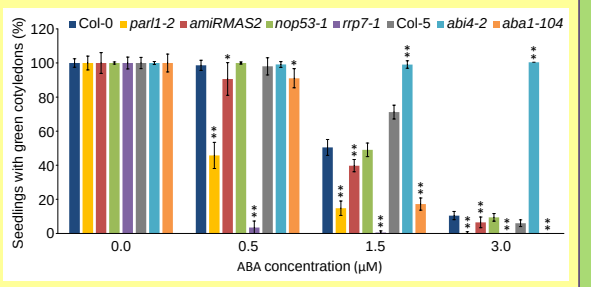

Figure 5.- Effects of ABA on *rrp7-1* and *nop53-1* seedling establishment and post-germination growth. Percentage of seedlings grown in media supplemented with different ABA concentrations that displayed green, fully expanded cotyledons, scored 10 das. Error bars indicate standard deviation. Asterisks indicate significant differences between a mutant and its wild type in Student's *t*-tests (*p<0.05 and **p<0.01).

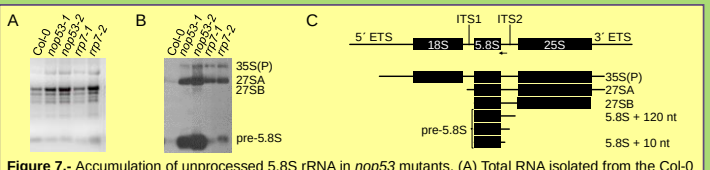

Figure 7.- Accumulation of unprocessed 5.8S rRNA in *nop53* mutants. (A) Total RNA isolated from the Col-0 wild type and the *nop53* and *rrp7* mutants, and (B) Northern analysis of 5.8S rRNA precursors. (C) Diagram illustrating the processing intermediates detected. Horizontal arrow indicate the position of the probe. ETS and ITS: external and internal transcribed spacers, respectively.

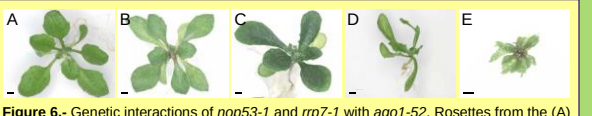

Figure 6.- Genetic interactions of *nop53-1* and *rrp7-1* with *ago1-52*. Rosettes from the (A) *nop53-1*, (B) *rrp7-1* and (C) *ago1-52* single mutants, and the (D) *nop53-1 ago1-52* and (E) *rrp7-1 ago1-52* double mutants. Pictures were taken (A, D) 21 and (B, C, E) 23 das. Scale bars: 1 mm.

REFERENCES

1.- Micol-Ponce, R., Aguilera, V., and Ponce, M.R. (2014). *Scientific Reports* **4**, 5533.

2.- Sánchez-García, A.B., Aguilera, V., Micol-Ponce, R., Jover-Gil, S., and Ponce, M.R. (2015). *Plant Cell* **27**, 1999-2015.

3.- Petricka, J.J., and Nelson, T.M. (2007). *Plant Physiology* **144**, 173-186.

4.- Pontvianne, F., Matía, I., Doue,t J., Tourmente, S., Medina, F.J., Echeverria, M., and Sáez-Vásquez, J. (2007). *Molecular Biology of the Cell* **18**, 369-379.

ACKNOWLEDGEMENTS

Research in the laboratory of M.R.P. is supported by grants from the Ministerio de Economía y Competitividad of Spain (BIO2014-56889-R) and the Generalitat Valenciana (PROMETEOII/2014/006).

The Arabidopsis RIBOSOMAL RNA PROCESSING7 nucleolar protein is required for 40S ribosome subunit biogenesis

Micol-Ponce, R., Sarmiento-Mañús, R., Ruiz-Bayón, A., Mora-Navarro, E., and Ponce, M.R.

Instituto de Bioingeniería, Universidad Miguel Hernández, Campus de Elche, 03202 Elche, Spain

NF-kappa B activating protein (NKAP) is a multifunctional protein that acts in splicing and transcriptional repression in animals. The Arabidopsis ortholog of NKAP is MORPHOLOGY OF argonaute1-52 SUPPRESSED2 (MAS2), which is required for 45S rDNA transcription and 45S pre-rRNA processing [1]. Ribosomal RNA processing protein 7 (Rrp7) participates in the biogenesis of the 40S ribosomal subunit in *Saccharomyces cerevisiae*.

We identified RRP7, the Arabidopsis ortholog of Rrp7, in a yeast two-hybrid screen for MAS2 interactors. We found RRP7 localized at the nucleolus. Lack of RRP7 function causes nucleolar hypertrophy, 18S rRNA altered processing, and nucleolar retention of mature and precursor 18S rRNA species. The pleiotropic phenotype of *rrp7* mutants includes altered shoot phyllotaxy, aberrant lateral organ venation pattern and ABA hypersensitivity at the seedling establishment stage.

The *RRP7* gene is coexpressed with genes encoding factors required for 45S pre-rRNA processing and ribosome subunit assembly, including *SMALL ORGAN4* (*SMO4*), which is required for 5.8S rRNA maturation. The Arabidopsis *NUCLEOLIN1* (*NUC1*) and *NUC2* redundant genes encode nucleolar proteins that participate in the epigenetic control of 45S rDNA expression [2]. We observed synergistic phenotypes in double mutant combinations of alleles of *RRP7* with alleles of *NUC1*, *NUC2*, *MAS2* or genes encoding components of the microRNA machinery. *rrp7* alleles seem epistatic to *smo4* alleles. The Arabidopsis genome contains hundreds of 45S rDNA genes, with four types of variants (*VAR*). *VAR* patterns of expression differ among accessions and developmental stages, and these patterns are altered in the *rrp7* and *smo4* mutants. Our results unveil the action and interactions of a key factor in 40S ribosome subunit biogenesis in Arabidopsis.

1. Sánchez-García, A.B., *et al.* (2015). *Plant Cell* 27, 1999-2015.
2. Pontvianne, F., *et al.* (2010). *PLOS Genet.* 6, e1001225.

2017
Plant Organ Growth Symposium 2017
Elche
Póster

The Arabidopsis RIBOSOMAL RNA PROCESSING7 nucleolar protein is required for 40S ribosome subunit biogenesis

Rosa Micol-Ponce, Raquel Sarmiento-Mañús, Alejandro Ruiz-Bayón, Eloy Mora-Navarro and María Rosa Ponce

Instituto de Bioingeniería, Universidad Miguel Hernández, Campus de Elche, 03202 Elche, Alicante, Spain.

rmicol@umh.es mrponce@umh.es http://genetica.umh.es

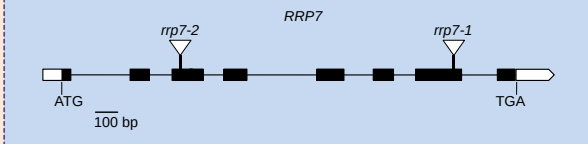

Figure 1.- Structure and mutant alleles of the *RRP7* gene. Exons and introns are depicted as black boxes and lines, respectively. White boxes indicate 5´- and 3´-UTRs. The predicted translation start (ATG) and stop (TGA) codons are indicated.

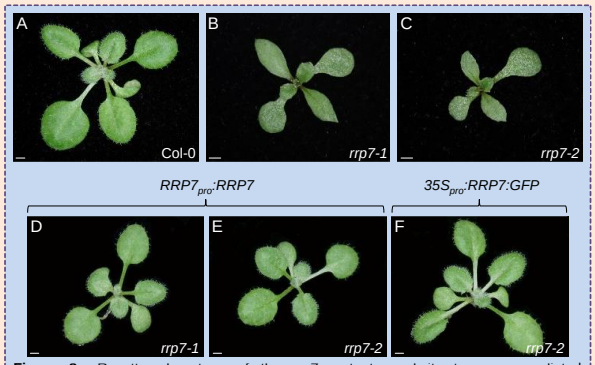

Figure 2.- Rosette phenotype of the *rrp7* mutants and its transgene-mediated complementation. (A-F) Rosettes of (A) Col-0, (B) *rrp7-1*, (C) *rrp7-2*, (D) *rrp7-1 RRP7pro:RRP7*, (E) *rrp7-2 RRP7pro:RRP7*, and (F) *rrp7-2 RRP7pro:RRP7:GFP* plants. All plants were homozygous for the mutations and transgenes shown. Pictures were taken 14 days after stratification (das). Scale bars: 1 mm.

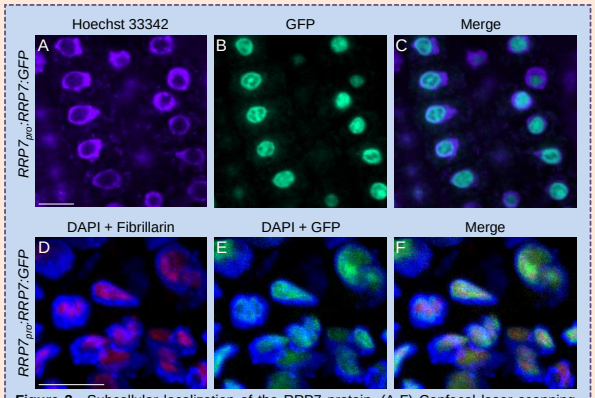

Figure 3.- Subcellular localization of the RRP7 protein. (A-F) Confocal laser scanning microscopy of roots of plants homozygous for the *RRP7proRRP7:GFP* transgene. Fluorescence signals correspond to: (A) Hoechst 33342, (B) GFP, (C) and their overlay. (D-F) Immunolocalization of Fibrillarin in the same plants. Fluorescence signals correspond to: (D) DAPI and the secondary antibody for Fibrillarin detection, (E) DAPI and GFP, (F) and their overlay. Scale bars: 10 µm.

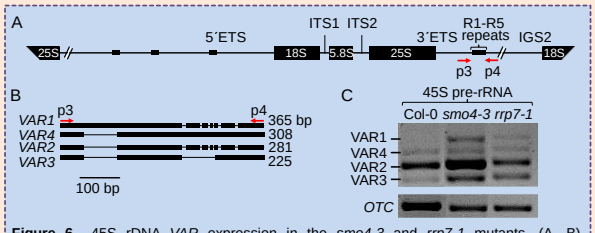

Figure 6.- 45S rDNA *VAR* expression in the *smo4-3* and *rrp7-1* mutants. (A, B) Schematic representation of (A) the 45S pre-RNA, and (B) its 3´ETS polymorphic region. (C) PCR analysis of the relative abundance of 45S rRNA variants in complementary DNA from Col-0, *smo4-3* and *rrp7-1*. The p3 and p4 primers shown in A and B were used.

ACKNOWLEDGEMENTS

Research in the laboratory of M.R.P. is supported by grants from the Ministerio de Economía y Competitividad of Spain (BIO2014-56889-R) and the Generalitat Valenciana (PROMETEOII/2014/006).

NF-kappa B activating protein (NKAP) is a multifunctional protein that acts in splicing and transcriptional repression in animals. The Arabidopsis ortholog of NKAP is MORPHOLOGY OF argonaute1-52 SUPPRESSED2 (MAS2), which is required for 45S rDNA transcription and 45S pre-rRNA processing. Ribosomal RNA processing protein 7 (Rrp7) participates in the biogenesis of the 40S ribosomal subunit in *Saccharomyces cerevisiae*.

We identified RRP7, the Arabidopsis ortholog of Rrp7, in a yeast two-hybrid screen for MAS2 interactors. The pleiotropic phenotype of *rrp7* mutants includes altered shoot phylotaxy, aberrant lateral organ venation patterns (Figures 1 and 2). To further confirm that the phenotype of *rrp7* mutants was caused by the absence of *RRP7* activity, we constructed *RRP7pro:RRP7* and *35Spro:RRP7:GFP* transgenes. Those transgenes were transferred into *rrp7* mutant plants and fully complemented their phenotypes (Figure 2). We found that RRP7 localizes to the nucleolus (Figure 3). Lack of RRP7 function causes nucleolar hypertrophy, altered processing of the 18S rRNA, and nucleolar retention of mature and precursor 18S rRNA species (Figure 4).

The *RRP7* gene is coexpressed with genes encoding factors required for 45S pre-rRNA processing and ribosome subunit assembly, including *SMALL ORGAN4* (*SMO4*), which is required for 5.8S rRNA maturation. The Arabidopsis *NUCLEOLIN1* (*NUC1*) and *NUC2* genes encode nucleolar proteins that have redundant functions in the epigenetic control of 45S rDNA expression. We observed synergistic phenotypes in double mutant combinations of alleles of *RRP7* with alleles of *NUC1*, *NUC2*, *MAS2*, or genes encoding components of the microRNA machinery (Figure 5). We also found that *rrp7* alleles are epistatic to *smo4* alleles.

The Arabidopsis genome contains hundreds of 45S rDNA genes, with four types of variants (*VAR*). *VAR* patterns of expression differ among accessions and developmental stages, and these patterns are altered in the *rrp7* and *smo4* mutants (Figure 6). Our results unveil the action and interactions of a key factor in 40S ribosome subunit biogenesis in Arabidopsis.

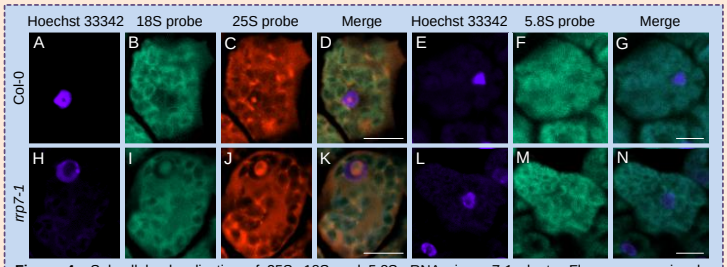

Figure 4.- Subcellular localization of 25S, 18S and 5.8S rRNAs in *rrp7-1* plants. Fluorescence signals correspond to: (A, E, H, L) Hoechst 33342, (B, I) 18S rRNA probe, (C, J) 25S rRNA probe, (F, M) 5.8S rRNA probe, and (D, K, G, N) their overlay. Scale bars: 10 µm.

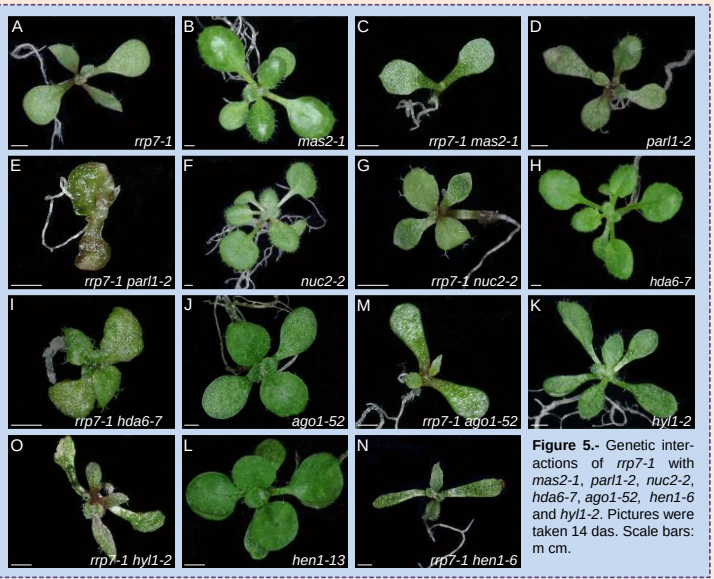

Figure 5.- Genetic interactions of *rrp7-1* with *mas2-1*, *parl1-2*, *nuc2-2*, *hda6-7*, *ago1-52*, *hen1-6* and *hyl1-2*. Pictures were taken 14 das. Scale bars: m cm.

Arabidopsis *SMALL ORGAN4* encodes a nucleolar and nucleoplasmic protein required for 5.8S rRNA maturation

Micol-Ponce, R., Sarmiento-Mañús, R., Fontcuberta-Cervera, S., and Ponce, M.R.

Instituto de Bioingeniería, Universidad Miguel Hernández, Campus de Elche, 03202 Elche, Spain

MORPHOLOGY OF argonaute1-52 SUPPRESSED2 (MAS2) is the Arabidopsis ortholog of metazoan NF-kappa B activating protein (NKAP). MAS2 is required for 45S rDNA transcription and 45S pre-rRNA processing [1], and NKAP is involved in splicing and transcriptional repression. In *Saccharomyces cerevisiae*, Nucleolar protein 53 (Nop53) participates in the biogenesis of the 60S ribosomal subunit.

The Arabidopsis ortholog of Nop53 is SMALL ORGAN4 (SMO4) [2], which we identified as a MAS2 interactor in a yeast two-hybrid screen. In a genetic screen for Arabidopsis mutants with altered leaf shape, we identified *denticulata2* (*den2*), which we found to be an allele of *SMO4*. The morphological phenotype caused by *den2* is similar to, but stronger than that of *smo4* insertional alleles; all these mutants exhibit reticulate, pointed, and dentate vegetative leaves.

Null *smo4* alleles cause accumulation of 5.8S rRNA precursors, as already described for its yeast and human orthologs. We found the Arabidopsis SMO4 protein localized mainly to the nucleolus but also to the nucleoplasm. The *SMO4* gene is coexpressed with genes encoding factors required for 45S pre-rRNA processing and ribosome subunit assembly, including *RIBOSOMAL RNA PROCESSING7* (*RRP7*), which is involved in 18S rRNA maturation. Our results on the morphological, cytological and molecular phenotypes caused by the lack of function of SMO4 shed light on the role of this protein in 60S ribosomal subunit biogenesis and confirm its interaction with MAS2.

1. Sánchez-García, A.B., *et al.* (2015). *Plant Cell* 27, 1999-2015.
2. Zhang, X.R., *et al.* (2015). *J. Integr. Plant Biol.* 57, 810-818.

2017
Plant Organ Growth Symposium 2017
Elche
Póster

Arabidopsis *SMALL ORGAN4* encodes a nucleolar and nucleoplasmic protein required for 5.8S rRNA maturation

Rosa Micol-Ponce, Raquel Sarmiento-Mañús, Sara Fontcuberta-Cervera, and María Rosa Ponce

Instituto de Bioingeniería, Universidad Miguel Hernández, Campus de Elche, 03202 Elche, Alicante, Spain.

rmicol@umh.es mrponce@umh.es http://genetica.umh.es

MORPHOLOGY OF argonaute1-52 SUPPRESSED2 (MAS2) is the Arabidopsis ortholog of metazoan NF-kappa B activating protein (NKAP). MAS2 is required for 45S rDNA transcription and 45S pre-rRNA processing, and NKAP is involved in splicing and transcriptional repression. In *Saccharomyces cerevisiae*, Nucleolar protein 53 (Nop53) participates in the biogenesis of the 60S ribosomal subunit.

The Arabidopsis ortholog of Nop53 is SMALL ORGAN4 (SMO4), which we identified as a MAS2 interactor in a yeast two-hybrid screen. In a genetic screen for Arabidopsis mutants with altered leaf shape, we identified *denticulata2* (*den2*), which we found to be an allele of *SMO4*. The morphological phenotype caused by *den2* is similar to, but stronger than that of *smo4* insertional alleles; all these mutants exhibit reticulate, pointed, and dentate vegetative leaves (Figures 1 and 2).

We found the Arabidopsis SMO4 protein localized mainly to the nucleolus but also to the nucleoplasm (Figure 4). Null *smo4* alleles cause accumulation of 5.8S rRNA precursors, as already described for its yeast and human orthologs (Figure 5). The *SMO4* gene is coexpressed with genes encoding factors required for 45S pre-rRNA processing and ribosome subunit assembly, including *RIBOSOMAL RNA PROCESSING7* (*RRP7*), which is involved in 18S rRNA maturation.

In addition, *smo4* alleles synergistically interact with *mas2-1*, as well as with mutant alleles of genes encoding nucleolins (Figure 6) and key components of the miRNA pathway (Figure 7). Our results on the morphological, cytological and molecular phenotypes caused by the lack of function of *SMO4* shed light on the role of this protein in 60S ribosomal subunit biogenesis and confirm its interaction with *MAS2*.

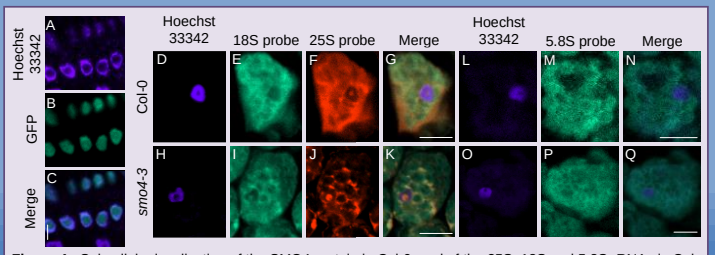

Figure 4.- Subcellular localization of the SMO4 protein in Col-0, and of the 25S, 18S and 5.8S rRNAs in Col-0 and *smo4-2*. (A-C) Confocal laser scanning microscopy of roots of plants homozygous for the *SMO4*$_{pro}$*SMO4:GFP* transgene. Fluorescence signals correspond to: (A) Hoechst 33342, (B) GFP, and (C) their overlay. (D-Q) Confocal laser scanning microscopy of roots of Col-0 and *smo4-3* plants. Fluorescence signals correspond to: (D, L, H, O) Hoechst 33342, (E, I) 18S probe, (F. J) 25S probe, (M, N) 5.8S probe, and (G, K, N, Q) their overlays. Scale bars: 10 µm.

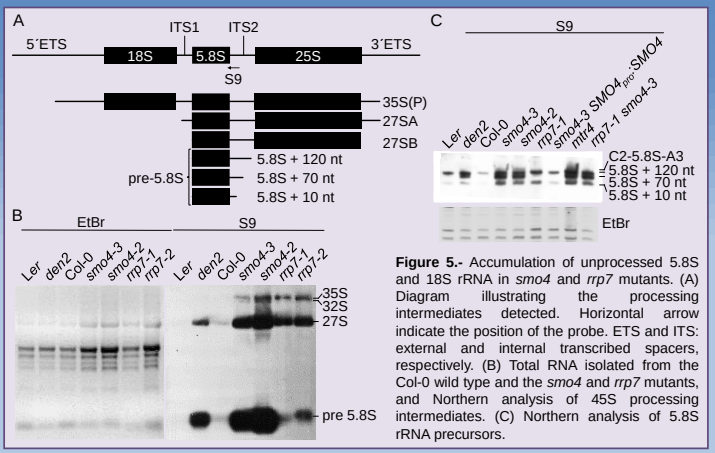

Figure 5.- Accumulation of unprocessed 5.8S and 18S rRNA in *smo4* and *rrp7* mutants. (A) Diagram illustrating the processing intermediates detected. Horizontal arrow indicate the position of the probe. ETS and ITS: external and internal transcribed spacers, respectively. (B) Total RNA isolated from the Col-0 wild type and the *smo4* and *rrp7* mutants, and Northern analysis of 45S processing intermediates. (C) Northern analysis of 5.8S rRNA precursors.

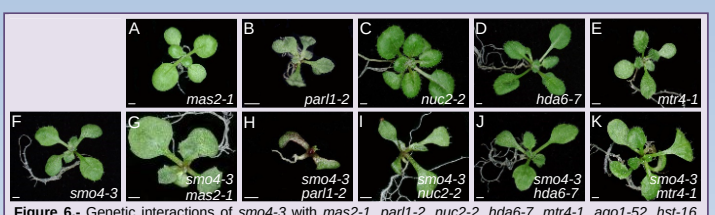

Figure 6.- Genetic interactions of *smo4-3* with *mas2-1*, *parl1-2*, *nuc2-2*, *hda6-7*, *mtr4-1*, *ago1-52*, *hst-16*, *hen1-13* and *hyl1-2*. Pictures were taken 14 das. Scale bars: 1 mm.

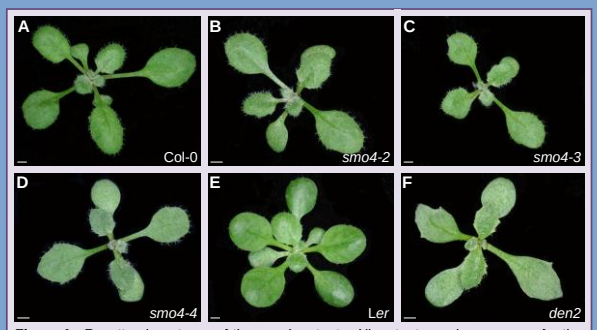

Figure 1.- Rosette phenotypes of the *smo4* mutants. All mutants are homozygous for the mutations indicated. Pictures were taken 14 days after stratification (das). Scale bars: 1 mm.

Figure 2.- Structure and mutant alleles of the *SMO4* gene. Exons and introns are depicted as black boxes and lines, respectively. White boxes represent the 5´- and 3´-UTRs. The predicted translation start (ATG) and stop (TGA) codons are indicated. A red arrow indicates the position of the *den2* point mutation.

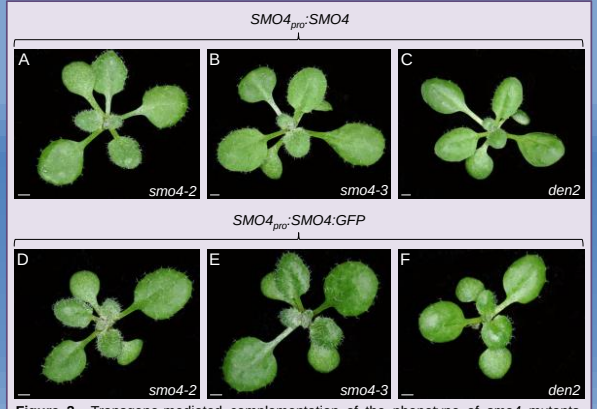

Figure 3.- Transgene-mediated complementation of the phenotype of *smo4* mutants. Plants were homozygous for the (A-C) *SMO4*$_{pro}$*:SMO4* and (D-F) *SMO4*$_{pro}$*:SMO4:GFP* transgenes. Pictures were taken 14 das. Scale bars: 1 mm.

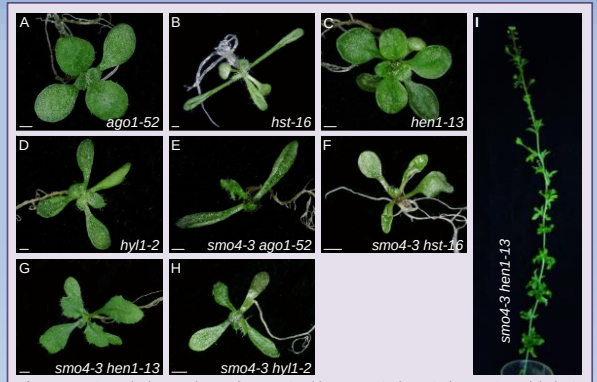

Figure 7.- Genetic interactions of *smo4-3* with *ago1-52*, *hst-16*, *hen1-13 and hyl1-2*. Pictures were taken (A-H) 14 das, and (I) 60 das. Scale bars: 1 mm.

ACKNOWLEDGEMENTS

Research in the laboratory of M.R.P. is supported by grants from the Ministerio de Economía y Competitividad of Spain (BIO2014-56889-R) and the Generalitat Valenciana (PROMETEOII/2014/006).

Characterization of the Arabidopsis *MORPHOLOGY OF ARGONAUTE1-52 SUPPRESSED5* gene

Cabezas-Fuster, A., Micol-Ponce, R., Senent-Valero, Y., and Ponce, M.R.

Instituto de Bioingeniería, Universidad Miguel Hernández, Campus de Elche, 03202 Elche, Alicante, Spain

ARGONAUTE1 (AGO1) functions as part of the RNA-induced silencing complex and *ago1* mutations affect leaf development and polarity. To examine AGO1 function in leaf development, we carried out a screen for genetic suppressors. To this end, we used ethyl methanesulfonate to mutagenize the Arabidopsis *ago1-52* line, which carries a hypomorphic, viable and recessive allele of *AGO1*. We screened 37,000 M_2 seeds, and isolated 23 viable double mutants exhibiting suppression of the leaf phenotype of *ago1-52*; the lines carrying second site mutations were named *mas* (*morphology of argonaute1-52 suppressed*) [1].

This screen identified six alleles of *MAS5* and positional cloning of the *mas5-1* mutation allowed us to identify a G→A transition (Lys→Glu) in AT1G80070 (*PRE-MRNA PROCESSING8; PRP8*), which encodes a key splicing factor. Null alleles of *PRP8* (*MAS5*) and its yeast and animal orthologs are embryonic lethal. Our *mas5* alleles might be neomorphic or antimorphic: they act as dominant suppressors of *ago1-52* but do not exhibit any visible phenotype in a wild-type genetic background.

The *ago1-52* allele carries a mutation that causes mis-splicing of its pre-mRNA, which finally produces a mixture of mutant and entirely wild-type AGO1 proteins; this aberrant splicing is not modified in the *ago1-52 mas5-1* double mutant plants. However, we observed a higher level of the wild-type AGO1 protein in *ago1-52 mas5-1* plants than in *ago1-52* plants.

We are studying the genetic interactions of *ago1-52* with *prp8* hypomorphic alleles obtained by other authors, and with mutations that cause mis-splicing, in order to ascertain the molecular nature of the suppression effect caused by *mas5* alleles on *ago1-52*.

1. Micol-Ponce, R*., et al.* (2015). *Sci. Rep*. 4, 5533.

2017

Plant Organ Growth Symposium 2017

Elche

Póster

Characterization of the Arabidopsis *MORPHOLOGY OF ARGONAUTE1-52 SUPRESSED5* gene

Adrián Cabezas-Fuster, Rosa Micol-Ponce, Yaiza Senent-Valero and María Rosa Ponce

Instituto de Bioingeniería, Universidad Miguel Hernández, Campus de Elche, 03202 Elche, Alicante, Spain

acabezas@umh.es mrponce@umh.es http://genetics.umh.es

ARGONAUTE1 (AGO1) functions as part of the RNA-induced silencing complex and *ago1* mutations affect leaf development and polarity. To examine AGO1 function in leaf development, we carried out a screen for genetic suppressors. To this end, we used ethyl methanesulfonate to mutagenize the Arabidopsis *ago1-52* line, which carries a hypomorphic, viable and recessive allele of *AGO1*[1]. We screened 37,000 M2 seeds, and isolated 23 viable double mutants exhibiting suppression of the leaf phenotype of *ago1-52*; the lines carrying second site mutations were named *mas* (*morphology of argonaute1-52 suppressed*)[2].

This screen identified six alleles of *MAS5* (Fig. 1) and positional cloning of the *mas5-1* mutation allowed us to identify a G→A transition (Lys→Glu) (Fig. 2) in AT1G80070 (*PRE-MRNA PROCESSING8; PRP8*), which encodes a key splicing factor (Fig. 3)[3]. Null alleles of *PRP8 (MAS5*) and its yeast and animal orthologs are embryonic lethal[4]. Our *mas5* alleles might be neomorphic or antimorphic: they act as dominant suppressors of *ago1-52* but do not exhibit any visible phenotype in a wild-type genetic background (Fig. 4).

The *ago1-52* allele carries a mutation that causes mis-splicing of its pre-mRNA, which finally produces a mixture of mutant and entirely wild-type AGO1 proteins; this aberrant splicing is not modified in the *ago1-52 mas5-1* double mutant plants (Fig. 5 and 6). However, we observed a higher level of the wild-type AGO1 protein in *ago1-52 mas5-1* plants than in *ago1-52* plants.

We are studying the genetic interactions of *ago1-52* with *prp8* hypomorphic alleles obtained by other authors, and with mutations that cause mis-splicing, in order to ascertain the molecular nature of the suppression effect caused by *mas5* alleles on *ago1-52*.

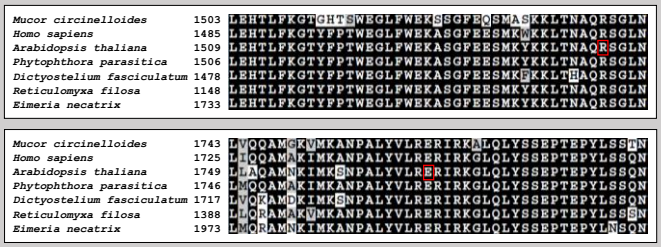

Figure 2.- Sequence conservation among eukaryotic PRP8 orthologs. Numbers indicate amino acid residues. Only the region harboring the amino acid changed (red rectangles) by *mas5-3* (1547) and *mas5-1* (1769) mutations is shown. Identical or similar residues shared by at least 50% of proteins are shaded black or grey, respectively. Sequences were obtained from UniProt (http://www.uniprot.org/), the aligned with ClustalX2 (http://www.clustal.org/clustal2/) and shaded with Boxshade 3.21 (http://www.ch.embnet.org/software/BOX_form.html).

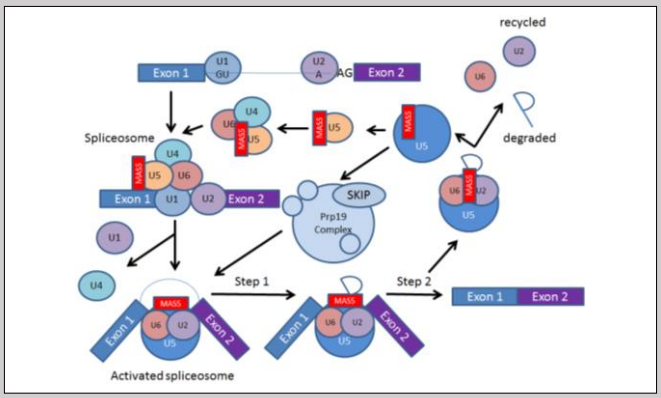

Figure 3.- Assembly and recycling of major spliceosome components. PRP8 appears here as MAS5. U1-U6 are small nuclear RNA–protein (snRNP) complexes formed by small nuclear RNAs (snRNAs) and proteins. The spliceosome is formed stepwise, through several presplicing complexes. Splicing involves two trans-esterification reactions that require PRP8. Following completion of the splicing reaction, spliceosome components are recycled and the intron is degraded. Adapted from Grainger and Beggs (2005)[4].

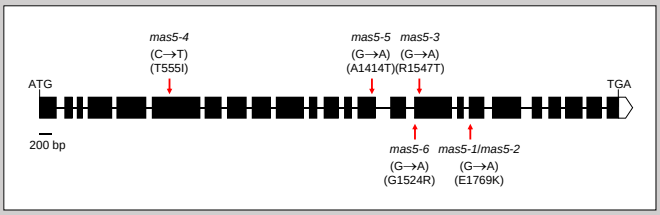

Figure 1.- Structure and mutant alleles of the *MAS5* gene. Exons and introns are depicted as black boxes and lines, respectively. White box indicates 3´-UTR. The predicted translation start (ATG) and stop (TGA) codons are indicated. Red arrows mark the positions of the point mutations in the *mas5* alleles, and the predicted nucleotide and amino acid substitutions in the *MAS5* gene and protein, respectively.

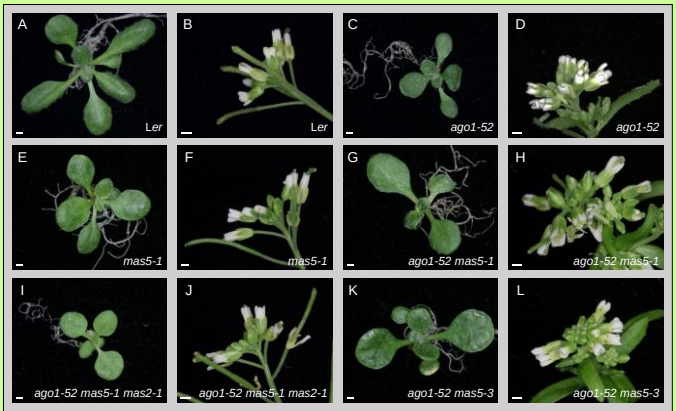

Figure 4.- Suppression of the phenotype of *ago1-52* by *mas5* alleles. (A, C, E, G, I, K) Rosettes and (B, D, F, H, J, L) inflorescences from (A, B) L*er* ,(C, D) *ago1-52*, (E, F) *mas5-1*, (G, H) *ago1-52 mas5-1*, (I, J) *ago1-52 mas5-1 mas2-1*, and (K, L) *ago1-52 mas5-3*. Pictures were taken (A, C, E, G, I, K) 14 and (B, D, F, H, J, L) 40 days after stratification (das). Scale bars: 1 mm.

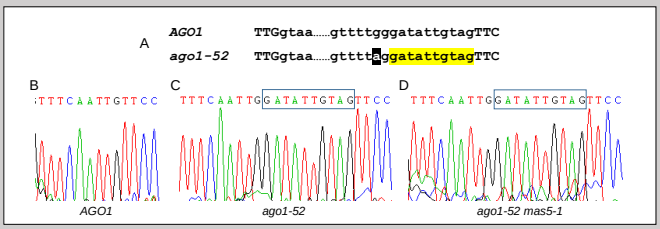

Figure 5.- The aberrant splicing of *ago1-52* seems not to be modified in the *ago1-52 mas5-1* double mutant. (A) Partial sequence of the wild type *AGO1* (L*er*) and the mutant *ago1-52* alleles. Exons are shown in uppercase and introns in lowercase letters. The nucleotide mutated in *ago1-52* is shaded black. The nucleotides highlighted in yellow (B) are absent from the mature mRNA of the wild-type *AGO1*, (C) but present in the mature mRNA of the *ago1-52* single mutants and (D) the *ago1-52 mas5-1* double mutant.

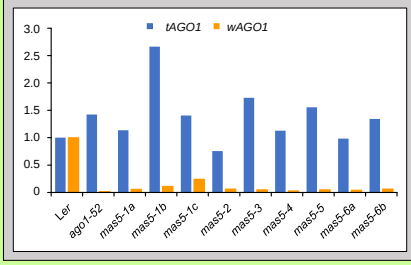

Figure 6.- RT-qPCR analysis of the modification of the relative levels of *tAGO1* (total *AGO1* mRNAs) and *wAGO1* (wild-type *AGO1* mRNAs) splice forms in the *mas5* suppressor lines identified. The *mas5-1a*, *mas5-1b* and *mas5-1c* lines carry the same *mas5-1* mutation; they were isolated from the same parental group. The *mas5-6a* and *mas5-6b* lines carry the same *mas5-6* mutation; they were isolated from the same parental group. RNA was extracted from plants collected 15 das.

ACKNOWLEDGMENTS

Research in the laboratory of M.R.P. is supported by grants from the Ministerio de Economía y Competitividad of Spain (BIO2014-56889-R) and the Generalitat Valenciana (PROMETEOII/2014/006).

REFERENCES

1.- Berná, G., Robles, P., and Micol, J.L. (1999). *Genetics*. **152**, 729-742.
2.- Micol-Ponce, R., Aguilera, V., and Ponce, M.R. (2014). *Sci Rep*. **4**, 5533.
3.- Grainger, R.J., and Beggs, J.D. (2005). *RNA* **11,** 533-537.
4.- Schwartz, B.W., Yeung, E.C., and Meinke, D.W. (1994). *Development* **120**, 3235-3245.

Genetic and physical interactions between CAX INTERACTING PROTEIN4 and MORPHOLOGY OF ARGONAUTE1-52 SUPPRESSED2 in Arabidopsis

Aceituno-Valenzuela, U., Ruiz-Bayón, A., Sarmiento-Mañús, R., Micol-Ponce, R., and Ponce, M.R.

Instituto de Bioingeniería, Universidad Miguel Hernández, Campus de Elche, 03202 Elche, Spain

The Arabidopsis ortholog of metazoan NF-kappa B Activating Protein is MORPHOLOGY OF ARGONAUTE1-52 SUPPRESSED2 (MAS2), an essential protein that seems to play a key role in the regulation of rRNA synthesis. By imaging of a MAS2:GFP fusion and fluorescence *in situ* hybridization, we found that MAS2 colocalizes with the 45S rDNA in nucleolar organizer regions. To identify MAS2 interactors, we performed a yeast two-hybrid screen; the most represented interactor found, in 23 of 55 positive clones, was CAX INTERACTING PROTEIN4 (CXIP4). This protein is of unknown function and was previously identified as interacting with the high-affinity vacuolar calcium antiporter CATION EXCHANGER1 (CAX1). CXIP4 is a plant-specific protein, with a conserved CCHC-type zinc finger motif (zinc knuckle), which is involved in DNA, RNA, and protein binding. In addition, the 30 N-terminal amino acids of CXIP4 show 70% similarity to mammalian Splicing regulatory protein, glutamine/lysine-rich 1 (SREK1)-interacting protein 1.

CXIP4 is a single-copy essential gene in Arabidopsis, as shown by its insertional allele *cxip4-1*, which causes embryonic lethality. To circumvent such lethality, we constructed artificial microRNAs (*amiR-CXIP4*) targeting the *CXIP4* mRNA. The a*miR-CXIP4* plants displayed pointed and reticulate leaves, a phenotype that is characteristic of mutants affected in genes encoding ribosomal proteins and other genes involved in translation.

Additional transgenes were obtained to complement the lethality of homozygous *cxip4-1* plants, and to visualize the expression pattern of *CXIP4* and the subcellular localization of CXIP4. We are also studying the genetic interactions between *CXIP4* and *MAS2*, and between *cxip4* alleles and alleles of genes encoding components of the microRNA pathway and ribosomal factors. Our preliminary results suggest that CXIP4 is involved in ribosome biogenesis or the control of translation.

2017

Plant Organ Growth Symposium 2017

Elche

Póster

Genetic and physical interactions between CAX INTERACTING PROTEIN4 and MORPHOLOGY OF ARGONAUTE1-52 SUPPRESSED2 in Arabidopsis

Uri Aceituno-Valenzuela, Alejandro Ruiz-Bayón, Raquel Sarmiento-Mañús, Rosa Micol-Ponce, and Maria Rosa Ponce

uaceituno@umh.es mrponce@umh.es

Instituto de Bioingeniería, Universidad Miguel Hernández, Campus de Elche, 03202 Elche, Alicante, Spain

The Arabidopsis ortholog of metazoan NF-kappa B Activating Protein is MORPHOLOGY OF ARGONAUTE1-52 SUPPRESSED2 (MAS2), an essential protein that seems to play a key role in the regulation of rRNA synthesis[1]. By imaging of a MAS2:GFP fusion and fluorescence *in situ* hybridization, we found that MAS2 colocalizes with the 45S rDNA in nucleolar organizer regions. To identify MAS2 interactors, we performed a yeast two-hybrid screen; the most represented interactor found, in 23 of 55 positive clones, was CAX INTERACTING PROTEIN4 (CXIP4). This protein is of unknown function and was previously identified as interacting with the high-affinity vacuolar calcium antiporter CATION EXCHANGER 1 (CAX1)[2]. CXIP4 is a plant-specific protein, with a conserved CCHC-type zinc finger motif (zinc knuckle), which is involved in DNA, RNA, and protein binding[3]. In addition, the 30 N-terminal amino acids of CXIP4 show 70% similarity to mammalian Splicing regulatory protein, glutamine/lysine-rich 1 (SREK1)-interacting protein 1 (SREK1IP1; Figure 1).

CXIP4 is a single-copy essential gene in Arabidopsis, as shown by its insertional allele *cxip4-1*, which causes embryonic lethality. (Figure 2).To circumvent such lethality, we constructed artificial microRNAs (*amiR-CXIP4*) targeting the *CXIP4* mRNA. The a*miR-CXIP4* plants displayed pointed and reticulate leaves, a phenotype that is characteristic of mutants affected in genes encoding ribosomal proteins and other genes involved in translation (Figure 3).

Additional transgenes were obtained to complement the lethality of homozygous *cxip4-1* plants, and to visualize the expression pattern of *CXIP4* (Figure 4). and the subcellular localization of CXIP4. We are also studying the genetic interactions between *CXIP4* and *MAS2*, and between *cxip4* alleles and alleles of genes encoding components of the microRNA pathway and ribosomal factors. Our preliminary results suggest that CXIP4 is involved in ribosome biogenesis or the control of translation.

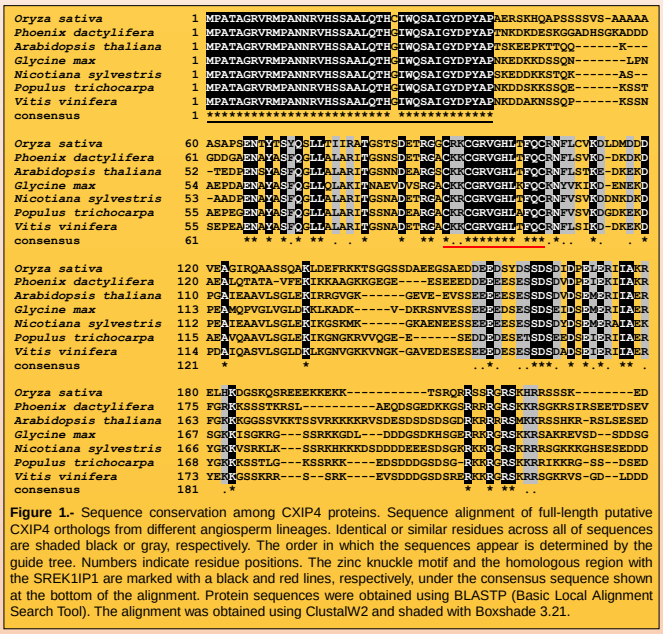

Figure 1.- Sequence conservation among CXIP4 proteins. Sequence alignment of full-length putative CXIP4 orthologs from different angiosperm lineages. Identical or similar residues across all of sequences are shaded black or gray, respectively. The order in which the sequences appear is determined by the guide tree. Numbers indicate residue positions. The zinc knuckle motif and the homologous region with the SREK1IP1 are marked with a black and red lines, respectively, under the consensus sequence shown at the bottom of the alignment. Protein sequences were obtained using BLASTP (Basic Local Alignment Search Tool). The alignment was obtained using ClustalW2 and shaded with Boxshade 3.21.

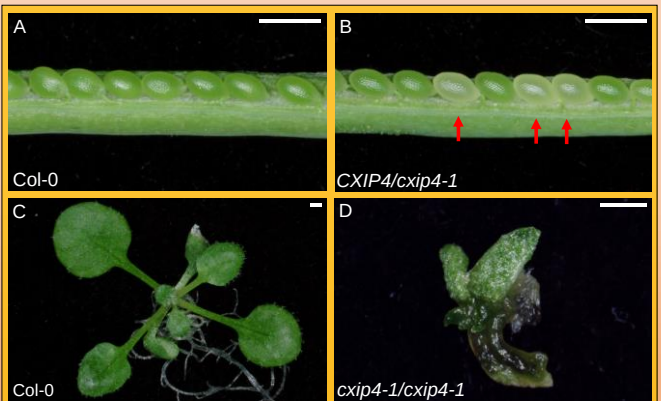

Figure 2.- Phenotypic effects of *CXIP4* loss of function. (A, B) Dissected immature siliques from (A) Col-0 and (B) *CXIP4/cxip4-1* plants. Red arrows indicate aborted seeds. (C, D) Two-week old rosettes from (C) Col-0 and (D) a *cxip4-1/cxip4-1* representative escaper plant. Scale bars indicate 1 mm. Ten siliques of five plants of each genotype were analysed. The percentage of clear seeds, carrying probably aborted seeds, was 4.1% ± 3.38 and 20.9% ± 4.63 in siliques of Col-0 and *CXIP4/cxip4-1* plants, respectively.These differences were significative in a Student's *t*-test (*p < 0.05).

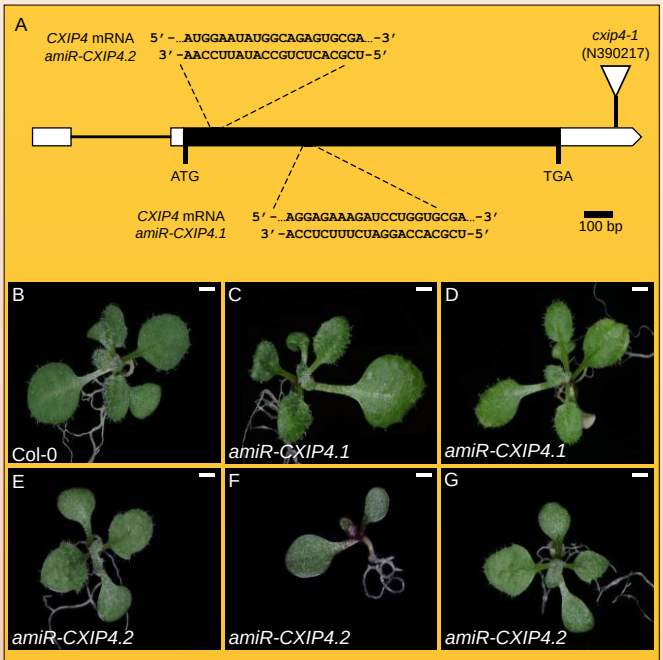

Figure 3.- Obtaining of amiRNAs to silence *CXIP4*. (A) Structure of the *CXIP4* and design of amiRNAs. Introns and exons are represented as black lines and boxes, respectively. Untranslated and coding regions are shown in white and black, respectively. The triangle indicates the T-DNA insertion carried by the *cxip4-1* lethal allele. (B-G) Sequences of amiRNAs and their pairing sequences in the *CXIP4* mRNA are shown. (B-G) Vegetative phenotypes of (B) Col-0 and several independent T2 individuals carrying constructs producing two different amiRNAs; (C, D) *amiRCXIP4.1* or (E-G) *amiR-CXIP4.2*. Pictures were taken 14 days after stratification (das). Scale bars: 1 mm.

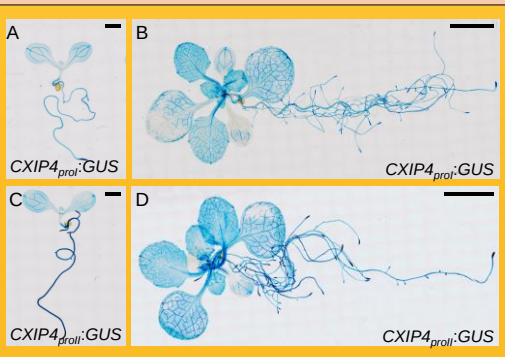

Figure 4.-Visualization of $CXIP4_{pro}$:*GUS* activity in wild-type plants. Two different promotor regions were used in the constructs, of 2104 (*proI*) and 971 (*proII*) bp. Plants were collected (A, C) 7 and (B, D) 14 das. Scale bars: (A,C) 1 mm and (B, D) 5 mm.

ACKNOWLEDGEMENTS

Research in the laboratory of M. R. P. was supported by grants from the Ministerio de Economía y Competitividad of Spain (BIO2014-56889-R) and the Generalitat Valenciana (PROMETEOII/2014/006). U.I.V. held predoctoral fellowships from the Generalitat Valenciana (GRISOLÍAP/2016/A/134)

REFERENCES

1.- Sánchez-García, A.B., Aguilera, V., Micol-Ponce, R., Jover-Gil, S., and Ponce, M.R. (2015). *Plant Cell* **27**, 1999-2015.

2.- Cheng, N.H., Liu, J.Z., Nelson, R.S., and Hirschi, K.D. (2004). *FEBS Letters* **559**, 99-106.

3.- Gamsjaeger *et,al.*(2007).*Trends Biochem. Sci.* **32**, 63-70,

VIII.- AGRADECIMIENTOS

II.- AGRADECIMIENTOS

La realización de esta Tesis ha sido posible gracias a la financiación de la investigación que se realiza en el laboratorio de María Rosa Ponce por la Generalitat Valenciana (PROMETEO/2009/112, ACOMP/2009/049 y PROMETEOII/2014/006) y el Ministerio de Economía, Industria y Competitividad (BIO2014-56889-R).

A mi directora, María Rosa Ponce, por enseñarme todo lo que sé de Genética, por transmitirme la ilusión por la ciencia y por creer en mí siempre, tanto dentro como fuera del laboratorio.

A José Luis Micol, por ayudarme siempre que lo he necesitado durante estos años y por sus aportaciones a nuestro trabajo.

A todos los que se han marchado del laboratorio pero me han ayudado durante mis primeros años (Rafa, Silvia, Sara, Leila, José María, Diana, Tania, Verónica, Bea, Paqui, Rubén, David E., Almudena Mollá, Almudena Ferrández, Ana Belén, Amani, Rebeca y Zeynep).

A mis alumnos y alumnas que me han ayudado a sacar el trabajo adelante (Lucía, Francisco, Alejandro, Noemi, Adrián, Eloy y Sara). En especial a Sara que ha pasado, y sigue pasando, mucho tiempo en el laboratorio y me ha ayudado mucho.

A mis compañeros actuales (José Manuel, Raquel, Tamara, Edu, María José, Juan, Sergio, Carla, Alejandro, Adrián, Uri, Riad, Lucía, Samuel y David Wilson), por hacer del laboratorio un ambiente tan agradable y cercano.

A José Manuel por estar siempre pendiente de todos tanto dentro como fuera del laboratorio.

A Raquel por ayudarme tanto en el laboratorio con las técnicas y las dudas que me han ido surgiendo.

A Leila, Rubén, Tamara, David Wilson y Edu por dejarme formar parte de sus vidas también fuera del laboratorio.

A Tamara por su amistad incondicional, por estar siempre ahí y por ser una de las mejores cosas que me llevo del laboratorio. Muchas gracias por todo.

A Luis Oñate por recibirme con los brazos abiertos en su laboratorio y enseñarme la técnica de un híbrido de la levadura.

A Javier Medina por sus conversaciones sobre el nucleolo y por dejarme aprender en su laboratorio la técnica de la inmunolocalización.

A mis padres por querer siempre lo mejor para mí y por haberme dejado formar parte de esto aunque en ocasiones no fuese lo más fácil.

A mi familia y amigos porque sin entender del todo en lo que trabajo se interesan por lo que hago.